bound on R_c such that $\bar{P}_e \to 0$ as $n \to \infty$. For unquantized (soft-decision) decoding, R_0 is given as

$$R_0 = \log_2 \frac{2}{1 + e^{-\mathscr{E}_c/N_0}} \tag{8-1-102}$$

where $\mathscr{E}_c/N_0 = R_c \gamma_b$ is the SNR per dimension. This result was derived in Section 7-2.

On the other hand, if the output of the demodulator is quantized to Q levels prior to decoding, the Chernoff bound may be used to upper-bound the ensemble average binary error probability $\overline{P_2(\mathbf{s}_i, \mathbf{s}_m)}$ defined in Section 7-2. The result of this derivation is the same upper bound on $\bar{P}_e$ given in (8-1-101) but with R_0 replaced by R_Q, where

$$R_Q = \max_{\{p_j\}} \left\{ -\log_2 \sum_{i=0}^{Q-1} \left[\sum_{j=0}^{1} p_j \sqrt{P(i \mid j)} \right]^2 \right\} \tag{8-1-103}$$

In (8-1-103), $\{p_j\}$ are the prior probabilities of the two signals at the input to the channel and $\{P(i \mid j)\}$ denote the transition probabilities of the channel. For example, in the case of a binary symmetric channel, we have $p_1 = p_0 = \frac{1}{2}$, $P(0 \mid 0) = P(1 \mid 1) = 1 - p$, and $P(0 \mid 1) = P(1 \mid 0) = p$. Hence,

$$R_Q = \log_2 \frac{2}{1 + \sqrt{4p(1-p)}} \qquad Q = 2 \tag{8-1-104}$$

where

$$p = Q(\sqrt{2\gamma_b R_c}) \tag{8-1-105}$$

A plot of R_Q versus $10 \log (\mathscr{E}_c/N_0)$ is illustrated in Fig. 8-1-15 for $Q = 2$ and $Q = \infty$ (soft-decision decoding). Note that the difference in decoder performance between unquantized soft-decision decoding and hard-decision decoding is approximately 2 dB. In fact, it is easily demonstrated again that as $\mathscr{E}_c/N_0 \to 0$, the loss in performance due to hard-decision decoding is

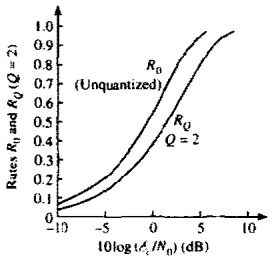

FIGURE 8-1-15 Comparison of R_0 (soft-decision decoding) with R_Q (hard-decision decoding) as a function of the SNR per dimension.

$10 \log_{10} \frac{1}{2}\pi \approx 2$ dB, which is the same decibel difference that was obtained in our comparison of the channel capacity relations. We mention that about 1 dB of this loss can be recovered by quantizing the output of the demodulator to three levels instead of two (see Problem 7-11). Additional improvements are possible by quantizing the output into more than three levels, as shown in Section 7-3.

8-1-7 Bounds on Minimum Distance of Linear Block Codes

The expressions for the probability of error derived in this chapter for soft-decision and hard-decision decoding of linear binary block codes clearly indicate the importance that the minimum distance parameter plays in the performance of the code. If we consider soft-decision decoding, for example, the upper bound on the error probability given by (8-1-52) indicates that, for a given code rate $R_c = k/n$, the probability of error in an AWGN channel decreases exponentially with $d_{\min}$. When this bound is used in conjunction with the lower bound on $d_{\min}$ given below, we obtain an upper bound on P_M that can be achieved by many known codes. Similarly, we may use the upper bound given by (8-1-82) for the probability of error for hard-decision decoding in conjunction with the lower bound on $d_{\min}$ to obtain an upper bound on the error probability for linear binary block codes on the binary symmetric channel.

On the other hand, an upper bound on $d_{\min}$ can be used to determine a lower bound on the probability of error achieved by the best code. For example, suppose that hard-decision decoding is employed. In this case, we have the two lower bounds on P_M given by (8-1-86) and (8-1-87), with the former being the tighter. When either one of these two bounds is used in conjunction with an upper bound on $d_{\min}$ the result is a lower bound on P_M for the best (n, k) code. Thus, upper and lower bounds on $d_{\min}$ are important in assessing the capabilities of codes.

A simple upper bound on the minimum distance of an (n, k) binary or non-binary linear block code was given in (8-1-14) as $d_{\min} \leq n - k + 1$. It is convenient to normalize this expression by the block size n. That is,

$$\frac{d_{\min}}{n} \leq (1 - R_c) + \frac{1}{n} \tag{8-1-106}$$

where R_c is the code rate. For large n, the factor $1/n$ can be neglected.

If a code has the largest possible distance, i.e., $d_{\min} = n - k + 1$, it is called a *maximum-distance-separable code*. Except for the trivial repetition-type codes, there are no binary maximum-separable codes. In fact, the upper bound in (8-1-106) is extremely loose for binary codes. On the other hand, nonbinary codes with $d_{\min} = n - k + 1$ do exist. For example, the Reed–Solomon codes, which comprise a subclass of BCH codes, are maximum-distance-separable.

In addition to the upper bound given above, there are several relatively

tight bounds on the minimum distance of linear block codes. We shall briefly describe four important bounds, three of which are upper bounds and the other a lower bound. The derivations of these bounds are lengthy and are not of particular interest in our subsequent discussion. The interested reader may refer to Chapter 4 of the book by Peterson and Weldon (1972) for those derivations.

One upper bound on the minimum distance can be obtained from the inequality in (8-1-83). By taking the logarithm of both sides of (8-1-83) and dividing by n, we obtain

$$1 - R_c \geq \frac{1}{n} \log_2 \sum_{i=0}^{t} \binom{n}{i} \tag{8-1-107}$$

Since the error-correcting capability of the code, measured by t, is related to the minimum distance, the above relation is an upper bound on the minimum distance. It is called the *Hamming upper bound.*

The asymptotic form of (8-1-107) is obtained by letting $n \to \infty$. Now, for any n, let t_0 be the largest integer t for which (8-1-107) holds. Then, it can be shown (Peterson and Weldon, 1972) that as $n \to \infty$, the ratio t/n for any (n, k) block code cannot exceed t_0/n, where t_0/n satisfies the equation

$$1 - R_c = H(t_0/n) \tag{8-1-108}$$

and $H(x)$ is the binary entropy function defined by (3-2-10).

The generalization of the Hamming bound to nonbinary codes is simply

$$1 - R_c \geq \frac{1}{n} \log_q \left[\sum_{i=0}^{t} \binom{n}{i} (q-1)^i \right] \tag{8-1-109}$$

Another upper bound, developed by Plotkin (1960), may be stated as follows. The number of check digits required to achieve a minimum distance $d_{\min}$ in an (n, k) linear block code satisfies the inequality

$$n - k \geq \frac{q d_{\min} - 1}{q - 1} - 1 - \log_q d_{\min} \tag{8-1-110}$$

where q is the alphabet size. When the code is binary, (8-1-110) may be expressed as

$$\frac{d_{\min}}{n} \left(1 - \frac{1}{2d_{\min}} \log_2 d_{\min} \right) \leq \frac{1}{2} \left(1 - R_c + \frac{2}{n} \right)$$

In the limit as $n \to \infty$ with $d_{\min}/n \leq \frac{1}{2}$, (8-1-110) reduces to

$$d_{\min}/n \leq \tfrac{1}{2}(1 - R_c) \tag{8-1-111}$$

Finally, there is another tight upper bound on the minimum distance obtained by Elias (Berlekamp, 1968). It may be expressed in its asymptotic form as

$$d_{\min}/n \leq 2A(1-A) \tag{8-1-112}$$

where the parameter A is related to the code rate through the equation

$$R_c = 1 + A\log_2 A + (1-A)\log_2(1-A), \quad 0 \leq A \leq \tfrac{1}{2} \tag{8-1-113}$$

Lower bounds on the minimum distance of (n, k) block codes also exist. In particular, binary block codes exist that have a normalized minimum distance that asymptotically satisfies the inequality

$$d_{\min}/n \geq \alpha \tag{8-1-114}$$

where α is related to the code rate through the equation

$$\begin{aligned} R_c &= 1 - H(\alpha) \\ &= 1 + \alpha\log_2 \alpha + (1-\alpha)\log_2(1-\alpha), \quad 0 \leq \alpha \leq \tfrac{1}{2} \end{aligned} \tag{8-1-115}$$

This lower bound is a special case of a lower bound developed by Gilbert (1952) and Varsharmov (1957), which applies to nonbinary and binary block codes.

The asymptotic bounds given above are plotted in Fig. 8-1-16 for binary codes. Also plotted in the figure for purposes of comparison are curves of the minimum distance as a function of code rate for BCH codes of block lengths $n = 31$ and 63. We observe that for $n = 31$ and 63, the normalized minimum distance falls well above the Varsharmov–Gilbert lower bound. As the block length n increases, the efficiency of the BCH codes diminishes. For example, when $n = 1023$, the curve for the normalized minimum distance falls close to

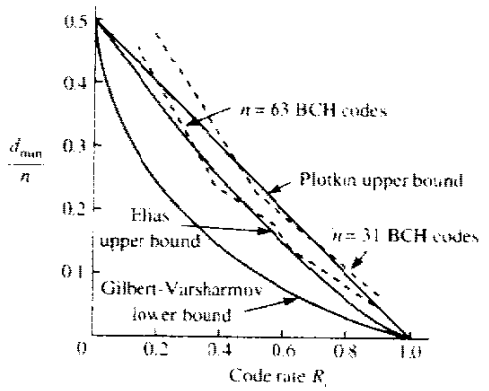

FIGURE 8-1-16 Upper and lower bounds on normalized minimum distance as a function of code rate.

the Varsharmov-Gilbert bound. As n increases beyond $n = 1023$, the normalized minimum distance of the BCH codes continues to decrease and falls below the Varsharmov-Gilbert bound. That is, $d_{\min}/n$ approaches zero as n tends to infinity. Consequently the BCH codes, which are the most important class of cyclic codes, are not very efficient at large block lengths.

8-1-8 Nonbinary Block Codes and Concatenated Block Codes

A nonbinary block code consists of a set of fixed-length code words in which the elements of the code words are selected from an alphabet of q symbols, denoted by $\{0, 1, 2, \ldots, q-1\}$. Usually, $q = 2^k$, so that k information bits are mapped into one of the q symbols. The length of the nonbinary code word is denoted by N and the number of information symbols encoded into a block of N symbols is denoted by K. The minimum distance of the nonbinary code is denoted by $D_{\min}$. A systematic (N, K) block code consists of K information symbols and $N - K$ parity check symbols.

Among the various types of nonbinary linear block codes, the Reed-Solomon codes are some of the most important for practical applications. As indicated previously, they comprise a subset of the BCH codes, which in turn are a class of cyclic codes. These codes are described by the parameters

$$\begin{aligned} N &= q - 1 = 2^k - 1 \\ K &= 1, 2, 3, \ldots, N - 1 \\ D_{\min} &= N - K + 1 \\ R_c &= K/N \end{aligned} \tag{8-1-116}$$

Such a code is guaranteed to correct up to

$$\begin{aligned} t &= \lfloor \tfrac{1}{2}(D_{min} - 1) \rfloor \\ &= \lfloor \tfrac{1}{2}(N - K) \rfloor \end{aligned} \tag{8-1-117}$$

symbol errors. Of course, these codes may be extended or shortened in the manner described previously for binary block codes.

The weight distribution $\{A_i\}$ of the class of Reed-Solomon codes is known. The coefficients in the weight enumerating polynomial are given as

$$A_i = \binom{N}{i}(q-1)\sum_{j=0}^{i-D}(-1)^j\binom{i-1}{j}q^{i-j-D}, \qquad i \geq D_{\min} \tag{8-1-118}$$

where $D \equiv D_{min}$ and $q = 2^k$.

One reason for the importance of the Reed-Solomon codes is their good

distance properties. A second reason for their importance is the existence of efficient hard-decision decoding algorithms, which make it possible to implement relatively long codes in many practical applications where coding is desirable.

A nonbinary code is particularly matched to an M-ary modulation technique for transmitting the 2^k possible symbols. Specifically, M-ary orthogonal signaling, e.g., M-ary FSK, is frequently used. Each of the 2^k symbols in the q-ary alphabet is mapped to one of the $M = 2^k$ orthogonal signals. Thus, the transmission of a code word is accomplished by transmitting N orthogonal signals, where each signal is selected from the set of $M = 2^k$ possible signals.

The optimum demodulator for such a signal corrupted by AWGN consists of M matched filters (or cross-correlators) whose outputs are passed to the decoder, either in the form of soft decisions or in the form of hard decisions. If hard decisions are made by the demodulator, the symbol error probability P_M and the code parameters are sufficient to characterize the performance of the decoder. In fact, the modulator, the AWGN channel, and the demodulator form an equivalent discrete (M-ary) input, discrete (M-ary) output, symmetric memoryless channel characterized by the transition probabilities $P_c = 1 - P_M$ and $P_M/(M-1)$. This channel model, which is illustrated in Fig. 8-1-17, is a generalization of the BSC.

The performance of the hard-decision decoder may be characterized by the following upper bound on the code word error probability:

$$P_e \leq \sum_{i=t+1}^{N} \binom{N}{i} P_M^i (1 - P_M)^{N-i} \tag{8-1-119}$$

where t is the number of errors guaranteed to be corrected by the code.

When a code word error is made, the corresponding symbol error probability is

$$P_{es} = \frac{1}{N} \sum_{i=t+1}^{N} i \binom{N}{i} P_M^i (1 - P_M)^{N-i} \tag{8-1-120}$$

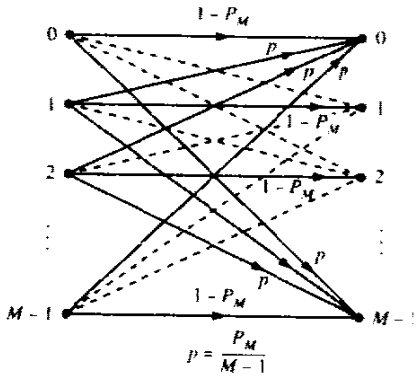

FIGURE 8-1-17 M-ary input, M-ary output, symmetric memoryless channel.

Furthermore, if the symbols are converted to binary digits, the bit error probability corresponding to (8-1-120) is

$$P_{eb} = \frac{2^{k-1}}{2^k - 1} P_{es} \tag{8-1-121}$$

Example 8-1-13

Let us evaluate the performance of an $N = 2^5 - 1 = 31$ Reed–Solomon code with $D_{\min} = 3$, 5, 9, and 17. The corresponding values of K are 29, 27, 23, and 15. The modulation is $M = 32$ orthogonal FSK with noncoherent detection at the receiver.

The probability of a symbol error is given by (5-4-46), and may be expressed as

$$P_M = \frac{1}{M} e^{-\gamma} \sum_{n=2}^{M} (-1)^n \binom{M}{n} e^{\gamma/n} \tag{8-1-122}$$

where γ is the SNR per code symbol. By using (8-1-122) in (8-1-120) and combining the result with (8-1-121), we obtain the bit error probability. The results of these computations are plotted in Fig. 8-1-18. Note that the more powerful codes (large $D_{\min}$) give poorer performance at low SNR per bit than the weaker codes. On the other hand, at high SNR, the more powerful codes give better performance. Hence, there are crossovers among the various codes, as illustrated for example in Fig. 8-1-18 for the $t = 1$ and $t = 8$ codes. Crossovers also occur among the $t = 1$, 2, and 4 codes at smaller values of SNR per bit. Similarly, the curves for $t = 4$ and 8 and for $t = 8$ and 2 cross in the region of high SNR. This is the characteristic behavior for noncoherent detection of the coded waveforms.

If the demodulator does not make a hard decision on each symbol, but

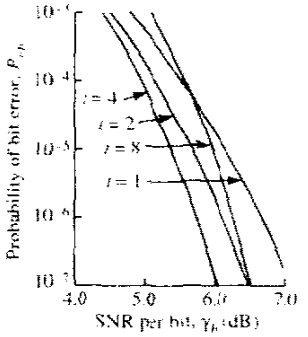

FIGURE 8-1-18 Performance of several $N = 31$, t-error correcting Reed–Solomon codes with 32-ary FSK modulation on an AWGN channel (noncoherent demodulation).

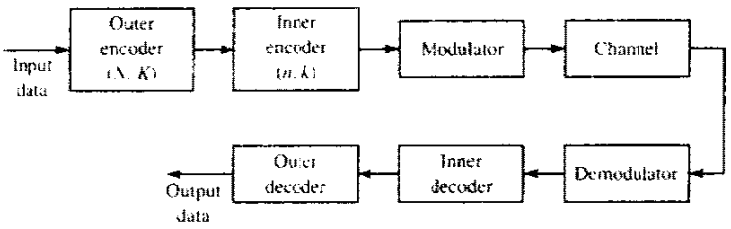

FIGURE 8-1-19 Block diagram of a communications system employing a concatenated code.

instead, passes the unquantized matched filter outputs to the decoder, soft-decision decoding can be performed. This decoding involves the formation of $q^K = 2^{kK}$ correlation metrics, where each metric corresponds to one of the q^K code words and consists of a sum of N matched filter outputs corresponding to the N code symbols. The matched filter outputs may be added coherently, or they may be envelope-detected and then added, or they may be square-law detected and then added. If coherent detection is used and the channel noise is AWGN, the computation of the probability of error is a straightforward extension of the binary case considered in Section 8-1-4. On the other hand, when envelope detection or square-law detection and noncoherent combining are used to form the decision variables, the computation of the decoder performance is considerably more complicated.

Concatenated Block Codes A concatenated code consists of two separate codes which are combined to form a larger code. Usually one code is selected to be nonbinary and the other is binary. The two codes are concatenated as illustrated in Fig. 8-1-19. The nonbinary (N, K) code forms the outer code and the binary code forms the inner code. Code words are formed by subdividing a block of kK information bits into K groups, called *symbols*, where each symbol consists of k bits. The K k-bit symbols are encoded into N k-bit symbols by the outer encoder, as is usually done with a nonbinary code. The inner encoder takes each k-bit symbol and encodes it into a binary block code of length n. Thus we obtain a concatenated block code having a block length of Nn bits and containing kK information bits. That is, we have created an equivalent (Nn, Kk) long binary code. The bits in each code word are transmitted over the channel by means of PSK or, perhaps, by FSK.

We also indicate that the minimum distance of the concatenated code is $d_{\min} D_{\min}$, where $D_{\min}$ is the minimum distance of the outer code and $d_{\min}$ is the minimum distance of the inner code. Furthermore, the rate of the concatenated code is Kk/Nn, which is equal to the product of the two code rates.

A hard-decision decoder for a concatenated code is conveniently separated into an inner decoder and an outer decoder. The inner decoder takes the hard decisions on each group of n bits, corresponding to a code word of the inner code, and makes a decision on the k information bits based on maximum-likelihood (minimum-distance) decoding. These k bits represent one symbol of

the outer code. When a block of N k-bit symbols are received from the inner decoder, the outer decoder makes a hard decision on the K k-bit symbols based on maximum-likelihood decoding.

Soft-decision decoding is also a possible alternative with a concatenated code. Usually, the soft-decision decoding is performed on the inner code, if it is selected to have relatively few code words, i.e., if 2^k is not too large. The outer code is usually decoded by means of hard-decision decoding, especially if the block length is long and there are many code words. On the other hand, there may be a significant gain in performance when soft-decision decoding is used on both the outer and inner codes, to justify the additional decoding complexity. This is the case in digital communications over fading channels, as we shall demonstrate in Chapter 14.

We conclude this subsection with the following example.

Example 8-1-14

Suppose that the (7, 4) Hamming code described in Examples 8-1-1 and 8-1-2 is used as the inner code in a concatenated code in which the outer code is a Reed–Solomon code. Since $k = 4$, we select the length of the Reed–Solomon code to be $N = 2^4 - 1 = 15$. The number of information symbols K per outer code word may be selected over the range $1 \leq K \leq 14$ in order to achieve a desired code rate.

8-1-9 Interleaving of Coded Data for Channels with Burst Errors

Most of the well-known codes that have been devised for increasing the reliability in the transmission of information are effective when the errors caused by the channel are statistically independent. This is the case for the AWGN channel. However, there are channels that exhibit bursty error characteristics. One example is the class of channels characterized by multipath and fading, which is described in detail in Chapter 14. Signal fading due to time-variant multipath propagation often causes the signal to fall below the noise level, thus resulting in a large number of errors. A second example is the class of magnetic recording channels (tape or disk) in which defects in the recording media result in clusters of errors. Such error clusters are not usually corrected by codes that are optimally designed for statistically independent errors.

Considerable work has been done on the construction of codes that are capable of correcting burst errors. Probably the best known burst error correcting codes are the subclass of cyclic codes called Fire codes, named after P. Fire (1959), who discovered them. Another class of cyclic codes for burst error correction were subsequently discovered by Burton (1969).

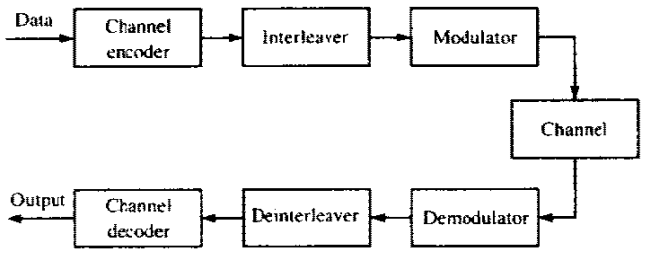

FIGURE 8-1-20 Block diagram of system employing interleaving for burst-error channel.

A *burst* of errors of length b is defined as a sequence of b-bit errors, the first and last of which are 1's. The *burst error correction capability* of a code is defined as one less than the length of the shortest uncorrectable burst. It is relatively easy to show that a systematic (n, k) code, which has $n - k$ parity check bits, can correct bursts of length $b \leq \lfloor \frac{1}{2}(n-k) \rfloor$.

An effective method for dealing with burst error channels is to interleave the coded data in such a way that the bursty channel is transformed into a channel having independent errors. Thus, a code designed for independent channel errors (short bursts) is used.

A block diagram of a system that employs interleaving is shown in Fig. 8-1-20. The encoded data are reordered by the interleaver and transmitted over the channel. At the receiver, after (either hard- or soft-decision) demodulation, the deinterleaver puts the data in proper sequence and passes it to the decoder. As a result of the interleaving/deinterleaving, error bursts are spread out in time so that errors within a code word appear to be independent.

The interleaver can take one of two forms: a block structure or a convolutional structure. A block *interleaver* formats the encoded data in a rectangular array of m rows and n columns. Usually, each row of the array constitutes a code word of length n. An *interleaver of degree m* consists of m rows (m code words) as illustrated in Fig. 8-1-21. The bits are read out

FIGURE 8-1-21 A block interleaver for coded data.

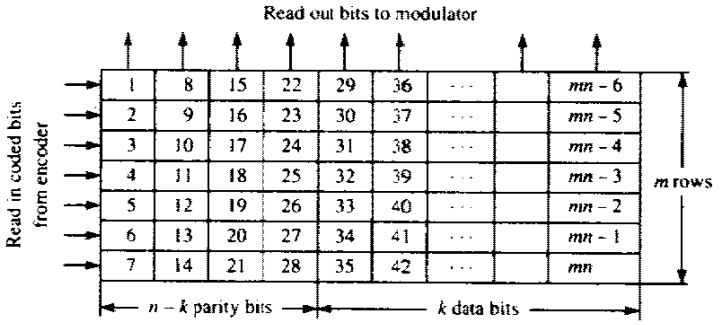

column-wise and transmitted over the channel. At the receiver, the deinterleaver stores the data in the same rectangular array format, but it is read out row-wise, one code word at a time. As a result of this reordering of the data during transmission, a burst of errors of length $l = mb$ is broken up into m bursts of length b. Thus, an (n, k) code that can handle burst errors of length $b \leq \lfloor \frac{1}{2}(n-k) \rfloor$ can be combined with an interleaver of degree m to create an interleaved (mn, mk) block code that can handle bursts of length mb.

A *convolutional interleaver* can be used in place of a block interleaver in much the same way. Convolutional interleavers are better matched for use with the class of convolutional codes that is described in the following section. Convolutional interleaver structures have been described by Ramsey (1970) and Forney (1971).

8-2 CONVOLUTIONAL CODES

A convolutional code is generated by passing the information sequence to be transmitted through a linear finite-state shift register. In general, the shift register consists of K (k-bit) stages and n linear algebraic function generators, as shown in Fig. 8-2-1. The input data to the encoder, which is assumed to be binary, is shifted into and along the shift register k bits at a time. The number of output bits for each k-bit input sequence is n bits. Consequently, the code rate is defined as $R_c = k/n$, consistent with the definition of the code rate for a block code. The parameter K is called the *constraint length* of the convolutional code.†

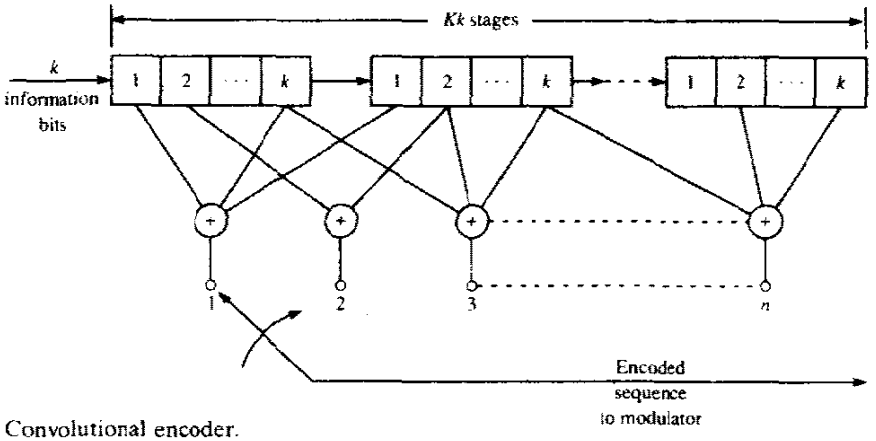

FIGURE 8-2-1 Convolutional encoder.

† In many cases, the constraint length of the code is given in bits rather than k-bit bytes. Hence the shift register may be called a *L-stage shift register*, where $L = Kk$. Furthermore, L may not be a multiple of k, in general.

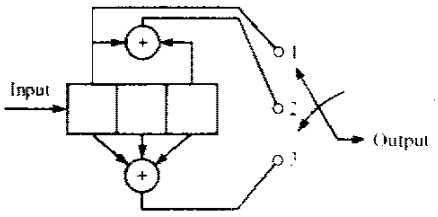

FIGURE 8-2-2 $K = 3$, $k = 1$, $n = 3$ convolutional encoder.

One method for describing a convolutional code is to give its generator matrix, just as we did for block codes. In general, the generator matrix for a convolutional code is semi-infinite since the input sequence is semi-infinite in length. As an alternative to specifying the generator matrix, we shall use a functionally equivalent representation in which we specify a set of n vectors, one vector for each of the n modulo-2 adders. Each vector has Kk dimensions and contains the connections of the encoder to that modulo-2 adder. A 1 in the ith position of the vector indicates that the corresponding stage in the shift register is connected to the modulo-2 adder and a 0 in a given position indicates that no connection exists between that stage and the modulo-2 adder.

To be specific, let us consider the binary convolutional encoder with constraint length $K = 3$, $k = 1$, and $n = 3$, which is shown in Fig. 8-2-2. Initially, the shift register is assumed to be in the all-zero state. Suppose the first input bit is a 1. Then the output sequence of 3 bits is 111. Suppose the second bit is a 0. The output sequence will then be 001. If the third bit is a 1, the output will be 100, and so on. Now, suppose we number the outputs of the function generators that generate each three-bit output sequence as 1, 2, and 3, from top to bottom, and similarly number each corresponding function generator. Then, since only the first stage is connected to the first function generator (no modulo-2 adder is needed), the generator is

$$\mathbf{g}_1 = [100]$$

The second function generator is connected to stages 1 and 3. Hence

$$\mathbf{g}_2 = [101]$$

Finally,

$$\mathbf{g}_3 = [111]$$

The generators for this code are more conveniently given in octal form as $(4, 5, 7)$. We conclude that, when $k = 1$, we require n generators, each of dimension K to specify the encoder.

For a rate k/n binary convolutional code with $k > 1$ and constraint length K, the n generators are Kk-dimensional vectors, as stated above. The following example illustrates the case in which $k = 2$ and $n = 3$.

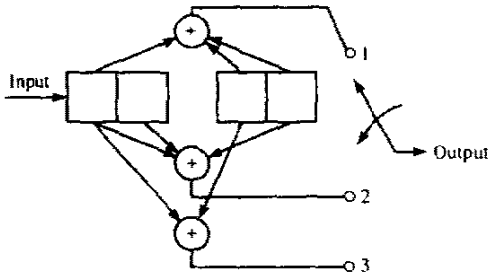

FIGURE 8-2-3 $K = 2$, $k = 2$, $n = 3$ convolutional encoder.

Example 8-2-1

Consider the rate 2/3 convolutional encoder illustrated in Fig. 8-2-3. In this encoder, two bits at a time are shifted into it and three output bits are generated. The generators are

$$\mathbf{g}_1 = [1011], \quad \mathbf{g}_2 = [1101], \quad \mathbf{g}_3 = [1010]$$

In octal form, these generators are (13, 15, 12).

There are three alternative methods that are often used to describe a convolutional code. These are the tree diagram, the trellis diagram, and the state diagram. For example, the tree diagram for the convolutional encoder shown in Fig. 8-2-2 is illustrated in Fig. 8-2-4. Assuming that the encoder is in the all-zero state initially, the diagram shows that, if the first input bit is a 0, the output sequence is 000 and, if the first bit is a 1; the output sequence is 111. Now, if the first input bit is a 1 and the second bit is a 0, the second set of three output bits is 001. Continuing through the tree, we see that if the third bit is a

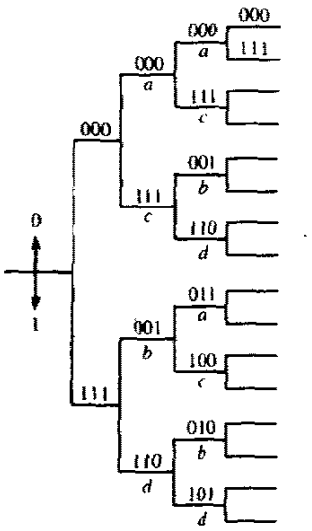

FIGURE 8-2-4 Tree diagram for rate 1/3, $K = 3$ convolutional code.

0 then the output is 011, while if the third bit is a 1 then the output is 100. Given that a particular sequence has taken us to a particular node in the tree, the branching rule is to follow the upper branch if the next input bit is a 0 and the lower branch if the bit is a 1. Thus, we trace a particular path through the tree that is determined by the input sequence.

Close observation of the tree that is generated by the convolutional encoder shown in Fig. 8-2-2 reveals that the structure repeats itself after the third stage. This behavior is consistent with the fact that the constraint length $K = 3$. That is, the three-bit output sequence at each stage is determined by the input bit and the two previous input bits, i.e., the two bits contained in the first two stages of the shift register. The bit in the last stage of the shift register is shifted out at the right and does not affect the output. Thus we may say that the three-bit output sequence for each input bit is determined by the input bit and the four possible states of the shift register, denoted as $a = 00$, $b = 01$, $c = 10$, $d = 11$. If we label each node in the tree to correspond to the four possible states in the shift register, we find that at the third stage there are two nodes with the label a, two with the label b, two with the label c, and two with the label d. Now we observe that all branches emanating from two nodes having the same label (same state) are identical in the sense that they generate identical output sequences. This means that the two nodes having the same label can be merged. If we do this to the tree shown in Fig. 8-2-4, we obtain another diagram, which is more compact, namely, a *trellis*. For example, the trellis diagram for the convolutional encoder of Fig. 8-2-2 is shown in Fig. 8-2-5. In drawing this diagram, we use the convention that a solid line denotes the output generated by the input bit 0 and a dotted line the output generated by the input bit 1. In the example being considered, we observe that, after the initial transient, the trellis contains four nodes at each stage, corresponding to the four states of the shift register, a, b, c, and d. After the second stage, each node in the trellis has two incoming paths and two outgoing paths. Of the two

FIGURE 8-2-5 Trellis diagram for rate 1/3, $K = 3$ convolutional code.

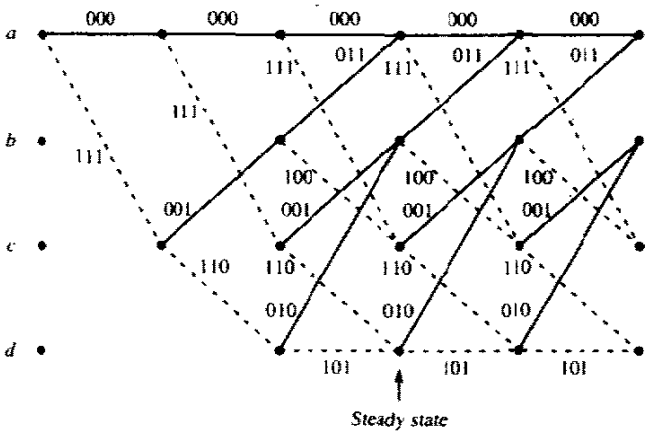

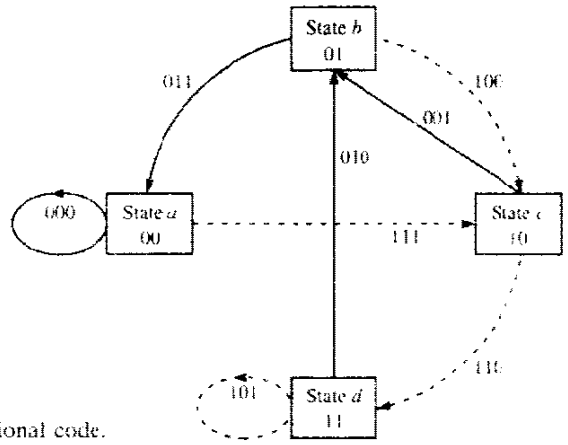

FIGURE 8-2-6 State diagram for rate 1/3, $K = 3$ convolutional code.

outgoing paths, one corresponds to the input bit 0 and the other to the path followed if the input bit is a 1.

Since the output of the encoder is determined by the input and the state of the encoder, an even more compact diagram than the trellis is the state diagram. The state diagram is simply a graph of the possible states of the encoder and the possible transitions from one state to another. For example the state diagram for the encoder shown in Fig. 8-2-2 is illustrated in Fig. 8-2-6. This diagram shows that the possible transitions are

$$a \xrightarrow{0} a,\ a \xrightarrow{1} c,\ b \xrightarrow{0} a,\ b \xrightarrow{1} c,\ c \xrightarrow{0} b,\ c \xrightarrow{1} d,\ d \xrightarrow{0} b,\ d \xrightarrow{1} d,$$

where $\alpha \xrightarrow{1} \beta$ denotes the transition from state α to β when the input bit is a 1. The three bits shown next to each branch in the state diagram represent the output bits. A dotted line in the graph indicates that the input bit is a 1, while the solid line indicates that the input bit is a 0.

Example 8-2-2

Let us consider the $k = 2$, rate 2/3 convolutional code described in Example 8-2-1 and shown in Fig. 8-2-3. The first two input bits may be 00, 01, 10, or 11. The corresponding output bits are 000, 010, 111, 101. When the next pair of input bits enter the encoder, the first pair is shifted to the second stage. The corresponding output bits depend on the pair of bits shifted into the second stage and the new pair of input bits. Hence, the tree diagram for this code, shown in Fig. 8-2-7, has four branches per node, corresponding to the four possible pairs of input symbols. Since the constraint length of the code is $K = 2$, the tree begins to repeat after the second stage. As illustrated in Fig. 8-2-7, all the branches emanating from nodes labeled a (state a) yield identical outputs. By merging the nodes having identical labels, we obtain the trellis, which is shown in Fig. 8-2-8. Finally, the state diagram for this code is shown in Fig. 8-2-9.

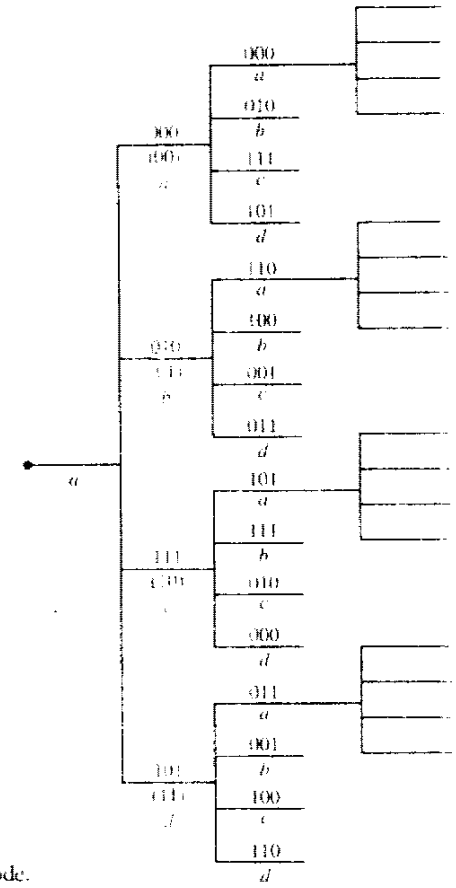

FIGURE 8-2-7 Tree diagram for $K = 2$, $k = 2$, $n = 3$ convolutional code.

To generalize, we state that a rate k/n, constraint length K, convolutional code is characterized by 2^k branches emanating from each node of the tree diagram. The trellis and the state diagrams each have $2^{k(K-1)}$ possible states. There are 2^k branches entering each state and 2^k branches leaving each state (in the trellis and tree, this is true after the initial transient).

The three types of diagrams described above are also used to represent nonbinary convolutional codes. When the number of symbols in the code alphabet is $q = 2^k$, $k > 1$, the resulting nonbinary code may also be represented as an equivalent binary code. The following example considers a convolutional code of this type.

Example 8-2-3

Let us consider the convolutional code generated by the encoder shown in Fig. 8-2-10. This code may be described as a binary convolutional code with parameters $K = 2$, $k = 2$, $n = 4$, $R_c = 1/2$, and having the generators

$$\mathbf{g}_1 = [1010], \quad \mathbf{g}_2 = [0101], \quad \mathbf{g}_3 = [1110], \quad \mathbf{g}_4 = [1001]$$

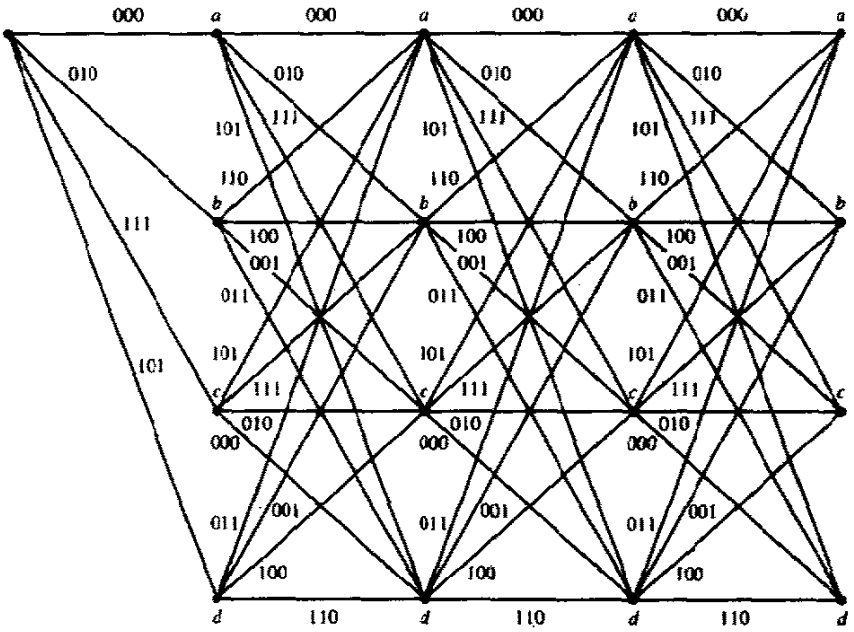

FIGURE 8-2-8 Trellis diagram for $K = 2$, $k = 2$, $n = 3$ convolutional code.

FIGURE 8-2-9 State diagram for $K = 2$, $k = 2$, $n = 3$ convolutional code.

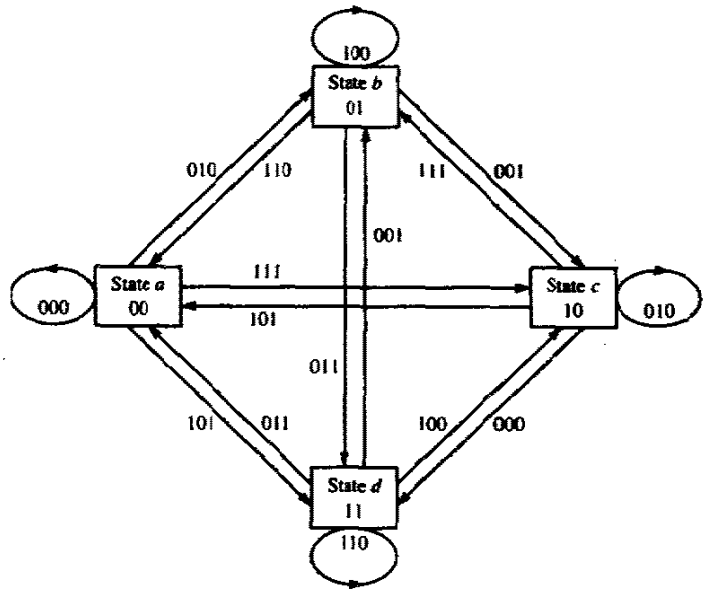

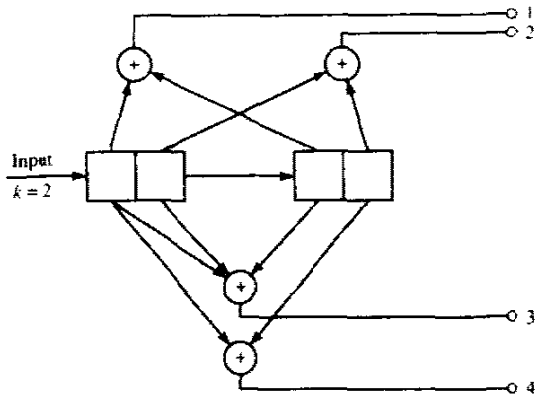

FIGURE 8-2-10 $K = 2$, $k = 2$, $n = 4$ convolutional encoder.

Except for the difference in rate, this code is similar in form to the rate 2/3, $k = 2$ convolutional code considered in Example 8-2-1.

Alternatively, the code generated by the encoder in Fig. 8-2-10 may be described as a nonbinary ($q = 4$) code with one quaternary symbol as an input and two quaternary symbols as an output. In fact, if the output of the encoder is treated by the modulator and demodulator as q-ary ($q = 4$) symbols that are transmitted over the channel by means of some M-ary ($M = 4$) modulation technique, the code is appropriately viewed as nonbinary.

In any case, the tree, the trellis, and the state diagrams are independent of how we view the code. That is, this particular code is characterized by a tree with four branches emanating from each node, or a trellis with four possible states and four branches entering and leaving each state or, equivalently, by a state diagram having the same parameters as the trellis.

8-2-1 The Transfer Function of a Convolutional Code

The distance properties and the error rate performance of a convolutional code can be obtained from its state diagram. Since a convolutional code is linear, the set of Hamming distances of the code sequences generated up to some stage in the tree, from the all-zero code sequence, is the same as the set of distances of the code sequences with respect to any other code sequence. Consequently, we assume without loss of generality that the all-zero code sequence is the input to the encoder.

The state diagram shown in Fig. 8-2-6 will be used to demonstrate the method for obtaining the distance properties of a convolutional code. First, we label the branches of the state diagram as either $D^0 = 1$, D^1, D^2, or D^3, where the exponent of D denotes the Hamming distance of the sequence of output bits corresponding to each branch from the sequence of output bits corresponding to the all-zero branch. The self-loop at node a can be eliminated, since it contributes nothing to the distance properties of a code sequence relative to

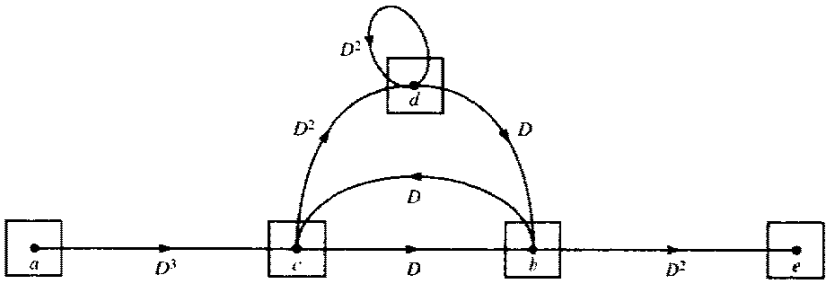

FIGURE 8-2-11 State diagram for rate 1/3, $K = 3$ convolutional code.

the all-zero code sequence. Furthermore, node a is split into two nodes, one of which represents the input and the other the output of the state diagram. Figure 8-2-11 illustrates the resulting diagram. We use this diagram, which now consists of five nodes because node a was split into two, to write the four state equations

$$\begin{aligned} X_c &= D^3 X_a + D X_b \\ X_b &= D X_c + D X_d \\ X_d &= D^2 X_c + D^2 X_d \\ X_e &= D^2 X_b \end{aligned} \tag{8-2-1}$$

The transfer function for the code is defined as $T(D) = X_e/X_a$. By solving the state equations given above, we obtain

$$\begin{aligned} T(D) &= \frac{D^6}{1 - 2D^2} \\ &= D^6 + 2D^8 + 4D^{10} + 8D^{12} + \cdots \\ &= \sum_{d=6}^{\infty} a_d D^d \end{aligned} \tag{8-2-2}$$

where, by definition,

$$a_d = \begin{cases} 2^{(d-6)/2} & (\text{even } d) \\ 0 & (\text{odd } d) \end{cases} \tag{8-2-3}$$

The transfer function for this code indicates that there is a single path of Hamming distance $d = 6$ from the all-zero path that merges with the all-zero path at a given node. From the state diagram shown in Fig. 8-2-6 or the trellis diagram shown in Fig. 8-2-5, it is observed that the $d = 6$ path is *acbe*. There is no other path from node a to node e having a distance $d = 6$. The second term in (8-2-2) indicates that there are two paths from node a to node e having a

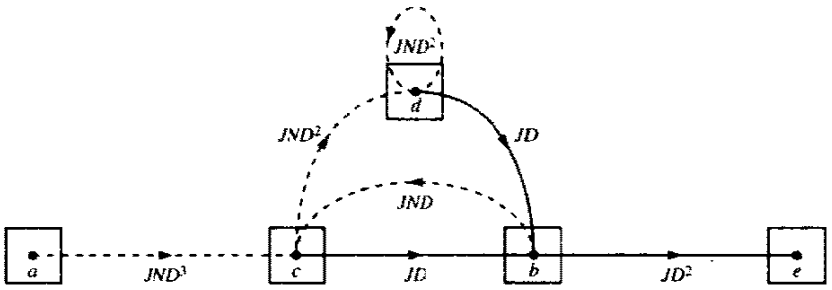

FIGURE 8-2-12 State diagram for rate 1/3, $K = 3$ convolutional code.

distance $d = 8$. Again, from the state diagram or the trellis, we observe that these paths are *acdbe* and *acbcbe*. The third term in (8-2-2) indicates that there are four paths of distance $d = 10$, and so forth. Thus the transfer function gives us the distance properties of the convolutional code. The minimum distance of the code is called the *minimum free distance* and denoted by d_{free}. In our example, $d_{\text{free}} = 6$.

The transfer function can be used to provide more detailed information than just the distance of the various paths. Suppose we introduce a factor N into all branch transitions caused by the input bit 1. Thus, as each branch is traversed, the cumulative exponent on N increases by one only if that branch transition is due to an input bit 1. Furthermore, we introduce a factor of J into each branch of the state diagram so that the exponent of J will serve as a counting variable to indicate the number of branches in any given path from node a to node e. For the rate 1/3 convolutional code in our example, the state diagram that incorporates the additional factors of J and N is shown in Fig. 8-2-12.

The state equations for the state diagram shown in Fig. 8-2-12 are

$$\begin{aligned} X_c &= JND^3X_a + JNDX_b \\ X_b &= JDX_c + JDX_d \\ X_d &= JND^2X_c + JND^2X_d \\ X_e &= JD^2X_b \end{aligned} \tag{8-2-4}$$

Upon solving these equations for the ratio X_e/X_a, we obtain the transfer function

$$\begin{aligned} T(D, N, J) &= \frac{J^3ND^6}{1 - JND^2(1 + J)} \\ &= J^3ND^6 + J^4N^2D^8 + J^5N^2D^8 + J^5N^3D^{10} \\ &\quad + 2J^6N^3D^{10} + J^7N^3D^{10} + \cdots \end{aligned} \tag{8-2-5}$$

This form for the transfer functions gives the properties of all the paths in

the convolutional code. That is, the first term in the expansion of $T(D, N, J)$ indicates that the distance $d = 6$ path is of length 3 and of the three information bits, one is a 1. The second and third terms in the expansion of $T(D, N, J)$ indicate that of the two $d = 8$ terms, one is of length 4 and the second has length 5. Two of the four information bits in the path having length 4 and two of the five information bits in the path having length 5 are 1s. Thus, the exponent of the factor J indicates the length of the path that merges with the all-zero path for the first time, the exponent of the factor N indicates the number of 1s in the information sequence for that path, and the exponent of D indicates the distance of the sequence of encoded bits for that path from the all-zero sequence.

The factor J is particularly important if we are transmitting a sequence of finite duration, say m bits. In such a case, the convolutional code is truncated after m nodes or m branches. This implies that the transfer function for the truncated code is obtained by truncating $T(D, N, J)$ at the term J^m. On the other hand, if we are transmitting an extremely long sequence, i.e., essentially an infinite-length sequence, we may wish to suppress the dependence of $T(D, N, J)$ on the parameter J. This is easily accomplished by setting $J = 1$. Hence, for the example given above, we have

$$\begin{aligned} T(D, N, 1) = T(D, N) &= \frac{ND^6}{1 - 2ND^2} \\ &= ND^6 + 2N^2D^8 + 4N^3D^{10} + \cdots \\ &= \sum_{d=6}^{\infty} a_d N^{(d-4)/2} D^d \end{aligned} \tag{8-2-6}$$

where the coefficients $\{a_d\}$ are defined by (8-2-3).

The procedure outlined above for determining the transfer function of a binary convolutional code is easily extended to nonbinary codes. In the following example, we determine the transfer function of the nonbinary convolutional code previously introduced in Example 8-2-3.

Example 8-2-4

The convolutional code shown in Fig. 8-2-10 has the parameters $K = 2$, $k = 2$, $n = 4$. In this example, we have a choice of how we label distances and count errors, depending on whether we treat the code as binary or nonbinary. Suppose we treat the code as nonbinary. Thus, the input to the encoder and the output are treated as quaternary symbols. In particular, if we treat the input and output as quaternary symbols 00, 01, 10, and 11, the distance measured in symbols between the sequences 0111 and 0000 is 2. Furthermore, suppose that an input symbol 00 is decoded as the symbol 11; then we have made one symbol error. This convention applied to the

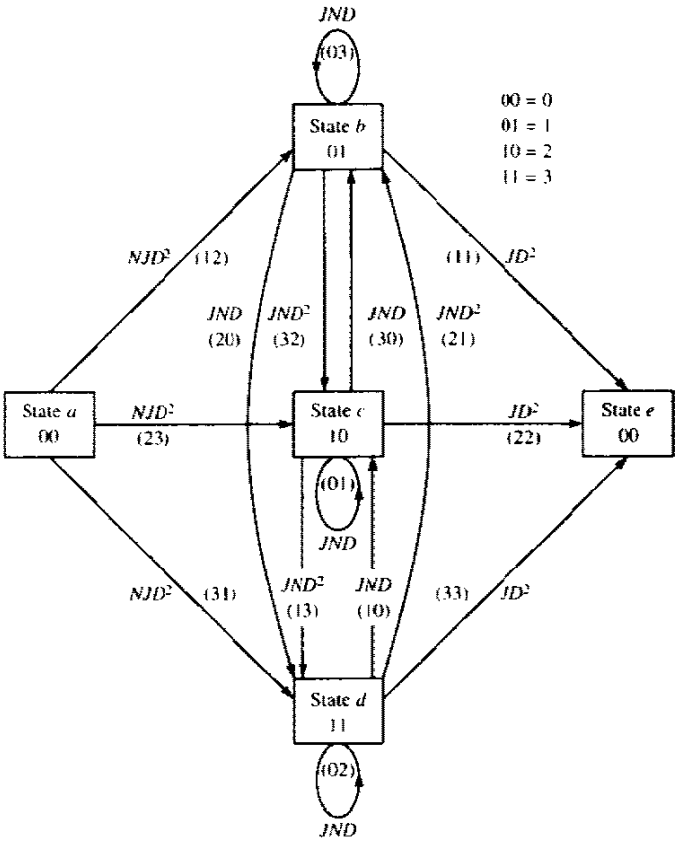

FIGURE 8-2-13 State diagram for $K = 2$, $k = 2$, rate 1/2 nonbinary code.

convolutional code shown in Fig. 8-2-10 results in the state diagram illustrated in Fig. 8-2-13, from which we obtain the state equations

$$\begin{aligned} X_b &= NJD^2X_a + NJDX_b + NJDX_c + NJD^2X_d \\ X_c &= NJD^2X_a + NJD^2X_b + NJDX_c + NJDX_d \\ X_d &= NJD^2X_a + NJDX_b + NJD^2X_c + NJDX_d \\ X_e &= JD^2(X_b + X_c + X_d) \end{aligned} \tag{8-2-7}$$

Solution of these equations leads to the transfer function

$$T(D, N, J) = \frac{3NJ^2D^4}{1 - 2NJD - NJD^2} \tag{8-2-8}$$

This expression for the transfer function is particularly appropriate when the quaternary symbols at the output of the encoder are mapped into a

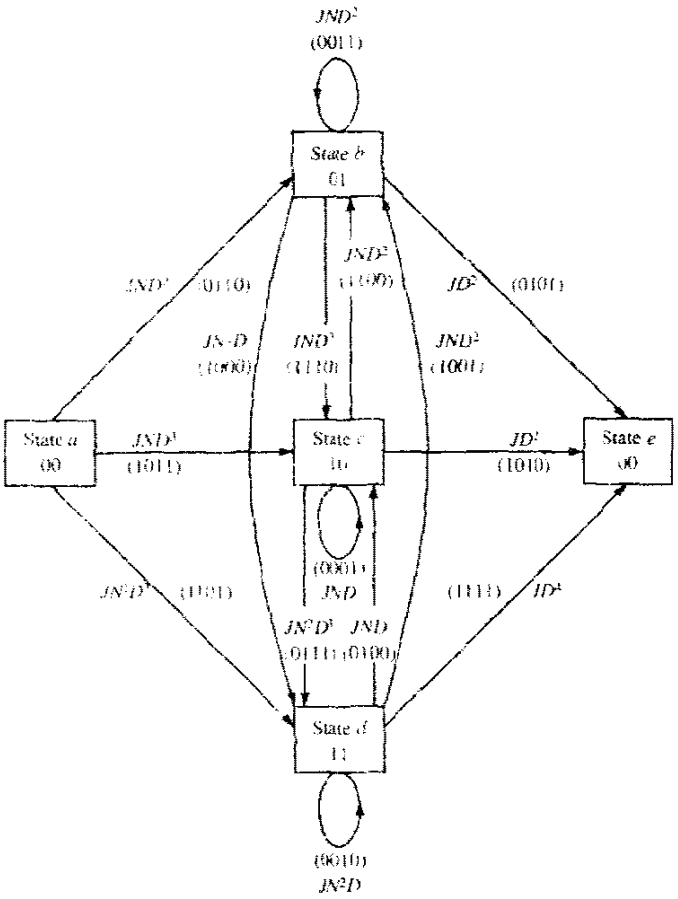

FIGURE 8-2-14 State diagram for $K = 2$, $k = 2$, rate 1/2 convolutional code with output treated as a binary sequence.

corresponding set of quaternary waveforms $s_m(t)$, $m = 1, 2, 3, 4$, e.g., four orthogonal waveforms. Thus, there is a one-to-one correspondence between code symbols and signal waveforms.

Alternatively, for example, the output of the encoder may be transmitted as a sequence of binary digits by means of binary PSK. In such a case, it is appropriate to measure distance in terms of bits. When this convention is employed, the state diagram is labeled as shown in Fig. 8-2-14. Solution of the state equations obtained from this state diagram yields a transfer function that is different from the one given in (8-2-8).

Some convolutional codes exhibit a characteristic behavior that is called *catastrophic error propagation*. When a code that has this characteristic is used on a binary symmetric channel, it is possible for a finite number of channel errors to cause an infinite number of decoding errors. Such a code can be

identified from its state diagram. It will contain a zero-distance path (a path with multiplier $D^0 = 1$) from some nonzero state back to the same state. This means that one can loop around this zero-distance path an infinite number of times without increasing the distance relative to the all-zero path. But, if this self-loop corresponds to the transmission of a 1, the decoder will make an infinite number of errors. Since such codes are easily recognized, they are easily avoided in practice.

8-2-2 Optimum Decoding of Convolutional Codes—The Viterbi Algorithm

In the decoding of a block code for a memoryless channel, we computed the distances (Hamming distance for hard-decision decoding and euclidean distance for soft-decision decoding) between the received code word and the 2^k possible transmitted code words. Then we selected the code word that was closest in distance to the received code word. This decision rule, which requires the computation of 2^k *metrics*, is optimum in the sense that it results in a minimum probability of error for the binary symmetric channel with $p < \frac{1}{2}$ and the additive white gaussian noise channel.

Unlike a block code, which has a fixed length n, a convolutional encoder is basically a finite-state machine. Hence the optimum decoder is a maximum-likelihood sequence estimator (MLSE) of the type described in Section 5-1-4 for signals with memory, such as NRZI and CPM. Therefore, optimum decoding of a convolutional code involves a search through the trellis for the most probable sequence. Depending on whether the detector following the demodulator performs hard or soft decisions, the corresponding metric in the trellis search may be either a Hamming metric or a euclidean metric, respectively. We elaborate below, using the trellis in Fig. 8-2-5 for the convolutional code shown in Fig. 8-2-2.

Consider the two paths in the trellis that begin at the initial state a and remerge at state a after three state transitions (three branches), corresponding to the two information sequences 000 and 100 and the transmitted sequences 000 000 000 and 111 001 011, respectively. We denote the transmitted bits by $\{c_{jm}, j = 1, 2, 3; m = 1, 2, 3\}$, where the index j indicates the jth branch and the index m the mth bit in that branch. Correspondingly, we define $\{r_{jm}, j = 1, 2, 3; m = 1, 2, 3\}$ as the output of the demodulator. If the detector performs hard-decision decoding, its output for each transmitted bit is either 0 or 1. On the other hand, if soft-decision decoding is employed and the coded sequence is transmitted by binary coherent PSK, the input to the decoder is

$$r_{jm} = \sqrt{\mathcal{E}_c}(2c_{jm} - 1) + n_{jm} \tag{8-2-9}$$

where n_{jm} represents the additive noise and $\mathcal{E}_c$ is the transmitted signal energy for each code bit.

A metric is defined for the jth branch of the ith path through the trellis as the logarithm of the joint probability of the sequence $\{r_{jm}, m = 1, 2, 3\}$

conditioned on the transmitted sequence $\{c_{jm}^{(i)},\ m = 1, 2, 3\}$ for the ith path. That is,

$$\mu_j^{(i)} = \log P(\mathbf{Y}_j \mid \mathbf{C}_j^{(i)}), \quad j = 1, 2, 3, \ldots \tag{8-2-10}$$

Furthermore, a metric for the ith path consisting of B branches through the trellis is defined as

$$PM^{(i)} = \sum_{j=1}^{B} \mu_j^{(i)} \tag{8-2-11}$$

The criterion for deciding between two paths through the trellis is to select the one having the larger metric. This rule maximizes the probability of a correct decision or, equivalently, it minimizes the probability of error for the sequence of information bits. For example, suppose that hard-decision decoding is performed by the demodulator, yielding the received sequence {101 000 100}. Let $i = 0$ denote the three-branch all-zero path and $i = 1$ the second three-branch path that begins in the initial state a and remerges with the all-zero path at state a after three transitions. The metrics for these two paths are

$$\begin{aligned} PM^{(0)} &= 6 \log (1 - p) + 3 \log p \\ PM^{(1)} &= 4 \log (1 - p) + 5 \log p \end{aligned} \tag{8-2-12}$$

where p is the probability of a bit error. Assuming that $p < \frac{1}{2}$, we find that the metric $PM^{(0)}$ is larger than the metric $PM^{(1)}$. This result is consistent with the observation that the all-zero path is at Hamming distance $d = 3$ from the received sequence, while the $i = 1$ path is at Hamming distance $d = 5$ from the received path. Thus, the Hamming distance is an equivalent metric for hard-decision decoding.

Similarly, suppose that soft-decision decoding is employed and the channel adds white gaussian noise to the signal. Then the demodulator output is described statistically by the probability density function

$$p(r_{jm} \mid c_{jm}^{(i)}) = \frac{1}{\sqrt{2\pi}\,\sigma} \exp\left\{ -\frac{[r_{jm} - \sqrt{\mathscr{E}_c}(2c_{jm}^{(i)} - 1)]^2}{2\sigma^2} \right\} \tag{8-2-13}$$

where $\sigma^2 = \frac{1}{2}N_0$ is the variance of the additive gaussian noise. If we neglect the terms that are common to all branch metrics, the branch metric for the jth branch of the ith path may be expressed as

$$\mu_j^{(i)} = \sum_{m=1}^{n} r_{jm}(2c_{jm}^{(i)} - 1) \tag{8-2-14}$$

where, in our example, $n = 3$. Thus the correlation metrics for the two paths under consideration are

$$\begin{aligned} CM^{(0)} &= \sum_{j=1}^{3} \sum_{m=1}^{3} r_{jm}(2c_{jm}^{(0)} - 1) \\ CM^{(1)} &= \sum_{j=1}^{3} \sum_{m=1}^{3} r_{jm}(2c_{jm}^{(1)} - 1) \end{aligned} \tag{8-2-15}$$

Having defined the branch metrics and path metrics computed by the decoder, we now consider the use of the Viterbi algorithm for optimum decoding of the convolutionally encoded information sequence. We consider the two paths described above, which merge at state a after three transitions. Note that any particular path through the trellis that stems from this node will add identical terms to the path metrics $CM^{(0)}$ and $CM^{(1)}$. Consequently, if $CM^{(0)} > CM^{(1)}$ at the merged node a after three transitions $CM^{(0)}$ will continue to be larger than $CM^{(1)}$ for any path that stems from node a. This means that the path corresponding to $CM^{(1)}$ can be discarded from further consideration. The path corresponding to the metric $CM^{(0)}$ is the *survivor*. Similarly, one of the two paths that merge at state b can be elminated on the basis of the two corresponding metrics. This procedure is repeated at state c and state d. As a result, after the first three transitions, there are four surviving paths, one terminating at each state, and a corresponding metric for each survivor. This procedure is repeated at each stage of the trellis as new signals are received in subsequent time intervals.

In general, when a binary convolutional code with $k = 1$ and constraint length K is decoded by means of the Viterbi algorithm, there are 2^{K-1} states. Hence, there are 2^{K-1} surviving paths at each stage and 2^{K-1} metrics, one for each surviving path. Furthermore, a binary convolutional code in which k bits at a time are shifted into an encoder that consists of K (k-bit) shift-register stages generates a trellis that has $2^{k(K-1)}$ states. Consequently, the decoding of such a code by means of the Viterbi algorithm requires keeping track of $2^{k(K-1)}$ surviving paths and $2^{k(K-1)}$ metrics. At each stage of the trellis, there are 2^k paths that merge at each node. Since each path that converges at a common node requires the computation of a metric, there are 2^k metrics computed for each node. Of the 2^k paths that merge at each node, only one survives, and this is the most-probable (minimum-distance) path. Thus the number of computations in decoding performed at each stage increases exponentially with k and K. The exponential increase in computational burden limits the use of the Viterbi algorithm to relatively small values of K and k.

The decoding delay in decoding a long information sequence that has been convolutionally encoded is usually too long for most practical applications. Moreover, the memory required to store the entire length of surviving sequences is large and expensive. As indicated in Section 5-1-4, a solution to this problem is to modify the Viterbi algorithm in a way which results in a fixed decoding delay without significantly affecting the optimal performance of the algorithm. Recall that the modification is to retain at any given time t only the most recent δ decoded information bits (symbols) in each surviving sequence. As each new information bit (symbol) is received, a final decision is made on the bit (symbol) received δ branches back in the trellis, by comparing the metrics in the surviving sequences and deciding in favor of the bit in the sequence having the largest metric. If δ is chosen sufficiently large, all surviving sequences will contain the identical decoded bit (symbol) δ branches back in time. That is, with high probability, all surviving sequences at time t stem from

the same node at $t - \delta$. It has been found experimentally (computer simulation) that a delay $\delta \geq 5K$ results in a negligible degradation in the performance relative to the optimum Viterbi algorithm.

8-2-3 Probability of Error for Soft-Decision Decoding

The topic of this subsection is the error rate performance of the Viterbi algorithm on an additive white gaussian noise channel with soft-decision decoding.

In deriving the probability of error for convolutional codes, the linearity property for this class of codes is employed to simplify the derivation. That is, we assume that the all-zero sequence is transmitted and we determine the probability of error in deciding in favor of another sequence. The coded binary digits for the jth branch of the convolutional code, denoted as $\{c_{jm}, m = 1, 2, \ldots, n\}$ and defined in Section 8-2-2, are assumed to be transmitted by binary PSK (or four-phase PSK) and detected coherently at the demodulator. The output of the demodulator, which is the input to the Viterbi decoder, is the sequence $\{r_{jm}, m = 1, 2, \ldots, n; j = 1, 2, \ldots\}$ where r_{jm} is defined in (8-2-9).

The Viterbi soft-decision decoder forms the branch metrics defined by (8-2-14) and from these computes the path metrics

$$CM^{(i)} = \sum_{j=1}^{B} \mu_j^{(i)} = \sum_{j=1}^{B} \sum_{m=1}^{n} r_{jm}(2c_{jm}^{(i)} - 1) \tag{8-2-16}$$

where i denotes any one of the competing paths at each node and B is the number of branches (information symbols) in a path. For example, the all-zero path, denoted as $i = 0$, has a path metric

$$\begin{aligned} CM^{(0)} &= \sum_{j=1}^{B} \sum_{m=1}^{n} (-\sqrt{\mathscr{E}_c} + n_{jm})(-1) \\ &= \sqrt{\mathscr{E}_c}\, Bn + \sum_{j=1}^{B} \sum_{m=1}^{n} n_{jm} \end{aligned} \tag{8-2-17}$$

Since the convolutional code does not necessarily have a fixed length, we derive its performance from the probability of error for sequences that merge with the all-zero sequence for the first time at a given node in the trellis. In particular, we define the first-event error probability as the probability that another path that merges with the all-zero path at node B has a metric that exceeds the metric of the all-zero path for the first time. Suppose the incorrect path, call it $i = 1$, that merges with the all-zero path differs from the all-zero path in d bits, i.e., there are d 1s in the path $i = 1$ and the rest are 0s. The probability of error in the pairwise comparison of the metrics $CM^{(0)}$ and $CM^{(1)}$ is

$$\begin{aligned} P_2(d) &= P(CM^{(1)} \geq CM^{(0)}) = P(CM^{(1)} - CM^{(0)} \geq 0) \\ P_2(d) &= P\left[2 \sum_{j=1}^{B} \sum_{m=1}^{n} r_{jm}(c_{jm}^{(1)} - c_{jm}^{(0)}) \geq 0\right] \end{aligned} \tag{8-2-18}$$

Since the coded bits in the two paths are identical except in the d positions, (8-2-18) can be written in the simpler form

$$P_2(d) = P\left(\sum_{l=1}^{d} r_l' \geq 0\right) \tag{8-2-19}$$

where the index l runs over the set of d bits in which the two paths differ and the set $\{r_l'\}$ represents the input to the decoder for these d bits.

The $\{r_l'\}$ are independent and identically distributed gaussian random variables with mean $-\sqrt{\mathscr{E}_c}$ and variance $\frac{1}{2}N_0$. Consequently the probability of error in the pairwise comparison of these two paths that differ in d bits is

$$\begin{aligned} P_2(d) &= Q\left(\sqrt{\frac{2\mathscr{E}_c}{N_0}d}\right) \\ &= Q(\sqrt{2\gamma_b R_c d}) \end{aligned} \tag{8-2-20}$$

where $\gamma_b = \mathscr{E}_b/N_0$ is the received SNR per bit and R_c is the code rate.

Although we have derived the first-event error probability for a path of distance d from the all-zero path, there are many possible paths with different distances that merge with the all-zero path at a given node B. In fact, the transfer function $T(D)$ provides a complete description of all the possible paths that merge with the all-zero path at node B and their distances. Thus we can sum the error probability in (8-2-20) over all possible path distances. Upon performing this summation, we obtain an upper bound on the first-event error probability in the form

$$\begin{aligned} P_e &\leq \sum_{d=d_{\text{free}}}^{\infty} a_d P_2(d) \\ &\leq \sum_{d=d_{\text{free}}}^{\infty} a_d Q(\sqrt{2\gamma_b R_c d}) \end{aligned} \tag{8-2-21}$$

where a_d denotes the number of paths of distance d from the all-zero path that merge with the all-zero path for the first time.

There are two reasons why (8-2-21) is an upper bound on the first-event error probability. One is that the events that result in the error probabilities $\{P_2(d)\}$ are not disjoint. This can be seen from observation of the trellis. Second, by summing over all possible $d \geq d_{\text{free}}$, we have implicitly assumed that the convolutional code has infinite length. If the code is truncated periodically after B nodes, the upper bound in (8-2-21) can be improved by summing the error events for $d_{\text{free}} \leq d \leq B$. This refinement has some merit in determining the performance of short convolutional codes, but the effect on performance is negligible when B is large.

The upper bound in (8-2-21) can be expressed in a slightly different form if the Q function is upper-bounded by an exponential. That is,

$$Q(\sqrt{2\gamma_b R_c d}) \leq e^{-\gamma_b R_c d} = D^d\big|_{D=e^{-\gamma_b R_c}} \tag{8-2-22}$$

If we use (8-2-22) in (8-2-21), the upper bound on the first-event error probability can be expressed as

$$P_e < T(D)\big|_{D=e^{-\gamma_b R_c}} \tag{8-2-23}$$

Although the first-event error probability provides a measure of the performance of a convolutional code, a more useful measure of performance is the bit error probability. This probability can be upper-bounded by the procedure used in bounding the first-event error probability. Specifically, we know that when an incorrect path is selected, the information bits in which the selected path differs from the correct path will be decoded incorrectly. We also know that the exponents in the factor N contained in the transfer function $T(D, N)$ indicate the number of information bit errors (number of 1s) in selecting an incorrect path that merges with the all-zero path at some node B. If we multiply the pairwise error probability $P_2(d)$ by the number of incorrectly decoded information bits for the incorrect path at the node where they merge, we obtain the bit error rate for that path. The average bit error probability is upper-bounded by multiplying each pairwise error probability $P_2(d)$ by the corresponding number of incorrectly decoded information bits, for each possible incorrect path that merges with the correct path at the Bth node, and summing over all d.

The appropriate multiplication factors corresponding to the number of information bit errors for each incorrectly selected path may be obtained by differentiating $T(D, N)$ with respect to N. In general, $T(D, N)$ can be expressed as

$$T(D, N) = \sum_{d=d_{\text{free}}}^{\infty} a_d D^d N^{f(d)} \tag{8-2-24}$$

where $f(d)$ denotes the exponent of N as a function of d. Taking the derivative of $T(D, N)$ with respect to N and setting $N = 1$, we obtain

$$\begin{aligned} \left.\frac{dT(D, N)}{dN}\right|_{N=1} &= \sum_{d=d_{\text{free}}}^{\infty} a_d f(d) D^d \\ &= \sum_{d=d_{\text{free}}}^{\infty} \beta_d D^d \end{aligned} \tag{8-2-25}$$

where $\beta_d = a_d f(d)$. Thus the bit error probability for $k = 1$ is upper-bounded by

$$\begin{aligned} P_b &< \sum_{d=d_{\text{free}}}^{\infty} \beta_d P_2(d) \\ &< \sum_{d=d_{\text{free}}}^{\infty} \beta_d Q(\sqrt{2\gamma_b R_c d}) \end{aligned} \tag{8-2-26}$$

If the Q function is upper-bounded by an exponential as indicated in (8-2-22) then (8-2-26) can be expressed in the simple form

$$P_b < \sum_{d=d_{free}}^{\infty} \beta_d D^d \Big|_{D=e^{-\gamma_b R_c}} < \frac{dT(D, N)}{dN}\Big|_{N=1, D=e^{-\gamma_b R_c}} \tag{8-2-27}$$

If $k > 1$, the equivalent bit error probability is obtained by dividing (8-2-26) and (8-2-27) by k.

The expressions for the probability of error given above are based on the assumption that the code bits are transmitted by binary coherent PSK. The results also hold for four-phase coherent PSK, since this modulation/demodulation technique is equivalent to two independent (phase-quadrature) binary PSK systems. Other modulation and demodulation techniques, such as coherent and noncoherent binary FSK, can be accommodated by recomputing the pairwise error probability $P_2(d)$. That is, a change in the modulation and demodulation technique used to transmit the coded information sequence affects only the computation of $P_2(d)$. Otherwise, the derivation for P_b remains the same.

Although the above derivation of the error probability for Viterbi decoding of a convolutional code applies to binary convolutional codes, it is relatively easy to generalize it to nonbinary convolutional codes in which each nonbinary symbol is mapped into a distinct waveform. In particular, the coefficients $\{\beta_d\}$ in the expansion of the derivative of $T(D, N)$, given in (8-2-25), represent the number of symbol errors in two paths separated in distance (measured in terms of symbols) by d symbols. Again, we denote the probability of error in a pairwise comparison of two paths that are separated in distance by d as $P_2(d)$. Then the symbol error probability, for a k-bit symbol, is upper-bounded by

$$P_M \leq \sum_{d=d_{free}}^{\infty} \beta_d P_2(d)$$

The symbol error probability can be converted into an equivalent bit error probability. For example, if 2^k orthogonal waveforms are used to transmit the k-bit symbols, the equivalent bit error probability is P_M multiplied by a factor $2^{k-1}/(2^k - 1)$, as shown in Chapter 5.

8-2-4 Probability of Error for Hard-Decision Decoding

We now consider the performance achieved by the Viterbi decoding algorithm on a binary symmetric channel. For hard-decision decoding of the convolutional code, the metrics in the Viterbi algorithm are the Hamming distances between the received sequence and the $2^{k(K-1)}$ surviving sequences at each node of the trellis.

As in our treatment of soft-decision decoding, we begin by determining the

first-event error probability. The all-zero path is assumed to be transmitted. Suppose that the path being compared with the all-zero path at some node B has distance d from the all-zero path. If d is odd, the all-zero path will be correctly selected if the number of errors in the received sequence is less than $\frac{1}{2}(d+1)$; otherwise, the incorrect path will be selected. Consequently, the probability of selecting the incorrect path is

$$P_2(d) = \sum_{k=(d+1)/2}^{d} \binom{d}{k} p^k (1-p)^{d-k} \tag{8-2-28}$$

where p is the probability of a bit error for the binary symmetric channel. If d is even, the incorrect path is selected when the number of errors exceeds $\frac{1}{2}d$. If the number of errors equals $\frac{1}{2}d$, there is a tie between the metrics in the two paths, which may be resolved by randomly selecting one of the paths; thus, an error occurs half the time. Consequently, the probability of selecting the incorrect path is

$$P_2(d) = \sum_{k=d/2+1}^{d} \binom{d}{k} p^k (1-p)^{d-k} + \frac{1}{2}\binom{d}{\frac{1}{2}d} p^{d/2}(1-p)^{d/2} \tag{8-2-29}$$

As indicated in Section 8-2-3, there are many possible paths with different distances that merge with the all-zero path at a given node. Therefore, there is no simple exact expression for the first-event error probability. However, we can overbound this error probability by the sum of the pairwise error probabilities $P_2(d)$ over all possible paths that merge with the all-zero path at the given node. Thus, we obtain the union bound

$$P_e < \sum_{d=d_{\text{free}}}^{\infty} a_d P_2(d) \tag{8-2-30}$$

where the coefficients $\{a_d\}$ represent the number of paths corresponding to the set of distances $\{d\}$. These coefficients are the coefficients in the expansion of the transfer function $T(D)$ or $T(D, N)$.

Instead of using the expressions for $P_2(d)$ given in (8-2-28) and (8-2-29), we can use the upper bound

$$P_2(d) < [4p(1-p)]^{d/2} \tag{8-2-31}$$

which was given in Section 8-1-5. Use of this bound in (8-2-30) yields a looser upper bound on the first-event error probability, in the form

$$\begin{aligned} P_e &< \sum_{d=d_{\text{free}}}^{\infty} a_d [4p(1-p)]^{d/2} \\ &< T(D)\big|_{D=\sqrt{4p(1-p)}} \end{aligned} \tag{8-2-32}$$

Let us now determine the probability of a bit error. As in the case of soft-decision decoding, we make use of the fact that the exponents in the factors of N that appear in the transfer function $T(D, N)$ indicate the number of nonzero information bits that are in error when an incorrect path is selected over the all-zero path. By differentiating $T(D, N)$ with respect to N and setting $N = 1$, the exponents of N become multiplication factors of the corresponding error-event probabilities $P_2(d)$. Thus, we obtain the expression for the upper bound on the bit error probability, in the form

$$P_b < \sum_{d=d_{free}}^{\infty} \beta_d P_2(d) \tag{8-2-33}$$

where the $\{\beta_d\}$ are the coefficients in the expansion of the derivative of $T(D, N)$, evaluated at $N = 1$. For $P_2(d)$, we may use either the expressions given in (8-2-28) and (8-2-29) or the upper bound in (8-2-31). If the latter is used, the upper bound on P_b can be expressed as

$$P_b < \left.\frac{dT(D, N)}{dN}\right|_{N=1, D=\sqrt{4p(1-p)}} \tag{8-2-34}$$

When $k > 1$, the results given in (8-2-33) and (8-2-34) for P_b should be divided by k.

A comparison of the error probability for the rate 1/3, $K = 3$ convolutional code with soft-decision decoding and hard-decision decoding is made in Fig. 8-2-15. Note that the Chernoff upper bound given by (8-2-34) is less than 1 dB above the tighter upper bound given by (8-2-33) in conjunction with (8-2-28) and (8-2-29). The advantage of the Chernoff bound is its computational

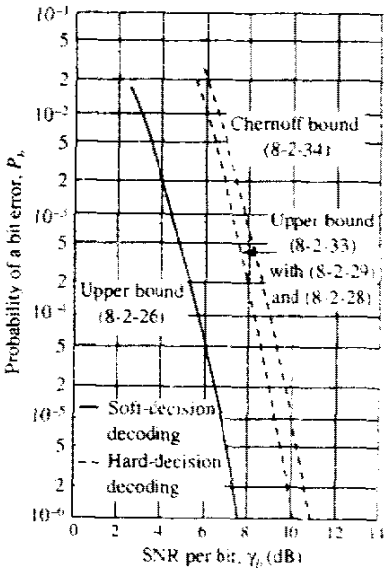

FIGURE 8-2-15 Comparison of soft-decision and hard-decision decoding for $K = 3$, $k = 1$, $n = 3$ convolutional code.

simplicity. In comparing the performance between soft-decision and hard-decision decoding, note that the difference obtained from the upper bounds is approximately 2.5 dB for $10^{-6} \leq P_b \leq 10^{-2}$.

Finally, we should mention that the ensemble average error rate performance of a convolutional code on a discrete memoryless channel, just as in the case of a block code, can be expressed in terms of the cutoff rate parameter R_0 as (for the derivation, see Viterbi and Omura, 1979).

$$\bar{P}_b < \frac{(q-1)q^{-KR_0/R_c}}{[1-q^{-(R_0-R_c)/R_c}]^2}, \qquad R_c \leq R_0$$

where q is the number of channel input symbols, K is the constraint length of the code, R_c is the code rate, and R_0 is the cutoff rate defined in Sections 7-2 and 8-1. Therefore, conclusions reached by computing R_0 for various channel conditions apply to both block codes and convolutional codes.

8-2-5 Distance Properties of Binary Convolutional Codes

In this subsection, we shall tabulate the minimum free distance and the generators for several binary, short-constraint-length convolutional codes for several code rates. These binary codes are optimal in the sense that, for a given rate and a given constraint length, they have the largest possible d_{free}. The generators and the corresponding values of d_{free} tabulated below have been obtained by Odenwalder (1970), Larsen (1973), Paaske (1974), and Daut *et al.* (1982) using computer search methods.

Heller (1968) has derived a relatively simple upper bound on the minimum free distance of a rate $1/n$ convolutional code. It is given by

$$d_{\text{free}} \leq \min_{l \geq 1} \left\lfloor \frac{2^{l-1}}{2^l - 1}(K + l - 1)n \right\rfloor \tag{8-2-35}$$

where $\lfloor x \rfloor$ denotes the largest integer contained in x. For purposes of comparison, this upper bound is also given in the tables for the rate $1/n$ codes. For rate k/n convolutional codes, Daut *et al.* (1982) has given a modification to Heller's bound. The values obtained from this upper bound for k/n codes are also tabulated.

Tables 8-2-1 to 8-2-7 list the parameter of rate $1/n$ convolutional codes for $n = 2, 3, \ldots, 8$. Tables 8-2-8 to 8-2-11 list the parameters of several rate k/n convolutional codes for $k \leq 4$ and $n \leq 8$.

8-2-6 Nonbinary Dual-k Codes and Concatenated Codes

Our treatment of convolutional codes thus far has been focused primarily on binary codes. Binary codes are particularly suitable for channels in which binary or quaternary PSK modulation and coherent demodulation is possible.

TABLE 8-2-1 RATE 1/2 MAXIMUM FREE DISTANCE CODE

Constraint length K	Generators in octal		d_{free}	Upper bound on d_{free}
3	5	7	5	5
4	15	17	6	6
5	23	35	7	8
6	53	75	8	8
7	133	171	10	10
8	247	371	10	11
9	561	753	12	12
10	1,167	1,545	12	13
11	2,335	3,661	14	14
12	4,335	5,723	15	15
13	10,533	17,661	16	16
14	21,675	27,123	16	17

Source: Odenwalder (1970) and Larsen (1973).

However, there are many applications in which PSK modulation and coherent demodulation is not suitable or possible. In such cases, other modulation techniques, e.g., M-ary FSK, are employed in conjunction with noncoherent demodulation. Nonbinary codes are particularly matched to M-ary signals that are demodulated noncoherently.

In this subsection, we describe a class of nonbinary convolutional codes, called *dual-k codes*, that are easily decoded by means of the Viterbi algorithm using either soft-decision or hard-decision decoding. They are also suitable either as an outer code or as an inner code in a concatenated code, as will also be described below.

TABLE 8-2-2 RATE 1/3 MAXIMUM FREE DISTANCE CODES

Constraint length K	Generators in octal			d_{free}	Upper bound on d_{free}
3	5	7	7	8	8
4	13	15	17	10	10
5	25	33	37	12	12
6	47	53	75	13	13
7	133	145	175	15	15
8	225	331	367	16	16
9	557	663	711	18	18
10	1,117	1,365	1,633	20	20
11	2,353	2,671	3,175	22	22
12	4,767	5,723	6,265	24	24
13	10,533	10,675	17,661	24	24
14	21,645	35,661	37,133	26	26

Sources: Odenwalder (1970) and Larsen (1973).

TABLE 8-2-3 RATE 1/4 MAXIMUM FREE DISTANCE CODES

Constraint length K	Generators in octal				d_{free}	Upper bound on d_{free}
3	5	7	7	7	10	10
4	13	15	15	17	13	15
5	25	27	33	37	16	16
6	53	67	71	75	18	18
7	135	135	147	163	20	20
8	235	275	313	357	22	22
9	463	535	733	745	24	24
10	1,117	1,365	1,633	1,653	27	27
11	2,387	2,353	2,671	3,175	29	29
12	4,767	5,723	6,265	7,455	32	32
13	11,145	12,477	15,537	16,727	33	33
14	21,113	23,175	35,527	35,537	36	36

Source: Larsen (1973).

TABLE 8-2-4 RATE 1/5 MAXIMUM FREE DISTANCE CODES

Constraint length K	Generators in octal					d_{free}	Upper bound on d_{free}
3	7	7	7	5	5	13	13
4	17	17	13	15	15	16	16
5	37	27	33	25	35	20	20
6	75	71	73	65	57	22	22
7	175	131	135	135	147	25	25
8	257	233	323	271	357	28	28

Source: Daut *et al.* (1982).

TABLE 8-2-5 RATE 1/6 MAXIMUM FREE DISTANCE CODES

Constraint length K	Generators in octal			d_{free}	Upper bound on d_{free}
3	7	7	7	16	16
	7	5	5		
4	17	17	13	20	20
	13	15	15		
5	37	35	27	24	24
	33	25	35		
6	73	75	55	27	27
	65	47	57		
7	173	151	135	30	30
	135	163	137		
8	253	375	331	34	34
	235	313	357		

Source: Daut *et al.* (1982).

TABLE 8-2-6 RATE 1/7 MAXIMUM FREE DISTANCE CODES

Constraint length K	Generators in octal				d_{free}	Upper bound on d_{free}
3	7	7	7	7	18	18
	5	5	5			
4	17	17	13	13	23	23
	13	15	15			
5	35	27	25	27	28	28
	33	35	37			
6	53	75	65	75	32	32
	47	67	57			
7	165	145	173	135	36	36
	135	147	137			
8	275	253	375	331	40	40
	235	313	357			

Source: Daut *et al.* (1982).

TABLE 8-2-7 RATE 1/8 MAXIMUM FREE DISTANCE CODES

Constraint length K	Generators in octal				d_{free}	Upper bound on d_{free}
3	7	7	5	5	21	21
	5	7	7	7		
4	17	17	13	13	26	26
	13	15	15	17		
5	37	33	25	25	32	32
	35	33	27	37		
6	57	73	51	65	36	36
	75	47	67	57		
7	153	111	165	173	40	40
	135	135	147	137		
8	275	275	253	371	45	45
	331	235	313	357		

Source: Daut *et al.* (1982).

TABLE 8-2-8 RATE 2/3 MAXIMUM FREE DISTANCE CODES

Constraint length K	Generators in octal			d_{free}	Upper bound on d_{free}
2	17	06	15	3	4
3	27	75	72	5	6
4	236	155	337	7	7

Source: Duat *et al.* (1982).

TABLE 8-2-9 RATE $k/5$ MAXIMUM FREE DISTANCE CODES

Rate	Constraint length K	Generators in octal					d_{free}	Upper bound on d_{free}
2/5	2	17	07	11	12	04	6	6
	3	27	71	52	65	57	10	10
	4	247	366	171	266	373	12	12
3/5	2	35	23	75	61	47	5	5
4/5	2	237	274	156	255	337	3	4

Source: Daut *et al.* (1982).

TABLE 8-2-10 RATE $k/7$ MAXIMUM FREE DISTANCE CODES

Rate	Constraint length K	Generators in octal				d_{free}	Upper bound on d_{free}
2/7	2	05	06	12	15	9	9
		15	13	17			
	3	33	55	72	47	14	14
		25	53	75			
	4	312	125	247	366	18	18
		171	266	373			
3/7	2	45	21	36	62	8	8
		57	43	71			
4/7	2	130	067	237	274	6	7
		156	255	337			

Source: Daut *et al.* (1982).

TABLE 8-2-11 RATES 3/4 AND 3/8 MAXIMUM FREE DISTANCE CODES

Rate	Constraint length K	Generators in octal				d_{free}	Upper bound on d_{free}
3/4	2	13	25	61	47	4	4
3/8	2	15	42	23	61	8	8
		51	36	75	47		

Source: Daut *et al.* (1982).

A dual-k rate 1/2 convolutional encoder may be represented as shown in Fig. 8-2-16. It consists of two ($K = 2$) k-bit shift-register stages and $n = 2k$ function generators. Its output is two k-bit symbols. We note that the code considered in Example 8-2-3 is a dual-2 convolutional code.

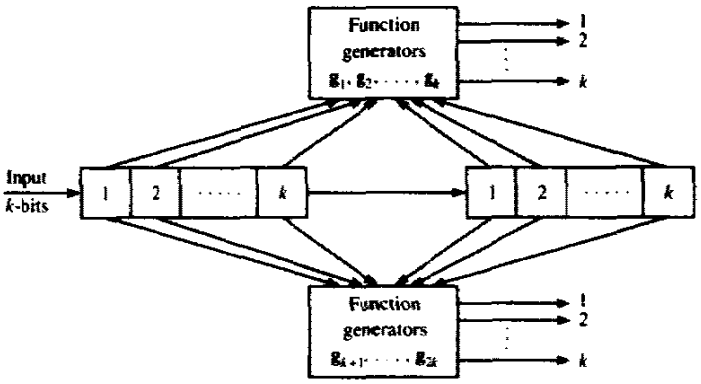

FIGURE 8-2-16 Encoder for rate 1/2 dual-k codes.

The $2k$ function generators for the dual-k codes have been given by Viterbi and Jacobs (1975). These may be expressed in the form

$$\begin{bmatrix} \leftarrow \mathbf{g}_1 \rightarrow \\ \leftarrow \mathbf{g}_2 \rightarrow \\ \vdots \\ \leftarrow \mathbf{g}_k \rightarrow \end{bmatrix} = \left[\begin{array}{ccccccc:ccc} 1 & 0 & 0 & \cdots & 0 & 1 & 0 & 0 & \cdots & 0 \\ 0 & 1 & 0 & \cdots & 0 & 0 & 1 & 0 & \cdots & 0 \\ \vdots & \vdots & \vdots & & \vdots & \vdots & \vdots & & & \vdots \\ 0 & 0 & 0 & \cdots & 1 & 0 & 0 & \cdots & 0 & 1 \end{array}\right] = [\mathbf{I}_k \quad \mathbf{I}_k]$$

$$\begin{bmatrix} \leftarrow \mathbf{g}_{k+1} \rightarrow \\ \leftarrow \mathbf{g}_{k+2} \rightarrow \\ \vdots \\ \leftarrow \mathbf{g}_{2k} \rightarrow \end{bmatrix} = \left[\begin{array}{ccccccc:ccccc} 1 & 1 & 0 & 0 & \cdots & & 0 & 1 & 0 & 0 & \cdots & 0 \\ 0 & 0 & 1 & 0 & \cdots & & 0 & 0 & 1 & 0 & \cdots & 0 \\ 0 & 0 & 0 & 1 & 0 & \cdots & 0 & 0 & 0 & 1 & 0 \cdots & 0 \\ 0 & 0 & 0 & & \cdots & 0 & 1 & & & & & \\ 1 & 0 & 0 & & \cdots & 0 & 0 & 0 & 0 & \cdots & 0 & 1 \end{array}\right]$$

$$= \left[\begin{array}{ccccccc:c} 1 & 1 & 0 & 0 & \cdots & & 0 & \\ 0 & 0 & 1 & 0 & \cdots & & 0 & \\ 0 & 0 & 0 & 1 & 0 & \cdots & 0 & \mathbf{I}_k \\ \hdashline 0 & 0 & 0 & & \cdots & 0 & 1 & \\ 1 & 0 & 0 & & \cdots & 0 & 0 & \end{array}\right] \tag{8-2-36}$$

where $\mathbf{I}_k$ denotes the $k \times k$ identity matrix.

The general form for the transfer function of a rate 1/2 dual-k code has been derived by Odenwalder (1976). It is expressed as

$$T(D, N, J) = \frac{(2^k - 1)D^4J^2N}{1 - NJ[2D + (2^k - 3)D^2]}$$

$$= \sum_{i=4}^{\infty} a_i D^i N^{f(i)} J^{h(i)} \tag{8-2-37}$$

where D represents the Hamming distance for the q-ary ($q = 2^k$) symbols, the $f(i)$ exponent on N represents the number of information symbol errors that are produced in selecting a branch in the tree or trellis other than a corresponding branch on the all-zero path, and the $h(i)$ exponent on J is equal to the number of branches in a given path. Note that the minimum free distance is $d_{\text{free}} = 4$ symbols ($4k$ bits).

Lower-rate dual-k convolutional codes can be generated in a number of ways, the simplest of which is to repeat each symbol generated by the rate 1/2 code r times, where $r = 1, 2, \ldots, m$ ($r = 1$ corresponds to each symbol appearing once). If each symbol in any particular branch of the tree or trellis or state diagram is repeated r times, the effect is to increase the distance parameter from D to D^r. Consequently the transfer function for a rate $1/2r$ dual-k code is

$$T(D, N, J) = \frac{(2^k - 1)D^{4r}J^2N}{1 - NJ[2D^r + (2^k - 3)D^{2r}]} \tag{8-2-38}$$

In the transmission of long information sequences, the path length parameter J in the transfer function may be suppressed by setting $J = 1$. The resulting transfer function $T(D, N)$ may be differentiated with respect to N, and N is set to unity. This yields

$$\begin{aligned} \left.\frac{dT(D,N)}{dN}\right|_{N=1} &= \frac{(2^k - 1)D^{4r}}{[1 - 2D^r - (2^k - 3)D^{2r}]^2} \\ &= \sum_{i=4r}^{\infty} \beta_i D^i \end{aligned} \tag{8-2-39}$$

where β_i represents the number of symbol errors associated with a path having distance D^i from the all-zero path, as described previously in Section 8-2-3. The expression in (8-2-39) may be used to evaluate the error probability for dual-k codes under various channel conditions.

Performance of Dual-k Codes with M-ary Modulation Suppose that a dual-k code is used in conjunction with M-ary orthogonal signaling at the modulator, where $M = 2^k$. Each symbol from the encoder is mapped into one of the M possible orthogonal waveforms. The channel is assumed to add white gaussian noise. The demodulator consists of M matched filters.

If the decoder performs hard-decision decoding, the performance of the code is determined by the symbol error probability P_M. This error probability has been computed in Chapter 5 for both coherent and noncoherent detection. From P_M, we can determine $P_2(d)$ according to (8-2-28) or (8-2-29), which is the probability of error in a pairwise comparison of the all-zero path with a path that differs in d symbols. The probability of a bit error is upper-bounded as

$$P_b < \frac{2^{k-1}}{2^k - 1} \sum_{d=4r}^{\infty} \beta_d P_2(d) \tag{8-2-40}$$

The factor $2^{k-1}/(2^k - 1)$ is used to convert the symbol error probability to the bit error probability.

Instead of hard-decision decoding, suppose that the decoder performs soft-decision decoding using the output of a demodulator that employs a square-law detector. The expression for the bit error probability given by (8-2-40) still applies, but now $P_2(d)$ is given by (see Section 12-1-1)

$$P_2(d) = \frac{1}{2^{2d-1}} \exp\left(-\tfrac{1}{2}\gamma_b R_c d\right) \sum_{i=0}^{d-1} K_i\left(\tfrac{1}{2}\gamma_b R_c d\right) \tag{8-2-41}$$

where

$$K_i = \frac{1}{i!} \sum_{l=0}^{d-1-i} \binom{2d-1}{l}$$

and $R_c = 1/2r$ is the code rate. This expression follows from the result (8-1-63).

Concatenated Codes In Section 8-1-8, we considered the concatenation of two block codes to form a long block code. Now that we have described convolutional codes, we broaden our viewpoint and consider the concatenation of a block code with a convolutional code or the concatenation of two convolutional codes.

As described previously, the outer code is usually chosen to be nonbinary, with each symbol selected from an alphabet of $q = 2^k$ symbols. This code may be a block code, such as a Reed–Solomon code, or a convolutional code, such as a dual-k code. The inner code may be either binary or nonbinary, and either a block or a convolutional code. For example, a Reed–Solomon code may be selected as the outer code and a dual-k code may be selected as the inner code. In such a concatenation scheme, the number of symbols in the outer (Reed–Solomon) code q equals 2^k, so that each symbol of the outer code maps into a k-bit symbol of the inner dual-k code. M-ary orthogonal signals may be used to transmit the symbols.

The decoding of such concatenated codes may also take a variety of different forms. If the inner code is a convolutional code having a short constraint length, the Viterbi algorithm provides an efficient means for decoding, using either soft-decision or hard-decision decoding.

If the inner code is a block code, and the decoder for this code performs soft-decision decoding, the outer decoder may also perform soft-decision decoding using as inputs the metrics corresponding to each word of the inner code. On the other hand, the inner decoder may make a hard decision after receipt of the code word and feed the hard decisions to the outer decoder. Then the outer decoder must perform hard-decision decoding.

The following example describes a concatenation code in which the outer code is a convolutional code and the inner code is a block code.

Example 8-2-5

Suppose we construct a concatenated code by selecting a dual-k code as the outer code and a Hadamard code as the inner code. To be specific, we select a rate 1/2 dual-5 code and a Hadamard (16, 5) inner code. The dual-5 rate

1/2 code has a minimum free distance $D_{free} = 4$ and the Hadamard code has a minimum distance $d_{min} = 8$. Hence, the concatenated code has an effective minimum distance of 32. Since there are 32 code words in the Hadamard code and 32 possible symbols in the outer code, in effect, each symbol from the outer code is mapped into one of the 32 Hadamard code words.

The probability of a symbol error in decoding the inner code may be determined from the results of the performance of block codes given in Sections 8-1-4 and 8-1-5 for soft-decision and hard-decision decoding, respectively. First, suppose that hard-decision decoding is performed in the inner decoder with the probability of a code word (symbol of outer code) error denoted as P_{32}, since $M = 32$. Then the performance of the outer code and, hence, the performance of the concatenated code is obtained by using this error probability in conjunction with the transfer function for the dual-5 code given by (8-2-37).

On the other hand, if soft-decision decoding is used on both the outer and the inner codes, the soft-decision metric from each received Hadamard code word is passed to the Viterbi algorithm, which computes the accumulated metrics for the competing paths through the trellis. We shall give numerical results on the performance of concatenated codes of this type in our discussion of coding for Rayleigh fading channels.

8-2-7 Other Decoding Algorithms for Convolutional Codes

The Viterbi algorithm described in Section 8-2-2 is the optimum decoding algorithm (in the sense of maximum-likelihood decoding of the entire sequence) for convolutional codes. However, it requires the computation of 2^{kK} metrics at each node of the trellis and the storage of $2^{k(K-1)}$ metrics and $2^{k(K-1)}$ surviving sequences, each of which may be about $5kK$ bits long. The computational burden and the storage required to implement the Viterbi algorithm make it impractical for convolutional codes with large constraint length.

Prior to the discovery of the optimum algorithm by Viterbi, a number of other algorithms had been proposed for decoding convolutional codes. The earliest was the sequential decoding algorithm originally proposed by Wozencraft (1957, 1961), and subsequently modified by Fano (1963).

The Fano sequential decoding algorithm searches for the most probable path through the tree or trellis by examining one path at a time. The increment added to the metric along each branch is proportional to the probability of the received signal for that branch, just as in Viterbi decoding, with the exception that an additional negative constant is added to each branch metric. The value of this constant is selected such that the metric for the correct path will increase on the average, while the metric for any incorrect path will decrease on the average. By comparing the metric of a candidate path with a moving (increasing) threshold, Fano's algorithm detects and discards incorrect paths.

To be more specific, let us consider a memoryless channel. The metric for

the ith path through the tree or trellis from the first branch to branch B may be expressed as

$$CM^{(i)} = \sum_{j=1}^{B} \sum_{m=1}^{n} \mu_{jm}^{(i)} \tag{8-2-42}$$

where

$$\mu_{jm}^{(i)} = \log_2 \frac{p(r_{jm} \mid c_{jm}^{(i)})}{p(r_{jm})} - \mathcal{K} \tag{8-2-43}$$

In (8-2-43), r_{jm} is the demodulator output sequence, $p(r_{jm} \mid c_{jm}^{(i)})$ denotes the pdf of r_{jm} conditional on the code bit $c_{jm}^{(i)}$ for the mth bit of the jth branch of the ith path, and $\mathcal{K}$ is a positive constant. $\mathcal{K}$ is selected as indicated above so that the incorrect paths will have a decreasing metric while the correct path will have an increasing metric on the average. Note that the term $p(r_{jm})$ in the denominator is independent of the code sequence, and, hence, may be subsumed in the constant factor.

The metric given by (8-2-43) is generally applicable for either hard- or soft-decision decoding. However, it can be considerably simplified when hard-decision decoding is employed. Specifically, if we have a BSC with transition (error) probability p, the metric for each received bit, consistent with the form in (8-2-43) is given by

$$\mu_{jm}^{(i)} = \begin{cases} \log_2 [2(1-p)] - R_c & \text{if } \tilde{r}_{jm} = c_{jm}^{(i)} \\ \log_2 2p - R_c & \text{if } \tilde{r}_{jm} \neq c_{jm}^{(i)} \end{cases} \tag{8-2-44}$$

where $\tilde{r}_{jm}$ is the hard-decision output from the demodulator and $c_{jm}^{(i)}$ is the mth code bit in the jth branch of the ith path in the tree and R_c is the code rate. Note that this metric requires some (approximate) knowledge of the error probability.

Example 8-2-6

Suppose we have a rate $R_c = 1/3$ binary convolutional code for transmitting information over a BSC with $p = 0.1$. By evaluating (8-2-44) we find that

$$\mu_{jm}^{(i)} = \begin{cases} 0.52 & \text{if } \tilde{r}_{jm} = c_{jm}^{(i)} \\ -2.65 & \text{if } \tilde{r}_{jm} \neq c_{jm}^{(i)} \end{cases} \tag{8-2-45}$$

To simplify the computations, the metric in (8-2-45) may be normalized. It is well approximated as

$$\mu_{jm}^{(i)} = \begin{cases} 1 & \text{if } \tilde{r}_{jm} = c_{jm}^{(i)} \\ -5 & \text{if } \tilde{r}_{jm} \neq c_{jm}^{(i)} \end{cases} \tag{8-2-46}$$

Since the code rate is 1/3, there are three output bits from the encoder for each input bit. Hence, the branch metric consistent with (8-2-46) is

$$\mu_j^{(i)} = 3 - 6d$$

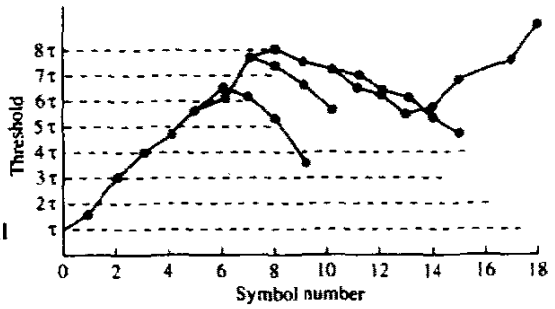

FIGURE 8-2-17 An example of the path search in sequential decoding. [*From Jordan (1966), © 1966 IEEE.*]

or, equivalently,

$$\mu_j^{(i)} = 1 - 2d \tag{8-2-47}$$

where d is the Hamming distance of the three received bits from the three branch bits. Thus, the metric $\mu_j^{(i)}$ is simply related to the Hamming distance of the received bits to the code bits in the jth branch of the ith path.

Initially, the decoder may be forced to start on the correct path by the transmission of a few known bits of data. Then it proceeds forward from node to node, taking the most probable (largest metric) branch at each node and increasing the threshold such that the threshold is never more than some preselected value, say τ, below the metric. Now suppose that the additive noise (for soft-decision decoding) or demodulation errors resulting from noise on the channel (for hard-decision decoding) cause the decoder to take an incorrect path because it appears more probable than the correct path. This is illustrated in Fig. 8-2-17. Since the metrics of an incorrect path decrease on the average, the metric will fall below the current threshold, say τ_0. When this occurs, the decoder backs up and takes alternative paths through the tree or trellis, in order of decreasing branch metrics, in an attempt to find another path that exceeds the threshold τ_0. If it is successful in finding an alternative path, it continues along that path, always selecting the most probable branch at each node. On the other hand, if no path exists that exceeds the threshold τ_0, the threshold is reduced by an amount τ and the original path is retraced. If the original path does not stay above the new threshold, the decoder resumes its backward search for other paths. This procedure is repeated, with the threshold reduced by τ for each repetition, until the decoder finds a path that remains above the adjusted threshold. A simplified flow diagram of Fano's algorithm is shown in Fig. 8-2-18.

The sequential decoding algorithm requires a buffer memory in the decoder to store incoming demodulated data during periods when the decoder is searching for alternate paths. When a search terminates, the decoder must be capable of processing demodulated bits sufficiently fast to empty the buffer prior to commencing a new search. Occasionally, during extremely long searches, the buffer may overflow. This causes loss of data, a condition that

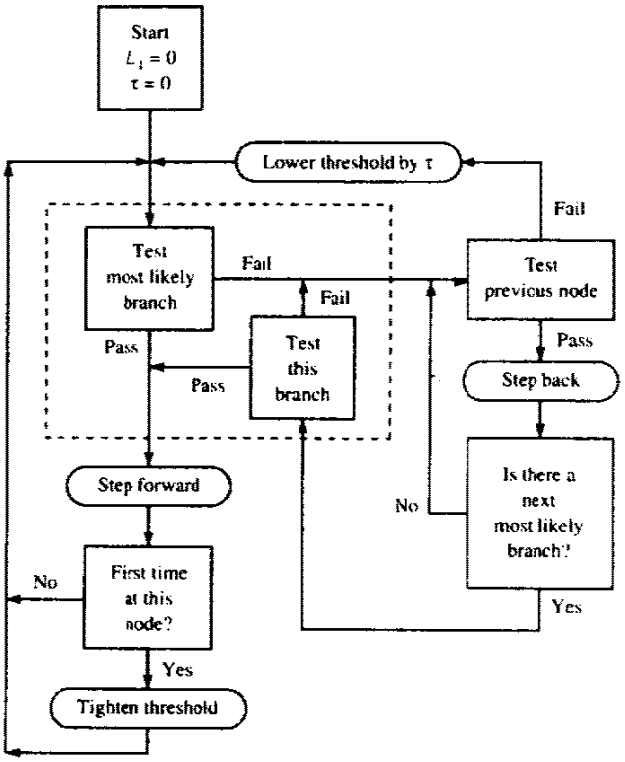

FIGURE 8-2-18 A simplified flow diagram of Fano's algorithm. [*From Jordan (1966), © 1966 IEEE.*]

can be remedied by retransmission of the lost information. In this regard, we should mention that the cutoff rate R_0 has special meaning in sequential decoding. It is the rate above which the average number of decoding operations per decoded digit becomes infinite, and it is termed the *computational cutoff rate* R_{comp}. In practice, sequential decoders usually operate at rates near R_0.

The Fano sequential decoding algorithm has been successfully implemented in several communication systems. Its error rate performance is comparable to that of Viterbi decoding. However, in comparison with Viterbi decoding, sequential decoding has a significantly larger decoding delay. On the positive side, sequential decoding requires less storage than Viterbi decoding and, hence, it appears attractive for convolutional codes with a large constraint length. The issues of computational complexity and storage requirements for sequential decoding are interesting and have been thoroughly investigated. For an analysis of these topics and other characteristics of the Fano algorithm, the interested reader may refer to Gallager (1968), Wozencraft and Jacobs (1965), Savage (1966), and Forney (1974).

Another type of sequential decoding algorithm, called a *stack algorithm*, has been proposed independently by Jelinek (1969) and Zigangirov (1966). In contrast to the Viterbi algorithm, which keeps track of $2^{(K-1)k}$ paths and

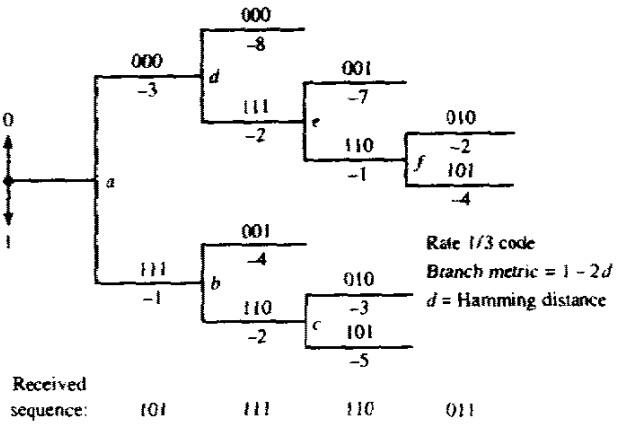

Stack with accumulated path metrics

Step *a*	Step *b*	Step *c*	Step *d*	Step *e*	Step *f*
-1	-2	-3	-2	-1	-2
-3	-3	-3	-3	-3	-3
	-4	-4	-4	-4	-4
		-5	-5	-5	-4
			-8	-7	-5
				-8	-7
					-8

FIGURE 8-2-19 A example of the stack algorithm for decoding a rate 1/3 convolutional code.

corresponding metrics, the stack sequential decoding algorithm deals with fewer paths and their corresponding metrics. In a stack algorithm, the more probable paths are ordered according to their metrics, with the path at the top of the stack having the largest metric. At each step of the algorithm, only the path at the top of the stack is extended by one branch. This yields 2^k successors and their corresponding metrics. These 2^k successors along with the other paths are then reordered according to the values of the metrics and all paths with metrics that fall below some preselected amount from the metric of the top path may be discarded. Then the process of extending the path with the largest metric is repeated. Figure 8-2-19 illustrates the first few steps in a stack algorithm.

It is apparent that when none of the 2^k extensions of the path with the largest metric remains at the top of the stack, the next step in the search involves the extension of another path that has climbed to the top of the stack. It follows that the algorithm does not necessarily advance by one branch through the trellis in every iteration. Consequently, some amount of storage must be provided for newly received signals and previously received signals in order to allow the algorithm to extend the search along one of the shorter paths, when such a path reaches the top of the stack.

In a comparison of the stack algorithm with the Viterbi algorithm, the stack algorithm requires fewer metric computations, but this computational saving is offset to a large extent by the computations involved in reordering the stack after every iteration. In comparison with the Fano algorithm, the stack algorithm is computationally simpler, since there is no retracing over the same path as is done in the Fano algorithm. On the other hand, the stack algorithm requires more storage than the Fano algorithm.

A third alternative to the optimum Viterbi decoder is a method called *feedback decoding* (Heller, 1975), which has been applied to decoding for a BSC (hard-decision decoding). In feedback decoding, the decoder makes a hard decision on the information bit at stage j based on metrics computed from stage j to stage $j+m$, where m is a preselected positive integer. Thus, the decision on the information bit is either 0 or 1 depending on whether the minimum Hamming distance path that begins at stage j and ends at stage $j+m$ contains a 0 or 1 in the branch emanating from stage j. Once a decision is made on the information bit at stage j, only that part of the tree that stems from the bit selected at stage j is kept (half the paths emanating from node j) and the remaining part is discarded. This is the feedback feature of the decoder.

The next step is to extend the part of the tree that has survived to stage $j+1+m$ and consider the paths from stage $j+1$ to $j+1+m$ in deciding on the bit at stage $j+1$. Thus, this procedure is repeated at every stage. The parameter m is simply the number of stages in the tree that the decoder looks ahead before making a hard decision. Since a large value of m results in a large amount of storage, it is desirable to select m as small as possible. On the other hand, m must be sufficiently large to avoid a severe degradation in performance. To balance these two conflicting requirements, m is usually selected in the range $K \leq m \leq 2K$, where K is the constraint length. Note that this decoding delay is significantly smaller than the decoding delay in a Viterbi decoder, which is usually about $5K$.

Example 8-2-7

Let us consider the use of a feedback decoder for the rate 1/3 convolutional code shown in Fig. 8-2-2. Figure 8-2-20 illustrates the tree diagram and the operation of the feedback decoder for $m = 2$. That is, in decoding the bit at branch j, the decoder considers the paths at branches j, $j+1$, and $j+2$. Beginning with the first branch, the decoder computes eight metrics (Hamming distances), and decides that the bit for the first branch is 0 if the minimum distance path is contained in the upper part of the tree, and 1 if the minimum distance path is contained in the lower part of the tree. In this example, the received sequence for the first three branches is assumed to be 101111110, so that the minimum distance path is in the upper part of the tree. Hence, the first output bit is 0.

The next step is to extend the upper part of the tree (the part of the tree that has survived) by one branch, and to compute the eight metrics for

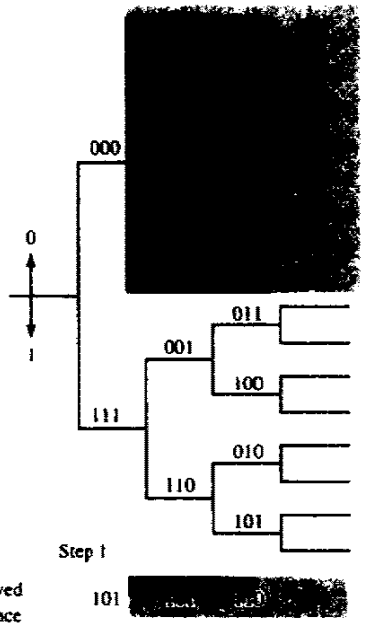

FIGURE 8-2-20 An example of feedback decoding for a rate 1/3 convolutional code.

Step 1 : Upper-tree metrics : 7,6,5,2* ; lower-tree metrics : 5,4,3,4 → 0
Step 2 : Upper-tree metrics : 7,6,5,6 ; lower-tree metrics : 3,6,1* ,2 → 1

branches 2, 3, and 4. For the assumed received sequence 111110011, the minimum-distance path is contained in the lower part of the section of the tree that survived from the first step. Hence, the second output bit is 1. The third step is to extend this lower part of the tree and to repeat the procedure described for the first two steps.

Instead of computing metrics as described above, a feedback decoder for the BSC may be efficiently implemented by computing the syndrome from the received sequence and using a table lookup method for correcting errors. This method is similar to the one described for decoding block codes. For some convolutional codes, the feedback decoder simplifies to a form called a *majority logic decoder* or a *threshold decoder* (Massey, 1963; Heller, 1975).

8-2-8 Practical Considerations in the Application of Convolutional Codes

Convolutional codes are widely used in many practical applications of communications system design. Viterbi decoding is predominantly used for short constraint lengths ($K \leq 10$), while sequential decoding is used for long constraint length codes, where the complexity of Viterbi decoding becomes prohibitive. The choice of constraint length is dictated by the desired coding gain.

From the error probability results for soft-decision decoding given by

TABLE 8-2-12 UPPER BOUNDS ON CODING GAIN FOR SOFT-DECISION DECODING OF SOME CONVOLUTION CODES

Rate 1/2 codes			Rate 1/3 codes		
Constraint length K	d_{free}	Upper bound (db)	Constraint length K	d_{free}	Upper bound (dB)
3	5	3.98	3	8	4.26
4	6	4.77	4	10	5.23
5	7	5.44	5	12	6.02
6	8	6.02	6	13	6.37
7	10	6.99	7	15	6.99
8	10	6.99	8	16	7.27
9	12	7.78	9	18	7.78
10	12	7.78	10	20	8.24

(8-2-26) it is apparent that the coding gain achieved by a convolutional code over an uncoded binary PSK or QPSK system is

$$\text{coding gain} \leq 10 \log_{10} (R_c d_{free})$$

We also know that the minimum free distance d_{free} can be increased either by decreasing the code rate or by increasing the constraint length, or both. Table 8-2-12 provides a list of upper bounds on the coding gain for several convolutional codes. For purposes of comparison, Table 8-2-13 lists the actual coding gains and the upper bounds for several short constraint length convolutional codes with Viterbi decoding. It should be noted that the coding gain increases toward the asymptotic limit as the SNR per bit increases.

These results are based on soft-decision Viterbi decoding. If hard-decision decoding is used, the coding gains are reduced by approximately 2 dB for the AWGN channel.

Larger coding gains than those listed in the above tables are achieved by

TABLE 8-2-13 CODING GAIN (dB) FOR SOFT-DECISION VITERBI DECODING

	$\mathcal{E}_b/N_0$ uncoded	$R_c = 1/3$		$R_c = 1/2$			$R_c = 2/3$		$R_c = 3/4$	
P_b	(dB)	$K = 7$	$K = 8$	$K = 5$	$K = 6$	$K = 7$	$K = 6$	$K = 8$	$K = 6$	$K = 9$
10^{-3}	6.8	4.2	4.4	3.3	3.5	3.8	2.9	3.1	2.6	2.6
10^{-5}	9.6	5.7	5.9	4.3	4.6	5.1	4.2	4.6	3.6	4.2
10^{-7}	11.3	6.2	6.5	4.9	5.3	5.8	4.7	5.2	3.9	4.8

Source: Jacobs (1974); © IEEE.

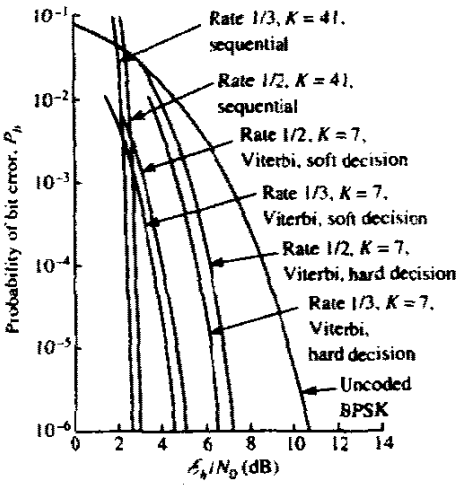

FIGURE 8-2-21 Performance of rate 1/2 and rate 1/3 Viterbi and sequential decoding. [*From Omura and Levitt (1982)* © *1982 IEEE.*]

employing long constraint length convolutional codes, e.g., $K = 50$, and decoding such codes by sequential decoding. Invariably, sequential decoders are implemented for hard-decision decoding to reduce complexity. Figure 8-2-21 illustrates the error rate performance of several constraint-length $K = 7$ convolutional codes for rates 1/2 and 1/3 and for sequential decoding (with hard decisions) of a rate 1/2 and a rate 1/3 constraint-length $K = 41$ convolutional codes. Note that the $K = 41$ codes achieve an error rate of 10^{-6} at 2.5 and 3 dB, which are within 4–4.5 dB of the channel capacity limit, i.e., in vicinity of the cutoff rate limit. However, the rate 1/2 and rate 1/3, $K = 7$ codes with soft-decision Viterbi decoding operate at about 5 and 4.4 dB at 10^{-6}, respectively. These short-constraint-length codes achieve a coding gain of about 6 dB at 10^{-6}, while the long constraint codes gain about 7.5–8 dB.

Two important issues in the implementation of Viterbi decoding are

1 the effect of path memory truncation, which is a desirable feature that ensures a fixed decoding delay, and

2 the degree of quantization of the input signal to the Viterbi decoder.

As a rule of thumb, we stated that path memory truncation to about five constraint lengths has been found to result in negligible performance loss. Figure 8-2-22 illustrates the performance obtained by simulation for rate 1/2, constraint-lengths $K = 3$, 5, and 7 codes with memory path length of 32 bits. In addition to path memory truncation, the computations were performed with eight-level (three bits) quantized input signals from the demodulator. The broken curves are performance results obtained from the upper bound in the bit error rate given by (8-2-26). Note that the simulation results are close to the theoretical upper bounds, which indicate that the degradation due to path memory truncation and quantization of the input signal has a minor effect on performance (0.20–0.30 dB).

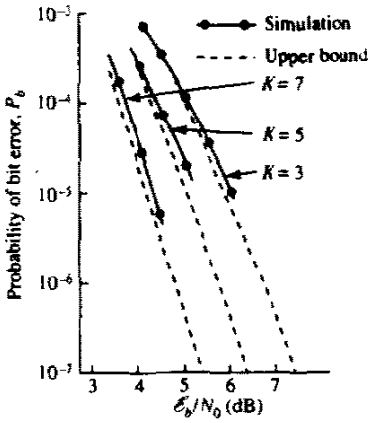

FIGURE 8-2-22 Bit error probability for rate 1/2 Viterbi decoding with eight-level quantized inputs to the decoder and 32-bit path memory. [*From Heller and Jacobs (1971). © 1971 IEEE.*]

Figure 8-2-23 illustrates the bit error rate performance obtained via simulation for hard-decision decoding of convolutional codes with $K = 3$–8. Note that with the $K = 8$ code, an error rate of 10^{-5} requires about 6 dB, which represents a coding gain of nearly 4 dB relative to uncoded QPSK.

The effect of input signal quantization is further illustrated in Fig. 8-2-24 for a rate 1/2, $K = 5$ code. Note that three-bit quantization (eight levels) is about 2 dB better than hard-decision decoding, which is the ultimate limit between soft-decision decoding and hard-decision decoding on the AWGN channel. The combined effect of signal quantization and path memory trunction for the rate 1/2, $K = 5$ code with 8-, 16-, and 32-bit path memories and either one- or three-bit quantization is shown in Fig. 8-2-25. It is apparent from these results that a path memory as short as three constraint lengths does not seriously degrade performance.

When the signal from the demodulator is quantized to more than two levels, another problem that must be considered is the spacing between quantization levels. Figure 8-2-26 illustrates the simulation results for an eight-level uniform quantizer as a function of the quantizer threshold spacing. We observe that

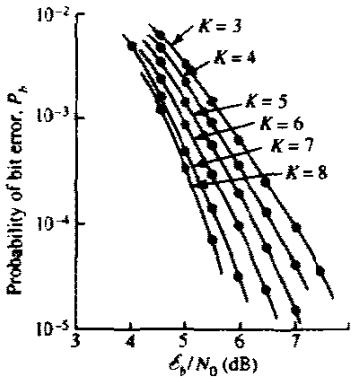

FIGURE 8-2-23 Performance of rate 1/2 codes with hard-decision Viterbi decoding and 32-bit path memory truncation. [*From Heller and Jacobs (1971). © 1971 IEEE.*]

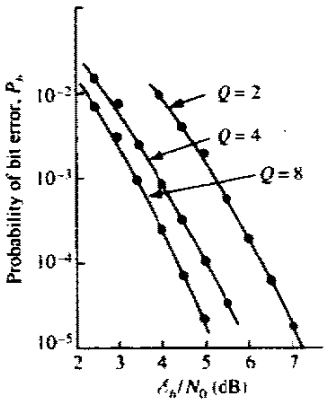

FIGURE 8-2-24 Performance of rate 1/2, $K = 5$ code with eight-, four-, and two-level quantization at the input to the Viterbi decoder. Path truncation length = 32 bits. [*From Heller and Jacobs (1971). © 1971 IEEE.*]

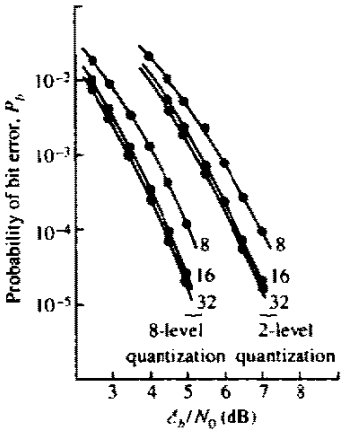

FIGURE 8-2-25 Performance of rate 1/2, $K = 5$ code with 32-, 16-, and 8-bit path memory truncation and eight- and two-level quantization. [*From Heller and Jacobs (1971). © 1971 IEEE.*]

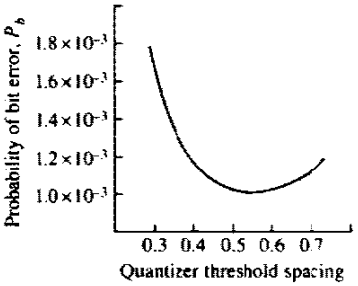

FIGURE 8-2-26 Error rate performance of rate 1/2, $K = 5$ Viterbi decoder for $\mathscr{E}_b/N_0 = 3.5$ dB and eight-level quantization as a function of quantizer threshold level spacing for equally spaced thresholds [*From Heller and Jacobs (1971). © 1971 IEEE.*]

there is an optimum spacing between thresholds (approximately equal to 0.5). However, the optimum is sufficiently broad (0.4–0.7) so that, once it is set, there is little degradation resulting from variations in the AGC level of the order of ±20%.

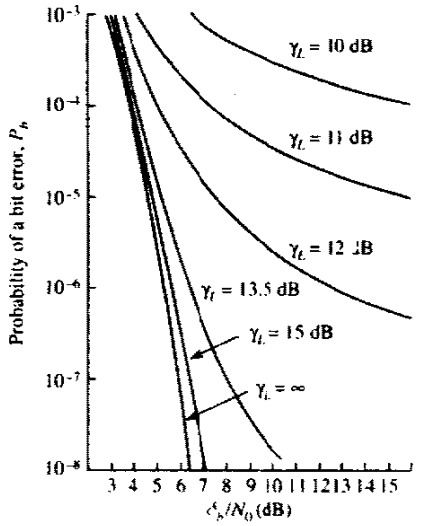

FIGURE 8-2-27 Performance of a rate 1/2, $K = 7$ code with Viterbi decoding and eight-level quantization as a function of the carrier phase tracking loop SNR γ_L. [*From Heller and Jacobs (1971). © 1971 IEEE.*]

Finally, we should point out some important results in the performance degradation due to carrier phase variations. Figure 8-2-27 illustrates the performance of a rate 1/2, $K = 7$ code with eight-level quantization and a carrier phase tracking loop SNR γ_L. Recall that in a PLL, the phase error has a variance that is inversely proportional to γ_L. The results in Fig. 8-2-27 indicate that the degradation is large when the loop SNR is small ($\gamma_L < 12$ dB), and causes the error rate performance to bottom out at relatively high error rate.

8-3 CODED MODULATION FOR BANDWIDTH-CONSTRAINED CHANNELS

In the treatment of block and convolutional codes in Sections 8-1 and 8-2, respectively, performance improvement was achieved by expanding the bandwidth of the transmitted signal by an amount equal to the reciprocal of the code rate. Recall for example that the improvement in performance achieved by an (n, k) binary block code with soft-decision decoding is approximately $10 \log_{10}(R_c d_{\min} - k \ln 2/\gamma_b)$ compared with uncoded binary or quaternary PSK. For example, when $\gamma_b = 10$ the (24, 12) extended Golay code gives a coding gain of 5 dB. This coding gain is achieved at a cost of doubling the bandwidth of the transmitted signal and, of course, at the additional cost in receiver implementation complexity. Thus, coding provides an effective method for trading bandwidth and implementation complexity against transmitter power. This situation applies to digital communications systems that are designed to operate in the power-limited region where $R/W < 1$.

In this section, we consider the use of coded signals for bandwidth-constrained channels. For such channels, the digital communications system is

designed to use bandwidth-efficient multilevel/phase modulation, such as PAM, PSK, DPSK, or QAM, and operates in the region where $R/W > 1$. When coding is applied to the bandwidth-constrained channel, a performance gain is desired without expanding the signal bandwidth. This goal can be achieved by increasing the number of signals over the corresponding uncoded system to compensate for the redundancy introduced by the code.

For example, suppose that a system employing uncoded four-phase PSK modulation achieves an $R/W = 2$ (bits/s)/Hz at an error probability of 10^{-6} For this error rate the SNR per bit is $\gamma_b = 10.5$ dB. We may try to reduce the SNR per bit by use of coded signals, but this must be done without expanding the bandwidth. If we choose a rate $R_c = 2/3$ code, it must be accompanied by an increase in the number of signal points from four (two bits per symbol) to eight (three bits per symbol). Thus, the rate 2/3 code used in conjunction with eight-phase PSK, for example, yields the same data throughput as uncoded four-phase PSK. However, we recall that an increase in the number of signal phases from four to eight requires an additional 4 dB approximately in signal power to maintain the same error rate. Hence, if coding is to provide a benefit, the performance gain of the rate 2/3 code must overcome this 4 dB penalty.

If the modulation is treated as a separate operation independent of the encoding, the use of very powerful codes (large-constraint-length convolutional codes or large-block-length block codes) is required to offset the loss and provide some significant coding gain. On the other hand, if the modulation is an integral part of the encoding process and is designed in conjunction with the code to increase the minimum euclidean distance between pairs of coded signals, the loss from the expansion of the signal set is easily overcome and a significant coding gain is achieved with relatively simple codes. The key to this integrated modulation and coding approach is to devise an effective method for mapping the coded bits into signal points such that the minimum euclidean distance is maximized. Such a method was developed by Ungerboeck (1982), based on the principle of *mapping by set partitioning*. We describe this principle by means of two examples.

Example 8-3-1: An 8-PSK Signal Constellation

Let us partition the eight-phase signal constellation shown in Fig. 8-3-1 into subsets of increasing minimum euclidean distance. In the eight-phase signal set, the signal points are located on a circle of radius $\sqrt{\mathscr{E}}$ and have a minimum distance separation of

$$d_0 = 2\sqrt{\mathscr{E}} \sin \tfrac{1}{8}\pi = \sqrt{(2 - \sqrt{2})\mathscr{E}} = 0.765\sqrt{\mathscr{E}}$$

In the first partitioning, the eight points are subdivided into two subsets of four points each, such that the minimum distance between points increases to $d_1 = \sqrt{2\mathscr{E}}$. In the second level of partitioning, each of the two subsets is subdivided into two subsets of two points, such that the minimum distance increases to $d_2 = 2\sqrt{\mathscr{E}}$. This results in four subsets of two points each.

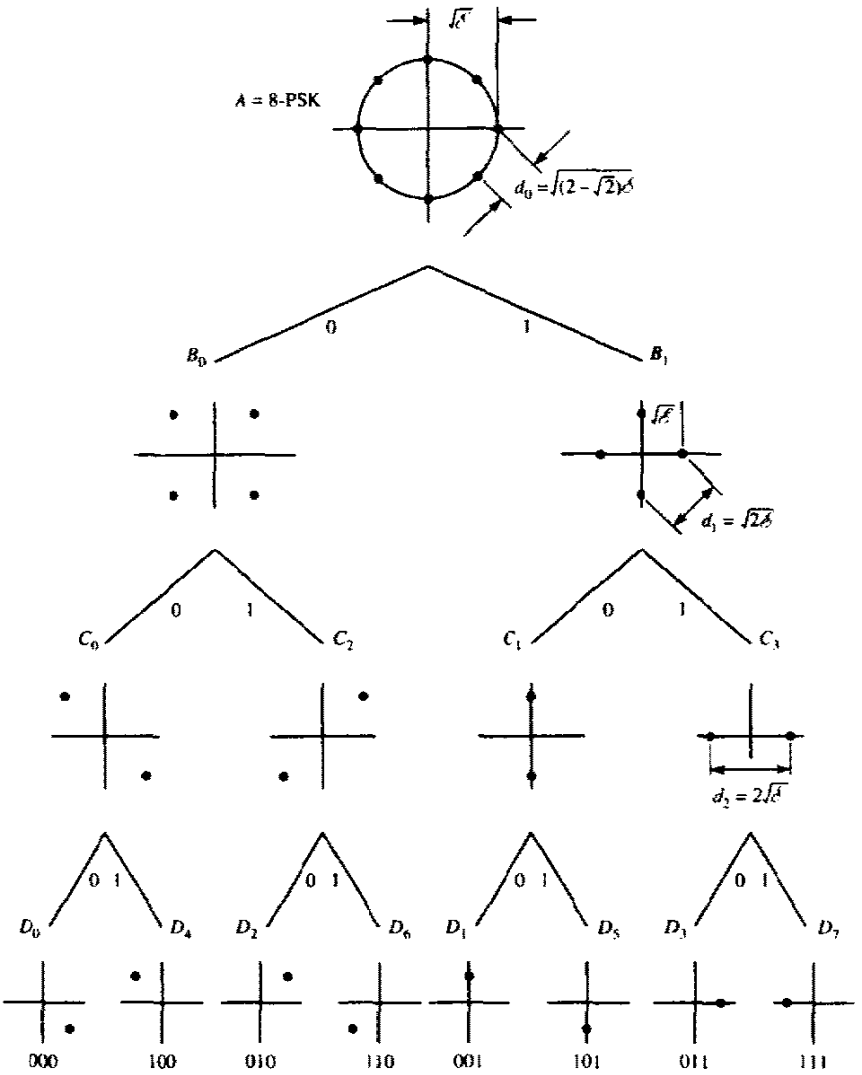

FIGURE 8-3-1 Set partitioning of an 8-PSK signal set.

Finally, the last stage of partitioning leads to eight subsets, where each subset contains a single point. Note that each level of partitioning increases the minimum euclidean distance between signal points. The results of these three stages of partitioning are illustrated in Fig. 8-3-1. The way in which the coded bits are mapped into the partitioned signal points is described below.

Example 8-3-2: A 16-QAM Signal Constellation

The 16-point rectangular signal constellation shown in Fig. 8-3-2 is first divided into two subsets by assigning alternate points to each subset as

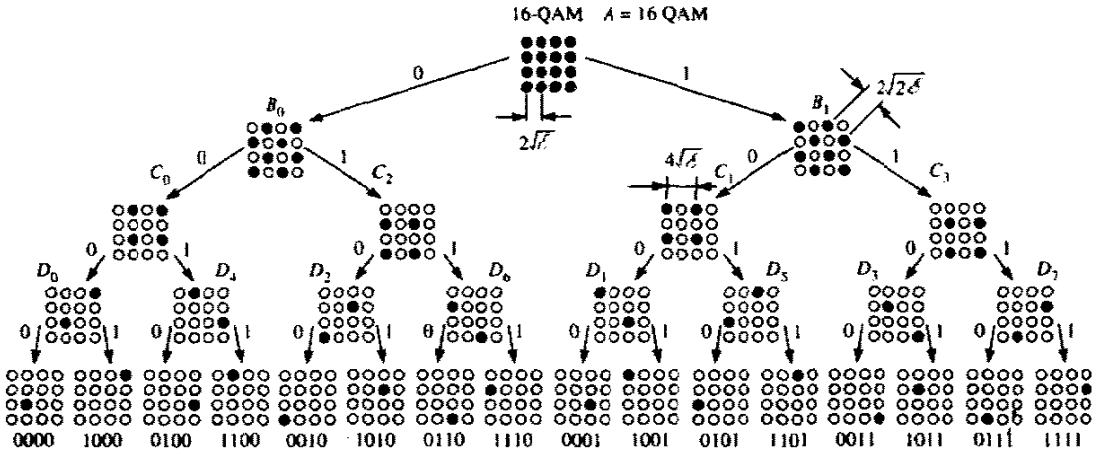

FIGURE 8-3-2 Set partitioning of 16-QAM signal.

illustrated in the figure. Thus, the distance between points is increased from $2\sqrt{\mathscr{E}}$ to $2\sqrt{2\mathscr{E}}$ by the first partitioning. Further partitioning of the two subsets leads to greater separation in euclidean distance between signal points as illustrated in Fig. 8-3-2. It is interesting to note that for the rectangular signal constellations, each level of partitioning increases the minimum euclidean distance by $\sqrt{2}$, i.e., $d_{i+1}/d_i = \sqrt{2}$ for all i.

In these two examples, the partitioning was carried out to the limit where each subset contains only a single point. In general, this may not be necessary. For example, the 16-point QAM signal constellation may be partitioned only twice, to yield four subsets of four points each. Similarly, the eight-phase PSK signal constellation can be partitioned twice, to yield four subsets of two points each.

The degree to which the signal is partitioned depends on the characteristics of the code. In general, the encoding process is performed as illustrated in Fig. 8-3-3. A block of m information bits is separated into two groups of length k_1

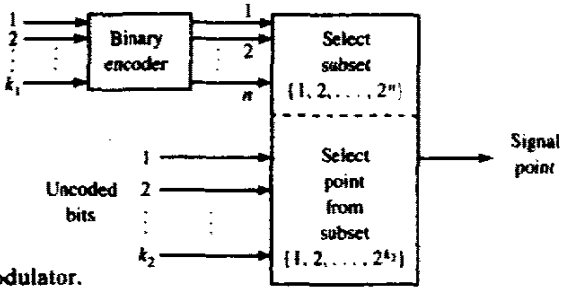

FIGURE 8-3-3 General structure of combined encoder/modulator.

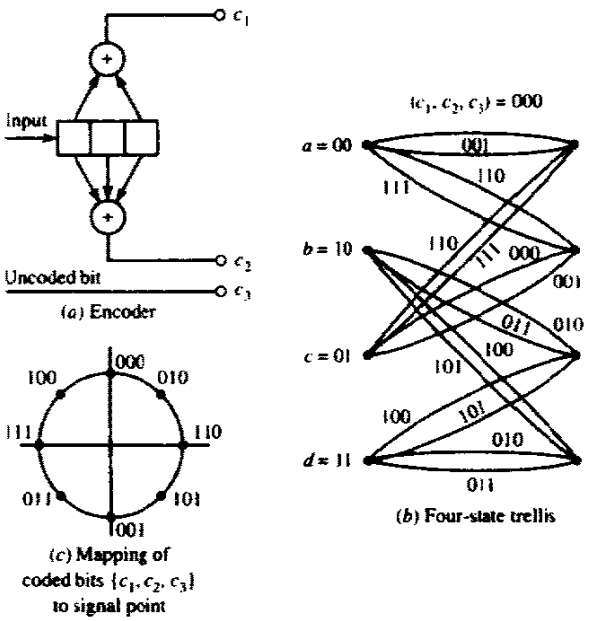

FIGURE 8-3-4 Four-state trellis-coded 8-PSK modulation.

and k_2. The k_1 bits are encoded into n bits while the k_2 bits are left uncoded. Then, the n bits from the encoder are used to select one of the 2^n possible subsets in the partitioned signal set while the k_2 bits are used to select one of the 2^{k_2} signal points in each subset. When $k_2 = 0$, all m information bits are encoded.

Example 8-3-3

Consider the use of the rate 1/2 convolutional code shown in Fig. 8-3-4 to encode one information bit while the second information bit is left uncoded. When used in conjunction with an eight-point signal constellation, e.g., eight-phase PSK or eight-point QAM, the two encoded bits are used to select one of the four subsets in the signal constellation, while the remaining information bit is used to select one of the two points within each subset. In this case, $k_1 = 1$ and $k_2 = 1$. The four-state trellis, which is shown in Fig. 8-3-4(b), is basically the trellis for the rate 1/2 convolution encoder with the addition of parallel paths in each transition to accommodate the uncoded bit c_3. Thus, the coded bits (c_1, c_2) are used to select one of the four subsets that contain two signal points each, while the uncoded bit is used to select one of the two signal points within each subset. Note that signal points within a subset are separated in distance by $d_2 = 2\sqrt{\mathcal{E}}$. Hence, the euclidean distance between parallel paths is d_2. The mapping of coded bits (c_1, c_2, c_3) to signal points is illustrated in Fig. 8-3-4(c). As an alternative coding scheme, we may use a rate 2/3 convolutional encoder, and, thus, encode

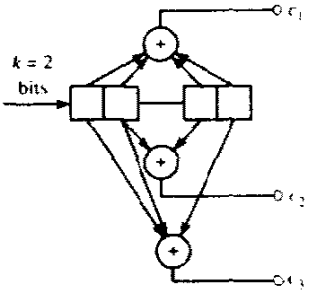

FIGURE 8-3-5 Rate 2/3 convolutional encoder for encoding both information bits.

both information bits as shown in Fig. 8-3-5. This encoding leads to an eight-state trellis and results in better performance, but also requires a more complex implementation of the decoder as described below.

Either block codes or convolutional codes may be used in conjunction with the partitioned signal constellation. In general, convolutional codes provide comparable coding gains to block codes and the availability of the Viterbi algorithm results in a simpler implementation for soft-decision decoding. For this reason, we limit our discussion to convolutional codes (linear trellis codes) and more generally to (nonlinear) trellis codes.

Trellis-Coded Modulation Let us consider the use of the 8-PSK signal constellation in conjunction with trellis codes. Uncoded four-phase PSK (4-PSK) is used as a reference in measuring coding gain. Uncoded 4-PSK employs the signal points in either subset B_0 or B_1 of Fig. 8-3-1, for which the minimum distance of the signal points is $\sqrt{2\mathscr{E}}$. Note that this signal corresponds to a trivial one-state trellis with four parallel state transitions as shown in Fig. 8-3-6(a). The subsets D_0, D_2, D_4, and D_6 are used as the signal points for the purpose of illustration.

For the coded 8-PSK modulation, we may use the four-state trellis shown in Fig. 8-3-6(b). Note that each branch in the trellis corresponds to one of the four subsets C_0, C_1, C_2, or C_3. For the eight-point constellation, each of the subsets C_0, C_1, C_2, and C_3, contains two signal points. Hence, the state transition C_0 contains the two signal points corresponding to the bits (000, 100) or (0, 4) in octal representation. Similarly, C_2 contains the two signal points corresponding to (010, 110), or to (2, 6) in octal, C_1 contains the points corresponding to (001, 101), or (1, 5) in octal, and C_3 contains the points corresponding to (011, 111), or (3, 7) in octal. Thus, each transition in the four-state trellis contains two parallel paths, as shown in more detail in Fig. 8-3-6(c). Note that any two signal paths that diverge from one state and remerge at the same state after more than one transition have a squared euclidean distance of $d_0^2 + 2d_1^2 = d_0^2 + d_2^2$ between them. For example, the

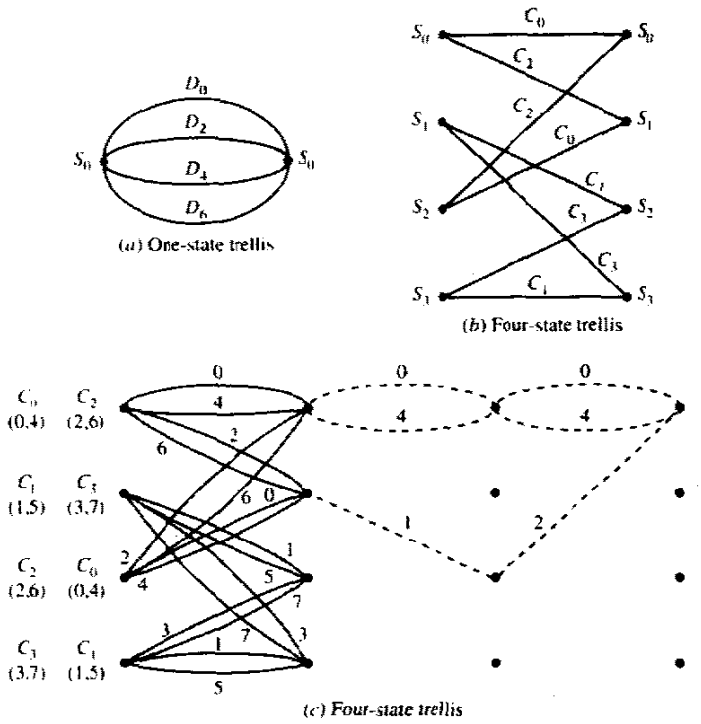

FIGURE 8-3-6 Uncoded 4-PSK and trellis-coded 8-PSK modulation.

signal paths 0, 0, 0 and 2, 1, 2 are separated by $d_0^2 + d_2^2 = [(0.765)^2 + 4]\mathscr{E} = 4.585\mathscr{E}$. On the other hand, the squared euclidean distance between parallel transitions is $d_2^2 = 4\mathscr{E}$. Hence, the minimum euclidean distance separation between paths that diverge from any state and remerge at the same state in the four-state trellis is $d_2 = 2\sqrt{\mathscr{E}}$. This minimum distance in the trellis code is called the *free euclidean distance* and denoted by D_{fed}.

In the four-state trellis of Fig. 8-3-6(b), $D_{\text{fed}} = 2\sqrt{\mathscr{E}}$. When compared with the euclidean distance $d_0 = \sqrt{2\mathscr{E}}$ for the uncoded 4-PSK modulation, we observe that the four-state trellis code gives a coding gain of 3 dB.

We should emphasize that the four-state trellis code illustrated in Fig. 8-3-6(b) is optimum in the sense that it provides the largest free euclidean distance. Clearly, many other four-state trellis codes can be constructed, including the one shown in Fig. 8-3-7, which consists of four distinct transitions from each state to all other states. However, neither this code nor any of the other possible four-state trellis codes gives a larger D_{fed}.

The construction of the optimum four-state trellis code for the eight-point constellation was performed on the basis of the following heuristic rules:

(a) Parallel transitions (when they occur) are assigned to signal points separated by the maximum euclidean distance, e.g., $d_2 = 2\sqrt{\mathscr{E}}$ for 8-PSK in the four subsets C_0, C_1, C_2, C_3.

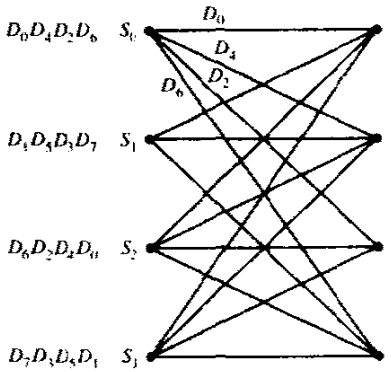

FIGURE 8-3-7 An alternative four-state trellis code.

(b) The transition originating from and merging into any state is assigned the subsets (C_0, C_2) or (C_1, C_3), which have a maximum distance $d_1 = \sqrt{2\mathscr{E}}$.

(c) The signal points should occur with equal frequency.

Note that rules (a) and (b) guarantee that the euclidean distance associated with single and multiple paths that diverge from any state and remerge in that state exceeds the euclidean distance of uncoded 4-PSK. Rule (c) guarantees that the trellis code will have a regular structure.

We should indicate that the specific mapping of coded bits into signal points, as illustrated in Fig. 8-3-1, where the eight signal points are represented in an equivalent binary form, is not important. Other mappings can be devised by permuting subsets in a way that preserves the main property of increased minimum distance among the subsets.

In the four-state trellis code, the parallel transitions were separated by the euclidean distance $2\sqrt{\mathscr{E}}$, which is also D_{fed}. Hence, the coding gain of 3 dB is limited by the distance of the parallel transitions. Larger gains in performance relative to uncoded 4-PSK can be achieved by using trellis codes with more states, which allow for the elimination of the parallel transitions. Thus, trellis codes with eight or more states would use distinct transitions to obtain a larger D_{fed}.

For example, in Fig. 8-3-8, we illustrate an eight-state trellis code due to Ungerboeck (1982) for the 8-PSK signal constellation. The state transitions for maximizing the free euclidean distance were determined from application of the three basic rules given above. In this case, note that the minimum squared euclidean distance is

$$D_{\text{fed}}^2 = d_0^2 + 2d_1^2 = 4.585\mathscr{E}$$

which, when compared with $d_0^2 = 2\mathscr{E}$ for uncoded 4-PSK, represents a gain of 3.6 dB. Ungerboeck (1982, 1987) has also found rate 2/3 trellis codes with 16, 32, 64, 128, and 256 states that achieve coding gains ranging from 4 to 5.75 dB for 8-PSK modulation.

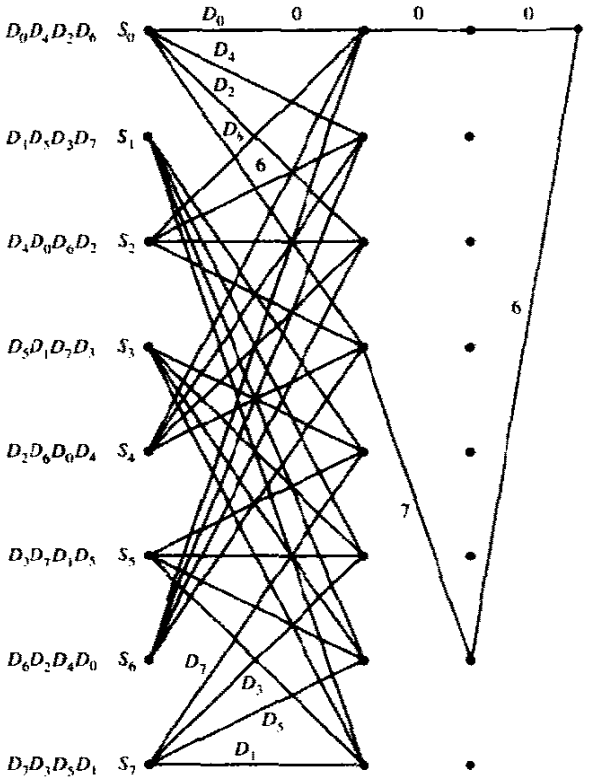

FIGURE 8-3-8 Eight-state trellis code for coded 8-PSK modulation.

The basic principle of set partitioning is easily extended to larger PSK signal constellations that yield greater bandwidth efficiency. For example, 3 (bits/s)/Hz can be achieved with either uncoded 8-PSK or with trellis-coded 16-PSK modulation. Ungerboeck (1987) has devised trellis codes and has evaluated the coding gains achieved by simple rate 1/2 and rate 2/3 convolutional codes for the 16-PSK signal constellations. The results are summarized below.

Soft-decision Viterbi decoding for trellis-coded modulation is accomplished in two steps. Since each branch in the trellis corresponds to a signal subset, the first step in decoding is to determine the best signal point within each subset, i.e., the point in each subset that is closest in distance to the received point. We may call this *subset decoding*. In the second step, the signal point selected from each subset and its squared distance metric are used for the corresponding branch in the Viterbi algorithm to determine the signal path through the code trellis that has the minimum sum of squared distances from the sequence of received (noisy channel output) signals.

The error rate performance of the trellis-coded signals in the presence of additive gaussian noise can be evaluated by following the procedure described in Section 8-2 for convolutional codes. Recall that this procedure involves the computation of the probability of error for all different error events and

summing these error event probabilities to obtain a union bound on the first-event error probability. Note, however, that, at high SNR, the first-event error probability is dominated by the leading term, which has the minimum distance D_{fed}. Consequently, at high SNR, the first-event error probability is well approximated as

$$P_e \approx N_{\text{fed}} Q\left(\sqrt{\frac{D_{\text{fed}}^2}{2N_0}}\right) \tag{8-3-1}$$

where N_{fed} denotes the number of signal sequences with distance D_{fed} that diverge at any state and remerge at that state after one or more transitions.

In computing the coding gain achieved by trellis-coded modulation, we usually focus on the gain achieved by increasing D_{fed} and neglect the effect of N_{fed}. However, trellis codes with a large number of states may result in a large N_{fed} that cannot be ignored in assessing the overall coding gain.

In addition to the trellis-coded PSK modulations described above, powerful trellis codes have also been developed for PAM and QAM signal constellations. Of particular practical importance is the class of trellis-coded two-dimensional rectangular signal constellations. Figure 8-3-9 illustrates these signal constellations for M-QAM where $M = 16$, 32, 64, and 128. The $M = 32$ and 128 constellations have a cross pattern and are sometimes called *cross-constellations*. The underlying rectangular grid containing the signal points in M-QAM is called a *lattice of type* Z_2 (the subscript indicates the dimensionality of the space). When set partitioning is applied to this class of signal constellations, the minimum euclidean distance between successive partitions is $d_{i+1}/d_i = \sqrt{2}$ for all i, as previously observed in Example 8-3-2.

FIGURE 8-3-9 Rectangular two-dimensional (QAM) signal constellations.

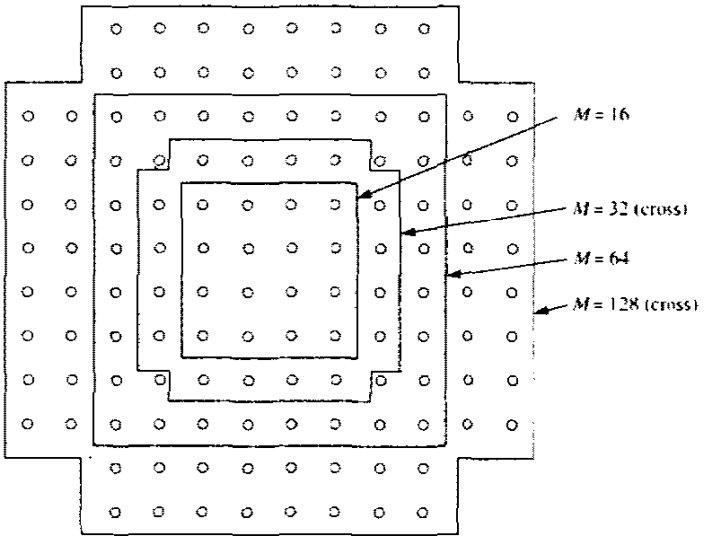

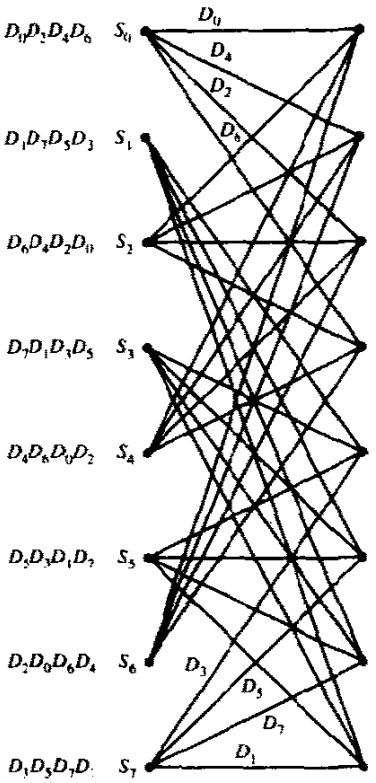

FIGURE 8-3-10 Eight-state trellis for rectangular QAM signal constellations.

Figure 8-3-10 illustrates an eight-state trellis code that can be used with any of the M-QAM rectangular signal constellations for which $M = 2^k$, where $k = 4, 5, 6, \ldots$, etc. With the eight-state trellis, we associate eight signal subsets, so that any of the M-QAM signals sets for $M \geq 16$ are suitable. For $M = 2^{m+1}$, two input bits ($k_1 = 2$) are encoded into $n = 3$ ($n = k_1 + 1$) bits that are used to select one of the eight states corresponding to the eight subsets. The additional $k_2 = m - k_1$ input bits are used to select signal points within a subset, and result in parallel transitions in the eight-state trellis. Hence, 16-QAM involves two parallel transitions in each branch of the trellis. More generally, the choice of an $M = 2^{m+1}$-point QAM signal constellation implies that the eight-state trellis contains 2^{m-2} parallel transitions in each branch.

The assignment of signal subsets to transitions is based on the same set of basic (heuristic) rules described above for the 8-PSK signal constellation. Thus, the four (branches) transitions originating from or leading to the same state are assigned either the subsets D_0, D_2, D_4, D_6 or D_1, D_3, D_5, D_7. Parallel transitions are assigned signal points contained within the corresponding subsets. This eight-state trellis code provides a coding gain of 4 dB. The euclidean distance of parallel transitions exceeds the free euclidean distance, and, hence, the code performance is not limited by parallel transitions.

Larger size trellis codes for M-QAM provide even larger coding gains. For

TABLE 8-3-1 CODING GAINS FOR TRELLIS-CODED PAM SIGNALS

Number of states	k_1	Code rate $\frac{k_1}{k_1+1}$	$m=1$ coding gain (dB) of 4-PAM versus uncoded 2-PAM	$m=2$ coding gain (dB) of 8-PAM versus uncoded 4-PAM	$m \to \infty$ asymptotic coding gain (dB)	$m \to \infty$ N_{fed}
4	1	1/2	2.55	3.31	3.52	4
8	1	1/2	3.01	3.77	3.97	4
16	1	1/2	3.42	4.18	4.39	8
32	1	1/2	4.15	4.91	5.11	12
64	1	1/2	4.47	5.23	5.44	36
128	1	1/2	5.05	5.81	6.02	66

Source: Ungerboeck (1987).

example, trellis codes with 2^ν states for an $M = 2^{m+1}$ QAM signal constellation can be constructed by convolutionally encoding k_1 input bits into $k_1 + 1$ output bits. Thus, a rate $R_c = k_1/(k_1 + 1)$ convolutional code is employed for this purpose. Usually, the choice of $k_1 = 2$ provides a significant fraction of the total coding gain that is achievable. The additional $k_2 = m - k_1$ input bits are uncoded, and are transmitted in each signal interval by selecting signal points within a subset.

Tables 8-3-1 to 8-3-3, taken from the paper by Ungerboeck (1987), provide a summary of coding gains achievable with trellis-coded modulation. Table 8-3-1 summarizes the coding gains achieved for trellis-coded (one-dimensional) PAM modulation with rate 1/2 trellis codes. Note that the coding gain with a 128-state trellis code is 5.8 dB for octal PAM, which is close to the channel cutoff rate R_0 and less than 4 dB from the channel capacity limit for error rates in the range of 10^{-6}–10^{-8}. We should also observe that the number of paths

TABLE 8-3-2 CODING GAINS FOR TRELLIS-CODED 16-PSK MODULATION

Number of states	k_1	Code rate $\frac{k_1}{k_1+1}$	$m=3$ coding gain (dB) of 16-PSK versus uncoded 8-PSK	$m \to \infty$ N_{fed}
4	1	1/2	3.54	4
8	1	1/2	4.01	4
16	1	1/2	4.44	8
32	1	1/2	5.13	8
64	1	1/2	5.33	2
128	1	1/2	5.33	2
256	2	2/3	5.51	8

Source: Ungerboeck (1987).

TABLE 8-3-3 CODING GAINS FOR TRELLIS-CODED QAM MODULATION

Number of states	k_1	Code rate $\frac{k_1}{k_1+1}$	$m=3$ gain (dB) of 16-QAM versus uncoded 8-QAM	$m=4$ gain (dB) of 32-QAM versus uncoded 16-QAM	$m=5$ gain (dB) of 64-QAM versus uncoded 32-QAM	$m=\infty$ asymptotic coding gain (dB)	N_{fed}
4	1	1/2	3.01	3.01	2.80	3.01	4
8	2	2/3	3.98	3.98	3.77	3.98	16
16	2	2/3	4.77	4.77	4.56	4.77	56
32	2	2/3	4.77	4.77	4.56	4.77	16
64	2	2/3	5.44	5.44	4.23	5.44	56
128	2	2/3	6.02	6.02	5.81	6.02	344
256	2	2/3	6.02	6.02	5.81	6.02	44

Source: Ungerboeck (1987).

N_{fed} with free euclidean distance D_{fed} becomes large with an increase in the number of states.

Table 8-3-2 lists the coding gain for trellis-coded 16-PSK. Again, we observe that the coding gain for eight or more trellis stages exceeds 4 dB, relative to uncoded 8-PSK. A simple rate 1/2 code yields 5.33 dB gain with a 128-stage trellis.

Table 8-3-3 contains the coding gains obtained with trellis-coded QAM signals. Relatively simple rate 2/3 trellis codes yield a gain of 6 dB with 128 trellis stages for $m = 3$ and 4.

The results in these tables clearly illustrate the significant coding gains that are achievable with relatively simple trellis codes. A 6 dB coding gain is close to the cutoff rate R_0 for the signal sets under consideration. Additional gains that would lead to transmission in the vicinity of the channel capacity bound are difficult to attain without a significant increase in coding/decoding complexity.

Since the channel capacity provides the ultimate limit on code performance, we should emphasize that continued partitioning of large signal sets quickly leads to signal point separation within any subset that exceeds the free euclidean distance of the code. In such cases, parallel transitions are no longer the limiting factor on D_{fed}. Usually, a partition to eight subsets is sufficient to obtain a coding gain of 5–6 dB with simple rate 1/2 or rate 2/3 trellis codes with either 64 or 128 trellis stages, as indicated in Tables 8-3-1 to 8-3-3.

Convolutional encoders for the linear trellis codes listed in Tables 8-3-1 to 8-3-3 for the M-PAM, M-PSK, and M-QAM signal constellations are given in the papers by Ungerboeck (1982, 1987). The encoders may be realized either with feedback or without feedback. For example Fig. 8-3-11 illustrates three feedback-free convolutional encoders corresponding to 4-, 8-, and 16-state trellis codes for 8-PSK and 16-QAM signal constellations. Equivalent realizations of these trellis codes based on systematic convolutional encoders with

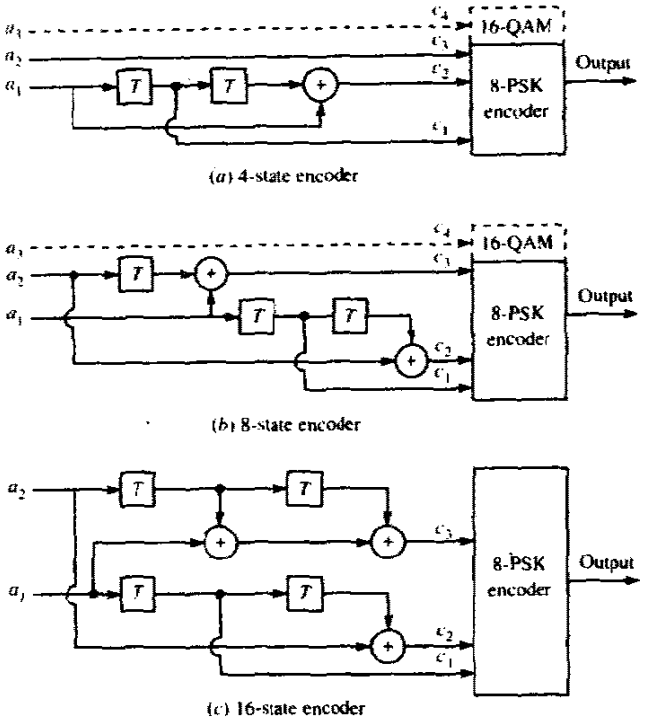

FIGURE 8-3-11 Minimal feedback-free convolutional encoders for 8-PSK and 16-QAM signals. [*From Ungerboeck (1982).* © *1982 IEEE.*]

feedback are shown in Fig. 8-3-12. Usually, the systematic convolutional encoders are preferred in practical applications.

A potential problem with linear trellis codes is that the modulated signal sets are not usually invariant to phase rotations. This poses a problem in practical applications where differential encoding is usually employed to avoid phase ambiguities when a receiver must recover the carrier phase after a temporary loss of signal. The problem of phase invariance and differential encoding/decoding was solved by Wei (1984a, b), who devised linear and nonlinear trellis codes that are rotationally invariant under either 180° or 90° phase rotations, respectively. For example, Fig. 8-3-13 illustrates a nonlinear eight-state convolutional encoder for a 32-QAM rectangular signal constellation that is invariant under 90° phase rotations. This trellis code has been adopted as an international standard for 9600 and 14,000 bits/s (high-speed) telephone line modems.

Trellis-coded modulation schemes have also been developed for multidimensional signals. In practical systems, multidimensional signals are transmitted as a sequence of either one-dimensional (PAM) or two-dimensional (QAM) signals. Trellis codes based on 4-, 8-, and 16-dimensional signal constellations have been constructed, and some of these codes have been

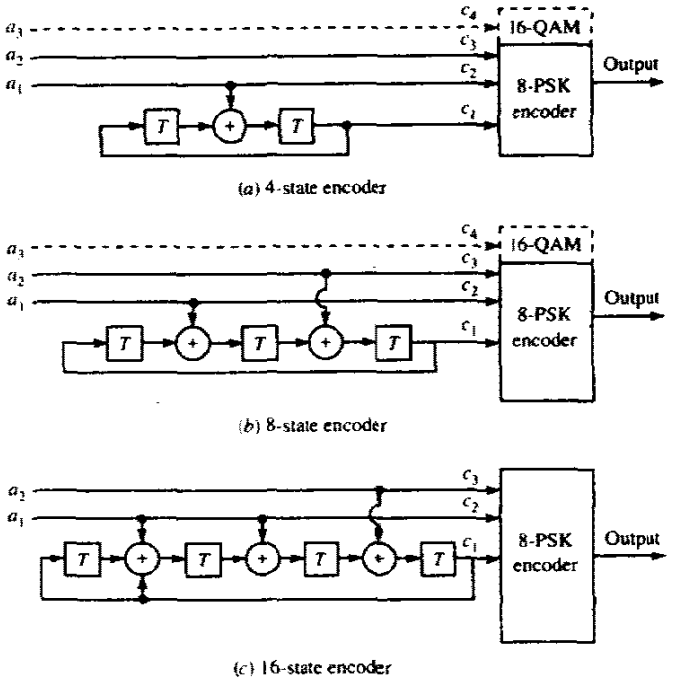

FIGURE 8-3-12 Equivalent realizations of systematic convolutional encoders with feedback for 8-PSK and 16-QAM. [*From Ungerboeck (1982).* © *1982 IEEE.*]

implemented in commercially available modems. A potential advantage of trellis-coded multidimensional signals is that we can use smaller constituent two-dimensional signal constellations that allow for a trade-off between coding gain and implementation complexity. The papers by Wei (1987), Ungerboeck (1987), Gersho and Lawrence (1984), and Forney *et al.* (1984) treat multidimensional signal constellations for trellis-coded modulation.

Finally, we should mention that a new design technique for trellis-coded modulation based on lattices and cosets of a sublattice has been described by Calderbank and Sloane (1987) and Forney (1988). This method for constructing trellis codes provides an alternative to the set partitioning method described above. However, the two methods are closely related. In this alternative method, a block of k_1 bits is fed to a convolutional encoder. Each block of k_1 input bits produces an output symbol that is a coset of the sublattice Λ', which is a subset of the chosen lattice. A second block of k_2 input bits is used to select one of the points in the coset at the output of the convolutional encoder. It is apparent that the cosets of the sublattice are akin to the subsets in set partitioning and the elements of the cosets are akin to the signal points within a subset. This new method has led to the discovery of new powerful trellis codes involving larger signal constellations, many of which are listed in the paper by Calderbank and Sloane (1987).

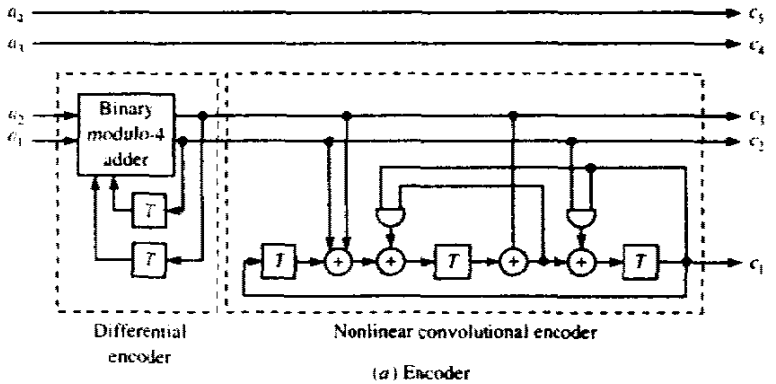

(a) Encoder

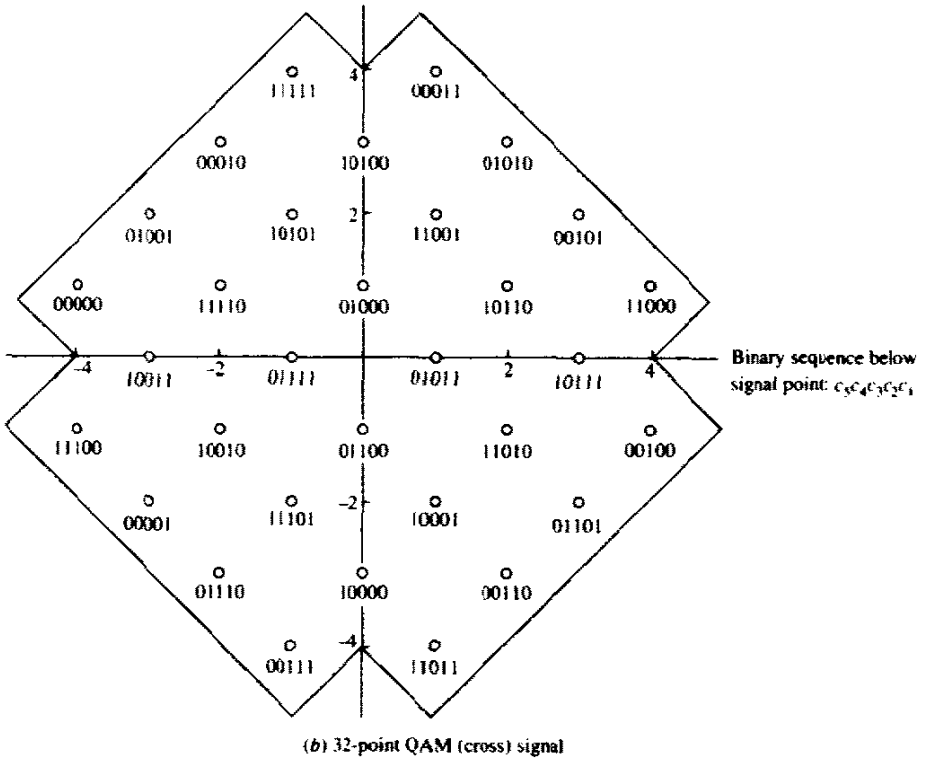

(b) 32-point QAM (cross) signal

FIGURE 8-3-13 Eight-state nonlinear convolutional encoder for 32-QAM signal set that exhibits invariance under 90° phase rotations.

8-4 BIBLIOGRAPHICAL NOTES AND REFERENCES

The pioneering work on coding and coded waveforms for digital communications was done by Shannon (1948a, b), Hamming (1950), and Golay (1949). These works were rapidly followed with papers on code performance by

Gilbert (1952), new codes by Muller (1954) and Reed (1954), and coding techniques for noisy channels by Elias (1954, 1955) and Slepian (1956).

During the period 1960–1970, there were a number of significant contributions in the development of coding theory and decoding algorithms. In particular, we cite the papers by Reed and Solomon (1960) on Reed–Solomon codes, the papers by Hocquenghem (1959) and Bose and Ray-Chaudhuri (1960a, b) on BCH codes, and the Ph.D dissertation of Forney (1966a) on concatenated codes. These works were followed by the papers of Goppa (1970, 1971) on the construction of a new class of linear cyclic codes, now called Goppa codes (see also Berlekamp, 1973), and the paper of Justesen (1972) on a constructive technique for asymptotically good codes. During this period, work on decoding algorithms was primarily focused on BCH codes. The first decoding algorithm for binary BCH codes was developed by Peterson (1960). A number of refinements and generalizations by Chien (1964), Forney (1965), Massey (1965), and Berlekamp (1968) led to the development of a computationally efficient algorithm for BCH codes, which is described in detail by Lin and Costello (1983).

In parallel with these developments on block codes are the developments in convolutional codes, which were invented by Elias (1955). The major problem in convolutional coding was decoding. Wozencraft and Reiffen (1961) described a sequential decoding algorithm for convolutional codes. This algorithm was later modified and refined by Fano (1963), and it is now called the *Fano algorithm*. Subsequently, the stack algorithm was devised by Ziganzirov (1966) and Jelinek (1969), and the Viterbi algorithm was devised by Viterbi (1967). The optimality and the relatively modest complexity for small constraint lengths have served to make the Viterbi algorithm the most popular in decoding of convolutional codes with $K \leq 10$.

One of the most important contributions in coding during the 1970s was the work of Ungerboeck and Csajka (1976) on coding for bandwidth-constrained channels. In this paper, it was demonstrated that a significant coding gain can be achieved through the introduction of redundancy in a bandwidth-constrained channel and trellis codes were described for achieving coding gains of 3–4 dB. This work has generated much interest among researchers and has led to a large number of publications over the past 10 years. A number of references can be found in the papers by Ungerboeck (1982, 1987) and Forney *et al.* (1984). Additional papers on coded modulation for bandwidth-constrained channels may also be found in the Special Issue on Voiceband Telephone Data Transmission, *IEEE Journal on Selected Areas in Communication* (September 1984). A comprehensive treatment of trellis-coded modulation is given in the book by Biglieri *et al.* (1991).

In addition to the references given above on coding, decoding, and coded signal design, we should mention the collection of papers published by the IEEE Press entitled *Key Papers in the Development of Coding Theory*, edited by Berlekamp (1974). This book contains important papers that were published in the first 25 years of coding theory. We should also cite the Special

Issue on Error-Correcting Codes, *IEEE Transactions on Communications* (October 1971).

PROBLEMS

8-1 The generator matrix for a linear binary code is

$$\mathbf{G} = \begin{bmatrix} 0 & 0 & 1 & 1 & 1 & 0 & 1 \\ 0 & 1 & 0 & 0 & 1 & 1 & 1 \\ 1 & 0 & 0 & 1 & 1 & 1 & 0 \end{bmatrix}$$

a Express **G** in systematic $[\mathbf{I} \mid \mathbf{P}]$ form.
b Determine the parity check matrix **H** for the code.
c Construct the table of syndromes for the code.
d Determine the minimum distance of the code.
e Demonstrate that the code word corresponding to the informatin sequence 101 is orthogonal to **H**.

8-2 List the code words generated by the matrices given in (8-1-35) and (8-1-37), and, thus, demonstrate that these matrices generate the same set of code words.

8-3 The weight distribution of Hamming codes is known. Expressed as a polynomial in powers of x, the weight distribution for the binary Hamming codes of block length n is

$$A(x) = \sum_{i=0}^{n} A_i x^i$$

$$= \frac{1}{n+1}\left[(1+x)^n + n(1+x)^{(n-1)/2}(1-x)^{(n+1)/2}\right]$$

where A_i is the number of code words of weight i. Use this formula to determine the weight distribution of the (7, 4) Hamming code and check your result with the list of code words given in Table 8-1-2.

8-4 The polynomial

$$g(p) = p^4 + p + 1$$

is the generator for the (15, 11) Hamming binary code.
a Determine a generator matrix **G** for this code in systematic form.
b Determine the generator polynomial for the dual code.

8-5 For the (7, 4) cyclic Hamming code with generator polynomial $g(p) = p^3 + p^2 + 1$, construct an (8, 4) extended Hamming code and list all the code words. What is $d_{\min}$ for the extended code?

8-6 An (8, 4) linear block code is constructed by shortening a (15, 11) Hamming code generated by the generator polynomial $g(p) = p^4 + p + 1$.
a Construct the code words of the (8, 4) code and list them.
b What is the minimum distance of the (8, 4) code?

8-7 The polynomial $p^{15} + 1$ when factored yields

$$p^{15} + 1 = (p^4 + p^3 + 1)(p^4 + p^3 + p^2 + p + 1)$$
$$\times (p^4 + p + 1)(p^2 + p + 1)(p + 1)$$

a Construct a systematic (15, 5) code using the generator polynomial

$$g(p) = (p^4 + p^3 + p^2 + p + 1)(p^4 + p + 1)(p^2 + p + 1)$$

b What is the minimum distance of the code?
c How many random errors per code word can be corrected?
d How many errors can be detected by this code?
e List the code words of a (15, 2) code constructed from the generator polynomial

$$g(p) = (p^{15} + 1)/(p^2 + p + 1)$$

and determine the minimum distance.

8-8 Construct the parity check matrices $\mathbf{H}_1$ and $\mathbf{H}_2$ corresponding to the generator matrices $\mathbf{G}_1$ and $\mathbf{G}_2$ given by (8-1-34) and (8-1-35), respectively.

8-9 Construct an extended (8, 4) code from the (7, 4) Hamming code by specifying the generator matrix and the parity check matrix.

8-10 A systematic (6, 3) code has the generator matrix

$$\mathbf{G} = \begin{bmatrix} 1 & 0 & 0 & 1 & 1 & 0 \\ 0 & 1 & 0 & 0 & 1 & 1 \\ 0 & 0 & 1 & 1 & 0 & 1 \end{bmatrix}$$

Construct the standard array and determine the correctable error patterns and their corresponding syndromes.

8-11 Construct the standard array for the (7, 3) code with generator matrix

$$\mathbf{G} = \begin{bmatrix} 1 & 0 & 0 & 1 & 0 & 1 & 1 \\ 0 & 1 & 0 & 1 & 1 & 1 & 0 \\ 0 & 0 & 1 & 0 & 1 & 1 & 1 \end{bmatrix}$$

and determine the correctable patterns and their corresponding syndromes.

8-12 Determine the correctable error patterns (of least weight) and their syndromes for the systematic (7, 4) cyclic Hamming code.

8-13 Prove that if the sum of two error patterns $\mathbf{e}_1$ and $\mathbf{e}_2$ is a valid code word $\mathbf{C}_j$ then each pattern has the same syndrome.

8-14 Let $g(p) = p^8 + p^6 + p^4 + p^2 + 1$ be a polynomial over the binary field.
a Find the lowest-rate cyclic code whose generator polynomial is $g(p)$. What is the rate of this code?
b Find the minimum distance of the code found in (a).
c What is the coding gain for the code found in (a).

8-15 The polynomial $g(p) = p + 1$ over the binary field is considered.
a Show that this polynomial can generate a cyclic code for any choice of n. Find the corresponding k.
b Find the systematic form of **G** and **H** for the code generated by $g(p)$.
c Can you say what type of code this generator polynomial generates?

8-16 Design a (6, 2) cyclic code by choosing the shortest possible generator polynomial.
a Determine the generator matrix **G** (in the systematic form) for this code and find all possible code words.
b How many errors can be corrected by this code?

8-17 Prove that any two n-tuples in the same row of a standard array add to produce a valid code word.

8-18 Beginning with a (15, 7) BCH code, construct a shortened (12, 4) code. Give the generator matrix for the shortened code.

8-19 In Section 8-1-2, it was indicated that when an (n, k) Hadamard code is mapped into waveforms by means of binary PSK, the corresponding $M = 2^k$ waveforms

are orthogonal. Determine the bandwidth expansion factor for the M orthogonal waveforms and compare this with the bandwidth requirements of orthogonal FSK detected coherently.

8-20 Show that the signaling waveforms generated from a maximum-length shift-register code by mapping each bit in a code word into a binary PSK signal are equicorrelated with correlation coefficient $\rho_s = -1/(M-1)$, i.e., the M waveforms form a simplex set.

8-21 Compute the error probability obtained with a (7, 4) Hamming code on an AWGN channel, both for hard-decision and soft-decision decoding. Use (8-1-50), (8-1-52), (8-1-82), (8-1-90), and (8-1-91).

8-22 Use the results in Section 2-1-6 to obtain the Chernoff bound for hard-decision decoding given by (8-1-89) and (8-1-90). Assume that the all-zero code word is transmitted and determine an upper bound on the probability that code word C_m, having weight w_m, is selected. This occurs if $\frac{1}{2}w_m$ or more bits are in error. To apply the Chernoff bound, define a sequence of w_m random variables as

$$X_i = \begin{cases} 1 & \text{with probability } p \\ -1 & \text{with probability } 1-p \end{cases}$$

where $i = 1, 2, \ldots, w_m$, and p is the probability of error. For the BSC, the $\{X_i\}$ are statistically independent.

8-23 A convolutional code is described by

$$\mathbf{g}_1 = [1 \quad 0 \quad 0], \quad \mathbf{g}_2 = [1 \quad 0 \quad 1], \quad \mathbf{g}_3 = [1 \quad 1 \quad 1]$$

a Draw the encoder corresponding to this code.
b Draw the state-transition diagram for this code.
c Draw the trellis diagram for this code.
d Find the transfer function and the free distance of this code.
e Verify whether or not this code is catastrophic.

8-24 The convolutional code of Problem 8-23 is used for transmission over a AWGN channel with hard-decision decoding. The output of the demodulator detector is (101001011110111 . . .). Using the Viterbi algorithm, find the transmitted sequence.

8-25 Repeat Problem 8-23 for a code with

$$\mathbf{g}_1 = [1 \quad 1 \quad 0], \quad \mathbf{g}_2 = [1 \quad 0 \quad 1], \quad \mathbf{g}_3 = [1 \quad 1 \quad 1]$$

8-26 The block diagram of a binary convolutional code is shown in Fig. P8-26.
a Draw the state diagram for the code.
b Find the transfer function of the code, $T(D)$.
c What is d_{free}, the minimum free distance of the code?

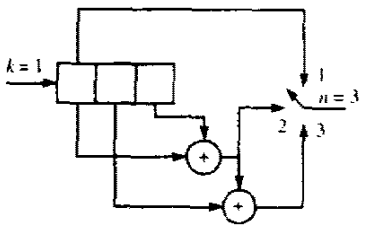

FIGURE P8-26

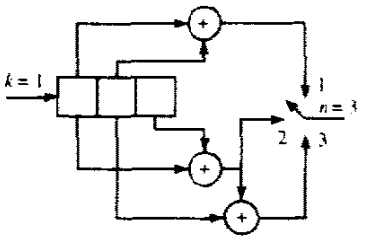

FIGURE P8-27

d Assume that a message has been encoded by this code and transmitted over a binary-symmetric channel with an error probability of $p = 10^{-5}$. If the received sequence is $\mathbf{r} = (110, 110, 110, 111, 010, 101, 101)$, using the Viterbi algorithm, find the transmitted bit sequence.

e Find an upper bound to the bit error probability of the code when the above binary-symmetric channel is employed. Make any reasonable approximation.

8-27 The block diagram of a (3, 1) convolutional code is shown in Fig. P8-27.

a Draw the state diagram of the code.

b Find the transfer function $T(D)$ of the code.

c Find the minimum free distance (d_{free}) of the code and show the corresponding path (at distance d_{free} from the all-zero code word) on the trellis.

d Assume that four information bits (x_1, x_2, x_3, x_4), followed by two zero bits, have been encoded and sent via a binary-symmetric channel with crossover probability equal to 0.1. The received sequence is (111, 111, 111, 111, 111, 111). Use the Viterbi decoding algorithm to find the most likely data sequence.

8-28 In the convolutional code generated by the encoder shown in Fig. P8-28.

a Find the transfer function of the code in the form $T(N, D)$.

b Find d_{free} of the code.

c If the code is used on a channel using hard-decision Viterbi decoding, assuming the crossover probability of the channel is $p = 10^{-6}$, use the hard-decision bound to find an upper bound on the average bit error probability of the code.

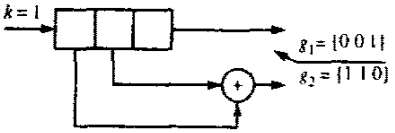

FIGURE P8-28

8-29 Figure P8-29 depicts a rate 1/2, constraint length $K = 2$, convolutional code.

a Sketch the tree diagram, the trellis diagram, and the state diagram.

b Solve for the transfer function $T(D, N, J)$ and, from this, specify the minimum free distance.

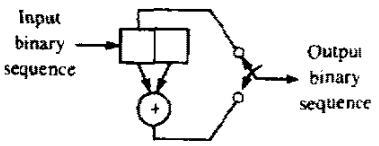

FIGURE P8-29

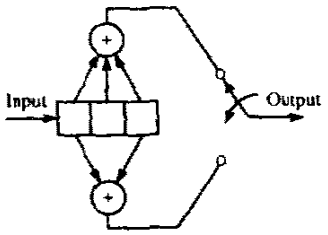

FIGURE P8-30

8-30 A rate 1/2, $K = 3$, binary convolutional encoder is shown in Fig. P8-30.
- **a** Draw the tree diagram, the trellis diagram, and the state diagram.
- **b** Determine the transfer function $T(D, N, J)$ and, from this, specify the minimum free distance.

8-31 Sketch the convolutional encoders for the following codes:
- **a** rate 1/2, $K = 5$, maximum free distance code (Table 8-2-1);
- **b** rate 1/3, $K = 5$, maximum free distance code (Table 8-2-2);
- **c** rate 2/3, $K = 2$, maximum free distance code (Table 8-2-8).

8-32 Draw the state diagram for the rate 2/3, $K = 2$, convolutional code indicated in Problem 8-31(c) and, for each transition, show the output sequence and the distance of the output sequence from the all-zero sequence.

8-33 Consider the $K = 3$, rate 1/2, convolutional code shown in Fig. P8-30. Suppose that the code is used on a binary symmetric channel and the received sequence for the first eight branches is 0001100000001001. Trace the decisions on a trellis diagram and label the survivors' Hamming distance metric at each node level. If a tie occurs in the metrics required for a decision, always choose the upper path (arbitrary choice).

8-34 Use the transfer function derived in Problem 8-30 for the $R_c = 1/2$, $K = 3$, convolutional code to compute the probability of a bit error for an AWGN channel with (a) hard-decision and (b) soft-decision decoding. Compare the performance by plotting the results of the computation on the same graph.

8-35 Use the generators given by (8-2-36) to obtain the encoder for a dual-3, rate 1/2 convolutional code. Determine the state diagram and derive the transfer function $T(D, N, J)$.

8-36 Draw the state diagram for the convolutional code generated by the encoder shown in Fig. P8-36 and, thus, determine if the code is catastrophic or noncatastrophic. Also, give an example of a rate 1/2, $K = 4$, convolutional encoder that exhibits catastrophic error propagation.

8-37 A trellis coded signal is formed as shown in Fig. P8-37 by encoding one bit by use

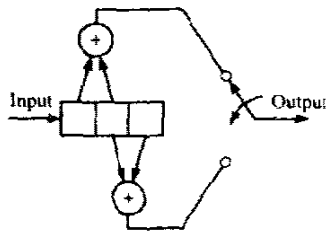

FIGURE P8-36

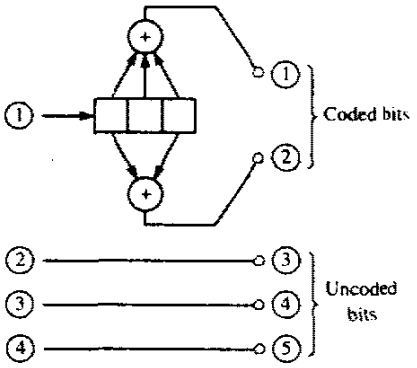

FIGURE P8-37

of a rate 1/2 convolutional code, while three additional information bits are left uncoded. Perform the set partitioning of a 32-QAM (cross) constellation and indicate the subsets in the partition. By how much is the distance between adjacent signal points increased as a result of partitioning?

8-38 Let $\mathbf{x}_1$ and $\mathbf{x}_2$ be two code words of length n with distance d and assume that these two code words are transmitted via a binary-symmetric channel with crossover probability p. Let $P(d)$ denote the error probability in transmission of these two code words.

a Show that

$$P(d) \leq \sum_{i=1}^{2^n} \sqrt{p(\mathbf{y}_i \mid \mathbf{x}_1)p(\mathbf{y}_i \mid \mathbf{x}_2)}$$

where the summation is over all binary sequences $\mathbf{y}_i$.

b From the above, conclude that

$$P(d) \leq [4p(1-p)]^{d/2}$$

9

SIGNAL DESIGN FOR BAND-LIMITED CHANNELS

In previous chapters, we considered the transmission of digital information through an additive gaussian noise channel. In effect, no bandwidth constraint was imposed on the signal design and the communication system design.

In this chapter, we consider the problem of signal design when the channel is band-limited to some specified bandwidth W Hz. Under this condition, the channel may be modeled as a linear filter having an equivalent lowpass frequency response $C(f)$ that is zero for $|f| > W$.

The first topic that is treated is the design of the signal pulse $g(t)$ in a linearly modulated signal, represented as

$$v(t) = \sum_n I_n g(t - nT)$$

that efficiently utilizes the total available channel bandwidth W. We shall see that when the channel is ideal for $|f| \leq W$, a signal pulse can be designed that allows us to transmit at symbol rates comparable to or exceeding the channel bandwidth W. On the other hand, when the channel is not ideal, signal transmission at a symbol rate equal to or exceeding W results in intersymbol interference (ISI) among a number of adjacent symbols.

The second topic that is treated in this chapter is the use of coding to shape the spectrum of the transmitted signal and, thus, to avoid the problem of ISI.

We begin our discussion with a general characterization of band-limited, linear filter channels.

9-1 CHARACTERIZATION OF BAND-LIMITED CHANNELS

Of the various channels available for digital communications, telephone channels are by far the most widely used. Such channels are characterized as

band-limited linear filters. This is certainly the proper characterization when frequency-division multiplexing (FDM) is used as a means for establishing channels in the telephone network. Recent additions to the telephone network employ pulse-code modulation (PCM) for digitizing and encoding the analog signal and time-division multiplexing (TDM) for establishing multiple channels. Nevertheless, filtering is still used on the analog signal prior to sampling and encoding. Consequently, even though the present telephone network employs a mixture of FDM and TDM for transmission, the linear filter model for telephone channels is still appropriate.

For our purposes, a band-limited channel such as a telephone channel will be characterized as a linear filter having an equivalent lowpass frequency response characteristic $C(f)$. Its equivalent lowpass impulse response is denoted by $c(t)$. Then, if a signal of the form

$$s(t) = \text{Re}\left[v(t)e^{j2\pi f_c t}\right] \tag{9-1-1}$$

is transmitted over a bandpass telephone channel, the equivalent lowpass received signal is

$$r_l(t) = \int_{-\infty}^{\infty} v(\tau)c(t-\tau)\,d\tau + z(t) \tag{9-1-2}$$

where the integral represents the convolution of $c(t)$ with $v(t)$, and $z(t)$ denotes the additive noise. Alternatively, the signal term can be represented in the frequency domain as $V(f)C(f)$, where $V(f)$ is the Fourier transform of $v(t)$.

If the channel is band-limited to W Hz then $C(f) = 0$ for $|f| > W$. As a consequence, any frequency components in $V(f)$ above $|f| = W$ will not be passed by the channel. For this reason, we limit the bandwidth of the transmitted signal to W Hz also.

Within the bandwidth of the channel, we may express the frequency response $C(f)$ as

$$C(f) = |C(f)|\,e^{j\theta(f)} \tag{9-1-3}$$

where $|C(f)|$ is the amplitude response characteristic and $\theta(f)$ is the phase response characteristic. Furthermore, the envelope delay characteristic is defined as

$$\tau(f) = -\frac{1}{2\pi}\frac{d\theta(f)}{df} \tag{9-1-4}$$

A channel is said to be *nondistorting* or *ideal* if the amplitude response $|C(f)|$ is constant for all $|f| \leq W$ and $\theta(f)$ is a linear function of frequency, i.e., $\tau(f)$ is a constant for all $|f| \leq W$. On the other hand, if $|C(f)|$ is not constant for all $|f| \leq W$, we say that the channel *distorts the transmitted signal* $V(f)$ *in amplitude*, and, if $\tau(f)$ is not constant for all $|f| \leq W$, we say that the channel *distorts the signal* $V(f)$ *in delay.*

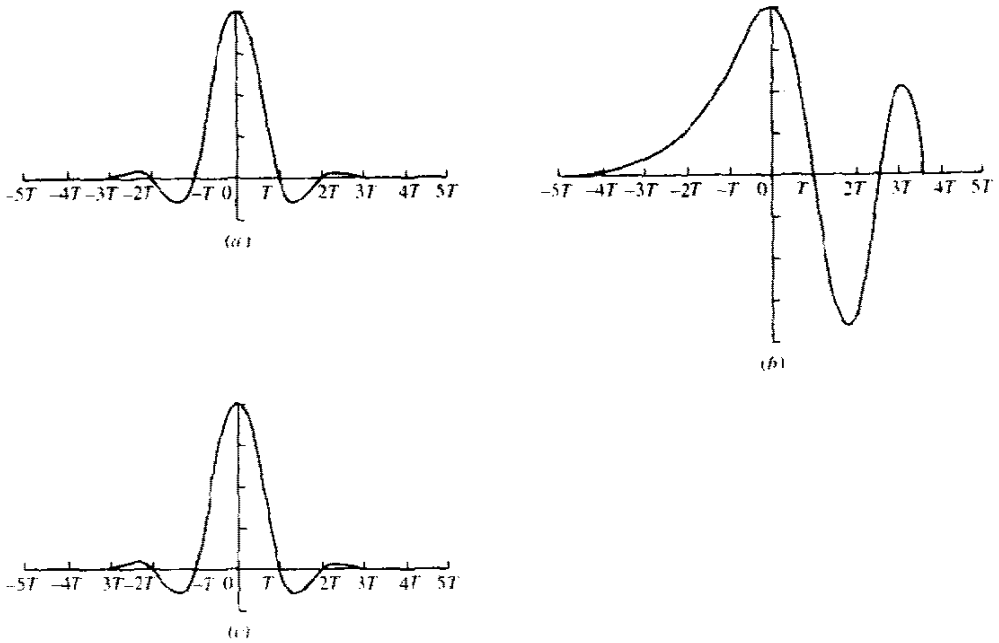

FIGURE 9-1-1 Effect of channel distortion: (*a*) channel input; (*b*) channel output; (*c*) equalizer output.

As a result of the amplitude and delay distortion caused by the nonideal channel frequency response characteristic $C(f)$, a succession of pulses transmitted through the channel at rates comparable to the bandwidth W are smeared to the point that they are no longer distinguishable as well-defined pulses at the receiving terminal. Instead, they overlap and, thus, we have intersymbol interference. As an example of the effect of delay distortion on a transmitted pulse, Fig. 9-1-1(*a*) illustrates a band-limited pulse having zeros periodically spaced in time at points labeled $\pm T$, $\pm 2T$, etc. If information is conveyed by the pulse amplitude, as in PAM, for example, then one can transmit a sequence of pulses, each of which has a peak at the periodic zeros of the other pulses. However, transmission of the pulse through a channel modeled as having a linear envelope delay characteristic $\tau(f)$ [quadratic phase $\theta(f)$] results in the received pulse shown in Fig. 9-1-1(*b*) having zero-crossings that are no longer periodically spaced. Consequently, a sequence of successive pulses would be smeared into one another and the peaks of the pulses would no longer be distinguishable. Thus, the channel delay distortion results in intersymbol interference. As will be discussed in Chapter 10, it is possible to compensate for the nonideal frequency response characteristic of the channel by use of a filter or equalizer at the demodulator. Figure 9-1-1(*c*) illustrates the output of a linear equalizer that compensates for the linear distortion in the channel.

The extent of the intersymbol interference on a telephone channel can be

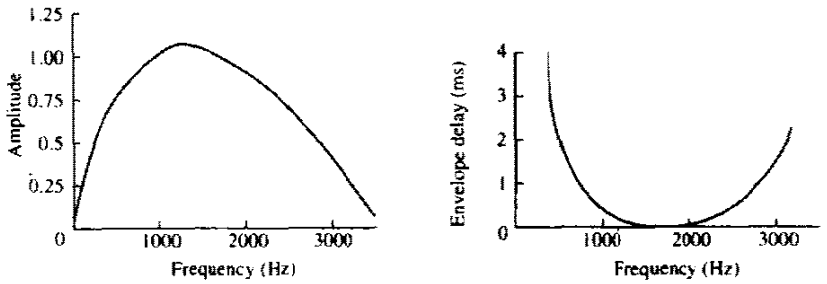

FIGURE 9-1-2 Average amplitude and delay characteristics of medium-range telephone channel.

appreciated by observing a frequency response characteristic of the channel. Figure 9-1-2 illustrates the measured average amplitude and delay as functions of frequency for a medium-range (180–725 mi) telephone channel of the switched telecommunications network as given by Duffy and Tratcher (1971). We observe that the usable band of the channel extends from about 300 Hz to about 3000 Hz. The corresponding impulse response of this average channel is shown in Fig. 9-1-3. Its duration is about 10 ms. In comparison, the transmitted symbol rates on such a channel may be of the order of 2500 pulses or symbols per second. Hence, intersymbol interference might extend over 20–30 symbols.

In addition to linear distortion, signals transmitted through telephone channels are subject to other impairments, specifically nonlinear distortion, frequency offset, phase jitter, impulse noise and thermal noise.

Nonlinear distortion in telephone channels arises from nonlinearities in

FIGURE 9-1-3 Impulse response of average channel with amplitude and delay shown in Fig. 9-1-2.

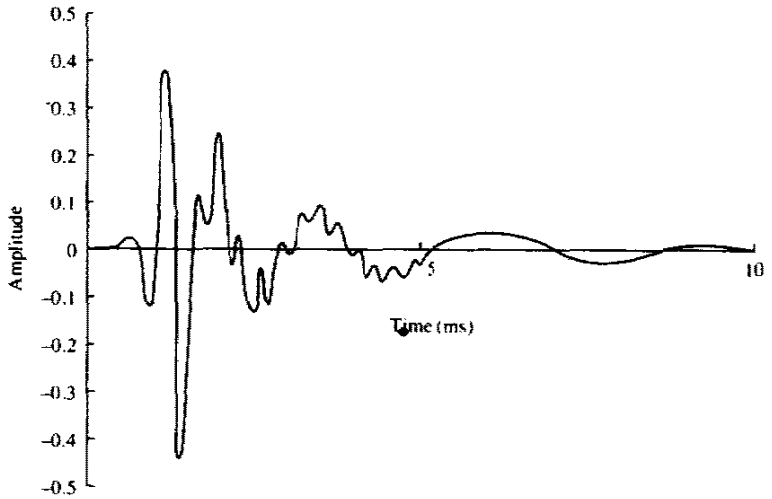

amplifiers and compandors used in the telephone system. This type of distortion is usually small and it is very difficult to correct.

A small *frequency offset*, usually less than 5 Hz, results from the use of carrier equipment in the telephone channel. Such an offset cannot be tolerated in high-speed digital transmission systems that use synchronous phase-coherent demodulation. The offset is usually compensated for by the carrier recovery loop in the demodulator.

Phase jitter is basically a low-index frequency modulation of the transmitted signal with the low frequency harmonics of the power line frequency (50–60 Hz). Phase jitter poses a serious problem in digital transmission of high rates. However, it can be tracked and compensated for, to some extent, at the demodulator.

Impulse noise is an additive disturbance. It arises primarily from the switching equipment in the telephone system. *Thermal* (gaussian) *noise* is also present at levels of 20–30 dB below the signal.

The degree to which one must be concerned with these channel impairments depends on the transmission rate over the channel and the modulation technique. For rates below 1800 bits/s ($R/W < 1$), one can choose a modulation technique, e.g., FSK, that is relatively insensitive to the amount of distortion encountered on typical telephone channels from all the sources listed above. For rates between 1800 and 2400 bits/s ($R/W \approx 1$), a more bandwidth-efficient modulation technique such as four-phase PSK is usually employed. At these rates, some form of compromise equalization is often employed to compensate for the average amplitude and delay distortion in the channel. In addition, the carrier recovery method is designed to compensate for the frequency offset. The other channel impairments are not that serious in their effects on the error rate performance at these rates. At transmission rates above 2400 bits/s ($R/W > 1$), bandwidth-efficient coded modulation techniques such as trellis-coded QAM, PAM, and PSK are employed. For such rates, special attention must be paid to linear distortion, frequency offset, and phase jitter. Linear distortion is usually compensated for by means of an adaptive equalizer. Phase jitter is handled by a combination of signal design and some type of phase compensation at the demodulator. At rates above 9600 bits/s, special attention must be paid not only to linear distortion, phase jitter, and frequency offset, but also to the other channel impairments mentioned above.

Unfortunately, a channel model that encompasses all the impairments listed above becomes difficult to analyze. For mathematical tractability the channel model that is adopted in this and the next two chapters is a linear filter that introduces amplitude and delay distortion and adds gaussian noise.

Besides the telephone channels, there are other physical channels that exhibit some form of time dispersion, and thus, introduce intersymbol interference. Radio channels such as shortwave ionospheric propagation (HF) and tropospheric scatter are two examples of time-dispersive channels. In these channels, time dispersion and, hence, intersymbol interference is the result of multiple propagation paths with different path delays. The number of paths

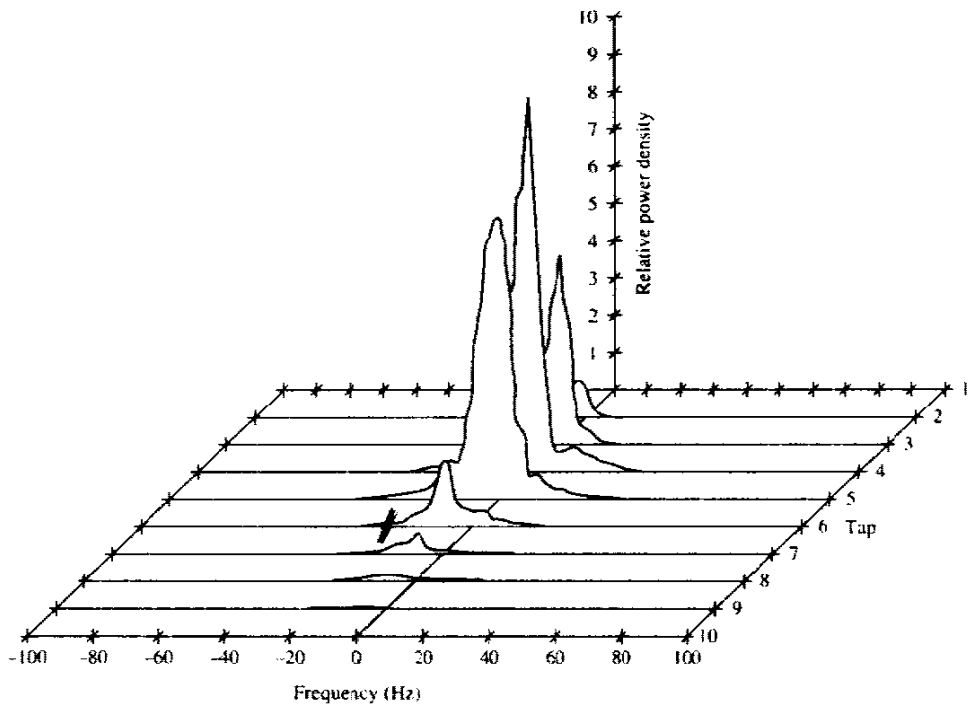

FIGURE 9-1-4 Scattering function of a medium-range tropospheric scatter channel.

and the relative time delays among the paths vary with time, and, for this reason, these radio channels are usually called *time-variant multipath channels*. The time-variant multipath conditions give rise to a wide variety of frequency response characteristics. Consequently the frequency response characterization that is used for telephone channels is inappropriate for time-variant multipath channels. Instead, these radio channels are characterized statistically, as explained in more detail in Chapter 14, in terms of the scattering function, which, in brief, is a two-dimensional representation of the average received signal power as a function of relative time delay and Doppler frequency.

For illustrative purposes, a scattering function measured on a medium-range (150 mi) trophospheric scatter channel is shown in Fig. 9-1-4. The total time duration (multipath spread) of the channel response is approximately 0.7 μs on the average, and the spread between "half-power points" in Doppler frequency is a little less than 1 Hz on the strongest path and somewhat larger on the other paths. Typically, if one is transmitting at a rate of 10^7 symbols/s over such a channel, the multipath spread of 0.7 μs will result in intersymbol interference that spans about seven symbols.

In this chapter, we deal exclusively with the linear time-invariant filter model for a band-limited channel. The adaptive equalization techniques presented in Chapters 10 and 11 for combating intersymbol interference are also applicable to time-invariant multipath channels, under the condition that

the time variations in the channel are relatively slow in comparison to the total channel bandwidth or, equivalently, to the symbol transmission rate over the channel.

9-2 SIGNAL DESIGN FOR BAND-LIMITED CHANNELS

It was shown in Chapter 4 that the equivalent lowpass transmitted signal for several different types of digital modulation techniques has the common form

$$v(t) = \sum_{n=0}^{\infty} I_n g(t - nT) \tag{9-2-1}$$

where $\{I_n\}$ represents the discrete information-bearing sequence of symbols and $g(t)$ is a pulse that, for the purposes of this discussion, is assumed to have a band-limited frequency response characteristic $G(f)$, i.e., $G(f) = 0$ for $|f| > W$. This signal is transmitted over a channel having a frequency response $C(f)$, also limited to $|f| \leq W$. Consequently, the received signal can be represented as

$$r(t) = \sum_{n=0}^{\infty} I_n h(t - nT) + z(t) \tag{9-2-2}$$

where

$$h(t) = \int_{-\infty}^{\infty} g(\tau)c(t - \tau)\, d\tau \tag{9-2-3}$$

and $z(t)$ represents the additive white Gaussian noise.

Let us suppose that the received signal is passed first through a filter and then sampled at a rate $1/T$ samples/s. We shall show in a subsequent section that the optimum filter from the point of view of signal detection is one matched to the received pulse. That is, the frequency response of the receiving filter is $H^*(f)$. We denote the output of the receiving filter as

$$y(t) = \sum_{n=0}^{\infty} I_n x(t - nT) + v(t) \tag{9-2-4}$$

where $x(t)$ is the pulse representing the response of the receiving filter to the input pulse $h(t)$ and $v(t)$ is the response of the receiving filter to the noise $z(t)$.

Now, if $y(t)$ is sampled at times $t = kT + \tau_0$, $k = 0, 1, \ldots$, we have

$$y(kT + \tau_0) \equiv y_k = \sum_{n=0}^{\infty} I_n x(kT - nT + \tau_0) + v(kT + \tau_0) \tag{9-2-5}$$

or, equivalently,

$$y_k = \sum_{n=0}^{\infty} I_n x_{k-n} + v_k, \qquad k = 0, 1, \ldots \tag{9-2-6}$$

where τ_0 is the transmission delay through the channel. The sample values can be expressed as

$$y_k = x_0\left(I_k + \frac{1}{x_0}\sum_{\substack{n=0\\ n\neq k}}^{\infty} I_n x_{k-n}\right) + v_k, \qquad k = 0, 1, \ldots \tag{9-2-7}$$

We regard x_0 as an arbitrary scale factor, which we arbitrarily set equal to unity for convenience. Then

$$y_k = I_k + \sum_{\substack{n=0\\ n\neq k}}^{\infty} I_n x_{k-n} + v_k \tag{9-2-8}$$

The term I_k represents the desired information symbol at the k th sampling instant, the term

$$\sum_{\substack{n=0\\ n\neq k}}^{\infty} I_n x_{k-n}$$

represents the intersymbol interference (ISI), and v_k is the additive gaussian noise variable at the kth sampling instant.

The amount of intersymbol interference and noise in a digital communications system can be viewed on an oscilloscope. For PAM signals, we can display the received signal $y(t)$ on the vertical input with the horizontal sweep rate set at $1/T$. The resulting oscilloscope display is called an *eye pattern* because of its resemblance to the human eye. For example, Fig. 9-2-1 illustrates the eye patterns for binary and four-level PAM modulation. The effect of ISI is to cause the eye to close, thereby reducing the margin for additive noise to cause errors. Figure 9-2-2 graphically illustrates the effect of intersymbol interference in reducing the opening of a binary eye. Note that intersymbol interference distorts the position of the zero-crossings and causes

FIGURE 9-2-1 Examples of eye patterns for binary and quaternary amplitude shift keying (or PAM).

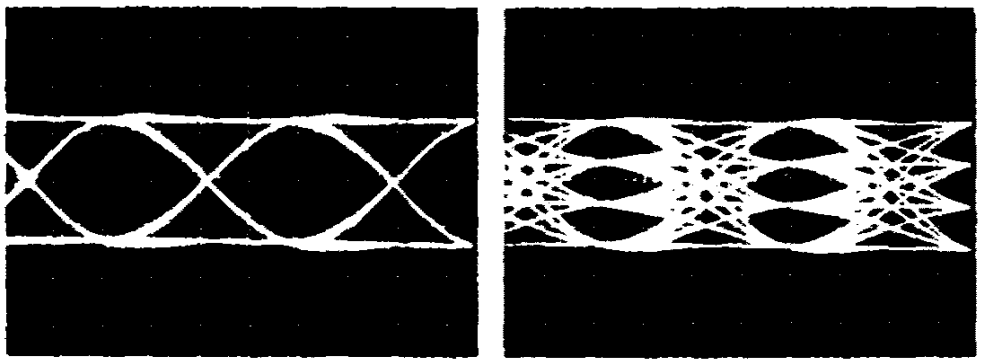

BINARY QUATERNARY

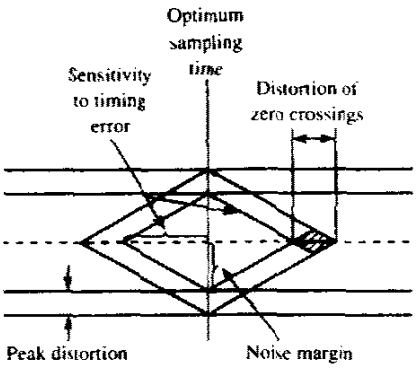

FIGURE 9-2-2 Effect of intersymbol interference on eye opening.

a reduction in the eye opening. Thus, it causes the system to be more sensitive to a synchronization error.

For PSK and QAM it is customary to display the "eye pattern" as a two-dimensional scatter diagram illustrating the sampled values $\{y_k\}$ that represent the decision variables at the sampling instants. Figure 9-2-3 illustrates such an eye pattern for an 8-PSK signal. In the absence of intersymbol interference and noise, the superimposed signals at the sampling instants would result in eight distinct points corresponding to the eight transmitted signal phases. Intersymbol interference and noise result in a deviation of the received samples $\{y_k\}$ from the desired 8-PSK signal. The larger the intersymbol interference and noise, the larger the scattering of the received signal samples relative to the transmitted signal points.

Below, we consider the problem of signal design under the condition that there is no intersymbol interference at the sampling instants.

9-2-1 DESIGN OF BAND-LIMITED SIGNALS FOR NO INTERSYMBOL INTERFERENCE—THE NYQUIST CRITERION

For the discussion in this section and in Section 9-2-2, we assume that the band-limited channel has ideal frequency response characteristics, i.e., $C(f) = 1$

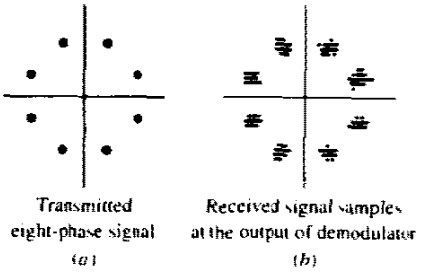

FIGURE 9-2-3 Two-dimensional digital "eye patterns."

for $|f| \leq W$. Then the pulse $x(t)$ has a spectral characteristic $X(f) = |G(f)|^2$, where

$$x(t) = \int_{-W}^{W} X(f) e^{j2\pi ft}\, df \tag{9-2-9}$$

We are interested in determining the spectral properties of the pulse $x(t)$ and, hence, the transmitted pulse $g(t)$, that results in no intersymbol interference. Since

$$y_k = I_k + \sum_{\substack{n=0 \\ n \neq k}}^{\infty} I_n x_{k-n} + v_k \tag{9-2-10}$$

the condition for no intersymbol interference is

$$x(t = kT) \equiv x_k = \begin{cases} 1 & (k = 0) \\ 0 & (k \neq 0) \end{cases} \tag{9-2-11}$$

Below, we derive the necessary and sufficient condition on $X(f)$ in order for $x(t)$ to satisfy the above relation. This condition is known as the *Nyquist pulse-shaping criterion* or *Nyquist condition for zero ISI* and is stated in the following theorem.

Theorem (Nyquist)

The necessary and sufficient condition for $x(t)$ to satisfy

$$x(nT) = \begin{cases} 1 & (n = 0) \\ 0 & (n \neq 0) \end{cases} \tag{9-2-12}$$

is that its Fourier transform $X(f)$ satisfy

$$\sum_{m=-\infty}^{\infty} X(f + m/T) = T \tag{9-2-13}$$

Proof

In general, $x(t)$ is the inverse Fourier transform of $X(f)$. Hence,

$$x(t) = \int_{-\infty}^{\infty} X(f) e^{j2\pi ft}\, df \tag{9-2-14}$$

At the sampling instants $t = nT$, this relation becomes

$$x(nT) = \int_{-\infty}^{\infty} X(f) e^{j2\pi fnT}\, df \tag{9-2-15}$$

Let us break up the integral in (9-2-15) into integrals covering the finite range of $1/T$. Thus, we obtain

$$\begin{aligned} x(nT) &= \sum_{m=-\infty}^{\infty} \int_{(2m-1)/2T}^{(2m+1)/2T} X(f)e^{j2\pi fnT}\,df \\ &= \sum_{m=-\infty}^{\infty} \int_{-1/2T}^{1/2T} X(f+m/T)e^{j2\pi fnT}\,dt \\ &= \int_{-1/2T}^{1/2T} \left[\sum_{m=-\infty}^{\infty} X(f+m/T)\right] e^{j2\pi fnT}\,df \\ &= \int_{-1/2T}^{1/2T} B(f)e^{j2\pi fnT}\,df \end{aligned} \tag{9-2-16}$$

where we have defined $B(f)$ as

$$B(f) = \sum_{m=-\infty}^{\infty} X(f+m/T) \tag{9-2-17}$$

Obviously $B(f)$ is a periodic function with period $1/T$, and, therefore, it can be expanded in terms of its Fourier series coefficients $\{b_n\}$ as

$$B(f) = \sum_{n=-\infty}^{\infty} b_n e^{j2\pi nfT} \tag{9-2-18}$$

where

$$b_n = T\int_{-1/2T}^{1/2T} B(f)e^{-j2\pi nfT}\,df \tag{9-2-19}$$

Comparing (9-2-19) and (9-2-16), we obtain

$$b_n = Tx(-nT) \tag{9-2-20}$$

Therefore, the necessary and sufficient condition for (9-2-10) to be satisfied is that

$$b_n = \begin{cases} T & (n=0) \\ 0 & (n\neq 0) \end{cases} \tag{9-2-21}$$

which, when substituted into (9-2-18), yields

$$B(f) = T \tag{9-2-22}$$

or, equivalently,

$$\sum_{m=-\infty}^{\infty} X(f+m/T) = T \tag{9-2-23}$$

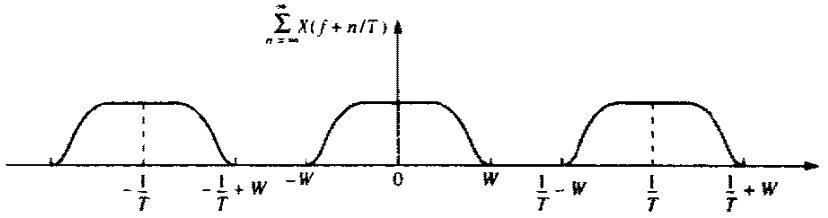

FIGURE 9-2-4 Plot of $B(f)$ for the case $T < 1/2W$.

This concludes the proof of the theorem.

Now suppose that the channel has a bandwidth of W. Then $C(f) \equiv 0$ for $|f| > W$ and, consequently, $X(f) = 0$ for $|f| > W$. We distinguish three cases.

1 When $T < 1/2W$, or, equivalently, $1/T > 2W$, since $B(f) = \sum_{n=-\infty}^{+\infty} X(f + n/T)$ consists of nonoverlapping replicas of $X(f)$, separated by $1/T$ as shown in Fig. 9-2-4, there is no choice for $X(f)$ to ensure $B(f) \equiv T$ in this case and there is no way that we can design a system with no ISI.

2 When $T = 1/2W$, or, equivalently, $1/T = 2W$ (the Nyquist rate), the replications of $X(f)$, separated by $1/T$, are as shown in Fig. 9-2-5. It is clear that in this case there exists only one $X(f)$ that results in $B(f) = T$, namely,

$$X(f) = \begin{cases} T & (|f| < W) \\ 0 & (\text{otherwise}) \end{cases} \tag{9-2-24}$$

which corresponds to the pulse

$$x(t) = \frac{\sin(\pi t/T)}{\pi t/T} \equiv \operatorname{sinc}\left(\frac{\pi t}{T}\right) \tag{9-2-25}$$

This means that the smallest value of T for which transmission with zero ISI is possible is $T = 1/2W$, and for this value, $x(t)$ has to be a sinc function. The difficulty with this choice of $x(t)$ is that it is noncausal and therefore nonrealizable. To make it realizable, usually a delayed version of it, i.e., $\operatorname{sinc}[\pi(t - t_0)/T]$ is used and t_0 is chosen such that for $t < 0$, we have $\operatorname{sinc}[\pi(t - t_0)/T] \approx 0$. Of course, with this choice of $x(t)$, the sampling time

FIGURE 9-2-5 Plot of $B(f)$ for the case $T = 1/2W$.

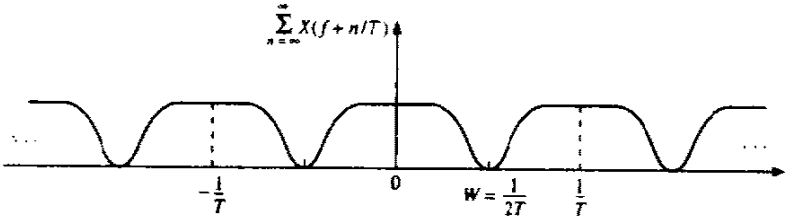

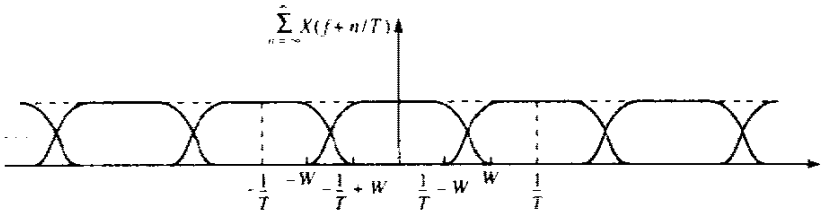

FIGURE 9-2-6 Plot of $B(f)$ for the case $T > 1/2W$.

must also be shifted to $mT + t_0$. A second difficulty with this pulse shape is that its rate of convergence to zero is slow. The tails of $x(t)$ decay as $1/t$; consequently, a small mistiming error in sampling the output of the matched filter at the demodulator results in an infinite series of ISI components. Such a series is not absolutely summable because of the $1/t$ rate of decay of the pulse, and, hence, the sum of the resulting ISI does not converge.

3 When $T > 1/2W$, $B(f)$ consists of overlapping replications of $X(f)$ separated by $1/T$, as shown in Fig. 9-2-6. In this case, there exist numerous choices for $X(f)$ such that $B(f) \equiv T$.

A particular pulse spectrum, for the $T > 1/2W$ case, that has desirable spectral properties and has been widely used in practice is the raised cosine spectrum. The raised cosine frequency characteristic is given as (see Problem 9-11)

$$X_{rc}(f) = \begin{cases} T & \left(0 \le |f| \le \dfrac{1-\beta}{2T}\right) \\ \dfrac{T}{2}\left\{1 + \cos\left[\dfrac{\pi T}{\beta}\left(|f| - \dfrac{1-\beta}{2T}\right)\right]\right\} & \left(\dfrac{1-\beta}{2T} \le |f| \le \dfrac{1+\beta}{2T}\right) \\ 0 & \left(|f| > \dfrac{1+\beta}{2T}\right) \end{cases} \tag{9-2-26}$$

where β is called the *rolloff factor*, and takes values in the range $0 \le \beta \le 1$. The bandwidth occupied by the signal beyond the Nyquist frequency $1/2T$ is called the *excess bandwidth* and is usually expressed as a percentage of the Nyquist frequency. For example, when $\beta = \frac{1}{2}$, the excess bandwidth is 50%, and when $\beta = 1$, the excess bandwidth is 100%. The pulse $x(t)$, having the raised cosine spectrum, is

$$\begin{aligned} x(t) &= \frac{\sin(\pi t/T)}{\pi t/T}\,\frac{\cos(\pi\beta t/T)}{1 - 4\beta^2 t^2/T^2} \\ &= \operatorname{sinc}(\pi t/T)\,\frac{\cos(\pi\beta t/T)}{1 - 4\beta^2 t^2/T^2} \end{aligned} \tag{9-2-27}$$

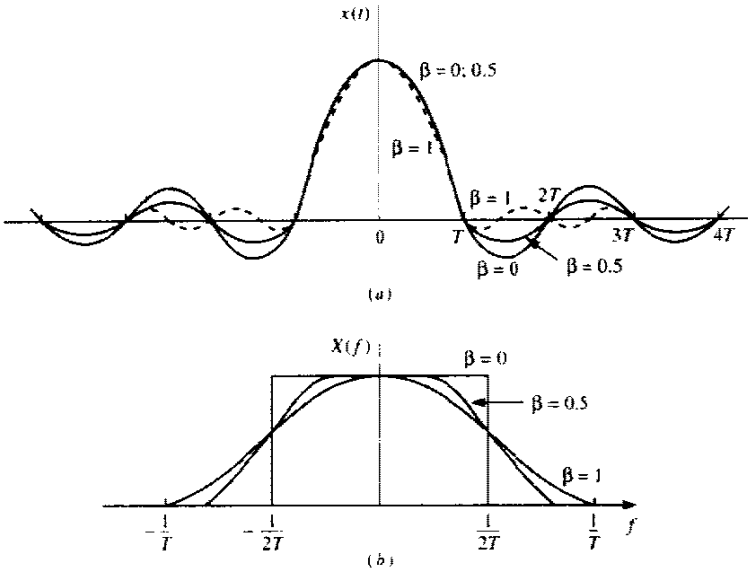

FIGURE 9-2-7 Pulses having a raised cosine spectrum.

Note that $x(t)$ is normalized so that $x(0) = 1$. Figure 9-2-7 illustrates the raised cosine spectral characteristics and the corresponding pulses for $\beta = 0$, $\frac{1}{2}$ and 1. Note that for $\beta = 0$, the pulse reduces to $x(t) = \text{sinc}(\pi t/T)$, and the symbol rate $1/T = 2W$. When $\beta = 1$, the symbol rate is $1/T = W$. In general, the tails of $x(t)$ decay as $1/t^3$ for $\beta > 0$. Consequently, a mistiming error in sampling leads to a series of ISI components that converges to a finite value.

Due to the smooth characteristics of the raised cosine spectrum, it is possible to design practical filters for the transmitter and the receiver that approximate the overall desired frequency response. In the special case where the channel is ideal, i.e., $C(f) = 1$, $|f| \leq W$, we have

$$X_{rc}(f) = G_T(f)G_R(f), \tag{9-2-28}$$

where $G_T(f)$ and $G_R(f)$ are the frequency responses of the two filters. In this case, if the receiver filter is matched to the transmitter filter, we have $X_{rc}(f) = G_T(f)G_R(f) = |G_T(f)|^2$. Ideally,

$$G_T(f) = \sqrt{|X_{rc}(f)|}\, e^{-j2\pi f t_0} \tag{9-2-29}$$

and $G_R(f) = G_T^*(f)$, where t_0 is some nominal delay that is required to ensure physical realizability of the filter. Thus, the overall raised cosine spectral characteristic is split evenly between the transmitting filter and the receiving filter. Note also that an additional delay is necessary to ensure the physical realizability of the receiving filter.

9-2-2 Design of Band-Limited Signals with Controlled ISI—Partial-Response Signals

As we have observed from our discussion of signal design for zero ISI, it is necessary to reduce the symbol rate $1/T$ below the Nyquist rate of $2W$ symbols/s to realize practical transmitting and receiving filters. On the other hand, suppose we choose to relax the condition of zero ISI and, thus, achieve a symbol transmission rate of $2W$ symbols/s. By allowing for a controlled amount of ISI, we can achieve this symbol rate.

We have already seen that the condition for zero ISI is $x(nT) = 0$ for $n \neq 0$. However, suppose that we design the band-limited signal to have controlled ISI at one time instant. This means that we allow one additional nonzero value in the samples $\{x(nT)\}$. The ISI that we introduce is deterministic or "controlled" and, hence, it can be taken into account at the receiver, as discussed below.

One special case that leads to (approximately), physically realizable transmitting and receiving filters is specified by the samples†

$$x(nT) = \begin{cases} 1 & (n = 0, 1) \\ 0 & (\text{otherwise}) \end{cases} \tag{9-2-30}$$

Now, using (9-2-20), we obtain

$$b_n = \begin{cases} T & (n = 0, -1) \\ 0 & (\text{otherwise}) \end{cases} \tag{9-2-31}$$

which, when substituted into (9-2-18), yields

$$B(f) = T + Te^{-j2\pi fT} \tag{9-2-32}$$

As in the preceding section, it is impossible to satisfy the above equation for $T < 1/2W$. However, for $T = 1/2W$, we obtain

$$\begin{aligned} X(f) &= \begin{cases} \dfrac{1}{2W}(1 + e^{-j\pi f/W}) & (|f| < W) \\ 0 & (\text{otherwise}) \end{cases} \\ &= \begin{cases} \dfrac{1}{W} e^{-j\pi f/2W} \cos \dfrac{\pi f}{2W} & (|f| < W) \\ 0 & (\text{otherwise}) \end{cases} \end{aligned} \tag{9-2-33}$$

Therefore, $x(t)$ is given by

$$x(t) = \text{sinc}\,(2\pi Wt) + \text{sinc}\,[2\pi(Wt - \tfrac{1}{2})] \tag{9-2-34}$$

This pulse is called a *duobinary signal pulse*. It is illustrated along with its

†It is convenient to deal with samples of $x(t)$ that are normalized to unity for $n = 0, 1$.

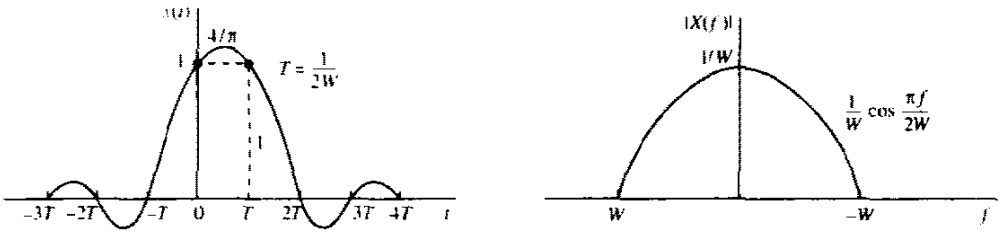

FIGURE 9-2-8 Time domain and frequency domain characteristics of a duobinary signal.

magnitude spectrum in Fig. 9-2-8. Note that the spectrum decays to zero smoothly, which means that physically realizable filters can be designed that approximate this spectrum very closely. Thus, a symbol rate of $2W$ is achieved.

Another special case that leads to (approximately) physically realizable transmitting and receiving filters is specified by the samples

$$x\left(\frac{n}{2W}\right) = x(nT) = \begin{cases} 1 & (n = -1) \\ -1 & (n = 1) \\ 0 & (\text{otherwise}) \end{cases} \tag{9-2-35}$$

The corresponding pulse $x(t)$ is given as

$$x(t) = \text{sinc}\left[\frac{\pi(t+T)}{T}\right] - \text{sinc}\left[\frac{\pi(t-T)}{T}\right] \tag{9-2-36}$$

and its spectrum is

$$X(f) = \begin{cases} \dfrac{1}{2W}(e^{j\pi f/W} - e^{-j\pi f/W}) = \dfrac{j}{W}\sin\dfrac{\pi f}{W} & |f| \leq W \\ 0 & |f| > W \end{cases} \tag{9-2-37}$$

This pulse and its magnitude spectrum are illustrated in Fig. 9-2-9. It is called a *modified duobinary signal pulse*. It is interesting to note that the spectrum of

FIGURE 9-2-9 Time domain and frequency domain characteristics of a modified duobinary signal.

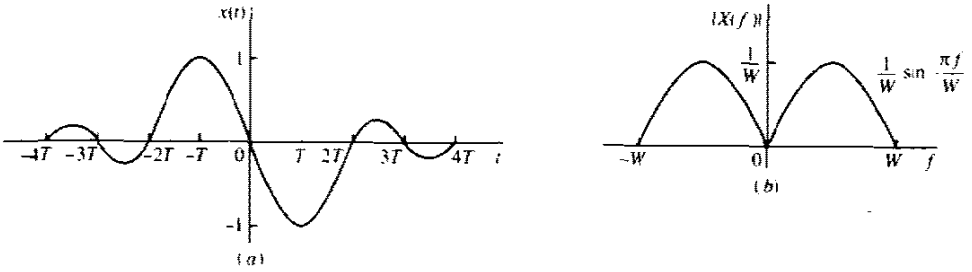

this signal has a zero at $f = 0$, making it suitable for transmission over a channel that does not pass d.c.

One can obtain other interesting and physically realizable filter characteristics, as shown by Kretzmer (1966) and Lucky *et al.* (1968), by selecting different values for the samples $\{x(n/2W)\}$ and more than two nonzero samples. However, as we select more nonzero samples, the problem of unraveling the controlled ISI becomes more cumbersome and impractical.

In general, the class of bandlimited signals pulses that have the form

$$x(t) = \sum_{n=-\infty}^{\infty} x\left(\frac{n}{2W}\right) \operatorname{sinc}\left[2\pi W\left(t - \frac{n}{2W}\right)\right] \tag{9-2-38}$$

and their corresponding spectra

$$X(f) = \begin{cases} \dfrac{1}{2W} \displaystyle\sum_{n=-\infty}^{\infty} x\left(\frac{n}{2W}\right) e^{-jn\pi f/W} & (|f| \leq W) \\ 0 & (|f| \leq W) \end{cases} \tag{9-2-39}$$

are called *partial-response signals* when controlled ISI is purposely introduced by selecting two or more nonzero samples from the set $\{x(n/2W)\}$. The resulting signal pulses allow us to transmit information symbols at the Nyquist rate of $2W$ symbols/s. The detection of the received symbols in the presence of controlled ISI is described below.

Alternative Characterization of Partial-Response Signals We conclude this subsection by presenting another interpretation of a partial-response signal. Suppose that the partial-response signal is generated, as shown in Fig. 9-2-10, by passing the discrete-time sequence $\{I_n\}$ through a discrete-time filter

FIGURE 9-2-10 An alternative method for generating a partial-response signal.

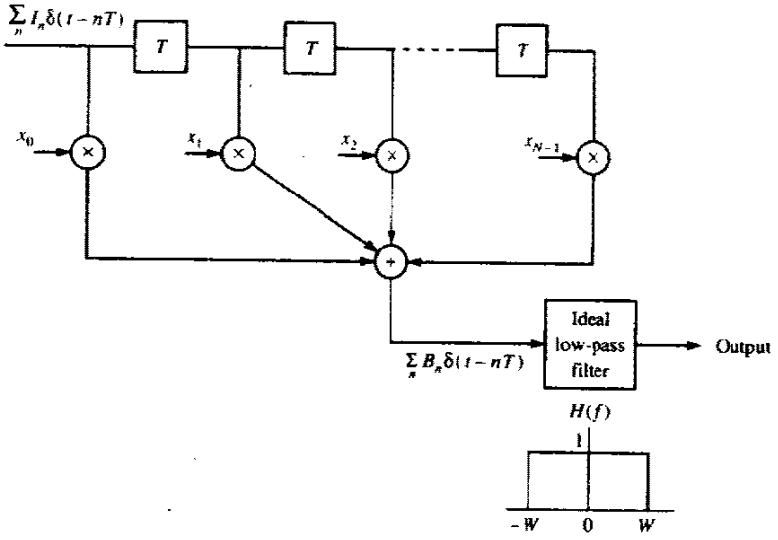

with coefficients $x_n \equiv x(n/2W)$, $n = 0, 1, \ldots, N-1$, and using the output sequence $\{B_n\}$ from this filter to excite periodically with an input $B_n\delta(t - nT)$ an analog filter having an impulse response $\text{sinc}(2\pi Wt)$. The resulting output signal is identical to the partial-response signal given by (9-2-38).

Since

$$B_n = \sum_{k=0}^{N-1} x_k I_{n-k} \tag{9-2-40}$$

the sequence of symbols $\{B_n\}$ is correlated as a consequence of the filtering performed on the sequence $\{I_n\}$. In fact, the autocorrelation function of the sequence $\{B_n\}$ is

$$\begin{aligned}\phi(m) &= E(B_n B_{n+m}) \\ &= \sum_{k=0}^{N-1}\sum_{l=0}^{N-1} x_k x_l E(I_{n-k} I_{n+m-l})\end{aligned} \tag{9-2-41}$$

When the input sequence is zero-mean and white,

$$E(I_{n-k} I_{n+m-l}) = \delta_{m+k-l} \tag{9-2-42}$$

where we have used the normalization $E(I_n^2) = 1$. Substitution of (9-2-42), into (9-2-41) yields the desired autocorrelation function for $\{B_n\}$ in the form

$$\phi(m) = \sum_{k=0}^{N-1-|m|} x_k x_{k+|m|}, \qquad m = 0, \pm 1, \ldots, \pm(N-1) \tag{9-2-43}$$

The corresponding power spectral density is

$$\begin{aligned}\Phi(f) &= \sum_{m=-(N-1)}^{N-1} \phi(m) e^{-j2\pi fmT} \\ &= \left| \sum_{m=0}^{N-1} x_m e^{-j2\pi fmT} \right|^2\end{aligned} \tag{9-2-44}$$

where $T = 1/2W$ and $|f| \leq 1/2T = W$.

9-2-3 Data Detection for Controlled ISI

In this section, we describe two methods for detecting the information symbols at the receiver when the received signal contains controlled ISI. One is a symbol-by-symbol detection method that is relatively easy to implement. The second method is based on the maximum-likelihood criterion for detecting a sequence of symbols. The latter method minimizes the probability of error but is a little more complex to implement. In particular, we consider the detection of the duobinary and the modified duobinary partial response signals. In both

cases, we assume that the desired spectral characteristic $X(f)$ for the partial response signal is split evenly between the transmitting and receiving filters, i.e., $|G_T(f)| = |G_R(f)| = |X(f)|^{1/2}$. This treatment is based on PAM signals, but it is easily generalized to QAM and PSK.

Symbol-by-Symbol Suboptimum Detection For the duobinary signal pulse, $x(nT) = 1$, for $n = 0, 1$, and zero otherwise. Hence, the samples at the output of the receiving filter (demodulator) have the form

$$y_m = B_m + v_m = I_m + I_{m-1} + v_m \tag{9-2-45}$$

where $\{I_m\}$ is the transmitted sequence of amplitudes and $\{v_m\}$ is a sequence of additive gaussian noise samples. Let us ignore the noise for the moment and consider the binary case where $I_m = \pm 1$ with equal probability. Then B_m takes on one of three possible values, namely, $B_m = -2, 0, 2$ with corresponding probabilities 1/4, 1/2, 1/4. If I_{m-1} is the detected symbol from the $(m-1)$ th signaling interval, its effect on B_m, the received signal in the m th signaling interval, can be eliminated by subtraction, thus allowing I_m to be detected. This process can be repeated sequentially for every received symbol.

The major problem with this procedure is that errors arising from the additive noise tend to propagate. For example, if I_{m-1} is in error, its effect on B_m is not eliminated but, in fact, it is reinforced by the incorrect subtraction. Consequently, the detection of B_m is also likely to be in error.

Error propagation can be avoided by *precoding* the data at the transmitter instead of eliminating the controlled ISI by subtraction at the receiver. The precoding is performed on the binary data sequence prior to modulation. From the data sequence $\{D_n\}$ of 1s and 0s that is to be transmitted, a new sequence $\{P_n\}$, called the *precoded sequence*, is generated. For the duobinary signal, the precoded sequence is defined as

$$P_m = D_m \ominus P_{m-1}, \qquad m = 1, 2, \ldots \tag{9-2-46}$$

where $\ominus$ denotes modulo-2 subtraction.† Then we set $I_m = -1$ if $P_m = 0$ and $I_m = 1$ if $P_m = 1$, i.e., $I_m = 2P_m - 1$. Note that this precoding operation is identical to that described in Section 4-3-2 in the context of our discussion of an NRZI signal.

The noise-free samples at the output of the receiving filter are given by

$$\begin{aligned} B_m &= I_m + I_{m-1} \\ &= (2P_m - 1) + (2P_{m-1} - 1) \\ &= 2(P_m + P_{m-1} - 1) \end{aligned} \tag{9-2-47}$$

Consequently,

$$P_m + P_{m-1} = \tfrac{1}{2}B_m + 1 \tag{9-2-48}$$

†Although this is identical to modulo-2 addition, it is convenient to view the precoding operation for duobinary in terms of modulo-2 subtraction.

TABLE 9-2-1 BINARY SIGNALING WITH DUOBINARY PULSES

Data sequence D_n		1	1	1	0	1	0	0	1	0	0	0	1	1	0	1
Precoded sequence P_n	0	1	0	1	1	0	0	0	1	1	1	1	0	1	1	0
Transmitted sequence I_m	−1	1	−1	1	1	−1	−1	−1	1	1	1	1	−1	1	1	−1
Received sequence B_n		0	0	0	2	0	−2	−2	0	2	2	2	0	0	2	0
Decoded sequence D_n		1	1	1	0	1	0	0	1	0	0	0	1	1	0	1

Since $D_m = P_m \oplus P_{m-1}$, it follows that the data sequence D_m is obtained from B_m using the relation

$$D_m = \tfrac{1}{2}B_m + 1 \pmod 2 \tag{9-2-49}$$

Consequently, if $B_m = \pm 2$ then $D_m = 0$, and if $B_m = 0$ then $D_m = 1$. An example that illustrates the precoding and decoding operations is given in Table 9-2-1. In the presence of additive noise, the sampled outputs from the receiving filter are given by (9-2-45). In this case $y_m = B_m + v_m$ is compared with the two thresholds set at $+1$ and -1. The data sequence $\{D_n\}$ is obtained according to the detection rule

$$D_m = \begin{cases} 1 & (|y_m| < 1) \\ 0 & (|y_m| \geq 1) \end{cases} \tag{9-2-50}$$

The extension from binary PAM to multilevel PAM signaling using the duobinary pulses is straightforward. In this case the M-level amplitude sequence $\{I_m\}$ results in a (noise-free) sequence

$$B_m = I_m + I_{m-1}, \qquad m = 1, 2, \ldots \tag{9-2-51}$$

which has $2M - 1$ possible equally spaced levels. The amplitude levels are determined from the relation

$$I_m = 2P_m - (M - 1) \tag{9-2-52}$$

where $\{P_m\}$ is the precoded sequence that is obtained from an M-level data sequence $\{D_m\}$ according to the relation

$$P_m = D_m \ominus P_{m-1} \pmod M \tag{9-2-53}$$

where the possible values of the sequence $\{D_m\}$ are $0, 1, 2, \ldots, M - 1$.

In the absence of noise, the samples at the output of the receiving filter may be expressed as

$$B_m = I_m + I_{m-1} = 2[P_m + P_{m-1} - (M - 1)] \tag{9-2-54}$$

TABLE 9-2-2 FOUR-LEVEL SIGNAL TRANSMISSION WITH DUOBINARY PULSES

Data sequence D_m		0	0	1	3	1	2	0	3	3	2	0	1	0
Precoded sequence P_m	0	0	0	1	2	3	3	1	2	1	1	3	2	2
Transmitted sequence I_m	−3	−3	−3	−1	1	3	3	−1	1	−1	−1	3	1	1
Received sequence B_m		−6	−6	−4	0	4	6	2	0	0	−2	2	4	2
Decoded sequence D_m		0	0	1	3	1	2	0	3	3	2	0	1	0

Hence,

$$P_m + P_{m-1} = \tfrac{1}{2}B_m + (M-1) \tag{9-2-55}$$

Since $D_m = P_m + P_{m-1} \pmod M$, it follows that

$$D_m = \tfrac{1}{2}B_m + (M-1) \pmod M \tag{9-2-56}$$

An example illustrating multilevel precoding and decoding is given in Table 9-2-2.

In the presence of noise, the received signal-plus-noise is quantized to the nearest of the possible signal levels and the rule given above is used on the quantized values to recover the data sequence.

In the case of the modified duobinary pulse, the controlled ISI is specified by the values $x(n/2W) = -1$, for $n = 1$, $x(n/2W) = 1$ for $n = -1$, and zero otherwise. Consequently, the noise-free sampled output from the receiving filter is given as

$$B_m = I_m - I_{m-2} \tag{9-2-57}$$

where the M-level sequence $\{I_m\}$ is obtained by mapping a precoded sequence according to the relation (9-2-52) and

$$P_m = D_m \oplus P_{m-2} \pmod M \tag{9-2-58}$$

From these relations, it is easy to show that the detection rule for recovering the data sequence $\{D_m\}$ from $\{B_m\}$ in the absence of noise is

$$D_m = \tfrac{1}{2}B_m \pmod M \tag{9-2-59}$$

As demonstrated above, the precoding of the data at the transmitter makes it possible to detect the received data on a symbol-by-symbol basis without having to look back at previously detected symbols. Thus, error propagation is avoided.

The symbol-by-symbol detection rule described above is not the optimum detection scheme for partial response signals due to the memory inherent in

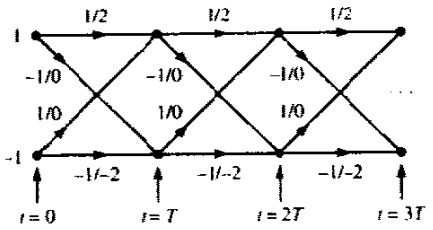

FIGURE 9-2-11 Trellis for duobinary partial response signal.

the received signal. Nevertheless, symbol-by-symbol detection is relatively simple to implement and is used in many practical applications involving duobinary and modified duobinary pulse signals. Its performance is evaluated in the following section.

Maximum-Likelihood Sequence Detection It is clear from the above discussion that partial-response waveforms are signal waveforms with memory. This memory is conveniently represented by a trellis. For example, the trellis for the duobinary partial-response signal for binary data transmission is illustrated in Fig. 9-2-11. For binary modulation, this trellis contains two states, corresponding to the two possible input values of I_m, i.e., $I_m = \pm 1$. Each branch in the trellis is labeled by two numbers. The first number on the left is the new data bit, i.e., $I_{m+1} = \pm 1$. This number determines the transition to the new state. The number on the right is the received signal level.

The duobinary signal has a memory of length $L = 1$. Hence, for binary modulation the trellis has $S_t = 2$ states. In general, for M-ary modulation, the number of trellis states is M^L.

The optimum maximum-likelihood (ML) sequence detector selects the most probable path through the trellis upon observing the received data sequence $\{y_m\}$ at the sampling instants $t = mT$, $m = 1, 2, \ldots$. In general, each node in the trellis will have M incoming paths and M corresponding metrics. One out of the M incoming paths is selected as the most probable, based on the values of the metrics and the other $M - 1$ paths and their metrics are discarded. The surviving path at each node is then extended to M new paths, one for each of the M possible input symbols, and the search process continues. This is basically the Viterbi algorithm for performing the trellis search.

For the class of partial response signals, the received sequence $\{y_m, 1 \leq m \leq N\}$ is generally described statistically by the joint pdf $f(\mathbf{y}_N \mid \mathbf{I}_N)$, where $\mathbf{y}_N = [y_1 \; y_2 \; \cdots \; y_N]'$ and $\mathbf{I}_N = [I_1 \; I_2 \; \cdots \; I_N]'$ and $N > L$. When the additive noise is zero-mean gaussian, $f(\mathbf{y}_N \mid \mathbf{I}_N)$ is a multivariate gaussian pdf, i.e.,

$$f(\mathbf{y}_N \mid \mathbf{I}_N) = \frac{1}{(2\pi \det \mathbf{C})^{N/2}} \exp\left[-\tfrac{1}{2}(\mathbf{y}_N - \mathbf{B}_N)'\mathbf{C}^{-1}(\mathbf{y}_N - \mathbf{B}_N)\right] \quad (9\text{-}2\text{-}60)$$

where $\mathbf{B}_N = [B_1 \; B_2 \; \cdots \; B_N]'$, is the mean of the vector $\mathbf{y}_N$ and $\mathbf{C}$ is the $N \times N$ covariance matrix of $\mathbf{y}_N$. Then, the ML sequence detector selects the sequence through the trellis that maximizes the pdf $f(\mathbf{y}_N \mid \mathbf{I}_N)$.

The computation for finding the most probable sequence through the trellis is simplified by taking the natural logarithms of $f(\mathbf{y}_N \mid \mathbf{I}_N)$. Thus,

$$\ln f(\mathbf{y}_N \mid \mathbf{I}_N) = -\tfrac{1}{2}N \ln (2\pi \det \mathbf{C}) - \tfrac{1}{2}(\mathbf{y}_N - \mathbf{B}_N)'\mathbf{C}^{-1}(\mathbf{y}_N - \mathbf{B}_N) \quad (9\text{-}2\text{-}61)$$

Given the received sequence $\{y_m\}$, the data sequence $\{I_m\}$ that maximizes $\ln f(\mathbf{y}_N \mid \mathbf{I}_N)$ is identical to the sequence $\{I_N\}$ that minimizes $(\mathbf{y}_N - \mathbf{B}_N)'\mathbf{C}^{-1}(\mathbf{y}_N - \mathbf{B}_N)$, i.e.

$$\hat{\mathbf{I}}_N = \arg\min_{\mathbf{I}_N} [(\mathbf{y}_N - \mathbf{B}_N)'\mathbf{C}^{-1}(\mathbf{y}_N - \mathbf{B}_N)] \quad (9\text{-}2\text{-}62)$$

The metric computations in the trellis search are complicated by the correlation of the noise samples at the output of the matched filter for the partial response signal. For example, in the case of the duobinary signal waveform, the correlation of the noise sequence $\{v_m\}$ is over two successive signal samples. Hence, v_m and v_{m+k} are correlated for $k = 1$ and uncorrelated for $k > 1$. In general, a partial response signal waveform with memory L will result in a correlated noise sequence at the output of the matched filter, which satisfies the condition $E[v_m v_{m+k}] = 0$ for $k > L$. In such a case, the Viterbi algorithm for performing the trellis search may be modified as described in Chapter 10.

Some simplification in the metric computations result if we ignore the noise correlation by assuming that $E(v_m v_{m+k}) = 0$ for $k > 0$. Then, by assumption, the covariance matrix $\mathbf{C} = \sigma_v^2 \mathbf{1}_N$, where $\sigma_v^2 = E[v_m^2]$ and $\mathbf{1}_N$ is the $N \times N$ identity matrix.† In this case, (9-2-62) simplifies to

$$\begin{aligned}\hat{\mathbf{I}}_N &= \arg\min_{\mathbf{I}_N} [(\mathbf{y}_N - \mathbf{B}_N)'(\mathbf{y}_N - \mathbf{B}_N)] \\ &= \arg\min_{\mathbf{I}_N} \left[\sum_{m=1}^{N} \left(y_m - \sum_{k=0}^{L} x_k I_{m-k} \right)^2 \right] \end{aligned} \quad (9\text{-}2\text{-}63)$$

where

$$B_m = \sum_{k=0}^{L} x_k I_{m-k}$$

and $x_k = x(kT)$ are the sampled values of the partial response signal waveform. In this case, the metric computations at each node of the trellis have the form

$$DM_m(\mathbf{I}_m) = DM_{m-1}(\mathbf{I}_{m-1}) + \left(y_m - \sum_{k=0}^{L} x_k I_{m-k} \right)^2 \quad (9\text{-}2\text{-}64)$$

where $DM_m(\mathbf{I}_m)$ are the distance metrics at time $t = mT$, $DM_{m-1}(\mathbf{I}_{m-1})$ are the distance metrics at time $t = (m-1)T$ and the second term on the right-hand side of (9-2-64) represents the new increments to the metrics based on the new received sample y_m.

†We are using $\mathbf{1}_N$ here to avoid confusion with $\mathbf{I}_N$.

As indicated in Section 5-1-4, ML sequence detection introduces a variable delay in detecting each transmitted information symbol. In practice, the variable delay is avoided by truncating the surviving sequences to N_t most recent symbols, where $N_t \gg 5L$, thus achieving a fixed delay. In the case that the M^L surviving sequences at time $t = mT$ disagree on the symbol I_{m-N_t}, the symbol in the most probable surviving sequence may be chosen. The loss in performance resulting from this truncation is negligible if $N_t > 5L$.

9-2-4 Signal Design for Channels with Distortion

In Sections 9-2-1 and 9-2-2, we described signal design criteria for the modulation filter at the transmitter and the demodulation filter at the receiver when the channel is ideal. In this section, we perform the signal design under the condition that the channel distorts the transmitted signal. We assume that the channel frequency response $C(f)$ is known for $|f| \leq W$ and that $C(f) = 0$ for $|f| > W$. The criterion for the optimization of the filter responses $G_T(f)$ and $G_R(f)$ is the maximization of the SNR at the output of the demodulation filter or equivalently, at the input to the detector. The additive channel noise is assumed to be gaussian with power spectral density $\Phi_{nn}(f)$. Figure 9-2-12 illustrates the overall system under consideration.

For the signal component at the output of the demodulator, we must satisfy the condition

$$G_T(f)C(f)G_R(f) = X_d(f)e^{-j2\pi f t_0}, \quad |f| \leq W \tag{9-2-65}$$

where $X_d(f)$ is the desired frequency response of the cascade of the modulator, channel, and demodulator, and t_0 is a time delay that is necessary to ensure the physical realizability of the modulation and demodulation filters. The desired frequency response $X_d(f)$ may be selected to yield either zero ISI or controlled ISI at the sampling instants. We shall carry out the optimization for zero ISI by selecting $X_d(f) = X_{rc}(f)$, where $X_{rc}(f)$ is the raised cosine spectrum with an arbitrary rolloff factor.

The noise at the output of the demodulation filter may be expressed as

$$v(t) = \int_{-\infty}^{\infty} n(t-\tau)g_R(\tau)\,d\tau \tag{9-2-66}$$

FIGURE 9-2-12 System model for the design of the modulation and demodulation filters.

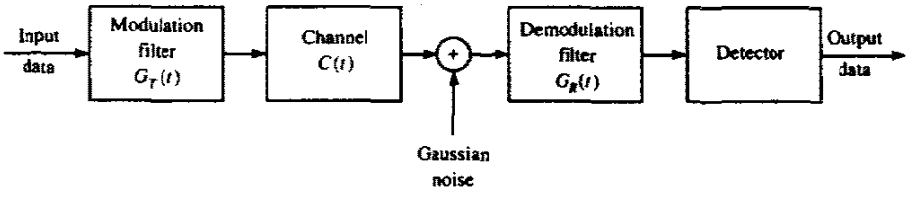

where $n(t)$ is the input to the filter. Since $n(t)$ is zero-mean gaussian, $v(t)$ is zero-mean gaussian, with a power spectral density

$$\Phi_{vv}(f) = \Phi_{nn}(f)\,|G_R(f)|^2 \tag{9-2-67}$$

For simplicity, we consider binary PAM transmission. Then, the sampled output of the matched filter is

$$y_m = x_0 I_m + v_m = I_m + v_m \tag{9-2-68}$$

where x_0 is normalized† to unity, $I_m = \pm d$, and v_m represents the noise term, which is zero-mean gaussian with variance

$$\sigma_v^2 = \int_{-\infty}^{\infty} \Phi_{nn}(f)\,|G_R(f)|^2\,df \tag{9-2-69}$$

Consequently, the probability of error is

$$P_2 = \frac{1}{\sqrt{2\pi}} \int_{d/\sigma_v}^{\infty} e^{-y^2/2}\,dy = Q(\sqrt{d^2/\sigma_v^2}) \tag{9-2-70}$$

The probability of error is minimized by maximizing the SNR $= d^2/\sigma_v^2$, or, equivalently, by minimizing the noise-to-signal ratio σ_v^2/d^2. But d^2 is related to the transmitted signal power as follows:

$$\begin{aligned} P_{av} &= \frac{E(I_m^2)}{T} \int_{-\infty}^{\infty} g_T^2(t)\,dt = \frac{d^2}{T} \int_{-\infty}^{\infty} g_T^2(t)\,dt \\ \frac{1}{d^2} &= \frac{1}{P_{av}T} \int_{-\infty}^{\infty} |G_T(f)|^2\,df \end{aligned} \tag{9-2-71}$$

However, $G_T(f)$ must be chosen to satisfy the zero ISI condition. Consequently,

$$|G_T(f)| = \frac{|X_{rc}(f)|}{|C(f)|\,|G_R(f)|}, \qquad |f| \leq W \tag{9-2-72}$$

and $G_T(f) = 0$ for $|f| \geq W$. Hence

$$\frac{1}{d^2} = \frac{1}{P_{av}T} \int_{-W}^{W} \frac{|X_{rc}(f)|^2}{|C(f)|^2\,|G_R(f)|^2}\,df \tag{9-2-73}$$

Therefore, the noise-to-signal ratio that must be minimized with respect to $|G_R(f)|$ for $|f| \leq W$ is

$$\frac{\sigma_v^2}{d^2} = \frac{1}{P_{av}T} \int_{-W}^{W} \Phi_{nn}(f)\,|G_R(f)|^2\,df \int_{-W}^{W} \frac{|X_{rc}(f)|^2}{|C(f)|^2\,|G_R(f)|^2}\,df \tag{9-2-74}$$

†By setting $x_0 = 1$ and $I_m = \pm d$, the scaling by x_0 is incorporated into the parameter d.

The optimum $|G_R(f)|$ can be found by applying the Cauchy–Schwartz inequality,

$$\int_{-\infty}^{\infty} |U_1(f)|^2\, df \int_{-\infty}^{\infty} |U_2(f)|^2\, df \geq \left[\int_{-\infty}^{\infty} |U_1(f)|\,|U_2(f)|\, df\right]^2 \tag{9-2-75}$$

where $|U_1(f)|$ and $|U_2(f)|$ are defined as

$$\begin{aligned} |U_1(f)| &= |\sqrt{\Phi_{nn}(f)}|\,|G_R(f)| \\ |U_2(f)| &= \frac{|X_{rc}(f)|}{|C(f)|\,|G_R(f)|} \end{aligned} \tag{9-2-76}$$

The minimum value of (9-2-74) is obtained when $|U_1(f)|$ is proportional to $|U_2(f)|$, or, equivalently, when

$$|G_R(f)| = K\frac{|X_{rc}(f)|^{1/2}}{[\Phi_{nn}(f)]^{1/4}\,|C(f)|^{1/2}}, \qquad |f| \leq W \tag{9-2-77}$$

where K is an arbitrary constant. The corresponding modulation filter has a magnitude characteristic

$$|G_T(f)| = \frac{1}{K}\frac{|X_{rc}(f)|^{1/2}\,[\Phi_{nn}(f)]^{1/4}}{|C(f)|^{1/2}}, \qquad |f| \leq W \tag{9-2-78}$$

Finally, the maximum SNR achieved by these optimum transmitting and receiving filters is

$$\frac{d^2}{\sigma_\nu^2} = \frac{P_{av}T}{\{\int_{-W}^{W} |X_{rc}(f)|\,[\Phi_{nn}(f)]^{1/2}\,|C(f)|^{-1}\, df\}^2} \tag{9-2-79}$$

We note that the optimum modulation and demodulation filters are specified in magnitude only. The phase characteristics for $G_T(f)$ and $G_R(f)$ may be selected so as to satisfy the condition in (9-2-65), i.e.,

$$\Theta_T(f) + \Theta_c(f) + \Theta_R(f) = 2\pi f t_0 \tag{9-2-80}$$

where $\Theta_T(f)$, $\Theta_c(f)$, and $\Theta_R(f)$ are the phase characteristics of the modulation filter, the channel, and the demodulation filter, respectively.

In the special case where the additive noise at the input to the demodulator is white gaussian with spectral density $\frac{1}{2}N_0$, the optimum filter characteristics specified by (9-2-77) and (9-2-78) reduce to

$$\begin{aligned} |G_R(f)| &= K_1\frac{|X_{rc}(f)|^{1/2}}{|C(f)|^{1/2}}, \qquad |f| \leq W \\ |G_T(f)| &= K_2\frac{|X_{rc}(f)|^{1/2}}{|C(f)|^{1/2}}, \qquad |f| \leq W \end{aligned} \tag{9-2-81}$$

where K_1 and K_2 are arbitrary scale factors. Note that, in this case, $|G_R(f)|$ is the matched filter to $|G_T(f)|$. The corresponding SNR at the detector, given by (9-2-79) reduces to

$$\frac{d^2}{\sigma_v^2} = \frac{2P_{av}T}{N_0}\left[\int_{-W}^{W} \frac{|X_{rc}(f)|}{|C(f)|}\,df\right]^{-2} \tag{9-2-82}$$

Example 9-2-1

Let us determine the optimum transmitting and receiving filters for a binary communication system that transmits data at a rate of 4800 bits/s over a channel with frequency (magnitude) response

$$|C(f)| = \frac{1}{\sqrt{1 + (f/W)^2}}, \qquad |f| \leq W \tag{9-2-83}$$

where $W = 4800$ Hz. The additive noise is zero-mean, white, gaussian with spectral density $\frac{1}{2}N_0 = 10^{-15}\,W/Hz$.

Since $W = 1/T = 4800$, we use a signal pulse with a raised cosine spectrum and $\beta = 1$. Thus,

$$\begin{aligned} X_{rc}(f) &= \tfrac{1}{2}T[1 + \cos(\pi T\,|f|)] \\ &= T\cos^2\left(\frac{\pi\,|f|}{9600}\right) \end{aligned} \tag{9-2-84}$$

Then,

$$|G_T(f) = |G_R(f)| = \left[1 + \left(\frac{f}{4800}\right)^2\right]^{1/4} \cos\left(\frac{\pi\,|f|}{9600}\right), \qquad |f| \leq 4800 \tag{9-2-85}$$

and $|G_T(f)| = |G_R(f)| = 0$, otherwise. Figure 9-2-13 illustrates the filter characteristic $G_T(f)$.

One can now use these optimum filters to determine the amount of transmitted energy $\mathscr{E}$ required to achieve a specified error probability. This problem is left as an exercise for the reader.

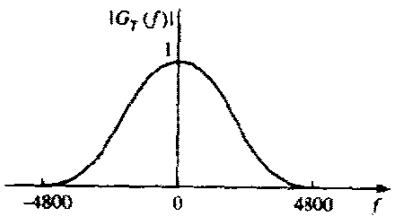

FIGURE 9-2-13 Frequency response of optimum transmitter filter.

9-3 PROBABILITY OF ERROR IN DETECTION OF PAM

In this section, we evaluate the performance of the receiver for demodulating and detecting an M-ary PAM signal in the presence of additive, white, gaussian noise at its input. First, we consider the case in which the transmitter and receiver filters $G_T(f)$ and $G_R(f)$ are designed for zero ISI. Then, we consider the case in which $G_T(f)$ and $G_R(f)$ are designed such that $x(t) = g_T(t) \star g_R(t)$ is either a duobinary signal or a modified duobinary signal.

9-3-1 Probability of Error for Detection of PAM with Zero ISI

In the absence of ISI, the received signal sample at the output of the receiving matched filter has the form

$$y_m = x_0 I_m + v_m \tag{9-3-1}$$

where

$$x_0 = \int_{-W}^{W} |G_T(f)|^2 \, df = \mathscr{E}_g \tag{9-3-2}$$

and v_m is the additive gaussian noise that has zero mean and variance

$$\sigma_v^2 = \tfrac{1}{2}\mathscr{E}_g N_0 \tag{9-3-3}$$

In general, I_m takes one of M possible equally spaced amplitude values with equal probability. Given a particular amplitude level, the problem is to determine the probability of error.

The problem of evaluating the probability of error for digital PAM in a band-limited, additive white gaussian noise channel, in the absence of ISI, is identical to the evaluation of the error probability for M-ary PAM as given in Section 5-2. The final result that is obtained from the derivation is

$$P_M = \frac{2(M-1)}{M} Q\left(\sqrt{\frac{2\mathscr{E}_g}{N_0}}\right) \tag{9-3-4}$$

But $\mathscr{E}_g = 3\mathscr{E}_{av}/(M^2-1)$, $\mathscr{E}_{av} = k\mathscr{E}_{bav}$ is the average energy per symbol and $\mathscr{E}_{bav}$ is the average energy per bit. Hence,

$$P_M = \frac{2(M-1)}{M} Q\left(\sqrt{\frac{6(\log_2 M)\mathscr{E}_{bav}}{(M^2-1)N_0}}\right) \tag{9-3-5}$$

This is exactly the form for the probability of error of M-ary PAM derived in Section 5-2 (see (5-2-46)). In the treatment of PAM given in this chapter, we imposed the additional constraint that the transmitted signal is band-limited to the bandwidth allocated for the channel. Consequently, the transmitted signal pulses were designed to be band-limited and to have zero ISI.

In contrast, no bandwidth constraint was imposed on the PAM signals considered in Section 5-2. Nevertheless, the receivers (demodulators and detectors) in both cases are optimum (matched filters) for the corresponding

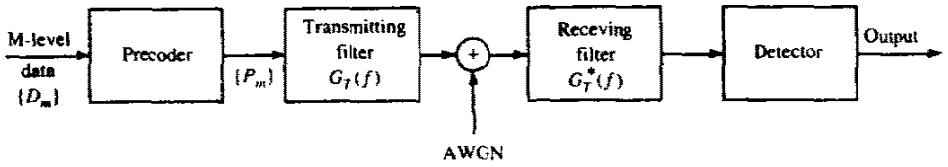

FIGURE 9-3-1 Block diagram of modulator and demodulator for partial-response signals.

transmitted signals. Consequently, no loss in error rate performance results from the bandwidth constraint when the signal pulse is designed for zero ISI and the channel does not distort the transmitted signal.

9-3-2 Probability of Error for Detection of Partial-Response Signals

In this section we determine the probability of error for detection of digital M-ary PAM signaling using duobinary and modified duobinary pulses. The channel is assumed to be an ideal bandlimited channel with additive white gaussian noise. The model for the communication system is shown in Fig. 9-3-1.

We consider two types of detectors. The first is the symbol-by-symbol detector and the second is the optimum ML sequence detector described in the previous section.

Symbol-by-Symbol Detector At the transmitter, the M-level data sequence $\{D_m\}$ is precoded as described previously. The precoder output is mapped into one of M possible amplitude levels. Then the transmitting filter with frequency response $G_T(f)$ has an output

$$v(t) = \sum_{n=-\infty}^{\infty} I_n g_T(t - nT) \tag{9-3-6}$$

The partial-response function $X(f)$ is divided equally between the transmitting and receiving filters. Hence, the receiving filter is matched to the transmitted pulse, and the cascade of the two filters results in the frequency characteristic

$$|G_T(f)G_R(f)| = |X(f)| \tag{9-3-7}$$

The matched filter output is sampled at $t = nT = n/2W$ and the samples are fed to the decoder. For the duobinary signal, the output of the matched filter at the sampling instant may be expressed as

$$y_m = I_m + I_{m-1} + \nu_m = B_m + \nu_m \tag{9-3-8}$$

where ν_m is the additive noise component. Similarly, the output of the matched filter for the modified duobinary signal is

$$y_m = I_m - I_{m-2} + \nu_m = B_m + \nu_m \tag{9-3-9}$$

For binary transmission, let $I_m = \pm d$, where $2d$ is the distance between signal levels. Then, the corresponding values of B_m are $(2d, 0, -2d)$. For M-ary PAM signal transmission, where $I_m = \pm d, \pm 3d, \ldots, \pm(M-1)d$, the received signal levels are $B_m = 0, \pm 2d, \pm 4d, \ldots, \pm 2(M-1)d$. Hence, the number of received levels is $2M-1$, and the scale factor d is equivalent to $x_0 = \mathscr{E}_g$.

The input transmitted symbols $\{I_m\}$ are assumed to be equally probable. Then, for duobinary and modified duobinary signals, it is easily demonstrated that, in the absence of noise, the received output levels have a (triangular) probability distribution of the form

$$P(B = 2md) = \frac{M - |m|}{M^2}, \qquad m = 0, \pm 1, \pm 2, \ldots, \pm(M-1) \tag{9-3-10}$$

where B denotes the noise-free received level and $2d$ is the distance between any two adjacent received signal levels.

The channel corrupts the signal transmitted through it by the addition of white gaussian noise with zero mean and power spectral density $\frac{1}{2}N_0$.

We assume that a symbol error occurs whenever the magnitude of the additive noise exceeds the distance d. This assumption neglects the rare event that a large noise component with magnitude exceeding d may result in a received signal level that yields a correct symbol decision. The noise component v_m is zero-mean gaussian with variance

$$\begin{aligned}\sigma_v^2 &= \tfrac{1}{2}N_0 \int_{-W}^{W} |G_R(f)|^2\, df \\ &= \tfrac{1}{2}N_0 \int_{-W}^{W} |X(f)|\, df = 2N_0/\pi\end{aligned} \tag{9-3-11}$$

for both the duobinary and the modified duobinary signals. Hence, an upper bound on the symbol probability of error is

$$\begin{aligned}P_M < & \sum_{m=-(M-2)}^{M-2} P(|y - 2md| > d \mid B = 2md) P(B = 2md) \\ & + 2P(y + 2(M-1)d > d \mid B = -2(M-1)d) P(B = -2(M-1)d) \\ = & P(|y| > d \mid b = 0)\left[2 \sum_{m=0}^{M-1} P(B = 2md) - P(B = 0) - P(B = -2(M-1)d)\right] \\ = & (1 - M^{-2}) P(|y| > d \mid B = 0)\end{aligned} \tag{9-3-12}$$

But

$$\begin{aligned}P(|y| > d \mid B = 0) &= \frac{2}{\sqrt{2\pi}\sigma_v} \int_d^{\infty} e^{-x^2/2\sigma_v^2}\, dx \\ &= 2Q(\sqrt{\pi d^2/2N_0})\end{aligned} \tag{9-3-13}$$

Therefore, the average probability of a symbol error is upper-bounded as

$$P_M < 2(1 - M^{-2})Q(\sqrt{\pi d^2/2N_0}) \tag{9-3-14}$$

The scale factor d in (9-3-14) can be eliminated by expressing it in terms of the average power transmitted into the channel. For the M-ary PAM signal in which the transmitted levels are equally probable, the average power at the output of the transmitting filter is

$$\begin{aligned} P_{av} &= \frac{E(I_m^2)}{T}\int_{-W}^{W} |G_T(f)|^2\, df \\ &= \frac{E(I_m^2)}{T}\int_{-W}^{W} |X(f)|\, df = \frac{4}{\pi T}E(I_m^2) \end{aligned} \tag{9-3-15}$$

where $E(I_m^2)$ is the mean square value of the M signal levels, which is

$$E(I_m^2) = \tfrac{1}{3}d^2(M^2 - 1) \tag{9-3-16}$$

Therefore,

$$d^2 = \frac{3\pi P_{av}T}{4(M^2 - 1)} \tag{9-3-17}$$

By substituting the value of d^2 from (9-3-17) into (9-3-14), we obtain the upper bound on the symbol error probability as

$$P_M < 2\left(1 - \frac{1}{M^2}\right)Q\left(\sqrt{\left(\frac{\pi}{4}\right)^2 \frac{6}{M^2 - 1}\frac{\mathscr{E}_{av}}{N_0}}\right) \tag{9-3-18}$$

where $\mathscr{E}_{av}$ is the average energy per transmitted symbol, which can be also expressed in terms of the average bit energy as $\mathscr{E}_{av} = k\mathscr{E}_{bav} = (\log_2 M)\mathscr{E}_{bav}$.

The expression in (9-3-18) for the probability of error of M-ary PAM holds for both duobinary and modified duobinary partial-response signals. If we compare this result with the error probability of M-ary PAM with zero ISI, which can be obtained by using a signal pulse with a raised cosine spectrum, we note that the performance of partial response duobinary or modified duobinary has a loss of $(\frac{1}{4}\pi)^2$, or 2.1 dB. This loss in SNR is due to the fact that the detector for the partial response signals makes decisions on a symbol-by symbol basis, thus ignoring the inherent memory contained in the received signal at the input to the detector.

Maximum-Likelihood Sequence Detector The ML sequence detector searches through the trellis for the most probable transmitted sequence $\{I_m\}$ as previously described in Section 9-2-3. At each stage of the search process the detector compares the metrics of paths that merge at each of the nodes and selects the path that is most probable at each node. The performance of the detector may be evaluated by determining the probability of error events, based on a euclidean distance metric, as was done for soft-decision decoding of convolutional codes. The general derivation is given in Section 10-1-4. In the

case of the duobinary and modified duobinary signals, it is demonstrated that the 2.1 dB loss inherent in the suboptimum symbol-by-symbol detector is completely recovered by the ML sequence detector.

9-3-3 Probability of Error for Optimum Signals in a Channel with Distortion

In Section 9-2-4, we derived the filter responses for the modulation and demodulation filters that maximize the SNR at the input to the detector when there is channel distortion. When the filters are designed for zero ISI at the sampling instants, the probability of error for M-ary PAM is

$$P_M = \frac{2(M-1)}{M} Q(\sqrt{d^2/\sigma_v^2}) \tag{9-3-19}$$

The parameter d is related to the average transmitted power as

$$\begin{aligned} P_{\text{av}} &= \frac{E[I_m^2]}{T} \int_{-W}^{W} |G_T(f)|^2 \, df \\ &= \frac{(M^2-1)d^2}{3T} \int_{-W}^{W} |G_T(f)|^2 \, df \end{aligned} \tag{9-3-20}$$

and the noise variance is given by (9-2-69). For AWGN, (9-3-19) may be expressed as

$$P_M = \frac{2(M-1)}{M} Q\left(\sqrt{\frac{6\mathscr{E}_{\text{av}}}{(M^2-1)N_0} \left[\int_{-W}^{W} \frac{|X_{rc}(f)|}{|C(f)|} df \right]^{-2}} \right) \tag{9-3-21}$$

Finally, we observe that the loss due to channel distortion is

$$20 \log_{10} \left[\int_{-W}^{W} \frac{|X_{rc}(f)|}{|C(f)|} df \right] \tag{9-3-22}$$

Note that when $C(f) = 1$ for $|f| \leq W$, the channel is ideal and

$$\int_{-W}^{W} X_{rc}(f) \, df = 1 \tag{9-3-23}$$

so that no loss is incurred. On the other hand, when there is amplitude distortion, $|C(f)| < 1$ for some range of frequencies in the band $|f| \leq W$ and, hence, there is a loss in SNR incurred, as given by (9-3-22). This loss is independent of channel phase distortion, because phase distortion has been perfectly compensated, as implied by (9-2-80). The loss given by (9-3-22) is due entirely to amplitude distortion and is a measure of the noise enhancement

resulting from the receiving filter, which compensates for the channel distortion.

9-4 MODULATION CODES FOR SPECTRUM SHAPING

We have observed that the power spectral density of a digital communication signal can be controlled and shaped by selecting the transmitted signal pulse $g(t)$ and by introducing correlation through coding, which is used to combat channel distortion and noise in transmission. Coding for spectrum shaping is introduced following the channel encoding so that the spectrum of the transmitted signal matches the spectral characteristics of a baseband or equivalent lowpass channel.

Codes that are used for spectrum shaping are generally called either *modulation codes,* or *line codes,* or *data translation codes.* Such codes generally place restrictions on the sequence of bits into the modulator and, thus, introduce correlation and, hence, memory into the transmitted signal. It is this type of coding that is treated in this section.

Modulation codes are usually employed in magnetic recording, in optical recording, and in digital communications over cable systems to achieve spectral shaping and to eliminate or minimize the d.c. content in the transmitted (or stored) baseband signal. In magnetic recording channels, the modulation code is designed to increase the distance between transitions in the recorded waveform and, thus, intersymbol interference effects are also reduced.

As an example of the use of a modulation code, let us consider a magnetic recording system, which consists of the elements shown in the block diagram of Fig. 9-4-1. The binary data sequence to be stored is used to generate a write current. This current may be viewed as the output for the "modulator." The most commonly used method to map the information sequence into the write current waveform is NRZI, which was described in Section 4-3-2. Recall that in NRZI, a transition from one amplitude to another (A to $-$A or $-$A to A) occurs only when the information bit is a 1. No transition occurs when the information bit is a 0, i.e., the amplitude level remains the same as in the previous signal interval. The positive amplitude pulse results in magnetizing

FIGURE 9-4-1 Block diagram of magnetic storage read/write system.

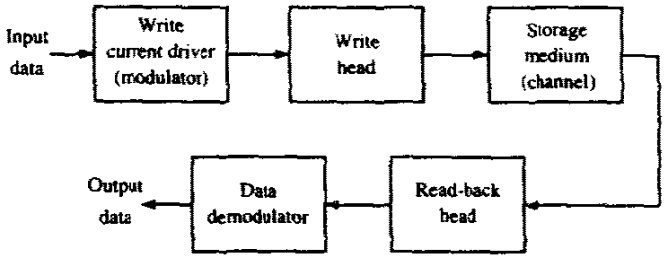

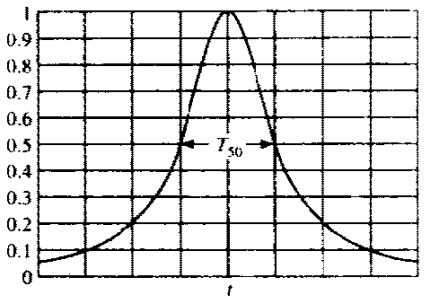

FIGURE 9-4-2 Read-back pulse in magnetic recording system.

the medium in one (direction) polarity and the negative pulse magnetizes the medium in the opposite (direction) polarity.

Since the input data sequence is basically random with equally probable 1 s and 0 s, we shall encounter level transitions from A to $-A$ or $-A$ to A with probability 1/2 for every data bit. The readback signal for a positive transition ($-A$ to A) is a pulse that is well-modeled mathematically as

$$g(t) = \frac{1}{1 + (2t/T_{50})^2} \tag{9-4-1}$$

where T_{50} is defined as the width of the pulse at its 50% amplitude level, as shown in Fig. 9-4-2. Similarly, the readback signal for a negative transition (A to $-A$) is the pulse $-g(t)$. The value of T_{50} is determined by the characteristics of the medium, the read/write heads, and the distance of the head to the medium.

Now, suppose we write a positive transition followed by a negative transition. Let's vary the time interval between the two transitions, which we denote as T_b (the bit time interval). Figure 9-4-3 illustrates the readback signal pulses, which are obtained by a superposition of $p(t)$ with $-p(t - T_b)$. The parameter $\Delta = T_{50}/T_b$ is defined as the *normalized density. The* closer the bit transitions (T_b small), the larger will be the value of the normalized density and, hence, the larger will be the packing density. We notice that as Δ is

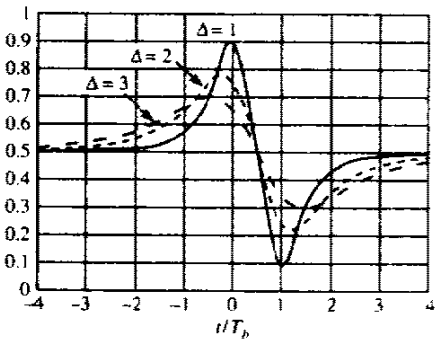

FIGURE 9-4-3 Read-back signal response to a pulse.

increased, the peak amplitudes of the readback signal are reduced and are also shifted in time from the desired time instants. In other words, the pulses interfere with one another, thus limiting the density with which we can write. This problem serves as a motivation to design modulation codes that take the original data sequence and transform (encode) it into another sequence that results in a write waveform in which amplitude transitions are spaced farther apart. For example, if we use NRZI, the encoded sequence into the modulator must contain one or more 0s between 1s.

The second problem encountered in magnetic recording is the need to avoid (or minimize) having a d.c. content in the modulated signal (the write current) due to the frequency response characteristics of the readback system and associated electronics. This requirement also arises in digital communication over cable channels. This problem can be overcome by altering (encoding) the data sequence into the modulator. A class of codes that satisfy these objectives are the modulation codes described below.

Runlength-Limited Codes Codes that have a restriction on the number of consecutive 1s or 0s in a sequence are generally called *runlength-limited codes*. These codes are generally described by two parameters, say d and κ, where d denotes the minimum number of 0s between two 1s in a sequence, and κ denotes the maximum number of 0s between two 1s in a sequence. When used with NRZI modulation, the effect of placing d zeros between successive 1s is to spread the transitions farther apart, thus reducing the overlap in the channel response due to successive transitions and hence reducing the intersymbol interference. Setting an upper limit κ on the runlength of 0s ensures that transitions occur frequently enough so that symbol timing information can be recovered from the received modulated signal. Runlength-limited codes are usually called (d, κ) codes.†

The (d, κ) code sequence constraints may be represented by a finite-state sequential machine with $\kappa + 1$ states, denoted as S_i, $1 \leq i \leq \kappa + 1$, as shown in Fig. 9-4-4. We observe that an output data bit 0 takes the sequence from state S_i to S_{i+1}, $i \leq \kappa$. The output data bit 1 takes the sequence to state S_1. The output bit from the encoder may be a 1 only when the sequence is in state S_i, $d + 1 \leq i \leq \kappa + 1$. When the sequence is in state $S_{\kappa+1}$, the output bit is always 1.

FIGURE 9-4-4 Finite-state sequential machine for a (d, κ)-coded sequence.

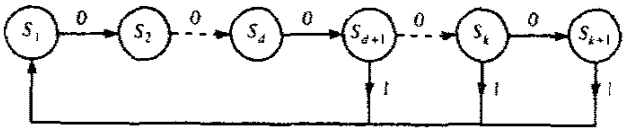

†In fact, they are usually called (d, k) codes, where k is the maximum runlength of zeros. We have substituted the Greek letter kappa κ for k, to avoid confusion with our previous use of k.

The finite-state sequential machine may also be represented by a *state transition matrix*, denoted as **D**, which is a square $(\kappa+1)\times(\kappa+1)$ with elements d_{ij}, where

$$d_{i1} = 1 \quad (i \geq d+1)$$
$$d_{ij} = \begin{cases} 1 & (j = i+1) \\ 0 & (\text{otherwise}) \end{cases} \tag{9-4-2}$$

Example 9-4-1

Let us determine the state transition matrix for a $(d, \kappa) = (1, 3)$ code. The $(1, 3)$ code has four states. From Fig. 9-4-4, we obtain its state transition matrix, which is

$$\mathbf{D} = \begin{bmatrix} 0 & 1 & 0 & 0 \\ 1 & 0 & 1 & 0 \\ 1 & 0 & 0 & 1 \\ 1 & 0 & 0 & 0 \end{bmatrix} \tag{9-4-3}$$

An important parameter of any (d, κ) code is the number of sequences of a certain length, say n, that satisfy the (d, κ) constraints. As n is allowed to increase, the number of sequences $N(n)$ that satisfy the (d, κ) constraint also increases. The number of information bits that can be uniquely represented with $N(n)$ code sequences is

$$k = \lfloor \log_2 N(n) \rfloor$$

where $\lfloor x \rfloor$ denotes the largest integer contained in x. The maximum code rate is then $R_c = k/n$.

The capacity of a (d, κ) code is defined as

$$C(d, \kappa) = \lim_{n \to \infty} \frac{1}{n} \log_2 N(n) \tag{9-4-4}$$

Clearly, $C(d, \kappa)$ is the maximum possible rate that can be achieved with the (d, κ) constraints. Shannon (1948) showed that the capacity is given as

$$C(d, \kappa) = \log_2 \lambda_{\max} \tag{9-4-5}$$

where $\lambda_{\max}$ is the largest real eigenvalue of the state transition matrix **D**.

Example 9-4-2

Let us determine the capacity of a $(d, \kappa) = (1, 3)$ code. Using the state-transition matrix given in Example 9-4-1 for the $(1, 3)$ code, we have

$$\det(\mathbf{D} - \lambda \mathbf{I}) = \det \begin{bmatrix} -\lambda & 1 & 0 & 0 \\ 1 & -\lambda & 1 & 0 \\ 1 & 0 & -\lambda & 1 \\ 1 & 0 & 0 & -\lambda \end{bmatrix}$$
$$= \lambda^4 - \lambda^2 - \lambda - 1 = 0 \tag{9-4-6}$$

TABLE 9-4-1 CAPACITY $C(d, \kappa)$ VERSUS RUNLENGTH PARAMETERS d AND κ

κ	$d=0$	$d=1$	$d=2$	$d=3$	$d=4$	$d=5$	$d=6$
2	.8791	.4057					
3	.9468	.5515	.2878				
4	.9752	.6174	.4057	.2232			
5	.9881	.6509	.4650	.3218	.1823		
6	.9942	.6690	.4979	.3746	.2269	.1542	
7	.9971	.6793	.5174	.4057	.3142	2281	.1335
8	.9986	.6853	.5293	.4251	.3432	.2709	.1993
9	.9993	.6888	.5369	.4376	.3620	.2979	.2382
10	.9996	.6909	.5418	.4460	.3746	.3158	.2633
11	.9998	.6922	.5450	.4516	.3833	.3285	.2804
12	.9999	.6930	.5471	.4555	.3894	.3369	.2924
13	.9999	.6935	.5485	.4583	.3937	.3432	.3011
14	.9999	.6938	.5495	.4602	.3968	.3478	.3074
15	.9999	.6939	.5501	.4615	.3991	.3513	.3122
∞	1.000	.6942	.5515	.4650	.4057	.3620	.3282

The maximum real root of this polynomial is found to be $\lambda_{max} = 1.4656$. Therefore, the capacity $C(1, 3) = \log_2 \lambda_{max} = 0.5515$.

The capacities of (d, κ) codes for $0 \leq d \leq 6$ and $2 \leq \kappa \leq 15$ are given in Table 9-4-1. We observe that $C(d, \kappa) < \frac{1}{2}$ for $d \geq 3$ and any value of κ. The most commonly used codes for magnetic recording employ $d \leq 2$; hence, their rate R_c is at least $\frac{1}{2}$.

Now let us turn our attention to the construction of some runlength-limited codes. In general, (d, κ) codes can be constructed either as fixed-length codes or as variable-length codes. In a fixed-length code, each bit or block of k bits is encoded into a block of $n > k$ bits.

In principle, the construction of a fixed-length code is straightforward. For a given block length n, we may select the subset of the 2^n code words that satisfy the specified runlength constraints. From this subset, we eliminate code words that do not satisfy the runlength constraints when concatenated. Thus, we obtain a set of code words that satisfy the constraints and can be used in the mapping of the input data bits to the encoder. The encoding and decoding operations can be performed by use of a look-up table.

Example 9-4-3

Let us construct a $d = 0$, $\kappa = 2$ code of length $n = 3$, and determine its efficiency. By listing all the code words, we find that the following five code words satisfy the (0, 2) constraint: (0 1 0), (0 1 1), (1 0 1), (1 1 0), (1 1 1). We may select any four of these code words and use then to encode the pairs of

data bits (00, 01, 10, 11). Thus, we have a rate $k/n = 2/3$ code that satisfies the $(0, 2)$ constraint.

The fixed-length code in this example is not very efficient. The capacity is $C(0, 2) = 0.8791$, so that this code has an *efficiency* of

$$\text{efficiency} = \frac{R_c}{C(d, \kappa)} = \frac{2/3}{0.8791} = 0.76$$

Surely, better $(0, 2)$ codes can be constructed by increasing the block length n.

In the following example, we place no restriction on the maximum runlength of zeros.

Example 9-4-4

Let us construct a $d = 1$, $\kappa = \infty$ code of length $n = 5$. In this case, we are placing no constraint on the number of consecutive zeros. To construct the code, we select from the set of 32 possible code words those that satisfy the $d = 1$ constraint. There are eight such code words, which implies that we can encode three information bits with each code word. The code is given in Table 9-4-2. Note that the first bit of each code word is a 0, whereas the last bit may be either 0 or 1. Consequently, the $d = 1$ constraint is satisfied when these code words are concatenated. This code has a rate $R_c = 3/5$. When compared with the capacity $C(1, \infty) = 0.6942$ obtained from Table 9-4-1, the code efficiency is 0.864, which is quite acceptable.

The code construction method described in the two examples above produces fixed-length (d, κ) codes that are *state-independent*. By state-independent, we mean that fixed-length code words can be concatenated without violating the (d, κ) constraints. In general, fixed-length state-independent (d, κ) codes require large block lengths, except in cases such as those in the examples above where d is small. Simpler (shorter-length) codes

TABLE 9-4-2 FIXED LENGTH $d = 1$, $\kappa = \infty$ CODE

Input data bits	Output coded sequence
0 0 0	0 0 0 0 0
0 0 1	0 0 0 0 1
0 1 0	0 0 0 1 0
0 1 1	0 0 1 0 0
1 0 0	0 0 1 0 1
1 0 1	0 1 0 0 0
1 1 0	0 1 0 0 1
1 1 1	0 1 0 1 0

are generally possible by allowing for state-dependence and for variable length code words. Below, we consider codes for which both the input blocks to the encoder and the output blocks may have variable length. For the code words to be uniquely decodable at the receiver, the variable-length code should satisfy the prefix condition, described in Chapter 3.

Example 9-4-5

A very simple uniquely decodable variable-length $d = 0$, $\kappa = 2$ code is

$$0 \rightarrow 01$$
$$10 \rightarrow 10$$
$$11 \rightarrow 11$$

The code in the above example has a fixed output block size but a variable input block size. In general, both the input and output blocks may be variable. The following example illustrates the latter case.

Example 9-4-6

Let us construct a (2, 7) variable block size code. The solution to this code construction is certainly not unique, nor is it trivial. We picked this example because the (2, 7) code has been widely used by IBM in many of its disk storage systems. The code is listed in Table 9-4-3. We observe that the input data blocks of 2, 3, and 4 bits are mapped into output data blocks of 4, 6, and 8 bits, respectively. Hence, the code rate is $R_c = 1/2$. Since this is the code rate for all code words, the code is called a *fixed-rate* code. This code has an efficiency of $0.5/0.5174 = 0.966$. Note that this code satisfies the prefix condition.

TABLE 9-4-3 CODE BOOK FOR VARIABLE-LENGTH (2, 7) CODE

Input data bits	Output coded sequence
1 0	1 0 0 0
1 1	0 1 0 0
0 1 1	0 0 0 1 0 0
0 1 0	0 0 1 0 0 0
0 0 0	1 0 0 1 0 0
0 0 1 1	0 0 1 0 0 1 0 0
0 0 1 0	0 0 0 0 1 0 0 0

TABLE 9-4-4 ENCODER FOR (1, 3) MILLER CODE

Input data bits	Output coded sequence
0	x 0
1	0 1

$x = 0$, if preceding input bit is 1
$x = 1$, if preceding input bit is 0

Another code that has been widely used in magnetic recording is the rate 1/2, $(d, \kappa) = (1, 3)$ code in Table 9-4-4. We observe that when the information bit is a 0, the first output bit is 1 if the previous input bit was 0, or a 0 if the previous input bit was a 1. When the information bit is a 1, the encoder output is 01. Decoding of this code is simple. The first bit of the two-bit block is redundant and may be discarded. The second bit is the information bit. This code is usually called the *Miller code*. We observe that this is a state-dependent code, which is described by the state diagram shown in Fig. 9-4-5. There are two states labeled S_1 and S_2 with transitions as shown in the figure. When the encoder is a state S_1, an input bit 1 results in the encoder staying in state S_1 and outputs 01. This is denoted as 1/01. If the input bit is a 0, the encoder enters state S_2 and outputs 00. This is denoted as 0/00. Similarly, if the encoder is in state S_2, an input bit 0 causes no transition and the encoder output is 10. On the other hand, if the input bit is a 1, the encoder enters state S_1 and outputs 01. Figure 9-4-6 shows the trellis for the Miller code.

The Mapping of Coded Bits into Signal Waveforms The output sequence from a (d, κ) encoder is mapped by the modulator into signal waveforms for transmission over the channel. If the binary digit 1 is mapped into a rectangular pulse of amplitude A and the binary digit 0 is mapped into a

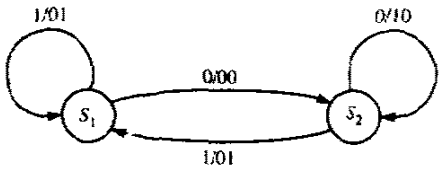

FIGURE 9-4-5 State diagrams for $d = 1$, $\kappa = 3$ (Miller) code.

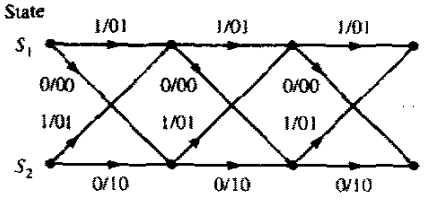

FIGURE 9-4-6 Trellis for $d = 1$, $\kappa = 3$ (Miller) code.

rectangular pulse of amplitude $-A$, the result is a (d, κ) coded NRZ modulated signal. Note that the duration of the rectangular pulses is $T_c = R_c/R_b = R_c T_b$, where R_b is the information (bit) rate into the encoder, T_b is the corresponding (uncoded) bit interval, and R_c is the code rate for the (d, κ) code.

When the (d, κ) code is a state-independent fixed-length code with code rate $R_c = k/n$, we may consider each n-bit block as generating one signal waveform of duration nT_c. Thus, we have $M = 2^k$ signal waveforms, one for each of the 2^k possible k-bit data blocks. These coded waveforms have the general form given by (4-3-6) and (4-3-38). In this case, there is no dependence between the transmission of successive waveforms.

In contrast to the situation considered above, the modulation signal is no longer memoryless when NRZI is used and/or the (d, κ) code is state-dependent. Let us consider the effect of mapping the coded bits into an NRZI signal waveform.

Recall that the state dependence in the NRZI signal is due to the differential encoding of the information sequence. The differential encoding is a form of precoding, which is described mathematically as

$$p_k = d_k \oplus p_{k-1}$$

where $\{d_k\}$ is the binary sequence into the precoder, $\{p_k\}$ is the output binary sequence from the precoder, and $\oplus$ denotes modulo-2 addition. This encoding is characterized by the state diagram shown in Fig. 9-4-7(a). Then, the sequence $\{p_k\}$ is transmitted by NRZ. Thus, when $p_k = 1$, the modulator output is a rectangular pulse of amplitude A, and when $p_k = 0$, the modulator

FIGURE 9-4-7 State and trellis diagrams for NRZI signal.

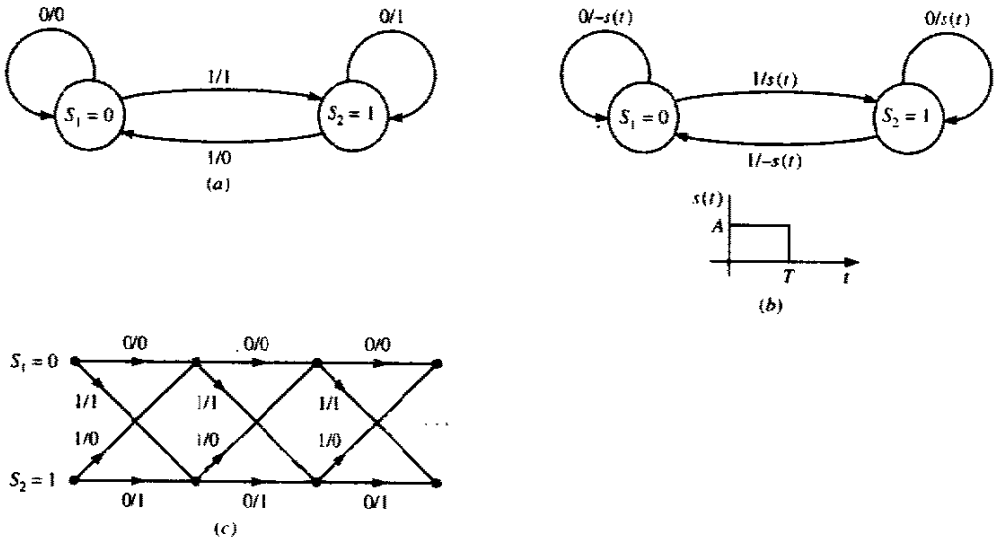

output is a rectangular pulse of amplitude $-A$. When the signal waveforms are superimposed on the state diagram of Fig. 9-4-7(a), we obtain the corresponding state diagram shown in Fig. 9-4-7(b). The corresponding trellis is shown in Fig. 9-4-7(c).

When the output of a state-dependent (d, κ) encoder is followed by an NRZI modulator, we may simply combine the two-state diagrams into a single-state diagram for the (d, κ) code with precoding. A similar combination can be performed with the corresponding trellises. The following example illustrates the approach for the (1, 3) Miller code followed by NRZI modulation.

Example 9-4-7

Let us determine the state diagram of the combined (1, 3) Miller code followed by the precoding inherent in NRZI modulation. Since the (1, 3) Miller code has two states and the precoder has two states, the state diagram for the combined encoder has four states, which we denote as $(S_M, S_N) = (\sigma_1, s_1), (\sigma_1, s_2), (\sigma_2, s_1), (\sigma_2, s_2)$, where $S_M = \{\sigma_1, \sigma_2\}$ represents the two states of the Miller code and $S_N = \{s_1, s_2\}$ represents the two states of the precoder for NRZI. For each data input bit into the Miller encoder, we obtain two output bits which are then precoded to yield two precoded output bits. The resulting state diagram is shown in Fig. 9-4-8, where the first bit denotes the information bit into the Miller encoder and the next two bits represent the corresponding output of the precoder.

The trellis diagram for the Miller precoded sequence may be obtained directly from the combined state diagram or from a combination of the trellises of the two codes. The result of this combination is the four-state trellis, one stage of which is shown in Fig. 9-4-9.

It is left as an exercise for the reader to show that the four signal waveforms obtained by mapping each pair of bits of the Miller-precoded sequence into an

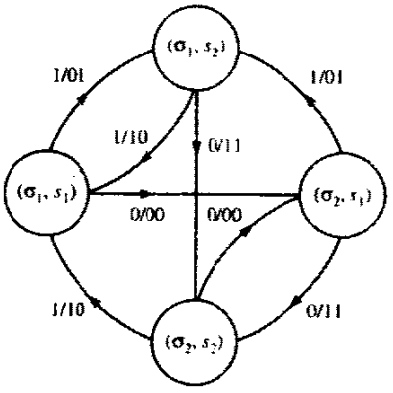

FIGURE 9-4-8 State diagram of the Miller code followed by the precoder.

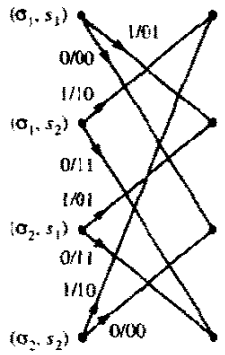

FIGURE 9-4-9 One stage of trellis diagram for the Miller code followed by the precoder.

NRZ signal are biorthogonal and that the resulting modulated signal waveform is identical to the delay modulation that was described in Section 4-3-2.

From the state diagram of a state-dependent runlength-limited code, one can obtain the transition probability matrix, as described in Section 4-3-2. Then, the power spectral density of the code may be determined, as shown in Section 4-4-3.

9-5 BIBLIOGRAPHICAL NOTES AND REFERENCES

The pioneering work on signal design for bandwidth-constrained channels was done by Nyquist (1928). The use of binary partial response signals was originally proposed by Lender (1963), and was later generalized by Kretzmer (1966). Other early work on problems dealing with intersymbol interference (ISI) and transmitter and receiver optimization with constraints on ISI was done by Gerst and Diamond (1961), Tufts (1965), Smith (1965), and Berger and Tufts (1967). "Faster than Nyquist" transmission has been studied by Mazo (1975) and Foschini (1984).

Modulation codes were also first introduced by Shannon (1948). Some of the early work on the construction of runlength-limited codes is found in the papers by Freiman and Wyner (1964), Gabor (1967), Franaszek (1968, 1969, 1970), Tang and Bahl (1970), and Jacoby (1977). More recent work is found in papers by Adler Coppersmith and Hassner (1983), and Karabed and Siegel (1991). The motivation for most of the work on runlength-limited codes was provided by applications to magnetic and optical recording. A well-written tutorial paper on runlength-limited codes has been published by Immink (1990).

PROBLEMS

9-1 A channel is said to be *distortionless* if the response $y(t)$ to an input $x(t)$ is $Kx(t - t_0)$, where K and t_0 are constants. Show that if the frequency response of the channel is $A(f)e^{j\theta(f)}$, where $A(f)$ and $\theta(f)$ are real, the necessary and

sufficient conditions for distortionless transmission are $A(f) = K$ and $\theta(f) = 2\pi f t_0 \pm n\pi$, $n = 0, 1, 2, \ldots$.

9-2 The raised-cosine spectral characteristic is given by (9-2-26).

a Show that the corresponding impulse response is

$$x(t) = \frac{\sin(\pi t/T)}{\pi t/T} \frac{\cos(\beta \pi t/T)}{1 - 4\beta^2 t^2/T^2}$$

b Determine the Hilbert transform of $x(t)$ when $\beta = 1$.

c Does $\hat{x}(t)$ possess the desirable properties of $x(t)$ that make it appropriate for data transmission? Explain.

d Determine the envelope of the SSB suppressed-carrier signal generated from $x(t)$.

9-3 **a** Show that (Poisson sum formula)

$$x(t) = \sum_{k=-\infty}^{\infty} g(t)h(t - kT) \Rightarrow X(f) = \frac{1}{T} \sum_{n=-\infty}^{\infty} H\left(\frac{n}{T}\right) G\left(f - \frac{n}{T}\right)$$

Hint: Make a Fourier-series expansion of the periodic factor

$$\sum_{k=-\infty}^{\infty} h(t - kT)$$

b Using the result in (a), verify the following versions of the Poisson sum:

$$\sum_{k=-\infty}^{\infty} h(kT) = \frac{1}{T} \sum_{n=-\infty}^{\infty} H\left(\frac{n}{T}\right) \tag{i}$$

$$\sum_{k=-\infty}^{\infty} h(t - kT) = \frac{1}{T} \sum_{n=-\infty}^{\infty} H\left(\frac{n}{T}\right) \exp\left(\frac{j2\pi nt}{T}\right) \tag{ii}$$

$$\sum_{k=-\infty}^{\infty} h(kT) \exp(-j2\pi kTf) = \frac{1}{T} \sum_{n=-\infty}^{\infty} H\left(f - \frac{n}{T}\right) \tag{iii}$$

c Derive the condition for no intersymbol interference (Nyquist criterion) by using the Poisson sum formula.

9-4 Suppose a digital communications system employs gaussian-shaped pulses of the form

$$x(t) = \exp(-\pi a^2 t^2)$$

To reduce the level of intersymbol interference to a relatively small amount, we impose the condition that $x(T) = 0.01$, where T is the symbol interval. The bandwidth W of the pulse $x(t)$ is defined as that value of W for which $X(W)/X(0) = 0.01$, where $X(f)$ is the Fourier transform of $x(t)$. Determine the value of W and compare this value to that of raised-cosine spectrum with 100% rolloff.

9-5 A band-limited signal having bandwidth W can be represented as

$$x(t) = \sum_{n=-\infty}^{\infty} x_n \frac{\sin[2\pi W(t - n/2W)]}{2\pi W(t - n/2W)}$$

a Determine the spectrum $X(f)$ and plot $|X(f)|$ for the following cases:

$$x_0 = 2, \quad x_1 = 1, \quad x_2 = -1, \quad x_n = 0, \quad n \neq 0, 1, 2 \tag{i}$$

$$x_{-1} = -1, \quad x_0 = 2, \quad x_1 = -1, \quad x_n = 0, \quad n \neq -1, 0, 1 \tag{ii}$$

b Plot $x(t)$ for these two cases.

c If these signals are used for binary signal transmission, determine the number of received levels possible at the sampling instants $t = nT = n/2W$, and the probabilities of occurrence of the received levels. Assume that the binary digits at the transmitter are equally probable.

9-6 A 4 kHz bandpass channel is to be used for transmission of data at a rate of 9600 bits/s. If $\frac{1}{2}N_0 = 10^{-10}$ W/Hz is the spectral density of the additive, zero-mean gaussian noise in the channel, design a QAM modulation and determine the average power that achieves a bit error probability of 10^{-6}. Use a signal pulse with a raised-cosine spectrum having a roll-off factor of at least 50%.

9-7 Determine the bit rate that can be transmitted through a 4 kHz voice-band telephone (bandpass) channel if the following modulation methods are used: (a) binary PAM; (b) four-phase PSK; (c) 8-point QAM; (d) binary orthogonal FSK, with noncoherent detection; (e) orthogonal four-FSK with noncoherent detection; (f) orthogonal 8-FSK with noncoherent detection. For (a)–(c), assume that the transmitter pulse shape has a raised-cosine spectrum with a 50% roll-off.

9-8 An ideal voice-band telephone line channel has a bandpass frequency response characteristic spanning the frequency range 600–3000 Hz.

a Design an $M = 4$ PSK (quadrature PSK or QPSK) system for transmitting data at a rate of 2400 bits/s and a carrier frequency $f_c = 1800$ Hz. For spectral shaping, use a raised-cosine frequency-response characteristic. Sketch a block diagram of the system and describe the functional operation of each block.

b Repeat (a) for a bit rate $R = 4800$ bits/s.

9-9 A voice-band telephone channel passes the frequencies in the band from 300 to 3300 Hz. It is desired to design a modem that transmits at a symbol rate of 2400 symbols/s, with the objective of achieving 9600 bits/s. Select an appropriate QAM signal constellation, carrier frequency, and the roll-off factor of a pulse with a raised cosine spectrum that utilizes the entire frequency band. Sketch the spectrum of the transmitted signal pulse and indicate the important frequencies.

9-10 A communication system for a voice-band (3 kHz) channel is designed for a received SNR at the detector of 30 dB when the transmitter power is $P_S = -3$ dBW. Determine the value of P_S if it is desired to expand the bandwidth of the system to 10 kHz, while maintaining the same SNR at the detector.

9-11 Show that a pulse having the raised cosine spectrum given by (9-2-26) satisfies the Nyquist criterion given by (9-2-13) for any value of the roll-off factor β.

9-12 Show that, for any value of β, the raised cosine spectrum given by (9-2-26) satisfies

$$\int_{-\infty}^{\infty} X_{rc}(f)\, df = 1$$

[*Hint:* Use the fact that $X_{rc}(f)$ satisfies the Nyquist criterion given by (9-2-13).]

9-13 The Nyquist criterion gives the necessary and sufficient condition for the spectrum $X(f)$ of the pulse $x(t)$ that yields zero ISI. Prove that for any pulse that is band-limited to $|f| < 1/T$, the zero-ISI condition is satisfied if Re $[X(f)]$, for $f > 0$, consists of a rectangular function plus an arbitrary odd function around $f = 1/2T$, and Im $[X(f)]$ is any arbitrary even function around $f = 1/2T$.

9-14 A voice-band telephone channel has a passband characteristic in the frequency range 300 Hz $< f <$ 3000 Hz.

a Select a symbol rate and a power efficient constellation size to achieve 9600 bits/s signal transmission.

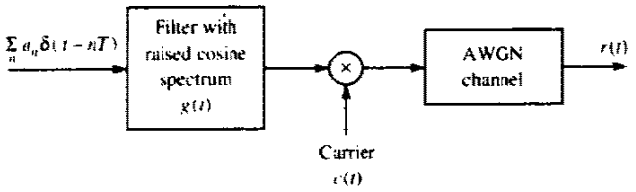

FIGURE P9-16

b If a square-root raised cosine pulse is used for the transmitter pulse $g(t)$, select the roll-off factor. Assume that the channel has an ideal frequency response characteristic.

9-15 Design an M-ary PAM system that transmits digital information over an ideal channel with bandwidth $W = 2400$ Hz. The bit rate is 14 400 bit/s. Specify the number of transmitted points, the number of received signal points using a duobinary signal pulse, and the required $\mathscr{E}_b$ to achieve an error probability of 10^{-6}. The additive noise is zero-mean gaussian with a power spectral density 10^{-4} W/Hz.

9-16 A binary PAM signal is generated by exciting a raised cosine roll-off filter with a 50% roll-off factor and is then DSB-SC amplitude-modulated on a sinusoidal carrier as illustrated in Fig. P9-16. The bit rate is 2400 bit/s.

a Determine the spectrum of the modulated binary PAM signal and sketch it.

b Draw the block diagram illustrating the optimum demodulator/detector for the received signal, which is equal to the transmitted signal plus additive white gaussian noise.

9-17 The elements of the sequence $\{a_n\}_{n=-\infty}^{\infty}$ are independent binary random variables taking values of ± 1 with equal probability. This data sequence is used to modulate the basic pulse $g(t)$ shown in Fig. P9-17(a). The modulated signal is

$$X(t) = \sum_{n=-\infty}^{+\infty} a_n g(t - nT)$$

a Find the power spectral density of $X(t)$.

b If $g_1(t)$ (shown in Fig. 9-17b) is used instead of $g(t)$, how would the power spectrum in (a) change?

c In (b) assume we want to have a null in the spectrum at $f = 1/3T$. This is done by a precoding of the form $b_n = a_n + \alpha a_{n-3}$. Find the α that provides the desired null.

d Is it possible to employ a precoding of the form $b_n = a_n + \sum_{i=1}^{N} \alpha_i a_{n-i}$ for some finite N such that the final power spectrum will be identical to zero for $1/3T \leq |f| \leq 1/2T$? If yes, how? If no, why? [*Hint:* Use properties of analytic functions.]

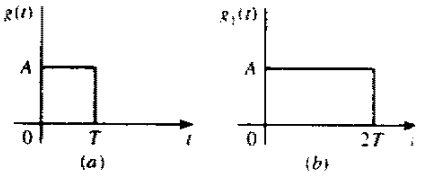

FIGURE P9-17

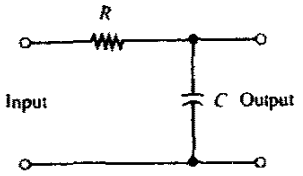

FIGURE P9-22

9-18 Consider the transmission of data via PAM over a voice-band telephone channel that has a bandwidth of 3000 Hz. Show how the symbol rate varies as a function of the excess bandwidth. In particular, determine the symbol rate for an excess bandwidth of 25%, 33%, 50%, 67%, 75%, and 100%.

9-19 The binary sequence 10010110010 is the input to a precoder whose output is used to modulate a duobinary transmitting filter. Construct a table as in Table 9-2-1 showing the precoded sequence, the transmitted amplitude levels, the received signal levels and the decoded sequence.

9-20 Repeat Problem 9-19 for a modified duobinary signal pulse.

9-21 A precoder for a partial response signal fails to work if the desired partial response at $n = 0$ is zero modulo M. For example, consider the desired response for $M = 2$:

$$x(nT) = \begin{cases} 2 & (n = 0) \\ 1 & (n = 1) \\ -1 & (n = 2) \\ 0 & \text{(otherwise)} \end{cases}$$

Show why this response cannot be precoded.

9-22 Consider the RC lowpass filter shown in Fig. P9-22, where $\tau = RC = 10^{-6}$.

a Determine and sketch the envelope (group) delay of the filter as a function of frequency.

b Suppose that the input to the filter is a lowpass signal of bandwidth $\Delta f = 1$ kHz. Determine the effect of the RC filter on this signal.

9-23 A microwave radio channel has a frequency response

$$C(f) = 1 + 0.3 \cos 2\pi fT$$

Determine the frequency response characteristic of the optimum transmitting and receiving filters that yield zero ISI at a rate of $1/T$ symbols/s and have a 50% excess bandwidth. Assume that the additive noise spectrum is flat.

9-24 $M = 4$ PAM modulation is used for transmitting at a bit rate of 9600 bit/s on a channel having a frequency response

$$C(f) = \frac{1}{1 + j(f/2400)}$$

for $|f| \leq 2400$, and $C(f) = 0$ otherwise. The additive noise is zero-mean, white Gaussian with power spectral density $\frac{1}{2}N_0$ W/Hz. Determine the (magnitude) frequency response characteristic of the optimum transmitting and receiving filters.

9-25 Determine the capacity of a $(0, 1)$ runlength-limited code. Compare its capacity with that of a $(1, \infty)$ code and explain the relationship.

9-26 A ternary signal format is designed for a channel that does not pass d.c. The

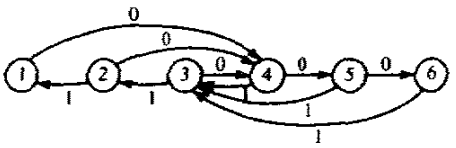

FIGURE P9-31

binary input information sequence is transmitted by mapping a 1 into either a positive pulse or a negative pulse, and a zero is transmitted by the absence of a pulse. Hence, for the transmission of 1s, the polarity of the pulses alternate. This is called an AMI (alternate mark inversion) code. Determine the capacity of the code.

9-27 Give an alternative description of the AMI code described in Problem 9-26 using the running digit sum (RDS) with the constraint that the RDS can take only the values 0 and +1.

9-28 (kBnT codes) From Problem 9-26, note that the AMI code is a "pseudo-ternary" code in that it transmits one bit per symbol using a ternary alphabet, which has the capacity of $\log_2 3 = 1.58$ bits. Such a code does not provide sufficient spectral shaping. Better spectral shaping is achieved by the class of block codes designated as kBnT, where k denotes the number of information bits and n denotes the number of ternary symbols per block. By selecting the largest k possible for each n, we obtain the following table:

k	n	Code
1	1	1B1T
3	2	3B2T
4	3	4B3T
6	4	6B4T

Determine the efficiency of these codes by computing the ratio of the code in bits/symbol divided by $\log_2 3$. Note that 1B1T is the AMI code.

9-29 This problem deals with the capacity of two (d, κ) codes.

a Determine the capacity of a (d, κ) code that has the following state transition matrix:

$$\mathbf{D} = \begin{bmatrix} 1 & 1 \\ 1 & 0 \end{bmatrix}$$

b Repeat (a) for

$$\mathbf{D} = \begin{bmatrix} 1 & 1 \\ 0 & 1 \end{bmatrix}$$

c Comment on the differences between (a) and (b).

9-30 A simplified model of the telegraph code consists of two symbols (Blahut, 1990). A dot consists of one time unit of line closure followed by one time unit of line

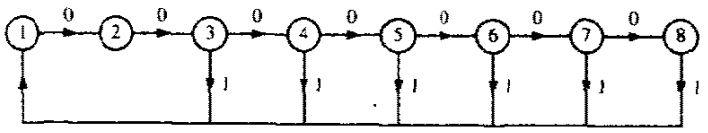

FIGURE P9-32

open. A dash consists of three units of line closure followed by one time unit of line open.

a Viewing this code as a constrained code with symbols of equal duration, give the constraints.

b Determine the state-transition matrix.

c Determine the capacity.

9-31 Determine the state-transition matrix for the runlength-constrained code described by the state diagram shown in Fig. P9-31. Sketch the corresponding trellis.

9-32 Determine the state-transition matrix for the $(2, 7)$ runlength-limited code specified by the state diagram shown in Fig. P9-32.

10

COMMUNICATION THROUGH BAND-LIMITED LINEAR FILTER CHANNELS

In Chapter 9, we focused on the design of the modulator and demodulator filters for band-limited channels. The design procedure was based on the assumption that the (ideal or non-ideal) channel response characteristic $C(f)$ was known a priori. However, in practical digital communications systems that are designed to transmit at high speed through band-limited channels, the frequency response $C(f)$ of the channel is not known with sufficient precision to design optimum filters for the modulator and demodulator. For example, in digital communication over the dial-up telephone network, the communication channel will be different every time we dial a number, because the channel route will be different. This is an example of a channel whose characteristics are unknown a priori. There are other types of channels, e.g., wireless channels such as radio channels and underwater acoustic channels, whose frequency response characteristics are time-variant. For such channels, it is not possible to design optimum fixed demodulation filters.

In this chapter, we consider the problem of receiver design in the presence of channel distortion, which is not known a priori, and AWGN. The channel distortion results in intersymbol interference, which, if left uncompensated, causes high error rates. The solution to the ISI problem is to design a receiver that employs a means for compensating or reducing the ISI in the received signal. The compensator for the ISI is called an *equalizer*.

Three types of equalization methods are treated in this chapter. One is based on the maximum-likelihood (ML) sequence detection criterion, which is optimum from a probability of error viewpoint. A second equalization method is based on the use of a linear filter with adjustable coefficients. The third equalization method that is described exploits the use of previous detected

symbols to suppress the ISI in the present symbol being detected, and it is called *decision-feedback equalization*. We begin with the derivation of the optimum detector for channels with ISI.

10-1 OPTIMUM RECEIVER FOR CHANNELS WITH ISI AND AWGN

In this section, we derive the structure of the optimum demodulator and detector for digital transmission through a nonideal, band-limited channel with additive gaussian noise. We begin with the transmitted (equivalent lowpass) signal given by (9-2-1). The received (equivalent lowpass) signal is expressed as

$$r_l(t) = \sum_n I_n h(t - nT) + z(t) \tag{10-1-1}$$

where $h(t)$ represents the response of the channel to the input signal pulse $g(t)$ and $z(t)$ represents the additive white gaussian noise.

First we demonstrate that the optimum demodulator can be realized as a filter matched to $h(t)$, followed by a sampler operating at the symbol rate $1/T$ and a subsequent processing algorithm for estimating the information sequence $\{I_n\}$ from the sample values. Consequently, the samples at the output of the matched filter are sufficient for the estimation of the sequence $\{I_n\}$.

10-1-1 Optimum Maximum-Likelihood Receiver

Let us expand the received signal $r_l(t)$ in the series

$$r_l(t) = \lim_{N\to\infty} \sum_{k=1}^{N} r_k f_k(t) \tag{10-1-2}$$

where $\{f_k(t)\}$ is a complete set of orthonormal functions and $\{r_k\}$ are the observable random variables obtained by projecting $r_l(t)$ onto the set $\{f_k(t)\}$. It is easily shown that

$$r_k = \sum_n I_n h_{kn} + z_k, \qquad k = 1, 2, \ldots \tag{10-1-3}$$

where h_{kn} is the value obtained from projecting $h(t - nT)$ onto $f_k(t)$, and z_k is the value obtained from projecting $z(t)$ onto $f_k(t)$. The sequence $\{z_k\}$ is gaussian with zero mean and covariance

$$\tfrac{1}{2}E(z_k^* z_m) = N_0 \delta_{km} \tag{10-1-4}$$

The joint probability density function of the random variables

$\mathbf{r}_N \equiv [r_1 \ r_2 \ \dots \ r_N]$ conditioned on the transmitted sequence $\mathbf{I}_p \equiv [I_1 \ I_2 \ \dots \ I_p]$, where $p \leq N$, is

$$p(\mathbf{r}_N \,|\, \mathbf{I}_p) = \left(\frac{1}{2\pi N_0}\right)^N \exp\left(-\frac{1}{2N_0}\sum_{k=1}^{N}\left|r_k - \sum_n I_n h_{kn}\right|^2\right) \tag{10-1-5}$$

In the limit as the number N of observable random variables approaches infinity, the logarithm of $p(\mathbf{r}_N \,|\, \mathbf{I}_p)$ is proportional to the metrics $PM(\mathbf{I}_p)$, defined as

$$\begin{aligned} PM(\mathbf{I}_p) &= -\int_{-\infty}^{\infty}\left|r_l(t) - \sum_n I_n h(t-nT)\right|^2 dt \\ &= -\int_{-\infty}^{\infty}|r_l(t)|^2\,dt + 2\,\mathrm{Re}\sum_n\left[I_n^*\int_{-\infty}^{\infty} r_l(t)h^*(t-nT)\,dt\right] \\ &\quad - \sum_n\sum_m I_n^* I_m \int_{-\infty}^{\infty} h^*(t-nT)h(t-mT)\,dt \end{aligned} \tag{10-1-6}$$

The maximum-likelihood estimates of the symbols $I_1, I_2, \dots, I_p$ are those that maximize this quantity. Note, however, that the integral of $|r_l(t)|^2$ is common to all metrics, and, hence, it may be discarded. The other integral involving $r(t)$ gives rise to the variables

$$y_n \equiv y(nT) = \int_{-\infty}^{\infty} r_l(t)h^*(t-nT)\,dt \tag{10-1-7}$$

These variables can be generated by passing $r(t)$ through a filter matched to $h(t)$ and sampling the output at the symbol rate $1/T$. The samples $\{y_n\}$ form a set of sufficient statistics for the computation of $PM(\mathbf{I}_p)$ or, equivalently, of the correlation metrics

$$CM(\mathbf{I}_p) = 2\,\mathrm{Re}\left(\sum_n I_n^* y_n\right) - \sum_n\sum_m I_n^* I_m x_{n-m} \tag{10-1-8}$$

where, by definition, $x(t)$ is the response of the matched filter to $h(t)$ and

$$x_n \equiv x(nT) = \int_{-\infty}^{\infty} h^*(t)h(t+nT)\,dt \tag{10-1-9}$$

Hence, $x(t)$ represents the output of a filter having an impulse response $h^*(-t)$ and an excitation $h(t)$. In other words, $x(t)$ represents the autocorrelation function of $h(t)$. Consequently, $\{x_n\}$ represents the samples of the autocorrelation function of $h(t)$, taken periodically at $1/T$. We are not particularly concerned with the noncausal characteristic of the filter matched to $h(t)$, since, in practice, we can introduce a sufficiently large delay to ensure causality of the matched filter.

If we substitute for $r_l(t)$ in (10-1-7) using (10-1-1), we obtain

$$y_k = \sum_n I_n x_{k-n} + \nu_k \tag{10-1-10}$$

where v_k denotes the additive noise sequence of the output of the matched filter, i.e.,

$$v_k = \int_{-\infty}^{\infty} z(t)h^*(t - kT)\,dt \tag{10-1-11}$$

The output of the demodulator (matched filter) at the sampling instants is corrupted by ISI as indicated by (10-1-10). In any practical system, it is reasonable to assume that the ISI affects a finite number of symbols. Hence, we may assume that $x_n = 0$ for $|n| > L$. Consequently, the ISI observed at the output of the demodulator may be viewed as the output of a finite state machine. This implies that the channel output with ISI may be represented by a trellis diagram, and the maximum-likelihood estimate of the information sequence $(I_1, I_2, \ldots, I_p)$ is simply the most probable path through the trellis given the received demodulator output sequence $\{y_n\}$. Clearly, the Viterbi algorithm provides an efficient means for performing the trellis search.

The metrics that are computed for the MLSE of the sequence $\{I_k\}$ are given by (10-1-8). It can be seen that these metrics can be computed recursively in the Viterbi algorithm, according to the relation

$$CM_n(\mathbf{I}_n) = CM_{n-1}(\mathbf{I}_{n-1}) + \text{Re}\left[I_n^*\left(2y_n - x_0 I_n - 2\sum_{m=1}^{L} x_m I_{n-m}\right)\right] \tag{10-1-12}$$

Figure 10-1-1 illustrates the block diagram of the optimum receiver for an AWGN channel with ISI.

10-1-2 A Discrete-Time Model for a Channel with ISI

In dealing with band-limited channels that result in ISI, it is convenient to develop an equivalent discrete-time model for the analog (continuous-time) system. Since the transmitter sends discrete-time symbols at a rate $1/T$ symbols/s and the sampled output of the matched filter at the receiver is also a discrete-time signal with samples occurring at a rate $1/T$ per second, it follows that the cascade of the analog filter at the transmitter with impulse response $g(t)$, the channel with impulse response $c(t)$, the matched filter at the receiver with impulse response $h^*(-t)$, and the sampler can be represented by

FIGURE 10-1-1 Optimum receiver for an AWGN channel with ISI.

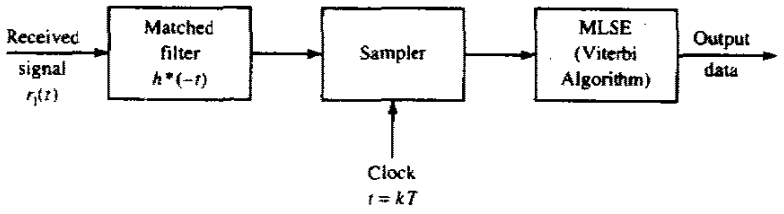

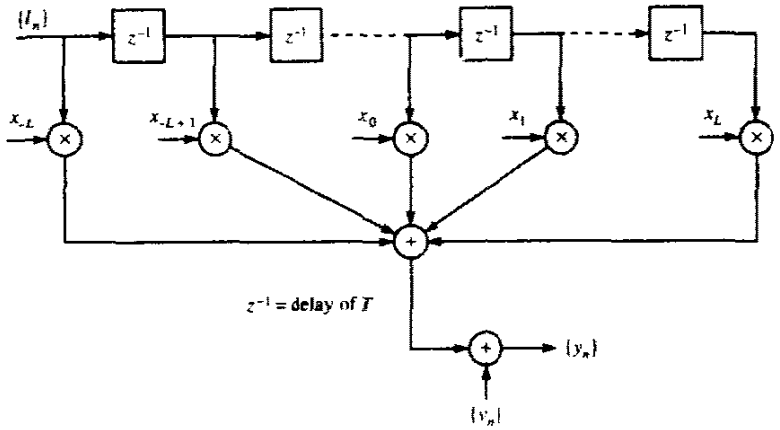

FIGURE 10-1-2 Equivalent discrete-time model of channel with intersymbol interference.

an equivalent discrete-time transversal filter having tap gain coefficients $\{x_k\}$. Consequently, we have an equivalent discrete-time transversal filter that spans a time interval of $2LT$ seconds. Its input is the sequence of information symbols $\{I_k\}$ and its output is the discrete-time sequence $\{y_k\}$ given by (10-1-10). The equivalent discrete-time model is shown in Fig. 10-1-2.

The major difficulty with this discrete-time model occurs in the evaluation of performance of the various equalization or estimation techniques that are discussed in the following sections. The difficulty is caused by the correlations in the noise sequence $\{v_k\}$ at the output of the matched filter. That is, the set of noise variables $\{v_k\}$ is a gaussian-distributed sequence with zero mean and autocorrelation function (see Problem 10-5)

$$\tfrac{1}{2}E(v_k^* v_j) = \begin{cases} N_0 x_{k-j} & (|k-j| \leq L) \\ 0 & (\text{otherwise}) \end{cases} \tag{10-1-13}$$

Hence, the noise sequence is correlated unless $x_k = 0$, $k \neq 0$. Since it is more convenient to deal with the white noise sequence when calculating the error rate performance, it is desirable to whiten the noise sequence by further filtering the sequence $\{y_k\}$. A discrete-time noise-whitening filter is determined as follows.

Let $X(z)$ denote the (two-sided) z transform of the sampled autocorrelation function $\{x_k\}$, i.e.,

$$X(z) = \sum_{k=-L}^{L} x_k z^{-k} \tag{10-1-14}$$

Since $x_k = x_{-k}^*$, it follows that $X(z) = X^*(z^{-1})$ and the $2L$ roots of $X(z)$ have the symmetry that if ρ is a root, $1/\rho^*$ is also a root. Hence, $X(z)$ can be factored and expressed as

$$X(z) = F(z)F^*(z^{-1}) \tag{10-1-15}$$

where $F(z)$ is a polynomial of degree L having the roots $\rho_1, \rho_2, \ldots, \rho_L$ and $F^*(z^{-1})$ is a polynomial of degree L having the roots $1/\rho_1^*, 1/\rho_2^*, \ldots, 1/\rho_L^*$. Then an appropriate noise-whitening filter has a z transform $1/F^*(z^{-1})$. Since there are 2^L possible choices for the roots of $F^*(z^{-1})$, each choice resulting in a filter characteristic that is identical in magnitude but different in phase from other choices of the roots, we propose to choose the unique $F^*(z^{-1})$ having minimum phase, i.e., the polynomial having all its roots inside the unit circle. Thus, when all the roots of $F^*(z^{-1})$ are inside the unit circle, $1/F^*(z^{-1})$ is a physically realizable, stable, recursive discrete-time filter.† Consequently, passage of the sequence $\{y_k\}$ through the digital filter $1/F^*(z^{-1})$ results in an output sequence $\{v_k\}$ that can be expressed as

$$v_k = \sum_{n=0}^{L} f_n I_{k-n} + \eta_k \tag{10-1-16}$$

where $\{\eta_k\}$ is a white gaussian noise sequence and $\{f_k\}$ is a set of tap coefficients of an equivalent discrete-time transversal filter having a transfer function $F(z)$. In general, the sequence $\{v_k\}$ is complex-valued.

In summary, the cascade of the transmitting filter $g(t)$, the channel $c(t)$, the matched filter $h^*(-t)$, the sampler, and the discrete-time noise-whitening filter $1/F^*(z^{-1})$ can be represented as an equivalent discrete-time transversal filter having the set $\{f_k\}$ as its tap coefficients. The additive noise sequence $\{\eta_k\}$ corrupting the output of the discrete-time transversal filter is a white gaussian noise sequence having zero mean and variance N_0. Figure 10-1-3 illustrates the model of the equivalent discrete-time system with white noise. We refer to this model as the *equivalent discrete-time white noise filter model.*

FIGURE 10-1-3 Equivalent discrete-time model of intersymbol interference channel with WGN.

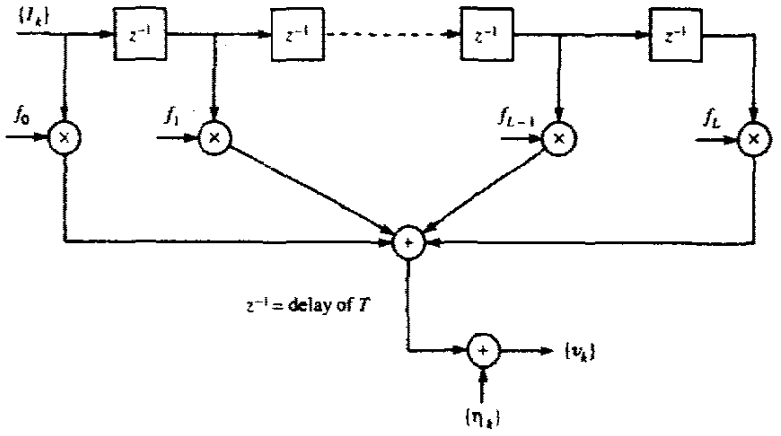

†By removing the stability condition, we can also show $F^*(z^{-1})$ to have roots on the unit circle.

Example 10-1-1

Suppose that the transmitter signal pulse $g(t)$ has duration T and unit energy and the received signal pulse is $h(t) = g(t) + ag(t - T)$. Let us determine the equivalent discrete-time white-noise filter model. The sample autocorrelation function is given by

$$x_k = \begin{cases} a^* & (k = -1) \\ 1 + |a|^2 & (k = 0) \\ a & (k = 1) \end{cases} \tag{10-1-17}$$

The z transform of x_k is

$$\begin{aligned} X(z) &= \sum_{k=-1}^{1} x_k z^{-k} \\ &= a^* z + (1 + |a|^2) + a z^{-1} \\ &= (a z^{-1} + 1)(a^* z + 1) \end{aligned} \tag{10-1-18}$$

Under the assumption that $|a| > 1$, one chooses $F(z) = az^{-1} + 1$, so that the equivalent transversal filter consists of two taps having tap gain coefficients $f_0 = 1$, $f_1 = a$. Note that the correlation sequence $\{x_k\}$ may be expressed in terms of the $\{f_n\}$ as

$$x_k = \sum_{n=0}^{L-k} f_n^* f_{n+k}, \qquad k = 0, 1, 2, \ldots, L \tag{10-1-19}$$

When the channel impulse response is changing slowly with time, the matched filter at the receiver becomes a time-variable filter. In this case, the time variations of the channel/matched-filter pair result in a discrete-time filter with time-variable coefficients. As a consequence, we have time-variable intersymbol interference effects, which can be modeled by the filter illustrated in Fig. 10-1-3, where the tap coefficients are slowly varying with time.

The discrete-time white noise linear filter model for the intersymbol interference effects that arise in high-speed digital transmission over nonideal band-limited channels will be used throughout the remainder of this chapter in our discussion of compensation techniques for the interference. In general, the compensation methods are called *equalization techniques* or *equalization algorithms.*

10-1-3 The Viterbi Algorithm for the Discrete-Time White Noise Filter Model

MLSE of the information sequence $\{I_k\}$ is most easily described in terms of the received sequence $\{v_k\}$ at the output of the whitening filter. In the presence of

intersymbol interference that spans $L + 1$ symbols (L interfering components), the MLSE criterion is equivalent to the problem of estimating the state of a discrete-time finite-state machine. The finite-state machine in this case is the equivalent discrete-time channel with coefficients $\{f_k\}$, and its state at any instant in time is given by the L most recent inputs, i.e., the state at time k is

$$S_k = (I_{k-1}, I_{k-2}, \ldots, I_{k-L}) \tag{10-1-20}$$

where $I_k = 0$ for $k \leq 0$. Hence, if the information symbols are M-ary, the channel filter has M^L states. Consequently, the channel is described by an M^L-state trellis and the Viterbi algorithm may be used to determine the most probable path through the trellis.

The metrics used in the trellis search are akin to the metrics used in soft-decision decoding of convolutional codes. In brief, we begin with the samples $v_1, v_2, \ldots, v_{L+1}$, from which we compute the M^{L+1} metrics

$$\sum_{k=1}^{L+1} \ln p(v_k \mid I_k, I_{k-1}, \ldots, I_{k-L}) \tag{10-1-21}$$

The M^{L+1} possible sequences of $I_{L+1}, I_L, \ldots, I_2, I_1$ are subdivided into M^L groups corresponding to the M^L states $(I_{L+1}, I_L, \ldots, I_2)$. Note that the M sequences in each group (state) differ in I_1 and correspond to the paths through the trellis that merge at a single node. From the M sequences in each of the M^L states, we select the sequence with the largest probability (with respect to I_1) and assign to the surviving sequence the metric

$$\begin{aligned} PM_1(\mathbf{I}_{L+1}) &\equiv PM_1(I_{L+1}, I_L, \ldots, I_2) \\ &= \max_{I_1} \sum_{k=1}^{L+1} \ln p(v_k \mid I_k, I_{k-1}, \ldots, I_{k-L}) \end{aligned} \tag{10-1-22}$$

The $M - 1$ remaining sequences from each of the M^L groups are discarded. Thus, we are left with M^L surviving sequences and their metrics.

Upon reception of v_{L+2}, the M^L surviving sequences are extended by one stage, and the corresponding M^{L+1} probabilities for the extended sequences are computed using the previous metrics and the new increment, which is $\ln p(v_{L+2} \mid I_{L+2}, I_{L+1}, \ldots, I_2)$. Again, the M^{L+1} sequences are subdivided into M^L groups corresponding to the M^L possible states $(I_{L+2}, \ldots, I_3)$ and the most probable sequence from each group is selected, while the other $M - 1$ sequences are discarded.

The procedure described continues with the reception of subsequent signal samples. In general, upon reception of v_{L+k}, the metrics†

$$PM_k(\mathbf{I}_{L+k}) = \max_{I_k} [\ln p(v_{L+k} \mid I_{L+k}, \ldots, I_k) + PM_{k-1}(\mathbf{I}_{L+k-1})] \tag{10-1-23}$$

†We observe that the metrics $PM_k(\mathbf{I})$ are simply related to the euclidean distance metrics $DM_k(\mathbf{I})$ when the additive noise is gaussian.

that are computed give the probabilities of the M^L surviving sequences. Thus, as each signal sample is received, the Viterbi algorithm involves first the computation of the M^{L+1} probabilities

$$\ln p(v_{L+k} \mid I_{L+k}, \ldots, I_k) + PM_{k-1}(\mathbf{I}_{L+k-1}) \tag{10-1-24}$$

corresponding to the M^{L+1} sequences that form the continuations of the M^L surviving sequences from the previous stage of the process. Then the M^{L+1} sequences are subdivided into M^L groups, with each group containing M sequences that terminate in the same set of symbols $I_{L+k}, \ldots, I_{k+1}$ and differ in the symbol I_k. From each group of M sequences, we select the one having the largest probability as indicated by (10-1-23), while the remaining $M-1$ sequences are discarded. Thus, we are left again with M^L sequences having the metrics $PM_k(\mathbf{I}_{L+k})$.

As indicated previously, the delay in detecting each information symbol is variable. In practice, the variable delay is avoided by truncating the surviving sequences to the q most recent symbols, where $q \gg L$, thus achieving a fixed delay. In the case that the M^L surviving sequences at time k disagree on the symbol I_{k-q}, the symbol in the most probable sequence may be chosen. The loss in performance resulting from this suboptimum decision procedure is negligible if $q \geq 5L$.

Example 10-1-2

For illustrative purposes, suppose that a duobinary signal pulse is employed to transmit four-level ($M = 4$) PAM. Thus, each symbol is a number selected from the set $\{-3, -1, 1, 3\}$. The controlled intersymbol interference in this partial response signal is represented by the equivalent discrete-time channel model shown in Fig. 10-1-4. Suppose we have received v_1 and v_2, where

$$\begin{aligned} v_1 &= I_1 + \eta_1 \\ v_2 &= I_2 + I_1 + \eta_2 \end{aligned} \tag{10-1-25}$$

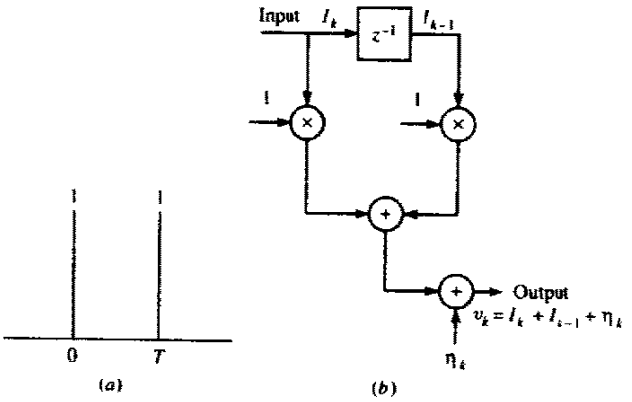

FIGURE 10-1-4 Equivalent discrete-time model for intersymbol interference resulting from a duobinary pulse.

and $\{\eta_i\}$ is a sequence of statistically independent zero-mean gaussian noise. We may now compute the 16 metrics

$$PM_1(I_2, I_1) = -\sum_{k=1}^{2}\left(v_k - \sum_{j=0}^{1} I_{k-j}\right)^2, \qquad I_1, I_2 = \pm 1, \pm 3 \qquad (10\text{-}1\text{-}26)$$

where $I_k = 0$ for $k \leq 0$.

Note that any subsequently received signals $\{v_i\}$ do not involve I_1. Hence, at this stage, we may discard 12 of the 16 possible pairs $\{I_1, I_2\}$. This step is illustrated by the tree diagram shown in Fig. 10-1-5. In other words, after computing the 16 metrics corresponding to the 16 paths in the tree diagram,

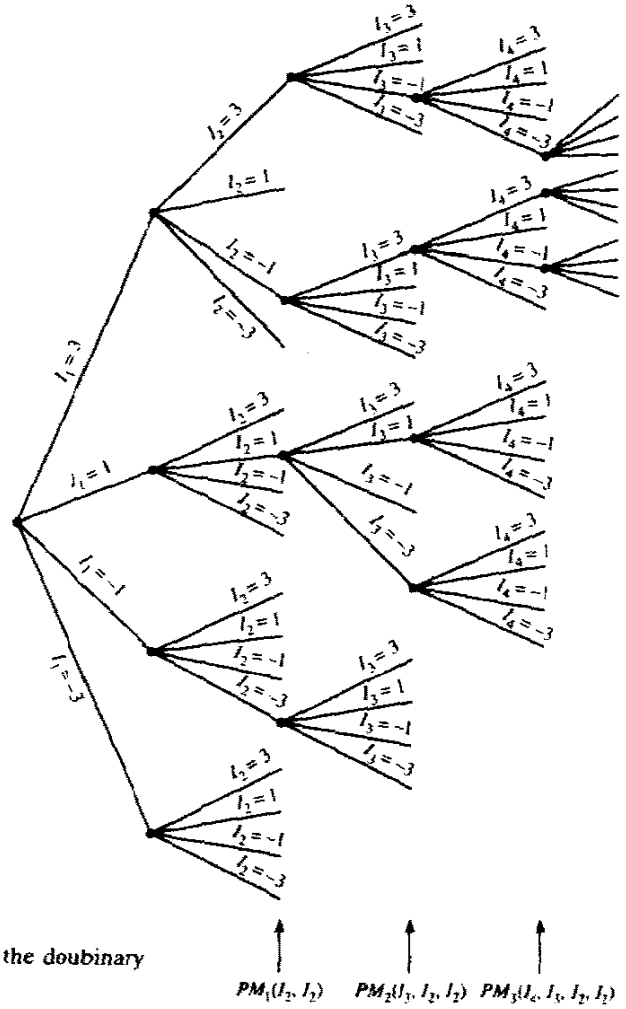

FIGURE 10-1-5 *Tree diagram for Viterbi decoding of the doubinary pulse.*

we discard three out of the four paths that terminate with $I_2 = 3$ and save the most probable of these four. Thus, the metric for the surviving path is

$$PM_1(I_2 = 3, I_1) = \max_{I_1} \left[-\sum_{k=1}^{2} \left(v_k - \sum_{j=0}^{1} I_{k-j} \right)^2 \right]$$

The process is repeated for each set of four paths terminating with $I_2 = 1$, $I_2 = -1$, and $I_2 = -3$. Thus four paths and their corresponding metrics survive after v_1 and v_2 are received.

When v_3 is received, the four paths are extended as shown in Fig. 10-1-5, to yield 16 paths and 16 corresponding metrics, given by

$$PM_2(I_3, I_2, I_1) = PM_1(I_2, I_1) - \left(v_3 - \sum_{j=0}^{1} I_{3-j} \right)^2 \qquad (10\text{-}1\text{-}27)$$

Of the four paths terminating with the $I_3 = 3$, we save the most probable. This procedure is again repeated for $I_3 = 1$, $I_3 = -1$, and $I_3 = -3$. Consequently, only four paths survive at this stage. The procedure is then repeated for each subsequently received signal v_k for $k > 3$.

10-1-4 Performance of MLSE for Channels with ISI

We shall now determine the probability of error for MLSE of the received information sequence when the information is transmitted via PAM and the additive noise is gaussian. The similarity between a convolutional code and a finite-duration intersymbol interference channel implies that the method for computing the error probability for the latter carries over from the former. In particular, the method for computing the performance of soft-decision decoding of a convolutional code by means of the Viterbi algorithm, described in Section 8-2-3, applies with some modification.

In PAM signaling with additive gaussian noise and intersymbol interference, the metrics used in the Viterbi algorithm may be expressed as in (10-1-23), or equivalently, as

$$PM_{k-L}(\mathbf{I}_k) = PM_{k-L-1}(\mathbf{I}_{k-1}) - \left(v_k - \sum_{j=0}^{L} f_j I_{k-j} \right)^2 \qquad (10\text{-}1\text{-}28)$$

where the symbols $\{I_n\}$ may take the values $\pm d, \pm 3d, \ldots, \pm(M-1)d$, and $2d$ is the distance between successive levels. The trellis has M^L states, defined at time k as

$$S_k(I_{k-1}, I_{k-2}, \ldots, I_{k-L}) \qquad (10\text{-}1\text{-}29)$$

Let the estimated symbols from the Viterbi algorithm be denoted by $\{\bar{I}_n\}$ and the corresponding estimated state at time k by

$$\bar{S}_k = (\bar{I}_{k-1}, \bar{I}_{k-2}, \ldots, \bar{I}_{k-L}) \qquad (10\text{-}1\text{-}30)$$

Now suppose that the estimated path through the trellis diverges from the correct path at time k and remerges with the correct path at time $k + l$. Thus, $\tilde{S}_k = S_k$ and $\tilde{S}_{k+l} = S_{k+l}$, but $\tilde{S}_m \neq S_m$ for $k < m < k + l$. As in a convolutional code, we call this an *error event*. Since the channel spans $L + 1$ symbols, it follows that $l \geq L + 1$.

For such an error event, we have $\tilde{I}_k \neq I_k$ and $\tilde{I}_{k+l-L-1} \neq I_{k+l-L-1}$, but $\tilde{I}_m = I_m$ for $k - L \leq m \leq k - 1$ and $k + l - L \leq m \leq k + l - 1$. It is convenient to define an error vector $\boldsymbol{\varepsilon}$ corresponding to this error event as

$$\boldsymbol{\varepsilon} = [\varepsilon_k \quad \varepsilon_{k+1} \quad \cdots \quad \varepsilon_{k+l-L-1}] \tag{10-1-31}$$

where the components of $\boldsymbol{\varepsilon}$ are defined as

$$\varepsilon_j = \frac{1}{2d}(I_j - \tilde{I}_j), \qquad j = k, k+1, \ldots, k+l-L-1 \tag{10-1-32}$$

The normalization factor of $2d$ in (10-1-32) results in elements ε_j that take on the values $\pm 1, \pm 2, \pm 3, \ldots, \pm(M-1)$. Moreover, the error vector is characterized by the properties that $\varepsilon_k \neq 0$, $\varepsilon_{k+l-L-1} \neq 0$, and there is no sequence of L consecutive elements that are zero. Associated with the error vector in (10-1-31) is the polynomial of degree $l - L - 1$,

$$\varepsilon(z) = \varepsilon_k + \varepsilon_{k+1}z^{-1} + \varepsilon_{k+2}z^{-2} + \ldots + \varepsilon_{k+l-L-1}z^{-(l-L-1)} \tag{10-1-33}$$

We wish to determine the probability of occurrence of the error event that begins at time k and is characterized by the error vector $\boldsymbol{\varepsilon}$ given in (10-1-31), or, equivalently, by the polymonial given in (10-1-33). To accomplish this, we follow the procedure developed by Forney (1972). Specifically, for the error event $\boldsymbol{\varepsilon}$ to occur, the following three subevents E_1, E_2, and E_3 must occur:

E_1: at time k, $\tilde{S}_k = S_k$;

E_2: the information symbols $I_k, I_{k+1}, \ldots, I_{k+l-L-1}$ when added to the scaled error sequence $2d(\varepsilon_k, \varepsilon_{k+1}, \ldots, \varepsilon_{k+l-L-1})$ must result in an allowable sequence, i.e., the sequence $\tilde{I}_k, \tilde{I}_{k+1}, \ldots, \tilde{I}_{k+l-L-1}$ must have values selected from $\pm d, \pm 3d, \pm \cdots \pm (M-1)d$;

E_3: for $k \leq m < k + l$, the sum of the branch metrics of the estimated path exceed the sum of the branch metrics of the correct path.

The probability of occurrence of E_3 is

$$P(E_3) = P\left[\sum_{i=k}^{k+l-1}\left(v_i - \sum_{j=0}^{L} f_j \tilde{I}_{i-j}\right)^2 < \sum_{i=k}^{k+l-1}\left(v_i - \sum_{j=0}^{L} f_j I_{i-j}\right)^2\right] \tag{10-1-34}$$

But

$$v_i = \sum_{j=0}^{L} f_j I_{i-j} + \eta_i \tag{10-1-35}$$

where $\{\eta_i\}$ is a real-valued white gaussian noise sequence. Substitution of (10-1-35) into (10-1-34) yields

$$P(E_3) = P\left[\sum_{i=k}^{k+l-1}\left(\eta_i + 2d\sum_{j=0}^{L} f_j\varepsilon_{i-j}\right)^2 < \sum_{i=k}^{k+l-1}\eta_i^2\right]$$

$$= P\left[4d\sum_{i=k}^{k+l-1}\eta_i\left(\sum_{j=0}^{L} f_j\varepsilon_{i-j}\right) < -4d^2\sum_{i=k}^{k+l-1}\left(\sum_{j=0}^{L} f_j\varepsilon_{i-j}\right)^2\right] \quad (10\text{-}1\text{-}36)$$

where $\varepsilon_j = 0$ for $j < k$ and $j > k + l - L - 1$. If we define

$$\alpha_i = \sum_{j=0}^{L} f_j\varepsilon_{i-j} \quad (10\text{-}1\text{-}37)$$

then (10-1-36) may be expressed as

$$P(E_3) = P\left(\sum_{i=k}^{k+l-1}\alpha_i\eta_i < -d\sum_{i=k}^{k+l-1}\alpha_i^2\right) \quad (10\text{-}1\text{-}38)$$

where the factor of $4d$ common to both terms has been dropped. Now (10-1-38) is just the probability that a linear combination of statistically independent guassian random variables is less than some negative number. Thus

$$P(E_3) = Q\left(\sqrt{\frac{2d^2}{N_0}\sum_{i=k}^{k+l-1}\alpha_i^2}\right) \quad (10\text{-}1\text{-}39)$$

For convenience, we define

$$\delta^2(\boldsymbol{\varepsilon}) = \sum_{i=k}^{k+l-1}\alpha_i^2 = \sum_{i=k}^{k+l-1}\left(\sum_{j=0}^{L} f_j\varepsilon_{i-j}\right)^2 \quad (10\text{-}1\text{-}40)$$

where $\varepsilon_j = 0$ for $j < k$ and $j > k + l - L - 1$. Note that the $\{\alpha_i\}$ resulting from the convolution of $\{f_i\}$ with $\{\varepsilon_j\}$ are the coefficients of the polynomial

$$\alpha(z) = F(z)\varepsilon(z)$$

$$= \alpha_k + \alpha_{k+1}z^{-1} + \ldots + \alpha_{k+l-1}z^{-(l-1)} \quad (10\text{-}1\text{-}41)$$

Furthermore, $\delta^2(\boldsymbol{\varepsilon})$ is simply equal to the coefficient of z^0 in the polynomial

$$\alpha(z)\alpha(z^{-1}) = F(z)F(z^{-1})\varepsilon(z)\varepsilon(z^{-1})$$

$$= X(z)\varepsilon(z)\varepsilon(z^{-1}) \quad (10\text{-}1\text{-}42)$$

We call $\delta^2(\boldsymbol{\varepsilon})$ the *euclidean weight* of the error event $\boldsymbol{\varepsilon}$.

An alternative method for representing the result of convolving $\{f_i\}$ with $\{\varepsilon_i\}$ is the matrix form

$$\boldsymbol{\alpha} = \mathbf{ef}$$

where $\boldsymbol{\alpha}$ is an l-dimensional vector, $\mathbf{f}$ is an $(L+1)$-dimensional vector, and $\mathbf{e}$ is an $l \times (L+1)$ matrix, defined as

$$\boldsymbol{\alpha} = \begin{bmatrix} \alpha_k \\ \alpha_{k+1} \\ \vdots \\ \alpha_{k+l-1} \end{bmatrix} \qquad \mathbf{f} = \begin{bmatrix} f_0 \\ f_1 \\ \vdots \\ f_L \end{bmatrix}$$

$$\mathbf{e} = \begin{bmatrix} \varepsilon_k & 0 & 0 & \cdots & 0 & \cdots & 0 \\ \varepsilon_{k+1} & \varepsilon_k & 0 & \cdots & 0 & \cdots & 0 \\ \varepsilon_{k+2} & \varepsilon_{k+1} & \varepsilon_k & \cdots & 0 & \cdots & 0 \\ \vdots & \vdots & \vdots & & \vdots & & \vdots \\ \varepsilon_{k+l-1} & \cdots & \cdots & \cdots & \cdots & \cdots & \varepsilon_{k+l-L-1} \end{bmatrix} \tag{10-1-43}$$

Then

$$\begin{aligned} \delta^2(\boldsymbol{\varepsilon}) &= \boldsymbol{\alpha}'\boldsymbol{\alpha} \\ &= \mathbf{f}'\mathbf{e}'\mathbf{ef} \\ &= \mathbf{f}'\mathbf{Af} \end{aligned} \tag{10-1-44}$$

where $\mathbf{A}$ is an $(L+1) \times (L+1)$ matrix of the form

$$\mathbf{A} = \mathbf{e}'\mathbf{e} = \begin{bmatrix} \beta_0 & \beta_1 & \beta_2 & \cdots & \beta_L \\ \beta_1 & \beta_0 & \beta_1 & \cdots & \beta_{L-1} \\ \beta_2 & \beta_1 & \beta_0 & \beta_1 & \beta_{L-2} \\ \vdots & \vdots & \vdots & \vdots & \vdots \\ \beta_L & \cdots & \cdots & \cdots & \beta_0 \end{bmatrix} \tag{10-1-45}$$

and

$$\beta_m = \sum_{i=k}^{k+l-1-m} \varepsilon_i \varepsilon_{i+m} \tag{10-1-46}$$

We may use either (10-1-40) and (10-1-41) or (10-1-45)–(10-1-46) in evaluating the error rate performance. We consider these computations later. For now we conclude that the probability of the subevent E_3, given by (10–1–39), may be expressed as

$$\begin{aligned} P(E_3) &= Q\left(\sqrt{\frac{2d^2}{N_0}\,\delta^2(\boldsymbol{\varepsilon})}\right) \\ &= Q\left(\sqrt{\frac{6}{M^2-1}\,\gamma_{\text{av}}\delta^2(\boldsymbol{\varepsilon})}\right) \end{aligned} \tag{10-1-47}$$

where we have used the relation

$$d^2 = \frac{3}{M^2-1}\,TP_{\text{av}} \tag{10-1-48}$$

to eliminate d^2 and $\gamma_{\text{av}} = TP_{\text{av}}/N_0$. Note that, in the absence of intersymbol

interference, $\delta^2(\boldsymbol{\varepsilon}) = 1$ and $P(E_3)$ is proportional to the symbol error probability of M-ary PAM.

The probability of the subevent E_2 depends only on the statistical properties of the input sequence. We assume that the information symbols are equally probable and that the symbols in the transmitted sequence are statistically independent. Then, for an error of the form $|\varepsilon_i| = j$, $j = 1, 2, \ldots, M-1$, there are $M - j$ possible values of I_i such that

$$I_i = \tilde{I}_i + 2d\varepsilon_i$$

Hence

$$P(E_2) = \prod_{i=0}^{l-L-1} \frac{M - |i|}{M} \tag{10-1-49}$$

The probability of the subevent E_1 is much more difficult to compute exactly because of its dependence on the subevent E_3. That is, we must compute $P(E_1 \mid E_3)$. However, $P(E_1 \mid E_3) = 1 - P_M$, where P_M is the symbol error probability. Hence $P(E_1 \mid E_3)$ is well approximated (and upper-bounded) by unity for reasonably low symbol error probabilities. Therefore, the probability of the error event $\boldsymbol{\varepsilon}$ is well approximated and upper-bounded as

$$P(\boldsymbol{\varepsilon}) \leq Q\left(\sqrt{\frac{6}{M^2-1}\gamma_{av}\delta^2(\boldsymbol{\varepsilon})}\right)\prod_{i=0}^{l-L-1}\frac{M-|i|}{M} \tag{10-1-50}$$

Let E be the set of all error events $\boldsymbol{\varepsilon}$ starting at time k and let $w(\boldsymbol{\varepsilon})$ be the corresponding number of nonzero components (Hamming weight or number of symbol errors) in each error event $\boldsymbol{\varepsilon}$. Then the probability of a symbol error is upper-bounded (union bound) as

$$\begin{aligned} P_M &\leq \sum_{\boldsymbol{\varepsilon}\in E} w(\boldsymbol{\varepsilon})P(\boldsymbol{\varepsilon}) \\ &\leq \sum_{\boldsymbol{\varepsilon}\in E} w(\boldsymbol{\varepsilon})Q\left(\sqrt{\frac{6}{M^2-1}\gamma_{av}\delta^2(\boldsymbol{\varepsilon})}\right)\prod_{i=0}^{l-L-1}\frac{M-|i|}{M} \end{aligned} \tag{10-1-51}$$

Now let D be the set of all $\delta(\boldsymbol{\varepsilon})$. For each $\delta \in D$, let E_δ be the subset of error events for which $\delta(\boldsymbol{\varepsilon}) = \delta$. Then (10-1-51) may be expressed as

$$\begin{aligned} P_M &\leq \sum_{\delta\in D} Q\left(\sqrt{\frac{6}{M^2-1}\gamma_{av}\delta^2}\right)\left[\sum_{\boldsymbol{\varepsilon}\in E_\delta} w(\boldsymbol{\varepsilon})\prod_{i=0}^{l-L-1}\frac{M-|i|}{M}\right] \\ &\leq \sum_{\delta\in D} K_\delta Q\left(\sqrt{\frac{6}{M^2-1}\gamma_{av}\delta^2}\right) \end{aligned} \tag{10-1-52}$$

where

$$K_\delta = \sum_{\boldsymbol{\varepsilon}\in E_\delta} w(\boldsymbol{\varepsilon})\prod_{i=0}^{l-L-1}\frac{M-|i|}{M} \tag{10-1-53}$$

The expression for the error probability in (10-1-52) is similar to the form of the error probability for a convolutional code with soft-decision decoding given

by (8-2-26). The weighting factors $\{K_\delta\}$ may be determined by means of the error state diagram, which is akin to the state diagram of a convolutional encoder. This approach has been illustrated by Forney (1972) and Viterbi and Omura (1979).

In general, however, the use of the error state diagram for computing P_M is tedious. Instead, we may simplify the computation of P_M by focusing on the dominant term in the summation of (10-1-52). Due to the exponential dependence of each term in the sum, the expression P_M is dominated by the term corresponding to the minimum value of δ, denoted as δ_{min}. Hence the symbol error probability may be approximated as

$$P_M \approx K_{\delta_{min}} Q\left(\sqrt{\frac{6}{M^2-1}\gamma_{av}\delta_{min}^2}\right) \tag{10-1-54}$$

where

$$K_{\delta_{min}} = \sum_{\epsilon \in E_{\delta_{min}}} w(\boldsymbol{\epsilon}) \prod_{i=0}^{l-L-1} \frac{M-|i|}{M} \tag{10-1-55}$$

In general, $\delta_{min}^2 \leq 1$. Hence, $10 \log \delta_{\min}^2$ represents the loss in SNR due to intersymbol interference.

The minimum value of δ may be determined either from (10-1-40) or from evaluation of the quadratic form in (10-1-44) for different error sequences. In the following two examples we use (10-1-40).

Example 10-1-3

Consider a two-path channel ($L = 1$) with arbitrary coefficients f_0 and f_1 satisfying the constraint $f_0^2 + f_1^2 = 1$. The channel characteristic is

$$F(z) = f_0 + f_1 z^{-1} \tag{10-1-56}$$

For an error event of length n,

$$\varepsilon(z) = \varepsilon_0 + \varepsilon_1 z^{-1} + \ldots + \varepsilon_{n-1} z^{-(n-1)}, \quad n \geq 1 \tag{10-1-57}$$

The product $\alpha(z) = F(z)\varepsilon(z)$ may be expressed as

$$\alpha(z) = \alpha_0 + \alpha_1 z^{-1} + \ldots + \alpha_n z^{-n} \tag{10-1-58}$$

where $\alpha_0 = \varepsilon_0 f_0$ and $\alpha_n = f_1 \varepsilon_{n-1}$. Since $\varepsilon_0 \neq 0$, $\varepsilon_{n-1} \neq 0$, and

$$\delta^2(\boldsymbol{\epsilon}) = \sum_{k=0}^{n} \alpha_k^2 \tag{10-1-59}$$

it follows that

$$\delta_{\min}^2 \geq f_0^2 + f_1^2 = 1$$

Indeed, $\delta_{\min}^2 = 1$ when a single error occurs, i.e. $\varepsilon(z) = \varepsilon_0$. Thus, we conclude that there is no loss in SNR in maximum-likelihood sequence

estimation of the information symbols when the channel dispersion has length 2.

Example 10-1-4

The controlled intersymbol interference in a partial response signal may be viewed as having been generated by a time-dispersive channel. Thus, the intersymbol interference from a duobinary pulse may be represented by the (normalized) channel characteristic

$$F(z) = \sqrt{\tfrac{1}{2}} + \sqrt{\tfrac{1}{2}} z^{-1} \tag{10-1-60}$$

Similarly, the representation for a modified duobinary pulse is

$$F(z) = \sqrt{\tfrac{1}{2}} - \sqrt{\tfrac{1}{2}} z^{-2} \tag{10-1-61}$$

The minimum distance $\delta_{\min}^2 = 1$ for any error event of the form

$$\varepsilon(z) = \pm(1 - z^{-1} - z^{-2} \ldots - z^{-(n-1)}), \quad n \geq 1 \tag{10-1-62}$$

for the channel given by (10-1-60) since

$$\alpha(z) = \pm\sqrt{\tfrac{1}{2}} \mp \sqrt{\tfrac{1}{2}} z^{-n}$$

Similarly, when

$$\varepsilon(z) = \pm(1 + z^{-2} - z^{-4} + \ldots + z^{-2(n-1)}), \quad n \geq 1 \tag{10-1-63}$$

$\delta_{\min}^2 = 1$ for the channel given by (10-1-61), since

$$\alpha(z) = \pm\sqrt{\tfrac{1}{2}} \mp \sqrt{\tfrac{1}{2}} z^{-2n}$$

Hence MLSE of these two partial response signals results in no loss in SNR. In contrast, the suboptimum symbol-by-symbol detection described previously resulted in a 2.1 dB loss.

The constant $K_{\delta_{\min}}$ is easily evaluated for these two signals. With precoding, the number of output symbol errors (Hamming weight) associated with the error events in (10-1-62) and (10-1-63) is two. Hence,

$$K_{\delta_{\min}} = 2 \sum_{n=1}^{\infty} \left(\frac{M-1}{M}\right)^n = 2(M-1) \tag{10-1-64}$$

On the other hand, without precoding, these error events result in n symbol errors, and, hence,

$$K_{\delta_{\min}} = 2 \sum_{n=1}^{\infty} n\left(\frac{M-1}{M}\right)^n = 2M(M-1) \tag{10-1-65}$$

As a final exercise, we consider the evaluation of $\delta_{\min}^2$ from the quadratic

form in (10-1-44). The matrix **A** of the quadratic form is positive-definite; hence, all its eigenvalues are positive. If $\{\mu_k(\boldsymbol{\varepsilon})\}$ are the eigenvalues and $\{\mathbf{v}_k(\boldsymbol{\varepsilon})\}$ are the corresponding orthonormal eigenvectors of **A** for an error event $\boldsymbol{\varepsilon}$ then the quadratic form in (10-1-44) can be expressed as

$$\delta^2(\boldsymbol{\varepsilon}) = \sum_{k=1}^{L+1} \mu_k(\boldsymbol{\varepsilon})[\mathbf{f}'\mathbf{v}_k(\boldsymbol{\varepsilon})]^2 \tag{10-1-66}$$

In other words, $\delta^2(\boldsymbol{\varepsilon})$ is expressed as a linear combination of the squared projections of the channel vector **f** onto the eigenvectors of **A**. Each squared projection in the sum is weighted by the corresponding eigenvalue $\mu_k(\boldsymbol{\varepsilon})$, $k = 1, 2, \ldots, L+1$. Then

$$\delta^2_{\min} = \min_{\boldsymbol{\varepsilon}} \delta^2(\boldsymbol{\varepsilon}) \tag{10-1-67}$$

It is interesting to note that the worst channel characteristic of a given length $L+1$ can be obtained by finding the eigenvector corresponding to the minimum eigenvalue. Thus, if $\mu_{\min}(\boldsymbol{\varepsilon})$ is the minimum eigenvalue for a given error event $\boldsymbol{\varepsilon}$ and $\mathbf{v}_{\min}(\boldsymbol{\varepsilon})$ is the corresponding eigenvector then

$$\mu_{min} = \min_{\boldsymbol{\varepsilon}} \mu_{min}(\boldsymbol{\varepsilon})$$

$$\mathbf{f} = \min_{\boldsymbol{\varepsilon}} \mathbf{v}_{\min}(\boldsymbol{\varepsilon})$$

and

$$\delta^2_{\min} = \mu_{\min}$$

Example 10-1-5

Let us determine the worst time-dispersive channel of length 3 ($L = 2$) by finding the minimum eigenvalue of **A** for different error events. Thus,

$$F(z) = f_0 + f_1 z^{-1} + f_2 z^{-2}$$

where f_0, f_1, and f_2 are the components of the eigenvector of **A** corresponding to the minimum eigenvalue. An error event of the form

$$\varepsilon(z) = 1 - z^{-1}$$

results in a matrix

$$\mathbf{A} = \begin{bmatrix} 2 & -1 & 0 \\ -1 & 2 & -1 \\ 0 & -1 & 2 \end{bmatrix}$$

which has the eigenvalues $\mu_1 = 2$, $\mu_2 = 2 + \sqrt{2}$, $\mu_3 = 2 - \sqrt{2}$. The eigenvector corresponding to μ_3 is

$$\mathbf{v}_3' = \begin{bmatrix} \frac{1}{2} & \frac{\sqrt{2}}{2} & \frac{1}{2} \end{bmatrix} \tag{10-1-68}$$

We may also consider the dual error event

$$\epsilon(z) = 1 + z^{-1}$$

which results in the matrix

$$\mathbf{A} = \begin{bmatrix} 2 & 1 & 0 \\ 1 & 2 & 1 \\ 0 & 1 & 2 \end{bmatrix}$$

This matrix has eigenvalues identical to those of the one for $\epsilon(z) = 1 - z^{-1}$ The corresponding eigenvector for $\mu_3 = 2 - \sqrt{2}$ is

$$\mathbf{v}_3' = [-\tfrac{1}{2} \quad \sqrt{\tfrac{1}{2}} \quad -\tfrac{1}{2}] \tag{10-1-69}$$

Any other error events lead to larger values for $\mu_{\min}$. Hence, $\mu_{\min} = 2 - \sqrt{2}$ and the worst-case channel is either

$$[\tfrac{1}{2} \quad \sqrt{\tfrac{1}{2}} \quad \tfrac{1}{2}] \quad \text{or} \quad [-\tfrac{1}{2} \quad \sqrt{\tfrac{1}{2}} \quad -\tfrac{1}{2}]$$

The loss in SNR from the channel is

$$-10 \log \delta_{\min}^2 = -10 \log \mu_{\min} = 2.3 \text{ dB}$$

Repetitions of the above computation for channels with $L = 3$, 4, and 5 yield the results given in Table 10-1-1.

10-2 LINEAR EQUALIZATION

The MLSE for a channel with ISI has a computational complexity that grows exponentially with the length of the channel time dispersion. If the size of the symbol alphabet is M and the number of interfering symbols contributing to ISI is L, the Viterbi algorithm computes M^{L+1} metrics for each new received symbol. In most channels of practical interest, such a large computational complexity is prohibitively expensive to implement.

In this and the following sections, we describe two suboptimum channel equalization approaches to compensate for the ISI. One approach employs a linear transversal filter, which is described in this section. These filter

TABLE 10-1-1 MAXIMUM PERFORMANCE LOSS AND CORRESPONDING CHANNEL CHARACTERISTICS

Channel length $L+1$	Performance loss $-10 \log \delta_{\min}^2$ (dB)	Minimum-distance channel
3	2.3	0.50, 0.71, 0.50
4	4.2	0.38, 0.60, 0.60, 0.38
5	5.7	0.29, 0.50, 0.58, 0.50, 0.29
6	7.0	0.23, 0.42, 0.52, 0.52, 0.42, 0.23

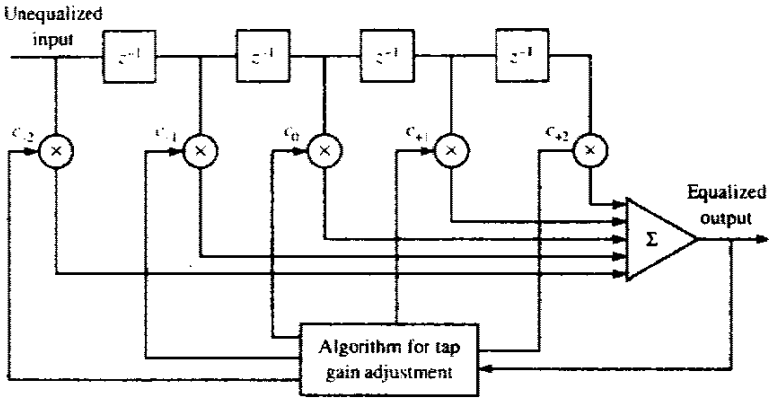

FIGURE 10-2-1 Linear transversal filter.

structures have a computational complexity that is a linear function of the channel dispersion length L.

The linear filter most often used for equalization is the transversal filter shown in Fig. 10-2-1. Its input is the sequence $\{v_k\}$ given in (10-1-16) and its output is the estimate of the information sequence $\{I_k\}$. The estimate of the k th symbol may be expressed as

$$\hat{I}_k = \sum_{j=-K}^{K} c_j v_{k-j} \tag{10-2-1}$$

where $\{c_j\}$ are the $2K + 1$ complex-valued tap weight coefficients of the filter. The estimate $\hat{I}_k$ is quantized to the nearest (in distance) information symbol to form the decision $\tilde{I}_k$. If $\tilde{I}_k$ is not identical to the transmitted information symbol I_k, an error has been made.

Considerable research has been performed on the criterion for optimizing the filter coefficients $\{c_k\}$. Since the most meaningful measure of performance for a digital communications system is the average probability of error, it is desirable to choose the coefficients to minimize this performance index. However, the probability of error is a highly nonlinear function of $\{c_j\}$. Consequently, the probability of error as a performance index for optimizing the tap weight coefficients of the equalizer is impractical.

Two criteria have found widespread use in optimizing the equalizer coefficients $\{c_j\}$. One is the peak distortion criterion and the other is the mean square error criterion.

10-2-1 Peak Distortion Criterion

The peak distortion is simply defined as the worst-case intersymbol interference at the output of the equalizer. The minimization of this performance index is called the *peak distortion criterion*. First we consider the minimization

of the peak distortion assuming that the equalizer has an infinite number of taps. Then we shall discuss the case in which the transversal equalizer spans a finite time duration.

We observe that the cascade of the discrete-time linear filter model having an impulse response $\{f_n\}$ and an equalizer having an impulse response $\{c_n\}$ can be represented by a single equivalent filter having the impulse response

$$q_n = \sum_{j=-\infty}^{\infty} c_j f_{n-j} \tag{10-2-2}$$

That is, $\{q_n\}$ is simply the convolution of $\{c_n\}$ and $\{f_n\}$. The equalizer is assumed to have an infinite number of taps. Its output at the k th sampling instant can be expressed in the form

$$\hat{I}_k = q_0 I_k + \sum_{n \neq k} I_n q_{k-n} + \sum_{j=-\infty}^{\infty} c_j \eta_{k-j} \tag{10-2-3}$$

The first term in (10-2-3) represents a scaled version of the desired symbol. For convenience, we normalize q_0 to unity. The second term is the intersymbol interference. The peak value of this interference, which is called the *peak distortion,* is

$$\begin{aligned} \mathscr{D}(\mathbf{c}) &= \sum_{\substack{n=-\infty \\ n \neq 0}}^{\infty} |q_n| \\ &= \sum_{\substack{n=-\infty \\ n \neq 0}}^{\infty} \left| \sum_{j=-\infty}^{\infty} c_j f_{n-j} \right| \end{aligned} \tag{10-2-4}$$

Thus, $\mathscr{D}(\mathbf{c})$ is a function of the equalizer tap weights.

With an equalizer having an infinite number of taps, it is possible to select the tap weights so that $\mathscr{D}(\mathbf{c}) = 0$, i.e., $q_n = 0$ for all n except $n = 0$. That is, the intersymbol interference can be completely eliminated. The values of the tap weights for accomplishing this goal are determined from the condition

$$q_n = \sum_{j=-\infty}^{\infty} c_j f_{n-j} = \begin{cases} 1 & (n = 0) \\ 0 & (n \neq 0) \end{cases} \tag{10-2-5}$$

By taking the z transform of (10-2-5), we obtain

$$Q(z) = C(z)F(z) = 1 \tag{10-2-6}$$

or, simply,

$$C(z) = \frac{1}{F(z)} \tag{10-2-7}$$

where $C(z)$ denotes the z transform of the $\{c_j\}$. Note that the equalizer, with transfer function $C(z)$, is simply the inverse filter to the linear filter model $F(z)$. In other words, complete elimination of the intersymbol interference requires the use of an inverse filter to $F(z)$. We call such a filter a *zero-forcing*

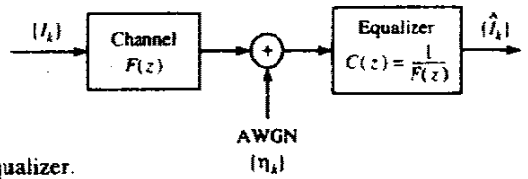

FIGURE 10-2-2 Block diagram of channel with zero-forcing equalizer.

filter. Figure 10-2-2 illustrates in block diagram the equivalent discrete-time channel and equalizer.

The cascade of the noise-whitening filter having the transfer function $1/F^*(z^{-1})$ and the zero-forcing equalizer having the transfer function $1/F(z)$ results in an equivalent zero-forcing equalizer having the transfer function

$$C'(z)=\frac{1}{F(z)F^*(z^{-1})}=\frac{1}{X(z)} \tag{10-2-8}$$

as shown in Fig. 10-2-3. This combined filter has as its input the sequence $\{y_k\}$ of samples from the matched filter, given by (10-1-10). Its output consists of the desired symbols corrupted only by additive zero-mean gaussian noise. The impulse response of the combined filter is

$$\begin{aligned} c'_k &= \frac{1}{2\pi j}\oint C'(z)z^{k-1}\,dz \\ &= \frac{1}{2\pi j}\oint \frac{z^{k-1}}{X(z)}\,dz \end{aligned} \tag{10-2-9}$$

where the integration is performed on a closed contour that lies within the region of convergence of $C'(z)$. Since $X(z)$ is a polynomial with $2L$ roots $(\rho_1, \rho_2, \ldots, \rho_L, 1/\rho_1^*, 1/\rho_2^*, \ldots, 1/\rho_L^*)$, it follows that $C'(z)$ must converge in an annular region in the z plane that includes the unit circle ($z = e^{j\theta}$). Consequently, the closed contour in the integral can be the unit circle.

The performance of the infinite-tap equalizer that completely eliminates the intersymbol interference can be expressed in terms of the signal-to-noise ratio (SNR) at its output. For mathematical convenience, we normalize the received

FIGURE 10-2-3 Block of channel with equivalent zero-forcing equalizer.

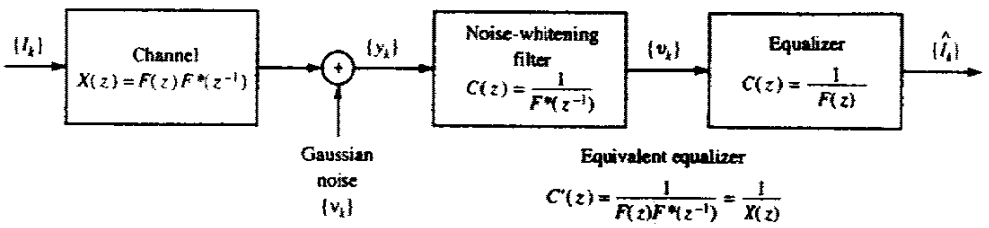

signal energy to unity.† This implies that $q_0 = 1$ and that the expected value of $|I_k|^2$ is also unity. Then the SNR is simply the reciprocal of the noise variance σ_n^2 at the output of the equalizer.

The value of σ_n^2 can be simply determined by observing that the noise sequence $\{v_k\}$ at the input to the equivalent zero-forcing equalizer $C'(z)$ has zero mean and a power spectral density

$$\Phi_{vv}(\omega) = N_0 X(e^{j\omega T}), \quad |\omega| \leq \frac{\pi}{T} \tag{10-2-10}$$

where $X(e^{j\omega T})$ is obtained from $X(z)$ by the substitution $z = e^{j\omega T}$. Since $C'(z) = 1/X(z)$, it follows that the noise sequence at the output of the equalizer has a power spectral density

$$\Phi_{nn}(\omega) = \frac{N_0}{X(e^{j\omega T})}, \quad |\omega| \leq \frac{\pi}{T} \tag{10-2-11}$$

Consequently, the variance of the noise variable at the output of the equalizer is

$$\begin{aligned} \sigma_n^2 &= \frac{T}{2\pi} \int_{-\pi/T}^{\pi/T} \Phi_{nn}(\omega)\, d\omega \\ &= \frac{TN_0}{2\pi} \int_{-\pi/T}^{\pi/T} \frac{d\omega}{X(e^{j\omega T})} \end{aligned} \tag{10-2-12}$$

and the SNR for the zero-forcing equalizer is

$$\begin{aligned} \gamma_\infty &= 1/\sigma_n^2 \\ &= \left[\frac{TN_0}{2\pi} \int_{-\pi/T}^{\pi/T} \frac{d\omega}{X(e^{j\omega T})} \right]^{-1} \end{aligned} \tag{10-2-13}$$

where the subscript on γ indicates that the equalizer has an infinite number of taps.

The spectral characteristics $X(e^{j\omega T})$ corresponding to the Fourier transform of the sampled sequence $\{x_n\}$ has an interesting relationship to the analog filter $H(\omega)$ used at the receiver. Since

$$x_k = \int_{-\infty}^{\infty} h^*(t) h(t + kT)\, dt$$

use of Parseval's theorem yields

$$x_k = \frac{1}{2\pi} \int_{-\infty}^{\infty} |H(\omega)|^2 e^{j\omega kT}\, d\omega \tag{10-2-14}$$

where $H(\omega)$ is the Fourier transform of $h(t)$. But the integral in (10-2-14) can be expressed in the form

$$x_k = \frac{1}{2\pi} \int_{-\pi/T}^{\pi/T} \left[\sum_{n=-\infty}^{\infty} \left| H\left(\omega + \frac{2\pi n}{T}\right) \right|^2 \right] e^{j\omega kT}\, d\omega \tag{10-2-15}$$

† This normalization is used throughout this chapter for mathematical convenience.

Now, the Fourier transform of $\{x_k\}$ is

$$X(e^{j\omega T}) = \sum_{k=-\infty}^{\infty} x_k e^{-j\omega kT} \tag{10-2-16}$$

and the inverse transform yields

$$x_k = \frac{T}{2\pi} \int_{-\pi/T}^{\pi/T} X(e^{j\omega T}) e^{j\omega kT}\, d\omega \tag{10-2-17}$$

From a comparison of (10-2-15) and (10-2-17), we obtain the desired relationship between $X(e^{j\omega T})$ and $H(\omega)$. That is,

$$X(e^{j\omega T}) = \frac{1}{T} \sum_{n=-\infty}^{\infty} \left| H\left(\omega + \frac{2\pi n}{T}\right)\right|^2, \quad |\omega| \leq \frac{\pi}{T} \tag{10-2-18}$$

where the right-hand side of (10-2-18) is called the *folded spectrum* of $|H(\omega)|^2$. We also observe that $|H(\omega)|^2 = X(\omega)$, where $X(\omega)$ is the Fourier transform of the waveform $x(t)$ and $x(t)$ is the response of the matched filter to the input $h(t)$. Therefore the right-hand side of (10-2-18) can also be expressed in terms of $X(\omega)$.

Substitution for $X(e^{j\omega T})$ in (10-2-13) using the result in (10-2-18) yields the desired expression for the SNR in the form

$$\gamma_\infty = \left[\frac{T^2 N_0}{2\pi} \int_{-\pi/T}^{\pi/T} \frac{d\omega}{\sum_{n=-\infty}^{\infty} |H(\omega + 2\pi n/T)|^2} \right]^{-1} \tag{10-2-19}$$

We observe that if the folded spectral characteristic of $H(\omega)$ possesses any zeros, the integrand becomes infinite and the SNR goes to zero. In other words, the performance of the equalizer is poor whenever the folded spectral characteristic possesses nulls or takes on small values. This behavior occurs primarily because the equalizer, in eliminating the intersymbol interference, enhances the additive noise. For example, if the channel contains a spectral null in its frequency response, the linear zero-forcing equalizer attempts to compensate for this by introducing an infinite gain at that frequency. But this compensates for the channel distortion at the expense of enhancing the additive noise. On the other hand, an ideal channel coupled with an appropriate signal design that results in no intersymbol interference will have a folded spectrum that satisfies the condition

$$\sum_{n=-\infty}^{\infty} \left| H\left(\omega + \frac{2\pi n}{T}\right)\right|^2 = T, \quad |\omega| \leq \frac{\pi}{T} \tag{10-2-20}$$

In this case, the SNR achieves its maximum value, namely,

$$\gamma_\infty = \frac{1}{N_0} \tag{10-2-21}$$

Finite-Length Equalizer Let us now turn our attention to an equalizer having $2K+1$ taps. Since $c_j = 0$ for $|j| > K$, the convolution of $\{f_n\}$ with $\{c_n\}$ is zero outside the range $-K \leq n \leq K+L-1$. That is, $q_n = 0$ for $n < -K$ and $n > K+L-1$. With q_0 normalized to unity, the peak distortion is

$$\mathcal{D}(\mathbf{c}) = \sum_{\substack{n=-K \\ n\neq 0}}^{K+L-1} |q_n| = \sum_{\substack{n=-K \\ n\neq 0}}^{K+L-1} \left| \sum_j c_j f_{n-j} \right| \tag{10-2-22}$$

Although the equalizer has $2K+1$ adjustable parameters, there are $2K+L$ nonzero values in the response $\{q_n\}$. Therefore, it is generally impossible to completely eliminate the intersymbol interference at the output of the equalizer. There is always some residual interference when the optimum coefficients are used. The problem is to minimize $\mathcal{D}(\mathbf{c})$ with respect to the coefficients $\{c_j\}$.

The peak distortion given by (10-2-22) has been shown by Lucky (1965) to be a convex function of the coefficients $\{c_j\}$. That is, it possesses a global minimum and no relative minima. Its minimization can be carried out numerically using, for example, the method of steepest descent. Little more can be said for the general solution to this minimization problem. However, for one special but important case, the solution for the minimization of $\mathcal{D}(\mathbf{c})$ is known. This is the case in which the distortion at the input to the equalizer, defined as

$$D_0 = \frac{1}{|f_0|} \sum_{n=1}^{L} |f_n| \tag{10-2-23}$$

is less than unity. This condition is equivalent to having the eye open prior to equalization. That is, the intersymbol interference is not severe enough to close the eye. Under this condition, the peak distortion $\mathcal{D}(\mathbf{c})$ is minimized by selecting the equalizer coefficients to force $q_n = 0$ for $1 \leq |n| \leq K$ and $q_0 = 1$. In other words, the general solution to the minimization of $\mathcal{D}(\mathbf{c})$, when $D_0 < 1$, is the zero-forcing solution for $\{q_n\}$ in the range $1 \leq |n| \leq K$. However, the values of $\{q_n\}$ for $K+1 \leq n \leq K+L-1$ are nonzero, in general. These nonzero values constitute the residual intersymbol interference at the output of the equalizer.

10-2-2 Mean Square Error (MSE) Criterion

In the MSE criterion, the tap weight coefficients $\{c_j\}$ of the equalizer are adjusted to minimize the mean square value of the error

$$\varepsilon_k = I_k - \hat{I}_k \tag{10-2-24}$$

where I_k is the information symbol transmitted in the k th signaling interval and $\hat{I}_k$ is the estimate of that symbol at the output of the equalizer, defined in

(10-2-1). When the information symbols $\{I_k\}$ are complex-valued, the performance index for the MSE criterion, denoted by J, is defined as

$$\begin{aligned} J &= E\,|\varepsilon_k|^2 \\ &= E\,|I_k - \hat{I}_k|^2 \end{aligned} \tag{10-2-25}$$

On the other hand, when the information symbols are real-valued, the performance index is simply the square of the real part of ε_k. In either case, J is a quadratic function of the equalizer coefficients $\{c_j\}$. In the following discussion, we consider the minimization of the complex-valued form given in (10-2-25).

Infinite-Length Equalizer First, we shall derive the tap weight coefficients that minimize J when the equalizer has an infinite number of taps. In this case, the estimate $\hat{I}_k$ is expressed as

$$\hat{I}_k = \sum_{j=-\infty}^{\infty} c_j v_{k-j} \tag{10-2-26}$$

Substitution of (10-2-26) into the expression for J given in (10-2-25) and expansion of the result yields a quadratic function of the coefficients $\{c_j\}$. This function can be easily minimized with respect to the $\{c_j\}$ to yield a set (infinite in number) of linear equations for the $\{c_j\}$. Alternatively, the set of linear equations can be obtained by invoking the orthogonality principle in mean square estimation. That is, we select the coefficients $\{c_j\}$ to render the error ε_k orthogonal to the signal sequence $\{v_{k-l}^*\}$ for $-\infty < l < \infty$. Thus,

$$E(\varepsilon_k v_{k-l}^*) = 0, \qquad -\infty < l < \infty \tag{10-2-27}$$

Substitution for ε_k in (10-2-27) yields

$$E\left[\left(I_k - \sum_{j=-\infty}^{\infty} c_j v_{k-j}\right) v_{k-l}^*\right] = 0$$

or, equivalently,

$$\sum_{j=-\infty}^{\infty} c_j E(v_{k-j} v_{k-l}^*) = E(I_k v_{k-l}^*), \qquad -\infty < l < \infty \tag{10-2-28}$$

To evaluate the moments in (10-2-28), we use the expression for v_k given in (10-1-16). Thus, we obtain

$$\begin{aligned} E(v_{k-j} v_{k-l}^*) &= \sum_{n=0}^{L} f_n^* f_{n+l-j} + N_0 \delta_{lj} \\ &= \begin{cases} x_{l-j} + N_0 \delta_{lj} & (|l-j| \le L) \\ 0 & (\text{otherwise}) \end{cases} \end{aligned} \tag{10-2-29}$$

and

$$E(I_k v_{k-l}^*) = \begin{cases} f_{-l}^* & (-L \le l \le 0) \\ 0 & (\text{otherwise}) \end{cases} \tag{10-2-30}$$

Now, if we substitute (10-2-29) and (10-2-30) into (10-2-28) and take the z transform of both sides of the resulting equation, we obtain

$$C(z)[F(z)F^*(z^{-1}) + N_0] = F^*(z^{-1}) \tag{10-2-31}$$

Therefore, the transfer function of the equalizer based on the MSE criterion is

$$C(z) = \frac{F^*(z^{-1})}{F(z)F^*(z^{-1}) + N_0} \tag{10-2-32}$$

When the noise-whitening filter is incorporated into $C(z)$, we obtain an equivalent equalizer having the transfer function

$$\begin{aligned} C'(z) &= \frac{1}{F(z)F^*(z^{-1}) + N_0} \\ &= \frac{1}{X(z) + N_0} \end{aligned} \tag{10-2-33}$$

We observe that the only difference between this expression for $C'(z)$ and the one based on the peak distortion criterion is the noise spectral density factor N_0 that appears in (10-2-33). When N_0 is very small in comparison with the signal, the coefficients that minimize the peak distortion $\mathcal{D}(\mathbf{c})$ are approximately equal to the coefficients that minimize the MSE performance index J. That is, in the limit as $N_0 \to 0$, the two criteria yield the same solution for the tap weights. Consequently, when $N_0 = 0$, the minimization of the MSE results in complete elimination of the intersymbol interference. On the other hand, that is not the case when $N_0 \neq 0$. In general, when $N_0 \neq 0$, there is both residual intersymbol interference and additive noise at the output of the equalizer.

A measure of the residual intersymbol interference and additive noise is obtained by evaluating the minimum value of J, denoted by $J_{\min}$, when the transfer function $C(z)$ of the equalizer is given by (10-2-32). Since $J = E|\varepsilon_k|^2 = E(\varepsilon_k I_k^*) - E(\varepsilon_k \hat{I}_k^*)$, and since $E(\varepsilon_k \hat{I}_k^*) = 0$ by virtue of the orthogonality conditions given in (10-2-27), it follows that

$$\begin{aligned} J_{\min} &= E(\varepsilon_k I_k^*) \\ &= E|I_k|^2 - \sum_{j=-\infty}^{\infty} c_j E(v_{k-j} I_k^*) \\ &= 1 - \sum_{j=-\infty}^{\infty} c_j f_{-j} \end{aligned} \tag{10-2-34}$$

This particular form for $J_{\min}$ is not very informative. More insight on the performance of the equalizer as a function of the channel characteristics is obtained when the summation in (10-2-34) is transformed into the frequency domain. This can be accomplished by first noting that the summation in (10-2-34) is the convolution of $\{c_j\}$ with $\{f_j\}$, evaluated at a shift of zero. Thus,

if $\{b_k\}$ denotes the convolution of these two sequences, the summation in (10-2-34) is simply equal to b_0. Since the z transform of the sequence $\{b_k\}$ is

$$\begin{aligned} B(z) &= C(z)F(z) \\ &= \frac{F(z)F^*(z^{-1})}{F(z)F^*(z^{-1}) + N_0} \\ &= \frac{X(z)}{X(z) + N_0} \end{aligned} \tag{10-2-35}$$

the term b_0 is

$$\begin{aligned} b_0 &= \frac{1}{2\pi j}\oint \frac{B(z)}{z}\,dz \\ &= \frac{1}{2\pi j}\oint \frac{X(z)}{z[X(z) + N_0]}\,dz \end{aligned} \tag{10-2-36}$$

The contour integral in (10-2-36) can be transformed into an equivalent line integral by the change of variable $z = e^{j\omega T}$. The result of this change of variable is

$$b_0 = \frac{T}{2\pi}\int_{-\pi/T}^{\pi/T} \frac{X(e^{j\omega T})}{X(e^{j\omega T}) + N_0}\,d\omega \tag{10-2-37}$$

Finally, substitution of the result in (10-2-37) for the summation in (10-2-34) yields the desired expression for the minimum MSE in the form

$$\begin{aligned} J_{\min} &= 1 - \frac{T}{2\pi}\int_{-\pi/T}^{\pi/T} \frac{X(e^{j\omega T})}{X(e^{j\omega T}) + N_0}\,d\omega \\ &= \frac{T}{2\pi}\int_{-\pi/T}^{\pi/T} \frac{N_0}{X(e^{j\omega T}) + N_0}\,d\omega \\ &= \frac{T}{2\pi}\int_{-\pi/T}^{\pi/T} \frac{N_0}{T^{-1}\sum_{n=-\infty}^{\infty} |H(\omega + 2\pi n/T)|^2 + N_0}\,d\omega \end{aligned} \tag{10-2-38}$$

In the absence of intersymbol interference, $X(e^{j\omega T}) = 1$ and, hence,

$$J_{\min} = \frac{N_0}{1 + N_0} \tag{10-2-39}$$

We observe that $0 \leq J_{\min} \leq 1$. Furthermore, the relationship between the output (normalized by the signal energy) SNR γ_∞ and $J_{\min}$ must be

$$\gamma_\infty = \frac{1 - J_{\min}}{J_{\min}} \tag{10-2-40}$$

More importantly, this relation between γ_∞ and $J_{\min}$ also holds when there is residual intersymbol interference in addition to the noise.

Finite-Length Equalizer Let us now turn our attention to the case in which the transversal equalizer spans a finite time duration. The output of the equalizer in the k th signaling interval is

$$\hat{I}_k = \sum_{j=-K}^{K} c_j v_{k-j} \tag{10-2-41}$$

The MSE for the equalizer having $2K + 1$ taps, denoted by $J(K)$, is

$$J(K) = E\,|I_k - \hat{I}_k|^2 = E\left|I_k - \sum_{j=-K}^{K} c_j v_{k-j}\right|^2 \tag{10-2-42}$$

Minimization of $J(K)$ with respect to the tap weights $\{c_j\}$ or, equivalently, forcing the error $\varepsilon_k = I_k - \hat{I}_k$ to be orthogonal to the signal samples v^*_{j-l}, $|l| \leq K$, yields the following set of simultaneous equations:

$$\sum_{j=-K}^{K} c_j \Gamma_{lj} = \xi_l, \qquad l = -K, \ldots, -1, 0, 1, \ldots, K \tag{10-2-43}$$

where

$$\Gamma_{lj} = \begin{cases} x_{l-j} + N_0 \delta_{lj} & (|l-j| \leq L) \\ 0 & (\text{otherwise}) \end{cases} \tag{10-2-44}$$

and

$$\xi_l = \begin{cases} f^*_{-l} & (-L \leq l \leq 0) \\ 0 & (\text{otherwise}) \end{cases} \tag{10-2-45}$$

It is convenient to express the set of linear equations in matrix form. Thus,

$$\boldsymbol{\Gamma}\mathbf{C} = \boldsymbol{\xi} \tag{10-2-46}$$

where $\mathbf{C}$ denotes the column vector of $2K + 1$ tap weight coefficients, $\boldsymbol{\Gamma}$ denotes the $(2K + 1) \times (2K + 1)$ Hermitian covariance matrix with elements Γ_{lj}, and $\boldsymbol{\xi}$ is a $(2K + 1)$-dimensional column vector with elements ξ_l. The solution of (10-2-46) is

$$\mathbf{C}_{\text{opt}} = \boldsymbol{\Gamma}^{-1}\boldsymbol{\xi} \tag{10-2-47}$$

Thus, the solution for $\mathbf{C}_{\text{opt}}$ involves inverting the matrix $\boldsymbol{\Gamma}$. The optimum tap weight coefficients given by (10-2-47) minimize the performance index $J(K)$, with the result that the minimum value of $J(K)$ is

$$\begin{aligned} J_{\min}(K) &= 1 - \sum_{j=-K}^{0} c_j f_{-j} \\ &= 1 - \boldsymbol{\xi}^{t*}\boldsymbol{\Gamma}^{-1}\boldsymbol{\xi} \end{aligned} \tag{10-2-48}$$

where $\boldsymbol{\xi}^t$ represents the transpose of the column vector $\boldsymbol{\xi}$. $J_{\min}(K)$ may be used

in (10-2-40) to compute the output SNR for the linear equalizer with $2K + 1$ tap coefficients.

10-2-3 Performance Characteristics of the MSE Equalizer

In this section, we consider the performance characteristics of the linear equalizer that is optimized by using the MSE criterion. Both the minimum MSE and the probability of error are considered as performance measures for some specific channels. We begin by evaluating the minimum MSE $J_{\min}$ and the output SNR γ_∞ for two specific channels. Then, we consider the evaluation of the probability of error.

Example 10-2-1

First, we consider an equivalent discrete-time channel model consisting of two components f_0 and f_1, which are normalized to $|f_0|^2 + |f_1|^2 = 1$. Then

$$F(z) = f_0 + f_1 z^{-1} \tag{10-2-49}$$

and

$$X(z) = f_0 f_1^* z + 1 + f_0^* f_1 z^{-1} \tag{10-2-50}$$

The corresponding frequency response is

$$\begin{aligned} X(e^{j\omega T}) &= f_0 f_1^* e^{j\omega T} + 1 + f_0^* f_1 e^{-j\omega T} \\ &= 1 + 2|f_0||f_1|\cos(\omega T + \theta) \end{aligned} \tag{10-2-51}$$

where θ is the angle of $f_0 f_1^*$. We note that this channel characteristic possesses a null at $\omega = \pi/T$ when $f_0 = f_1 = \sqrt{\frac{1}{2}}$.

A linear equalizer with an infinite number of taps, adjusted on the basis of the MSE criterion, will have the minimum MSE given by (10-2-38). Evaluation of the integral in (10-2-38) for the $X(e^{j\omega T})$ given in (10-2-51) yields the result

$$\begin{aligned} J_{\min} &= \frac{N_0}{\sqrt{N_0^2 + 2N_0(|f_0|^2 + |f_1|^2) + (|f_0|^2 - |f_1|^2)^2}} \\ &= \frac{N_0}{\sqrt{N_0^2 + 2N_0 + (|f_0|^2 - |f_1|^2)^2}} \end{aligned} \tag{10-2-52}$$

Let us consider the special case in which $f_0 = f_1 = \sqrt{\frac{1}{2}}$. The minimum MSE is $J_{\min} = N_0/\sqrt{N_0^2 + 2N_0}$ and the corresponding output SNR is

$$\begin{aligned} \gamma_\infty &= \sqrt{1 + \frac{2}{N_0}} - 1 \\ &\approx \left(\frac{2}{N_0}\right)^{1/2}, \quad N_0 \ll 1 \end{aligned} \tag{10-2-53}$$

This result should be compared with the output SNR of $1/N_0$ obtained in

the case of no intersymbol interference. A significant loss in SNR occurs from this channel.

Example 10-2-2

As a second example, we consider an exponentially decaying characteristic of the form

$$f_k = \sqrt{1-a^2}\,a^k, \qquad k = 0, 1, \ldots$$

where $a < 1$. The Fourier transform of this sequence is

$$X(e^{j\omega T}) = \frac{1-a^2}{1+a^2-2a\cos\omega T} \tag{10-2-54}$$

which is a function that contains a minimum at $\omega = \pi/T$.

The output SNR for this channel is

$$\gamma_\infty = \left(\sqrt{1+2N_0\frac{1+a^2}{1-a^2}+N_0^2}-1\right)^{-1}$$

$$\approx \frac{1-a^2}{(1+a^2)N_0}, \qquad N_0 \ll 1 \tag{10-2-55}$$

Therefore, the loss in SNR due to the presence of the interference is

$$10\log_{10}\left(\frac{1-a^2}{1+a^2}\right)$$

Probability of Error Performance of Linear MSE Equalizer Above, we discussed the performance of the linear equalizer in terms of the minimum achievable MSE $J_{\min}$ and the output SNR γ that is related to $J_{\min}$ through the formula in (10-2-40). Unfortunately, there is no simple relationship between these quantities and the probability of error. The reason is that the linear MSE equalizer contains some residual intersymbol interference at its output. This situation is unlike that of the infinitely long zero-forcing equalizer, for which there is no residual interference, but only gaussian noise. The residual interference at the output of the MSE equalizer is not well characterized as an additional gaussian noise term, and, hence, the output SNR does not translate easily into an equivalent error probability.

One approach to computing the error probability is a brute force method that yields an exact result. To illustrate this method, let us consider a PAM signal in which the information symbols are selected from the set of values $2n - M - 1$, $n = 1, 2, \ldots, M$, with equal probability. Now consider the decision on the symbol I_n. The estimate of I_n is

$$\hat{I}_n = q_0 I_n + \sum_{k\neq n} I_k q_{n-k} + \sum_{j=-K}^{K} c_j \eta_{n-j} \tag{10-2-56}$$

where $\{q_n\}$ represent the convolution of the impulse response of the equalizer and equivalent channel, i.e.,

$$q_n = \sum_{k=-K}^{K} c_k f_{n-k} \tag{10-2-57}$$

and the input signal to the equalizer is

$$v_k = \sum_{j=0}^{L} f_j I_{k-j} + \eta_k \tag{10-2-58}$$

The first term in the right-hand side of (10-2-56) is the desired symbol, the middle term is the intersymbol interference, and the last term is the gaussian noise. The variance of the noise is

$$\sigma_n^2 = N_0 \sum_{j=-K}^{K} c_j^2 \tag{10-2-59}$$

For an equalizer with $2K + 1$ taps and a channel response that spans $L + 1$ symbols, the number of symbols involved in the intersymbol interference is $2K + L$.

Define

$$\mathscr{D} = \sum_{k \neq n} I_k q_{n-k} \tag{10-2-60}$$

For a particular sequence of $2K + L$ information symbols, say the sequence $\mathbf{I}_J$, the intersymbol interference term $\mathscr{D} \equiv D_J$ is fixed. The probability of error for a fixed D_J is

$$\begin{aligned} P_M(D_J) &= 2\frac{(M-1)}{M} P(N + D_J > q_0) \\ &= \frac{2(M-1)}{M} Q\left(\sqrt{\frac{(q_0 - D_J)^2}{\sigma_n^2}}\right) \end{aligned} \tag{10-2-61}$$

where N denotes the additive noise term. The average probability of error is obtained by averaging $P_M(D_J)$ over all possible sequences $\mathbf{I}_J$. That is,

$$\begin{aligned} P_M &= \sum_{\mathbf{I}_J} P_M(D_J) P(\mathbf{I}_J) \\ &= \frac{2(M-1)}{M} \sum_{\mathbf{I}_J} Q\left(\sqrt{\frac{(q_0 - D_J)^2}{\sigma_n^2}}\right) P(\mathbf{I}_J) \end{aligned} \tag{10-2-62}$$

When all the sequences are equally likely,

$$P(\mathbf{I}_J) = \frac{1}{M^{2K+L}} \tag{10-2-63}$$

The conditional error probability terms $P_M(D_J)$ are dominated by the sequence that yields the largest value of D_J. This occurs when $I_n = \pm(M-1)$

and the signs of the information symbols match the signs of the corresponding $\{q_n\}$. Then,

$$D_f^* = (M-1)\sum_{k\neq 0}|q_k|$$

and

$$P_M(D_f^*) = \frac{2(M-1)}{M}Q\left(\sqrt{\frac{q_0^2}{\sigma_n^2}\left(1-\frac{M-1}{q_0}\sum_{k\neq 0}|q_k|\right)^2}\right) \qquad (10\text{-}2\text{-}64)$$

Thus, an upper bound on the average probability of error for equally likely symbol sequences is

$$P_M \leq P_M(D_f^*) \qquad (10\text{-}2\text{-}65)$$

If the computation of the exact error probability in (10-2-62) proves to be too cumbersome and too time consuming because of the large number of terms in the sum and if the upper bound is too loose, one can resort to one of a number of different approximate methods that have been devised, which are known to yield tight bounds on P_M. A discussion of these different approaches would take us too far afield. The interested reader is referred to the papers by Saltzberg (1968), Lugannani (1969), Ho and Yeh (1970), Shimbo and Celebiler (1971), Glave (1972), Yao (1972), and Yao and Tobin (1976).

As an illustration of the performance limitations of a linear equalizer in the presence of severe intersymbol interference, we show in Fig. 10-2-4 the probability of error for binary (antipodal) signaling, as measured by Monte Carlo simulation, for the three discrete-time channel characteristic shown in

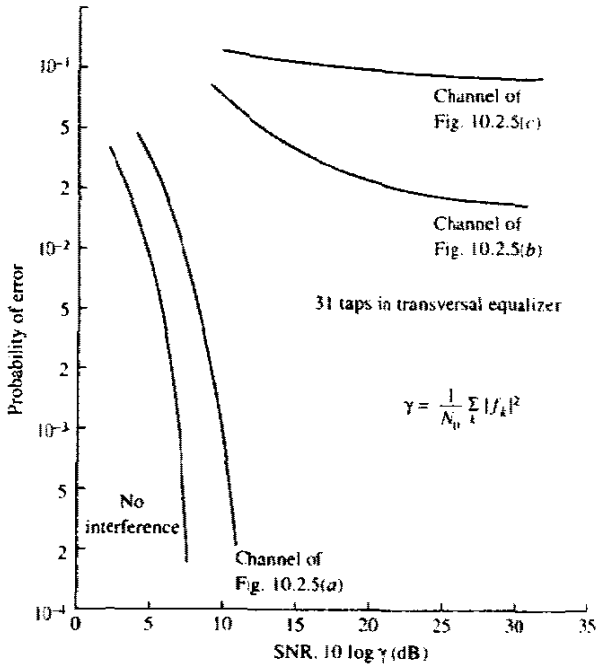

FIGURE 10-2-4 Error rate performance of linear MSE equalizer.

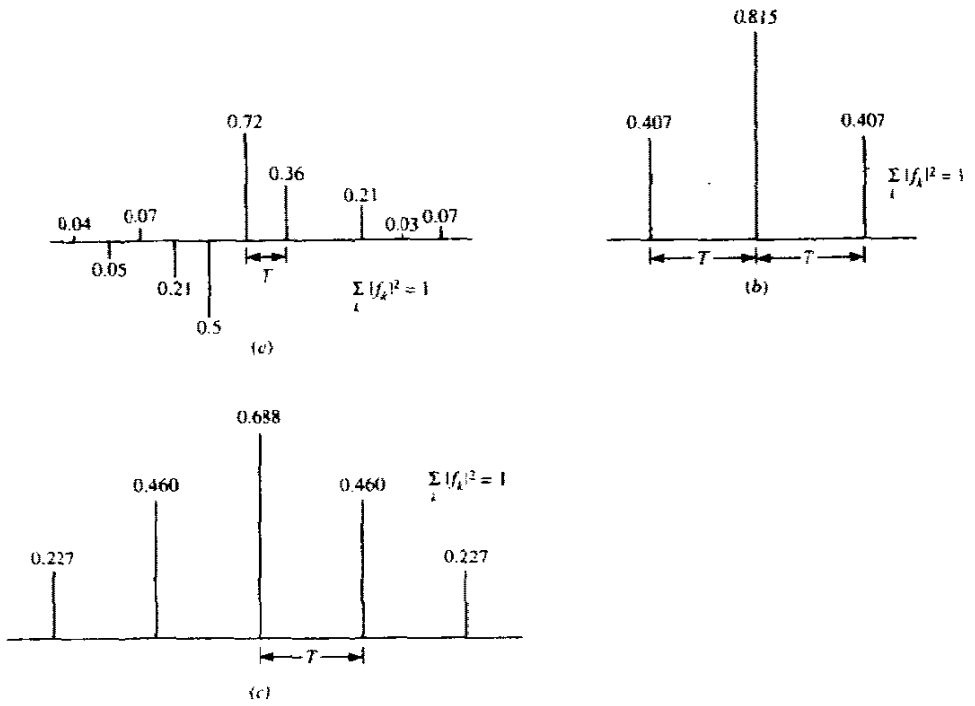

FIGURE 10-2-5 Three discrete-time channel characteristics.

Fig. 10-2-5. For purposes of comparison, the performance obtained for a channel with no intersymbol interference is also illustrated in Fig. 10-2-4. The equivalent discrete-time channel shown in Fig. 10-2-5(a) is typical of the response of a good quality telephone channel. In contrast, the equivalent discrete-time channel characteristics shown in Fig. 10-2-5(b) and (c) result in severe intersymbol interference. The spectral characteristics $|X(e^{j\omega})|$ for the three channels, illustrated in Fig. 10-2-6, clearly show that the channel in Fig. 10-2-5(c) has the worst spectral characteristic. Hence the performance of the linear equalizer for this channel is the poorest of the three cases. Next in performance is the channel shown in Fig. 10-2-5(b), and finally, the best performance is obtained with the channel shown in Fig. 10-2-5(a). In fact, the error rate of the latter is within 3 dB of the error rate achieved with no interference.

One conclusion reached from the results on output SNR γ_x and the limited probability of error results illustrated in Fig. 10-2-4 is that a linear equalizer yields good performance on channels such as telephone lines, where the spectral characteristics of the channels are well behaved and do not exhibit spectral nulls. On the other hand, a linear equalizer is inadequate as a compensator for the intersymbol interference on channels with spectral nulls, which may be encountered in radio transmission.

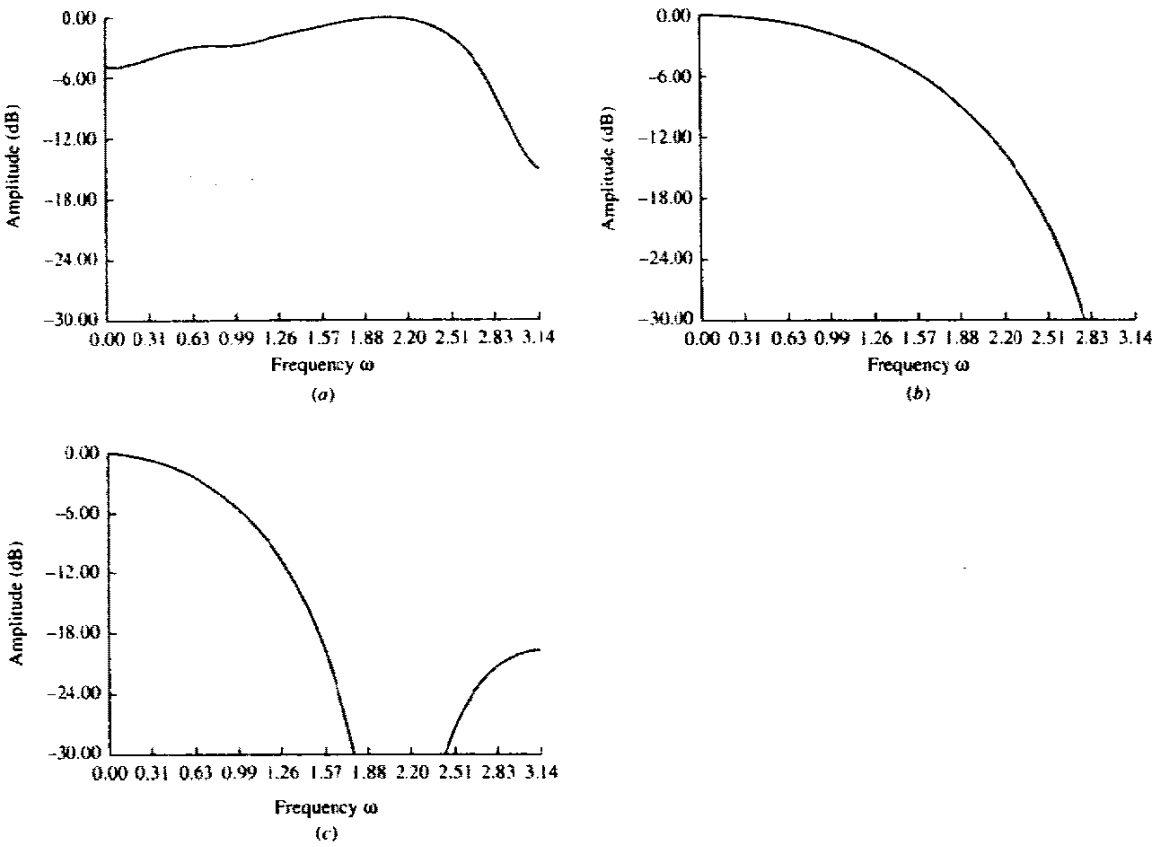

FIGURE 10-2-6 Amplitude spectra for the channels shown in Figs 10-2-5(*a*), (*b*), and (*c*), respectively.

The basic limitation of the linear equalizer to cope with severe ISI has motivated a considerable amount of research into nonlinear equalizers with low computational complexity. The decision-feedback equalizer described in Section 10-3 is shown to be an effective solution to this problem.

10-2-4 Fractionally Spaced Equalizers

In the linear equalizer structures that we have described in the previous section, the equalizer taps are spaced at the reciprocal of the symbol rate, i.e., at the reciprocal of the signaling rate $1/T$. This tap spacing is optimum if the equalizer is preceded by a filter matched to the channel distorted transmitted pulse. When the channel characteristics are unknown, the receiver filter is usually matched to the transmitted signal pulse and the sampling time is optimized for this suboptimum filter. In general, this approach leads to an equalizer performance that is very sensitive to the choice of sampling time.

The limitations of the symbol rate equalizer are most easily evident in the

frequency domain. From (9-2-5), the spectrum of the signal at the input to the equalizer may be expressed as

$$Y_T(f) = \frac{1}{T}\sum_n X\left(f - \frac{n}{T}\right)e^{j2\pi(f-n/T)\tau_0} \tag{10-2-66}$$

where $Y_T(f)$ is the folded or aliased spectrum, where the folding frequency is $1/2T$. Note that the received signal spectrum is dependent on the choice of the sampling delay τ_0. The signal spectrum at the output of the equalizer is $C_T(f)Y_T(f)$, where

$$C_T(f) = \sum_{k=-K}^{K} c_k e^{-j2\pi fkT} \tag{10-2-67}$$

It is clear from these relationships that the symbol rate equalizer can only compensate for the frequency response characteristics of the aliased received signal. It cannot compensate for the channel distortion inherent in $X(f)e^{j2\pi f\tau_0}$.

In contrast to the symbol rate equalizer, a *fractionally spaced equalizer* (FSE) is based on sampling the incoming signal at least as fast as the Nyquist rate. For example, if the transmitted signal consists of pulses having a raised cosine spectrum with a roll-off factor β, its spectrum extends to $F_{\max} = (1+\beta)/2T$. This signal can be sampled at the receiver at a rate

$$2F_{\max} = \frac{1+\beta}{T} \tag{10-2-68}$$

and then passed through an equalizer with tap spacing of $T/(1+\beta)$. For example, if $\beta = 1$, we would have a $\frac{1}{2}T$-spaced equalizer. If $\beta = 0.5$, we would have a $\frac{2}{3}T$-spaced equalizer, and so forth. In general, then, a digitally implemented fractionally spaced equalizer has tap spacing of MT/N where M and N are integers and $N > M$. Usually, a $\frac{1}{2}T$-spaced equalizer is used in many applications.

Since the frequency response of the FSE is

$$C_{T'}(f) = \sum_{k=-K}^{K} c_k e^{-j2\pi fkT'} \tag{10-2-69}$$

where $T' = MT/N$, it follows that $C_{T'}(f)$ can equalize the received signal spectrum beyond the Nyquist frequency $f = 1/2T$ to $f = (1+\beta)/T = N/MT$ The equalized spectrum is

$$\begin{aligned} C_{T'}(f)Y_{T'}(f) &= C_{T'}(f)\sum_n X\left(f - \frac{n}{T'}\right)e^{j2\pi(f-n/T')\tau_0} \\ &= C_{T'}(f)\sum_n X\left(f - \frac{nN}{MT}\right)e^{j2\pi(f-nN/MT)\tau_0} \end{aligned} \tag{10-2-70}$$

Since $X(f) = 0$ for $|f| > N/MT$, (10-2-70) may be expressed as

$$C_{T'}(f)Y_{T'}(f) = C_{T'}(f)X(f)e^{j2\pi f\tau_0}, \quad |f| \leq \frac{1}{2T'} \tag{10-2-71}$$

Thus, we observe that the FSE compensates for the channel distortion in the received signal before the aliasing effects due to symbol rate sampling. In other words, $C_T(f)$ can compensate for any arbitrary timing phase.

The FSE output is sampled at the symbol rate $1/T$ and has the spectrum

$$\sum_k C_T\left(f - \frac{k}{T}\right) X\left(f - \frac{k}{T}\right) e^{j2\pi(f - k/T)\tau_0} \tag{10-2-72}$$

In effect, the optimum FSE is equivalent to the optimum linear receiver consisting of the matched filter followed by a symbol rate equalizer.

Let us now consider the adjustment of the tap coefficients in the FSE. The input to the FSE may be expressed as

$$y\left(\frac{kMT}{N}\right) = \sum_n I_n x\left(\frac{kMT}{N} - nT\right) + v\left(\frac{kMT}{N}\right) \tag{10-2-73}$$

In each symbol interval, the FSE produces an output of the form

$$\hat{I}_k = \sum_{n=-K}^{K} c_n y\left(kT - \frac{nMT}{N}\right) \tag{10-2-74}$$

where the coefficients of the equalizer are selected to minimize the MSE. This optimization leads to a set of linear equations for the equalizer coefficients that have the solution

$$\mathbf{C}_{\text{opt}} = \mathbf{A}^{-1}\boldsymbol{\alpha} \tag{10-2-75}$$

where $\mathbf{A}$ is the covariance matrix of the input data and $\boldsymbol{\alpha}$ is the vector of cross-correlations. These equations are identical in form to those for the symbol rate equalizer, but there are some subtle differences. One is that $\mathbf{A}$ is Hermitian, but not Toeplitz. In addition, $\mathbf{A}$ exhibits periodicities that are inherent in a cyclostationary process, as shown by Qureshi (1985). As a result of the fractional spacing, some of the eigenvalues of $\mathbf{A}$ are nearly zero. Attempts have been made by Long *et al.* (1988a, b) to exploit this property in the coefficient adjustment.

An analysis of the performance of fractionally spaced equalizers, including their convergence properties, is given in a paper by Ungerboeck (1976). Simulation results demonstrating the effectiveness of the FSE over a symbol rate equalizer have also been given in the papers by Qureshi and Forney (1977) and Gitlin and Weinstein (1981). We cite two examples from these papers. First, Fig. 10-2-7 illustrates the performance of the symbol rate equalizer and a $\frac{1}{2}T$-FSE for a channel with high-end amplitude distortion, whose characteristics are also shown in this figure. The symbol-spaced equalizer was preceded with a filter matched to the transmitted pulse that had a (square-root) raised cosine spectrum with a 20% roll-off ($\beta = 0.2$). The FSE did not have any filter preceding it. The symbol rate was 2400 symbols/s and the modulation was QAM. The received SNR was 30 dB. Both equalizers had 31 taps; hence, the $\frac{1}{2}T$-FSE spanned one-half of the time interval of the

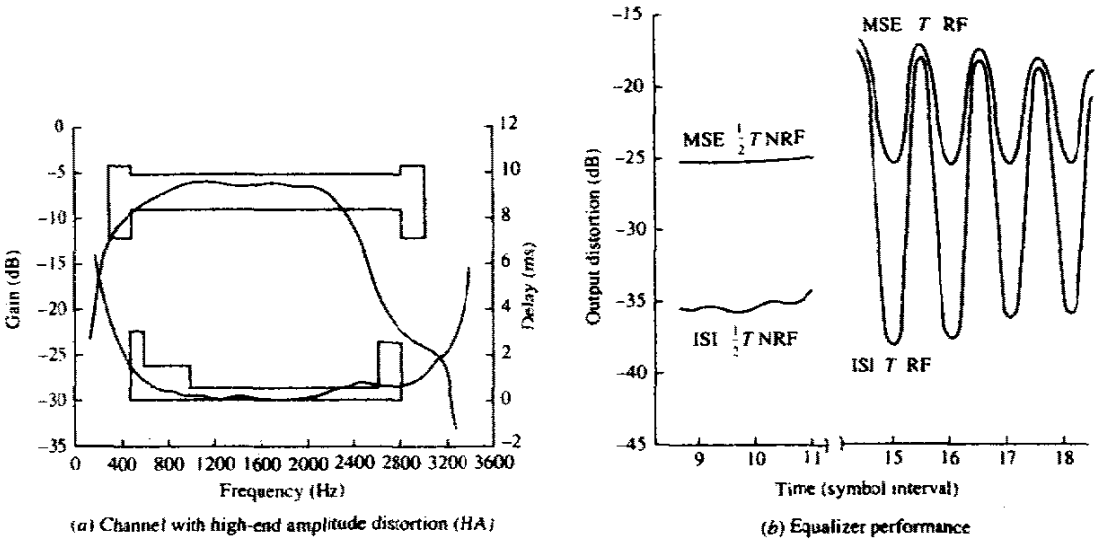

(*a*) Channel with high-end amplitude distortion (*HA*)

(*b*) Equalizer performance

FIGURE 10-2-7 T and $\frac{1}{2}T$ equalizer performance as a function of timing phase for 2400 symbols per second. (NRF indicates no receiver filter.) [*From Qureshi and Forney (1977). © 1977 IEEE.*]

symbol rate equalizer. Nevertheless, the FSE outperformed the symbol rate equalizer when the latter was optimized at the best sampling time. Furthermore, the FSE did not exhibit any sensitivity to timing phase, as illustrated in Fig. 10-2-7.

Similar results were obtained by Gitlin and Weinstein. For a channel with poor envelope delay characteristics, the SNR performance of the symbol rate equalizer and a $\frac{1}{2}T$-FSE are illustrated in Fig. 10-2-8. In this case, both equalizers had the same time span. The T-spaced equalizer had 24 taps while the FSE had 48 taps. The symbol rate was 2400 symbols/s and the data rate was 9600 bits/s with 16-QAM modulation. The signal pulse had a raised cosine spectrum with $\beta = 0.12$. Note again that the FSE outperformed the T-spaced equalizer by several decibels, even when the latter was adjusted for optimum

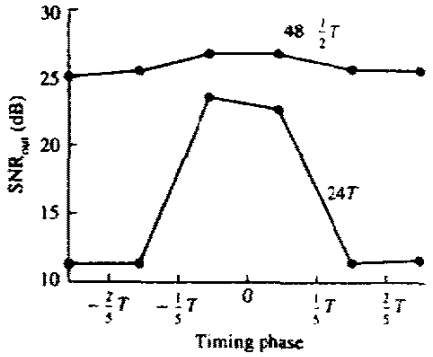

FIGURE 10-2-8 Performance of T and $\frac{1}{2}T$ equalizers as a function of timing phase for 2400 symbols/s 16-QAM on a channel with poor envelope delay. [*From Gitlin and Weinstein (1981). Reprinted with permission from* Bell System Technical Journal. *© 1981 AT & T.*]

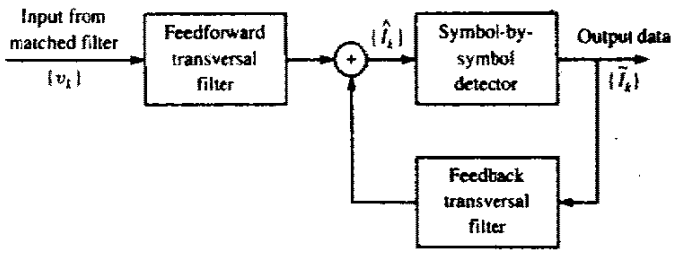

FIGURE 10-3-1 Structure of decision-feedback equalizer.

sampling. The results in these two papers clearly demonstrate the superior performance achieved with a fractionally spaced equalizer.

10-3 DECISION-FEEDBACK EQUALIZATION

The *decision-feedback equalizer* (DFE), depicted in Fig. 10-3-1, consists of two filters, a feedforward filter and a feedback filter. As shown, both have taps spaced at the symbol interval T. The input to the feedforward section is the received signal sequence $\{v_k\}$. In this respect, the feedforward filter is identical to the linear transversal equalizer described in Section 10-2. The feedback filter has as its input the sequence of decisions on previously detected symbols. Functionally, the feedback filter is used to remove that part of the intersymbol interference from the present estimate caused by previously detected symbols.

10-3-1 Coefficient Optimization

From the description given above, it follows that the equalizer output can be expressed as

$$\hat{I}_k = \sum_{j=-K_1}^{0} c_j v_{k-j} + \sum_{j=1}^{K_2} c_j \tilde{I}_{k-j} \tag{10-3-1}$$

where $\hat{I}_k$ is an estimate of the k th information symbol, $\{c_j\}$ are the tap coefficients of the filter, and $\{\tilde{I}_{k-1}, \ldots, \tilde{I}_{k-K_2}\}$ are previously detected symbols. The equalizer is assumed to have $(K_1 + 1)$ taps in its feedforward section and K_2 in its feedback section. It should be observed that this equalizer is nonlinear because the feedback filter contains previously detected symbols $\{\tilde{I}_k\}$.

Both the peak distortion criterior and the MSE criterion result in a mathematically tractable optimization of the equalizer coefficients, as can be concluded from the papers by George *et al.* (1971). Price (1972), Salz (1973), and Proakis (1975). Since the MSE criterion is more prevalent in practice, we focus our attention on it. Based on the assumption that previously detected symbols in the feedback filter are correct, the minimization of MSE

$$J(K_1, K_2) = E\,|I_k - \hat{I}_k|^2 \tag{10-3-2}$$

leads to the following set of linear equations for the coefficients of the feedforward filter:

$$\sum_{j=-K_1}^{0} \psi_{lj} c_j = f^*_{-l}, \qquad l = -K_1, \ldots, -1, 0 \tag{10-3-3}$$

where

$$\psi_{lj} = \sum_{m=0}^{-l} f^*_m f_{m+l-j} + N_0 \delta_{lj}, \qquad l, j = -K_1, \ldots, -1, 0 \tag{10-3-4}$$

The coefficients of the feedback filter of the equalizer are given in terms of the coefficients of the feedforward section by the following expression:

$$c_k = -\sum_{j=-K_1}^{0} c_j f_{k-j}, \qquad k = 1, 2, \ldots, K_2 \tag{10-3-5}$$

The values of the feedback coefficients result in complete elimination of intersymbol interference from previously detected symbols, provided that previous decisions are correct and that $K_2 \geq L$ (see Problem 10-9).

10-3-2 Performance Characteristics of DFE

We now turn our attention to the performance achieved with decision-feedback equalization. The exact evaluation of the performance is complicated to some extent by occasional incorrect decisions made by the detector, which then propagate down the feedback section. In the absence of decision errors, the minimum MSE is given as

$$J_{\min}(K_1) = 1 - \sum_{j=-K_1}^{0} c_j f_{-j} \tag{10-3-6}$$

By going to the limit ($K_1 \to \infty$) of an infinite number of taps in the feedforward filter, we obtain the smallest achievable MSE, denoted as $J_{\min}$. With some effort $J_{\min}$ can be expressed in terms of the spectral characteristics of the channel and additive noise, as shown by Salz (1973). This more desirable form for $J_{\min}$ is

$$J_{\min} = \exp\left\{\frac{T}{2\pi}\int_{-\pi/T}^{\pi/T} \ln\left[\frac{N_0}{X(e^{j\omega T}) + N_0}\right] d\omega\right\} \tag{10-3-7}$$

The corresponding output SNR is

$$\begin{aligned}\gamma_\infty &= \frac{1 - J_{\min}}{J_{\min}} \\ &= -1 + \exp\left\{\frac{T}{2\pi}\int_{-\pi/T}^{\pi/T} \ln\left[\frac{N_0 + X(e^{j\omega T})}{N_0}\right] d\omega\right\}\end{aligned} \tag{10-3-8}$$

We observe again that, in the absence of intersymbol interference, $X(e^{j\omega T}) = 1$ and, hence, $J_{\min} = N_0/(1 + N_0)$. The corresponding output SNR is $\gamma_\infty = 1/N_0$.

Example 10-3-1

It is interesting to compare the value of $J_{\min}$ for the decision-feedback equalizer with the value of $J_{\min}$ obtained with the linear MSE equalizer. For example, ler us consider the discrete-time equivalent channel consisting of two taps f_0 and f_1. The minimum MSE for this channel is

$$\begin{aligned} J_{\min} &= \exp\left\{\frac{T}{2\pi}\int_{-\pi/T}^{\pi/T} \ln\left[\frac{N_0}{1+N_0+2|f_0||f_1|\cos(\omega T+\theta)}\right]d\omega\right\} \\ &= N_0 \exp\left[-\frac{1}{2\pi}\int_{-\pi}^{\pi} \ln(1+N_0+2|f_0||f_1|\cos\omega)\,d\omega\right] \\ &= \frac{2N_0}{1+N_0+\sqrt{(1+N_0)^2-4|f_0 f_1|^2}} \end{aligned} \tag{10-3-9}$$

Note that $J_{\min}$ is maximized when $|f_0| = |f_1| = \sqrt{\frac{1}{2}}$. Then

$$\begin{aligned} J_{\min} &= \frac{2N_0}{1+N_0+\sqrt{(1+N_0)^2-1}} \\ &\approx 2N_0, \qquad N_0 \ll 1 \end{aligned} \tag{10-3-10}$$

The corresponding output SNR is

$$\gamma_\infty \approx \frac{1}{2N_0}, \qquad N_0 \ll 1 \tag{10-3-11}$$

Therefore, there is a 3 dB degradation in output SNR due to the presence of intersymbol interference. In comparison, the performance loss for the linear equalizer is very severe. Its output SNR as given by (10-2-53) is $\gamma_\infty \approx (2/N_0)^{1/2}$ for $N_0 \ll 1$.

Example 10-3-2

Consider the exponentially decaying channel characteristic of the form

$$f_k = (1-a^2)^{1/2}a^k, \qquad k = 0, 1, 2, \ldots \tag{10-3-12}$$

where $a < 1$. The output SNR of the decision-feedback equalizer is

$$\begin{aligned} \gamma_\infty &= -1 + \exp\left\{\frac{1}{2\pi}\int_{-\pi}^{\pi} \ln\left[\frac{1+a^2+(1-a^2)/N_0-2a\cos\omega}{1+a^2-2a\cos\omega}\right]d\omega\right\} \\ &= -1 + \frac{1}{2N_0}\{1-a^2+N_0(1+a^2)+\sqrt{[1-a^2+N_0(1+a^2)]^2-4a^2N_0^2}\} \\ &\approx \frac{(1-a^2)[1+N_0(1+a^2)/(1-a^2)]-N_0}{N_0} \\ &\approx \frac{1-a^2}{N_0}, \qquad N_0 \ll 1 \end{aligned} \tag{10-3-13}$$

Thus, the loss in SNR is $10 \log_{10}(1 - a^2)$ dB. In comparison, the linear equalizer has a loss of $10 \log_{10}[(1 - a^2)/(1 + a^2)]$ dB.

These results illustrate the superiority of the decision-feedback equalizer over the linear equalizer when the effect of decision errors on performance is neglected. It is apparent that a considerable gain in performance can be achieved relative to the linear equalizer by the inclusion of the decision-feedback section, which eliminates the intersymbol interference from previously detected symbols.

One method of assessing the effect of decision errors on the error rate performance of the decision-feedback equalizer is Monte Carlo simulation on a digital computer. For purposes of illustration, we offer the following results for binary PAM signaling through the equivalent discrete-time channel models shown in Figs 10-2-5(*b*) and (*c*).

The results of the simulation are displayed in Fig. 10-3-2. First of all, a comparison of these results with those presented in Fig. 10-2-4 leads us to conclude that the decision-feedback equalizer yields a significant improvement in performance relative to the linear equalizer having the same number of taps. Second, these results indicate that there is still a significant degradation in performance of the decision-feedback equalizer due to the residual intersymbol interference, especially on channels with severe distortion such as the one

FIGURE 10-3-2 *Performance of decision-feedback equalizer with and without error propagation.*

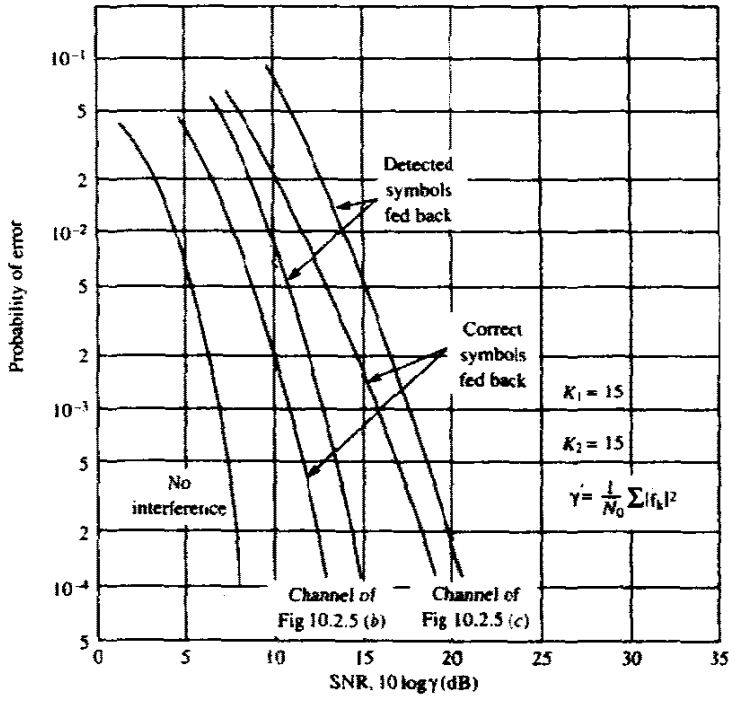

shown in Fig. 10-2-5(*c*). Finally, the performance loss due to incorrect decisions being fed back is 2 dB, approximately, for the channel responses under consideration. Additional results on the probability of error for a decision-feedback equalizer with error propagation may be found in the papers by Duttweiler *et al.* (1974) and Beaulieu (1992).

The structure of the DFE that is analyzed above employs a T-spaced filter for the feedforward section. The optimality of such a structure is based on the assumption that the analog filter preceding the DFE is matched to the channel-corrupted pulse response and its output is sampled at the optimum time instant. In practice, the channel response is not known a priori, so it is not possible to design an ideal matched filter. In view of this difficulty, it is customary in practical applications to use a fractionally spaced feedforward filter. Of course, the feedback filter tap spacing remains at T. The use of the FSE for the feedforward filter eliminates the system sensitivity to a timing error.

Performance Comparison with MLSE We conclude this subsection on the performance of the DFE by comparing its performance against that of MLSE. For the two-path channel with $f_0 = f_1 = \sqrt{\frac{1}{2}}$, we have shown that MLSE suffers no SNR loss while the decision-feedback equalizer suffers a 3 dB loss. On channels with more distortion, the SNR advantage of MLSE over decision-feedback equalization is even greater. Figure 10-3-3 illustrates a comparison of the error rate performance of these two equalization techniques, obtained via Monte Carlo simulation, for binary PAM and the channel characteristics shown in Figs 10-2-5(*b*) and (*c*). The error rate curves for the two methods have different slopes; hence the difference in SNR increases as the error

FIGURE 10-3-3 Comparison of performance between MLSE and decision-feedback equalization for channel characteristics shown (*a*) in Fig. 10-2-5(*b*) and (*b*) in Fig. 10-2-5(*c*).

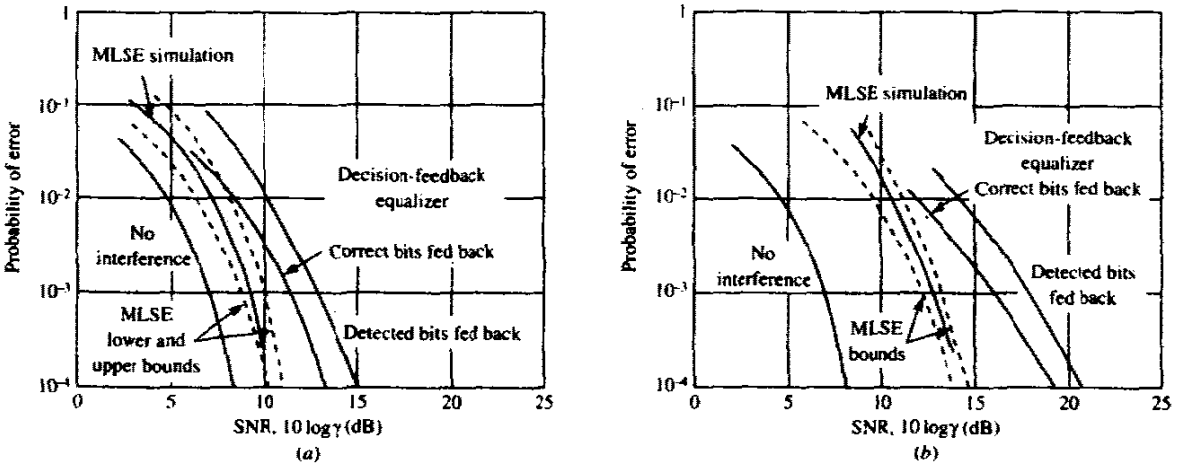

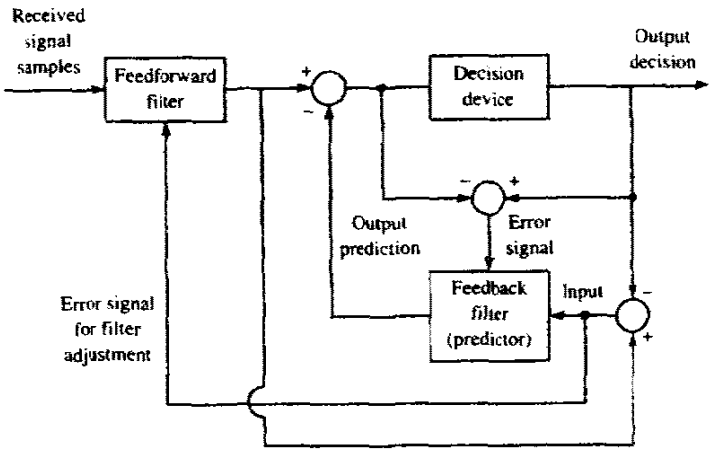

FIGURE 10-3-4 Block diagram of predictive DFE.

probability decreases. As a benchmark, the error rate for the AWGN channel with no intersymbol interference is also shown in Fig. 10-3-3.

10-3-3 Predictive Decision-Feedback Equalizer

Belfiore and Park (1979) proposed another DFE structure that is equivalent to the one shown in Fig. 10-3-1 under the condition that the feedforward filter has an infinite number of taps. This structure consists of a FSE as a feedforward filter and a linear predictor as a feedback filter, as shown in the configuration given in Fig. 10-3-4. Let us briefly consider the performance characteristics of this equalizer.

First of all, the noise at the output of the infinite length feedforward filter has the power spectral density

$$\frac{N_0 X(e^{j\omega T})}{|N_0 + X(e^{j\omega T})|^2}, \qquad |\omega| \leq \frac{\pi}{T} \tag{10-3-14}$$

The residual intersymbol interference has the power spectral density

$$\left|1 - \frac{X(e^{j\omega T})}{N_0 + X(e^{j\omega T})}\right|^2 = \frac{N_0^2}{|N_0 + X(e^{j\omega T})|^2}, \qquad |\omega| \leq \frac{\pi}{T} \tag{10-3-15}$$

The sum of these two spectra represents the power spectral density of the total noise and intersymbol interference at the output of the feedforward filter. Thus, on adding (10-3-14) and (10-3-15), we obtain

$$E(\omega) = \frac{N_0}{N_0 + X(e^{j\omega T})}, \qquad |\omega| \leq \frac{\pi}{T} \tag{10-3-16}$$

As we have observed previously, if $X(e^{j\omega T}) = 1$, the channel is ideal and,

hence, it is not possible to reduce the MSE any further. On the other hand, if there is channel distortion, the power in the error sequence at the output of the feedforward filter can be reduced by means of linear prediction based on past values of the error sequence.

If $\mathcal{B}(\omega)$ represents the frequency response of the infinite length feedback predictor, i.e.,

$$\mathcal{B}(\omega) = \sum_{n=1}^{\infty} b_n e^{-j\omega nT} \tag{10-3-17}$$

then the error at the output of the predictor is

$$E(\omega) - E(\omega)\mathcal{B}(\omega) = E(\omega)[1 - \mathcal{B}(\omega)] \tag{10-3-18}$$

The minimization of the mean square value of this error, i.e.,

$$J = \frac{1}{2\pi}\int_{-\pi/T}^{\pi/T} |1 - \mathcal{B}(\omega)|^2 |E(\omega)|^2 \, d\omega \tag{10-3-19}$$

over the predictor coefficients $\{b_n\}$ yields the optimum predictor in the form

$$\mathcal{B}(\omega) = 1 - \frac{G(\omega)}{g_0} \tag{10-3-20}$$

where $G(\omega)$ is the solution to the spectral factorization

$$G(\omega)G^*(-\omega) = \frac{1}{|E(\omega)|^2} \tag{10-3-21}$$

and

$$G(\omega) = \sum_{n=0}^{\infty} g_n e^{-j\omega nT} \tag{10-3-22}$$

The output of the infinite length linear predictor is a white noise sequence with power spectral density $1/g_0^2$ and the corresponding minimum MSE is given by (10-3-7). Therefore, the MSE performance of the infinite-length predictive DFE is identical to the conventional DFE.

Although these two DFE structures result in equivalent performance if their lengths are infinite, the predictive DFE is suboptimum if the lengths of the two filters are finite. The reason for the optimality of the conventional DFE is relatively simple. The optimization of its tap coefficients in the feedforward and feedback filters is done jointly. Hence, it yields the minimum MSE. On the other hand, the optimizations of the feedforward filter and the feedback predictor in the predictive DFE are done separately. Hence, its MSE is at least as large as that of the conventional DFE. In spite of this suboptimality of the predictive DFE, it is suitable as an equalizer for trellis-coded signals, where the conventional DFE is not as suitable, as described in the next chapter.

10-4 BIBLIOGRAPHICAL NOTES AND REFERENCES

Channel equalization for digital communications was developed by Lucky (1965, 1966), who focused on linear equalizers that were optimized using the peak distortion criterion. The mean square error criterion for optimization of the equalizer coefficients was proposed by Widrow (1966).

Decision-feedback equalization was proposed and analyzed by Austin (1967). Analyses of the performance of the DFE can be found in the papers by Monsen (1971), George *et al.* (1971), Price (1972), Salz (1973), Duttweiler *et al.* (1974), and Altekar and Beaulieu (1993).

The use of the Viterbi algorithm as the optimal maximum-likelihood sequence estimator for symbols corrupted by ISI was proposed and analyzed by Forney (1972) and Omura (1971). Its use for carrier-modulated signals was considered by Ungerboeck (1974) and MacKenchnie (1973).

PROBLEMS

10-1 In a binary PAM system, the input to the detector is

$$y_m = a_m + n_m + i_m$$

where $a_m = \pm 1$ is the desired signal, n_m is a zero-mean Gaussian random variable with variance σ_n^2, and i_m represents the ISI due to channel distortion. The ISI term is a random variable that takes the values $-\frac{1}{2}$, 0, and $\frac{1}{2}$ with probabilities $\frac{1}{4}$, $\frac{1}{2}$, and $\frac{1}{4}$, respectively. Determine the average probability of error as a function of σ_n^2.

10-2 In a binary PAM system, the clock that specifies the sampling of the correlator output is offset from the optimum sampling time by 10%.

a If the signal pulse used is rectangular, determine the loss in SNR due to the mistiming.

b Determine the amount of ISI introduced by the mistiming and determine its effect on performance.

10-3 The frequency response characteristic of a lowpass channel can be approximated by

$$H(f) = \begin{cases} 1 + \alpha \cos 2\pi f t_0 & (|\alpha| < 1,\ |f| \le W) \\ 0 & (\text{otherwise}) \end{cases}$$

where W is the channel bandwidth. An input signal $s(t)$ whose spectrum is bandlimited to W Hz is passed through the channel.

a Show that

$$y(t) = s(t) + \tfrac{1}{2}\alpha[s(t - t_0) + s(t + t_0)]$$

Thus, the channel produces a pair of echoes.

b Suppose that the received signal $y(t)$ is passed through a filter matched to $s(t)$. Determine the output of the matched filter at $t = kT$, $k = 0, \pm 1, \pm 2, \ldots$, where T is the symbol duration.

c What is the ISI pattern resulting from the channel if $t_0 = T$?

10-4 A wireline channel of length 1000 km is used to transmit data by means of binary

PAM. Regenerative repeaters are spaced 50 km apart along the system. Each segment of the channel has an ideal (constant) frequency response over the frequency band $0 \leq f \leq 1200$ Hz and an attenuation of 1 dB/km. The channel noise is AWGN.

a What is the highest bit rate that can be transmitted without ISI?

b Determine the required $\mathscr{E}_b/N_0$ to achieve a bit error of $P_2 = 10^{-7}$ for each repeater.

c Determine the transmitted power at each repeater to achieve the desired $\mathscr{E}_b/N_0$, where $N_0 = 4.1 \times 10^{-21}$ W/Hz.

10-5 Prove the relationship in (10-1-13) for the autocorrelation of the noise at the output of the matched filter.

10-6 In the case of PAM with correlated noise, the correlation metrics in the Viterbi algorithm may be expressed in general as (Ungerboeck, 1974)

$$CM(\mathbf{I}) = 2\sum_n I_n r_n - \sum_n \sum_m I_n I_m x_{n-m}$$

where $x_n = x(nT)$ is the sampled signal output of the matched filter, $\{I_n\}$ is the data sequence, and $\{r_n\}$ is the received signal sequence at the output of the matched filter. Determine the metric for the duobinary signal.

10-7 Consider the use of a (square-root) raised cosine signal pulse with a roll-off factor of unity for transmission of binary PAM over an ideal bandlimited channel that passes the pulse without distortion. Thus, the transmitted signal is

$$v(t) = \sum_{k=-\infty}^{\infty} I_k g_T(t - kT_b)$$

where the signal interval $T_b = \frac{1}{2}T$. Thus, the symbol rate is double of that for no ISI.

a Determine the ISI values at the output of a matched filter demodulator.

b Sketch the trellis for the maximum-likelihood sequence detector and label the states.

10-8 A binary antipodal signal is transmitted over a nonideal band-limited channel, which introduces ISI over two adjacent symbols. For an isolated transmitted signal pulse $s(t)$, the (noise-free) output of the demodulator is $\sqrt{\mathscr{E}_b}$ at $t = T$, $\sqrt{\mathscr{E}_b}/4$ at $t = 2T$, and zero for $t = kT$, $k > 2$, where $\mathscr{E}_b$ is the signal energy and T is the signaling interval.

a Determine the average probability of error, assuming that the two signals are equally probable and the additive noise is white and gaussian.

b By plotting the error probability obtained in (a) and that for the case of no ISI, determine the relative difference in SNR of the error probability of 10^{-6}.

10-9 Derive the expression in (10-3-5) for the coefficients in the feedback filter of the DFE.

10-10 Binary PAM is used to transmit information over an unequalized linear filter channel. When $a = 1$ is transmitted, the noise-free output of the demodulator is

$$x_m = \begin{cases} 0.3 & (m = 1) \\ 0.9 & (m = 0) \\ 0.3 & (m = -1) \\ 0 & \text{(otherwise)} \end{cases}$$

a Design a three-tap zero-forcing linear equalizer so that the output is

$$q_m = \begin{cases} 1 & (m = 0) \\ 0 & (m = \pm 1) \end{cases}$$

b Determine q_m for $m = \pm 2, \pm 3$, by convolving the impulse response of the equalizer with the channel response.

10-11 The transmission of a signal pulse with a raised cosine spectrum through a channel results in the following (noise-free) sampled output from the demodulator:

$$x_k = \begin{cases} -0.5 & (k = -2) \\ 0.1 & (k = -1) \\ 1 & (k = 0) \\ -0.2 & (k = 1) \\ 0.05 & (k = 2) \\ 0 & (\text{otherwise}) \end{cases}$$

a Determine the tap coefficients of a three-tap linear equalizer based on the zero-forcing criterion.

b For the coefficients determined in (a), determine the output of the equalizer for the case of the isolated pulse. Thus, determine the residual ISI and its span in time.

10-12 A nonideal band-limited channel introduces ISI over three successive symbols. The (noise-free) response of the matched filter demodulator sampled at the sampling time kT is

$$\int_{-\infty}^{\infty} s(t)s(t - kT)\,dt = \begin{cases} \mathscr{E}_b & (k = 0) \\ 0.9\mathscr{E}_b & (k = \pm 1) \\ 0.1\mathscr{E}_b & (k = \pm 2) \\ 0 & (\text{otherwise}) \end{cases}$$

a Determine the tap coefficients of a three-tap linear equalizer that equalizes the channel (received signal) response to an equivalent partial response (duobinary) signal

$$y_k = \begin{cases} \mathscr{E}_b & (k = 0, 1) \\ 0 & (\text{otherwise}) \end{cases}$$

b Suppose that the linear equalizer in (a) is followed by a Viterbi sequence detector for the partial signal. Give an estimate of the error probability if the additive noise is white and gaussian, with power spectral density $\frac{1}{2}N_0$ W/Hz.

***10-13** Determine the tap weight coefficients of a three-tap zero-forcing equalizer if the ISI spans three symbols and is characterized by the values $x(0) = 1, x(-1) = 0.3$, $x(1) = 0.2$. Also determine the residual ISI at the output of the equalizer for the optimum tap coefficients.

10-14 In line-of-sight microwave radio transmission, the signal arrives at the receiver via two propagation paths: the direct path and a delayed path that occurs due to signal reflection from surrounding terrain. Suppose that the received signal has the form

$$r(t) = s(t) + \alpha s(t - T) + n(t)$$

where $s(t)$ is the transmitted signal, α is the attenuation ($\alpha < 1$) of the secondary path and $n(t)$ is AWGN.

a Determine the output of the demodulator at $t = T$ and $t = 2T$ that employs a filter matched to $s(t)$.

b Determine the probability of error for a symbol-by-symbol detector if the transmitted signal is binary antipodal and the detector ignores the ISI.

c What is the error-rate performance of a simple (one-tap) DFE that estimates α and removes the ISI? Sketch the detector structure that employs a DFE.

10-15 Repeat Problem 10-10 using the MMSE as the criterion for optimizing the tap coefficients. Assume that the noise power spectral density is 0.1 W/Hz.

10-16 In a magnetic recording channel, where the readback pulse resulting from a positive transition in the write current has the form

$$p(t) = \left[1 + \left(\frac{2t}{T_{50}}\right)^2\right]^{-1}$$

a linear equalizer is used to equalize the pulse to a partial response. The parameter T_{50} is defined as the width of the pulse at the 50% amplitude level. The bit rate is $1/T_b$ and the ratio of $T_{50}/T_b = \Delta$ is the normalized density of the recording. Suppose the pulse is equalized to the partial-response values

$$x(nT) = \begin{cases} 1 & (n = -1, 1) \\ 2 & (n = 0) \\ 0 & \text{(otherwise)} \end{cases}$$

where $x(t)$ represents the equalized pulse shape.

a Determine the spectrum $X(f)$ of the band-limited equalized pulse.

b Determine the possible output levels at the detector, assuming that successive transitions can occur at the rate $1/T_b$.

c Determine the error rate performance of the symbol-by-symbol detector for this signal, assuming that the additive noise is zero-mean gaussian with variance σ^2.

10-17 Sketch the trellis for the Viterbi detector of the equalized signal in Problem 10-16 and label all the states. Also, determine the minimum euclidean distance between merging paths.

10-18 Consider the problem of equalizing the discrete-time equivalent channel shown in Fig. P10-18. The information sequence $\{I_n\}$ is binary (± 1) and uncorrelated.

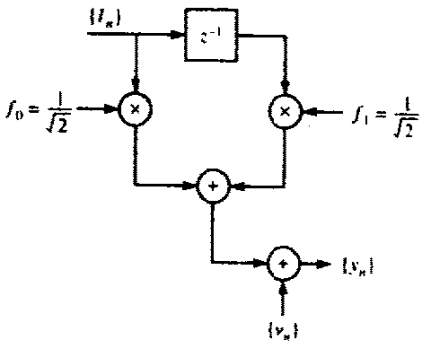

FIGURE P10-18

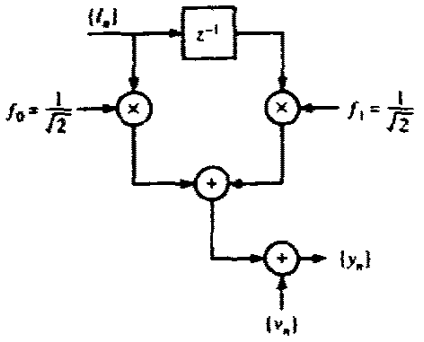

FIGURE P10-21

The additive noise $\{v_n\}$ is white and real-valued, with variance N_0. The received sequence $\{y_n\}$ is processed by a linear three-tap equalizer that is optimized on the basis of the MSE criterion.

a Determine the optimum coefficients of the equalizer as a function of N_0.

b Determine the three eigenvalues λ_1, λ_2, and λ_3 of the covariance matrix Γ and the corresponding (normalized to unit length) eigenvectors $\mathbf{v}_1$, $\mathbf{v}_2$, $\mathbf{v}_3$.

c Determine the minimum MSE for the three-tap equalizer as a function of N_0.

d Determine the output SNR for the three-tap equalizer as a function of N_0. How does this compare with the output SNR for the infinite-tap equalizer? For example, evaluate the output SNR for these two equalizers when $N_0 = 0.1$.

10-19 Use the orthogonality principle to derive the equations for the coefficients in a decision-feedback equalizer based on the MSE criterion and given by (10-3-3) and (10-3-5).

10-20 Suppose that the discrete-time model for the intersymbol interference is characterized by the tap coefficients $f_0, f_1, \ldots, f_L$. From the equations for the tap coefficients of a decision-feedback equalizer (DFE), show that only L taps are needed in the feedback filter of the DFE. That is, if $\{c_k\}$ are the coefficients of the feedback filter then $c_k = 0$ for $k \geq L + 1$.

10-21 Consider the channel model shown in Fig. P10-21. $\{v_n\}$ is a real-valued white-noise sequence with zero mean and variance N_0. Suppose the channel is to be equalized by DFE having a two-tap feedforward filter (c_0, c_{-1}) and a one-tap feedback filter (c_1). The $\{c_i\}$ are optimized using the MSE criterion.

a Determine the optimum coefficients and their approximate values for $N_0 \ll 1$.

b Determine the exact value of the minimum MSE and a first-order approximation appropriate to the case $N_0 \ll 1$.

c Determine the exact value of the output SNR for the three-tap equalizer as a function of N_0 and a first-order approximation appropriate to the case $N_0 \ll 1$.

d Compare the results in (b) and (c) with the performance of the infinite-tap DFE.

e Evaluate and compare the exact values of the output SNR for the three-tap and infinite-tap DFE in the special cases where $N_0 = 0.1$ and 0.01. Comment on how well the three-tap equalizer performs relative to the infinite-tap equalizer.

10-22 A pulse and its (raised-cosine) spectral characteristic are shown in Fig. P10-22. This pulse is used for transmitting digital information over a band-limited channel at a rate $1/T$ symbols/s.

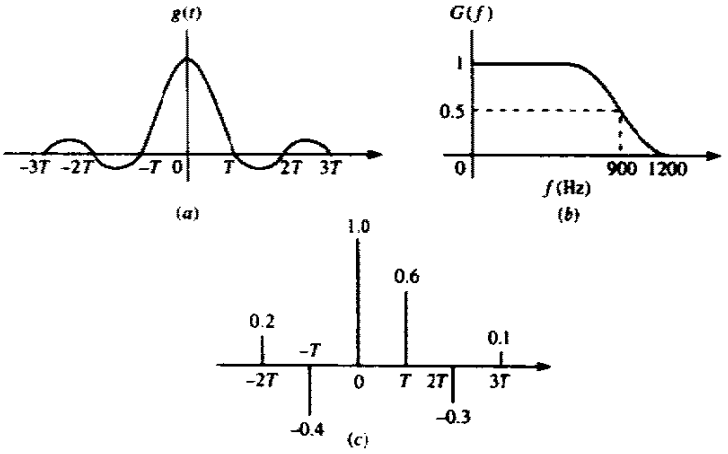

FIGURE P10-22

a What is the roll-off factor β?
b What is the pulse rate?
c The channel distorts the signal pulses. Suppose the sampled values of the filtered received pulse $x(t)$ are as shown in Fig. P10-22(*c*) It is obvious that there are five interfering signal components. Give the sequence of +1s and −1s that will cause the largest (destructive or constructive) interference and the corresponding value of the interference (the peak distortion).
d What is the probability of occurrence of the worst sequence obtained in (c), assuming that all binary digits are equally probable and independent?

10-23 A time-dispersive channel having an impulse response $h(t)$ is used to transmit four-phase PSK at a rate $R = 1/T$ symbols/s. The equivalent discrete-time channel is shown in Fig. P10-23. The sequence $\{\eta_k\}$ is a white noise sequence having zero mean and variance $\sigma^2 = N_0$.

a What is the sampled autocorrelation function sequence $\{x_k\}$ defined by

$$x_k = \int_{-\infty}^{\infty} h^*(t)h(t + kT)\,dt$$

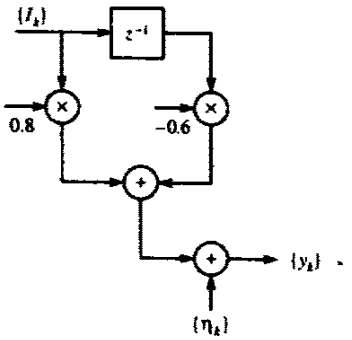

FIGURE P10-23

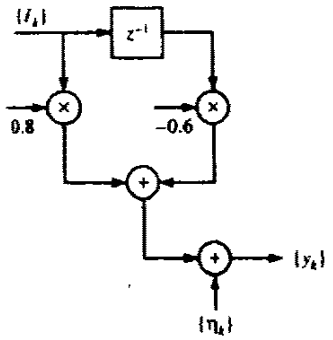

FIGURE P10-24

for this channel?

b The minimum MSE performance of a linear equalizer and a decision-feedback equalizer having an infinite number of taps depends on the *folded spectrum of the channel*

$$\frac{1}{T}\sum_{n=-\infty}^{\infty}\left|H\left(\omega+\frac{2\pi n}{T}\right)\right|^2$$

where $H(\omega)$ is the Fourier transform of $h(t)$. Determine the folded spectrum of the channel given above.

c Use your answer in (b) to express the minimum MSE of a linear equalizer in terms of the folded spectrum of the channel. (You may leave your answer in integral form.)

d Repeat (c) for an infinite-tap decision-feedback equalizer.

10-24 Consider a four-level PAM system with possible transmitted levels, 3, 1, −1, and −3. The channel through which the data are transmitted introduces intersymbol interference over two successive symbols. The equivalent discrete-time channel model is shown in Fig. P10-24. $\{\eta_k\}$ is a sequence of real-valued independent zero-mean gaussian noise variables with variance $\sigma^2 = N_0$. The received sequence is

$$\begin{aligned} y_1 &= 0.8I_1 + n_1 \\ y_2 &= 0.8I_2 - 0.6I_1 + n_2 \\ y_3 &= 0.8I_3 - 0.6I_2 + n_3 \\ &\vdots \\ y_k &= 0.8I_k - 0.6I_{k-1} + n_k \end{aligned}$$

a Sketch the tree structure, showing the possible signal sequences for the received signals y_1, y_2 and y_3.

b Suppose the Viterbi algorithm is used to detect the information sequence. How many probabilities must be computed at each stage of the algorithm?

c How many surviving sequences are there in the Viterbi algorithm for this channel?

d Suppose that the received signals are

$$y_1 = 0.5, \quad y_2 = 2.0, \quad y_3 = -1.0$$

Determine the surviving sequences through stage y_3 and the corresponding metrics.

e Give a tight upper bound for the probability of error for four-level PAM transmitted over this channel.

10-25 A transversal equalizer with K taps has an impulse response

$$e(t) = \sum_{k=0}^{K-1} c_k \delta(t - kT)$$

where T is the delay between adjacent taps, and a transfer function

$$E(z) = \sum_{k=0}^{K-1} c_k z^{-k}$$

The *discrete Fourier transform* (DFT) of the equalizer coefficients $\{c_k\}$ is defined as

$$E_n \equiv E(z)|_{z=e^{j2\pi n/K}} = \sum_{k=0}^{K-1} c_k e^{-j2\pi kn/K}, \quad n = 0, 1, \ldots, K-1$$

The *inverse DFT* is defined as

$$b_k = \frac{1}{K} \sum_{n=0}^{K-1} E_n e^{j2\pi nk/K}, \quad k = 0, 1, \ldots, K-1$$

a Show that $b_k = c_k$, by substituting for E_n in the above expression.

b From the relations given above, derive an equivalent filter structure having the z transform

$$E(z) = \underbrace{\frac{1 - z^{-K}}{K}}_{E_1(z)} \sum_{n=0}^{K-1} \underbrace{\frac{E_n}{1 - e^{j2\pi n/K} z^{-1}}}_{E_2(z)}$$

c If $E(z)$ is considered as two separate filters $E_1(z)$ and $E_2(z)$ in cascade, sketch a block diagram for each of the filters, using z^{-1} to denote a unit of delay.

d In the transversal equalizer, the adjustable parameters are the equalizer coefficients $\{c_k\}$. What are the adjustable parameters of the equivalent equalizer in (b), and how are they related to $\{c_k\}$?

11

ADAPTIVE EQUALIZATION

In Chapter 10, we introduced both optimum and suboptimum receivers that compensate for ISI in the transmission of digital information through band-limited, nonideal channels. The optimum receiver employed maximum-likelihood sequence estimation for detecting the information sequence from the samples of the demodulation filter. The suboptimum receivers employed either a linear equalizer or a decision-feedback equalizer.

In the development of the three equalization methods, we implicitly assumed that the channel characteristics, either the impulse response or the frequency response, were known at the receiver. However, in most communication systems that employ equalizers, the channel characteristics are unknown a priori and, in many cases, the channel response is time-variant. In such a case, the equalizers are designed to be adjustable to the channel response and, for time-variant channels, to be adaptive to the time variations in the channel response.

In this chapter, we present algorithms for automatically adjusting the equalizer coefficients to optimize a specified performance index and to adaptively compensate for time variations in the channel characteristics. We also analyze the performance characteristics of the algorithm, including their rate of convergence and their computational complexity.

11-1 ADAPTIVE LINEAR EQUALIZER

In the case of the linear equalizer, recall that we considered two different criteria for determining the values of the equalizer coefficients $\{c_k\}$. One criterion was based on the minimization of the peak distortion at the output of

the equalizer, which is defined by (10-2-4). The other criterion was based on the minimization of the mean-square error at the output of the equalizer, which is defined by (10-2-25). Below, we describe two algorithms for performing the optimization automatically and adaptively.

11-1-1 The Zero-Forcing Algorithm

In the peak-distortion criterion, the peak distortion $\mathcal{D}(\mathbf{c})$, given by (10-2-22), is minimized by selecting the equalizer coefficients $\{c_k\}$. In general, there is no simple computational algorithm for performing this optimization, except in the special case where the peak distortion at the input to the equalizer, defined as $\mathcal{D}_0$ in (10-2-23), is less than unity. When $\mathcal{D}_0 < 1$, the distortion $\mathcal{D}(\mathbf{c})$ at the output of the equalizer is minimized by forcing the equalizer response $q_n = 0$, for $1 \leq |n| \leq K$, and $q_0 = 1$. In this case, there is a simple computational algorithm, called the zero-forcing algorithm, that achieves these conditions.

The zero-forcing solution is achieved by forcing the cross-correlation between the error sequence $\varepsilon_k = I_k - \hat{I}_k$ and the desired information sequence $\{I_k\}$ to be zero for shifts in the range $0 \leq |n| \leq K$. The demonstration that this leads to the desired solution is quite simple. We have

$$\begin{aligned} E(\varepsilon_k I_{k-j}^*) &= E[(I_k - \hat{I}_k) I_{k-j}^*] \\ &= E(I_k I_{k-j}^*) - E(\hat{I}_k I_{k-j}^*), \quad j = -K, \ldots, K \end{aligned} \tag{11-1-1}$$

We assume that the information symbols are uncorrelated, i.e., $E(I_k I_j^*) = \delta_{kj}$, and that the information sequence $\{I_k\}$ is uncorrelated with the additive noise sequence $\{\eta_k\}$. For $\hat{I}_k$, we use the expression given in (10-2-41). Then, after taking the expected values in (11-1-1), we obtain

$$E(\varepsilon_k I_{k-j}^*) = \delta_{j0} - q_j, \quad j = -K, \ldots, K \tag{11-1-2}$$

Therefore, the conditions

$$E(\varepsilon_k I_{k-j}^*) = 0, \quad j = -K, \ldots, K \tag{11-1-3}$$

are fulfilled when $q_0 = 1$ and $q_n = 0$, $1 \leq |n| \leq K$.

When the channel response is unknown, the cross-correlations given by (11-1-1) are also unknown. This difficulty can be circumvented by transmitting a known training sequence $\{I_k\}$ to the receiver, which can be used to estimate the cross-correlation by substituting time averages for the ensemble averages given in (11-1-1). After the initial training, which will require the transmission of a training sequence of some predetermined length that equals or exceeds the equalizer length, the equalizer coefficients that satisfy (11-1-3) can be determined.

A simple recursive algorithm for adjusting the equalizer coefficients is

$$c_j^{(k+1)} = c_j^{(k)} + \Delta \varepsilon_k I_{k-j}^*, \quad j = -K, \ldots, -1, 0, 1, \ldots, K \qquad (11\text{-}1\text{-}4)$$

where $c_j^{(k)}$ is the value of the jth coefficient at time $t = kT$, $\varepsilon_k = I_k - \hat{I}_k$ is the error signal at time $t = kT$, and Δ is a scale factor that controls the rate of adjustment, as will be explained later in this section. This is the *zero-forcing algorithm*. The term $\varepsilon_k I_{k-j}^*$ is an estimate of the cross-correlation (ensemble average) $E(\varepsilon_k I_{k-j}^*)$. The averaging operation of the cross-correlation is accomplished by means of the recursive first-order difference equation algorithm in (11-1-4), which represents a simple discrete-time integrator.

Following the training period, after which the equalizer coefficients have converged to their optimum values, the decisions at the output of the detector are generally sufficiently reliable so that they may be used to continue the coefficient adaptation process. This is called a *decision-directed mode* of adaptation. In such a case, the cross-correlations in (11-1-4) involve the error signal $\tilde{\varepsilon}_k = \tilde{I}_k - \hat{I}_k$ and the detected output sequence $\tilde{I}_{k-j}$, $j = -K, \ldots, K$. Thus, in the adaptive mode, (11-1-4) becomes

$$c_j^{(k+j)} = c_j^{(k)} + \Delta \tilde{\varepsilon}_k \tilde{I}_{k-j}^* \qquad (11\text{-}1\text{-}5)$$

Figure 11-1-1 illustrates the zero-forcing equalizer in the training mode and the adaptive mode of operation.

The characteristics of the zero-forcing algorithm are similar to those of the LMS algorithm, which minimizes the MSE and which is described in detail in the following section.

FIGURE 11-1-1 An adaptive zero-forcing equalizer.

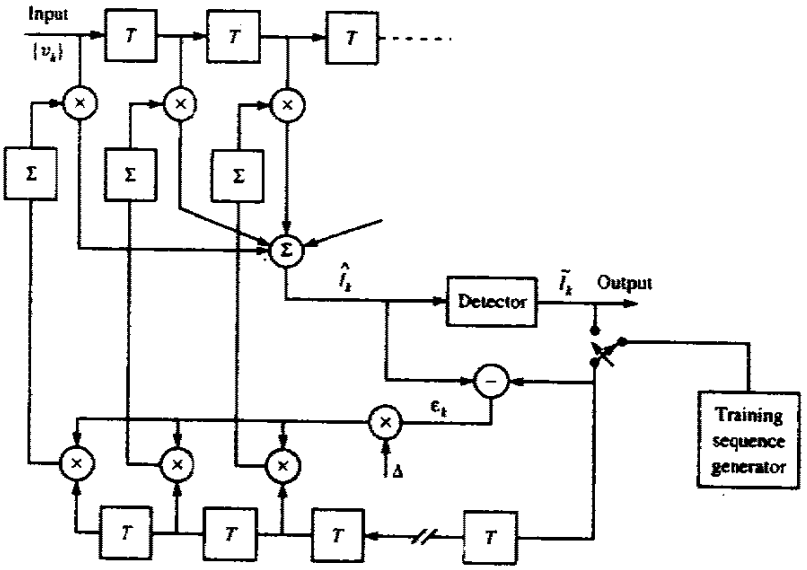

11-1-2 The LMS Algorithm

In the minimization of the MSE, treated in Section 10-2-2, we found that the optimum equalizer coefficients are determined from the solution of the set of linear equations, expressed in matrix form as

$$\mathbf{\Gamma C} = \boldsymbol{\xi} \tag{11-1-6}$$

where $\mathbf{\Gamma}$ is the $(2K+1)\times(2K+1)$ covariance matrix of the signal samples $\{v_k\}$, $\mathbf{C}$ is the column vector of $(2K+1)$ equalizer coefficients, and $\boldsymbol{\xi}$ is a $(2K+1)$-dimensional column vector of channel filter coefficients. The solution for the optimum equalizer coefficients vector $\mathbf{C}_{opt}$ can be determined by inverting the covariance matrix $\mathbf{\Gamma}$, which can be efficiently performed by use of the Levinson–Durbin algorithm described in Appendix A.

Alternatively, an iterative procedure that avoids the direct matrix inversion may be used to compute $\mathbf{C}_{opt}$. Probably the simplest iterative procedure is the method of steepest descent, in which one begins by arbitrarily choosing the vector $\mathbf{C}$, say as $\mathbf{C}_0$. This initial choice of coefficients corresponds to some point on the quadratic MSE surface in the $(2K+1)$-dimensional space of coefficients. The gradient vector $\mathbf{G}_0$, having the $2K+1$ gradient components $\frac{1}{2}\,\partial J/\partial c_{0k}$, $k=-K,\ldots,-1,0,1,\ldots,K$, is then computed at this point on the MSE surface, and each tap weight is changed in the direction opposite to its corresponding gradient component. The change in the jth tap weight is proportional to the size of the jth gradient component. Thus, succeeding values of the coefficient vector $\mathbf{C}$ are obtained according to the relation

$$\mathbf{C}_{k+1} = \mathbf{C}_k - \Delta\mathbf{G}_k, \qquad k = 0, 1, 2, \ldots \tag{11-1-7}$$

where the gradient vector $\mathbf{G}_k$ is

$$\mathbf{G}_k = \frac{1}{2}\frac{dJ}{d\mathbf{C}_k} = \mathbf{\Gamma C}_k - \boldsymbol{\xi} = -E(\varepsilon_k \mathbf{V}_k^*) \tag{11-1-8}$$

The vector $\mathbf{C}_k$ represents the set of coefficients at the kth iteration, $\varepsilon_k = I_k - \hat{I}_k$ is the error signal at the kth iteration, $\mathbf{V}_k$ is the vector of received signal samples that make up the estimate $\hat{I}_k$, i.e., $\mathbf{V}_k = [v_{k+K} \ \ldots \ v_k \ \ldots \ v_{k-K}]'$, and Δ is a positive number chosen small enough to ensure convergence of the iterative procedure. If the minimum MSE is reached for some $k = k_0$, then $\mathbf{G}_k = \mathbf{0}$, so that no further change occurs in the tap weights. In general, $J_{min}(K)$ cannot be attained for a finite value of k_0 with the steepest-descent method. It can, however, be approached as closely as desired for some finite value of k_0.

The basic difficulty with the method of steepest descent for determining the optimum tap weights is the lack of knowledge of the gradient vector $\mathbf{G}_k$, which depends on both the covariance matrix $\mathbf{\Gamma}$ and the vector $\boldsymbol{\xi}$ of cross-correlations. In turn, these quantities depend on the coefficients $\{f_k\}$ of the equivalent discrete-time channel model and on the covariance of the information sequence and the additive noise, all of which may be unknown at the receiver

in general. To overcome the difficulty, estimates of the gradient vector may be used. That is, the algorithm for adjusting the tap weight coefficients may be expressed in the form

$$\hat{\mathbf{C}}_{k+1} = \hat{\mathbf{C}}_k - \Delta\hat{\mathbf{G}}_k \tag{11-1-9}$$

where $\hat{\mathbf{G}}_k$ denotes an estimate of the gradient vector $\mathbf{G}_k$ and $\hat{\mathbf{C}}_k$ denotes the estimate of the vector of coefficients.

From (11-1-8) we note that $\mathbf{G}_k$ is the negative of the expected value of the $\varepsilon_k\mathbf{V}_k^*$. Consequently, an estimate of $\mathbf{G}_k$ is

$$\hat{\mathbf{G}}_k = -\varepsilon_k\mathbf{V}_k^* \tag{11-1-10}$$

Since $E(\hat{\mathbf{G}}_k) = \mathbf{G}_k$, the estimate $\hat{\mathbf{G}}_k$ is an unbiased estimate of the true gradient vector $\mathbf{G}_k$. Incorporation of (11-1-10) into (11-1-9) yields the algorithm

$$\hat{\mathbf{C}}_{k+1} = \hat{\mathbf{C}}_k + \Delta\varepsilon_k\mathbf{V}_k^* \tag{11-1-11}$$

This is the basic LMS (least-mean-square) algorithm for recursively adjusting the tap weight coefficients of the equalizer first proposed by Widrow and Hoff (1960). It is illustrated in the equalizer shown in Fig. 11-1-2.

The basic algorithm given by (11-1-11) and some of its possible variations have been incorporated into many commercial adaptive equalizers that are

FIGURE 11-1-2 Linear adaptive equalizer based on MSE criterion.

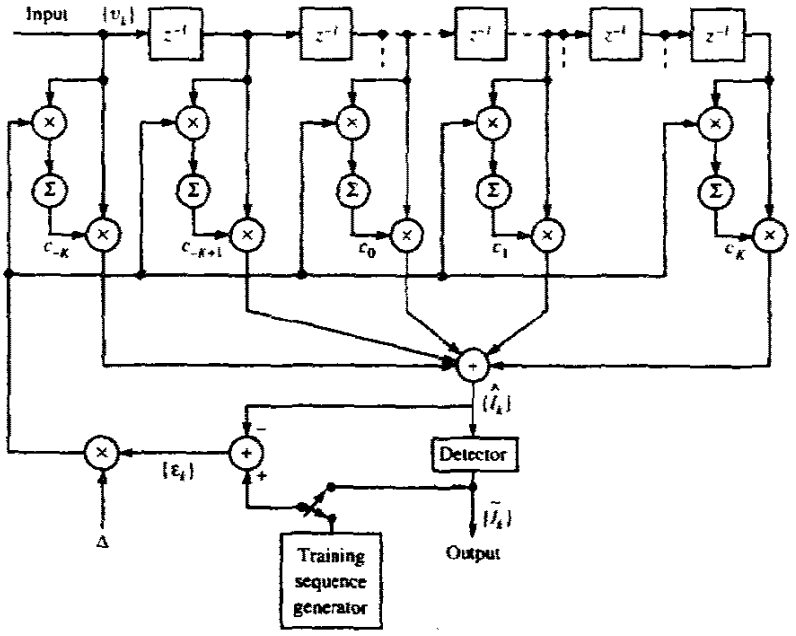

used in high-speed modems. Three variations of the basic algorithm are obtained by using only sign information contained in the error signal ε_k and/or in the components of $\mathbf{V}_k$. Hence, the three possible variations are

$$c_{(k+1)j} = c_{kj} + \Delta \operatorname{csgn}(\varepsilon_k) v^*_{k-j}, \quad j = -K, \ldots, -1, 0, 1, \ldots, K \tag{11-1-12}$$

$$c_{(k+1)j} = c_{kj} + \Delta \varepsilon_k \operatorname{csgn}(v^*_{k-j}), \quad j = -K, \ldots, -1, 0, 1, \ldots, K \tag{11-1-13}$$

$$c_{(k+1)j} = c_{kj} + \Delta \operatorname{csgn}(\varepsilon_k) \operatorname{csgn}(v^*_{k-j}), \quad j = -K, \ldots, -1, 0, 1, \ldots, K \tag{11-1-14}$$

where csgn (x) is defined as

$$\operatorname{csgn}(x) = \begin{cases} 1+j & (\operatorname{Re}(x) > 0, \operatorname{Im}(x) > 0) \\ 1-j & (\operatorname{Re}(x) > 0, \operatorname{Im}(x) < 0) \\ -1+j & (\operatorname{Re}(x) < 0, \operatorname{Im}(x) > 0) \\ -1-j & (\operatorname{Re}(x) < 0, \operatorname{Im}(x) < 0) \end{cases} \tag{11-1-15}$$

(Note that in (11-1-15), $j \equiv \sqrt{-1}$, as distinct from the index j in (11-1-12)–(11-1-14).) Clearly, the algorithm in (11-1-14) is the most easily implemented, but it gives the slowest rate of convergence to the others.

Several other variations of the LMS algorithm are obtained by averaging or filtering the gradient vectors over several iterations prior to making adjustments of the equalizer coefficients. For example, the average over N gradient vectors is

$$\bar{\mathbf{G}}_{mN} = -\frac{1}{N} \sum_{n=0}^{N-1} \varepsilon_{mN+n} \mathbf{V}^*_{mN+n} \tag{11-1-16}$$

and the corresponding recursive equation for updating the equalizer coefficients once very N iterations is

$$\hat{\mathbf{C}}_{(k+1)N} = \hat{\mathbf{C}}_{kN} - \Delta \bar{\mathbf{G}}_{kN} \tag{11-1-17}$$

In effect, the averaging operation performed in (11-1-16) reduces the noise in the estimate of the gradient vector, as shown by Gardner (1984).

An alternative approach is to filter the noisy gradient vectors by a lowpass filter and use the output of the filter as an estimate of the gradient vector. For example, a simple lowpass filter for the noisy gradients yields as an output

$$\bar{\mathbf{G}}_k = w \bar{\mathbf{G}}_{k-1} + (1-w) \hat{\mathbf{G}}_k, \quad \bar{\mathbf{G}}(0) = \hat{\mathbf{G}}(0) \tag{11-1-18}$$

where the choice of $0 \leq w < 1$ determines the bandwidth of the lowpass filter. When w is close to unity, the filter bandwidth is small and the effective averaging is performed over many gradient vectors. On the other hand, when w is small, the lowpass filter has a large bandwidth and, hence, it provides little averaging of the gradient vectors. With the filtered gradient vectors given by

(11-1-18) in place of $\mathbf{G}_k$, we obtain the filtered gradient LMS algorithm given by

$$\hat{\mathbf{C}}_{k+1} = \hat{\mathbf{C}}_k - \Delta\tilde{\mathbf{G}}_k \tag{11-1-19}$$

In the above discussion, it has been assumed that the receiver has knowledge of the transmitted information sequence in forming the error signal between the desired symbol and its estimate. Such knowledge can be made available during a short training period in which a signal with a known information sequence is transmitted to the receiver for initially adjusting the tap weights. The length of this sequence must be at least as long as the length of the equalizer so that the spectrum of the transmitted signal adequately covers the bandwidth of the channel being equalized.

In practice, the training sequence is often selected to be a periodic pseudo-random sequence, such as a maximum length shift-register sequence whose period N is equal to the length of the equalizer ($N = 2K + 1$). In this case, the gradient is usually averaged over the length of the sequence as indicated in (11-1-16) and the equalizer is adjusted once a period according to (11-1-17). A practical scheme for continuous adjustment of the tap weights may be either a decision-directed mode of operation in which decisions on the information symbols are assumed to be correct and used in place of I_k in forming the error signal ε_k, or one in which a known pseudo-random-probe sequence is inserted in the information-bearing signal either additively or by interleaving in time and the tap weights adjusted by comparing the received probe symbols with the known transmitted probe symbols. In the decision-directed mode of operation, the error signal becomes $\tilde{\varepsilon}_k = \tilde{I}_k - \hat{I}_k$, where $\tilde{I}_k$ is the decision of the receiver based on the estimate $\hat{I}_k$. As long as the receiver is operating at low error rates, an occasional error will have a negligible effect on the convergence of the algorithm.

If the channel response changes, this change is reflected in the coefficients $\{f_k\}$ of the equivalent discrete-time channel model. It is also reflected in the error signal ε_k, since it depends on $\{f_k\}$. Hence, the tap weights will be changed according to (11-1-11) to reflect the change in the channel. A similar change in the tap weights occurs if the statistics of the noise or the information sequence change. Thus, the equalizer is adaptive.

11-1-3 Convergence Properties of the LMS Algorithm

The convergence properties of the LMS algorithm given by (11-1-11) are governed by the step-size parameter Δ. We shall now consider the choice of the parameter Δ to ensure convergence of the steepest-descent algorithm in (11-1-7), which employs the exact value of the gradient.

From (11-1-7) and (11-1-8), we have

$$\begin{aligned}\mathbf{C}_{k+1} &= \mathbf{C}_k - \Delta\mathbf{G}_k \\ &= (\mathbf{I} - \Delta\Gamma)\mathbf{C}_k + \Delta\boldsymbol{\xi}\end{aligned} \tag{11-1-20}$$

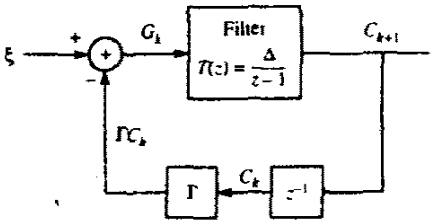

FIGURE 11-1-3 Closed-loop control system representation of recursive equation in (11-1-20).

where $\mathbf{I}$ is the identity matrix, Γ is the autocorrelation matrix of the received signal, $\mathbf{C}_k$ is the $(2K+1)$-dimensional vector of equalizer tap gains, and $\boldsymbol{\xi}$ is the vector of cross-correlations given by (10-2-45). The recursive relation in (11-1-20) can be represented as a closed-loop control system as shown in Fig. 11-1-3. Unfortunately, the set of $2K+1$ first-order difference equations in (11-1-20) are coupled through the autocorrelation matrix Γ. In order to solve these equations and, thus, establish the convergence properties of the recursive algorithm, it is mathematically convenient to decouple the equations by performing a linear transformation. The appropriate transformation is obtained by noting that the matrix Γ is Hermitian and, hence, can be represented as

$$\Gamma = \mathbf{U}\Lambda\mathbf{U}'^{*} \tag{11-1-21}$$

where $\mathbf{U}$ is the normalized modal matrix of Γ and Λ is a diagonal matrix with diagonal elements equal to the eigenvalues of Γ.

When (11-1-21) is substituted into (11-1-20) and if we define the transformed (orthogonalized) vectors $\mathbf{C}_k^o = \mathbf{U}'^{*}\mathbf{C}_k$ and $\boldsymbol{\xi}^o = \mathbf{U}'^{*}\boldsymbol{\xi}$, we obtain

$$\mathbf{C}_{k+1}^o = (\mathbf{I} - \Delta\Lambda)\mathbf{C}_k^o + \Delta\boldsymbol{\xi}^o \tag{11-1-22}$$

This set of first order difference equations is now decoupled. Their convergence is determined from the homogeneous equation

$$\mathbf{C}_{k+1}^o = (\mathbf{I} - \Delta\Lambda)\mathbf{C}_k^o \tag{11-1-23}$$

We see that the recursive relation will converge provided that all the poles lie inside the unit circle, i.e.,

$$|1 - \Delta\lambda_k| < 1, \qquad k = -K, \ldots, -1, 0, 1, \ldots, K \tag{11-1-24}$$

where $\{\lambda_k\}$ is the set of $2K+1$ (possibly nondistinct) eigenvalues of Γ. Since Γ is an autocorrelation matrix, it is positive-definite and, hence, $\lambda_k > 0$ for all k. Consequently convergence of the recursive relation in (11-1-22) is ensured if Δ satisfies the inequality

$$0 < \Delta < \frac{2}{\lambda_{\max}} \tag{11-1-25}$$

where $\lambda_{\max}$ is the largest eigenvalue of Γ.

Since the largest eigenvalue of a positive-definite matrix is less than the sum

of all the eigenvalues of the matrix and, furthermore, since the sum of the eigenvalues of a matrix is equal to its trace, we have the following simple upper bound on λ_{max}:

$$\lambda_{max} < \sum_{k=-K}^{K} \lambda_k = \text{tr}\,\Gamma = (2K+1)\Gamma_{kk}$$
$$= (2K+1)(x_0 + N_0) \tag{11-1-26}$$

From (11-1-23) and (11-1-24) we observe that rapid convergence occurs when $|1 - \Delta\lambda_k|$ is small, i.e., when the pole positions are far from the unit circle. But we cannot achieve this desirable condition and still satisfy (11-1-25) if there is a large difference between the largest and smallest eigenvalues of Γ. In other words, even if we select Δ to be near the upper bound given in (11-1-25), the convergence rate of the recursive MSE algorithm is determined by the smallest eigenvalue λ_{min}. Consequently, the ratio $\lambda_{max}/\lambda_{min}$ ultimately determines the convergence rate. If $\lambda_{max}/\lambda_{min}$ is small, Δ can be selected so as to achieve rapid convergence. However, if the ratio $\lambda_{max}/\lambda_{min}$ is large, as is the case when the channel frequency response has deep spectral nulls, the convergence rate of the algorithm will be slow.

11-1-4 Excess MSE Due to Noisy Gradient Estimates

The recursive algorithm in (11-1-11) for adjusting the coefficients of the linear equalizer employs unbiased noisy estimates of the gradient vector. The noise in these estimates causes random fluctuations in the coefficients about their optimal values and, thus, leads to an increase in the MSE at the output of the equalizer. That is, the final MSE is $J_{min} + J_\Delta$, where J_Δ is the variance of the measurement noise. The term J_Δ due to the estimation noise has been termed *excess means-square error* by Widrow (1966).

The total MSE at the output of the equalizer for any set of coefficients $\mathbf{C}$ can be expressed as

$$J = J_{min} + (\mathbf{C} - \mathbf{C}_{opt})'^{*}\Gamma(\mathbf{C} - \mathbf{C}_{opt}) \tag{11-1-27}$$

where $\mathbf{C}_{opt}$ represents the optimum coefficients, which satisfy (11-1-6). This expression for the MSE can be simplified by performing the linear orthogonal transformation used above to establish convergence. The result of this transformation applied to (11-1-27) is

$$J = J_{min} + \sum_{k=-K}^{K} \lambda_k E\,|c_k^o - c_{k\,opt}^o|^2 \tag{11-1-28}$$

where the $\{c_k^o\}$ are the set of transformed equalizer coefficients. The excess MSE is the expected value of the second term in (11-1-28), i.e.,

$$J_\Delta = \sum_{k=-K}^{K} \lambda_k E\,|c_k^o - c_{k\,opt}^o|^2 \tag{11-1-29}$$

It has been shown by Widrow (1970, 1975) that the excess MSE is

$$J_\Delta = \Delta^2 J_{\min} \sum_{k=-K}^{K} \frac{\lambda_k^2}{1-(1-\Delta\lambda_k)^2} \tag{11-1-30}$$

The expression in (11-1-30) can be simplified when Δ is selected such that $\Delta\lambda_k \ll 1$ for all k. Then

$$\begin{aligned} J_\Delta &\approx \tfrac{1}{2}\Delta J_{\min} \sum_{k=-K}^{K} \lambda_k \\ &\approx \tfrac{1}{2}\Delta J_{\min} \operatorname{tr} \Gamma \\ &\approx \tfrac{1}{2}\Delta(2K+1)J_{\min}(x_0+N_0) \end{aligned} \tag{11-1-31}$$

Note that $x_0 + N_0$ represents the received signal plus noise power.

It is desirable to have $J_\Delta < J_{\min}$. That is, Δ should be selected such that

$$\frac{J_\Delta}{J_{\min}} \approx \tfrac{1}{2}\Delta(2K+1)(x_0+N_0) < 1$$

or, equivalently,

$$\Delta < \frac{2}{(2K+1)(x_0+N_0)} \,. \tag{11-1-32}$$

For example, if Δ is selected as

$$\Delta = \frac{0.2}{(2K+1)(x_0+N_0)} \tag{11-1-33}$$

the degradation in the output SNR of the equalizer due to the excess MSE is less than 1 dB.

The analysis given above on the excess mean square error is based on the assumption that the mean value of the equalizer coefficients has converged to the optimum value $\mathbf{C}_{\text{opt}}$. Under this condition, the step size Δ should satisfy the bound in (11-1-32). On the other hand, we have determined that convergence of the mean coefficient vector requires that $\Delta < 2/\lambda_{\max}$. While a choice of Δ near the upper bound $2/\lambda_{\max}$ may lead to initial convergence of the deterministic (known) steepest-descent gradient algorithm, such a large value of Δ will usually result in instability of the LMS stochastic gradient algorithm.

The initial convergence or transient behavior of the LMS algorithm has been investigated by several researchers. Their results clearly indicate that the step size must be reduced in direct proportion to the length of the equalizer as specified by (11-1-32). Hence, the upper bound given by (11-1-32) is also necessary to ensure the initial convergence of the LMS algorithm. The papers by Gitlin and Weinstein (1979) and Ungerboeck (1972) contain analyses of the transient behavior and the convergence properties of the LMS algorithm.

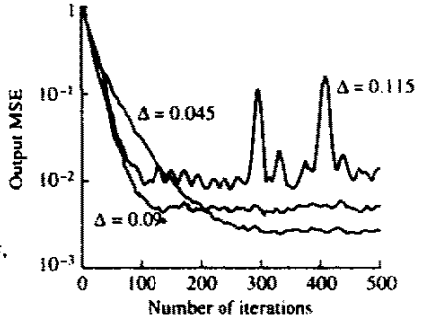

FIGURE 11-1-4 Initial convergence characteristics of the LMS algorithm with different step sizes. [*From* Digital Signal Processing, *by J. G. Proakis and D. G. Manolakis, 1988. Macmillan Publishing Company. Reprinted with permission of the publisher.*]

The following example serves to reinforce the important points made above regarding the initial convergence of the LMS algorithm.

Example 11-1-1

The LMS algorithm was used to adaptively equalize a communication channel for which the autocorrelation matrix $\mathbf{\Gamma}$ has an eigenvalue spread of $\lambda_{max}/\lambda_{min} = 11$. The number of taps selected for the equalizer was $2K + 1 = 11$. The input signal plus noise power $x_0 + N_0$ was normalized to unity. Hence, the upper bound on Δ given by (11-1-32) is 0.18. Figure 11-1-4 illustrates the initial convergence characteristics of the LMS algorithm for $\Delta = 0.045$, 0.09, and 0.115, by averaging the (estimated) MSE in 200 simulations. We observe that by selecting $\Delta = 0.09$ (one-half of the upper bound) we obtain relatively fast initial convergence. If we divide Δ by a factor of 2 to $\Delta = 0.045$, the convergence rate is reduced but the excess mean square error is also reduced, so that the LMS algorithm performs better in steady state (in a time-invariant signal environment). Finally, we note that a choice of $\Delta = 0.115$, which is still far below the upper bound, causes large undesirable fluctuations in the output MSE of the algorithm.

In a digital implementation of the LMS algorithm, the choice of the step-size parameter becomes even more critical. In an attempt to reduce the excess mean square error, it is possible to reduce the step-size parameter to the point where the total mean square error actually increases. This condition occurs when the estimated gradient components of the vector $\varepsilon_k \mathbf{V}_k^*$ after multiplication by the small step-size parameter Δ are smaller than one-half of the least significant bit in the fixed-point representation of the equalizer coefficients. In such a case, adaptation ceases. Consequently, it is important for the step size to be large enough to bring the equalizer coefficients in the vicinity of $\mathbf{C}_{opt}$. If it is desired to decrease the step size significantly, it is necessary to increase the precision in the equalizer coefficients. Typically, 16

bits of precision may be used for the coefficients, with about 10–12 of the most significant bits used for arithmetic operations in the equalization of the data. The remaining least significant bits are required to provide the necessary precision for the adaptation process. Thus, the scaled, estimated gradient components $\Delta\varepsilon\mathbf{V}_k^*$ usually affect only the least-significant bits in any one iteration. In effect, the added precision also allows for the noise to be averaged out, since many incremental changes in the least-significant bits are required before any change occurs in the upper more significant bits used in arithmetic operations for equalizing the data. For an analysis of roundoff errors in a digital implementation of the LMS algorithm, the reader is referred to the papers by Gitlin and Weinstein (1979), Gitlin *et al.* (1982), and Caraiscos and Liu (1984).

As a final point, we should indicate that the LMS algorithm is appropriate for tracking slowly time-invariant signal statistics. In such a case, the minimum MSE and the optimum coefficient vector will be time-variant. In other words, $J_{\min}(n)$ is a function of time and the $(2K+1)$-dimensional error surface is moving with the time index n. The LMS algorithm attempts to follow the moving minimum $J_{\min}(n)$ in the $(2K+1)$-dimensional space, but it is always lagging behind due to its use of (estimated) gradient vectors. As a consequence, the LMS algorithm incurs another form of error, called the *lag error*, whose mean square value decreases with an increase in the step size Δ. The total MSE error can now be expressed as

$$J_{\text{total}} = J_{\min}(n) + J_\Delta + J_l$$

where J_l denotes the mean square error due to the lag.

In any given nonstationary adaptive equalization problem, if we plot the errors J_Δ and J_l as a function of Δ, we expect these errors to behave as illustrated in Fig. 11-1-5. We observe that J_Δ increases with an increase in Δ while J_l decreases with an increase in Δ. The total error will exhibit a minimum, which will determine the optimum choice of the step-size parameter.

When the statistical time variations of the signal occur rapidly, the lag error

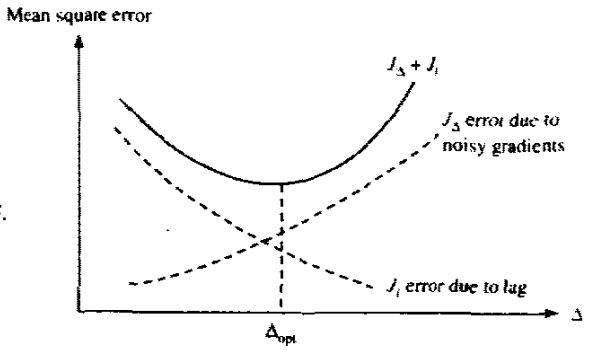

FIGURE 11-1-5 Excess mean square error J_Δ and lag error J_l as a function of the step size. [*From* Digital Signal Processing, *by J. G. Proakis and D. G. Manolakis, 1988, Macmillan Publishing Company. Reprinted with permission of the publisher.*]

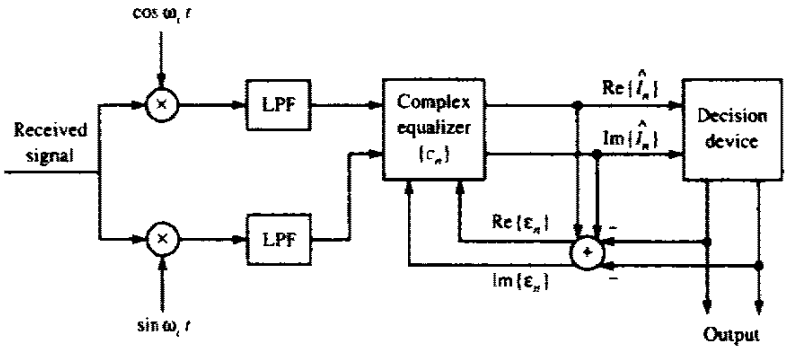

FIGURE 11-1-6 QAM signal demodulation.

will dominate the performance of the adaptive equalizer. In such a case, $J_l \gg J_{\min} + J_\Delta$, even when the largest possible value of Δ is used. When this condition occurs, the LMS algorithm is inappropriate for the application and one must rely on the more complex recursive least-squares algorithms described in Section 11-4 to obtain faster convergence and tracking.

11-1-5 Baseband and Passband Linear Equalizers

Our treatment of adaptive linear equalizers has been in terms of equivalent lowpass signals. However, in a practical implementation, the linear adaptive equalizer shown in Fig. 11-1-2 can be realized either at baseband or at bandpass. For example Fig. 11-1-6 illustrates the demodulation of QAM (or multiphase PSK) by first translating the signal to baseband and equalizing the baseband signal with an equalizer having complex-valued coefficients. In effect, the complex equalizer with complex-valued (in-phase and quadrature components) input is equivalent to four parallel equalizers with real-valued tap coefficients as shown in Fig. 11-1-7.

As an alternative, we may equalize the signal at passband. This is

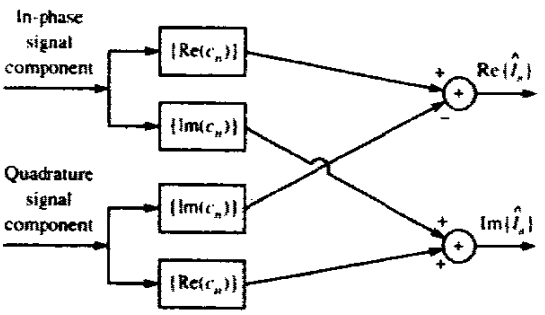

FIGURE 11-1-7 Complex-valued baseband equalizer for QAM signals.

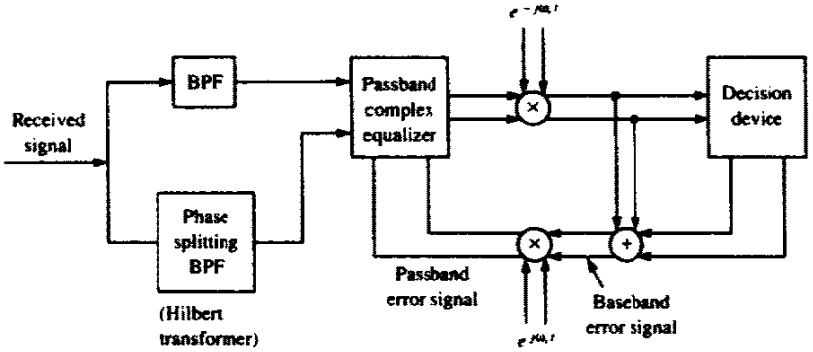

FIGURE 11-1-8 QAM or PSK signal equalization at passband.

accomplished as shown in Fig. 11-1-8 for a two-dimensional signal constellation such as QAM and PSK. The received signal is filtered and, in parallel, it is passed through a Hilbert transformer, called a *phase-splitting filter*. Thus, we have the equivalent of in-phase and quadrature components at passband, which are fed to a passband complex equalizer. Following the equalization, the signal is down-converted to a baseband and detected. The error signal generated for the purpose of adjusting the equalizer coefficients is formed at baseband and frequency-translated to passband as illustrated in Fig. 11-1-8.

11-2 ADAPTIVE DECISION-FEEDBACK EQUALIZER

As in the case of the linear adaptive equalizer, the coefficients of the feedforward filter and the feedback filter in a decision-feedback equalizer may be adjusted recursively, instead of inverting a matrix as implied by (10-3-3). Based on the minimization of the MSE at the output of the DFE, the steepest-descent algorithm takes the form

$$\mathbf{C}_{k+1} = \mathbf{C}_k + \Delta E(\varepsilon_k \mathbf{V}_k^*) \tag{11-2-1}$$

where $\mathbf{C}_k$ is the vector of equalizer coefficients in the kth signal interval, $E(\varepsilon_k \mathbf{V}_k^*)$ is the cross-correlation of the error signal $\varepsilon_k = I_k - \hat{I}_k$ with $\mathbf{V}_k$ and $\mathbf{V}_k = [v_{k+K_1} \cdots v_k \; I_{k-1} \cdots I_{k-K_2}]^t$, representing the signal values in the feedforward and feedback filters at time $t = kT$. The MSE is minimized when the cross-correlation vector $E(\varepsilon_k \mathbf{V}_k^*) = \mathbf{0}$ as $k \to \infty$.

Since the exact cross-correlation vector is unknown at any time instant, we use as an estimate the vector $\varepsilon_k \mathbf{V}_k^*$ and average out the noise in the estimate through the recursive equation

$$\hat{\mathbf{C}}_{k+1} = \hat{\mathbf{C}}_k + \Delta \varepsilon_k \mathbf{V}_k^* \tag{11-2-2}$$

This is the LMS algorithm for the DFE.

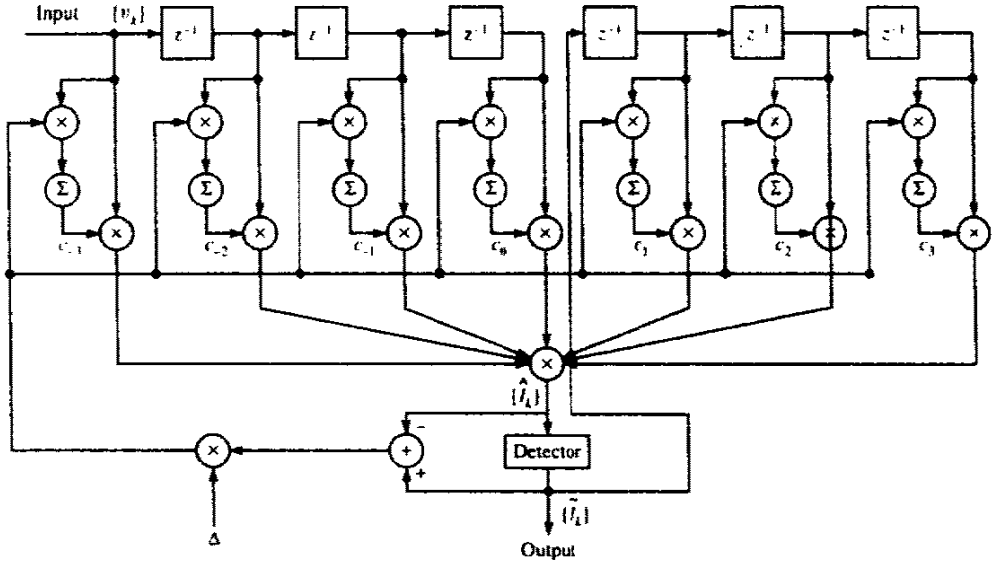

FIGURE 11-2-1 Decision-feedback equalizer.

As in the case of a linear equalizer, we may use a training sequence to adjust the coefficients of the DFE initially. Upon convergence to the (near-) optimum coefficients (minimum MSE), we may switch to a decision-directed mode where the decisions at the output of the detector are used in forming the error signal ε_k and fed to the feedback filter. This is the adaptive mode of the DFE, which is illustrated in Fig 11-2-1. In this case, the recursive equation for adjusting the equalizer coefficient is

$$\tilde{\mathbf{C}}_{k+1} = \tilde{\mathbf{C}}_k + \Delta \tilde{\varepsilon}_k \mathbf{V}_k^* \tag{11-2-3}$$

where $\tilde{\varepsilon}_k = \tilde{I}_k - \hat{I}_k$ and $\mathbf{V}_k = [v_{k+K_1} \cdots v_k \ \tilde{I}_{k-1} \cdots \tilde{I}_{k-K_2}]^t$.

The performance characteristics of the LMS algorithm for the DFE are basically the same as the development given in Sections 11-1-3 and 11-1-4 for the linear adaptive equalizer.

11-2-1 Adaptive Equalization of Trellis-Coded Signals

Bandwidth efficient trellis-coded modulation that was described in Section 8-3 is frequently used in digital communications over telephone channels to reduce the required SNR per bit for achieving a specified error rate. Channel distortion of the trellis-coded signal forces us to use adaptive equalization in order to reduce the intersymbol interference. The output of the equalizer is then fed to the Viterbi decoder, which performs soft-decision decoding of the trellis-coded signal.

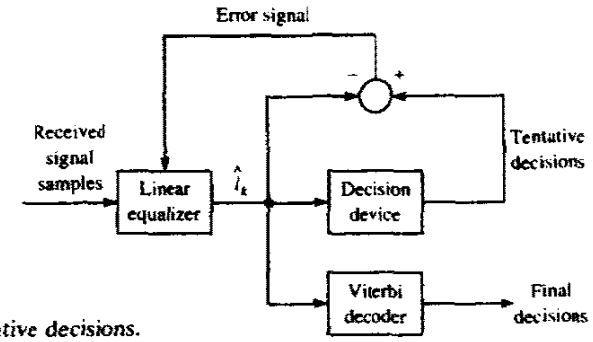

FIGURE 11-2-2 Adjustment of equalizer based on tentative decisions.

The question that arises regarding such a receiver is how do we adapt the equalizer in a data transmission mode? One possibility is to have the equalizer make its own decisions at its output solely for the purpose of generating an error signal for adjusting its tap coefficients, as shown in the block diagram in Fig. 11-2-2. The problem with this approach is that such decisions are generally unreliable, since the pre-decoding coded symbol SNR is relatively low. A high error rate would cause a significant degradation in the operation of the equalizer, which would ultimately affect the reliability of the decisions at the output of the decoder. The more desirable alternative is to use the post-decoding decisions from the Viterbi decoder, which are much more reliable, to continuously adapt the equalizer. This approach is certainly preferable and viable when a linear equalizer is used prior to the Viterbi decoder. The decoding delay inherent in the Viterbi decoder can be overcome by introducing an identical delay in the tap weight adjustment of the equalizer coefficients as shown in Fig. 11-2-3. The major price that must be paid for the added delay is that the step-size parameter in the LMS algorithm must be reduced, as described by Long *et al.* (1987, 1989), in order to achieve stability in the algorithm.

In channels with one or more in-band spectral nulls, the linear equalizer is

FIGURE 11-2-3 Adjustment of equalizer based on decisions from the Viterbi decoder.

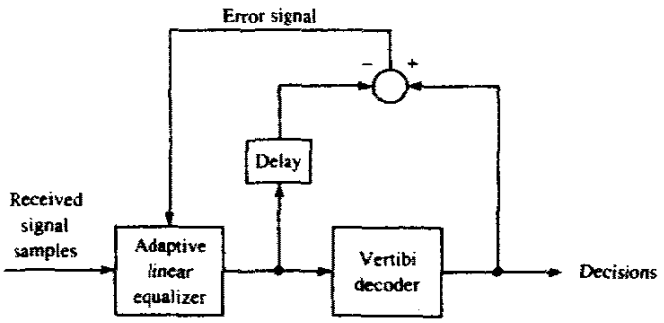

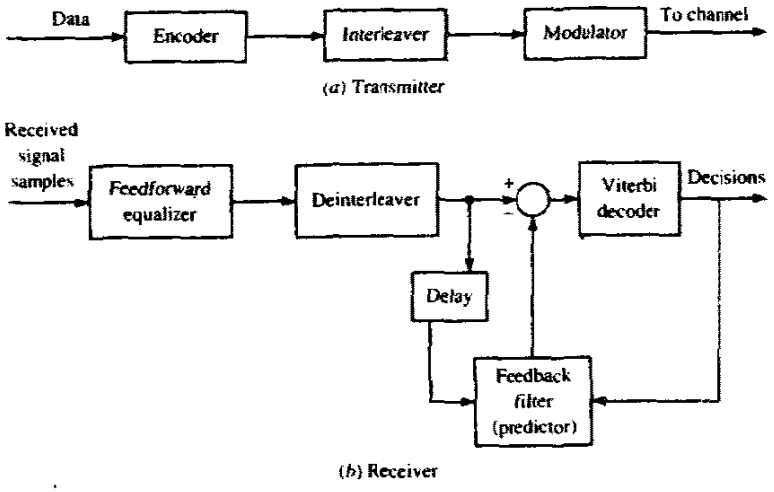

FIGURE 11-2-4 Use of predictive DFE with interleaving and trellis-coded modulation.

no longer adequate for compensating the channel intersymbol interference. Instead, we should like to use a DFE. But the DFE requires reliable decisions in its feedback filter in order to cancel out the intersymbol interference from previously detected symbols. Tentative decisions prior to decoding would be highly unreliable and, hence, inappropriate. Unfortunately, the conventional DFE cannot be cascaded with the Viterbi algorithm in which post-decoding decisions from the decoder are fed back to the DFE.

One alternative is to use the predictive DFE described in Section 10-3-3. In order to accommodate for the decoding delay as it affects the linear predictor, we introduce a periodic interleaver/deinterleaver pair that has the same delay as the Viterbi decoder and, thus, makes it possible to generate the appropriate error signal to the predictor as illustrated in the block diagram of Fig. 11-2-4. The novel way in which a predictive DFE can be combined with Viterbi decoding to equalize trellis-coded signals is described and analyzed by Eyuboglu (1988). This same idea has been carried over to the equalization of fading multipath channels by Zhou *et al.* (1988, 1990), but the structure of the DFE was modified to use recursive least-squares lattice-type filters, which provide faster adaptation to the time variations encountered in the channel.

11-3 AN ADAPTIVE CHANNEL ESTIMATOR FOR ML SEQUENCE DETECTION

The ML sequence detection criterion implemented via the Viterbi algorithm as embodied in the metric computation given by (10-1-23) and the probabilistic symbol-by-symbol detection algorithm described in Section 5-1-5 require knowledge of the equivalent discrete-time channel coefficients $\{f_k\}$. To accommodate a channel that is unknown or slowly time-varying, one may include a

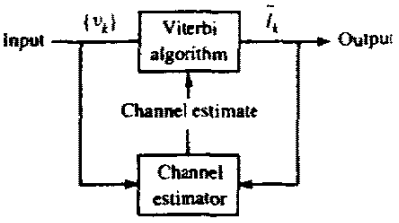

FIGURE 11-3-1 Block diagram of method for estimating the channel characteristics for the Viterbi algorithm.

channel estimator connected in parallel with the detection algorithm, as shown in Fig. 11-3-1. The channel estimator, which is shown in Fig. 11-3-2 is identical in structure to the linear transversal equalizer discussed previously in Section 11-1. In fact, the channel estimator is a replica of the equivalent discrete-time channel filter that models the intersymbol interference. The estimated tap coefficients, denoted by $\{\hat{f}_k\}$, are adjusted recursively to minimize the MSE between the actual received sequence and the output of the estimator. For example, the steepest-descent algorithm in a decision-directed mode of operation is

$$\hat{\mathbf{f}}_{k+1} = \hat{\mathbf{f}}_k + \Delta \varepsilon_k \tilde{\mathbf{I}}_k^* \tag{11-3-1}$$

where $\hat{\mathbf{f}}_k$ is the vector of tap gain coefficients at the kth iteration, Δ is the step size, $\varepsilon_k = v_k - \hat{v}_k$ is the error signal, and $\tilde{\mathbf{I}}_k$ denotes the vector of detected information symbols in the channel estimator at the kth iteration.

We now show that when the MSE between v_k and $\hat{v}_k$ is minimized, the resulting values of the tap gain coefficients of the channel estimator are the values of the discrete-time channel model. For mathematical tractability, we assume that the detected information sequence $\{\tilde{I}_k\}$ is correct, i.e., $\{\tilde{I}_k\}$ is

FIGURE 11-3-2 Adaptive transversal filter for estimating the channel dispersion.

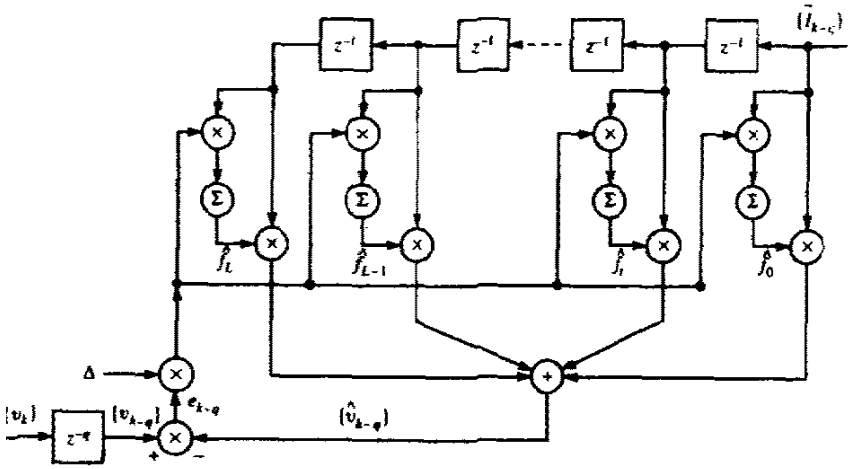

identical to the transmitted sequence $\{I_k\}$. This is a reasonable assumption when the system is operating at a low probability of error. Thus, the MSE between the received signal v_k and the estimate $\hat{v}_k$ is

$$J(\hat{\mathbf{f}}) = E\left(\left|v_k - \sum_{j=0}^{N-1} \hat{f}_j I_{k-j}\right|^2\right) \tag{11-3-2}$$

The tap coefficients $\{\hat{f}_k\}$ that minimize $J(\hat{\mathbf{f}})$ in (11-3-2) satisfy the set of N linear equations

$$\sum_{j=0}^{N-1} \hat{f}_j \phi_{kj} = d_k, \qquad k = 0, 1, \ldots, N-1 \tag{11-3-3}$$

where

$$\phi_{kj} = E(I_k I_j^*), \qquad d_k = \sum_{j=0}^{N-1} f_j \phi_j \tag{11-3-4}$$

From (11-3-3) and (11-3-4), we conclude that, as long as the information sequence $\{I_k\}$ is uncorrelated, the optimum coefficients are exactly equal to the respective values of the equivalent discrete-time channel. It is also apparent that when the number of taps N in the channel estimator is greater than or equal to $L+1$, the optimum tap gain coefficients $\{\hat{f}_k\}$ are equal to the respective values of the $\{f_k\}$, even when the information sequence is correlated. Subject to the above conditions, the minimum MSE is simply equal to the noise variance N_0.

In the above discussion, the estimated information sequence at the output of the Viterbi algorithm or the probabilistic symbol-by-symbol algorithm was used in making adjustments of the channel estimator. For startup operation, one may send a short training sequence to perform the initial adjustment of the tap coefficients, as is usually done in the case of the linear transversal equalizer. In an adaptive mode of operation, the receiver simply uses its own decisions to form an error signal.

11-4 RECURSIVE LEAST-SQUARES ALGORITHMS FOR ADAPTIVE EQUALIZATION

The LMS algorithm that we described in Sections 11-1 and 11-2 for adaptively adjusting the tap coefficients of a linear equalizer or a DFE is basically a (stochastic) steepest-descent algorithm in which the true gradient vector is approximated by an estimate obtained directly from the data.

The major advantage of the steepest-descent algorithm lies in its computational simplicity. However, the price paid for the simplicity is slow convergence, especially when the channel characteristics result in an autocorrelation matrix Γ whose eigenvalues have a large spread, i.e., $\lambda_{max}/\lambda_{min} \gg 1$. Viewed in another way, the gradient algorithm has only a single adjustable parameter for

controlling the convergence rate, namely, the parameter Δ. Consequently the slow convergence is due to this fundamental limitation.

In order to obtain faster convergence, it is necessary to devise more complex algorithms involving additional parameters. In particular, if the matrix $\mathbf{\Gamma}$ is $N \times N$ and has eigenvalues $\lambda_1, \lambda_2, \ldots, \lambda_N$, we may use an algorithm that contains N parameters—one for each of the eigenvalues. The optimum selection of these parameters to achieve rapid convergence is a topic of this section.

In deriving faster converging algorithms, we shall adopt a least-squares approach. Thus, we shall deal directly with the received data in minimizing the quadratic performance index, whereas previously we minimized the expected value of the squared error. Put simply, this means that the performance index is expressed in terms of a time average instead of a statistical average.

It is convenient to express the recursive least-squares algorithms in matrix form. Hence, we shall define a number of vectors and matrices that are needed in this development. In so doing, we shall change the notation slightly. Specifically, the estimate of the information symbol at time t, where t is an integer, from a linear equalizer is now expressed as

$$\tilde{I}(t) = \sum_{j=-K}^{K} c_j(t-1) v_{t-j}$$

By changing the index j on $c_j(t-1)$ to run from $j=0$ to $j=N-1$ and simultaneously defining

$$y(t) = v_{t+K}$$

the estimate $\tilde{I}(t)$ becomes

$$\begin{aligned} \tilde{I}(t) &= \sum_{j=0}^{N-1} c_j(t-1) y(t-j) \\ &= \mathbf{C}_N(t-1)\mathbf{Y}_N(t) \end{aligned} \tag{11-4-1}$$

where $\mathbf{C}_N(t-1)$ and $\mathbf{Y}_N(t)$ are, respectively, the column vectors of the equalizer coefficients $c_j(t-1)$, $j=0, 1, \ldots, N-1$, and the input signals $y(t-j)$, $j=0, 1, 2, \ldots, N-1$.

Similarly, in the decision-feedback equalizer, we have tap coefficients $c_j(t)$, $j=0, 1, \ldots, N-1$, where the first K_1+1 are the coefficients of the feedforward filter and the remaining $K_2 = N - K_1 - 1$ are the coefficients of the feedback filter. The data in the estimate $\hat{I}(t)$ is $v_{t+K_1}, \ldots, v_{t+1}, \tilde{I}_{t-1}, \ldots, \tilde{I}_{t-K_2}$, where $\tilde{I}_{t-j}$, $1 \leq j \leq K_2$, denote the decisions on previously detected symbols. In this development, we neglect the effect of decision errors in the algorithms. Hence, we assume that $\tilde{I}_{t-j} = I_{t-j}$, $1 \leq j \leq K_2$. For notational convenience, we also define

$$y(t-j) = \begin{cases} v_{t+K_1-j} & (0 \leq j \leq K_1) \\ I_{t+K_1-j} & (K_1 < j \leq N-1) \end{cases} \tag{11-4-2}$$

Thus,

$$\begin{aligned}\mathbf{Y}_N(t) &= [y(t) \quad y(t-1) \quad \cdots \quad y(t-N+1)]' \\ &= [v_{t+K_1} \quad \cdots \quad v_{t+1} \quad v_t \quad I_{t-1} \quad \cdots \quad I_{t-K_2}]' \end{aligned} \tag{11-4-3}$$

11-4-1 Recursive Least-Squares (Kalman) Algorithm

The recursive least-squares (RLS) estimation of $\hat{I}(t)$ may be formulated as follows. Suppose we have observed the vectors $\mathbf{Y}_N(n)$, $n = 0, 1, \ldots, t$, and we wish to determine the coefficient vector $\mathbf{C}_N(t)$ of the equalizer (linear or decision-feedback) that minimizes the time-average weighted squared error

$$\mathscr{E}_N^{LS} = \sum_{n=0}^{t} w^{t-n} |e_N(n, t)|^2 \tag{11-4-4}$$

where the error is defined as

$$e_N(n, t) = I(n) - \mathbf{C}_N'(t)\mathbf{Y}_N(n) \tag{11-4-5}$$

and w represents a weighting factor $0 < w < 1$. Thus we introduce exponential weighting into past data, which is appropriate when the channel characteristics are time-variant. Minimization of $\mathscr{E}_N^{LS}$ with respect to the coefficient vector $\mathbf{C}_N(t)$ yields the set of linear equations

$$\mathbf{R}_N(t)\mathbf{C}_N(t) = \mathbf{D}_N(t) \tag{11-4-6}$$

where $\mathbf{R}_N(t)$ is the signal correlation matrix defined as

$$\mathbf{R}_N(t) = \sum_{n=0}^{t} w^{t-n}\mathbf{Y}_N^*(n)\mathbf{Y}_N^t(n) \tag{11-4-7}$$

and $\mathbf{D}_N(t)$ is the cross-correlation vector

$$\mathbf{D}_N(t) = \sum_{n=0}^{t} w^{t-n} I(n)\mathbf{Y}_N^*(n) \tag{11-4-8}$$

The solution of (11-4-6) is

$$\mathbf{C}_N(t) = \mathbf{R}_N^{-1}(t)\mathbf{D}_N(t) \tag{11-4-9}$$

The matrix $\mathbf{R}_N(t)$ is akin to the statistical autocorrelation matrix Γ_N, while the vector $\mathbf{D}_N(t)$ is akin to the cross-correlation vector ξ_N, defined previously. We emphasize, however, that $\mathbf{R}_N(t)$ is not a Toeplitz matrix. We also should mention that, for small values of t, $\mathbf{R}_N(t)$ may be ill conditioned; hence, it is customary to initially add the matrix $\delta\mathbf{I}_N$ to $\mathbf{R}_N(t)$, where δ is a small positive

constant and $\mathbf{I}_N$ is the identity matrix. With exponential weighting into the past, the effect of adding $\delta\mathbf{I}_N$ dissipates with time.

Now suppose we have the solution (11-4-9) for time $t-1$, i.e., $\mathbf{C}_N(t-1)$, and we wish to compute $\mathbf{C}_N(t)$. It is inefficient and, hence, impractical to solve the set of N linear equations for each new signal component that is received. To avoid this, we proceed as follows. First, $\mathbf{R}_N(t)$ may be computed recursively as

$$\mathbf{R}_N(t) = w\mathbf{R}_N(t-1) + \mathbf{Y}_N^*(t)\mathbf{Y}_N'(t) \tag{11-4-10}$$

We call (11-4-10) the *time-update equation* for $\mathbf{R}_N(t)$.

Since the inverse of $\mathbf{R}_N(t)$ is needed in (11-4-9), we use the matrix-inverse identity

$$\mathbf{R}_N^{-1}(t) = \frac{1}{w}\left[\mathbf{R}_N^{-1}(t-1) - \frac{\mathbf{R}_N^{-1}(t-1)\mathbf{Y}_N^*(t)\mathbf{Y}_N'(t)\mathbf{R}_N^{-1}(t-1)}{w + \mathbf{Y}_N'(t)\mathbf{R}_N^{-1}(t-1)\mathbf{Y}_N^*(t)}\right] \tag{11-4-11}$$

Thus $\mathbf{R}_N^{-1}(t)$ may be computed recursively according to (11-4-11).

For convenience, we define $\mathbf{P}_N(t) = \mathbf{R}_N^{-1}(t)$. It is also convenient to define an N-dimensional vector, called the *Kalman gain vector*, as

$$\mathbf{K}_N(t) = \frac{1}{w + \mu_N(t)}\mathbf{P}_N(t-1)\mathbf{Y}_N^*(t) \tag{11-4-12}$$

where $\mu_N(t)$ is a scalar defined as

$$\mu_N(t) = \mathbf{Y}_N'(t)\mathbf{P}_N(t-1)\mathbf{Y}_N^*(t) \tag{11-4-13}$$

With these definitions, (11-4-11) becomes

$$\mathbf{P}_N(t) = \frac{1}{w}[\mathbf{P}_N(t-1) - \mathbf{K}_N(t)\mathbf{Y}_N'(t)\mathbf{P}_N(t-1)] \tag{11-4-14}$$

Suppose we postmultiply both sides of (11-4-14) by $\mathbf{Y}_N^*(t)$. Then

$$\begin{aligned}\mathbf{P}_N(t)\mathbf{Y}_N^*(t) &= \frac{1}{w}[\mathbf{P}_N(t-1)\mathbf{Y}_N^*(t) - \mathbf{K}_N(t)\mathbf{Y}_N'(t)\mathbf{P}_N(t-1)\mathbf{Y}_N^*(t)] \\ &= \frac{1}{w}\{[w + \mu_N(t)]\mathbf{K}_N(t) - \mathbf{K}_N(t)\mu_N(t)\} \\ &= \mathbf{K}_N(t)\end{aligned} \tag{11-4-15}$$

Therefore, the Kalman gain vector may also be defined as $\mathbf{P}_N(t)\mathbf{Y}_N(t)$.

Now we use the matrix inversion identity to derive an equation for obtaining $\mathbf{C}_N(t)$ from $\mathbf{C}_N(t-1)$. Since

$$\mathbf{C}_N(t) = \mathbf{P}_N(t)\mathbf{D}_N(t)$$

and

$$\mathbf{D}_N(t) = w\mathbf{D}_N(t-1) + I(t)\mathbf{Y}_N^*(t) \tag{11-4-16}$$

we have

$$\begin{aligned}\mathbf{C}_N(t) &= \frac{1}{w}[\mathbf{P}_N(t-1) - \mathbf{K}_N(t)\mathbf{Y}_N'(t)\mathbf{P}_N(t-1)][w\mathbf{D}_N(t-1) + I(t)\mathbf{Y}_N^*(t)] \\ &= \mathbf{P}_N(t-1)\mathbf{D}_N(t-1) + \frac{1}{w}I(t)\mathbf{P}_N(t-1)\mathbf{Y}_N^*(t) \\ &\quad - \mathbf{K}_N(t)\mathbf{Y}_N'(t)\mathbf{P}_N(t-1)\mathbf{D}_N(t-1) \\ &\quad - \frac{1}{w}I(t)\mathbf{K}_N(t)\mathbf{Y}_N'(t)\mathbf{P}_N(t-1)\mathbf{Y}_N^*(t) \\ &= \mathbf{C}_N(t-1) + \mathbf{K}_N(t)[I(t) - \mathbf{Y}_N'(t)\mathbf{C}_N(t-1)] \end{aligned} \tag{11-4-17}$$

Note that $\mathbf{Y}_N'(t)\mathbf{C}_N(t-1)$ is the output of the equalizer at time t, i.e.,

$$\hat{I}(t) = \mathbf{Y}_N'(t)\mathbf{C}_N(t-1) \tag{11-4-18}$$

and

$$e_N(t, t-1) = I(t) - \hat{I}(t) \equiv e_N(t) \tag{11-4-19}$$

is the error between the desired symbol and the estimate. Hence, $\mathbf{C}_N(t)$ is updated recursively according to the relation

$$\mathbf{C}_N(t) = \mathbf{C}_N(t-1) + \mathbf{K}_N(t)e_N(t) \tag{11-4-20}$$

The residual MSE resulting from this optimization is

$$\mathcal{E}_{N\min}^{LS} = \sum_{n=0}^{t} w^{t-n}|I(n)|^2 - \mathbf{C}_N'(t)\mathbf{D}_N^*(t) \tag{11-4-21}$$

To summarize, suppose we have $\mathbf{C}_N(t-1)$ and $\mathbf{P}_N(t-1)$. When a new signal component is received, we have $\mathbf{Y}_N(t)$. Then the recursive computation for the time update of $\mathbf{C}_N(t)$ and $\mathbf{P}_N(t)$ proceeds as follows:

- compute output:

$$\hat{I}(t) = \mathbf{Y}_N'(t)\mathbf{C}_N(t-1)$$

- compute error:

$$e_N(t) = I(t) - \hat{I}(t)$$

- compute Kalman gain vector:

$$\mathbf{K}_N(t) = \frac{\mathbf{P}_N(t-1)\mathbf{Y}_N'(t)}{w + \mathbf{Y}_N'(t)\mathbf{P}_N(t-1)\mathbf{Y}_N^*(t)}$$

- update inverse of the correlation matrix:

$$\mathbf{P}_N(t) = \frac{1}{w}[\mathbf{P}_N(t-1) - \mathbf{K}_N(t)\mathbf{Y}_N'(t)\mathbf{P}_N(t-1)]$$

- update coefficients:

$$\begin{aligned}\mathbf{C}_N(t) &= \mathbf{C}_N(t-1) + \mathbf{K}_N(t)e_N(t) \\ &= \mathbf{C}_N(t-1) + \mathbf{P}_N(t)\mathbf{Y}^*(t)e_N(t)\end{aligned} \tag{11-4-22}$$

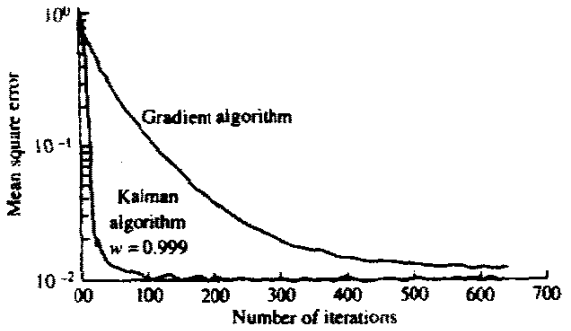

FIGURE 11-4-1 Comparison of convergence rate for the Kalman and gradient algorithms.

The algorithm described by (11-4-22) is called the *RLS direct form* or *Kalman algorithm*. It is appropriate when the equalizer has a transversal (direct-form) structure.

Note that the equalizer coefficients change with time by an amount equal to the error $e_N(t)$ multiplied by the Kalman gain vector $\mathbf{K}_N(t)$. Since $\mathbf{K}_N(t)$ is N-dimensional, each tap coefficient in effect is controlled by one of the elements of $\mathbf{K}_N(t)$. Consequently rapid convergence is obtained. In contrast, the steepest-descent algorithm, expressed in our present notation, is

$$\mathbf{C}_N(t) = \mathbf{C}_N(t-1) + \Delta \mathbf{Y}_N^*(t) e_N(t) \tag{11-4-23}$$

and the only variable parameter is the step size Δ.

Figure 11-4-1 illustrates the initial convergence rate of these two algorithms for a channel with fixed parameters $f_0 = 0.26$, $f_1 = 0.93$, $f_2 = 0.26$, and a linear equalizer with 11 taps. The eigenvalue ratio for this channel is $\lambda_{max}/\lambda_{min} = 11$. All the equalizer coefficients were initialized to zero. The steepest-descent algorithm was implemented with $\Delta = 0.020$. The superiority of the Kalman algorithm is clearly evident. This is especially important in tracking a time-variant channel. For example, the time variations in the characteristics of an (ionospheric) high-frequency (HF) radio channel are too rapid to be equalized by the gradient algorithm, but the Kalman algorithm adapts sufficiently rapidly to track such variations.

In spite of its superior tracking performance, the Kalman algorithm described above have two disadvantages. One is its complexity. The second is its sensitivity to roundoff noise that accumulates due to the recursive computations. The latter may cause instabilities in the algorithm.

The number of computations or operations (multiplications, divisions, and subtractions) in computing the variables in (11-4-22) is proportional to N^2. Most of these operations are involved in the updating of $\mathbf{P}_N(t)$. This part of the computation is also susceptible to roundoff noise. To remedy that problem, algorithms have been developed that avoid the computation of $\mathbf{P}_N(t)$ according to (11-4-14). The basis of these algorithms lies in the decomposition of $\mathbf{P}_N(t)$ in the form

$$\mathbf{P}_N(t) = \mathbf{S}_N(t)\mathbf{A}_N(t)\mathbf{S}_N'(t) \tag{11-4-24}$$

where $\mathbf{S}_N(t)$ is a lower-triangular matrix whose diagonal elements are unity, and $\mathbf{\Lambda}_N(t)$ is a diagonal matrix. Such a decomposition is called a *square-root factorization* (see Bierman, 1977). This factorization is described in Appendix D. In a square-root algorithm, $\mathbf{P}_N(t)$ is not updated as in (11-4-14) nor is it computed. Instead, the time updating is performed on $\mathbf{S}_N(t)$ and $\mathbf{\Lambda}_N(t)$.

Square-root algorithms are frequently used in control systems applications in which Kalman filtering is involved. In digital communications, the square-root Kalman algorithm has been implemented in a decision-feedback-equalized PSK modem designed to transmit at high speed over HF radio channels with a nominal 3 kHz bandwidth. This algorithm is described in the paper by Hsu (1982). It has a computational complexity of $1.5N^2 + 6.5N$ (complex-valued multiplications and divisions per output symbol). It is also numerically stable and exhibits good numerical properties. For a detailed discussion of square-root algorithms in sequential estimation, the reader is referred to the book by Bierman (1977).

It is also possible to derive RLS algorithms with computational complexities that grow linearly with the number N of equalizer coefficients. Such algorithms are generally called *fast RLS algorithms* and have been described in the papers by Carayannis *et al.* (1983), Cioffi and Kailath (1984), and Slock and Kailath (1988).

11-4-2 Linear Prediction and the Lattice Filter

In Chapter 3, we considered the linear prediction of a signal, in the context of speech encoding. In this section, we shall establish the connection between linear prediction and a lattice filter.

The linear prediction problem may be stated as follows: given a set of data $y(t-1), y(t-2), \ldots, y(t-p)$, predict the value of the next data point $y(t)$. The predictor of order p is

$$\hat{y}(t) = \sum_{k=1}^{p} a_{pk}\, y(t-k) \tag{11-4-25}$$

Minimization of the MSE, defined as

$$\begin{aligned} \mathscr{E}_p &= E[y(t) - \hat{y}(t)]^2 \\ &= E\left[y(t) - \sum_{k=1}^{p} a_{pk}\, y(t-k)\right]^2 \end{aligned} \tag{11-4-26}$$

with respect to the predictor coefficients $\{a_{pk}\}$ yields the set of linear equations

$$\sum_{k=1}^{p} a_{pk}\, \phi(k-l) = \phi(l), \qquad l = 1, 2, \ldots, p \tag{11-4-27}$$

where

$$\phi(l) = E[y(t)y(t+l)]$$

These are called the *normal equations* or the *Yule–Walker equations*.

The matrix $\mathbf{\Phi}$ with elements $\phi(k-l)$ is a Toeplitz matrix, and, hence, the Levinson–Durbin algorithm described in Appendix A provides an efficient means for solving the linear equations recursively, starting with a first-order predictor and proceeding recursively to the solution of the coefficients for the predictor of order p. The recursive relations for the Levinson–Durbin algorithm are

$$\begin{aligned} a_{11} &= \frac{\phi(1)}{\phi(0)}, \qquad \mathscr{E}_0 = \phi(0) \\ a_{mm} &= \frac{\phi(m) - \mathbf{A}'_m \boldsymbol{\phi}'_{m-1}}{\mathscr{E}_{m-1}} \\ a_{mk} &= a_{m-1\,k} - a_{mm} a_{m-1\,m-k} \\ \mathscr{E}_m &= \mathscr{E}_{m-1}(1 - a_{mm}^2) \end{aligned} \tag{11-4-28}$$

for $m = 1, 2, \ldots, p$, where the vectors $\mathbf{A}_{m-1}$ and $\boldsymbol{\phi}'_{m-1}$ are defined as

$$\begin{aligned} \mathbf{A}_{m-1} &= [a_{m-1\,1} \quad a_{m-1\,2} \quad \cdots \quad a_{m-1\,m-1}]' \\ \boldsymbol{\phi}'_{m-1} &= [\phi(m-1) \quad \phi(m-2) \quad \ldots \quad \phi(1)]' \end{aligned}$$

The linear prediction filter of order m may be realized as a transversal filter with transfer function

$$A_m(z) = 1 - \sum_{k=1}^{m} a_m z^{-k} \tag{11-4-29}$$

Its input is the data $\{y(t)\}$ and its output is the error $e(t) = y(t) - \hat{y}(t)$. The prediction filter can also be realized in the form of a lattice, as we now demonstrate.

Our starting point is the use of the Levinson–Durbin algorithm for the predictor coefficients a_{mk} in (11-4-29). This substitution yields

$$\begin{aligned} A_m(z) &= 1 - \sum_{k=1}^{m-1} (a_{m-1\,k} - a_{mm} a_{m-1\,m-k}) z^{-k} - a_{mm} z^{-m} \\ &= 1 - \sum_{k=1}^{m-1} a_{m-1\,k} z^{-k} - a_{mm} z^{-m} \left(1 - \sum_{k=1}^{m-1} a_{m-1\,k} z^{k}\right) \\ &= A_{m-1}(z) - a_{mm} z^{-m} A_{m-1}(z^{-1}) \end{aligned} \tag{11-4-30}$$

Thus we have the transfer function of the mth-order predictor in terms of the transfer function of the $(m-1)$th-order predictor.

Now suppose we define a filter with transfer function $G_m(z)$ as

$$G_m(z) = z^{-m} A_m(z^{-1}) \tag{11-4-31}$$

Then (11-4-30) may be expressed as

$$A_m(z) = A_{m-1}(z) - a_{mm} z^{-1} G_{m-1}(z) \tag{11-4-32}$$

Note that $G_{m-1}(z)$ represents a transversal filter with tap coefficients $(-a_{m-1\,m-1}, -a_{m-1\,m-2}, \cdots, -a_{m-1\,1}, 1)$, while the coefficients of $A_{m-1}(z)$ are exactly the same except that they are given in reverse order.

More insight into the relationship between $A_m(z)$ and $G_m(z)$ can be obtained by computing the output of these two filters to an input sequence $y(t)$. Using z-transform relations, we have

$$A_m(z)Y(z) = A_{m-1}(z)Y(z) - a_{mm}z^{-1}G_{m-1}(z)Y(z) \tag{11-4-33}$$

We define the outputs of the filters as

$$\begin{aligned} F_m(z) &= A_m(z)Y(z) \\ B_m(z) &= G_m(z)Y(z) \end{aligned} \tag{11-4-34}$$

Then (11-4-33) becomes

$$F_m(z) = F_{m-1}(z) - a_{mm}z^{-1}B_{m-1}(z) \tag{11-4-35}$$

In the time domain, the relation in (11-4-35) becomes

$$f_m(t) = f_{m-1}(t) - a_{mm}b_{m-1}(t-1), \qquad m \geq 1 \tag{11-4-36}$$

where

$$f_m(t) = y(t) - \sum_{k=1}^{m-1} a_{mk}\,y(t-k) \tag{11-4-37}$$

$$b_m(t) = y(t-m) - \sum_{k=1}^{m-1} a_{mk}\,y(t-m+k) \tag{11-4-38}$$

To elaborate, $f_m(t)$ in (11-4-37) represents the error of an mth-order forward predictor, while $b_m(t)$ represents the error of an mth-order backward predictor.

The relation in (11-4-36) is one of two that specifies a lattice filter. The second relation is obtained from $G_m(z)$ as follows:

$$\begin{aligned} G_m(z) &= z^{-m}A_m(z^{-1}) \\ &= z^{-m}[A_{m-1}(z^{-1}) - a_{mm}z^{m}A_{m-1}(z)] \\ &= z^{-1}G_{m-1}(z) - a_{mm}A_{m-1}(z) \end{aligned} \tag{11-4-39}$$

Now, if we multiply both sides of (11-4-39) by $Y(z)$ and express the result in terms of $F_m(z)$ and $B_m(z)$ using the definitions in (11-4-34), we obtain

$$B_m(z) = z^{-1}B_{m-1}(z) - a_{mm}F_{m-1}(z) \tag{11-4-40}$$

By transforming (11-4-40) into the time domain, we obtain the second relation that corresponds to the lattice filter, namely,

$$b_m(t) = b_{m-1}(t-1) - a_{mm}f_{m-1}(t), \qquad m \geq 1 \tag{11-4-41}$$

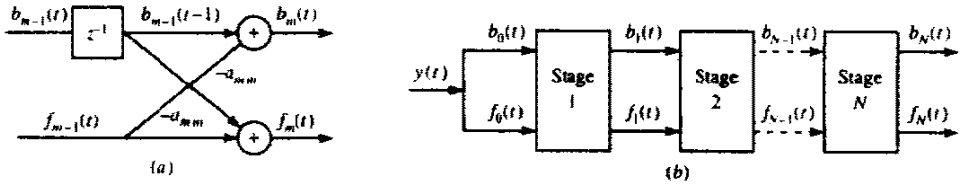

FIGURE 11-4-2 A lattice filter.

The initial condition is

$$f_0(t) = b_0(t) = y(t) \tag{11-4-42}$$

The lattice filter described by the recursive relations in (11-4-36) and (11-4-41) is illustrated in Fig. 11-4-2. Each stage is characterized by its own multiplication factor $\{a_{ii}\}$, $i = 1, 2, \ldots, m$, which is defined in the Levinson–Durbin algorithm. The forward and backward errors $f_m(t)$ and $b_m(t)$ are usually called the *residuals*. The mean square value of these residuals is

$$\mathscr{E}_m = E[f_m^2(t)] = E[b_m^2(t)] \tag{11-4-43}$$

$\mathscr{E}_m$ is given recursively, as indicated in the Levinson–Durbin algorithm, by

$$\begin{aligned} \mathscr{E}_m &= \mathscr{E}_{m-1}(1 - a_{mm}^2) \\ &= \mathscr{E}_0 \prod_{i=1}^{m} (1 - a_{ii}^2) \end{aligned} \tag{11-4-44}$$

where $\mathscr{E}_0 = \phi(0)$.

The residuals $\{f_m(t)\}$ and $\{b_m(t)\}$ satisfy a number of interesting properties, as described by Makhoul (1978). Most important of these are the orthogonality properties

$$\begin{aligned} E[b_m(t)b_n(t)] &= \mathscr{E}_m \delta_{mn} \\ E[f_m(t+m)f_n(t+n)] &= \mathscr{E}_m \delta_{mn} \end{aligned} \tag{11-4-45}$$

Furthermore, the cross-correlation between $f_m(t)$ and $b_n(t)$ is

$$E[f_m(t)b_n(t)] = \begin{cases} a_{nn}\mathscr{E}_m & (m \geq n) \\ 0 & (m < n) \end{cases} \qquad m, n \geq 0 \tag{11-4-46}$$

As a consequence of the orthogonality properties of the residuals, the different sections of the lattice exhibit a form of independence that allows us to add or delete one or more of the last stages without affecting the parameters of the remaining stages. Since the residual mean square error $\mathscr{E}_m$ decreases monotonically with the number of sections, $\mathscr{E}_m$ can be used as a performance index in determining where the lattice should be terminated.

From the above discussion, we observe that a linear prediction filter can be implemented either as a linear transversal filter or as a lattice filter. The lattice filter is order-recursive, and, as a consequence, the number of sections it contains can be easily increased or decreased without affecting the parameters

of the remaining sections. In contrast, the coefficients of a transversal filter obtained on the basis of the RLS criterion are interdependent. This means that an increase or a decrease in the size of the filter results in a change in all coefficients. Consequently, the Kalman algorithm described in Section 11-4-1 is recursive in time but not in order.

Based on least-squares optimization, RLS lattice algorithms have been developed whose computational complexity grow linearly with the number N of filter coefficients (lattice stages). Hence, the lattice equalizer structure is computationally competitive with the direct-form fast RLS equalizer algorithms. RLS lattice algorithms are described in the papers by Morf *et al.* (1973), Satorius and Alexander (1979), Satorius and Pack (1981), Ling and Proakis (1984), and Ling *et al.* (1986).

RLS lattice algorithms have the distinct feature of being numerically robust to round-off error inherent in digital implementations of the algorithm. A treatment of their numerical properties may be found in the papers by Ling *et al.* (1984, 1986).

11-5 SELF-RECOVERING (BLIND) EQUALIZATION

In the conventional zero-forcing or minimum MSE equalizers, we assumed that a known training sequence is transmitted to the receiver for the purpose of initially adjusting the equalizer coefficients. However, there are some applications, such as multipoint communication networks, where it is desirable for the receiver to synchronize to the received signal and to adjust the equalizer without having a known training sequence available. Equalization techniques based on initial adjustment of the coefficients without the benefit of a training sequence are said to be *self-recovering* or *blind*.

Beginning with the paper by Sato (1975), three different classes of adaptive blind equalization algorithms have been developed over the past two decades. One class of algorithms is based on steepest descent for adaptation of the equalizer. A second class of algorithms is based on the use of second- and higher-order (generally, fourth-order) statistics of the received signal to estimate the channel characteristics and to design the equalizer. More recently, a third class of blind equalization algorithms based on the maximum-likelihood criterion have been investigated. In this section, we briefly describe these approaches and give several relevant references to the literature.

11-5-1 Blind Equalization Based on Maximum-Likelihood Criterion

It is convenient to use the equivalent, discrete-time channel model described in Section 10-1-2. Recall that the output of this channel model with ISI is

$$v_n = \sum_{k=0}^{L} f_k I_{n-k} + \eta_n \tag{11-5-1}$$

where $\{f_k\}$ are the equivalent discrete-time channel coefficients, $\{I_n\}$ represents the information sequence, and $\{\eta_n\}$ is a white gaussian noise sequence.

For a block of N received data points, the (joint) probability density function of the received data vector $\mathbf{v} = [v_1\ v_2\ \ldots\ v_N]'$ conditioned on knowing the impulse response vector $\mathbf{f} = [f_0\ f_1\ \ldots\ f_L]'$ and the data vector $\mathbf{I} = [I_1\ I_2\ \ldots\ I_N]'$ is

$$p(\mathbf{v} \mid \mathbf{f}, \mathbf{I}) = \frac{1}{(2\pi\sigma^2)^N} \exp\left(-\frac{1}{2\sigma^2} \sum_{n=1}^{N} \left| v_n - \sum_{k=0}^{L} f_k I_{n-k} \right|^2\right) \tag{11-5-2}$$

The joint maximum-likelihood estimates of $\mathbf{f}$ and $\mathbf{I}$ are the values of these vectors that maximize the joint probability density function $p(\mathbf{v} \mid \mathbf{f}, \mathbf{I})$ or, equivalently, the values of $\mathbf{f}$ and $\mathbf{I}$ that minimize the term in the exponent. Hence, the ML solution is simply the minimum over $\mathbf{f}$ and $\mathbf{I}$ of the metric

$$\begin{aligned} DM(\mathbf{I}, \mathbf{f}) &= \sum_{n=1}^{N} \left| v_n - \sum_{k=0}^{L} f_k I_{n-k} \right|^2 \\ &= \|\mathbf{v} - \mathbf{A}\mathbf{f}\|^2 \end{aligned} \tag{11-5-3}$$

where the matrix $\mathbf{A}$ is called the *data matrix* and is defined as

$$\mathbf{A} = \begin{bmatrix} I_1 & 0 & 0 & \ldots & 0 \\ I_2 & I_1 & 0 & \ldots & 0 \\ I_3 & I_2 & I_1 & \ldots & 0 \\ \vdots & \vdots & \vdots & & \vdots \\ I_N & I_{N-1} & I_{N-2} & \ldots & I_{N-L} \end{bmatrix} \tag{11-5-4}$$

We make several observations. First of all, we note that when the data vector $\mathbf{I}$ (or the data matrix $\mathbf{A}$) is known, as is the case when a training sequence is available at the receiver, the ML channel impulse response estimate obtained by minimizing (11-5-3) over $\mathbf{f}$ is

$$\mathbf{f}_{ML}(\mathbf{I}) = (\mathbf{A}'\mathbf{A})^{-1}\mathbf{A}'\mathbf{v} \tag{11-5-5}$$

On the other hand, when the channel impulse response $\mathbf{f}$ is known, the optimum ML detector for the data sequence $\mathbf{I}$ performs a trellis search (or tree search) by utilizing the Viterbi algorithm for the ISI channel.

When neither $\mathbf{I}$ nor $\mathbf{f}$ are known, the minimization of the performance index $DM(\mathbf{I}, \mathbf{f})$ may be performed jointly over $\mathbf{I}$ and $\mathbf{f}$. Alternatively, $\mathbf{f}$ may be estimated from the probability density function $p(\mathbf{v} \mid \mathbf{f})$, which may be obtained by averaging $p(\mathbf{v}, \mathbf{f} \mid \mathbf{I})$ over all possible data sequences. That is,

$$\begin{aligned} p(\mathbf{v} \mid \mathbf{f}) &= \sum_{m} p(\mathbf{v}, \mathbf{I}^{(m)} \mid \mathbf{f}) \\ &= \sum_{m} p(\mathbf{v} \mid \mathbf{I}^{(m)}, \mathbf{f}) P(\mathbf{I}^{(m)}) \end{aligned} \tag{11-5-6}$$

where $P(\mathbf{I}^{(m)})$ is the probability of the sequence $\mathbf{I} = \mathbf{I}^{(m)}$, for $m = 1, 2, \ldots, M^N$ and M is the size of the signal constellation.

Channel Estimation Based on Average over Data Sequences As indicated in the above discussion, when both $\mathbf{I}$ and $\mathbf{f}$ are unknown, one approach is to estimate the impulse response $\mathbf{f}$ after averaging the probability density $p(\mathbf{v}, \mathbf{I} \mid \mathbf{f})$ over all possible data sequences. Thus, we have

$$\begin{aligned} p(\mathbf{v} \mid \mathbf{f}) &= \sum_m p(\mathbf{v} \mid \mathbf{I}^{(m)}, \mathbf{f}) P(\mathbf{I}^{(m)}) \\ &= \sum_m \left[\frac{1}{(2\pi\sigma^2)^N} \exp\left(-\frac{\|\mathbf{v} - \mathbf{A}^{(m)}\mathbf{f}\|^2}{2\sigma^2} \right) \right] P(\mathbf{I}^{(m)}) \end{aligned} \tag{11-5-7}$$

Then, the estimate of $\mathbf{f}$ that maximizes $p(\mathbf{v} \mid \mathbf{f})$ is the solution of the equation

$$\begin{aligned} \frac{\partial p(\mathbf{v} \mid \mathbf{f})}{\partial \mathbf{f}} &= \sum_m P(\mathbf{I}^{(m)}) \\ (\mathbf{A}^{(m)t}\mathbf{A}^{(m)}\mathbf{f} - \mathbf{A}^{(m)t}\mathbf{v}) \exp\left(-\frac{\|\mathbf{v} - \mathbf{A}^{(m)}\mathbf{f}\|^2}{2\sigma^2} \right) &= 0 \end{aligned} \tag{11-5-8}$$

Hence, the estimate of $\mathbf{f}$ may be expressed as

$$\begin{aligned} \mathbf{f} = &\left[\sum_m P(\mathbf{I}^{(m)}) \mathbf{A}^{(m)t}\mathbf{A}^{(m)} g(\mathbf{v}, \mathbf{A}^{(m)}, \mathbf{f}) \right]^{-1} \\ &\times \sum_m P(\mathbf{I}^{(m)}) g(\mathbf{v}, \mathbf{A}^{(m)}, \mathbf{f}) \mathbf{A}^{(m)t}\mathbf{v} \end{aligned} \tag{11-5-9}$$

where the function $g(\mathbf{v}, \mathbf{A}^{(m)}, \mathbf{f})$ is defined as

$$g(\mathbf{v}, \mathbf{A}^{(m)}, \mathbf{f}) = \exp\left(-\frac{\|\mathbf{v} - \mathbf{A}^{(m)}\mathbf{f}\|^2}{2\sigma^2} \right) \tag{11-5-10}$$

The resulting solution for the optimum $\mathbf{f}$ is denoted by $\mathbf{f}_{ML}$.

Equation (11-5-9) is a nonlinear equation for the estimate of the channel impulse response, given the received signal vector $\mathbf{v}$. It is generally difficult to obtain the optimum solution by solving (11-5-9) directly. On the other hand, it is relatively simple to devise a numerical method that solves for $\mathbf{f}_{ML}$ recursively. Specifically, we may write

$$\begin{aligned} \mathbf{f}^{(k+1)} = &\left[\sum_m P(\mathbf{I}^{(m)}) \mathbf{A}^{(m)t}\mathbf{A}^{(m)} g(\mathbf{v}, \mathbf{A}^{(m)}, \mathbf{f}^{(k)}) \right]^{-1} \\ &\times \sum_m P(\mathbf{I}^{(m)}) g(\mathbf{v}, \mathbf{A}^{(m)}, \mathbf{f}^{(k)}) \mathbf{A}^{(m)t}\mathbf{v} \end{aligned} \tag{11-5-11}$$

Once $\mathbf{f}_{ML}$ is obtained from the solution of (11-5-9) or (11-5-11), we may

simply use the estimate in the minimization of the metric $DM(\mathbf{I}, \mathbf{f}_{ML})$, given by (11-5-3), over all the possible data sequences. Thus, $\mathbf{I}_{ML}$ is the sequence $\mathbf{I}$ that mimimizes $DM(\mathbf{I}, \mathbf{f}_{ML})$, i.e.,

$$\min_{\mathbf{I}} DM(\mathbf{I}, \mathbf{f}_{ML}) = \min_{\mathbf{I}} \|\mathbf{v} - \mathbf{A}\mathbf{f}_{ML}\|^2 \tag{11-5-12}$$

We know that the Viterbi algorithm is the computationally efficient algorithm for performing the minimization of $DM(\mathbf{I}, \mathbf{f}_{ML})$ over $\mathbf{I}$.

This algorithm has two major drawbacks. First, the recursion for $\mathbf{f}_{LM}$ given by (11-5-11) is computationally intensive. Second, and, perhaps, more importantly, the estimate $\mathbf{f}_{ML}$ is not as good as the maximum-likelihood estimate $\mathbf{f}_{ML}(\mathbf{I})$ that is obtained when the sequence $\mathbf{I}$ is known. Consequently, the error rate performance of the blind equalizer (the Viterbi algorithm) based on the estimate $\mathbf{f}_{ML}$ is poorer than that based on $\mathbf{f}_{ML}(\mathbf{I})$. Next, we consider joint channel and data estimation.

Joint Channel and Data Estimation Here, we consider the joint optimization of the performance index $DM(\mathbf{I}, \mathbf{f})$ given by (11-5-3). Since the elements of the impulse response vector $\mathbf{f}$ are continuous and the elements of the data vector $\mathbf{I}$ are discrete, one approach is to determine the maximum-likelihood estimate of $\mathbf{f}$ for each possible data sequence and, then, to select the data sequence that minimizes $DM(\mathbf{I}, \mathbf{f})$ for each corresponding channel estimate. Thus, the channel estimate corresponding to the mth data sequence $\mathbf{I}^{(m)}$ is

$$\mathbf{f}_{ML}(\mathbf{I}^{(m)}) = (\mathbf{A}^{(m)t}\mathbf{A}^{(m)})^{-1}\mathbf{A}^{(m)t}\mathbf{v}. \tag{11-5-13}$$

For the mth data sequence, the metric $DM(\mathbf{I}, \mathbf{f})$ becomes

$$DM(\mathbf{I}^{(m)}, \mathbf{f}_{ML}(\mathbf{I}^{(m)})) = \|\mathbf{v} - \mathbf{A}^{(m)}\mathbf{f}_{ML}(\mathbf{I}^{(m)})\|^2 \tag{11-5-14}$$

Then, from the set of M^N possible sequences, we select the data sequence that minimizes the cost function in (11-5-14), i.e., we determine

$$\min_{\mathbf{I}^{(m)}} DM(\mathbf{I}^{(m)}, \mathbf{f}_{ML}(\mathbf{I}^{(m)})) \tag{11-5-15}$$

The approach described above is an exhaustive computational search method with a computational complexity that grows exponentially with the length of the data block. We may select $N = L$, and, thus, we shall have one channel estimate for each of the M^L surviving sequences. Thereafter, we may continue to maintain a separate channel estimate for each surviving path of the Viterbi algorithm search through the trellis.

A similar approach has been proposed by Seshadri (1991). In essence, Seshadri's algorithm is a type of generalized Viterbi algorithm (GVA) that retains $K \geq 1$ best estimates of the transmitted data sequence into each state

of the trellis and the corresponding channel estimates. In Seshadri's GVA, the search is identical to the conventional VA from the beginning up to the L stage of the trellis, i.e., up to the point where the received sequence $(v_1, v_2, \ldots, v_L)$ has been processed. Hence, up to the L stage, an exhaustive search is performed. Associated with each data sequence $\mathbf{I}^{(m)}$, there is a corresponding channel estimate $\mathbf{f}_{ML}(\mathbf{I}^{(m)})$. From this stage on, the search is modified, to retain $K \geq 1$ surviving sequences and associated channel estimates per state instead of only one sequence per state. Thus, the GVA is used for processing the received signal sequence $\{v_n, n \geq L+1\}$. The channel estimate is updated recursively at each stage using the LMS algorithm to further reduce the computational complexity. Simulation results given in the paper by Seshadri (1991) indicate that this GVA blind equalization algorithm performs rather well at moderate signal-to-noise ratios with $K = 4$. Hence, there is a modest increase in the computational complexity of the GVA compared with that for the conventional VA. However, there are additional computations involved with the estimation and updating of the channel estimates $\mathbf{f}(\mathbf{I}^{(m)})$ associated with each of the surviving data estimates.

An alternative joint estimation algorithm that avoids the least-squares computation for channel estimation has been devised by Zervas *et al.* (1991). In this algorithm, the order for performing the joint minimization of the performance index $DM(\mathbf{I}, \mathbf{f})$ is reversed. That is, a channel impulse response, say $\mathbf{f} = \mathbf{f}^{(1)}$ is selected and then the conventional VA is used to find the optimum sequence for this channel impulse response. Then, we may modify $\mathbf{f}^{(1)}$ in some manner to $\mathbf{f}^{(2)} = \mathbf{f}^{(1)} + \Delta\mathbf{f}^{(1)}$ and repeat the optimization over the data sequences $\{\mathbf{I}^{(m)}\}$.

Based on this general approach, Zervas developed a new ML blind equalization algorithm, which is called a *quantized-channel algorithm*. The algorithm operates over a grid in the channel space, which becomes finer and finer by using the ML criterion to confine the estimated channel in the neighborhood of the original unknown channel. This algorithm leads to an efficient parallel implementation, and its storage requirements are only those of the VA.

11-5-2 Stochastic Gradient Algorithm

Another class of blind equalization algorithms are stochastic-gradient iterative equalization schemes that apply a memoryless nonlinearity in the output of a linear FIR equalization filter in order to generate the "desired response" in each iteration.

Let us begin with an initial guess of the coefficients of the optimum equalizer, which we denote by $\{c_n\}$. Then, the convolution of the channel response with the equalizer response may be expressed as

$$\{c_n\} \star \{f_n\} = \{\delta_n\} + \{e_n\} \tag{11-5-16}$$

where $\{\delta_n\}$ is the unit sample sequence and $\{e_n\}$ denotes the error sequence

that results from our initial guess of the equalizer coefficients. If we convolve the equalizer impulse response with the received sequence $\{v_n\}$, we obtain

$$\begin{aligned}\{\hat{I}_n\} &= \{v_n\} \star \{c_n\} \\ &= \{I_n\} \star \{f_n\} \star \{c_n\} + \{\eta_n\} \star \{c_n\} \\ &= \{I_n\} \star (\{\delta_n\} + \{e_n\}) + \{\eta_n\} \star \{c_n\} \\ &= \{I_n\} + \{I_n\} \star \{e_n\} + \{\eta_n\} \star \{c_n\}\end{aligned} \tag{11-5-17}$$

The term $\{I_n\}$ in (11-5-17) represents the desired data sequence, the term $\{I_n\} \star \{e_n\}$ represents the residual ISI, and the term $\{\eta_n\} \star \{c_n\}$ represents the additive noise. Our problem is to utilize the deconvolved sequence $\{\hat{I}_n\}$ to find the "best" estimate of a desired response, denoted in general by $\{d_n\}$. In the case of adaptive equalization using a training sequence, $\{d_n\} = \{I_n\}$. In a blind equalization mode, we shall generate a desired response from $\{\hat{I}_n\}$.

The mean square error (MSE) criterion may be employed to determine the "best" estimate of $\{I_n\}$ from the observed equalizer output $\{\hat{I}_n\}$. Since the transmitted sequence $\{I_n\}$ has a nongaussian pdf, the MSE estimate is a nonlinear transformation of $\{\hat{I}_n\}$. In general, the "best" estimate $\{d_n\}$ is given by

$$\begin{aligned} d_n &= g(\hat{I}_n) && \text{(memoryless)} \\ d_n &= g(\hat{I}_n, \hat{I}_{n-1}, \ldots, \hat{I}_{n-m}) && (m\text{th-order memory}) \end{aligned} \tag{11-5-18}$$

where $g(\ )$ is a nonlinear function. The sequence $\{d_n\}$ is then used to generate an error signal, which is fed back into the adaptive equalization filter, as shown in Fig. 11-5-1.

A well-known classical estimation problem is the following. If the equalizer output $\hat{I}_n$ is expressed as

$$\hat{I}_n = I_n + \tilde{\eta}_n \tag{11-5-19}$$

where $\tilde{\eta}_n$ is assumed to be zero-mean gaussian (the central limit theorem may

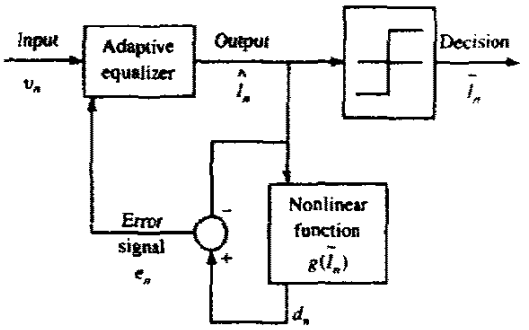

FIGURE 11-5-1 Adaptive blind equalization with stochastic gradient algorithms.

TABLE 11-5-1 STOCHASTIC GRADIENT ALGORITHMS FOR BLIND EQUALIZATION

Equalizer tap coefficients	$\{c_n, 0 \le n \le N-1\}$
Received signal sequence	$\{v_n\}$
Equalizer output sequence	$\{\hat{I}_n\} = \{v_n\} \star \{c_n\}$
Equalizer error sequence	$\{e_n\} = g(\hat{I}_n) - \hat{I}_n$
Tap coefficient update equation	$\mathbf{c}_{n+1} = \mathbf{c}_n + \Delta \mathbf{v}_n^* e_n$

Algorithm	Nonlinearity: $g(\hat{I}_n)$
Godard	$\frac{\hat{I}_n}{\lvert\hat{I}_n\rvert}(\lvert\hat{I}_n\rvert + R_2\lvert\hat{I}_n\rvert - \lvert\hat{I}_n\rvert^3), R_2 = \frac{E\{\lvert I_n\rvert^4\}}{E\{\lvert I_n\rvert^2\}}$
Sato	$\zeta \operatorname{csgn}(\hat{I}_n), \zeta = \frac{E\{[\operatorname{Re}(I_n)]^2\}}{E\{\lvert\operatorname{Re}(I_n)\rvert\}}$
Benveniste–Goursat	$\hat{I}_n + k_1(\hat{I}_n - I_n) + k_2\lvert\hat{I}_n - \hat{I}_n\rvert\,[\zeta \operatorname{csgn}(\hat{I}_n) - \hat{I}_n]$, k_1 and k_2 are positive constants
Stop-and-Go	$\hat{I}_n + \frac{1}{2}A(\hat{I}_n - \hat{I}_n) + \frac{1}{2}B(\hat{I}_n - \hat{I}_n)^*$ $(A, B) = (2, 0), (1, 1), (1, -1)$, or $(0, 0)$, depending on the signs of decision-directed error $\hat{I}_n - \hat{I}_n$ and the error $\zeta \operatorname{csgn}(\hat{I}_n) - \hat{I}_n$

be invoked here for the residual ISI and the additive noise), $\{I_n\}$ and $\{\tilde{\eta}_n\}$ are statistically independent, and $\{I_n\}$ are statistically independent and identically distributed random variables, then the MSE estimate of $\{I_n\}$ is

$$d_n = E(I_n \mid \hat{I}_n) \tag{11-5-20}$$

which is a nonlinear function of the equalizer output when $\{I_n\}$ is nongaussian.

Table 11-5-1 illustrates the general form of existing blind equalization algorithms that are based on LMS adaptation. We observe that the basic difference among these algorithms lies in the choice of the memoryless nonlinearity. The most widely used algorithm in practice is the *Godard algorithm*, sometimes also called the *constant-modulus algorithm* (CMA).

It is apparent from Table 11-5-1 that the output sequence $\{d_n\}$ obtained by taking a nonlinear function of the equalizer output plays the role of the desired response or a training sequence. It is also apparent that these algorithms are simple to implement, since they are basically LMS-type algorithms. As such, we expect that the convergence characteristics of these algorithms will depend on the autocorrelation matrix of the received data $\{v_n\}$.

With regard to convergence, the adaptive LMS-type algorithms converge in the mean when

$$E[v_n g^*(\hat{I}_n)] = E[v_n \hat{I}_n^*] \tag{11-5-21}$$

and, in the mean square sense, when (superscript H denotes the conjugate transpose)

$$\begin{aligned} E[\mathbf{c}_n^H \mathbf{v}_n g^*(\hat{I}_n)] &= E[\mathbf{c}_n^H \mathbf{v}_n \hat{I}_n^*] \\ E[\hat{I}_n g^*(\hat{I}_n)] &= E[\lvert\hat{I}_n\rvert^2] \end{aligned} \tag{11-5-22}$$

Therefore, it is required that the equalizer output $\{\hat{I}_n\}$ satisfy (11-5-22). Note that (11-5-22) states that the autocorrelation of $\{\hat{I}_n\}$ (the right-hand side) equals the cross-correlation between $\hat{I}_n$ and a nonlinear transformation of $\hat{I}_n$ (left-hand side). Processes that satisfy this property are called *Bussgang* (1952), as named by Bellini (1986). In summary, the algorithms given in Table 11-5-1 converge when the equalizer output sequence $\hat{I}_n$ satisfies the Bussgang property.

The basic limitation of stochastic gradient algorithms is their relatively slow convergence. Some improvement in the convergence rate can be achieved by modifying the adaptive algorithms from LMS-type to recursive-least-square (RLS) type.

Godard Algorithm As indicated above, the Godard blind equalization algorithm is a steepest-descent algorithm that is widely used in practice when a training sequence is not available. Let us describe this algorithm in more detail.

Godard considered the problem of combined equalization and carrier phase recovery and tracking. The carrier phase tracking is performed at baseband, following the equalizer as shown in Fig. 11-5-2. Based on this structure, we may express the equalizer output as

$$\hat{I}_k = \sum_{n=-K}^{K} c_n v_{k-n} \tag{11-5-23}$$

and the input to the decision device as $\hat{I}_k \exp(-j\hat{\phi}_k)$, where $\hat{\phi}_k$ is the carrier phase estimate in the kth symbol interval.

If the desired symbol were known, we could form the error signal

$$\varepsilon_k = I_k - \hat{I}_k e^{-j\hat{\phi}_k} \tag{11-5-24}$$

and minimize the MSE with respect to $\hat{\phi}_k$ and $\{c_n\}$, i.e.,

$$\min_{\hat{\phi}_k, \mathbf{C}} E(|I_k - \hat{I}_k e^{-j\hat{\phi}_k}|^2) \tag{11-5-25}$$

FIGURE 11-5-2 Godard scheme for combined adaptive (blind) equalization and carrier phase tracking.

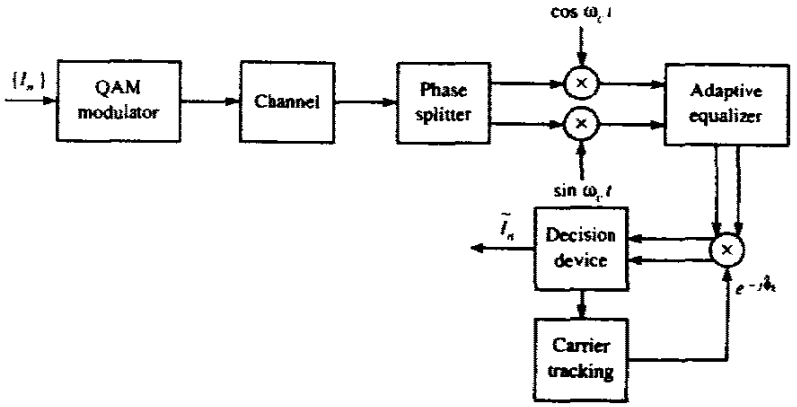

This criterion leads us to use the LMS algorithm for recursively estimating $\mathbf{C}$ and ϕ_k. The LMS algorithm based on knowledge of the transmitted sequence is

$$\hat{\mathbf{C}}_{k+1} = \hat{\mathbf{C}}_k + \Delta_c(I_k - \hat{I}_k e^{-j\hat{\phi}_k})\mathbf{V}_k^* e^{j\hat{\phi}_k} \tag{11-5-26}$$

$$\hat{\phi}_{k+1} = \hat{\phi}_k + \Delta_\phi \operatorname{Im}(I_k \hat{I}_k^* e^{j\hat{\phi}_k}) \tag{11-5-27}$$

where Δ_c and Δ_ϕ are the step-size parameters for the two recursive equations. Note that these recursive equations are coupled together. Unfortunately, these equations will not converge, in general, when the desired symbol sequence $\{I_k\}$ is unknown.

The approach proposed by Godard is to use a criterion that depends on the amount of intersymbol interference at the output of the equalizer but one that is independent of the QAM signal constellation and the carrier phase. For example, a cost function that is independent of carrier phase and has the property that its minimum leads to a small MSE is

$$G^{(p)} = E(|\hat{I}_k|^p - |I_k|^p)^2 \tag{11-5-28}$$

where p is a positive and real integer. Minimization of $G^{(p)}$ with respect to the equalizer coefficients results in the equalization of the signal amplitude only. Based on this observation, Godard selected a more general cost function, called the *dispersion of order p*, defined as

$$D^{(p)} = E(|\hat{I}_k|^p - R_p)^2 \tag{11-5-29}$$

where R_p is a positive real constant. As in the case of $G^{(p)}$, we observe that $D^{(p)}$ is independent of the carrier phase.

Minimization of $D^{(p)}$ with respect to the equalizer coefficients can be performed recursively according to the steepest-descent algorithm

$$\mathbf{C}_{k+1} = \mathbf{C}_k - \Delta_p \frac{dD^{(p)}}{d\mathbf{C}_k} \tag{11-5-30}$$

where Δ_p is the step-size parameter. By differentiating $D^{(p)}$ and dropping the expectation operation, we obtain the following LMS-type algorithm for adjusting the equalizer coefficients:

$$\hat{\mathbf{C}}_{k+1} = \hat{\mathbf{C}}_k + \Delta_p \mathbf{V}_k^* \hat{I}_k |\hat{I}_k|^{p-2}(R_p - |\hat{I}_k|^p) \tag{11-5-31}$$

where Δ_p is the step-size parameter and the optimum choice of R_p is

$$R_p = \frac{E(|I_k|^{2p})}{E(|I_k|^p)} \tag{11-5-32}$$

As expected, the recursion in (11-5-31) for $\hat{\mathbf{C}}_k$ does not require knowledge of the carrier phase. Carrier phase tracking may be carried out in a decision-directed mode according to (11-5-27).

Of particular importance is the case $p = 2$, which leads to the relatively simple algorithm

$$\begin{aligned}\hat{\mathbf{C}}_{k+1} &= \hat{\mathbf{C}}_k + \Delta_p \mathbf{V}_k^* \hat{I}_k (R_2 - |\hat{I}_k|^2) \\ \hat{\phi}_{k+1} &= \hat{\phi}_k + \Delta_\phi \operatorname{Im}(\tilde{I}_k \hat{I}_k^* e^{j\hat{\phi}_k})\end{aligned} \tag{11-5-33}$$

where $\tilde{I}_k$ is the output decision based on $\hat{I}_k$, and

$$R_2 = \frac{E(|I_k|^4)}{E(|I_k|^2)} \tag{11-5-34}$$

Convergence of the algorithm given in (11-5-33) was demonstrated in the paper by Godard (1980). Initially, the equalizer coefficients were set to zero except for the center (reference) tap, which was set according to the condition

$$|c_0|^2 > \frac{E\,|I_k|^4}{2\,|x_0|^2\,[E(|I_k|^2)]^2} \tag{11-5-35}$$

which is sufficient, but not necessary, for convergence of the algorithm. Simulation results performed by Godard on simulated telephone channels with typical frequency response characteristics and transmission rates of 7200–12 000 bits/s indicate that the algorithm in (11-5-31) performs well and leads to convergence in 5000–20 000 iterations, depending on the signal constellation. Initially, the eye pattern was closed prior to equalization. The number of iterations required for convergence is about an order of magnitude greater than the number required to equalize the channels with a known training sequence. No apparent difficulties were encountered in using the decision-directed phase estimation algorithm in (11-5-33) from the beginning of the equalizer adjustment process.

11-5-3 Blind Equalization Algorithms Based on Second- and Higher-Order Signal Statistics

It is well known that second-order statistics (autocorrelation) of the received signal sequence provide information on the magnitude of the channel characteristics, but not on the phase. However, this statement is not correct if the autocorrelation function of the received signal is periodic, as is the case for a digitally modulated signal. In such a case, it is possible to obtain a measurement of the amplitude and the phase of the channel from the received signal. This cyclostationarity property of the received signal forms the basis for a channel estimation algorithm devised by Tong *et al.* (1993).

It is also possible to estimate the channel response from the received signal by using higher-order statistical methods. In particular, the impulse response of a linear, discrete-time-invariant system can be obtained explicitly from cumulants of the received signal, provided that the channel input is nongaussian. We describe the following simple method for estimation of the channel

impulse response from fourth-order cumulants of the received signal sequence. The fourth-order cumulant is defined as

$$\begin{aligned} c(v_k, v_{k+m}, v_{k+n}, v_{k+l}) \equiv c_v(m, n, l) \\ = E(v_k\, v_{k+m}\, v_{k+n}\, v_{k+l}) \\ - E(v_k\, v_{k+m})E(v_{k+n}\, v_{k+l}) \\ - E(v_k\, v_{k+n})E(v_{k+m}\, v_{k+l}) \\ - E(v_k\, v_{k+l})E(v_{k+m}\, v_{k+n}) \end{aligned} \tag{11-5-36}$$

(The fourth-order cumulant of a gaussian signal process is zero.) Consequently, it follows that

$$c_r(m, n, l) = c(I_k, I_{k+m}, I_{k+n}, I_{k+l}) \sum_{k=0}^{\infty} f_k f_{k+m} f_{k+n} f_{k+l} \tag{11-5-37}$$

For a statistically independent and identically distributed input sequence $\{I_n\}$ to the channel, $c(I_k, I_{k+m}, I_{k+n}, I_{k+l}) = k$, a constant, called the *kurtosis*. Then, if the length of the channel response is $L + 1$, we may let $m = n = l = -L$ so that

$$c_r(-L, -L, -L) = kf_L f_0^3 \tag{11-5-38}$$

Similarly, if we let $m = 0$, $n = L$ and $l = p$, we obtain

$$c_r(0, L, p) = kf_L f_0^2 f_p \tag{11-5-39}$$

If we combine (11-5-38) and (11-5-39), we obtain the impulse response within a scale factor as

$$f_p = f_0 \frac{c_r(0, L, p)}{c_r(-L, -L, -L)}, \qquad p = 1, 2, \ldots, L \tag{11-5-40}$$

The cumulants $c_r(m, n, l)$ are estimated from sample averages of the received signal sequence $\{v_n\}$.

Another approach based on higher-order statistics is due to Hatzinakos and Nikias (1991). They have introduced the first polyspectra-based adaptive blind equalization method named the *tricepstrum equalization algorithm* (TEA). This method estimates the channel response characteristics by using the complex cepstrum of the fourth-order cumulants (tricepstrum) of the received signal sequence $\{v_n\}$. TEA depends only on fourth-order cumulants of $\{v_n\}$ and is capable of separately reconstructing the minimum-phase and maximum-phase characteristics of the channel. The channel equalizer coefficients are then computed from the measured channel characteristics. The basic approach used in TEA is to compute the tricepstrum of the received sequence $\{v_n\}$, which is the inverse (three-dimensional) Fourier transform of the logarithm of the trispectrum of $\{v_n\}$. (The *trispectrum* is the three-dimensional discrete Fourier transform of the fourth-order cumulant sequence $c_r(m, n, l)$). The equalizer coefficients are then computed from the cepstral coefficients.

By separating the channel estimation from the channel equalization, it is possible to use any type of equalizer for the ISI, i.e., either linear, or decision-feedback, or maximum-likelihood sequence detection. The major disadvantage with this class of algorithms is the large amount of data and the inherent computational complexity involved in the estimation of the higher-order moments (cumulants) of the received signal.

In conclusion, we have provided an overview of three classes of blind equalization algorithms that find applications in digital communications. Of the three families of algorithms described, those based on the maximum-likelihood criterion for jointly estimating the channel impulse response and the data sequence are optimal and require relatively few received signal samples for performing channel estimation. However, the computational complexity of the algorithms is large when the ISI spans many symbols. On some channels, such as the mobile radio channel, where the span of the ISI is relatively short, these algorithms are simple to implement. However, on telephone channels, where the ISI spans many symbols but is usually not too severe, the LMS-type (stochastic gradient) algorithms are generally employed.

11-6 BIBLIOGRAPHICAL NOTES AND REFERENCES

Adaptive equalization for digital communications was developed by Lucky (1965, 1966). His algorithm was based on the peak distortion criterion and led to the zero-forcing algorithm. Lucky's work was a major breakthrough, which led to the rapid development of high-speed modems within five years of publication of his work. Concurrently, the LMS algorithm was devised by Widrow (1966), and its use for adaptive equalization for complex-valued (in-phase and quadrature components) signals was described and analyzed in a tutorial paper by Proakis and Miller (1969).

A tutorial treatment of adaptive equalization algorithms that were developed during the period 1965–1975 is given by Proakis (1975). A more recent tutorial treatment of adaptive equalization is given in the paper by Qureshi (1985). The major breakthrough in adaptive equalization techniques, beginning with the work of Lucky in 1965 coupled with the development of trellis-coded modulation, which was proposed by Ungerboeck and Csajka (1976), has led to the development of commercially available high speed modems with a capability of speeds of 9600–28 800 bits/s on telephone channels.

The use of a more rapidly converging algorithm for adaptive equalization was proposed by Godard (1974). Our derivation of the RLS (Kalman) algorithm, described in Section 11-4-1, follows the approach outlined by Picinbono (1978). RLS lattice algorithms for general signal estimation applications were developed by Morf *et al.* (1977, 1979). The applications of these algorithms have been investigated by several researchers, including Makhoul (1978), Satorius and Pack (1981), Satorius and Alexander (1979), and Ling and Proakis (1982, 1984a–c, 1985). The fast RLS Kalman algorithm for adaptive equalization was first described by Falconer and Liung (1978). The above

references are just a few of the important papers that have been published on RLS algorithms for adaptive equalization and other applications.

Sato's (1975) original work on blind equalization was focused on PAM (one-dimensinal) signal constellations. Subsequently it was generalized to two-dimensional and multidimensional signal constellations in the algorithms devised by Godard (1980), Benveniste and Goursat (1984), Sato (1986), Foschini (1985), Picchi and Prati (1987), and Shalvi and Weinstein (1990). Blind equalization methods based on the use of second- and higher-order moments of the received signal were proposed by Hatzinakos and Nikias (1991) and Tong *et al.* (1994). The use of the maximum-likelihood criterion for joint channel estimation and data detection has been investigated and treated in papers by Seshadri (1991), Ghosh and Weber (1991), Zervas *et al.* (1991) and Raheli *et al.* (1995). Finally, the convergence characteristics of stochastic gradient blind equalization algorithms have been investigated by Ding (1990), Ding *et al.* (1989), and Johnson (1991).

PROBLEMS

11-1 An equivalent discrete-time channel with white gaussian noise is shown in Fig. P11-1.

a Suppose we use a linear equalizer to equalize the channel. Determine the tap coefficients c_{-1}, c_0, c_1 of a three-tap equalizer. To simplify the computation, let the AWGN be zero.

b The tap coefficients of the linear equalizer in (a) are determined recursively via the algorithm

$$\mathbf{C}_{k+1} = \mathbf{C}_k - \Delta \mathbf{g}_k, \qquad \mathbf{C}_k = [c_{-1k} \quad c_{0k} \quad c_{1k}]'$$

where $\mathbf{g}_k = \Gamma \mathbf{C}_k - \mathbf{b}$ is the gradient vector and Δ is the step size. Determine the range of values of Δ to ensure convergence of the recursive algorithm. To simplify the computation, let the AWGN be zero.

c Determine the tap weights of a DFE with two feedforward taps and one feedback gap. To simplify the computation, let the AWGN be zero.

11-2 Refer to Problem 10-18 and answer the following questions.

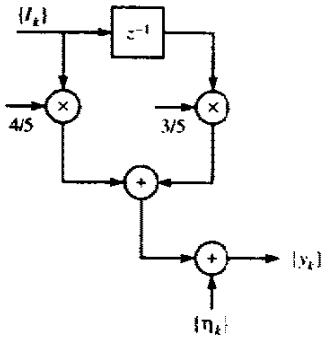

FIGURE P11-1

a Determine the maximum value of Δ that can be used to ensure that the equalizer coefficients converge during operation in the adaptive mode.

b What is the variance of the self-noise generated by the three-tap equalizer when operating in an adaptive mode, as a function of Δ? Suppose it is desired to limit the variance of the self-noise to 10% of the minimum MSE for the three-tap equalizer when $N_0 = 0.1$. What value of Δ would you select?

c If the optimum coefficients of the equalizer are computed recursively by the method of steepest descent, the recursive equation can be expressed in the form

$$\mathbf{C}_{(n+1)} = (\mathbf{I} - \Delta\Gamma)\mathbf{C}_{(n)} + \Delta\boldsymbol{\xi}$$

where $\mathbf{I}$ is the identity matrix. The above represents a set of three coupled first-order difference equations. They can be decoupled by a linear transformation that diagonalizes the matrix Γ. That is, $\Gamma = \mathbf{U}\Lambda\mathbf{U}'$ where Λ is the diagonal matrix having the eigenvalues of Γ as its diagonal elements and $\mathbf{U}$ is the (normalized) modal matrix that can be obtained from your answer to 10-18(b). Let $\mathbf{C}' = \mathbf{U}'\mathbf{C}$ and determine the steady-state solution for $\mathbf{C}'$. From this, evaluate $\mathbf{C} = (U')^{-1}\mathbf{C}' = \mathbf{U}\mathbf{C}'$ and, thus, show that your answer agrees with the result obtained in 10-18(a).

11-3 When a periodic pseudo-random sequence of length N is used to adjust the coefficients of an N-tap linear equalizer, the computations can be performed efficiently in the frequency domain by use of the discrete Fourier transform (DFT). Suppose that $\{y_n\}$ is a sequence of N received samples (taken at the symbol rate) at the equalizer input. Then the computation of the equalizer coefficients is performed as follows.

a Compute the DFT of one period of the equalizer input sequence $\{y_n\}$, i.e.,

$$Y_k = \sum_{n=0}^{N-1} y_n e^{-j2\pi nk/N}$$

b Compute the desired equalizer spectrum

$$C_k = \frac{X_k Y_k^*}{|Y_k|^2}, \qquad k = 0, 1, \ldots, N-1$$

where $\{X_i\}$ is the precomputed DFT of the training sequence.

c Compute the inverse DFT of $\{C_k\}$ to obtain the equalizer coefficients $\{c_n\}$. Show that this procedure in the absence of noise yields an equalizer whose frequency response is equal to the frequency response of the inverse folded channel spectrum at the N uniformly spaced frequencies $f_k = k/NT$, $k = 0, 1, \ldots, N-1$.

11-4 Show that the gradient vector in the minimization of the MSE may be expressed as

$$\mathbf{G}_k = -E(\varepsilon_k \mathbf{V}_k^*)$$

where the error $\varepsilon_k = I_k - \hat{I}_k$, and the estimate of $\mathbf{G}_k$, i.e.,

$$\hat{\mathbf{G}}_k = -\varepsilon_k \mathbf{V}_k^*$$

satisfies the condition that $E(\hat{\mathbf{G}}_k) = \mathbf{G}_k$.

11-5 The *tap-leakage LMS algorithm* proposed in the paper by Gitlin *et al.* (1982) may be expressed as

$$\mathbf{C}_N(n+1) = w\mathbf{C}_N(n) + \Delta\varepsilon(n)\mathbf{V}_N^*(n)$$

where $0 < w < 1$, Δ is the step size, and $\mathbf{V}_M(n)$ is the data vector at time n. Determine the condition for the convergence of the mean value of $\mathbf{C}_N(n)$.

11-6 Consider the random process

$$x(n) = gv(n) + w(n), \quad n = 0, 1, \ldots, M-1$$

where $v(n)$ is a known sequence, g is a random variable with $E(g) = 0$, and $E(g^2) = G$. The process $w(n)$ is a white noise sequence with

$$\gamma_{ww}(m) = \sigma_w^2 \delta_m$$

Determine the coefficients of the linear estimator for g, that is,

$$\hat{g} = \sum_{n=0}^{M-1} h(n)x(n)$$

that minimize the mean square error

11-7 A digital transversal filter can be realized in the frequency-sampling form with system function (see Problem 10-25)

$$H(z) = \frac{1 - z^{-M}}{M} \sum_{k=0}^{M-1} \frac{H_k}{1 - e^{j2\pi k/M} z^{-1}}$$
$$= H_1(z)H_2(z)$$

where $H_1(z)$ is the comb filter, $H_2(z)$ is the parallel bank of resonators, and $\{H_k\}$ are the values of the discrete Fourier transform (DFT).

a Suppose that this structure is implemented as an adaptive filter using the LMS algorithm to adjust the filter (DFT) parameters $\{H_k\}$. Give the time-update equation for these parameters. Sketch the adaptive filter structure.

b Suppose that this structure is used as an adaptive channel equalizer in which the desired signal is

$$d(n) = \sum_{k=0}^{M-1} A_k \cos \omega_k n, \quad \omega_k = \frac{2\pi k}{M}$$

With this form for the desired signal, what advantages are there in the LMS adaptive algorithm for the DFT coefficients $\{H_k\}$ over the direct-form structure with coefficients $\{h(n)\}$? (see Proakis, 1970).

11-8 Consider the performance index

$$J = h^2 + 40h + 28$$

Suppose that we search for the minimum of J by using the steepest-descent algorithm

$$h(n+1) = h(n) - \tfrac{1}{2}\Delta g(n)$$

where $g(n)$ is the gradient.

a Determine the range of values of Δ that provides an overdamped system for the adjustment process.

b Plot the expression for J as a function of n for a value of Δ in this range.

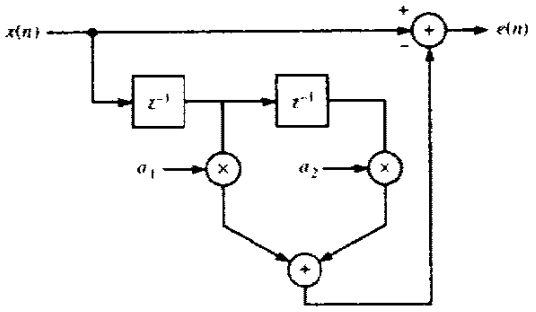

FIGURE P11-9

11-9 Determine the coefficients a_1 and a_2 for the linear predictor shown in Fig. P11-9, given that the autocorrelation $\gamma_{xx}(m)$ of the input signal is

$$\gamma_{xx}(m) = b^{|m|}, \quad 0 < b < 1$$

11-10 Determine the lattice filter and its optimum reflection coefficients corresponding to the linear predictor in Problem 11-9.

11-11 Consider the adaptive FIR filter shown in Fig. P11-11. The system $C(z)$ is characterized by the system function

$$C(z) = \frac{1}{1 - 0.9z^{-1}}$$

Determine the optimum coefficients of the adaptive transversal (FIR) filter $B(z) = b_0 + b_1 z^{-1}$ that minimize the mean square error. The additive noise is white with variance $\sigma_w^2 = 0.1$.

11-12 An $N \times N$ correlation matrix $\mathbf{\Gamma}$ has eigenvalues $\lambda_1 > \lambda_2 > \ldots > \lambda_N > 0$ and associated eigenvectors $\mathbf{v}_1, \mathbf{v}_2, \ldots, \mathbf{v}_N$. Such a matrix can be represented as

$$\mathbf{\Gamma} = \sum_{i=1}^{N} \lambda_i \mathbf{v}_i \mathbf{v}_i^{*t}$$

a If $\mathbf{\Gamma} = \mathbf{\Gamma}^{1/2}\mathbf{\Gamma}^{1/2}$, where $\mathbf{\Gamma}^{1/2}$ is the square root of $\mathbf{\Gamma}$, show that $\mathbf{\Gamma}^{1/2}$ can be represented as

$$\mathbf{\Gamma}^{1/2} = \sum_{i=1}^{N} \lambda_i^{1/2} \mathbf{v}_i \mathbf{v}_i^{*t}$$

b Using this representation, determine a procedure for computing $\mathbf{\Gamma}^{1/2}$.

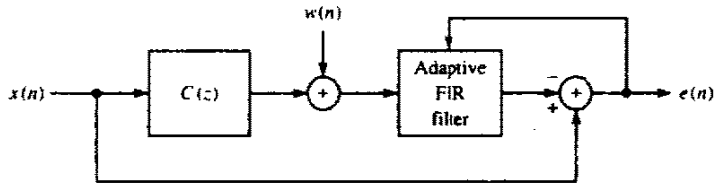

FIGURE P11-11

12

MULTICHANNEL AND MULTICARRIER SYSTEMS

In some applications, it is desirable to transmit the same information-bearing signal over several channels. This mode of transmission is used primarily in situations where there is a high probability that one or more of the channels will be unreliable from time to time. For example, radio channels such as ionospheric scatter and tropospheric scatter suffer from signal fading due to multipath, which renders the channels unreliable for short periods of time. As another example, multichannel signaling is sometimes employed in military communication systems as a means of overcoming the effects of jamming of the transmitted signal. By transmitting the same information over multiple channels, we are providing signal diversity, which the receiver can exploit to recover the information.

Another form of multichannel communications is multiple carrier transmission, where the frequency band of the channel is subdivided into a number of subchannels and information is transmitted on each of the subchannels. A rationale for subdividing the frequency band of a channel into a number of narrowband channels is given below.

In this chapter, we consider both multichannel signal transmission and multicarrier transmission. We begin with a treatment of multichannel transmission.

12-1 MULTICHANNEL DIGITAL COMMUNICATION IN AWGN CHANNELS

In this section, we confine our attention to multichannel signaling over fixed channels that differ only in attenuation and phase shift. The specific model for

the multichannel digital signaling system may be described as follows. The signal waveforms, in general are expressed as

$$s_m^{(n)}(t) = \text{Re}\left[s_{lm}^{(n)}(t)e^{j2\pi f_c t}\right], \quad 0 \le t \le T$$
$$n = 1, 2, \ldots, L, \quad m = 1, 2, \ldots, M \quad (12\text{-}1\text{-}1)$$

where L is the number of channels and M is the number of waveforms. The waveforms are assumed to have equal energy and to be equally probable a priori. The waveforms $\{s_m^{(n)}(t)\}$ transmitted over the L channels are scaled by the factors $\{\alpha_n\}$, phase-shifted by $\{\phi_n\}$, and corrupted by additive noise. The equivalent lowpass signals received from the L channels may be expressed as

$$r_l^{(n)}(t) = \alpha_n e^{j\phi_n} s_{lm}^{(n)}(t) + z_n(t), \quad 0 \le t \le T$$
$$n = 1, 2, \ldots, L, \quad m = 1, 2, \ldots, M \quad (12\text{-}1\text{-}2)$$

where $\{s_{lm}^{(n)}(t)\}$ are the equivalent lowpass transmitted waveforms and $\{z_n(t)\}$ represent the additive noise processes on the L channels. We assume that $\{z_n(t)\}$ are mutually statistically independent and identically distributed gaussian noise random processes.

We consider two types of processing at the receiver, namely, coherent detection and noncoherent detection. The receiver for coherent detection estimates the channel parameters $\{\alpha_n\}$ and $\{\phi_n\}$ and uses the estimates in computing the decision variables. Suppose we define $g_n = \alpha_n e^{-j\phi_n}$ and let $\hat{g}_n$ be the estimate of g_n. The multichannel receiver correlates each of the L received signals with a replica of the corresponding transmitted signals, multiplies each of the correlator outputs by the corresponding estimates $\{\hat{g}_n^*\}$, and sums the resulting signals. Thus, the decision variables for coherent detection are the correlation metrics

$$CM_m = \sum_{n=1}^{L} \text{Re}\left[\hat{g}_n^* \int_0^T r_l^{(n)}(t) s_{lm}^{(n)*}(t)\, dt\right], \quad m = 1, 2, \ldots, M \quad (12\text{-}1\text{-}3)$$

In noncoherent detection, no attempt is made to estimate the channel parameters. The demodulator may base its decision either on the sum of the envelopes (envelope detection) or the sum of the squared envelopes (square-law detection) of the matched filter outputs. In general, the performance obtained with envelope detection differs little from the performance obtained with square-law detection in AWGN. However, square-law detection of multichannel signaling in AWGN channels is considerably easier to analyze than envelope detection. Therefore, we confine our attention to square-law detection of the received signals of the L channels, which produces the decision variables

$$CM_m = \sum_{n=1}^{L} \left| \int_0^T r_l^{(n)}(t) s_{lm}^{(n)*}(t)\, dt \right|^2, \quad m = 1, 2, \ldots, M \quad (12\text{-}1\text{-}4)$$

Let us consider binary signaling first, and assume that $s_{l1}^{(n)}$, $n = 1, 2, \ldots, L$

are the L transmitted waveforms. Then an error is committed if $CM_2 > CM_1$, or, equivalently, if the difference $D = CM_1 - CM_2 < 0$. For noncoherent detection, this difference may be expressed as

$$D = \sum_{n=1}^{L} (|X_n|^2 - |Y_n|^2) \tag{12-1-5}$$

where the variables $\{X_n\}$ and $\{Y_n\}$ are defined as

$$\begin{aligned} X_n &= \int_0^T r_l^{(n)}(t) s_{l1}^{(n)*}(t)\, dt, \quad n = 1, 2, \ldots, L \\ Y_n &= \int_0^T r_l^{(n)}(t) s_{l2}^{(n)*}(t)\, dt, \quad n = 1, 2, \ldots, L \end{aligned} \tag{12-1-6}$$

The $\{X_n\}$ are mutually independent and identically distributed gaussian random variables. The same statement applies to the variables $\{Y_n\}$. However, for any n, X_n and Y_n may be correlated. For coherent detection, the difference $D = CM_1 - CM_2$ may be expressed as

$$D = \tfrac{1}{2} \sum_{n=1}^{L} (X_n Y_n^* + X_n^* Y_n) \tag{12-1-7}$$

where, by definition,

$$\begin{aligned} Y_n &= \hat{g}_n, \quad n = 1, 2, \ldots, L \\ X_n &= \int_0^T r_l^{(n)}(t) [s_{l1}^{(n)*}(t) - s_{l2}^{(n)*}(t)]\, dt \end{aligned} \tag{12-1-8}$$

If the estimates $\{\hat{g}_n\}$ are obtained from observation of the received signal over one or more signaling intervals, as described in Appendix C, their statistical characteristics are described by the gaussian distribution. Then the $\{Y_n\}$ are characterized as mutually independent and identically distributed gaussian random variables. The same statement applies to the variables $\{X_n\}$. As in noncoherent detection, we allow for correlation between X_n and Y_n, but not between X_m and Y_n for $m \neq n$.

12-1-1 Binary Signals

In Appendix B, we derive the probability that the general quadratic form

$$D = \sum_{n=1}^{L} (A |X_n|^2 + B |Y_n|^2 + C X_n Y_n^* + C^* X_n^* Y_n) \tag{12-1-9}$$

in complex-valued gaussian random variables is less than zero. This probability, which is given in (B-21) of Appendix B, is the probability of error for

binary multichannel signaling in AWGN. A number of special cases are of particular importance.

If the binary signals are antipodal and the estimates of $\{g_n\}$ are perfect, as in coherent PSK, the probability of error takes the simple form

$$P_b = Q(\sqrt{2\gamma_b}) \tag{12-1-10}$$

where

$$\gamma_b = \frac{\mathscr{E}}{N_0} \sum_{n=1}^{L} |g_n|^2$$
$$= \frac{\mathscr{E}}{N_0} \sum_{n=1}^{L} \alpha_n^2 \tag{12-1-11}$$

is the SNR per bit. If the channels are all identical, $\alpha_n = \alpha$ for all n and, hence,

$$\gamma_b = \frac{L\mathscr{E}}{N_0} \alpha^2 \tag{12-1-12}$$

We observe that $L\mathscr{E}$ is the total transmitted signal energy for the L signals. The interpretation of this result is that the receiver combines the energy from the L channels in an optimum manner. That is, there is no loss in performance in dividing the total transmitted signal energy among the L channels. The same performance is obtained as in the case in which a single waveform having energy $L\mathscr{E}$ is transmitted on one channel. This behavior holds true only if the estimates $\hat{g}_n = g_n$, for all n. If the estimates are not perfect, a loss in performance occurs, the amount of which depends on the quality of the estimates, as described in Appendix C.

Perfect estimates for $\{g_n\}$ constitute an extreme case. At the other extreme, we have binary DPSK signaling. In DPSK, the estimates $\{\hat{g}_n\}$ are simply the (normalized) signal-plus-noise samples at the outputs of the matched filters in the previous signaling interval. This is the poorest estimate that one might consider using in estimating $\{g_n\}$. For binary DPSK, the probability of error obtained from (B-21) is

$$P_b = \frac{1}{2^{2L-1}} e^{-\gamma_b} \sum_{n=1}^{L-1} c_n \gamma_b^n \tag{12-1-13}$$

where, by definition,

$$c_n = \frac{1}{n!} \sum_{k=0}^{L-1-n} \binom{2L-1}{k} \tag{12-1-14}$$

and γ_b is the SNR per bit defined in (12-1-11) and, for identical channels in (12-1-12). This result can be compared with the single-channel ($L = 1$) error probability. To simplify the comparison, we assume that the L channels have identical attenuation factors. Thus, for the same value of γ_b, the performance of the multichannel system is poorer than that of the single-channel system. That is, splitting the total transmitted energy among L channels results in a loss in performance, the amount of which depends on L.

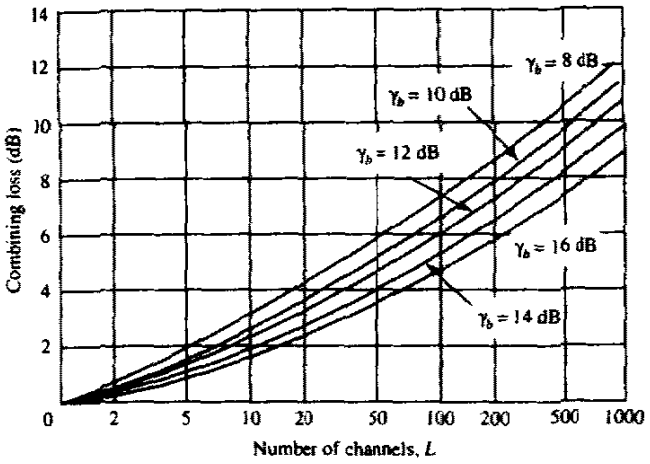

FIGURE 12-1-1 Combining loss in noncoherent detection and combination of binary multichannel signals.

A loss in performance also occurs in square-law detection of orthogonal signals transmitted over L channels. For binary orthogonal signaling, the expression for the probability of error is identical in form to that for binary DPSK given in (12-1-13), except that γ_b is replaced by $\frac{1}{2}\gamma_b$. That is, binary orthogonal signaling with noncoherent detection is 3 dB poorer than binary DPSK. However, the loss in performance due to noncoherent combination of the signals received on the L channels is identical to that for binary DPSK.

Figure 12-1-1 illustrates the loss resulting from noncoherent (square-law) combining of the L signals as a function of L. The probability of error is not shown, but it can be easily obtained from the curve of the expression

$$P_b = \tfrac{1}{2}e^{-\gamma_b} \tag{12-1-15}$$

which is the error probability of binary DPSK shown in Fig. 5-2-12 and then degrading the required SNR per bit, γ_b, by the noncoherent combining loss corresponding to the value of L.

12-1-2 M-ary Orthogonal Signals

Now let us consider M-ary orthogonal signaling with square-law detection and combination of the signals on the L channels. The decision variables are given by (12-1-4). Suppose that the signals $s_1^{(n)}(t)$, $n = 1, 2, \ldots, L$, are transmitted over the L AWGN channels. Then, the decision variables are expressed as

$$\begin{aligned} U_1 &= \sum_{n=1}^{L} |2\mathcal{E}\alpha_n + N_{n1}|^2 \\ U_m &= \sum_{n=1}^{L} |N_{nm}|^2, \quad m = 2, 3, \ldots, M \end{aligned} \tag{12-1-16}$$

where the $\{N_{nm}\}$ are complex-valued zero-mean gaussian random variables with variance $\sigma^2 = \frac{1}{2}E(|N_{nm}|^2) = 2\mathscr{E}N_0$. Hence U_1 is described statistically as a noncentral chi-square random variable with $2L$ degrees of freedom and noncentrality parameter

$$s^2 = \sum_{n=1}^{L} (2\mathscr{E}\alpha_n)^2 = 4\mathscr{E}^2 \sum_{n=1}^{L} \alpha_n^2 \tag{12-1-17}$$

Using (2-1-118), we obtain the pdf of U_1 as

$$p(u_1) = \frac{1}{4\mathscr{E}N_0}\left(\frac{u_1}{s^2}\right)^{(L-1)/2} \exp\left(-\frac{s^2+u_1}{4\mathscr{E}N_0}\right) I_{L-1}\left(\frac{s\sqrt{u_1}}{2\mathscr{E}N_0}\right), \quad u_1 \geq 0 \tag{12-1-18}$$

On the other hand, the $\{U_m\}$, $m = 2, 3, \ldots, M$, are statistically independent and identically chi-square-distributed random variables, each having $2L$ degrees of freedom. Using (2-1-110), we obtain the pdf for U_m as

$$p(u_m) = \frac{1}{(4\mathscr{E}N_0)^L(L-1)!} u_m^{L-1} e^{-u_m/4\mathscr{E}N_0}, \quad u_m \geq 0$$

$$m = 2, 3, \ldots, M \tag{12-1-19}$$

The probability of a symbol error is

$$\begin{aligned} P_M &= 1 - P_c \\ &= 1 - P(U_2 < U_1, U_3 < U_1, \ldots, U_M < U_1) \\ &= 1 - \int_0^\infty [P(U_2 < u_1 \mid U_1 = u_1)]^{M-1} p(u_1)\, du_1 \end{aligned} \tag{12-1-20}$$

But

$$P(U_2 < u_1 \mid U_1 = u_1) = 1 - \exp\left(-\frac{u_1}{4\mathscr{E}N_0}\right) \sum_{k=0}^{L-1} \frac{1}{k!}\left(\frac{u_1}{4\mathscr{E}N_0}\right)^k \tag{12-1-21}$$

Hence,

$$\begin{aligned} P_M &= 1 - \int_0^\infty \left[1 - e^{-u_1/4\mathscr{E}N_0} \sum_{k=0}^{L-1} \frac{1}{k!}\left(\frac{u_1}{4\mathscr{E}N_0}\right)^k\right]^{M-1} p(u_1)\, du_1 \\ &= 1 - \int_0^\infty \left(1 - e^{-v} \sum_{k=0}^{L-1} \frac{v^k}{k!}\right)^{M-1} \left(\frac{v}{\gamma}\right)^{(L-1)/2} e^{-(\gamma+v)} I_{L-1}(2\sqrt{\gamma v})\, dv \end{aligned} \tag{12-1-22}$$

where

$$\gamma = \mathscr{E} \sum_{n=1}^{L} \alpha_n^2 / N_0$$

The integral in (12-1-22) can be evaluated numerically. It is also possible to expand the term $(1-x)^{M-1}$ in (12-1-22) and carry out the integration term by term. This approach yields an expression for P_M in terms of finite sums.

An alternative approach is to use the union bound

$$P_M < (M-1)P_2(L) \tag{12-1-23}$$

where $P_2(L)$ is the probability of error in choosing between U_1 and any one of the $M-1$ decision variables $\{U_m\}$, $m = 2, 3, \ldots, M$. From our previous discussion on the performance of binary orthogonal signaling, we have

$$P_2(L) = \frac{1}{2^{2L-1}} e^{-k\gamma_b/2} \sum_{n=0}^{L-1} c_n (\tfrac{1}{2}k\gamma_b)^n \tag{12-1-24}$$

where c_n is given by (12-1-14). For relatively small values of M, the union bound in (12-1-23) is sufficiently tight for most practical applications.

12-2 MULTICARRIER COMMUNICATIONS

From our treatment of nonideal linear filter channels in Chapters 10 and 11, we have observed that such channels introduce ISI, which degrades performance compared with the ideal channel. The degree of performance degradation depends on the frequency response characteristics. Furthermore, the complexity of the receiver increases as the span of the ISI increases.

Given a particular channel characteristic, the communication system designer must decide how to efficiently utilize the available channel bandwidth in order to transmit the information reliably within the transmitter power constraint and receiver complexity constraints. For a nonideal linear filter channel, one option is to employ a single carrier system in which the information sequence is transmitted serially at some specified rate R symbols/s. In such a channel, the time dispersion is generally much greater than the symbol rate and, hence, ISI results from the nonideal frequency response characteristics of the channel. As we have observed, an equalizer is necessary to compensate for the channel distortion.

An alternative approach to the design of a bandwidth-efficient communication system in the presence of channel distortion is to subdivide the available channel bandwidth into a number of subchannels, such that each subchannel is nearly ideal. To elaborate, suppose that $C(f)$ is the frequency response of a nonideal, band-limited channel with a bandwidth W, and that the power spectral density of the additive gaussian noise is $\Phi_{nn}(f)$. Then, we divide the bandwidth W into $N = W/\Delta f$ subbands of width Δf, where Δf is chosen sufficiently small that $|C(f)|^2/\Phi_{nn}(f)$ is approximately a constant within each subband. Furthermore, we shall select the transmitted signal power to be distributed in frequency as $P(f)$, subject to the constraint that

$$\int_W P(f)\, df \leq P_{\text{av}} \tag{12-2-1}$$

where, P_{av} is the available average power of the transmitter. Let us evaluate the capacity of the nonideal additive gaussian noise channel.

12-2-1 Capacity of a Nonideal Linear Filter Channel

Recall that the capacity of an ideal, band-limited, AWGN channel is

$$C = W \log_2\left(1 + \frac{P_{av}}{WN_0}\right) \tag{12-2-2}$$

where C is the capacity in bits/s, W is the channel bandwidth, and P_{av} is the average transmitted power. In a multicarrier system, with Δf sufficiently small, the subchannel has capacity

$$C_i = \Delta f \log_2\left[1 + \frac{\Delta f P(f_i)|C(f)|^2}{\Delta f \Phi_{nn}(f_i)}\right] \tag{12-2-3}$$

Hence, the total capacity of the channel is

$$C = \sum_{i=1}^{N} C_i = \Delta f \sum_{i=1}^{N} \log_2\left[1 + \frac{P(f_i)|C(f_i)|^2}{\Phi_{nn}(f_i)}\right] \tag{12-2-4}$$

In the limit as $\Delta f \to 0$, we obtain the capacity of the overall channel in bits/s as

$$C = \int_W \log_2\left[1 + \frac{P(f)|C(f)|^2}{\Phi_{nn}(f)}\right] df \tag{12-2-5}$$

Under the constraint on $P(f)$ given by (12-2-1), the choice of $P(f)$ that maximizes C may be determined by maximizing the integral

$$\int_W \left\{\log_2\left[1 + \frac{P(f)|C(f)|^2}{\Phi_{nn}(f)}\right] + \lambda P(f)\right\} df \tag{12-2-6}$$

where λ is a Lagrange multiplier, which is chosen to satisfy the constraint. By using the calculus of variations to perform the maximization, we find that the optimum distribution of transmitted signal power is the solution to the equation

$$\frac{1}{|C(f)|^2 P(f) + \Phi_{nn}(f)} + \lambda = 0 \tag{12-2-7}$$

Therefore, $P(f) + \Phi_{nn}(f)/|C(f)|^2$ must be a constant, whose value is adjusted to satisfy the average power constraint in (12-2-1). That is,

$$P(f) = \begin{cases} K - \Phi_{nn}(f)/|C(f)|^2 & (f \in W) \\ 0 & (f \notin W) \end{cases} \tag{12-2-8}$$

This expression for the channel capacity of a nonideal linear filter channel with additive gaussian noise is due to Shannon (1949). The basic interpretation of this result is that the signal power should be high when the channel SNR $|C(f)|^2/\Phi_{nn}(f)$ is high, and low when the channel SNR is low. This result on

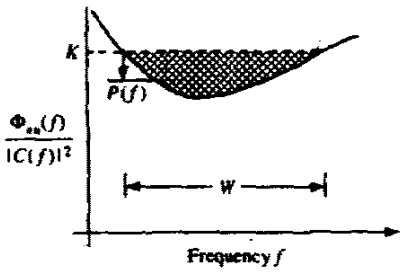

FIGURE 12-2-1 The optimum water-pouring spectrum.

the transmitted power distribution is illustrated in Fig. 12-2-1. Observe that if $\Phi_{nn}(f)/|C(f)|^2$ is interpreted as the bottom of a bowl of unit depth, and we pour an amount of water equal to P_{av} into the bowl, the water will distribute itself in the bowl so as to achieve capacity. This is called the *water-filling interpretation* of the optimum power distribution as a function of frequency.

It is interesting to note that the channel capacity is the smallest when the channel SNR $|C(f)|^2/\Phi_{nn}(f)$ is a constant for all $f \in W$. In this case, $P(f)$ is a constant for all $f \in W$. Equivalently, if the channel frequency response is ideal, i.e., $C(f) = 1$ for $f \in W$, then the worst gaussian noise power distribution, from the viewpoint of maximizing capacity, is white gaussian noise.

The above development suggests that multicarrier modulation that divides the available channel bandwidth into subbands of relatively narrow width $\Delta f = W/N$ provides a solution that could yield transmission rates close to capacity. The signal in each subband may be independently coded and modulated at a synchronous symbol rate of $1/\Delta f$, with the optimum power allocation $P(f)$. If Δf is small enough then $C(f)$ is essentially constant across each subband, so that no equalization is necessary because the ISI is negligible.

Multicarrier modulation has been used in modems for both radio and telephone channels. Multicarrier modulation has also been proposed for future digital audio broadcast applications.

A particularly suitable application of multicarrier modulation is in digital transmission over copper wire subscriber loops. The typical channel attenuation characteristics for such subscriber lines are illustrated in Fig. 12-2-2. We

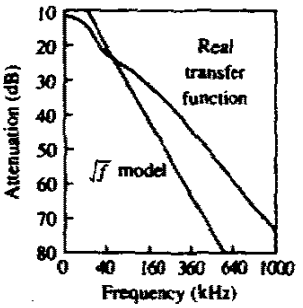

FIGURE 12-2-2 Attenuation characteristic of a 24 gauge 12 kft PIC loop. [*From Werner (1991)* © *IEEE.*]

observe that the attenuation increases rapidly as a function of frequency. This characteristic makes it extremely difficult to achieve a high transmission rate with a single modulated carrier and an equalizer at the receiver. The ISI penalty in performance is very large. On the other hand, multicarrier modulation with optimum power distribution provides the potential for a higher transmission rate.

The dominant noise in transmission over subscriber lines is crosstalk interference from signals carried on other telephone lines located in the same cable. The power distribution of this type of noise is also frequency-dependent, which can be taken into consideration in the allocation of the available transmitted power.

A design procedure for a multicarrier QAM system for a nonideal linear filter channel has been given by Kalet (1989). In this procedure, the overall bit rate is maximized, through the design of an optimal power division among the subcarriers and an optimum selection of the number of bits per symbol (sizes of the QAM signal constellations) for each subcarrier, under an average power constraint and under the constraint that the symbol error probabilities for all subcarriers are equal.

Below, we present an implementation of a multicarrier QAM modulator and demodulator that is based on the discrete Fourier transform (DFT) for the generation of the multiple carriers.

12-2-2 An FFT-Based Multicarrier System

In this section, we describe a multicarrier communication system that employs the fast Fourier transform (FFT) algorithm to synthesize the signal at the transmitter and to demodulate the received signal at the receiver. The FFT is simply the efficient computational tool for implementing the discrete fourier transform (DFT).

Figure 12-2-3 illustrates a block diagram of a multicarrier communication

FIGURE 12-2-3 Multicarrier communication system.

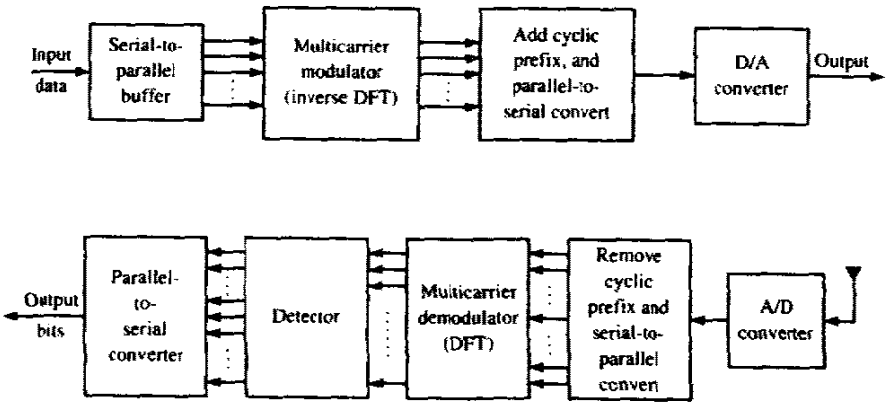

system. A serial-to-parallel buffer segments the information sequence into frames of N_f bits. The N_f bits in each frame are parsed into $\tilde{N}$ groups, where the ith group is assigned $\tilde{n}_i$ bits, and

$$\sum_{i=1}^{\tilde{N}} \tilde{n}_i = N_f \tag{12-2-9}$$

Each group may be encoded separately, so that the number of output bits from the encoder for the ith group is $n_i \geq \tilde{n}_i$.

It is convenient to view the multicarrier modulation as consisting of $\tilde{N}$ independent QAM channels, each operating at the same symbol rate $1/T$, but each channel having a distinct QAM constellation, i.e., the ith channel will employ $M_i = 2^{\tilde{n}_i}$ signal points. We denote the complex-valued signal points corresponding to the information symbols on the subchannels by X_k, $k = 0, 1, \ldots, \tilde{N} - 1$. In order to modulate the $\tilde{N}$ subcarriers by the information symbols $\{X_k\}$, we employ the inverse DFT (IDFT).

However, if we compute the $\tilde{N}$-point IDFT of $\{X_k\}$, we shall obtain a complex-valued time series, which is not equivalent to $\tilde{N}$ QAM-modulated subcarriers. Instead, we create $N = 2\tilde{N}$ information symbols by defining

$$X_{N-k} = X_k^*, \quad k = 1, \ldots, \tilde{N} - 1 \tag{12-2-10}$$

and $X_0' = \text{Re}\,(X_0)$, $X_{\tilde{N}} = \text{Im}\,(X_0)$. Thus, the symbol X_0 is split into two parts, both real. Then, the N-point IDFT yields the real-valued sequence

$$x_n = \frac{1}{\sqrt{N}} \sum_{k=0}^{N-1} X_k e^{j2\pi nk/N}, \quad n = 0, 1, \ldots, N - 1 \tag{12-2-11}$$

where $1/\sqrt{N}$ is simply a scale factor.

The sequence $\{x_n, 0 \leq n \leq N - 1\}$ corresponds to the samples of the sum $x(t)$ of $\tilde{N}$ subcarrier signals, which is expressed as

$$x(t) = \frac{1}{\sqrt{N}} \sum_{k=0}^{N-1} X_k e^{j2\pi kt/T}, \quad 0 \leq t \leq T \tag{12-2-12}$$

where T is the symbol duration. We observe that the subcarrier frequencies are $f_k = k/T$, $k = 0, 1, \ldots, \tilde{N}$. Furthermore, the discrete-time sequence $\{x_n\}$ in (12-2-10) represents the samples of $x(t)$ taken at times $t = nT/N$ where $n = 0, 1, \ldots, N - 1$.

The computation of the IDFT of the data $\{X_k\}$ as given in (12-2-10) may be viewed as multiplication of each data point X_k by a corresponding vector

$$\mathbf{v}_k = [v_{k0} \quad v_{k1} \quad \cdots \quad v_{k(N-1)}] \tag{12-2-13}$$

where

$$v_{kn} = \frac{1}{\sqrt{N}} e^{j(2\pi/N)kn} \tag{12-2-14}$$

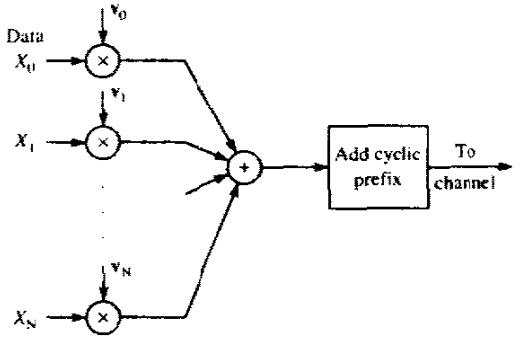

FIGURE 12-2-4 Signal synthesis for multicarrier modulation based on inverse DFT.

as illustrated in Fig. 12-2-4. In any case, the computation of the DFT is performed efficiently by the use of the FFT algorithm.

In practice, the signal samples $\{x_n\}$ are passed through a D/A converter whose output, ideally, would be the signal waveform $x(t)$. The output of the channel is the waveform

$$r(t) = x(t) \bigstar h(t) + n(t) \tag{12-2-15}$$

where $h(t)$ is the impulse response of the channel and $\bigstar$ denotes convolution. By selecting the bandwidth Δf of each subchannel to be very small, the symbol duration $T = 1/\Delta f$ is large compared with the channel time dispersion. To be specific, let us assume that the channel dispersion spans $\nu + 1$ signal samples where $\nu \ll N$. One way to avoid the effect of ISI is to insert a time guard band of duration $\nu T/N$ between transmissions of successive blocks.

An alternative method that avoids ISI is to append a cyclic prefix to each block of N signal samples $\{x_0, x_1, \ldots, x_{N-1}\}$. The cyclic prefix for this block of samples consists of the samples $x_{N-\nu}, x_{N-\nu+1}, \ldots, x_{N-1}$. These new samples are appended to the beginning of each block. Note that the addition of the cyclic prefix to the block of data increases the length of the block to $N + \nu$ samples, which may be indexed from $n = -\nu, \ldots, N-1$, where the first ν samples constitute the prefix. Then, if $\{h_n, 0 \leq n \leq \nu\}$ denotes the sampled channel impulse response, its convolution with $\{x_n, -\nu \leq n \leq N-1\}$ produces $\{r_n\}$, the received sequence. We are interested in the samples of $\{r_n\}$ for $0 \leq n \leq N-1$, from which we recover the transmitted sequence by using the N-point DFT for demodulation. Thus, the first ν samples of $\{r_n\}$ are discarded.

From a frequency-domain viewpoint, when the channel impulse response is $\{h_n, 0 \leq n \leq \nu\}$, its frequency response at the subcarrier frequencies $f_k = k/N$ is

$$H_k \equiv H\left(\frac{2\pi k}{N}\right) = \sum_{n=0}^{\nu} h_n e^{-j2\pi nk/N} \tag{12-2-16}$$

Due to the cyclic prefix, successive blocks (frames) of the transmitted

information sequence do not interfere and, hence, the demodulated sequence may be expressed as

$$\hat{X}_k = H_k X_k + \eta_k, \quad k = 0, 1, \ldots, N-1 \tag{12-2-17}$$

where $\{\hat{X}_k\}$ is the output of the N-point DFT demodulator, and η_k is the additive noise corrupting the signal. We note that by selecting $N \gg \nu$, the rate loss due to the cyclic prefix can be rendered negligible.

As shown in Fig. 12-2-3, the information is demodulated by computing the DFT of the received signal after it has been passed through an A/D converter. The DFT computation may be viewed as a multiplication of the received signal samples $\{r_n\}$ from the A/D converter by $\mathbf{v}_n^*$, where $\mathbf{v}_n$ is defined in (12-2-12). As in the case of the modulator, the DFT computation at the demodulator is performed efficiently by use of the FFT algorithm.

It is a simple matter to estimate and compensate for the channel factors $\{H_k\}$ prior to passing the data to the detector and decoder. A training signal consisting of either a known modulated sequence on each of the subcarriers or unmodulated subcarriers may be used to measure the $\{H_k\}$ at the receiver. If the channel parameters vary slowly with time, it is also possible to track the time variations by using the decisions at the output of the detector or the decoder, in a decision-directed fashion. Thus, the multicarrier system can be rendered adaptive.

Multicarrier QAM modulation of the type described above has been implemented for a variety of applications, including high-speed transmission over telephone lines, such as digital subscriber lines.

Other types of implementation besides the DFT are possible. For example, a digital filter bank that basically performs the DFT may be substituted for the FFT-based implementation when the number of subcarriers is small, e.g., $N \leq 32$. For a large number of subcarriers, e.g., $N > 32$, the FFT-based systems are computatively more efficient.

One limitation of the DFT-type modulators and demodulators arises from the relatively large sidelobes in frequency that are inherent in DFT-type filter banks. The first sidelobe is only 13 dB down from the peak at the desired subcarrier. Consequently, the DFT-based implementations are vulnerable to interchannel interference (ICI) unless a full cyclic prefix is used. If ICI is a problem, due to channel anomalies, one may resort to other types of digital filter banks that have much lower sidelobes. In particular, the class of multirate digital filter banks that have the perfect reconstruction property associated with wavelet-based filters appear to be an attractive alternative (see Tzannes *et al.*, 1994; Rizos *et al.*, 1994).

12-3 BIBLIOGRAPHICAL NOTES AND REFERENCES

Multichannel signal transmission is commonly used on time-varying channels to overcome the effects of signal fading. This topic is treated in some detail in Chapter 14, where we provide a number of references to published work. Of

particular relevance to the treatment of multichannel digital communications given in this chapter are the two publications by Price (1962a,b).

There is a large amount of literature on multicarrier digital communication systems. Such systems have been implemented and used for over 30 years. One of the earliest systems, described by Doeltz *et al.* (1957) and called Kineplex, was used for digital transmission in the HF band. Other early work on multicarrier system design has been reported in the papers by Chang (1966) and Saltzburg (1967). The use of the DFT for modulation and demodulation of multicarrier systems was proposed by Weinstein and Ebert (1971).

Of particular interest in recent years is the use of multicarrier digital transmission for data, facsimile, and video on a variety of channels, including the narrowband (4 kHz) switched telephone network, the 48 kHz group telephone band, digital subscriber lines, cellular radio, and audio broadcast. The interested reader may refer to the many papers in the literature. We cite as examples the papers by Hirosaki *et al.* (1981, 1986), Chow *et al.* (1991), and the survey paper by Bingham (1990). The paper by Kalet (1989) gives a design procedure for optimizing the rate in a multicarrier QAM system given constraints on transmitter power and channel characteristics. Finally, we cite the book by Vaidyanathan (1993) and the papers by Tzannes *et al.* (1994) and Rizos *et al.* (1994) for a treatment of multirate digital filter banks.

PROBLEMS

12-1 $X_1, X_2, \ldots, X_N$ are a set of N statistically independent and identically distributed real gaussian random variables with moments $E(X_i) = m$ and var $(X_i) = \sigma^2$.

a Define

$$U = \sum_{n=1}^{N} X_n$$

Evaluate the SNR of U, which is defined as

$$(\text{SNR})_U = \frac{[E(U)]^2}{2\sigma_U^2}$$

where σ_U^2 is the variance of U.

b Define

$$V = \sum_{n=1}^{N} X_n^2$$

Evaluate the SNR of V, which is defined as

$$(\text{SNR})_V = \frac{[E(V)]^2}{2\sigma_V^2}$$

where σ_V^2 is the variance of V.

c Plot $(\text{SNR})_U$ and $(\text{SNR})_V$ versus m^2/σ^2 on the same graph and, thus, compare the SNRs graphically.

d What does the result in (c) imply regarding coherent detection and combining versus square-law detection and combining of multichannel signals?

12-2 A binary communication system transmits the same information on two diversity channels. The two received signals are

$$r_1 = \pm\sqrt{\mathscr{E}_b} + n_1$$
$$r_2 = \pm\sqrt{\mathscr{E}_b} + n_2$$

where $E(n_1) = E(n_2) = 0$, $E(n_1^2) = \sigma_1^2$ and $E(n_2^2) = \sigma_2^2$, and n_1 and n_2 are uncorrelated gaussian variables. The detector bases its decision on the linear combination of r_1 and r_2, i.e.,

$$r = r_1 + kr_2$$

a Determine the value of k that minimizes the probability of error.

b Plot the probability of error for $\sigma_1^2 = 1$, $\sigma_2^2 = 3$, and either $k = 1$ or k is the optimum value found in (a). Compare the results.

12-3 Assess the cost of the cyclic prefix (used in multitone modulation to avoid ISI) in terms of

a extra channel bandwidth;

b extra signal energy.

12-4 Let $x(n)$ be a finite-duration signal with length N and let $X(k)$ be its N-point DFT. Suppose we pad $x(n)$ with L zeros and compute the $(N + L)$-point DFT, $X'(k)$. What is the relationship between $X(0)$ and $X'(0)$? If we plot $|X(k)|$ and $|X'(k)|$ on the same graph, explain the relationships between the two graphs.

12-5 Show that the sequence $\{x_n\}$ given by (12-2-11) corresponds to the samples of the signal $x(t)$ given by (12-2-12).

12-6 Show that the IDFT of a sequence $\{X_k, 0 \leq k \leq N-1\}$ can be computed by passing the sequence $\{X_k\}$ through a bank of N linear discrete-time filters with system functions

$$H_n(z) = \frac{1}{1 - e^{j2\pi n/N} z^{-1}}$$

12-7 Plot $P_2(L)$ for $L = 1$ and $L = 2$ as a function of $10 \log \gamma_b$ and determine the loss in SNR due to the combining loss for $\gamma_b = 10$.

13

SPREAD SPECTRUM SIGNALS FOR DIGITAL COMMUNICATIONS

Spread spectrum signals used for the transmission of digital information are distinguished by the characteristic that their bandwidth W is much greater than the information rate R in bits/s. That is, the bandwidth expansion factor $B_e = W/R$ for a spread spectrum signal is much greater than unity. The large redundancy inherent in spread spectrum signals is required to overcome the severe levels of interference that are encountered in the transmission of digital information over some radio and satellite channels. Since coded waveforms are also characterized by a bandwidth expansion factor greater than unity and since coding is an efficient method for introducing redundancy, it follows that coding is an important element in the design of spread spectrum signals.

A second important element employed in the design of spread spectrum signals is pseudo-randomness, which makes the signals appear similar to random noise and difficult to demodulate by receivers other than the intended ones. This element is intimately related with the application or purpose of such signals.

To be specific, spread spectrum signals are used for

- combatting or suppressing the detrimental effects of interference due to jamming, interference arising from other users of the channel, and self-interference due to multipath propagation;
- hiding a signal by transmitting it at low power and, thus, making it difficult for an unintended listener to detect in the presence of background noise;
- achieving message privacy in the presence of other listeners.

In applications other than communications, spread spectrum signals are used

to obtain accurate range (time delay) and range rate (velocity) measurements in radar and navigation. For the sake of brevity, we shall limit our discussion to digital communications applications.

In combatting intentional interference (jamming), it is important to the communicators that the jammer who is trying to disrupt the communication does not have prior knowledge of the signal characteristics except for the overall channel bandwidth and the type of modulation, (PSK, FSK, etc.) being used. If the digital information is just encoded as described in Chapter 8, a sophisticated jammer can easily mimic the signal emitted by the transmitter and, thus, confuse the receiver. To circumvent this possibility, the transmitter introduces an element of unpredictability or randomness (pseudo-randomness) in each of the transmitted coded signal waveforms that is known to the intended receiver but not to the jammer. As a consequence, the jammer must synthesize and transmit an interfering signal without knowledge of the pseudo-random pattern.

Interference from the other users arises in multiple-access communication systems in which a number of users share a common channel bandwidth. At any given time, a subset of these users may transmit information simultaneously over the common channel to corresponding receivers. Assuming that all the users employ the same code for the encoding and decoding of their respective information sequences, the transmitted signals in this common spectrum may be distinguished from one another by superimposing a different pseudo-random pattern, also called a *code*, in each transmitted signal. Thus, a particular receiver can recover the transmitted information intended for it by knowing the pseudo-random pattern, i.e., the key, used by the corresponding transmitter. This type of communication technique, which allows multiple users to simultaneously use a common channel for transmission of information, is called *code division multiple access* (CDMA). CDMA will be considered in Sections 13-2 and 13-3.

Resolvable multipath components resulting from time-dispersive propagation through a channel may be viewed as a form of self-interference. This type of interference may also be suppressed by the introduction of a pseudo-random pattern in the transmitted signal, as will be described below.

A message may be hidden in the background noise by spreading its bandwidth with coding and transmitting the resultant signal at a low average power. Because of its low power level, the transmitted signal is said to be "covert." It has a low probability of being intercepted (detected) by a casual listener and, hence, is also called a *low-probability-of-intercept* (LPI) signal.

Finally, message privacy may be obtained by superimposing a pseudo-random pattern on a transmitted message. The message can be demodulated by the intended receivers, who know the pseudo-random pattern or key used at the transmitter, but not by any other receivers who do not have knowledge of the key.

In the following sections, we shall describe a number of different types of spread spectrum signals, their characteristics, and their application. The

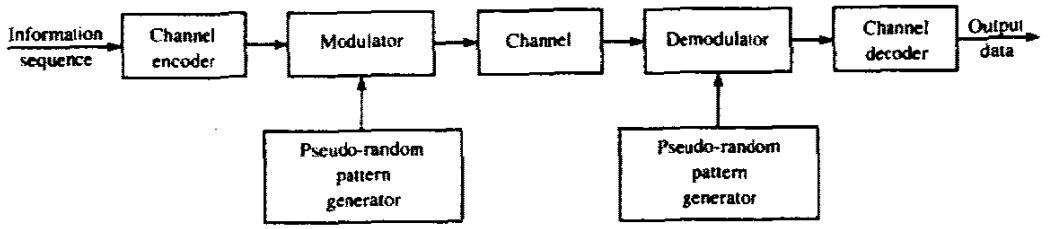

FIGURE 13-1-1 Model of spread spectrum digital communication system.

emphasis will be on the use of spread spectrum signals for combatting, jamming (antijam or AJ signals), for CDMA, and for LPI. Before discussing the signal design problem, however, we shall briefly describe the types of channel characteristics assumed for the applications cited above.

13-1 MODEL OF SPREAD SPECTRUM DIGITAL COMMUNICATION SYSTEM

The block diagram shown in Fig. 13-1-1 illustrates the basic elements of a spread spectrum digital communication system with a binary information sequence at its input at the transmitting end and at its output at the receiving end. The channel encoder and decoder and the modulator and demodulator are basic elements of the system, which were treated in Chapters 5, 7 and 8. In addition to these elements, we have two identical pseudo-random pattern generators, one that interfaces with the modulator at the transmitting end and a second that interfaces with the demodulator at the receiving end. The generators generate a pseudo-random or pseudo-noise (PN) binary-valued sequence, which is impressed on the transmitted signal at the modulator and removed from the received signal at the demodulator.

Synchronization of the PN sequence generated at the receiver with the PN sequence contained in the incoming received signal is required in order to demodulate the received signal. Initially, prior to the transmission of information, synchronization may be achieved by transmitting a fixed pseudo-random bit pattern that the receiver will recognize in the presence of interference with a high probability. After time synchronization of the generators is established, the transmission of information may commence.

Interference is introduced in the transmission of the information-bearing signal through the channel. The characteristics of the interference depend to a large extent on its origin. It may be categorized as being either broadband or narrowband relative to the bandwidth of the information-bearing signal, and either continuous or pulsed (discontinuous) in time. For example, a jamming signal may consist of one or more sinusoids in the bandwidth used to transmit the information. The frequencies of the sinusoids may remain fixed or they may change with time according to some rule. As a second example, the interference generated in CDMA by other users of the channel may be either

broadband or narrowband, depending on the type of spread spectrum signal that is employed to achieve multiple access. If it is broadband, it may be characterized as an equivalent additive white gaussian noise. We shall consider these types of interference and some others in the following sections.

Our treatment of spread spectrum signals will focus on the performance of the digital communication system in the presence of narrowband and broadband interference. Two types of modulation are considered: PSK and FSK. PSK is appropriate in applications where phase coherence between the transmitted signal and the received signal can be maintained over a time interval that is relatively long compared to the reciprocal of the transmitted signal bandwidth. On the other hand, FSK modulation is appropriate in applications where such phase coherence cannot be maintained due to time-variant effects on the communications link. This may be the case in a communications link between two high-speed aircraft or between a high-speed aircraft and a ground terminal.

The PN sequence generated at the modulator is used in conjunction with the PSK modulation to shift the phase of the PSK signal pseudo-randomly as described in Section 13-2. The resulting modulated signal is called a *direct sequence* (DS) or a *pseudo-noise* (PN) spread spectrum signal. When used in conjunction with binary or M-ary ($M > 2$) FSK, the pseudo-random sequence selects the frequency of the transmitted signal pseudo-randomly. The resulting signal is called a *frequency-hopped* (FH) spread spectrum signal. Although a number of other types of spread spectrum signals will be briefly described, the emphasis of our treatment will be on PN and FH spread spectrum signals.

13-2 DIRECT SEQUENCE SPREAD SPECTRUM SIGNALS

In the model shown in Fig. 13-1-1, we assume that the information rate at the input to the encoder is R bits/s and the available channel bandwidth is W Hz. The modulation is assumed to be binary PSK. In order to utilize the entire available channel bandwidth, the phase of the carrier is shifted pseudo-randomly according to the pattern from the PN generator at a rate W times/s. The reciprocal of W, denoted by T_c, defines the duration of a rectangular pulse, which is called a *chip* while T_c is called the *chip interval*. The pulse is the basic element in a DS spread spectrum signal.

If we define $T_b = 1/R$ to be the duration of a rectangular pulse corresponding to the transmission time of an information bit, the bandwidth expansion factor W/R may be expressed as

$$B_e = \frac{W}{R} = \frac{T_b}{T_c} \tag{13-2-1}$$

In practical systems, the ratio T_b/T_c is an integer,

$$L_c = \frac{T_b}{T_c} \tag{13-2-2}$$

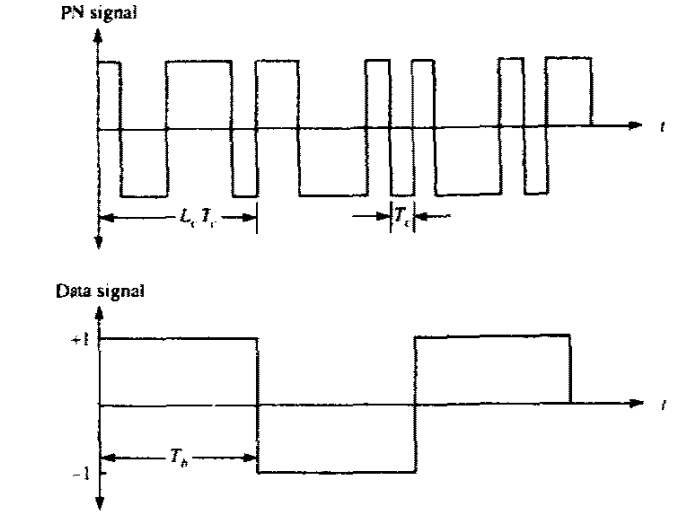

(a) PN and data signals

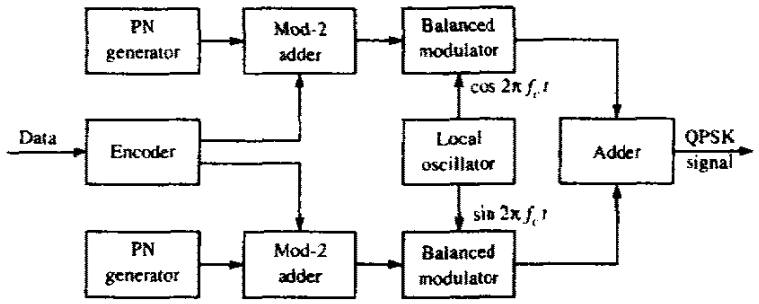

(b) DS-QPSK modulator

FIGURE 13-2-1 The PN and data signals (*a*) and the QPSK modulator (*b*) for a DS spread spectrum system.

which is the number of chips per information bit. That is, L_c is the number of phase shifts that occur in the transmitted signal during the bit duration $T_b = 1/R$. Figure 13-2-1(*a*) illustrates the relationships between the PN signal and the data signal.

Suppose that the encoder takes k information bits at a time and generates a binary linear (n, k) block code. The time duration available for transmitting the n code elements is kT_b s. The number of chips that occur in this time interval is kL_c. Hence, we may select the block length of the code as $n = kL_c$. If the encoder generates a binary convolutional code of rate k/n, the number of chips in the time interval kT_b is also $n = kL_c$. Therefore, the following discussion applies to both block codes and convolutional codes.

One method for impressing the PN sequence on the transmitted signal is to

alter directly the coded bits by modulo-2 addition with the PN sequence.† Thus, each coded bit is altered by its addition with a bit from the PN sequence. If b_i represents the ith bit of the PN sequence and c_i is the corresponding bit from the encoder, the modulo-2 sum is

$$a_i = b_i \oplus c_i \tag{13-2-3}$$

Hence, $a_i = 1$ if either $b_i = 1$ and $c_i = 0$ or $b_i = 0$ and $c_i = 1$; also, $a_i = 0$ if either $b_i = 1$ and $c_i = 1$ or $b_i = 0$ and $c_i = 0$. We may say that $a_i = 0$ when $b_i = c_i$ and $a_i = 1$ when $b_i \neq c_i$. The sequence $\{a_i\}$ is mapped into a binary PSK signal of the form $s(t) = \pm \text{Re}\,[g(t)e^{j2\pi f_c t}]$ according to the convention

$$g_i(t) = \begin{cases} g(t - iT_c) & (a_i = 0) \\ -g(t - iT_c) & (a_i = 1) \end{cases} \tag{13-2-4}$$

where $g(t)$ represents a pulse of duration T_c s and arbitrary shape.

The modulo-2 addition of the coded sequence $\{c_i\}$ and the sequence $\{b_i\}$ from the PN generator may also be represented as a multiplication of two waveforms. To demonstrate this point, suppose that the elements of the coded sequence are mapped into a binary PSK signal according to the relation

$$c_i(t) = (2c_i - 1)g(t - iT_c) \tag{13-2-5}$$

Similarly, we define a waveform $p_i(t)$ as

$$p_i(t) = (2b_i - 1)p(t - iT_c) \tag{13-2-6}$$

where $p(t)$ is a rectangular pulse of duration T_c. Then the equivalent lowpass transmitted signal corresponding to the ith coded bit is

$$\begin{aligned} g_i(t) &= p_i(t)c_i(t) \\ &= (2b_i - 1)(2c_i - 1)g(t - iT_c) \end{aligned} \tag{13-2-7}$$

This signal is identical to the one given by (13-2-4), which is obtained from the sequence $\{a_i\}$. Consequently, modulo-2 addition of the coded bits with the PN sequence followed by a mapping that yields a binary PSK signal is equivalent to multiplying a binary PSK signal generated from the coded bits with a sequence of unit amplitude rectangular pulses, each of duration T_c, and with a polarity which is determined from the PN sequence according to (13-2-6). Although it is easier to implement modulo-2 addition followed by PSK modulation instead of waveform multiplication, it is convenient, for purposes of demodulation, to consider the transmitted signal in the multiplicative form

† When four-phase PSK is desired, one PN sequence is added to the information sequence carried on the in-phase signal component and a second PN sequence is added to the information sequence carried on the quadrature component. In many PN-spread spectrum systems, the same binary information sequence is added to the two PN sequences to form the two quadrature components. Thus, a four-phase PSK signal is generated with a binary information stream.

given by (13-2-7). A functional block diagram of a four-phase PSK DS spread spectrum modulator is shown in Fig. 13-2-1(*b*).

The received equivalent lowpass signal for the ith code element is†

$$\begin{aligned} r_i(t) &= p_i(t)c_i(t) + z(t), \qquad iT_c \leq t \leq (i+1)T_c \\ &= (2b_i - 1)(2c_i - 1)g(t - iT_c) + z(t) \end{aligned} \tag{13-2-8}$$

where $z(t)$ represents the interference or jamming signal corrupting the information-bearing signal. The interference is assumed to be a stationary random process with zero mean.

If $z(t)$ is a sample function from a complex-valued gaussian process, the optimum demodulator may be implemented either as a filter matched to the waveform $g(t)$ or as a correlator, as illustrated by the block diagrams in Fig. 13-2-2. In the matched filter realization, the sampled output from the matched filter is multiplied by $2b_i - 1$, which is obtained from the PN generator at the

FIGURE 13-2-2 Possible demodulator structures for PN spread spectrum signals.

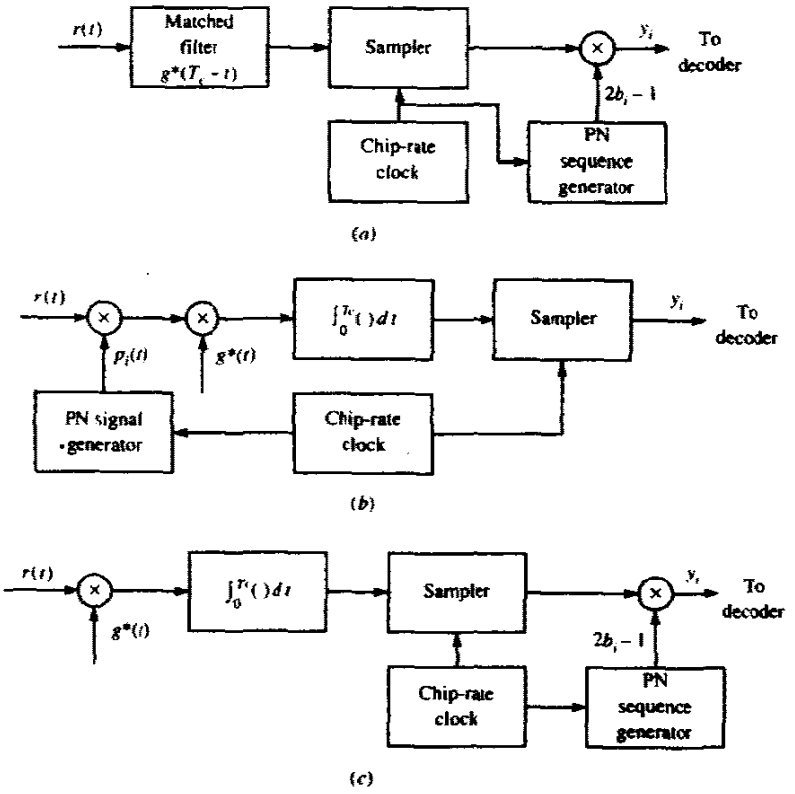

† *For simplicity, we assume that the channel attenuation* $\alpha = 1$ *and the phase shift of the channel is zero. Since coherent PSK detection is assumed, any arbitrary channel phase shift is compensated for in the demodulation.*

demodulator when the PN generator is properly synchronized. Since $(2b_i - 1)^2 = 1$ when $b_i = 0$ and $b_i = 1$, the effect of the PN sequence on the received coded bits is thus removed.

In Fig. 13-2-2, we also observe that the cross-correlation can be accomplished in either one of two ways. The first, illustrated in Fig. 13-2-2(b), involves premultiplying $r_i(t)$ with the waveform $p_i(t)$ generated from the output of the PN generator and then cross-correlating with $g^*(t)$ and sampling the output in each chip interval. The second method, illustrated in Fig. 13-2-2(c), involves cross-correlation with $g^*(t)$ first, sampling the output of the correlator and, then, multiplying this output with $2b_i - 1$, which is obtained from the PN generator.

If $z(t)$ is not a gaussian random process, the demodulation methods illustrated in Fig. 13-2-2 are no longer optimum. Nevertheless, we may still use any of these three demodulator structures to demodulate the received signal. When the statistical characteristics of the interference $z(t)$ are unknown a priori, this is certainly one possible approach. An alternative method, which is described later, utilizes an adaptive filter prior to the matched filter or correlator to suppress narrowband interference. The rationale for this second method is also described later.

In Section 13-2-1, we derive the error rate performance of the DS spread spectrum system in the presence of wideband and narrowband interference. The derivations are based on the assumption that the demodulator is any of the three equivalent structures shown in Fig. 13-2-2.

13-2-1 Error Rate Performance of the Decoder

Let the unquantized output of the demodulator be denoted by y_j, $1 \leq j \leq n$. First we consider a linear binary (n, k) block code and, without loss of generality, we assume that the all-zero code word is transmitted.

A decoder that employs soft-decision decoding computes the correlation metrics

$$CM_i = \sum_{j=1}^{n} (2c_{ij} - 1)y_j, \qquad i = 1, 2, \ldots, 2^k \tag{13-2-9}$$

where c_{ij} denotes the jth bit in the ith code word. The correlation metric corresponding to the all-zero code word is

$$\begin{aligned} CM_1 &= 2n\mathscr{E}_c + \sum_{j=1}^{n} (2c_{1j} - 1)(2b_j - 1)v_j \\ &= 2n\mathscr{E}_c - \sum_{j=1}^{n} (2b_j - 1)v_j \end{aligned} \tag{13-2-10}$$

where v_j, $1 \leq j \leq n$, is the additive noise term corrupting the jth coded bit and $\mathscr{E}_c$ is the chip energy. It is defined as

$$v_j = \text{Re}\left\{\int_0^{T_c} g^*(t)z[t + (j-1)T_c]\,dt\right\}, \qquad j = 1, 2, \ldots, n \tag{13-2-11}$$

Similarly, the correlation metric corresponding to code word $\mathbf{C}_m$ having weight w_m is

$$CM_m = 2\mathscr{E}_c n\left(1 - \frac{2w_m}{n}\right) + \sum_{j=1}^{n} (2c_{mj} - 1)(2b_j - 1)v_j \qquad (13\text{-}2\text{-}12)$$

Following the procedure used in Section 8-1-4, we shall determine the probability that $CM_m > CM_1$. The difference between CM_1 and CM_m is

$$\begin{aligned} D &= CM_1 - CM_m \\ &= 4\mathscr{E}_c w_m - 2\sum_{j=1}^{n} c_{mj}(2b_j - 1)v_j \end{aligned} \qquad (13\text{-}2\text{-}13)$$

Since the code word $\mathbf{C}_m$ has weight w_m, there are w_m nonzero components in the summation of noise terms contained in (13-2-13). We shall assume that the minimum distance of the code is sufficiently large that we can invoke the central limit theorem for the summation of noise components. This assumption is valid for PN spread spectrum signals that have a bandwidth expansion of 20 or more.† Thus, the summation of noise components is modeled as a gaussian random variable. Since $E(2b_j - 1) = 0$ and $E(v_j) = 0$, the mean of the second term in (13-2-13) is also zero.

The variance is

$$\sigma_m^2 = 4\sum_{j=1}^{n}\sum_{i=1}^{n} c_{mi}c_{mj}E[(2b_j - 1)(2b_i - 1)]E(v_i v_j) \qquad (13\text{-}2\text{-}14)$$

The sequence of binary digits from the PN generator are assumed to be uncorrelated. Hence,

$$E[(2b_j - 1)(2b_i - 1)] = \delta_{ij} \qquad (13\text{-}2\text{-}15)$$

and

$$\sigma_m^2 = 4w_m E(v^2) \qquad (13\text{-}2\text{-}16)$$

where $E(v^2)$ is the second moment of any one element from the set $\{v_j\}$. This moment is easily evaluated to yield

$$\begin{aligned} E(v^2) &= \int_0^{T_c}\int_0^{T_c} g^*(t)g(\tau)\phi_{zz}(t - \tau)\,dt\,d\tau \\ &= \int_{-\infty}^{\infty} |G(f)|^2\,\Phi_{zz}(f)\,df \end{aligned} \qquad (13\text{-}2\text{-}17)$$

† Typically, the bandwidth expansion factor in a spread spectrum signal is of the order of 100 and higher.

where $\phi_{zz}(\tau) = \frac{1}{2}E[z^*(t)z(t+\tau)]$ is the autocorrelation function and $\Phi_{zz}(f)$ is the power spectral density of the interference $z(t)$.

We observe that when the interference is spectrally flat within the bandwidth† occupied by the transmitted signal, i.e.,

$$\Phi_{zz}(f) = J_0 \qquad |f| \leq \tfrac{1}{2}W \tag{13-2-18}$$

the second moment in (13-2-17) is $E(\nu^2) = 2\mathscr{E}_c J_0$, and, hence, the variance of the interference term in (13-2-16) becomes

$$\sigma_m^2 = 8\mathscr{E}_c J_0 w_m \tag{13-2-19}$$

In this case, the probability that $D < 0$ is

$$P_2(m) = Q\left(\sqrt{\frac{2\mathscr{E}_c}{J_0} w_m}\right) \tag{13-2-20}$$

But the energy per coded bit $\mathscr{E}_c$ may be expressed in terms of the energy per information bit $\mathscr{E}_b$ as

$$\mathscr{E}_c = \frac{k}{n}\mathscr{E}_b = R_c\mathscr{E}_b \tag{13-2-21}$$

With this substitution, (13-2-20) becomes

$$\begin{aligned} P_2(m) &= Q\left(\sqrt{\frac{2\mathscr{E}_b}{J_0} R_c w_m}\right) \\ &= Q(\sqrt{2\gamma_b R_c w_m}) \end{aligned} \tag{13-2-22}$$

where $\gamma_b = \mathscr{E}_b/J_0$ is the SNR per information bit. Finally, the code word error probability may be upper-bounded by the union bound as

$$P_m \leq \sum_{m=2}^{M} Q(\sqrt{2\gamma_b R_c w_m}) \tag{13-2-23}$$

where $M = 2^k$. Note that this expression is identical to the probability of a code word error for soft-decision decoding of a linear binary block code in an AWGN channel.

Although we have considered a binary block code in the derivation given above, the procedure is similar for an (n, k) convolutional code. The result of such a derivation is the following upper bound on the equivalent bit error probability:

$$P_b \leq \frac{1}{k}\sum_{d=d_{\text{free}}}^{\infty} \beta_d Q(\sqrt{2\gamma_b R_c d}) \tag{13-2-24}$$

The set of coefficients $\{\beta_d\}$ is obtained from an expansion of the derivative of the transfer function $T(D, N)$, as described in Section 8-2-3.

Next, we consider a narrowband interference centered at the carrier (at d.c.

† If the bandwidth of the bandpass channel is W, that of the equivalent low-pass channel is $\frac{1}{2}W$.

for the equivalent lowpass signal). We may fix the total (average) jamming power to $J_{av} = J_0 W$, where J_0 is the value of the power spectral density of an equivalent wideband interference (jamming signal). The narrowband interference is characterized by the power spectral density

$$\Phi_{zz}(f) = \begin{cases} \dfrac{J_{av}}{W_1} = \dfrac{J_0 W}{W_1} & (|f| \leq \frac{1}{2}W_1) \\ 0 & (|f| > \frac{1}{2}W_1) \end{cases} \tag{13-2-25}$$

where $W \gg W_1$.

Substitution of (13-2-25) for $\Phi_{zz}(f)$ into (13-2-17) yields

$$E(v^2) = \frac{J_{av}}{W_1} \int_{-W_1/2}^{W_1/2} |G(f)|^2 \, df \tag{13-2-26}$$

The value of $E(v^2)$ depends on the spectral characteristics of the pulse $g(t)$. In the following example, we consider two special cases.

Example 13-2-1

Suppose that $g(t)$ is a rectangular pulse as shown in Fig. 13-2-3(a) and $|G(f)|^2$ is the corresponding energy density spectrum shown in Fig. 13-2-3(b). For the narrowband interference given by (13-2-26), the variance of the total interference is

$$\begin{aligned} \sigma_m^2 &= 4w_m E(v^2) \\ &= \frac{8\mathscr{E}_c w_m T_c J_{av}}{W_1} \int_{-W_1/2}^{W_1/2} \left(\frac{\sin \pi f T_c}{\pi f T_c} \right)^2 df \\ &= \frac{8\mathscr{E}_c w_m J_{av}}{W_1} \int_{-\beta/2}^{\beta/2} \left(\frac{\sin \pi x}{\pi x} \right)^2 dx \end{aligned} \tag{13-2-27}$$

FIGURE 13-2-3 Rectangular pulse and its energy density spectrum.

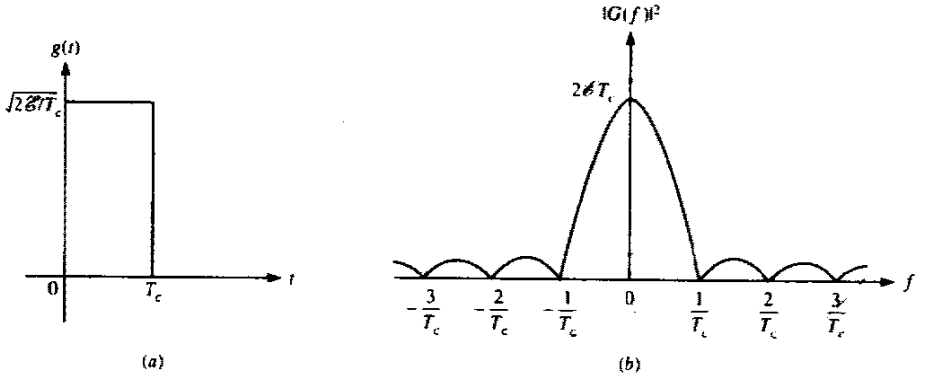

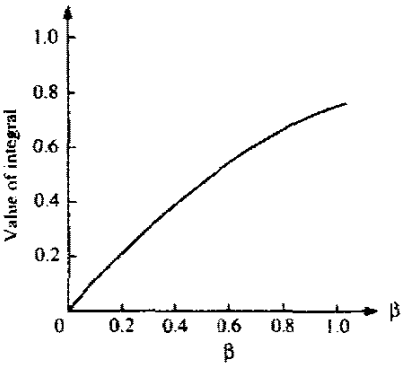

FIGURE 13-2-4 Plot of the value of the integral in (13-2-27).

where $\beta = W_1 T_c$. Figure 13-2-4 illustrates the value of this integral for $0 \leq \beta \leq 1$. We observe that the value of the integral is upper-bounded by $W_1 T_c$. Hence, $\sigma_m^2 \leq 8\mathscr{E}_c w_m T_c J_{av}$.

In the limit as W_1 becomes zero, the interference becomes an impulse at the carrier. In this case the interference is a pure frequency tone and it is usually called a *CW jamming signal*. The power spectral density is

$$\Phi_{zz}(f) = J_{av}\delta(f) \tag{13-2-28}$$

and the corresponding variance for the decision variable $D = CM_1 - CM_m$ is

$$\begin{aligned}\sigma_m^2 &= 4w_m J_{av} |G(0)|^2 \\ &= 8w_m \mathscr{E}_c T_c J_{av}\end{aligned} \tag{13-2-29}$$

The probability of a code word error for CW jamming is upper-bounded as

$$P_M \leq \sum_{m=2}^{M} Q\left(\sqrt{\frac{2\mathscr{E}_c}{J_{av}T_c} w_m}\right) \tag{13-2-30}$$

But $\mathscr{E}_c = R_c \mathscr{E}_b$. Furthermore, $T_c \approx 1/W$ and $J_{av}/W = J_0$. Therefore (13-2-30) may be expressed as

$$P_M \leq \sum_{m=2}^{M} Q\left(\sqrt{\frac{2\mathscr{E}_b}{J_0} R_c w_m}\right) \tag{13-2-31}$$

which is the result obtained previously for broadband interference. This result indicates that a CW jammer has the same effect on performance as an equivalent broadband jammer. This equivalence is discussed further below.

Example 13-2-2

Let us determine the performance of the DS spread spectrum system in the presence of a CW jammer of average power J_{av} when the transmitted signal pulse $g(t)$ is one-half cycle of a sinusoid as illustrated in Fig. 13-2-5, i.e.,

$$g(t) = \sqrt{\frac{4\mathscr{E}_c}{T_c}} \sin\frac{\pi t}{T_c}, \quad 0 \leq t \leq T_c \tag{13-2-32}$$

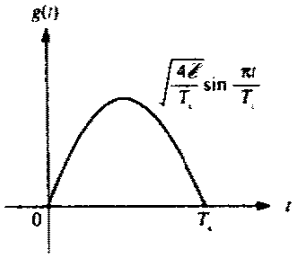

FIGURE 13-2-5 A sinusoidal signal pulse.

The variance of the interference of this pulse is

$$\sigma_m^2 = 4w_m J_{av} |G(0)|^2$$

$$= \frac{64}{\pi^2} \mathscr{E}_c T_c J_{av} w_m \tag{13-2-33}$$

Hence, the upper bound on the code word error probability is

$$P_M \leq \sum_{m=2}^{M} Q\left(\sqrt{\frac{\pi^2 \mathscr{E}_b}{4J_{av} T_c} R_c w_m} \right) \tag{13-2-34}$$

We observe that the performance obtained with this pulse is 0.9 dB better than that obtained with a rectangular pulse. Recall that this pulse shape when used in offset QPSK results in an MSK signal. MSK modulation is frequently used in DS spread spectrum systems.

The Processing Gain and the Jamming Margin An interesting interpretation of the performance characteristics for the DS spread spectrum signal is obtained by expressing the signal energy per bit $\mathscr{E}_b$ in terms of the average power. That is, $\mathscr{E}_b = P_{av} T_b$, where P_{av} is the average signal power and T_b is the bit interval. Let us consider the performance obtained in the presence of CW jamming for the rectangular pulse treated in Example 13-2-1. When we substitute for $\mathscr{E}_b$ and J_0 into (13-2-31), we obtain

$$P_M \leq \sum_{m=2}^{M} Q\left(\sqrt{\frac{2P_{av}}{J_{av}} \frac{T_b}{T_c} R_c w_m} \right) = \sum_{m=2}^{M} Q\left(\sqrt{\frac{2P_{av}}{J_{av}} L_c R_c w_m} \right) \tag{13-2-35}$$

where L_c is the number of chips per information bit and P_{av}/J_{av} is the signal-to-jamming power ratio.

An identical result is obtained with broadband jamming for which the performance is given by (13-2-23). For the signal energy per bit, we have

$$\mathscr{E}_b = P_{av} T_b = \frac{P_{av}}{R} \tag{13-2-36}$$

where R is the information rate in bits/s. The power spectral density for the jamming signal may be expressed as

$$J_0 = \frac{J_{av}}{W} \tag{13-2-37}$$

Using the relation in (13-2-36) and (13-2-37), the ratio $\mathscr{E}_b/J_0$ may be expressed as

$$\frac{\mathscr{E}_b}{J_0} = \frac{P_{av}/R}{J_{av}/W} = \frac{W/R}{J_{av}/P_{av}} \tag{13-2-38}$$

The ratio J_{av}/P_{av} is the jamming-to-signal power ratio, which is usually greater than unity. The ratio $W/R = T_b/T_c = B_c = L_c$ is just the bandwidth expansion factor, or, equivalently, the number of chips per information bit. This ratio is usually called the *processing gain* of the DS spread spectrum system. It represents the advantage gained over the jammer that is obtained by expanding the bandwidth of the transmitted signal. If we interpret $\mathscr{E}_b/J_0$ as the SNR required to achieve a specified error rate performance and W/R as the available bandwidth expansion factor, the ratio J_{av}/P_{av} is called the *jamming margin* of the DS spread spectrum system. In other words, the jamming margin is the largest value that the ratio J_{av}/P_{av} can take and still satisfy the specified error probability.

The performance of a soft-decision decoder for a linear (n, k) binary code, expressed in terms of the processing gain and the jamming margin, is

$$P_m \leq \sum_{m=2}^{M} Q\left(\sqrt{\frac{2W/R}{J_{av}/P_{av}} R_c w_m}\right) \leq (M-1)Q\left(\sqrt{\frac{2W/R}{J_{av}/P_{av}} R_c d_{min}}\right) \tag{13-2-39}$$

In addition to the processing gain W/R and J_{av}/P_{av}, we observe that the performance depends on a third factor, namely, $R_c w_m$. This factor is the *coding gain*. A lower bound on this factor is $R_c d_{min}$. Thus the jamming margin achieved by the DS spread spectrum signal depends on the processing gain and the coding gain.

Uncoded DS Spread Spectrum Signals The performance results given above for DS spread spectrum signals generated by means of an (n, k) code may be specialized to a trivial type of code, namely, a binary repetition code. For this case, $k = 1$ and the weight of the nonzero code word is $w = n$. Thus, $R_c w = 1$ and, hence, the performance of the binary signaling system reduces to

$$\begin{aligned} P_2 &= Q\left(\sqrt{\frac{2\mathscr{E}_b}{J_0}}\right) \\ &= Q\left(\sqrt{\frac{2W/R}{J_{av}/P_{av}}}\right) \end{aligned} \tag{13-2-40}$$

Note that the trivial (repetition) code gives no coding gain. It does result in a processing gain of W/R.

Example 13-2-3

Suppose that we wish to achieve an error rate performance of 10^{-6} or less with an uncoded DS spread spectrum system. The available bandwidth expansion factor is $W/R = 1000$. Let us determine the jamming margin.

The $\mathscr{E}_b/J_0$ required to achieve a bit error probability of 10^{-6} with uncoded binary PSK is 10.5 dB. The processing gain is $10 \log_{10} 1000 = 30$ dB. Hence the maximum jamming-to-signal power that can be tolerated, i.e., the jamming margin, is

$$10 \log_{10} \frac{J_{av}}{P_{av}} = 30 - 10.5 = 19.5 \text{ dB}$$

Since this is the jamming margin achieved with an uncoded DS spread spectrum system, it may be increased by coding the information sequence.

There is another way to view the modulation and demodulation processes for the uncoded (repetition code) DS spread spectrum system. At the modulator, the signal waveform generated by the repetition code with rectangular pulses, for example, is identical to a unit amplitude rectangular pulse $s(t)$ of duration T_b or its negative, depending on whether the information bit is 1 or 0, respectively. This may be seen from (13-2-7), where the coded chips $\{c_i\}$ within a single information bit are either all 1s or 0s. The PN sequence multiplies either $s(t)$ or $-s(t)$. Thus, when the information bit is a 1, the L_c PN chips generated by the PN generator are transmitted with the same polarity. On the other hand, when the information bit is a 0, the L_c PN chips when multiplied by $-s(t)$ are reversed in polarity.

The demodulator for the repetition code, implemented as a correlator, is illustrated in Fig. 13-2-6. We observe that the integration interval in the integrator is the bit interval T_b. Thus, the decoder for the repetition code is eliminated and its function is subsumed in the demodulator.

Now let us qualitatively assess the effect of this demodulation process on

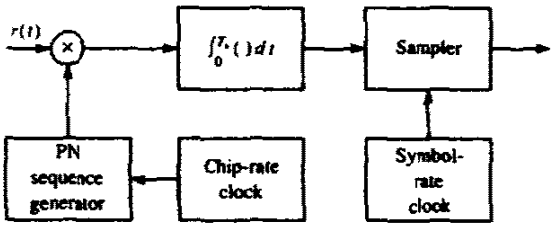

FIGURE 13-2-6 Correlation-type demodulator for a repetition code.

the interference $z(t)$. The multiplication of $z(t)$ by the output of the PN generator, which is expressed as

$$w(t) = \sum_i (2b_i - 1)p(t - iT_c)$$

yields

$$v(t) = w(t)z(t)$$

The waveforms $w(t)$ and $z(t)$ are statistically independent random processes each with zero mean and autocorrelation functions $\phi_{ww}(\tau)$ and $\phi_{zz}(\tau)$, respectively. The product $v(t)$ is also a random process having an autocorrelation function equal to the product of $\phi_{ww}(\tau)$ with $\phi_{zz}(\tau)$. Hence, the power spectral density of the process $v(t)$ is equal to the convolution of the power spectral density of $w(t)$ with the power spectral density of $z(t)$.

The effect of convolving the two spectra is to spread the power in bandwidth. Since the bandwidth of $w(t)$ occupies the available channel bandwith W, the result of convolution of the two spectra is to spread the power spectral density of $z(t)$ over the frequency band of width W. If $z(t)$ is a narrowband process, i.e., its power spectral density has a width much less than W, the power spectral density of the process $v(t)$ will occupy a bandwidth equal to at least W.

The integrator used in the cross-correlation shown in Fig. 13-2-6 has a bandwidth approximately equal to $1/T_b$. Since $1/T_b \ll W$, only a fraction of the total interference power appears at the output of the correlator. This fraction is approximately equal to the ratio of bandwidths $1/T_b$ to W. That is,

$$\frac{1/T_b}{W} = \frac{1}{WT_b} = \frac{T_c}{T_b} = \frac{1}{L_c}$$

In other words, the multiplication of the interference with the signal from the PN generator spreads the interference to the signal bandwidth W, and the narrowband integration following the multiplication sees only the fraction $1/L_c$ of the total interference. Thus, the performance of the uncoded DS spread spectrum system is enhanced by the processing gain L_c.

Linear Code Concatenated with a Binary Repetition Code As illustrated above, a binary repetition code provides a margin against an interference or jamming signal but yields no coding gain. To obtain an improvement in performance, we may use a linear (n_1, k) block or convolutional code, where $n_1 \leq n = kL_c$. One possibility is to select $n_1 < n$ and to repeat each code bit n_2 times such that $n = n_1 n_2$. Thus, we can construct a linear (n_1, k) code by concatenating the (n_1, k) code with a binary $(n_2, 1)$ repetition code. This may be viewed as a trivial form of code concatenation where the outer code is the (n_1, k) code and the inner code is the repetition code.

Since the repetition code yields no coding gain, the coding gain achieved by the combined code must reduce to that achieved by the (n_1, k) outer code. It

is demonstrated that this is indeed the case. The coding gain of the overall combined code is

$$R_c w_m = \frac{k}{n} w_m, \qquad m = 2, 3, \ldots, 2^k$$

But the weights $\{w_m\}$ for the combined code may be expressed as

$$w_m = n_2 w_m^0$$

where $\{w_m^0\}$ are the weights of the outer code. Therefore, the coding gain of the combined code is

$$R_c w_m = \frac{k}{n_1 n_2} n_2 w_m^0 = \frac{k}{n_1} w_m^0 = R_c^0 w_m^0 \tag{13-2-41}$$

which is just the coding gain obtained from the outer code.

A coding gain is also achieved if the (n_1, k) outer code is decoded using hard decisions. The probability of a bit error obtained with the $(n_2, 1)$ repetition code (based on soft-decision decoding) is

$$p = Q\left(\sqrt{\frac{2n_2 \mathscr{E}_c}{J_0}}\right) = Q\sqrt{\frac{2\mathscr{E}_b}{J_0} R_c^0}\Big)$$

$$= Q\left(\sqrt{\frac{2W/R}{J_{av}/P_{av}} R_c^0}\right) \tag{13-2-42}$$

Then the code word error probability for a linear (n_1, k) block code is upper-bounded as

$$P_M \leq \sum_{m=t+1}^{n_1} \binom{n_1}{m} p^m (1-p)^{n_1 - m} \tag{13-2-43}$$

where $t = \lfloor \frac{1}{2}(d_{\min} - 1) \rfloor$, or as

$$P_M \leq \sum_{m=2}^{M} [4p(1-p)]^{w_m^0/2} \tag{13-2-44}$$

where the latter is a Chernoff bound. For an (n_1, k) binary convolutional code, the upper bound on the bit error probability is

$$P_b \leq \sum_{d=d_{\text{free}}}^{\infty} \beta_d P_2(d) \tag{13-2-45}$$

where $P_2(d)$ is defined by (8-2-28) for odd d and by (8-2-29) for even d.

Concatenated Coding for DS Spread Spectrum Systems It is apparent from the above discussion that an improvement in performance can be obtained by replacing the repetition code by a more powerful code that will

yield a coding gain in addition to the processing gain. Basically, the objective in a DS spread spectrum system is to construct a long, low-rate code having a large minimum distance. This may be best accomplished by using code concatenation. When binary PSK is used in conjunction with DS spread spectrum, the elements of a concatenated code word must be expressed in binary form.

Best performance is obtained when soft-decision decoding is used on both the inner and outer codes. However, an alternative, which usually results in reduced complexity for the decoder, is to employ soft-decision decoding on the inner code and hard-decision decoding on the outer code. The expressions for the error rate performance of these decoding schemes depend, in part, on the type of codes (block or convolutional) selected for the inner and outer codes. For example, the concatenation of two block codes may be viewed as an overall long binary (n, k) block code having a performance given by (13-2-39). The performance of other code combinations may also be readily derived. For the sake of brevity, we shall not consider such code combinations.

13-2-2 Some Applications of DS Spread Spectrum Signals

In this subsection, we shall briefly consider the use of coded DS spread spectrum signals for three specific applications. One is concerned with providing immunity against a jamming signal. In the second, a communication signal is hidden in the background noise by transmitting the signal at a very low power level. The third application is concerned with accommodating a number of simultaneous signal transmissions on the same channel, i.e., CDMA.

Antijamming Application In Section 13-2-1, we derived the error rate performance for a DS spread spectrum signal in the presence of either a narrow band or a wideband jamming signal. As examples to illustrate the performance of a digital communications system in the presence of a jamming signal, we shall select three codes. One is the Golay (24, 12), which is characterized by the weight distribution given in Table 8-1-1 and has a minimum distance $d_{\min} = 8$. The second code is an expurgated Golay (24, 11) obtained by selecting 2048 code words of constant weight 12. Of course this expurgated code is nonlinear. These two codes will be used in conjunction with a repetition code. The third code to be considered is a maximum-length shift-register code.

The error rate performance of the Golay (24, 12) with soft-decision decoding is

$$P_M \leq \left[759Q\left(\sqrt{\frac{8W/R}{J_{av}/P_{av}}}\right) + 2576Q\left(\sqrt{\frac{12W/R}{J_{av}/P_{av}}}\right) + 759Q\left(\sqrt{\frac{16W/R}{J_{av}/P_{av}}}\right) + Q\left(\sqrt{\frac{24W/R}{J_{av}/P_{av}}}\right)\right] \tag{13-2-46}$$

where W/R is the processing gain and J_{av}/P_{av} is the jamming margin. Since $n = n_1 n_2 = 12W/R$ and $n_1 = 24$, each coded bit is, in effect, repeated $n_2 = W/2R$ times. For example, if $W/R = 100$ (a processing gain of 20 dB), the block length of the repetition code is $n_2 = 50$.

If hard-decision decoding is used, the probability of error for a coded bit is

$$p = Q\left(\sqrt{\frac{W/R}{J_{av}/P_{av}}}\right) \tag{13-2-47}$$

and the corresponding probability of a code word error is upper-bounded as

$$P_M \leq \sum_{m=4}^{24} \binom{24}{m} p^m (1-p)^{24-m} \tag{13-2-48}$$

As an alternative, we may use the Chernoff bound for hard-decision decoding, which is

$$\begin{aligned} P_M \leq\ & 759[4p(1-p)]^4 + 2576[4p(1-p)]^6 \\ & + 759[4p(1-p)]^8 + [4p(1-p)]^{12} \end{aligned} \tag{13-2-49}$$

Figure 13-2-7 illustrates the performance of the Golay (24, 12) as a function of the jamming margin J_{av}/P_{av}, with the processing gain as a parameter. The Chernoff bound was used to compute the error probability for hard-decision decoding. The error probability for soft-decision decoding is dominated by the term

$$759Q\left(\sqrt{\frac{8W/R}{J_{av}/P_{av}}}\right)$$

and that for hard-decision decoding is dominated by the term $759[4p(1-p)]^4$. Hence, the coding gain for soft-decision decoding † is at most $10 \log 4 = 6$ dB. We note that the two curves corresponding to $W/R = 1000$ (30 dB) are identical in shape to the ones for $W/R = 100$ (20 dB), except that the latter are shifted by 10 dB to the right relative to the former. This shift is simply the difference in processing gain between these two DS spread spectrum signals.

The error rate performance of the expurgated Golay (24, 11) is upper-bounded as

$$P_M \leq 2047Q\left(\sqrt{\frac{11W/R}{J_{av}/P_{av}}}\right) \tag{13-2-50}$$

for soft-decision decoding and as‡

$$P_M \leq 2047[4p(1-p)]^6 \tag{13-2-51}$$

† The coding gain is less than 6 dB due to the multiplicative factor of 759, which increases the error probability relative to the performance of the binary uncoded system.

‡ We remind the reader that the union bound is not very tight for large signal sets.

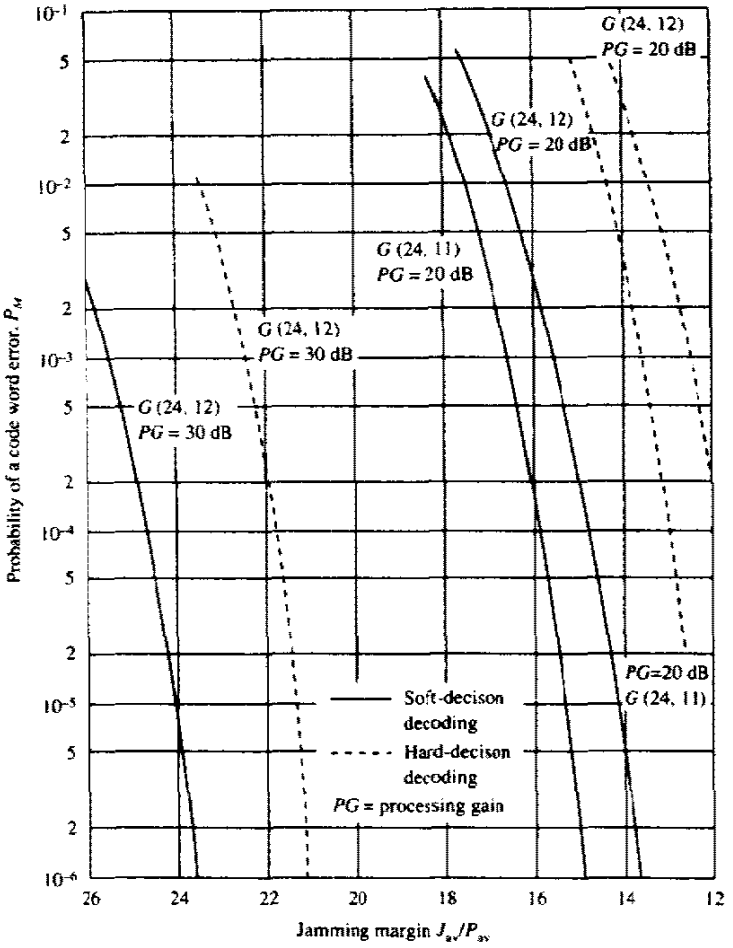

FIGURE 13-2-7 Performance of Golay codes used in DS spread spectrum signal.

for hard-decision decoding, where p is given as

$$p = Q\left(\sqrt{\frac{11W/R}{J_{av}/P_{av}}}\right) \tag{13-2-52}$$

The performance characteristics of this code are also plotted in Fig. 13-2-7 for $W/R = 100$. We observe that this expurgated Golay (24, 11) code performs about 1 dB better than the Golay (24, 12) code.

Instead of using a block code concatenated with a low-rate $(1/n_2)$ repetition code, let us consider using a single low-rate code. A particularly suitable set of low-rate codes is the set of maximum-length shift-register codes described in Section 8-1-3. We recall that for this set of codes,

$$\begin{aligned}(n, k) &= (2^m - 1, m)\\ d_{\min} &= 2^{m-1}\end{aligned} \tag{13-2-53}$$

All code words except the all-zero word have an identical weight of 2^{m-1}. Hence, the error rate for soft-decision decoding is upper-bounded as†

$$P_M \leq (M-1)Q\left(\sqrt{\frac{2W/R}{J_{av}/P_{av}} R_c d_{min}}\right)$$

$$\leq 2^m Q\left(\sqrt{\frac{2W/R}{J_{av}/P_{av}} \frac{m2^{m-1}}{2^m-1}}\right)$$

$$\leq 2^m \exp\left(-\frac{W/R}{J_{av}/P_{av}} \frac{m2^{m-1}}{2^m-1}\right) \qquad (13\text{-}2\text{-}54)$$

For moderate values of m, $R_c d_{min} \approx \frac{1}{2}m$ and, hence, (13-2-54) may be expressed as

$$P_M \leq 2^m Q\left(\sqrt{\frac{W/R}{J_{av}/P_{av}} m}\right) \leq 2^m \exp\left(-\frac{mW/R}{2J_{av}P_{av}}\right) \qquad (13\text{-}2\text{-}55)$$

Hence, the coding gain is at most $10 \log \frac{1}{2}m$.

For example, if we select $m = 10$ then $n = 2^{10} - 1 = 1023$. Since $n = kW/R = mW/R$, it follows that $W/R \approx 102$. Thus, we have a processing gain of about 20 dB and a coding gain of 7 dB. This performance is comparable to that obtained with the expurgated Golay (24, 11) code. Higher coding gains can be achieved with larger values of m.

If hard-decision decoding is used for the maximum-length shift-register codes, the error rate is upper-bounded by the Chernoff bound as

$$P_M \leq (M-1)[4p(1-p)]^{d_{min}/2} = (2^m - 1)[4p(1-p)]^{2^{m-2}} \qquad (13\text{-}2\text{-}56)$$

where p is given as

$$p = Q\left(\sqrt{\frac{2W/R}{J_{av}/P_{av}} R_c}\right) = Q\left(\sqrt{\frac{2W/R}{J_{av}/P_{av}} \frac{m}{2^m-1}}\right) \qquad (13\text{-}2\text{-}57)$$

For $m = 10$, the code word error rate P_M is comparable to that obtained with the expurgated Golay (24, 11) code for hard-decision decoding.

The reslts given above illustrate the performance that can be obtained with a single level of coding. Greater coding gains can be achieved with concatenated codes.

† The $M = 2^m$ waveforms generated by a maximum-length shift-register code form a simplex set (see Problem 8-13). The exact expression for the error probability, given in Section 5-2-4, may be used for large values of M, where the union bound becomes very loose.

Low-Detectability Signal Transmission In this application, the signal is purposely transmitted at a very low power level relative to the background channel noise and thermal noise that is generated in the front end of the receiver. If the DS spread spectrum signal occupies a bandwidth W and the spectral density of the additive noise is N_0 W/Hz, the average noise power in the bandwidth W is $N_{av} = WN_0$.

The average received signal power at the intended receiver is P_{av}. If we wish to hide the presence of the signal from receivers that are in the vicinity of the intended receiver, the signal is transmitted at a low power level such that $P_{av}/N_{av} \ll 1$. The intended receiver can recover the information-bearing signal with the aid of the processing gain and the coding gain. However, any other receiver that has no prior knowledge of the PN sequence is unable to take advantage of the processing gain and the coding gain. Hence, the presence of the information-bearing signal is difficult to detect. We say that the signal has a *low probability* of being *intercepted* (LPI) and it is called an *LPI signal.*

The probability of error results given in Section 13-2-1 also apply to the demodulation and decoding of LPI signals at the intended receiver.

Code Division Multiple Access The enhancement in performance obtained from a DS spread spectrum signal through the processing gain and coding gain can be used to enable many DS spread spectrum signals to occupy the same channel bandwidth provided that each signal has its own distinct PN sequence. Thus, it is possible to have several users transmit messages simultaneously over the same channel bandwidth. This type of digital communication in which each user (transmitter-receiver pair) has a distinct PN code for transmitting over a common channel bandwidth is called either *code division multiple access* (CDMA) or *spread spectrum multiple access* (SSMA).

In the demodulation of each PN signal, the signals from the other simultaneous users of the channel appear as an additive interference. The level of interference varies, depending on the number of users at any given time. A major advantage of CDMA is that a large number of users can be accommodated if each transmits messages for a short period of time. In such a multiple access system, it is relatively easy either to add new users or to decrease the number of users without disrupting the system.

Let us determine the number of simultaneous signals that can be supported in a CDMA system.† For simplicity, we assume that all signals have identical average powers. Thus, if there are N_u simultaneous users, the desired signal-to-noise interference power ratio at a given receiver is

$$\frac{P_{av}}{J_{av}} = \frac{P_{av}}{(N_u - 1)P_{av}} = \frac{1}{N_u - 1} \tag{13-2-58}$$

† In this section the interference from other users is treated as a random process. This is the case if there is no cooperation among the users. In Chapter 15 we consider CDMA transmission in which interference from other users is known and is suppressed by the receiver.

Hence, the performance for soft-decision decoding at the given receiver is upper-bounded as

$$P_M \leq \sum_{m=2}^{M} Q\left(\sqrt{\frac{2W/R}{N_u - 1} R_c w_m}\right) \leq (M-1)Q\left(\sqrt{\frac{2W/R}{N_u - 1} R_c d_{\min}}\right) \tag{13-2-59}$$

In this case, we have assumed that the interference from other users is gaussian.

As an example, suppose that the desired level of performance (error probability of 10^{-6}) is achieved when

$$\frac{W/R}{N_u - 1} R_c d_{\min} = 20$$

Then the maximum number of users that can be supported in the CDMA system is

$$N_u = \frac{W/R}{20} R_c d_{\min} + 1 \tag{13-2-60}$$

If $W/R = 100$ and $R_c d_{\min} = 4$, as obtained with the Golay (24, 12) code, the maximum number is $N_u = 21$. If $W/R = 1000$ and $R_c d_{\min} = 4$, this number becomes $N_u = 201$.

In determining the maximum number of simultaneous users of the channel, we have implicitly assumed that the PN code sequences are mutually orthogonal and the interference from other users adds on a power basis only. However, orthogonality among a number of PN code sequences is not easily achieved, especially if the number of PN code sequences required is large. In fact, the selection of a good set of PN sequences for a CDMA system is an important problem that has received considerable attention in the technical literature. We shall briefly discuss this problem in Section 13-2-3.

13-2-3 Effect of Pulsed Interference on DS Spread Spectrum Systems

Thus far, we have considered the effect of continuous interference or jamming on a DS spread spectrum signal. We have observed that the processing gain and coding gain provide a means for overcoming the detrimental effects of this type of interference. However, there is a jamming threat that has a dramatic effect on the performance of a DS spread spectrum system. That jamming signal consists of pulses of spectrally flat noise that covers the entire signal bandwidth W. This is usually called *pulsed interference* or *partial-time jamming*.

Suppose the jammer has an average power J_{av} in the signal bandwidth W. Hence $J_0 = J_{av}/W$. Instead of transmitting continuously, the jammer transmits pulses at a power J_{av}/α for α% of the time, i.e., the probability that the jammer is transmitting at a given instant is α. For simplicity, we assume that

an interference pulse spans an integral number of signaling intervals and, thus, it affects an integral number of bits. When the jammer is not transmitting, the transmitted bits are assumed to be received error-free, and when the jammer is transmitting, the probability of error for an uncoded DS spread spectrum system is $Q(\sqrt{2\alpha\mathscr{E}_b/J_0})$. Hence, the average probability of a bit error is

$$P_2(\alpha) = \alpha Q(\sqrt{2\alpha\mathscr{E}_b/J_0}) = \alpha Q\left(\sqrt{\frac{2\alpha W/R}{J_{av}/P_{av}}}\right) \tag{13-2-61}$$

The jammer selects the duty cycle α to maximize the error probability. On differentiating (13-2-61) with respect to α, we find that the worst-case pulse jamming occurs when

$$\alpha^* = \begin{cases} \dfrac{0.71}{\mathscr{E}_b/J_0} & (\mathscr{E}_b/J_0 \geq 0.71) \\ 1 & (\mathscr{E}_b/J_0 < 0.71) \end{cases} \tag{13-2-62}$$

and the corresponding error probability is

$$P_2 = \begin{cases} \dfrac{0.083}{\mathscr{E}_b/J_0} = \dfrac{0.083 J_{av}/P_{av}}{W/R} & (\mathscr{E}_b/J_0 > 0.71) \\ Q\left(\sqrt{\dfrac{2W/R}{J_{av}/P_{av}}}\right) & (\mathscr{E}_b/J_0 < 0.71) \end{cases} \tag{13-2-63}$$

The error rate performance given by (13-2-61) for $\alpha = 1.0$, 0.1, and 0.01 along with the worst-case performance based on α^* is plotted in Fig. 13-2-8.

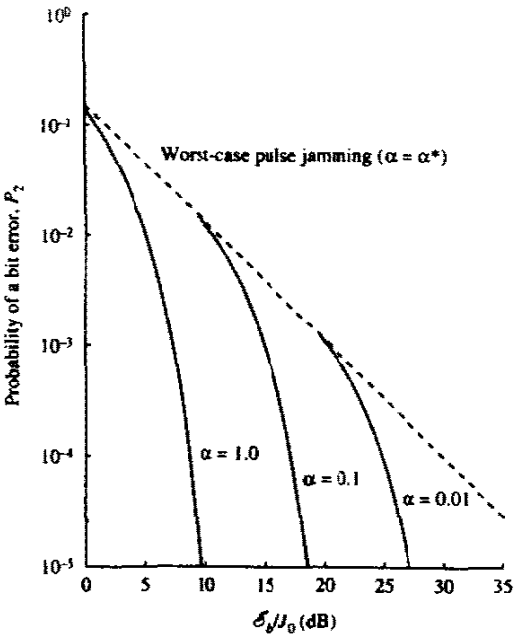

FIGURE 13-2-8 Performance of DS binary PSK with pulse jamming.

By comparing the error rate for continuous gaussian noise jamming with worst-case pulse jamming, we observe a large difference in performance, which is approximately 40 dB at an error rate of 10^{-6}.

We should point out that the above analysis applies when the jammer pulse duration is equal to or greater than the bit duration. In addition, we should indicate that practical considerations may prohibit the jammer from achieving high peak power (small values of α). Nevertheless, the error probability given by (13-2-63) serves as an upper bound on the performance of the uncoded binary PSK in worst-case pulse jamming. Clearly, the performance of the DS spread spectrum system in the presence of such jamming is extremely poor.

If we simply add coding to the DS spread spectrum system, the improvement over the uncoded system is the coding gain. Thus, $\mathscr{E}_b/J_0$ is reduced by the coding gain, which in most cases is limited to less than 10 dB. The reason for the poor performance is that the jamming signal pulse duration may be selected to affect many consecutive coded bits when the jamming signal is turned on. Consequently, the code word error probability is high due to the burst characteristics of the jammer.

In order to improve the performance, we should interleave the coded bits prior to transmission over the channel. The effect of the interleaving, as discussed in Section 8-1-9, is to make the coded bits that are hit by the jammer statistically independent.

The block diagram of the digital communication system that includes interleaving/deinterleaving is shown in Fig. 13-2-9. Also shown is the possibility that the receiver knows the jammer state, i.e., that it knows when the jammer is on or off. Knowledge of the jammer state (called *side information*) is sometimes available from channel measurements of noise power levels in adjacent frequency bands. In our treatment, we consider two

FIGURE 13-2-9 Block diagram of AJ communication system.

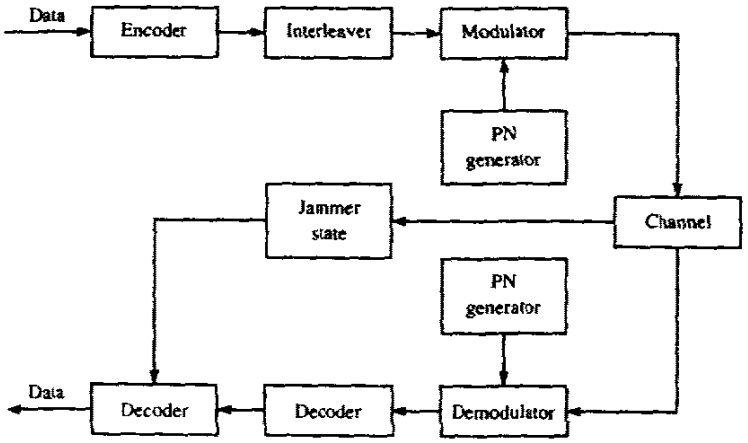

extreme cases, namely, no knowledge of the jammer state or complete knowledge of the jammer state. In any case, the random variable ζ representing the jammer state is characterized by the probabilities

$$P(\zeta = 1) = \alpha, \quad P(\zeta = 0) = 1 - \alpha$$

When the jammer is on, the channel is modeled as an AWGN with power spectral density $N_0 = J_0/\alpha = J_{av}/\alpha W$; and when the jammer is off, there is no noise in the channel. Knowledge of the jammer state implies that the decoder knows when $\zeta = 1$ and when $\zeta = 0$, and uses this information in the computation of the correlation metrics. For example, the decoder may weight the demodulator output for each coded bit by the reciprocal of the noise power level in the interval. Alternatively, the decoder may give zero weight (erasure) to a jammed bit.

First, let us consider the effect of jamming without knowledge of the jammer state. The interleaver/deinterleaver pair is assumed to result in statistically independent jammer hits of the coded bits. As an example of the performance achieved with coding, we cite the performance results from the paper of Martin and McAdam (1980). There the performance of binary convolutional codes is evaluated for worst-case pulse jamming. Both hard and soft-decision Viterbi decoding are considered. Soft decisions are obtained by quantizing the demodulator output to eight levels. For this purpose, a uniform quantizer is used for which the threshold spacing is optimized for the pulse jammer noise level. The quantizer plays the important role of limiting the size of the demodulator output when the pulse jammer is on. The limiting action ensures that any hit on a coded bit does not heavily bias the corresponding path metrics.

The optimum duty cycle for the pulse jammer in the coded system is generally inversely proportional to the SNR, but its value is different from that given by (13-2-62) for the uncoded system. Figure 13-2-10 illustrates graphically the optimal jammer duty cycle for both hard- and soft-decision decoding of the rate 1/2 convolutional codes. The corresponding error rate results for this worst-case pulse jammer are illustrated in Figs 13-2-11 and 13-2-12 for rate 1/2 codes with constraint lengths $3 \leq K \leq 9$. For example, note that at $P_2 = 10^{-6}$, the $K = 7$ convolutional code with soft-decision decoding requires $\mathscr{E}_b/J_0 = 7.6$ dB, whereas hard-decision decoding requires $\mathscr{E}_b/J_0 = 11.7$ dB. This 4.1 dB difference in SNR is relatively large. With continuous gaussian noise, the corresponding SNRs for an error rate of 10^{-6} are 5 dB for soft-decision decoding and 7 dB for hard-decision decoding. Hence, the worst-case pulse jammer has degraded the performance by 2.6 dB for soft-decision decoding and by 4.7 dB for hard-decision decoding. These levels of degradation increase as the constraint length of the convolutional code is decreased. The important point, however, is that the loss in SNR due to jamming has been reduced from 40 dB for the uncoded system to less than 5 dB for the coded system based on a $K = 7$, rate 1/2 convolutional code.

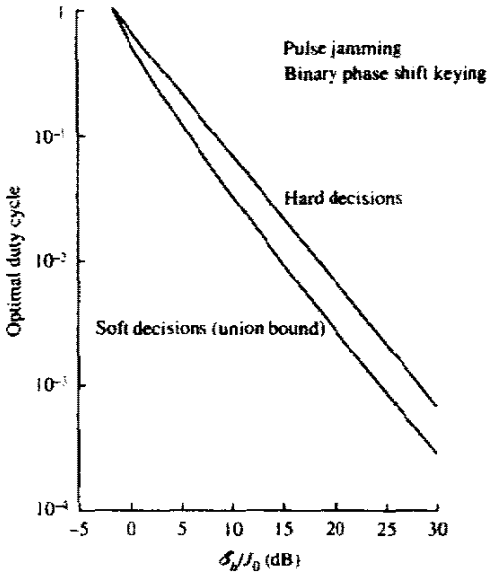

FIGURE 13-2-10 Optimal duty cycle for pulse jammer. [*From Martin and McAdam (1980). © 1980 IEEE.*]

A simpler method for evaluating the performance of a coded AJ communication system is to use the cutoff rate parameter R_0 as proposed by Omura and Levitt (1982). For example, with binary-coded modulation, the cutoff rate may be expressed as

$$R_0 = 1 - \log(1 + D_\alpha) \tag{13-2-64}$$

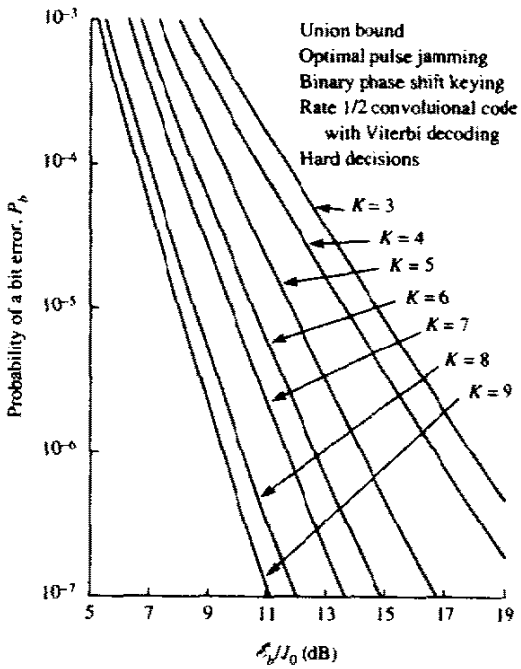

FIGURE 13-2-11 Performance of rate 1/2 convolutional codes with hard-decision Viterbi decoding binary PSK with optimal pulse jamming. [*From Martin and McAdam (1980). © 1980 IEEE.*]

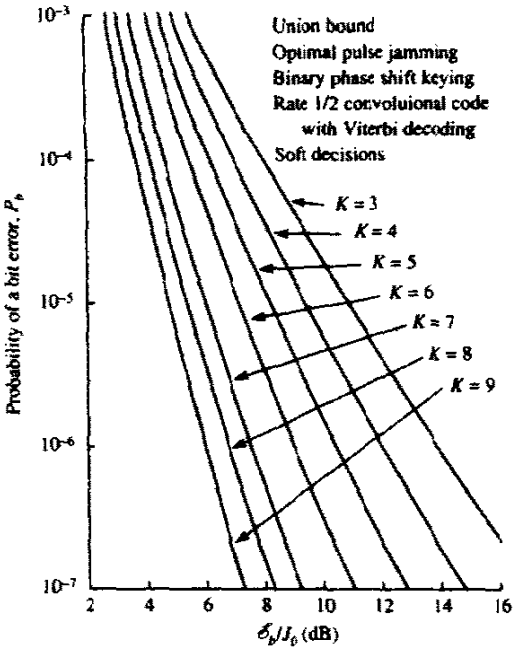

FIGURE 13-2-12 Performance of rate 1/2 convolutional codes with soft-decision Viterbi decoding binary PSK with optimal pulse jamming. [*From Martin and McAdam (1980). © 1980 IEEE.*]

where the factor D_α depends on the channel noise characteristics and the decoder processing. Recall that for binary PSK in an AWGN channel and soft-decision decoding,

$$D_\alpha = e^{-\mathscr{E}_c/N_0} \tag{13-2-65}$$

where $\mathscr{E}_c$ is the energy per coded bit; and for hard-decision decoding,

$$D_\alpha = \sqrt{4p(1-p)} \tag{13-2-66}$$

where p is the probability of a coded bit error. Here, we have $N_0 \equiv J_0$.

For a coded binary PSK, with pulse jamming, Omura and Levitt (1982) have shown that

$$D_\alpha = \alpha e^{-\alpha \mathscr{E}_c/N_0} \quad \text{for soft-decision decoding with knowledge of jammer state} \tag{13-2-67}$$

$$D_\alpha = \min_{\lambda \geq 0} \{[\alpha \exp(\lambda^2 \mathscr{E}_c N_0/\alpha) + 1 - \alpha] \exp(-2\lambda \mathscr{E}_c)\}$$

for soft-decision decoding with no knowledge of jammer state (13-2-68)

$$D_\alpha = \alpha\sqrt{4p(1-p)} \quad \text{for hard-decision decoding with knowledge of the jammer state} \tag{13-2-69}$$

$$D_\alpha = \sqrt{4\alpha p(1-\alpha p)} \quad \text{for hard-decision decoding with no knowledge of the jammer state} \tag{13-2-70}$$

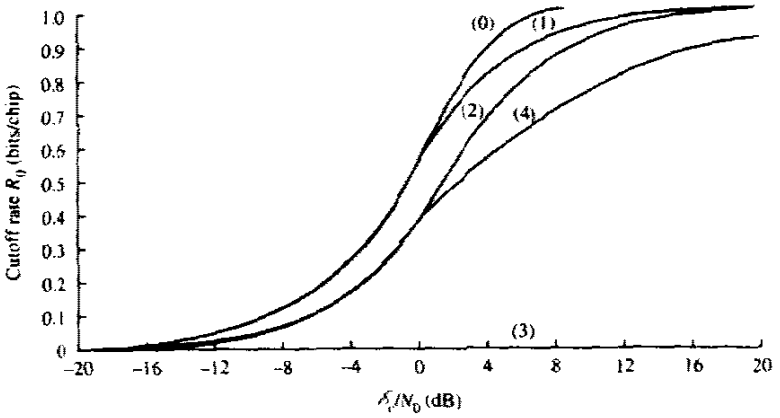

Key
(0) Soft-decision decoding in AWGN ($\alpha=1$)
(1) Soft-decision with jammer state information
(2) Hard-decision with jammer state information
(3) Soft-decision with no jammer state information
(4) Hard-decision with no jammer state information

FIGURE 13-2-13 Cutoff rate for coded DS binary PSK modulation. [*From Omura and Levitt (1982). © 1982 IEEE.*]

where the probability of error for hard-decision decoding of binary PSK is

$$p = Q\left(\sqrt{\frac{2\alpha\mathscr{E}_c}{N_0}}\right)$$

The graphs for R_0 as a function of $\mathscr{E}_c/N_0$ are illustrated in Fig. 13-2-13 for the cases given above. Note that these graphs represent the cutoff rate for the worst-case value of $\alpha = \alpha^*$ that maximizes D_α (minimizes R_0) for each value of $\mathscr{E}_c/N_0$. Furthermore, note that with soft-decision decoding and no knowledge of the jammer state, $R_0 = 0$. This situation results from the fact that the demodulator output is not quantized.

The graphs in Fig. 13-2-13 may be used to evaluate the performance of coded systems. To demonstrate the procedure, suppose that we wish to determine the SNR required to achieve an error probability of 10^{-6} with coded binary PSK in worst-case pulse jamming. To be specific, we assume that we have a rate 1/2, $K = 7$ convolutional code. We begin with the performance of the rate 1/2, $K = 7$ convolutional code with soft-decision decoding in an AWGN channel. At $P_2 = 10^{-6}$, the SNR required is found from Fig. 8-2-21 to be

$$\mathscr{E}_b/N_0 = 5 \text{ dB}$$

Since the code is rate 1/2, we have

$$\mathscr{E}_c/N_0 = 2 \text{ dB}$$

Now, we go to the graphs in Fig. 13-2-13 and find that for the AWGN channel (*reference system*) with $\mathscr{E}_c/N_0 = 2$ dB, the corresponding value of the cutoff rate is

$$R_0 = 0.74 \text{ bits/symbol}$$

If we have another channel with different noise characteristics (a worst-case pulse noise channel) but with the same value of the cutoff rate R_0, then the upper bound on the bit error probability is the same, i.e., 10^{-6} in this case. Consequently, we can use this rate to determine the SNR required for the worst-case pulse jammer channel. From the graphs in Fig. 13-2-13, we find that

$$\frac{\mathscr{E}_c}{J_0} = \begin{cases} 10 \text{ dB} & \text{for hard-decision decoding with no knowledge of jammer state} \\ 5 \text{ dB} & \text{for hard-decision decoding with knowledge of jammer state} \\ 3 \text{ dB} & \text{for soft-decision decoding with knowledge of jammer state} \end{cases}$$

Therefore, the corresponding values of $\mathscr{E}_b/J_0$ for the rate 1/2, $K = 7$ convolutional are 13, 8, and 6 dB, respectively.

This general approach may be used to generate error rate graphs for coded binary signals in a worst-case pulse jamming channel by using corresponding error rate graphs for the AWGN channel. The approach we describe above is easily generalized to M-ary coded signals as indicated by Omura and Levitt (1982).

By comparing the cutoff rate for coded DS binary PSK modulation shown in Fig. 13-2-13, we note that for rates below 0.7, there is no penalty in SNR with soft-decision decoding and jammer state information compared with the performance on the AWGN channel ($\alpha = 1$). On the other hand, at $R_0 = 0.7$, there is a 6 dB difference in performance between the SNR in an AWGN channel and that required for hard-decision decoding with no jammer state information. At rates below 0.4, there is no penalty in SNR with hard-decision decoding if the jammer state is unknown. However, there is the expected 2 dB loss in hard-decision decoding compared with soft-decision decoding in the AWGN channel.

13-2-4 Generation of PN Sequences

The generation of PN sequences for spread spectrum applications is a topic that has received considerable attention in the technical literature. We shall briefly discuss the construction of some PN sequences and present a number of important properties of the autocorrelation and cross-correlation functions of such sequences. For a comprehensive treatment of this subject, the interested reader may refer to the book by Golomb (1967).

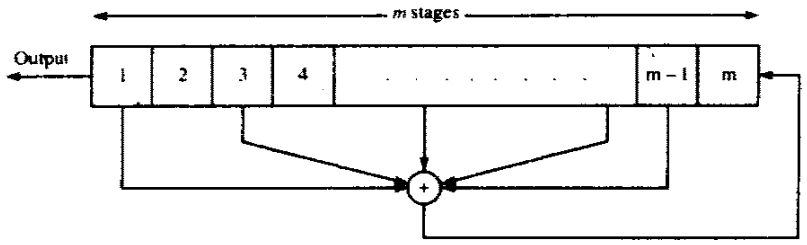

FIGURE 13-2-14 General m-stage shift register with linear feedback.

By far the most widely known binary PN sequences are the maximum-length shift-register sequences introduced in Section 8-1-3 in the context of coding and suggested again in Section 13-2-2 for use as low-rate codes. A maximum-length shift-register sequence, or m-sequence for short, has length $n = 2^m - 1$ bits and is generated by an m-stage shift register with linear feedback as illustrated in Fig. 13-2-14. The sequence is periodic with period n. Each period of the sequence contains 2^{m-1} ones and $2^{m-1} - 1$ zeros.

In DS spread spectrum applications the binary sequence with elements $\{0, 1\}$ is mapped into a corresponding sequence of positive and negative pulses according to the relation

$$p_i(t) = (2b_i - 1)p(t - iT)$$

where $p_i(t)$ is the pulse corresponding to the element b_i in the sequence with elements $\{0, 1\}$. Equivalently, we may say that the binary sequence with elements $\{0, 1\}$ is mapped into a corresponding binary sequence with elements $\{-1, 1\}$. We shall call the equivalent sequence with elements $\{-1, 1\}$ a *bipolar sequence*, since it results in pulses of positive and negative amplitudes.

An important characteristic of a periodic PN sequence is its periodic autocorrelation function, which is usually defined in terms of the bipolar sequence as

$$\phi(j) = \sum_{i=1}^{n} (2b_i - 1)(2b_{i+j} - 1), \qquad 0 \leq j \leq n - 1 \tag{13-2-71}$$

where n is the period. Clearly, $\phi(j + rn) = \phi(j)$ for any integer value r.

Ideally, a pseudo-random sequence should have an autocorrelation function with the property that $\phi(0) = n$ and $\phi(j) = 0$ for $1 \leq j \leq n - 1$. In the case of m sequences, the periodic autocorrelation function is

$$\phi(j) = \begin{cases} n & (j = 0) \\ -1 & (1 \leq j \leq n - 1) \end{cases} \tag{13-2-72}$$

For large values of n, i.e., for long m sequences, the size of the off-peak values of $\phi(j)$ relative to the peak value $\phi(j)/\phi(0) = -1/n$ is small and, from a practical viewpoint, inconsequential. Therefore, m sequences are almost ideal when viewed in terms of their autocorrelation function.

In antijamming applications of PN spread spectrum signals, the period of the sequence must be large in order to prevent the jammer from learning the feedback connections of the PN generator. However, this requirement is impractical in most cases because the jammer can determine the feedback connections by observing only $2m$ chips from the PN sequence. This vulnerability of the PN sequence is due to the linearity property of the generator. To reduce the vulnerability to a jammer, the output sequences from several stages of the shift register or the outputs from several distinct m sequences are combined in a nonlinear way to produce a nonlinear sequence that is considerably more difficult for the jammer to learn. Further reduction in vulnerability is achieved by frequently changing the feedback connections and/or the number of stages in the shift register according to some prearranged plan formulated between the transmitter and the intended receiver.

In some applications, the cross-correlation properties of PN sequences are as important as the autocorrelation properties. For example, in CDMA, each user is assigned a particular PN sequence. Ideally, the PN sequences among users should be mutually orthogonal so that the level of interference experienced by any one user from transmissions of other users adds on a power basis. However, the PN sequences used in practice exhibit some correlation.

To be specific, we consider the class of m sequences. It is known (Sarwate and Pursley, 1980) that the periodic cross-correlation function between any pair of m sequences of the same period can have relatively large peaks. Table 13-2-1 lists the peak magnitude $\phi_{\max}$ for the periodic cross-correlation between pairs of m sequences for $3 \leq m \leq 12$. The table also shows the number of m sequences of length $n = 2^m - 1$ for $3 \leq m \leq 12$. As we can see, the number of m sequences of length n increases rapidly with m. We also observe that, for most sequences, the peak magnitude $\phi_{\max}$ of the cross-correlation function is a large percentage of the peak value of the autocorrelation function.

Such high values for the cross-correlations are undesirable in CDMA.

TABLE 13-2-1 PEAK CROSS-CORRELATION OF m SEQUENCES AND GOLD SEQUENCES

m	$n = 2^m - 1$	Number of m sequences	Peak cross-correlation $\phi_{\max}$	$\phi_{\max}/\phi(0)$	$t(m)$	$t(m)/\phi(0)$
3	7	2	5	0.71	5	0.71
4	15	2	9	0.60	9	0.60
5	31	6	11	0.35	9	0.29
6	63	6	23	0.36	17	0.27
7	127	18	41	0.32	17	0.13
8	255	16	95	0.37	33	0.13
9	511	48	113	0.22	33	0.06
10	1023	60	383	0.37	65	0.06
11	2047	176	287	0.14	65	0.03
12	4095	144	1407	0.34	129	0.03

Although it is possible to select a small subset of m sequences that have relatively smaller cross-correlation peak values, the number of sequences in the set is usually too small for CDMA applications.

PN sequences with better periodic cross-correlation properties than m sequences have been given by Gold (1967, 1968) and Kasami (1966). They are derived from m sequences as described below.

Gold and Kasami proved that certain pairs of m sequences of length n exhibit a three-valued cross-correlation function with values $\{-1, -t(m), t(m)-2\}$, where

$$t(m) = \begin{cases} 2^{(m+1)/2} + 1 & (\text{odd } m) \\ 2^{(m+2)/2} + 1 & (\text{even } m) \end{cases} \tag{13-2-73}$$

For example, if $m = 10$ then $t(10) = 2^6 + 1 = 65$ and the three possible values of the periodic cross-correlation function are $\{-1, -65, 63\}$. Hence the maximum cross-correlation for the pair of m sequences is 65, while the peak for the family of 60 possible sequences generated by a 10-stage shift register with different feedback connections is $\phi_{\max} = 383$—about a sixfold difference in peak values. Two m sequences of length n with a periodic cross-correlation function that takes on the possible values $\{-1, -t(m), t(m)-2\}$ are called *preferred sequences.*

From a pair of preferred sequences, say $\mathbf{a} = [a_1 a_2 \ldots a_n]$ and $\mathbf{b} = [b_1 b_2 \ldots b_n]$, we construct a set of sequences of length n by taking the modulo-2 sum of $\mathbf{a}$ with the n cyclicly shifted versions of $\mathbf{b}$ or vice versa. Thus, we obtain n new periodic sequences† with period $n = 2^m - 1$. We may also include the original sequences $\mathbf{a}$ and $\mathbf{b}$ and, thus, we have a total of $n+2$ sequences. The $n+2$ sequences constructed in this manner are called *Gold sequences.*

Example 13-2-4

Let us consider the generation of Gold sequences of length $n = 31 = 2^5 - 1$. As indicated above for $m = 5$, the cross-correlation peak is

$$t(5) = 2^3 + 1 = 9$$

Two preferred sequences, which may be obtained from Peterson and Weldon (1972), are described by the polynomials

$$g_1(p) = p^5 + p^2 + 1$$
$$g_2(p) = p^5 + p^4 + p^2 + p + 1$$

† An equivalent method for generating the n new sequences is to employ a shift register of length $2m$ with feedback connections specified by the polynomial $h(p) = g_1(p)g_2(p)$, where $g_1(p)$ and $g_2(p)$ are the polynomials that specify the feedback connections of the m-stage shift registers that generate the m sequences $\mathbf{a}$ and $\mathbf{b}$.

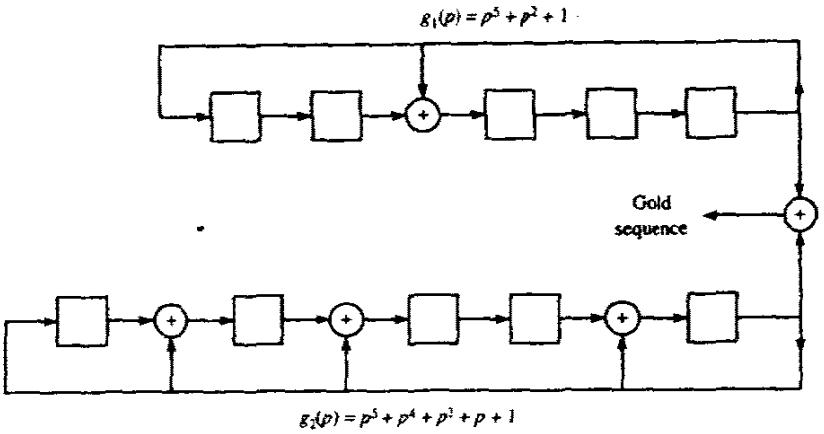

FIGURE 13-2-15 *Generation of Gold sequences of length 31.*

The shift registers for generating the two m sequences and the corresponding Gold sequences are shown in Fig. 13-2-15. In this case, there are 33 different sequences, corresponding to the 33 relative phases of the two m sequences. Of these, 31 sequences are non-maximal-length sequences.

With the exception of the sequences **a** and **b**, the set of Gold sequences does not comprise maximum-length shift-register sequences of length n. Hence, their autocorrelation functions are not two-valued. Gold (1968) has shown that the cross-correlation function for any pair of sequences from the set of $n+2$ Gold sequences is three-valued with possible values $\{-1, -t(m), t(m)-2\}$, where $t(m)$ is given by (13-2-73). Similarly, the off-peak autocorrelation function for a Gold sequence takes on values from the set $\{-1, -t(m), t(m)-2\}$. Hence, the off-peak values of the autocorrelation function are upper-bounded by $t(m)$.

The values of the off-peak autocorrelation function and the peak cross-correlation function, i.e., $t(m)$, for Gold sequences is listed in Table 13-2-1. Also listed are the values normalized by $\phi(0)$.

It is interesting to compare the peak cross-correlation value of Gold sequences with a known lower bound on the cross-correlation between any pair of binary sequences of period n in a set of M sequences. A lower bound developed by Welch (1974) for ϕ_{max} is

$$\phi_{max} \geq n\sqrt{\frac{M-1}{Mn-1}} \tag{13-2-74}$$

which, for large values of n and M, is well approximated as $\sqrt{n}$. For Gold sequences, $n = 2^m - 1$ and, hence, the lower bound is $\phi_{max} \approx 2^{m/2}$. This bound is lower by $\sqrt{2}$ for odd m and by 2 for even m relative to $\phi_{max} = t(m)$ for Gold sequences.

A procedure similar to that used for generating Gold sequences will generate a smaller set of $M = 2^{m/2}$ binary sequences of period $n = 2^m - 1$, where m is even. In this procedure, we begin with an m sequence **a** and we form a binary sequence **b** by taking every $2^{m/2} + 1$ bit of **a**. Thus, the sequence **b** is formed by decimating **a** by $2^{m/2} + 1$. It can be verified that the resulting **b** is periodic with period $2^{m/2} - 1$. For example, if $m = 10$, the period of **a** is $n = 1023$ and the period of **b** is 31. Hence, if we observe 1023 bits of the sequence **b**, we shall see 33 repetitions of the 31-bit sequence. Now, by taking $n = 2^m - 1$ bits of the sequences **a** and **b**, we form a new set of sequences by adding, modulo-2, the bits from **a** and the bits from **b** and all $2^{m/2} - 2$ cyclic shifts of the bits from **b**. By including **a** in the set, we obtain a set of $2^{m/2}$ binary sequences of length $n = 2^m - 1$. These are called *Kasami sequences*. The autocorrelation and cross-correlation functions of these sequences take on values from the set $\{-1, -(2^{m/2} + 1), 2^{m/2} - 1\}$. Hence, the maximum cross-correlation value for any pair of sequences from the set is

$$\phi_{\max} = 2^{m/2} + 1 \tag{13-2-75}$$

This value of $\phi_{\max}$ satisfies the Welch lower bound for a set of $2^{m/2}$ sequences of length $n = 2^m - 1$. Hence, the Kasami sequences are optimal.

Besides the well-known Gold and Kasami sequences, there are other binary sequences appropriate for CDMA applications. The interested reader may refer to the work of Scholtz (1979), Olsen (1977), and Sarwate and Pursley (1980).

Finally, we wish to indicate that, although we have discussed the periodic cross-correlation function between pairs of periodic sequences, many practical CDMA systems may use information bit durations that encompass only fractions of a periodic sequence. In such cases, it is the partial-period cross-correlation between two sequences that is important. A number of papers deal with this problem, including those by Lindholm (1968), Wainberg and Wolf (1970), Fredricsson (1975), Bekir *et al.* (1978), and Pursley (1979).

13-3 FREQUENCY-HOPPED SPREAD SPECTRUM SIGNALS

In a *frequency-hopped* (FH) spread spectrum communications system the available channel bandwidth is subdivided into a large number of contiguous frequency slots. In any signaling interval, the transmitted signal occupies one or more of the available frequency slots. The selection of the frequency slot(s) in each signaling interval is made pseudo-randomly according to the output from a PN generator. Figure 13-3-1 illustrates a particular frequency-hopped pattern in the time-frequency plane.

A block diagram of the transmitter and receiver for a frequency-hopped spread spectrum system is shown in Fig. 13-3-2. The modulation is usually either binary or M-ary FSK. For example, if binary FSK is employed, the modulator selects one of two frequencies corresponding to the transmission of

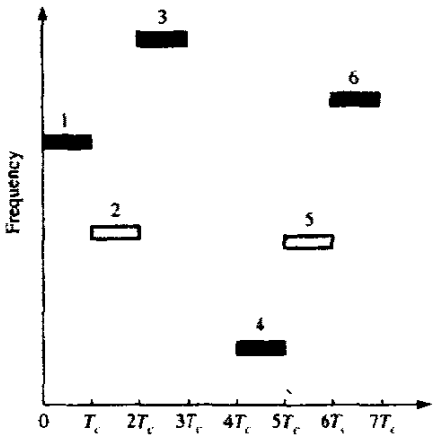

FIGURE 13-3-1 An example of a frequency-hopped (FH) pattern.

either a 1 or a 0. The resulting FSK signal is translated in frequency by an amount that is determined by the output sequence from the PN generator, which, in turn, is used to select a frequency that is synthesized by the frequency synthesizer. This frequency is mixed with the output of the modulator and the resultant frequency-translated signal is transmitted over the channel. For example, m bits from the PN generator may be used to specify $2^m - 1$ possible frequency translations.

At the receiver, we have an identical PN generator, synchronized with the received signal, which is used to control the output of the frequency synthesizer. Thus, the pseudo-random frequency translation introduced at the transmitter is removed at the receiver by mixing the synthesizer output with the received signal. The resultant signal is demodulated by means of an FSK demodulator. A signal for maintaining synchronism of the PN generator with the frequency-translated received signal is usually extracted from the received signal.

Although PSK modulation gives better performance than FSK in an

FIGURE 13-3-2 Block diagram of a FH spread spectrum system.

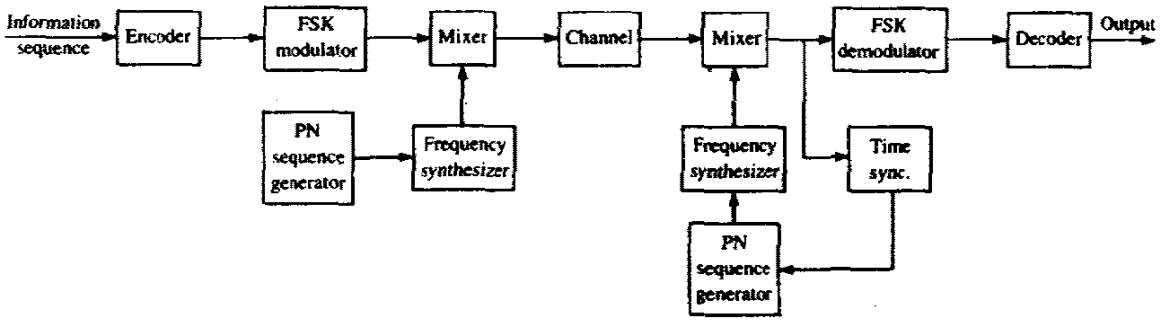

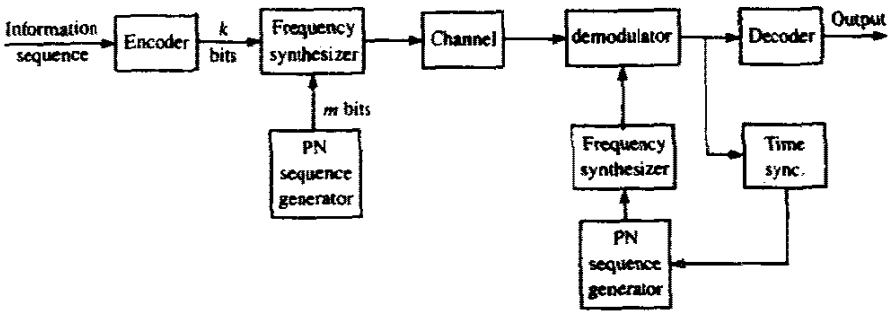

FIGURE 13-3-3 Block diagram of an independent tone FH spread spectrum system.

AWGN channel, it is difficult to maintain phase coherence in the synthesis of the frequencies used in the hopping pattern and, also, in the propagation of the signal over the channel as the signal is hopped from one frequency to another over a wide bandwidth. Consequently, FSK modulation with noncoherent detection is usually employed with FH spread spectrum signals.

In the frequency-hopping system depicted in Fig. 13-3-2, the carrier frequency is pseudo-randomly hopped in every signaling interval. The M information-bearing tones are contiguous and separated in frequency by $1/T_c$, where T_c is the signaling interval. This type of frequency hopping is called *block hopping.*

Another type of frequency hopping that is less vulnerable to some jamming strategies is independent tone hopping. In this scheme, the M possible tones from the modulator are assigned widely dispersed frequency slots. One method for accomplishing this is illustrated in Fig. 13-3-3. Here, the m bits from the PN generator and the k information bits are used to specify the frequency slots for the transmitted signal.

The frequency-hopping rate is usually selected to be either equal to the (coded or uncoded) symbol rate or faster than that rate. If there are multiple hops per symbol, we have a fast-hopped signal. On the other hand, if the hopping is performed at the symbol rate, we have a slow-hopped signal.

Fast frequency hopping is employed in AJ applications when it is necessary to prevent a type of jammer, called a *follower jammer,* from having sufficient time to intercept the frequency and retransmit it along with adjacent frequencies so as to create interfering signal components. However, there is a penalty incurred in subdividing a signal into several frequency-hopped elements because the energy from these separate elements is combined noncoherently. Consequently, the demodulator incurs a penalty in the form of a noncoherent combining loss as described in Section 12-1.

FH spread spectrum signals are used primarily in digital communications systems that require AJ projection and in CDMA, where many users share a common bandwidth. In most cases, a FH signal is preferred over a DS spread spectrum signal because of the stringent synchronization requirements

inherent in DS spread spectrum signals. Specifically, in a DS system, timing and synchronization must be established to within a fraction of the chip interval $T_c \approx 1/W$. On the other hand, in an FH system, the chip interval is the time spent in transmitting a signal in a particular frequency slot of bandwidth $B \ll W$. But this interval is approximately $1/B$, which is much larger than $1/W$. Hence the timing requirements in a FH system are not as stringent as in a PN system.

In Sections 13-3-2 and 13-3-3, we shall focus on the AJ and CDMA applications of FH spread spectrum signals. First, we shall determine the error rate performance of an uncoded and a coded FH signal in the presence of broadband AWGN interference. Then we shall consider a more serious type of interference that arises in AJ and CDMA applications, called *partial-band interference*. The benefits obtained from coding for this type of interference are determined. We conclude the discussion in Section 13-3-3 with an example of an FH CDMA system that was designed for use by mobile users with a satellite serving as the channel.

13-3-1 Performance of FH Spread Spectrum Signals in AWGN Channel

Let us consider the performance of a FH spread spectrum signal in the presence of broadband interference characterized statistically as AWGN with power spectral density J_0. For binary orthogonal FSK with noncoherent detection and slow frequency hopping (1 hop/bit), the probability of error, derived in Section 5-4-1, is

$$P_2 = \tfrac{1}{2} e^{-\gamma_b/2} \tag{13-3-1}$$

where $\gamma_b = \mathscr{E}_b/J_0$. On the other hand, if the bit interval is subdivided into L subintervals and FH binary FSK is transmitted in each subinterval, we have a fast FH signal. With square-law combining of the output signals from the corresponding matched filters for the L subintervals, the error rate performance of the FH signal, obtained from the results in Section 12-1, is

$$P_2(L) = \frac{1}{2^{2L-1}} e^{-\gamma_b/2} \sum_{i=0}^{L-1} K_i (\tfrac{1}{2}\gamma_b)^i \tag{13-3-2}$$

where the SNR per bit is $\gamma_b = \mathscr{E}_b/J_0 = L\gamma_c$, γ_c is the SNR per chip in the L-chip symbol, and

$$K_i = \frac{1}{i!} \sum_{r=0}^{L-1-i} \binom{2L-1}{r} \tag{13-3-3}$$

We recall that, for a given SNR per bit γ_b, the error rate obtained from (13-3-2) is larger than that obtained from (13-3-1). The difference in SNR for a given error rate and a given L is called the *noncoherent combining loss*, which was described and illustrated in Section 12-1.

Coding improves the performance of the FH spread spectrum system by an

amount, which we call the *coding gain*, that depends on the code parameters. Suppose we use a linear binary (n, k) block code and binary FSK modulation with one hop per coded bit for transmitting the bits. With soft-decision decoding of the square-law -demodulated FSK signal, the probability of a code word error is upper-bounded as

$$P_M \leq \sum_{m=2}^{M} P_2(m) \tag{13-3-4}$$

where $P_2(m)$ is the error probability in deciding between the mth code word and the all-zero code word when the latter has been transmitted. The expression for $P_2(m)$ was derived in Section 8-1-4 and has the same form as (13-3-2) and (13-3-3), with L being replaced by w_m and γ_b by $\gamma_b R_c w_m$, where w_m is the weight of the mth code word and R_c is the code rate. The product $R_c w_m$, which is not less than $R_c d_{\min}$, represents the coding gain. Thus, we have the performance of a block coded FH system with slow frequency hopping in broadband interference.

The probability of error for fast frequency hopping with n_2 hops per coded bit is obtained by reinterpreting the binary event probability $P_2(m)$ in (13-3-4). The n_2 hops per coded bit may be interpreted as a repetition code, which, when combined with a nontrivial (n_1, k) binary linear code having weight distribution $\{w_m\}$, yields an $(n_1 n_2, k)$ binary linear code with weight distribution $\{n_2 w_m\}$. Hence, $P_2(m)$ has the form given in (13-3-2), with L replaced by $n_2 w_m$ and γ_b by $\gamma_b R_c n_2 w_m$, where $R_c = k/n_1 n_2$. Note that $\gamma_b R_c n_2 w_m = \gamma_b w_m k/n_1$, which is just the coding gain obtained from the nontrivial (n_1, k) code. Consequently, the use of the repetition code will result in an increase in the noncoherent combining loss.

With hard-decision decoding and slow frequency hopping, the probability of a coded bit error at the output of the demodulator for noncoherent detection is

$$p = \tfrac{1}{2} e^{-\gamma_b R_c/2} \tag{13-3-5}$$

The code word error probability is easily upper-bounded, by use of the Chernoff bound, as

$$P_M \leq \sum_{m=2}^{M} [4p(1-p)]^{w_m/2} \tag{13-3-6}$$

However, if fast frequency hopping is employed with n_2 hops per coded bit, and the square-law-detected outputs from the corresponding matched filters for the n_2 hops are added as in soft-decision decoding to form the two decision variables for the coded bits, the bit error probability p is also given by (13-3-2), with L replaced by n_2 and γ_b replaced by $\gamma_b R_c n_2$, where R_c is the rate of the nontrivial (n_1, k) code. Consequently, the performance of the fast FH system in broadband interference is degraded relative to the slow FH system by an amount equal to the noncoherent combining loss of the signals received from the n_2 hops.

We have observed that for both hard-decision and soft-decision decoding, the use of the repetition code in a fast-frequency-hopping system yields no coding gain. The only coding gain obtained comes from the (n_1, k) block code. Hence, the repetition code is inefficient in a fast FH system with noncoherent combining. A more efficient coding method is one in which either a single low-rate binary code or a concatenated code is employed. Additional improvements in performance may be obtained by using nonbinary codes in conjunction with M-ary FSK. Bounds on the error probability for this case may be obtained from the results given in Section 12-1.

Although we have evaluated the performance of linear block codes only in the above discussion, it is relatively easy to derive corresponding performance results for binary convolutional codes. We leave as an exercise for the reader the derivation of the bit error probability for soft-decision Viterbi decoding and hard-decision Viterbi decoding of FH signals corrupted by broadband interference.

Finally, we observe that $\mathscr{E}_b$, the energy per bit, can be expressed as $\mathscr{E}_b = P_{av}/R$, where R is the information rate in bits per second and $J_0 = J_{av}/W$. Therefore, γ_b may be expressed as

$$\gamma_b = \frac{\mathscr{E}_b}{J_0} = \frac{W/R}{J_{av}/P_{av}} \tag{13-3-7}$$

In this expression, we recognize W/R as the processing gain and J_{av}/P_{av} as the jamming margin for the FH spread spectrum signal.

13-3-2 Performance of FH Spread Spectrum Signals in Partial-Band Interference

The partial-band interference considered in this subsection is modeled as a zero-mean gaussian random process with a flat power spectral density over a fraction α of the total bandwidth W and zero elsewhere. In the region or regions where the power spectral density is nonzero, its value is $\Phi_{zz}(f) = J_0/\alpha$, $0 < \alpha \leq 1$. This model of the interference may be applied to a jamming signal or to interference from other users in a FH CDMA system.

Suppose that the partial-band interference comes from a jammer who may select α to optimize the effect on the communications system. In an uncoded pseudo-randomly hopped (slow-hopping) FH system with binary FSK modulation and noncoherent detection, the received signal will be jammed with probability α and it will not be jammed with probability $1 - \alpha$. When it is jammed, the probability of error is $\frac{1}{2}\exp(-\mathscr{E}_b\alpha/2J_0)$, and when it is not jammed, the demodulation is error-free. Consequently, the average probability of error is

$$P_2(\alpha) = \tfrac{1}{2}\alpha \exp\left(-\frac{\alpha\mathscr{E}_b}{2J_0}\right) \tag{13-3-8}$$

where $\mathscr{E}_b/J_0$ may also be expressed as $(W/R)/(J_{av}/P_{av})$.

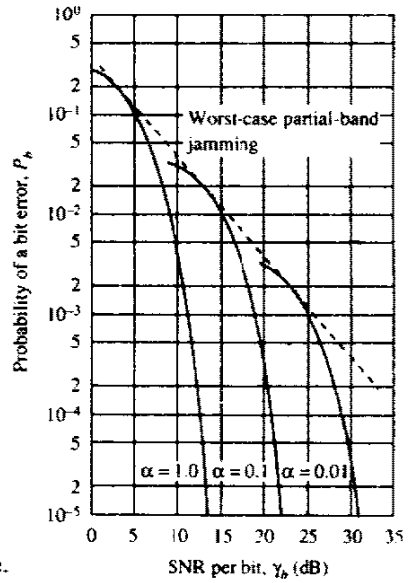

FIGURE 13-3-4 Performance of binary FSK with partial-band interference.

Figure 13-3-4 illustrates the error rate as a function of $\mathscr{E}_b/J_0$ for several values of α. The jammer's optimum strategy is to select the value of α that maximizes the error probability. By differentiating $P_2(\alpha)$ and solving for the extremum with the restriction that $0 \leq \alpha \leq 1$, we find that

$$\alpha^* = \begin{cases} \dfrac{1}{\mathscr{E}_b/2J_0} = 2\dfrac{J_{av}/P_{av}}{W/R} & (\mathscr{E}_b/J_0 \geq 2) \\ 1 & (\mathscr{E}_b/J_0 < 2) \end{cases} \tag{13-3-9}$$

The corresponding error probability for the worst-case partial-band jammer is

$$P_2 = \frac{e^{-1}}{\mathscr{E}_b/J_0} = \left[e\left(\frac{W/R}{J_{av}/P_{av}}\right)\right]^{-1} \tag{13-3-10}$$

Whereas the error probability decreases exponentially for full-band jamming, we now find that the error probability decreases only inversely with $\mathscr{E}_b/J_0$ for the worst-case partial-band jamming. This result is similar to the error rate performance of binary FSK in a Rayleigh fading channel (see Section 14-3) and to the uncoded DS spread spectrum system corrupted by worst-case pulse jamming (see Section 13-2-3).

As we shall demonstrate below, signal diversity obtained by means of coding provides a significant improvement in performance relative to uncoded signals. This same approach to signal design is also effective for signaling over a fading channel, as we shall demonstrate in Chapter 14.

To illustrate the benefits of diversity in a FH spread spectrum signal with partial-band interference, we assume that the same information symbol is

transmitted by binary FSK on L independent frequency hops. This may be accomplished by subdividing the signaling interval into L subintervals, as described previously for fast frequency hopping. After the hopping pattern is removed, the signal is demodulated by passing it through a pair of matched filters whose outputs are square-law-detected and sampled at the end of each subinterval. The square-law-detected signals corresponding to the L frequency hops are weighted and summed to form the two decision variables (metrics), which are denoted as U_1 and U_2.

When the decision variable U_1 contains the signal components, U_1 and U_2 may be expressed as

$$U_1 = \sum_{k=1}^{L} \beta_k |2\mathscr{E}_c + N_{1k}|^2$$
$$U_2 = \sum_{k=1}^{L} \beta_k |N_{2k}|^2 \qquad (13\text{-}3\text{-}11)$$

where $\{\beta_k\}$ represent the weighting coefficients, $\mathscr{E}_c$ is the signal energy per chip in the L-chip symbol, and $\{N_{jk}\}$ represent the additive gaussian noise terms at the output of the matched filters.

The coefficients are optimally selected to prevent the jammer from saturating the combiner should the transmitted frequencies be successfully hit in one or more hops. Ideally, β_k is selected to be equal to the reciprocal of the variance of the corresponding noise terms $\{N_k\}$. Thus, the noise variance for each chip is normalized to unity by this weighting and the corresponding signal is also scaled accordingly. This means that when the signal frequencies on a particular hop are jammed, the corresponding weight is very small. In the absence of jamming on a given hop, the weight is relatively large. In practice, for partial-bound noise jamming, the weighting may be accomplished by use of an AGC having a gain that is set on the basis of noise power measurements obtained from frequency bands adjacent to the transmitted tones. This is equivalent to having side information (knowledge of jammer state) at the decoder.

Suppose that we have broadband gaussian noise with power spectral density N_0 and partial-band interference, over αW of the frequency band, which is also gaussian with power spectral density J_0/α. In the presence of partial-band interference, the second moments of the noise terms N_{1k} and N_{2k} are

$$\sigma_k^2 = \tfrac{1}{2}E(|N_{1k}|^2) = \tfrac{1}{2}E(|N_{2k}|^2) = 2\mathscr{E}_c\left(N_0 + \frac{J_0}{\alpha}\right) \qquad (13\text{-}3\text{-}12)$$

In this case, we select $\beta_k = 1/\sigma_k^2 = [2\mathscr{E}_c(N_0 + J_0/\alpha)]^{-1}$. In the absence of partial-band interference, $\sigma_k^2 = 2\mathscr{E}_c N_0$ and, hence, $\beta_k = (2\mathscr{E}_c N_0)^{-1}$. Note that β_k is a random variable.

An error occurs in the demodulation if $U_2 > U_1$. Although it is possible to determine the exact error probability, we shall resort to the Chernoff bound,

which yields a result that is much easier to evaluate and interpret. Specifically, the Chernoff (upper) bounds in the error probability is

$$\begin{aligned} P_2 &= P(U_2 - U_1 > 0) \leq E\{\exp[\nu(U_2 - U_1)]\} \\ &= E\left\{\exp\left[-\nu \sum_{k=1}^{L} \beta_k (|2\mathscr{E}_c + N_{1k}|^2 - |N_{2k}|^2)\right]\right\} \end{aligned} \tag{13-3-13}$$

where ν is a variable that is optimized to yield the tightest possible bound.

The averaging in (13-3-13) is performed with respect to the statistics of the noise components and the statistics of the weighting coefficients $\{\beta_k\}$, which are random as a consequence of the statistical nature of the interference. Keeping the $\{\beta_k\}$ fixed and averaging over the noise statistics first, we obtain

$$\begin{aligned} P_2(\boldsymbol{\beta}) &= E\left[\exp\left(-\nu \sum_{k=1}^{L} \beta_k |2\mathscr{E}_c + N_{1k}|^2 + \nu \sum_{k=1}^{L} \beta_k |N_{2k}|^2\right)\right] \\ &= \prod_{k=1}^{L} E[\exp(-\nu\beta_k |2\mathscr{E}_c + N_{1k}|^2)] E[\exp(\nu\beta_k |N_{2k}|^2)] \\ &= \prod_{k=1}^{L} \frac{1}{1-4\nu^2} \exp\left(\frac{-4\mathscr{E}_c^2 \beta_k \nu}{1+2\nu}\right) \end{aligned} \tag{13-3-14}$$

Since the FSK tones are jammed with probability α, it follows that $\beta_k = [2\mathscr{E}(N_0 + J_0/\alpha)]^{-1}$ with probability α and $(2\mathscr{E}_c N_0)^{-1}$ with probability $1-\alpha$. Hence, the Chernoff bound is

$$\begin{aligned} P_2 &\leq \prod_{k=1}^{L} \left\{\frac{\alpha}{1-4\nu^2} \exp\left[\frac{-2\mathscr{E}_c \nu}{(N_0 + J_0/\alpha)(1+2\nu)}\right] + \frac{1-\alpha}{1-4\nu^2} \exp\left[\frac{-2\mathscr{E}_c \nu}{N_0(1+2\nu)}\right]\right\} \\ &= \left\{\frac{\alpha}{1-4\nu^2} \exp\left[\frac{-2\mathscr{E}_c \nu}{(N_0 + J_0/\alpha)(1+2\nu)}\right] + \frac{1-\alpha}{1-4\nu^2} \exp\left[\frac{-2\mathscr{E}_c \nu}{N_0(1+2\nu)}\right]\right\}^L \end{aligned} \tag{13-3-15}$$

The next step is to optimize the bound in (13-3-15) with respect to the variable ν. In its present form, however, the bound is messy to manipulate. A significant simplification occurs if we assume that $J_0/\alpha \gg N_0$, which renders the second term in (13-3-15) negligible compared with the first. Alternatively, we let $N_0 = 0$, so that the bound on P_2 reduces to

$$P_2 \leq \left\{\frac{\alpha}{1-4\nu^2} \exp\left[\frac{-2\alpha\nu\mathscr{E}_c}{J_0(1+2\nu)}\right]\right\}^L \tag{13-3-16}$$

The minimum value of this bound with respect to ν and the maximum with respect to α (worst-case partial-band interference) is easily shown to occur when $\alpha = 3J_0/\mathscr{E}_c \leq 1$ and $\nu = \frac{1}{4}$. For these values of the parameters, (13-3-16) reduces to

$$P_2 \leq P_2(L) = \left(\frac{4}{e\gamma_c}\right)^L = \left(\frac{1.47}{\gamma_c}\right)^L, \qquad \gamma_c = \frac{\mathscr{E}_c}{J_0} = \frac{\mathscr{E}_b}{LJ_0} \geq 3 \tag{13-3-17}$$

where γ_c is the SNR per chip in the L-chip symbol. Equivalently,

$$P_2 \leq \left[\frac{1.47(J_{av}/P_{av})}{W/R}\right]^L, \quad \frac{W/R}{L(J_{av}/P_{av})} \geq 3 \tag{13-3-18}$$

The result in (13-3-17) was first derived by Viterbi and Jacobs (1975).

We observe that the probability of error for the worst-case partial-band interference decreases exponentially with an increase in the SNR per chip γ_c. This result is very similar to the performance characteristics of diversity techniques for Rayleigh fading channels (see Section 14-4). We may express the right-hand side of (13-3-17) in the form

$$P_2(L) = \exp[-\gamma_b h(\gamma_c)] \tag{13-3-19}$$

where the function $h(\gamma_c)$ is defined as

$$h(\gamma_c) = -\frac{1}{\gamma_c}\left[\ln\left(\frac{4}{\gamma_c}\right) - 1\right] \tag{13-3-20}$$

A plot of $h(\gamma_c)$ is given in Fig. 13-3-5. We observe that the function has a maximum value of $\frac{1}{4}$ at $\gamma_c = 4$. Consequently, there is an optimum SNR per chip of $10 \log \gamma_c = 6$ dB. At the optimum SNR, the error rate is upper-bounded as

$$P_2 \leq P_2(L_{opt}) = e^{-\gamma_b/4} \tag{13-3-21}$$

When we compare the error probability bound in (13-3-21) with the error probability for binary FSK in spectrally flat noise, which is given by (13-3-1), we see that the combined effect of worst-case partial-band interference and the noncoherent combining loss in the square-law combining of the L chips is 3 dB. We emphasize, however, that for a given $\mathscr{E}_b/J_0$, the loss is greater when the order of diversity is not optimally selected.

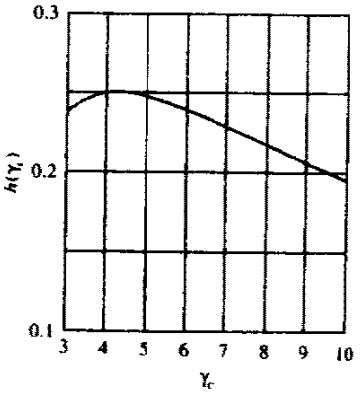

FIGURE 13-3-5 Graph of the function $h(\gamma_c)$.

Coding provides a means for improving the performance of the frequency-hopped system corrupted by partial-band interference. In particular, if a block orthogonal code is used, with $M = 2^k$ code words and Lth-order diversity per code word, the probability of a code word error is upper-bounded as

$$P_M \leq (2^k - 1)P_2(L) = (2^k - 1)\left(\frac{1.47}{\gamma_c}\right)^L = (2^k - 1)\left(\frac{1.47}{k\gamma_b/L}\right)^L \quad (13\text{-}3\text{-}22)$$

and the equivalent bit error probability is upper-bounded as

$$P_b \leq 2^{k-1}\left(\frac{1.47}{k\gamma_b/L}\right)^L \quad (13\text{-}3\text{-}23)$$

Figure 13-3-6 illustrates the probability of a bit error for $L = 1, 2, 4, 8$ and

FIGURE 13-3-6 Performance of binary and octal FSK with L-order diversity for a channel with worst-case partial-band interference.

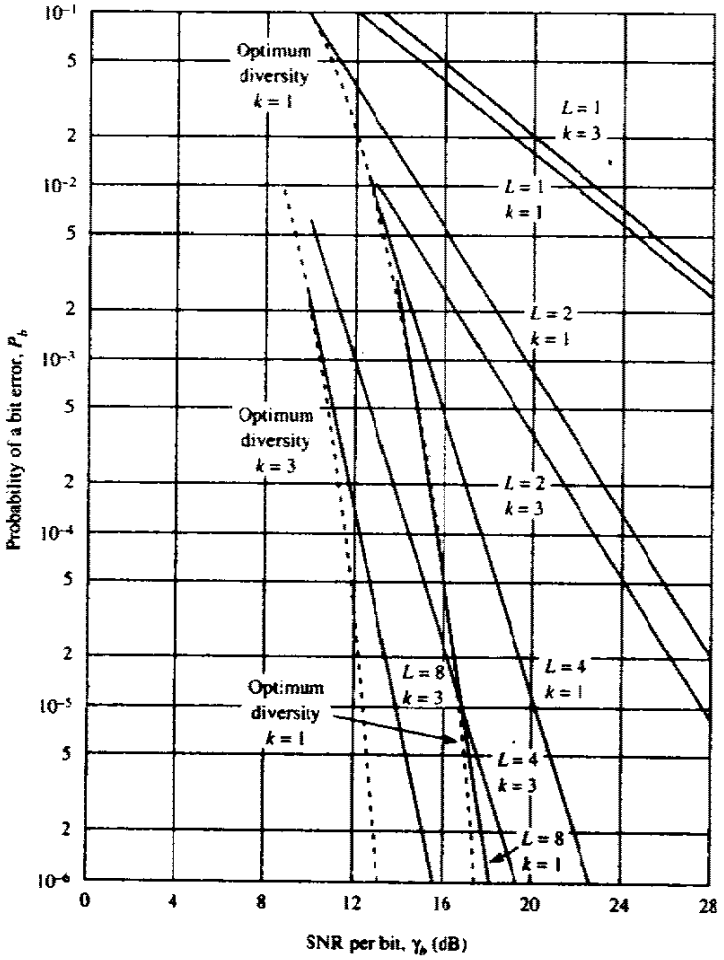

$k = 1, 3$. With an optimum choice of diversity, the upper bound can be expressed as

$$P_b \leq 2^{k-1} \exp(-\tfrac{1}{4}k\gamma_b) = \tfrac{1}{2}\exp[-k(\tfrac{1}{4}\gamma_b - \ln 2)] \qquad (13\text{-}3\text{-}24)$$

Thus, we have an improvement in performance by an amount equal to $10 \log [k(1 - 2.77/\gamma_b)]$. For example, if $\gamma_b = 10$ and $k = 3$ (octal modulation) then the gain is 3.4 dB, while if $k = 5$ then the gain is 5.6 dB.

Additional gains can be achieved by employing concatenated codes in conjunction with soft-decision decoding. In the example below, we employ a dual-k convolutional code as the outer code and a Hadamard code as the inner code on the channel with partial-band interference.

Example 13-3-1

Suppose we use a Hadamard $H(n, k)$ constant weight code with on-off keying (OOK) modulation for each code bit. The minimum distance of the code is $d_{\min} = \frac{1}{2}n$, and, hence, the effective order of diversity obtained with OOK modulation is $\frac{1}{2}d_{\min} = \frac{1}{4}n$. There are $\frac{1}{2}n$ frequency-hopped tones transmitted per code word. Hence,

$$\gamma_c = \frac{k}{\frac{1}{2}n}\gamma_b = 2R_c\gamma_b \qquad (13\text{-}3\text{-}25)$$

when this code is used alone. The bit error rate performance for soft-decision decoding of these codes for the partial-band interference channel is upper-bounded as

$$P_b \leq 2^{k-1}P_2(\tfrac{1}{2}d_{\min}) = 2^{k-1}\left(\frac{1.47}{2R_c\gamma_b}\right)^{n/4} \qquad (13\text{-}3\text{-}26)$$

Now, if a Hadamard (n, k) code is used as the inner code and a rate 1/2 dual-k convolutional code (see Section 8-2-6) is the outer code, the bit error performance in the presence of worst-case partial-band interference is (see (8-2-40))

$$P_b \leq \frac{2^{k-1}}{2^k - 1}\sum_{m=4}^{\infty}\beta_m P_2(\tfrac{1}{2}md_{\min}) = \frac{2^{k-1}}{2^k - 1}\sum_{m=4}^{\infty}\beta_m P_2(\tfrac{1}{4}mn) \qquad (13\text{-}3\text{-}27)$$

where $P_2(L)$ is given by (13-3-17) with

$$\gamma_c = \frac{k}{n}\gamma_b = R_c\gamma_b \qquad (13\text{-}3\text{-}28)$$

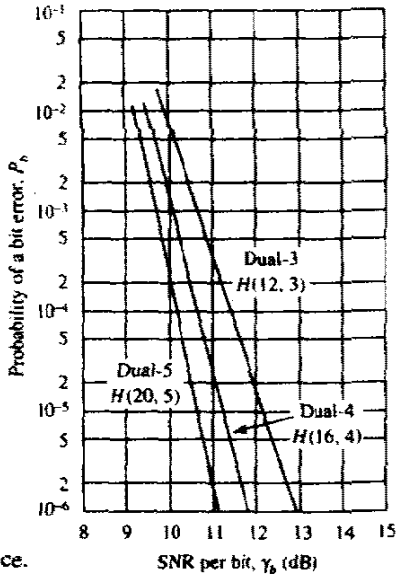

FIGURE 13-3-7 Performance of dual-k codes concatenated with Hadamard codes for a channel with worst-case partial-band interference.

Figure 13-3-7 illustrates the performance of the dual-k codes for $k = 5$, 4, and 3 concatenated with the Hadamard $H(20, 5)$, $H(16, 4)$, and $H(12, 3)$ codes, respectively.

In the above discussion, we have focused on soft-decision decoding. On the other hand, the performance achieved with hard-decision decoding is significantly (several decibels) poorer than that obtained with soft-decision decoding. In a concatenated coding scheme, however, a mixture involving soft-decision decoding of the inner code and hard-decision decoding of the outer code represents a reasonable compromise between decoding complexity and performance.

Finally, we wish to indicate that another serious threat in a FH spread spectrum system is partial-band multitone jamming. This type of interference is similar in effect to partial-band spectrally flat noise jamming. Diversity obtained through coding is an effective means for improving the performance of the FH system. An additional improvement is achieved by properly weighting the demodulator outputs so as to suppress the effects of the jammer.

13-3-3 A CDMA System Based on FH Spread Spectrum Signals

In Section 13-2-2, we considered a CDMA system based on use of DS spread spectrum signals. As previously indicated, it is also possible to have a CDMA system based on FH spread spectrum signals. Each transmitter–receiver pair in such a system is assigned its own pseudo-random frequency-hopping pattern.

Aside from this distinguishing feature, the transmitters and receivers of all the users may be identical in that they may have identical encoders, decoders, modulators, and demodulators.

CDMA systems based on FH spread spectrum signals are particularly attractive for mobile (land, air, sea) users because timing requirements are not as stringent as in a PN spread spectrum signal. In addition, frequency synthesis techniques and associated hardware have been developed that make it possible to frequency-hop over bandwidths that are significantly larger than those currently possible with DS spread spectrum systems. Consequently, larger processing gains are possible with FH. The capacity of CDMA with FH is also relatively high. Viterbi (1978) has shown that with dual-k codes and M-ary FSK modulation, it is possible to accomodate up to $\frac{3}{8}W/R$ simultaneous users who transmit at an information rate R bits/s over a channel with bandwidth W.

One of the earliest CDMA systems based on FH coded spread spectrum signals was built to provide multiple-access tactical satellite communications for small mobile (land, sea, air) terminals each of which transmitted relatively short messages over the channel intermittently. The system was called the *Tactical Transmission System* (TATS) and it is described in a paper by Drouilhet and Bernstein (1969).

An octal Reed–Solomon (7, 2) code is used in the TATS system. Thus, two 3 bit information symbols from the input to the encoder are used to generate a seven-symbol code word. Each 3 bit coded symbol is transmitted by means of octal FSK modulation. The eight possible frequencies are spaced $1/T_c$ Hz apart, where T_c is the time (chip) duration of a single frequency transmission. In addition to the seven symbols in a code word, an eighth symbol is included. That symbol and its corresponding frequency are fixed and transmitted at the beginning of each code word for the purpose of providing timing and frequency synchronization† at the receiver. Consequently, each code word is transmitted in $8T_c$ s.

TATS was designed to transmit at information rates of 75 and 2400 bits/s. Hence, $T_c = 10$ ms and 312.5 μs, respectively. Each frequency tone corresponding to a code symbol is frequency-hopped. Hence, the hopping rate is 100 hops/s at the 75 bits/s rate and 3200 hops/s at the 2400 bits/s rate.

There are $M = 2^6 = 64$ code words in the Reed–Solomon (7, 2) code and the minimum distance of the code is $d_{\min} = 6$. This means that the code provides an effective order of diversity equal to 6.

At the receiver, the received signal is first dehopped and then demodulated by passing it through a parallel bank of eight matched filters, where each filter is tuned to one of the eight possible frquencies. Each filter output is envelope-detected, quantized to 4 bits (one of 16 levels), and fed to the decoder. The decoder takes the 56 filter outputs corresponding to the

† Since mobile users are involved, there is a Doppler frequency offset associated with transmission. This frequency offset must be tracked and compensated for in the demodulation of the signal. The sync symbol is used for this purpose.

reception of each seven-symbol code word and forms 64 decision variables corresponding to the 64 possible code words in the (7, 2) code by linearly combining the appropriate envelope detected outputs. A decision is made in favor of the code word having the largest decision variable.

By limiting the matched filter outputs to 16 levels, interference (crosstalk) from other users of the channel causes a relatively small loss in performance (0.75 dB with strong interference on one chip and 1.5 dB with strong interference on two chips out of the seven). The AGC used in TATS has a time constant greater than the chip interval T_c, so that no attempt is made to perform optimum weighting of the demodulator outputs as described in Section 13-3-2.

The derivation of the error probability for the TATS signal in AWGN and worst-case partial-band interference is left as an exercise for the reader (Problems 13-23 and 13-24).

13-4 OTHER TYPES OF SPREAD SPECTRUM SIGNALS

DS and FH are the most common forms of spread spectrum signals used in practice. However, other methods may be used to introduce pseudo-randomness in a spread spectrum signal. One method, which is analogous to FH, is *time* hopping (TH). In TH, a time interval, which is selected to be much larger than the reciprocal of the information rate, is subdivided into a large number of time slots. The coded information symbols are transmitted in a pseudo-randomly selected time slot as a block of one or more code words. PSK modulation may be used to transmit the coded bits.

For example, suppose that a time interval T is subdivided into 1000 time slots of width $T/1000$ each. With an information bit rate of R bits/s, the number of bits to be transmitted in T s is RT. Coding increases this number to RT/R_c bits, where R_c is the coding rate. Consequently, in a time interval of $T/1000$ s, we must transmit RT/R_c bits. If binary PSK is used as the modulation method, the bit rate is $1000R/R_c$ and the bandwidth required is approximately $W = 1000R/R_c$.

A block diagram of a transmitter and a receiver for a TH spread spectrum system is shown in Fig. 13-4-1. Due to the burst characteristics of the transmitted signal, buffer storage must be provided at the transmitter in a TH system, as shown in Fig. 13-4-1. A buffer may also be used at the receiver to provide a uniform data stream to the user.

Just as partial-band interference degrades an uncoded FH spread spectrum system, partial-time (pulsed) interference has a similar effect on a TH spread spectrum system. Coding and interleaving are effective means for combatting this type of interference, as we have already demonstrated for FH and DS systems. Perhaps the major disadvantage of a TH system is the stringent timing requirements compared not only with FH but, also, with DS.

Other types of spread spectrum signals can be obtained by combining DS,

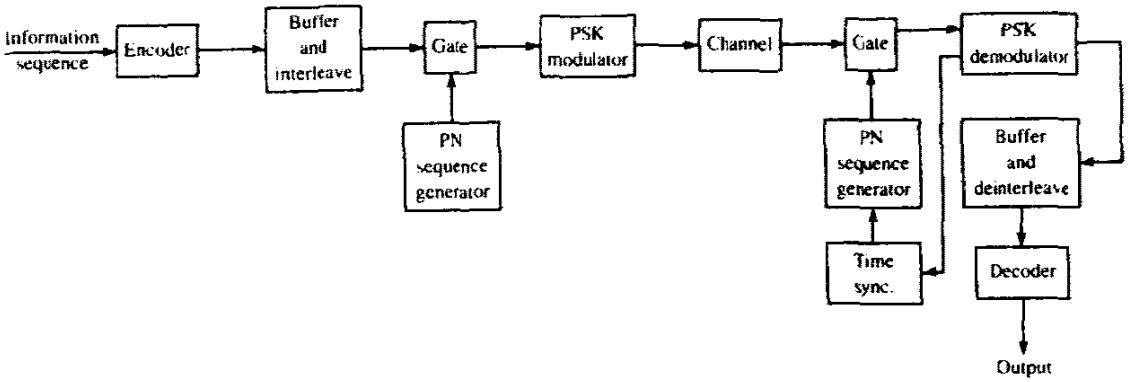

FIGURE 13-4-1 Block diagram of time-hopping (TH) spread spectrum system.

FH, and TH. For example, we may have a hybrid DS/FH, which means that a PN sequence is used in combination with frequency hopping. The signal transmitted on a single hop consists of a DS spread spectrum signal which is demodulated coherently. However, the received signals from different hops are combined noncoherently (envelope or square-law combining). Since coherent detection is performed within a hop, there is an advantage obtained relative to a pure FH system. However, the price paid for the gain in performance is an increase in complexity, greater cost, and more stringent timing requirements.

Another possible hybrid spread spectrum signal is DS/TH. This does not seem to be as practical as DS/FH, primarily because of an increase in system complexity and more stringent timing requirements.

13-5 SYNCHRONIZATION OF SPREAD SPECTRUM SYSTEMS

Time synchronization of the receiver to the received spread spectrum signal may be separated into two phases. There is an initial acquisition phase and a tracking phase after the signal has been initially acquired.

Acquisition In a direct sequence spread spectrum system, the PN code must be time-synchronized to within a small fraction of the chip interval $T_c \approx 1/W$. The problem of initial synchronization may be viewed as one in which we attempt to synchronize in time the receiver clock to the transmitter clock. Usually, extremely accurate and stable time clocks are used in spread spectrum systems. Consequently, accurate time clocks result in a reduction of the time uncertainty between the receiver and the transmitter. However, there is always an initial timing uncertainty due to range uncertainty between the transmitter and the receiver. This is especially a problem when communication is taking place between two mobile users. In any case, the usual procedure for establishing initial synchronization is for the transmitter to send a known

pseudo-random data sequence to the receiver. The receiver is continuously in a search mode looking for this sequence in order to establish initial synchronization.

Let us suppose that the initial timing uncertainty is T_u and the chip duration is T_c. If initial synchronization is to take place in the presence of additive noise and other interference, it is necessary to dwell for $T_d = NT_c$ in order to test synchronism at each time instant. If we search over the time uncertainty interval in (coarse) time steps of $\frac{1}{2}T_c$ then the time required to establish initial synchronization is

$$T_{init\ sync} = \frac{T_u}{\frac{1}{2}T_c} NT_c = 2NT_u \tag{13-5-1}$$

Clearly, the synchronization sequence transmitted to the receiver must be at least as long as $2NT_c$ in order for the receiver to have sufficient time to perform the necessary search in a serial fashion.

In principle, matched filtering or cross-correlation are optimum methods for establishing initial synchronization. A filter matched to the known data waveform generated from the known pseudo-random sequence continuously looks for exceedence of a predetermined threshold. When this occurs, initial synchronization is established and the demodulator enters the "data receive" mode.

Alternatively, we may use a *sliding correlator* as shown in Fig. 13-5-1. The correlator cycles through the time uncertainty, usually in discrete time intervals of $\frac{1}{2}T_c$, and correlates the received signal with the known synchronization sequence. The cross-correlation is performed over the time interval NT_c (N chips) and the correlator output is compared with a threshold to determine if the known signal sequence is present. If the threshold is not exceeded, the known reference sequence is advanced in time by $\frac{1}{2}T_c$ s and the correlation process is repeated. These operations are performed until a signal is detected or until the search has been performed over the time uncertainty interval T_u. In the latter case, the search process is then repeated.

A similar process may also be used for FH signals. In this case, the problem is to synchronize the PN code that controls the hopped frequency pattern. To accomplish this initial synchronization, a known frequency hopped signal is

FIGURE 13-5-1 A sliding correlator for DS signal acquisition.

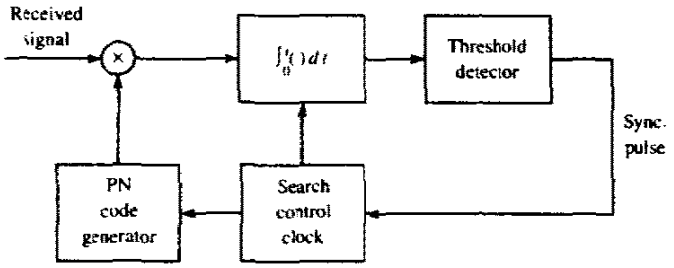

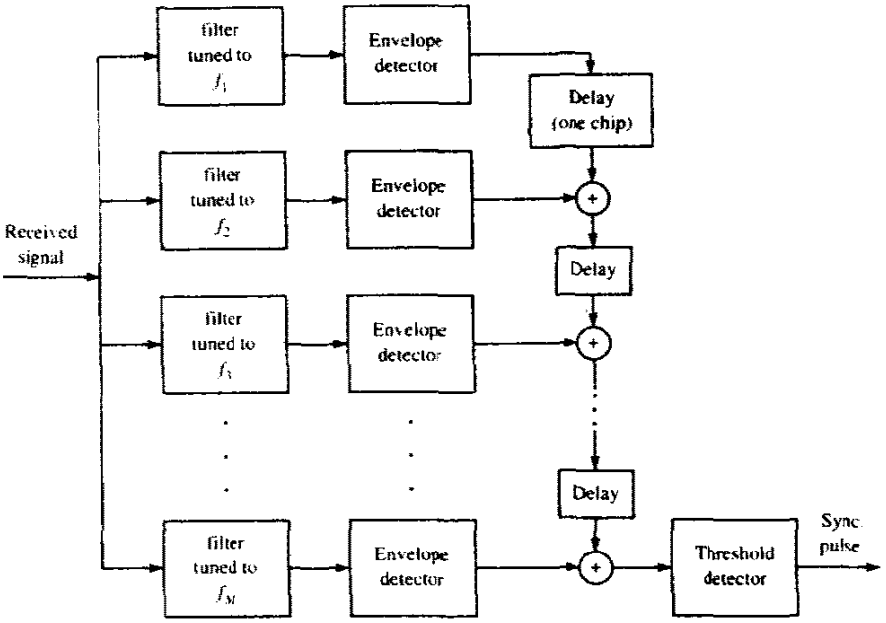

FIGURE 13-5-2 System for acquisition of a FH signal.

transmitted to the receiver. The initial acquisition system at the receiver looks for this known FH signal pattern. For example, a bank of matched filters tuned to the transmitted frequencies in the known pattern may be employed. Their outputs must be properly delayed, envelope- or square-law-detected, weighted, if necessary, and added (noncoherent integration) to produce the signal output which is compared with a threshold. A signal present is declared when the threshold is exceeded. The search process is usually performed continuously in time until a threshold is exceeded. A block diagram illustrating this signal acquisition scheme is given in Fig. 13-5-2. As an alternative, a single matched-filter–envelope detector pair may be used, preceded by a frequency-hopping pattern generator and followed by a post-detection integrator and a threshold detector. This configuration, shown in Fig. 13-5-3, is based on a serial search and is akin to the sliding correlator for DS spread spectrum signals.

The sliding correlator for the DS signals or its counterpart shown in Fig. 13-5-3 for FH signals basically perform a serial search that is generally time-consuming. As an alternative, one may introduce some degree of parallelism by having two or more such correlators operating in parallel and searching over nonoverlapping time slots. In such a case, the search time is reduced at the expense of a more complex and costly implementation. Figure 13-5-2 represents such a parallel realization for the FH signals.

During the search mode, there may be false alarms that occur at the designed false alarm rate of the system. To handle the occasional false alarms, it is necessary to have an additional method or circuit that checks to confirm

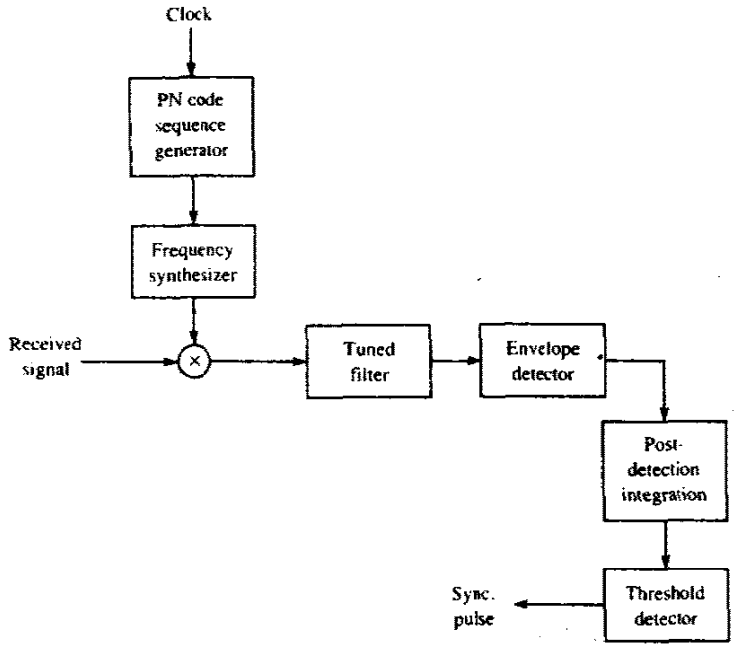

FIGURE 13-5-3 Alternative system for acquisition of a FH signal.

that the received signal at the output of the correlator remains above the threshold. With such a detection strategy, a large noise pulse that causes a false alarm will cause only a temporary exceedence of the threshold. On the other hand, when a signal is present, the correlator or matched filter output will stay above the threshold for the duration of the transmitted signal. Thus, if confirmation fails, the search is resumed.

Another initial search strategy, called a *sequential search*, has been investigated by Ward (1965, 1977). In this method, the dwell time at each delay in the search process is made variable by employing a correlator with a variable integration period whose (biased) output is compared with two thresholds. Thus, there are three possible decisions:

1 if the upper threshold is exceed by the correlator output, initial synchronization is declared established;

2 if the correlator output falls below the lower threshold, the signal is declared absent at that delay and the search process resumes at a different delay;

3 if the correlator output falls between the two thresholds, the integration time is increased by one chip and the resulting output is compared with the two thresholds again.

Hence, steps 1, 2, and 3 are repeated for each chip interval until the correlator output either exceeds the upper threshold or falls below the lower threshold.

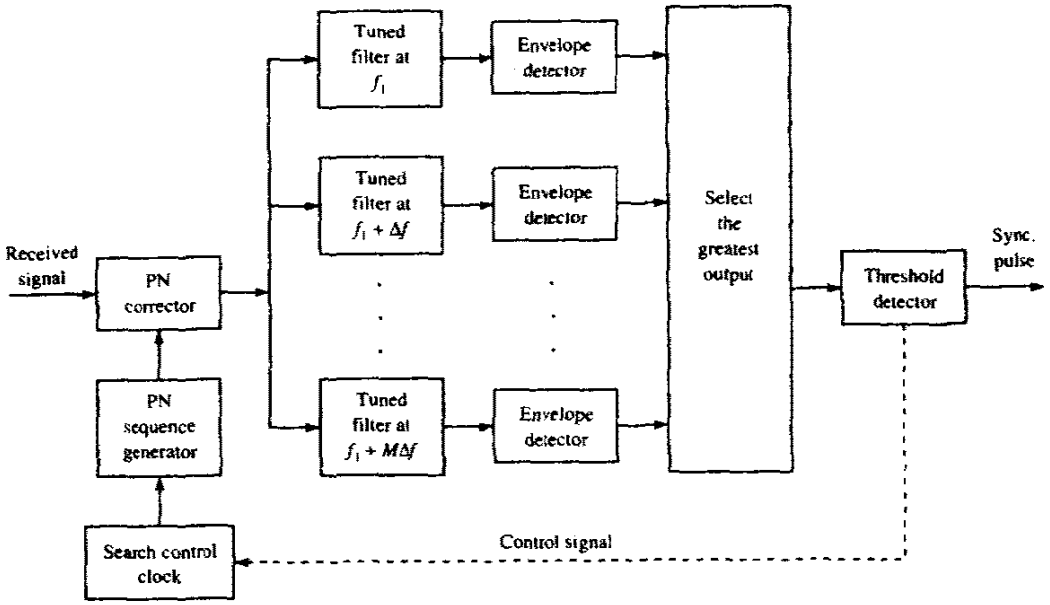

FIGURE 13-5-4 Initial search for Doppler frequency offset in a DS system.

The sequential search method falls in the class of sequential estimation methods proposed by Wald (1947), which are known to result in a more efficient search in the sense that the average search time is minimized. Hence, the search time for a sequential search is less than that for the fixed dwell time integrator.

In the above discussion, we have considered only time uncertainty in establishing initial synchronization. However, another aspect of initial synchronization is frequency uncertainty. If the transmitter and/or the receiver are mobile, the relative velocity between them results in a Doppler frequency shift in the received signal relative to the transmitted signal. Since the receiver does not usually know the relative velocity, a priori, the Doppler frequency shift is unknown and must be determined by means of a frequency search method. Such a search is usually accomplished in parallel over a suitably quantized frequency uncertainty interval and serially over the time uncertainty interval. A block diagram of this scheme is shown in Fig. 13-5-4. Appropriate Doppler frequency search methods can also be devised for FH signals.

Tracking Once the signal is acquired, the initial search process is stopped and fine synchronization and tracking begins. The tracking maintains the PN code generator at the receiver in synchronism with the incoming signal. Tracking includes both fine chip synchronization and, for coherent demodulation, carrier phase tracking.

The commonly used tracking loop for a DS spread spectrum signal is the

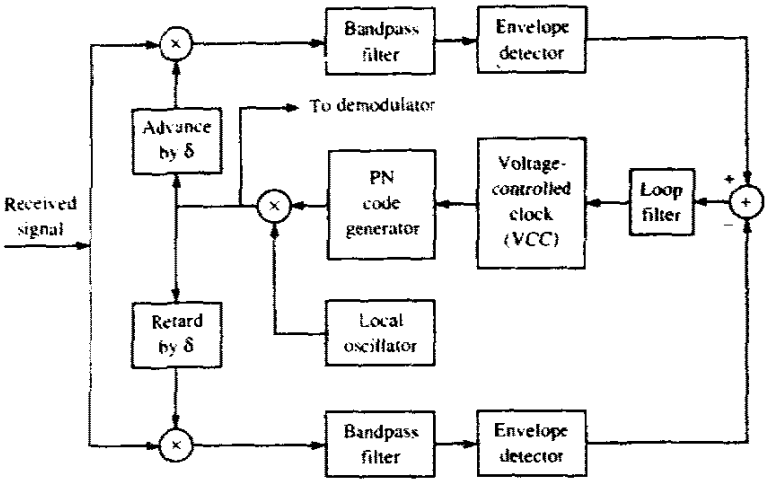

FIGURE 13-5-5 Delay-locked loop (DLL) for PN code tracking.

delay-locked loop (DLL), which is shown in Fig. 13-5-5. In this tracking loop, the received signal is applied to two multipliers, where it is multiplied by two outputs from the local PN code generator, which are delayed relative to each other by an amount $2\delta \leq T_c$. Thus, the product signals are the cross-correlations between the received signal and the PN sequence at the two values of delay. These products are bandpass-filtered and envelope- (or square-law-) detected and then subtracted. This difference signal is applied to the loop filter that drives the voltage controlled clock (VCC). The VCC serves as the clock for the PN code signal generator.

If the synchronism is not exact, the filtered output from one correlator will exceed the other and the VCC will be appropriately advanced or delayed. At the equilibrium point, the two filtered correlator outputs will be equally displaced from the peak value, and the PN code generator output will be exactly synchronized to the received signal that is fed to the demodulator. We observe that this implementation of the DLL for tracking a DS signal is equivalent to the early–late gate bit tracking synchronizer previously discussed in Section 6-3-2 and shown in Fig. 6-3-5.

An alternative method for time tracking a DS signal is to use a *tau-dither loop* (TDL), illustrated by the block diagram in Fig. 13-5-6. The TDL employs a single "arm" instead of the two "arms" shown in Fig. 13-5-5. By providing a suitable gating waveform, it is possible to make this "single-arm" implementation appear to be equivalent to the "two-arm" realization. In this case, the cross-correlation is regularly sampled at two values of delay, by stepping the code clock forward or backward in time by an amount δ. The envelope of the cross-correlation that is sampled at $\pm\delta$ has an amplitude modulation whose phase relative to the tau-dither modulator determines the sign of the tracking error.

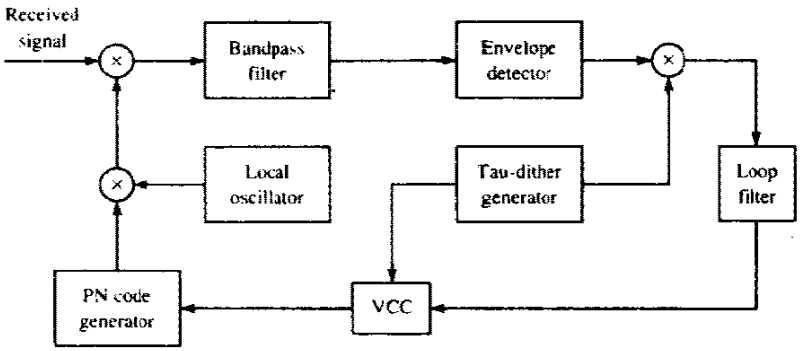

FIGURE 13-5-6 Tau-dither loop (TDL).

A major advantage of the TDL is the less costly implementation resulting from elimination of one of the two arms that are employed in the conventional DLL. A second and less apparent advantage is that the TDL does not suffer from performance degradation that is inherent in the DLL when the amplitude gain in the two arms is not properly balanced.

The DLL (and its equivalent, the TDL) generate an error signal by sampling the signal correlation function at $\pm\delta$ off the peak as shown in Fig. 13-5-7(*a*). This generates an error signal as shown in Fig. 13-5-7(*b*). The analysis of the performance of the DLL is similar to that for the phase-locked loop (PLL) carried out in Section 6-3. If it were not for the envelope detectors in the two arms of the DLL, the loop would resemble a Costas loop. In general, the variance of the time estimation error in the DLL is inversely proportional to the loop SNR, which depends on the input SNR to the loop and the loop bandwidth. Its performance is somewhat degraded as in the squaring PLL by the nonlinearities inherent in the envelope detectors, but this degradation is relatively small.

FIGURE 13-5-7 Autocorrelation function and tracking error signal for DLL.

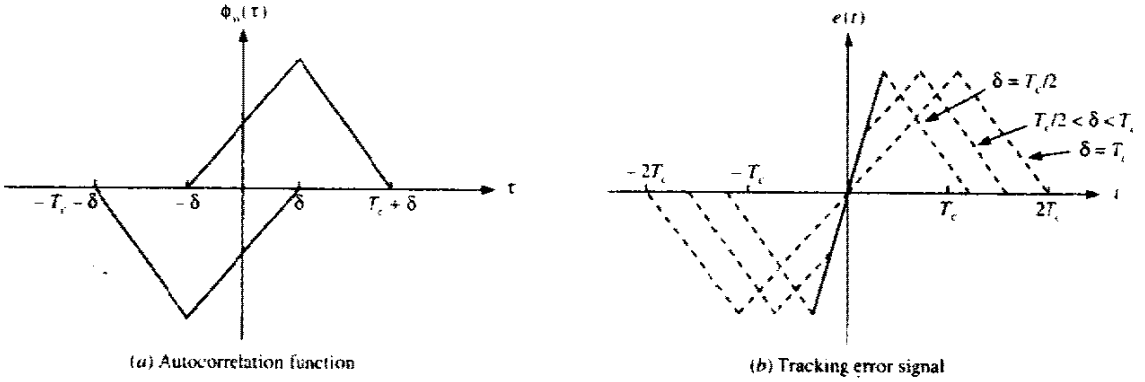

(*a*) Autocorrelation function

(*b*) Tracking error signal

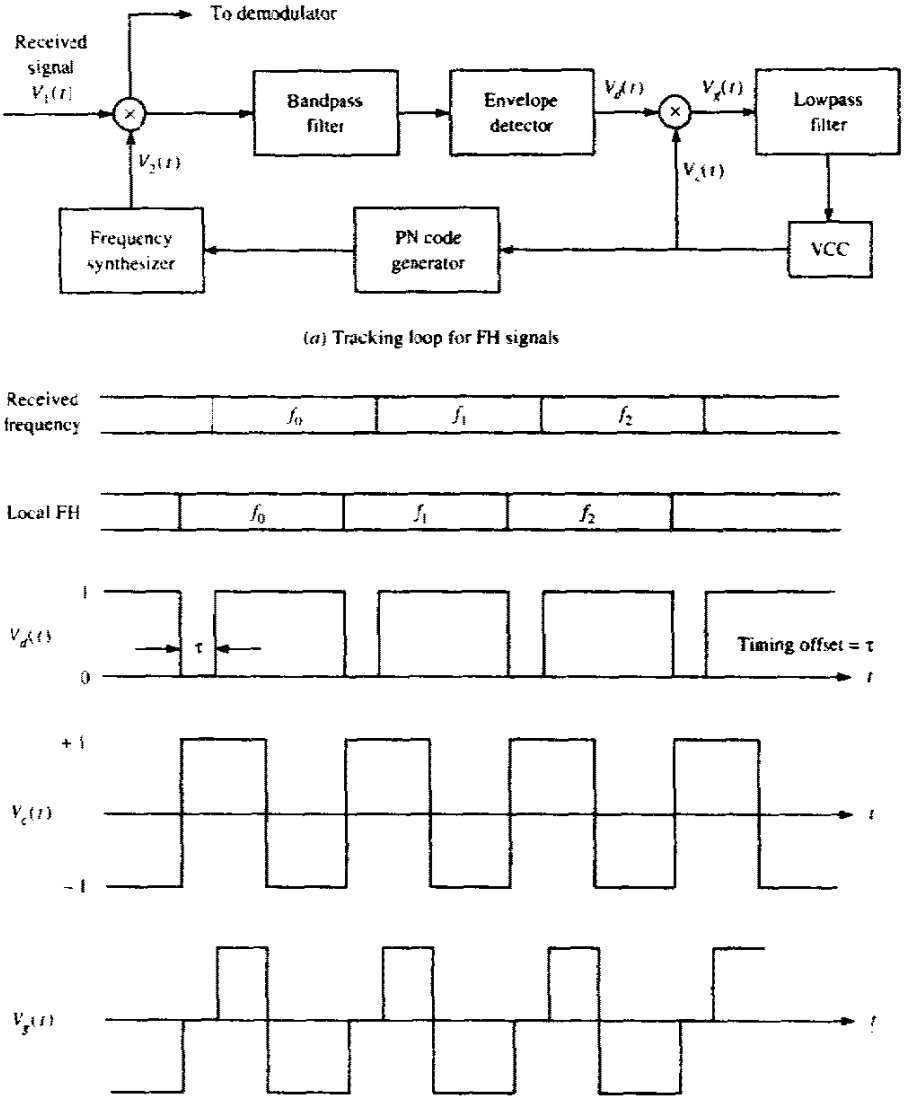

(*a*) Tracking loop for FH signals

(*b*) Wavefront for tracking an FH signal

FIGURE 13-5-8 Trracking method for FH signals. [*From Pickholtz* et al. *(1982). © 1982 IEEE.*]

A typical tracking technique for FH spread spectrum signals is illustrated in Fig. 13-5-8(*a*). This method is also based on the premise that, although initial acquisition has been achieved, there is a small timing error between the received signal and the receiver clock. The bandpass filter is tuned to a single intermediate frequency and its bandwidth is of the order of $1/T_c$, where T_c is the chip interval. Its output is envelope-detected and then multiplied by the clock signal to produce a three-level signal, as shown in Fig. 13-5-8(*b*), which

drives the loop filter. Note that when the chip transitions from the locally generated sinusoidal waveform do not occur at the same time as the transitions in the incoming signal, the output of the loop filter will be either negative or positive, depending on whether the VCC is lagging or advanced relative to the timing of the input signal. This error signal from the loop filter will provide the control signal for adjusting the VCC timing signal so as to drive the frequency synthesized pulsed sinusoid to proper synchronism with the received signal.

13-6 BIBLIOGRAPHICAL NOTES AND REFERENCES

The introductory treatment of spread spectrum signals and their performance that we have given in this chapter is necessarily brief. Detailed and more specialized treatments of signal acquisition techniques, code tracking methods, and hybrid spread spectrum systems, as well as other general topics on spread spectrum signals and systems, can be found in the vast body of technical literature that now exists on the subject.

Historically, the primary application of spread spectrum communications has been in the development of secure (AJ) digital communication systems for military use. In fact, prior to 1970, most of the work on the design and development of spread spectrum communications was classified. Since then, this trend has been reversed. The open literature now contains numerous publications on all aspects of spread spectrum signal analysis and design. Moreover, we have recently seen publications dealing with the application of spread spectrum signaling techniques to commercial communications such as interoffice radio communications (see Pahlavan, 1985) and mobile-user radio communications (see Yue, 1983).

A historical perspective on the development of spread spectrum communication systems covering the period 1920–1960 is given in a paper by Scholtz (1982). Tutorial treatments focusing on the basic concepts are found in the papers by Scholtz (1977) and Pickholtz *et al.* (1982). These papers also contain a large number of references to previous work. In addition, there are two papers by Viterbi (1979, 1985) that provide a basic review of the performance characteristics of DS and FH signaling techniques.

Comprehensive treatments of various aspects of analysis and design of spread spectrum signals and systems, including synchronization techniques are now available in the texts by Simon *et al.* (1985), Ziemer and Peterson (1985), and Holmes (1982). In addition to these texts, there are several special issues of the *IEEE Transactions on Communications* devoted to spread spectrum communications (August 1977 and May 1982) and the *IEEE Transactions on Selected Areas in Communication* (September 1985, May 1989, May 1990, and June 1993). These issues contain a collection of papers devoted to a variety of topics, including multiple access techniques, synchronization techniques, and performance analyses with various types of interference. A number of important papers that have been published in IEEE journals have also been reprinted in book form by the IEEE Press (Dixon, 1976; Cook *et al.* 1983).

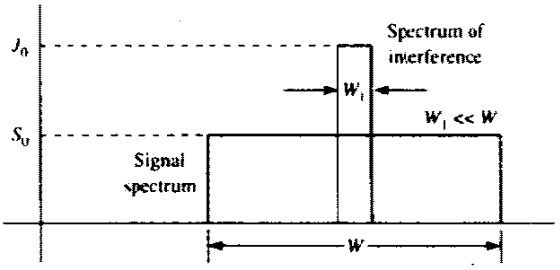

FIGURE P13-2

Finally, we recommend the book by Golomb (1967) as a basic reference on shift register sequences for the reader who wishes to delve deeper into this topic.

PROBLEMS

13-1 Following the procedure outlined in Example 13-2-2, determine the error rate performance of a DS spread spectrum system in the presence of CW jamming when the signal pulse is

$$g(t) = \sqrt{\frac{16\mathscr{E}_c}{3T_c}} \cos^2\left[\frac{\pi}{T_c}(t - \tfrac{1}{2}T_c)\right], \quad 0 \le t \le T_c$$

13-2 The sketch in Fig. P13-2 illustrates the power spectral densities of a PN spread spectrum signal and narrowband interference in an uncoded (trivial repetition code) digital communication system. Referring to Fig. 13-2-6, which shows the demodulator for this signal, sketch the (approximate) spectral characteristics of the signal and the interference after the multiplication of $r(t)$ with the output of the PN generator. Determine the fraction of the total interference that appears at the output of the correlator when the number of PN chips per bit is L_c.

13-3 Consider the concatenation of a Reed-Solomon (31, 3) ($q = 32$-ary alphabet) as the outer code with a Hadamard (16, 5) binary code as the inner code in a DS spread spectrum system. Assume that soft-decision decoding is performed on both codes. Determine an upper (union) bound on the probability of a bit error based on the minimum distance of the concatenated code.

13-4 The Hadamard $(n, k) = (2^m, m + 1)$ codes are low-rate codes with $d_{\min} = 2^{m-1}$. Determine the performance of this class of codes for DS spread spectrum signals with binary PSK modulation and either soft-decision or hard-decision decoding.

13-5 A rate 1/2 convolutional code with $d_{\text{free}} = 10$ is used to encode a data sequence occurring at a rate of 1000 bits/s. The modulation is binary PSK. The DS spread-spectrum sequence has a chip rate of 10 MHz.

a Determine the coding gain.

b Determine the processing gain.

c Determine the jamming margin assuming an $\mathscr{E}_b/J_0 = 10$.

13-6 A total of 30 equal-power users are to share a common communication channel by CDMA. Each user transmits information at a rate of 10 kbits/s via DS spread-spectrum and binary PSK. Determine the minimum chip rate to obtain a bit error

probability of 10^{-5}. Additive noise at the receiver may be ignored in this computation.

13-7 A CDMA system is designed based on DS spread spectrum with a processing gain of 1000 and binary PSK modulation. Determine the number of users if each user has equal power and the desired level of performance is an error probability of 10^{-6}. Repeat the computation if the processing gain is changed to 500.

13-8 A DS spread-spectrum system transmits at a rate of 1000 bits/s in the presence of a tone jammer. The jammer power is 20 dB greater than the desired signal and the required $\mathscr{E}_b/J_0$ to achieve satisfactory performance is 10 dB.

a Determine the spreading bandwidth required to meet the specifications.

b If the jammer is a pulse jammer, determine the pulse duty cycle that results in worst-case jamming and the corresponding probability of error.

13-9 A CDMA system consists of 15 equal-power users that transmit information at a rate of 10 000 bits/s, each using a DS spread spectrum signal operating at a chip rate of 1 MHz. The modulation is binary PSK.

a Determine the $\mathscr{E}_b/J_0$, where J_0 is the spectral density of the combined interference.

b What is the processing gain?

c How much should the processing gain be increased to allow for doubling the number of users without affecting the output SNR?

13-10 A DS binary PSK spread spectrum signal has a processing gain of 500. What is the jamming margin against a continuous-tone jammer if the desired error probability is 10^{-5}?

13-11 Repeat Problem 13-10 if the jammer is a pulsed-noise jammer with a duty cycle of 1%.

13-12 Consider the DS spread spectrum signal

$$c(t) = \sum_{n=-\infty}^{\infty} c_n p(t - nT_c)$$

where c_n is a periodic m sequence with a period $N = 127$ and $p(t)$ is a rectangular pulse of duration $T_c = 1\ \mu$s. Determine the power spectral density of the signal $c(t)$.

13-13 Suppose that $\{c_{1i}\}$ and $\{c_{2i}\}$ are two binary $(0, 1)$ periodic sequences with periods N_1 and N_2, respectively. Determine the period of the sequence obtained by forming the modulo-2 sum of $\{c_{1i}\}$ and $\{c_{2i}\}$.

13-14 An $m = 10$ ML shift register is used to generate the pseudorandom sequence in a DS spread spectrum system. The chip duration is $T_c = 1\ \mu$s, and the bit duration is $T_b = NT_c$, where N is the length (period) of the m sequence.

a Determine the processing gain of the system in dB.

b Determine the jamming margin if the required $\mathscr{E}_b/J_0 = 10$ and the jammer is a tone jammer with an average power J_{av}.

13-15 A FH binary orthogonal FSK system employs an $m = 15$ stage linear feedback shift register that generates an ML sequence. Each state of the shift register selects one of L nonoverlapping frequency bands in the hopping pattern. The bit rate is 100 bits/s and the hop rate is once per bit. The demodulator employs noncoherent detection.

a Determine the hopping bandwidth for this channel.

b What is the processing gain?

c What is the probability of error in the presence of AWGN?

13-16 Consider the FH binary orthogonal FSK system described in Problem 13-15. Suppose that the hop rate is increased to 2 hops/bit. The receiver uses square-law combining to combine the signal over the two hops.
- **a** Determine the hopping bandwidth for the channel.
- **b** What is the processing gain?
- **c** What is the error probability in the presence of AWGN?

13-17 In a fast FH spread-spectrum system, the information is transmitted via FSK, with noncoherent detection. Suppose there are $N = 3$ hops/bit, with hard-decision decoding of the signal in each hop.
- **a** Determine the probability of error for this system in an AWGN channel with power spectral density $\frac{1}{2}N_0$ and an SNR = 13 dB (total SNR over the three hops).
- **b** Compare the result in (a) with the error probability of a FH spread-spectrum system that hops once per bit.

13-18 A slow FH binary FSK system with noncoherent detection operates at $\mathscr{E}_b/J_0 = 10$, with a hopping bandwidth of 2 GHz, and a bit rate of 10 kbits/s.
- **a** What is the processing gain for the system?
- **b** If the jammer operates as a partial-band jammer, what is the bandwidth occupancy for worst-case jamming?
- **c** What is the probability of error for the worst-case partial-band jammer?

13-19 Determine the error probability for a FH spread spectrum signal in which a binary convolutional code is used in combination with binary FSK. The interference on the channel is AWGN. The FSK demodulator outputs are square-law detected and passed to the decoder, which performs optimum soft-decision Viterbi decoding as described in Section 8-2. Assume that the hopping rate is 1 hop per coded bit.

13-20 Repeat Problem 13-19 for hard-decision Viterbi decoding.

13-21 Repeat Problem 13-19 when fast frequency hopping is performed at a hopping rate of L hops per coded bit.

13-22 Repeat Problem 13-19 when fast frequency hopping is performed with L hops per coded bit and the decoder is a hard-decision Viterbi decoder. The L chips per coded bit are square-law-detected and combined prior to the hard decision.

13-23 The TATS signal described in Section 13-3-3 is demodulated by a parallel bank of eight matched filters (octal FSK), and each filter output is square-law-detected. The eight outputs obtained in each of seven signal intervals (56 total outputs) are used to form the 64 possible decision variables corresponding to the Reed-Solomon (7, 2) code. Determine an upper (union) bound of the code word error probability for AWGN and soft-decision decoding.

13-24 Repeat Problem 13-23 for the worst-case partial-band interference channel.

13-25 Derive the results in (13-2-62) and (13-2-63) from (13-2-61).

13-26 Show that (13-3-14) follows from (13-3-13).

13-27 Derive (13-3-17) from (13-3-16).

13-28 The generator polynomials for constructing Gold code sequences of length $n = 7$ are

$$g_1(p) = p^3 + p + 1$$
$$g_2(p) = p^3 + p^2 + 1$$

Generate all the Gold codes of length 7 and determine the cross-correlations of one sequence with each of the others.

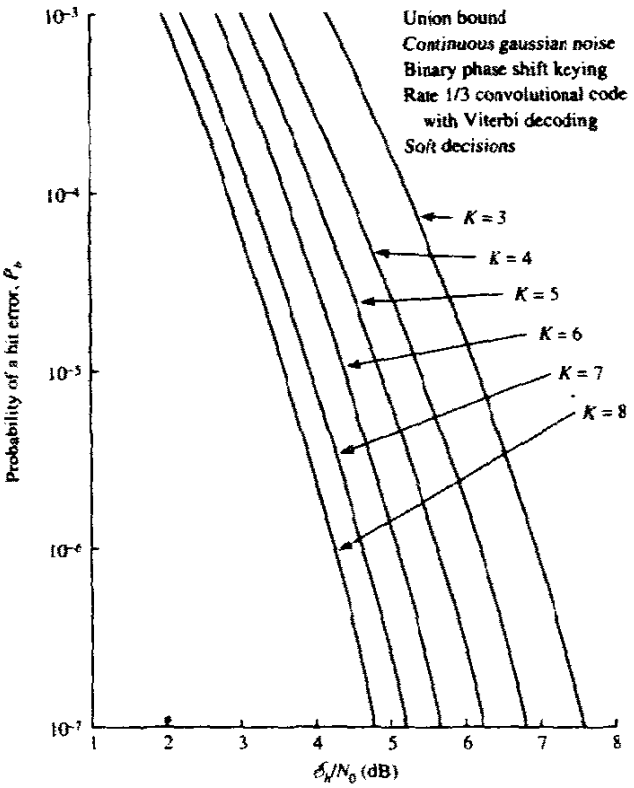

FIGURE P13-29

13-29 In Section 13-2-3, we demonstrated techniques for evaluating the error probability of a coded system with interleaving in pulse interference by using the cutoff rate parameter R_0. Use the error probability curves given in Fig. P13-29 for rate 1/2 and 1/3 convolutional codes with soft-decision Viterbi decoding to determine the corresponding error rates for a coded system in pulse interference. Perform this computation for $K = 3$, 5, and 7.

13-30 In coded and interleaved DS binary PSK modulation with pulse jamming and soft-decision decoding, the cutoff rate is

$$R_{0_s} = 1 - \log_2 (1 + \alpha e^{-\alpha \mathscr{E}_c/N_0})$$

where α is the fraction of the time the system is being jammed, $\mathscr{E}_c = \mathscr{E}_b R$, R is the bit rate, and $N_0 \equiv J_0$.

a Show that the SNR per bit, $\mathscr{E}_b/N_0$, can be expressed as

$$\frac{\mathscr{E}_b}{N_0} = \frac{1}{\alpha R} \ln \frac{\alpha}{2^{1-R_0} - 1}$$

b Determine the value of α that maximizes the required $\mathscr{E}_b/N_0$ (worst-case pulse jamming) and the resulting maximum value of $\mathscr{E}_b/N_0$.

b Plot the graph of $10 \log (\mathscr{E}_b/rN_0)$ versus R_0, where $r = R_0/R$, for worst-case pulse jamming and for AWGN ($\alpha = 1$). What conclusions do you reach regarding the effect of worst-case pulse jamming?

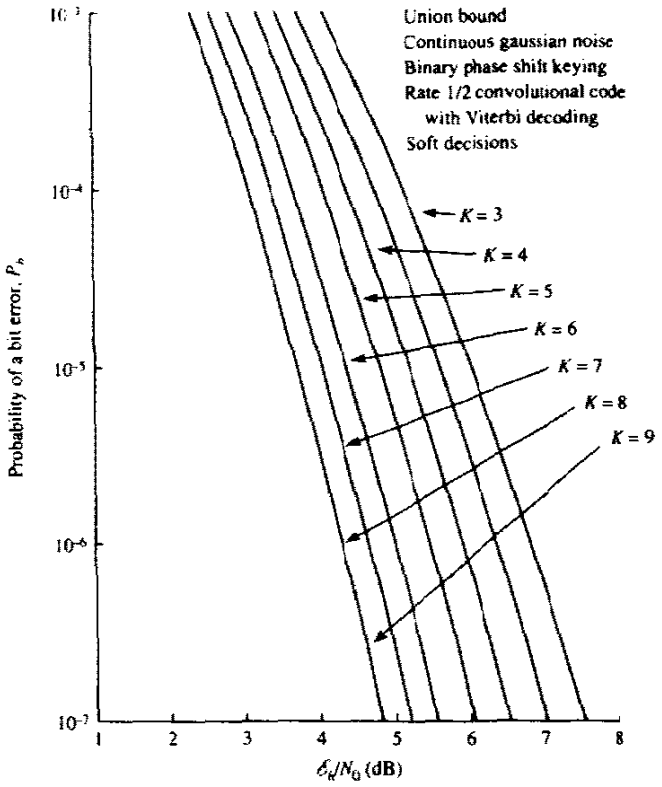

FIGURE P13-29 *(Continued).*

13-31 In a coded and interleaved frequency-hopped q-ary FSK modulation with partial band jamming and coherent demodulation with soft-decision decoding, the cutoff rate is

$$R_0 = \log_2\left[\frac{q}{1+(q-1)\alpha e^{-\alpha \mathscr{E}_c/2N_0}}\right]$$

where α is the fraction of the band being jammed, $\mathscr{E}_c$ is the chip (or tone) energy, and $N_0 = J_0$.

a Show that the SNR per bit can be expressed as

$$\frac{\mathscr{E}_b}{N_0} = \frac{2}{\alpha R}\ln\frac{(q-1)\alpha}{q2^{-R_0}-1}$$

b Determine the value of α that maximizes the required $\mathscr{E}_b/N_0$ (worst-case partial band jamming) and the resulting maximum value of $\mathscr{E}_b/N_0$.

c Define $r = R_0/R$ in the result for $\mathscr{E}_b/N_0$ from (b), and plot $10\log(\mathscr{E}_b/rN_0)$ versus the normalized cutoff rate $R_0/\log_2 q$ for $q = 2, 4, 8, 16, 32$. Compare these graphs with the results of Problem 13-30(c). What conclusions do you reach regarding the effect of worst-case partial band jamming? What is the effect of increasing the alphabet size q? What is the penalty in SNR between the results in Problem 13-30(c) and q-ary FSK as $q \to \infty$?

14

DIGITAL COMMUNICATION THROUGH FADING MULTIPATH CHANNELS

The previous chapters have described the design and performance of digital communications systems for transmission on either the classical AWGN channel or a linear filter channel with AWGN. We observed that the distortion inherent in linear filter channels requires special signal design techniques and rather sophisticated adaptive equalization algorithms in order to achieve good performance.

In this chapter, we consider the signal design, receiver structure, and receiver performance for more complex channels, namely, channels having randomly time-variant impulse responses. This characterization serves as a model for signal transmission over many radio channels such as shortwave ionospheric radio communication in the 3–30 MHz frequency band (HF), tropospheric scatter (beyond-the-horizon) radio communications in the 300–3000 MHz frequency band (UHF) and 3000–30 000 MHz frequency band (SHF), and ionospheric forward scatter in the 30–300 MHz frequency band (VHF). The time-variant impulse responses of these channels are a consequence of the constantly changing physical characteristics of the media. For example, the ions in the ionospheric layers that reflect the signals transmitted in the HF frequency band are always in motion. To the user of the channel, the motion of the ions appears to be random. Consequently, if the same signal is transmitted at HF in two widely separated time intervals, the two received signals will be different. The time-varying responses that occur are treated in statistical terms.

We shall begin our treatment of digital signalling over fading multipath channels by first developing a statistical characterization of the channel. Then we shall evaluate the performance of several basic digital signaling techniques for communication over such channels. The performance results will demons-

trate the severe penalty in SNR that must be paid as a consequence of the fading characteristics of the received signal. We shall then show that the penalty in SNR can be dramatically reduced by means of efficient modulation/coding and demodulation/decoding techniques.

14-1 CHARACTERIZATION OF FADING MULTIPATH CHANNELS

If we transmit an extremely short pulse, ideally an impulse, over a time-varying multipath channel, the received signal might appear as a train of pulses, as shown in Fig. 14-1-1. Hence, one characteristic of a multipath medium is the time spread introduced in the signal that is transmitted through the channel.

A second characteristic is due to the time variations in the structure of the medium. As a result of such time variations, the nature of the multipath varies with time. That is, if we repeat the pulse-sounding experiment over and over, we shall observe changes in the received pulse train, which will include changes in the sizes of the individual pulses, changes in the relative delays among the pulses, and, quite often, changes in the number of pulses observed in the received pulse train as shown in Fig. 14-1-1. Moreover, the time variations appear to be unpredictable to the user of the channel. Therefore, it is reasonable to characterize the time-variant multipath channel statistically.

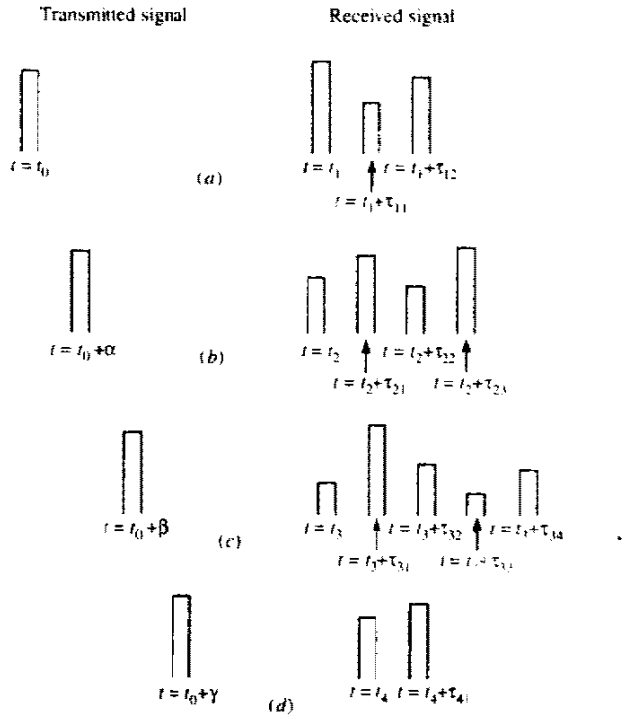

FIGURE 14-1-1 Example of the response of a time-variant multipath channel to a very narrow pulse.

Toward this end, let us examine the effects of the channel on a transmitted signal that is represented in general as

$$s(t) = \text{Re}\,[s_l(t)e^{j2\pi f_c t}] \tag{14-1-1}$$

We assume that there are multiple propagation paths. Associated with each path is a propagation delay and an attenuation factor. Both the propagation delays and the attenuation factors are time-variant as a result of changes in the structure of the medium. Thus, the received bandpass signal may be expressed in the form

$$x(t) = \sum_n \alpha_n(t)s(t - \tau_n(t)) \tag{14-1-2}$$

where $\alpha_n(t)$ is the attenuation factor for the signal received on the nth path and $\tau_n(t)$ is the propagation delay for the nth path. Substitution for $s(t)$ from (14-1-1) into (14-1-2) yields the result

$$x(t) = \text{Re}\left\{\left[\sum_n \alpha_n(t)e^{-j2\pi f_c \tau_n(t)}s_l(t - \tau_n(t))\right]e^{j2\pi f_c t}\right\} \tag{14-1-3}$$

It is apparent from (14-1-3) that the equivalent lowpass received signal is

$$r_l(t) = \sum_n \alpha_n(t)e^{-j2\pi f_c \tau_n(t)}s_l(t - \tau_n(t)) \tag{14-1-4}$$

Since $r_l(t)$ is the response of an equivalent lowpass channel to the equivalent lowpass signal $s_l(t)$, it follows that the equivalent lowpass channel is described by the time-variant impulse response

$$c(\tau; t) = \sum_n \alpha_n(t)e^{-j2\pi f_c \tau_n(t)}\delta(\tau - \tau_n(t)) \tag{14-1-5}$$

For some channels, such as the tropospheric scatter channel, it is more appropriate to view the received signal as consisting of a continuum of multipath components. In such a case, the received signal $x(t)$ is expressed in the integral form

$$x(t) = \int_{-\infty}^{\infty} \alpha(\tau; t)s(t - \tau)\,d\tau \tag{14-1-6}$$

where $\alpha(\tau; t)$ denotes the attenuation of the signal components at delay τ and at time instant t. Now substitution for $s(t)$ from (14-1-1) into (14-1-6) yields

$$x(t) = \text{Re}\left\{\left[\int_{-\infty}^{\infty} \alpha(\tau; t)e^{-j2\pi f_c \tau}s_l(t - \tau)\,d\tau\right]e^{j2\pi f_c t}\right\} \tag{14-1-7}$$

Since the integral in (14-1-7) represents the convolution of $s_l(t)$ with an equivalent lowpass time-variant impulse response $c(\tau; t)$, it follows that

$$c(\tau; t) = \alpha(\tau; t)e^{-j2\pi f_c \tau} \tag{14-1-8}$$

where $c(\tau; t)$ represents the response of the channel at time t due to an impulse applied at time $t - \tau$. Thus (14-1-8) is the appropriate definition of the equivalent lowpass impulse response when the channel results in continuous multipath and (14-1-5) is appropriate for a channel that contains discrete multipath components.

Now let us consider the transmission of an unmodulated carrier at frequency f_c. Then $s_l(t) = 1$ for all t, and, hence, the received signal for the case of discrete multipath, given by (14-1-4), reduces to

$$r_l(t) = \sum_n \alpha_n(t) e^{-j2\pi f_c \tau_n(t)}$$

$$= \sum_n \alpha_n(t) e^{-j\theta_n(t)} \tag{14-1-9}$$

where $\theta_n(t) = 2\pi f_c \tau_n(t)$. Thus, the received signal consists of the sum of a number of time-variant vectors (phasors) having amplitudes $\alpha_n(t)$ and phases $\theta_n(t)$. Note that large dynamic changes in the medium are required for $\alpha_n(t)$ to change sufficiently to cause a significant change in the received signal. On the other hand, $\theta_n(t)$ will change by 2π rad whenever τ_n changes by $1/f_c$. But $1/f_c$ is a small number and, hence, θ_n can change by 2π rad with relatively small motions of the medium. We also expect the delays $\tau_n(t)$ associated with the different signal paths to change at different rates and in an unpredictable (random) manner. This implies that the received signal $r_l(t)$ in (14-1-9) can be modeled as a random process. When there are a large number of paths, the central limit theorem can be applied. That is, $r_l(t)$ may be modeled as a complex-valued gaussian random process. This means that the time-variant impulse response $c(\tau; t)$ is a complex-valued gaussian random process in the t variable.

The multipath propagation model for the channel embodied in the received signal $r_l(t)$, given in (14-1-9), results in signal fading. The fading phenomenon is primarily a result of the time variations in the phases $\{\theta_n(t)\}$. That is, the randomly time-variant phases $\{\theta_n(t)\}$ associated with the vectors $\{\alpha_n e^{-j\theta_n}\}$ at times result in the vectors adding destructively. When that occurs, the resultant received signal $r_l(t)$ is very small or practically zero. At other times, the vectors $\{\alpha_n e^{-j\theta_n}\}$ add constructively, so that the received signal is large. Thus, the amplitude variations in the received signal, termed *signal fading*, are due to the time-variant multipath characteristics of the channel.

When the impulse response $c(\tau; t)$ is modeled as a zero-mean complex-valued gaussian process, the envelope $|c(\tau; t)|$ at any instant t is Rayleigh-distributed. In this case the channel is said to be a *Rayleigh fading channel*. In the event that there are fixed scatterers or signal reflectors in the medium, in addition to randomly moving scatterers, $c(\tau; t)$ can no longer be modeled as having zero mean. In this case, the envelope $|c(\tau; t)|$ has a Rice distribution and the channel is said to be a *Ricean fading channel*. Another probability distribution function that has been used to model the envelope of fading

signals is the Nakagami-m distribution. These fading channel models are considered in Section 14-1-2.

14-1-1 Channel Correlation Functions and Power Spectra

We shall now develop a number of useful correlation functions and power spectral density functions that define the characteristics of a fading multipath channel. Our starting point is the equivalent lowpass impulse response $c(\tau; t)$, which is characterized as a complex-valued random process in the t variable. We assume that $c(\tau; t)$ is wide-sense-stationary. Then we define the autocorrelation function of $c(\tau; t)$ as

$$\phi_c(\tau_1, \tau_2; \Delta t) = \tfrac{1}{2}E[c^*(\tau_1; t)c(\tau_2; t + \Delta t)] \tag{14-1-10}$$

In most radio transmission media, the attenuation and phase shift of the channel associated with path delay τ_1 is uncorrelated with the attenuation and phase shift associated with path delay τ_2. This is usually called *uncorrelated scattering*. We make the assumption that the scattering at two different delays is uncorrelated and incorporate it into (14-1-10) to obtain

$$\tfrac{1}{2}E[c^*(\tau_1; t)c(\tau_2; t + \Delta t)] = \phi_c(\tau_1; \Delta t)\delta(\tau_1 - \tau_2) \tag{14-1-11}$$

If we let $\Delta t = 0$, the resulting autocorrelation function $\phi_c(\tau; 0) \equiv \phi_c(\tau)$ is simply the average power output of the channel as a function of the time delay τ. For this reason, $\phi_c(\tau)$ is called the *multipath intensity profile* or *the delay power spectrum* of the channel. In general, $\phi_c(\tau; \Delta t)$ gives the average power output as a function of the time delay τ and the difference Δt in observation time.

In practice, the function $\phi_c(\tau; \Delta t)$ is measured by transmitting very narrow pulses or, equivalently, a wideband signal and cross-correlating the received signal with a delayed version of itself. Typically, the measured function $\phi_c(\tau)$ may appear as shown in Fig. 14-1-2. The range of values of τ over which $\phi_c(\tau)$

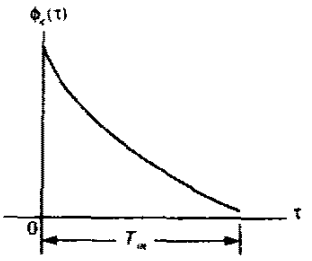

FIGURE 14-1-2 Multipath intensity profile.

is essentially nonzero is called the *multipath spread of the channel* and is denoted by T_m.

A completely analogous characterization of the time-variant multipath channel begins in the frequency domain. By taking the Fourier transform of $c(\tau; t)$ we obtain the time-variant transfer function $C(f; t)$, where f is the frequency variable. Thus,

$$C(f; t) = \int_{-\infty}^{\infty} c(\tau; t) e^{-j2\pi f\tau}\, d\tau \tag{14-1-12}$$

If $c(\tau; t)$ is modeled as a complex-valued zero-mean gaussian random process in the t variable, it follows that $C(f; t)$ also has the same statistics. Under the assumption that the channel is wide-sense-stationary, we define the autocorrelation function

$$\phi_C(f_1, f_2; \Delta t) = \tfrac{1}{2} E[C^*(f_1; t) C(f_2; t + \Delta t)] \tag{14-1-13}$$

Since $C(f; t)$ is the Fourier transform of $c(\tau; t)$, it is not surprising to find that $\phi_C(f_1, f_2; \Delta t)$ is related to $\phi_C(\tau; \Delta t)$ by the Fourier transform. The relationship is easily established by substituting (14-1-12) into (14-1-13). Thus,

$$\begin{aligned}
\phi_C(f_1, f_2; \Delta t) &= \tfrac{1}{2} \int_{-\infty}^{\infty} \int_{-\infty}^{\infty} E[c^*(\tau_1; t) c(\tau_2; t + \Delta t)] e^{j2\pi(f_1\tau_1 - f_2\tau_2)}\, d\tau_1\, d\tau_2 \\
&= \int_{-\infty}^{\infty} \int_{-\infty}^{\infty} \phi_c(\tau_1; \Delta t) \delta(\tau_1 - \tau_2) e^{j2\pi(f_1\tau_1 - f_2\tau_2)}\, d\tau_1\, d\tau_2 \\
&= \int_{-\infty}^{\infty} \phi_c(\tau_1; \Delta t) e^{j2\pi(f_1 - f_2)\tau_1}\, d\tau_1 \\
&= \int_{-\infty}^{\infty} \phi_c(\tau_1; \Delta t) e^{-j2\pi\, \Delta f \tau_1}\, d\tau_1 \equiv \phi_C(\Delta f; \Delta t)
\end{aligned} \tag{14-1-14}$$

where $\Delta f = f_2 - f_1$. From (14-1-14), we observe that $\phi_C(\Delta f; \Delta t)$ is the Fourier transform of the multipath intensity profile. Furthermore, the assumption of uncorrelated scattering implies that the autocorrelation function of $C(f; t)$ in frequency is a function of only the frequency difference $\Delta f = f_2 - f_1$. Therefore, it is appropriate to call $\phi_C(\Delta f; \Delta t)$ the *spaced-frequency, spaced-time correlation function of the channel.* It can be measured in practice by transmitting a pair of sinusoids separated by Δf and cross-correlating the two separately received signals with a relative delay Δt.

Suppose we set $\Delta t = 0$ in (14-1-14). Then, with $\phi_C(\Delta f; 0) \equiv \phi_c(\Delta f)$ and $\phi_c(\tau; 0) \equiv \phi_c(\tau)$, the transform relationship is simply

$$\phi_C(\Delta f) = \int_{-\infty}^{\infty} \phi_c(\tau) e^{-j2\pi\, \Delta f \tau}\, d\tau \tag{14-1-15}$$

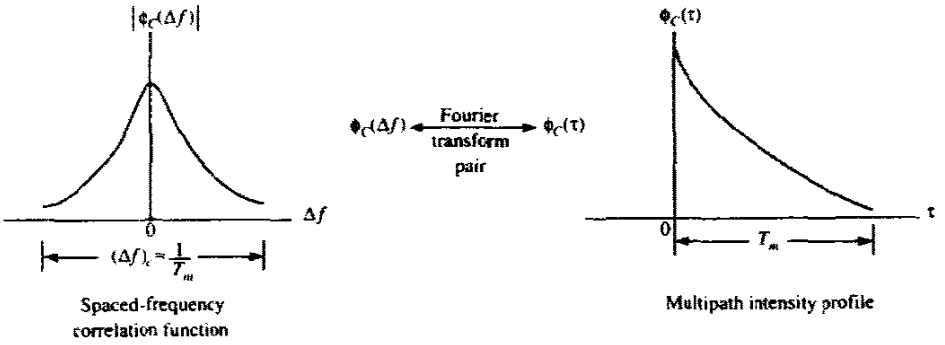

FIGURE 14-1-3 Relationship between $\phi_C(\Delta f)$ and $\phi_c(\tau)$.

The relationship is depicted graphically in Fig. 14-1-3. Since $\phi_C(\Delta f)$ is an autocorrelation function in the frequency variable, it provides us with a measure of the frequency coherence of the channel. As a result of the Fourier transform relationship between $\phi_C(\Delta f)$ and $\phi_c(\tau)$, the reciprocal of the multipath spread is a measure of the *coherence bandwidth of the channel.* That is,

$$(\Delta f)_c \approx \frac{1}{T_m} \tag{14-1-16}$$

where $(\Delta f)_c$ denotes the coherence bandwidth. Thus, two sinusoids with frequency separation greater than $(\Delta f)_c$ are affected differently by the channel. When an information-bearing signal is transmitted through the channel, if $(\Delta f)_c$ is small in comparison to the bandwidth of the transmitted signal, the channel is said to be *frequency-selective.* In this case, the signal is severely distorted by the channel. On the other hand, if $(\Delta f)_c$ is large in comparison with the bandwidth of the transmitted signal, the channel is said to be *frequency-nonselective.*

We now focus our attention on the time variations of the channel as measured by the parameter Δt in $\phi_C(\Delta f; \Delta t)$. The time variations in the channel are evidenced as a Doppler broadening and, perhaps, in addition as a Doppler shift of a spectral line. In order to relate the Doppler effects to the time variations of the channel, we define the Fourier transform of $\phi_C(\Delta f; \Delta t)$ with respect to the variable Δt to be the function $S_C(\Delta f; \lambda)$. That is,

$$S_C(\Delta f; \lambda) = \int_{-\infty}^{\infty} \phi_C(\Delta f; \Delta t) e^{-j2\pi\lambda\,\Delta t}\, d\Delta t \tag{14-1-17}$$

With Δf set to zero and $S_C(0; \lambda) \equiv S_C(\lambda)$, the relation in (14-1-17) becomes

$$S_C(\lambda) = \int_{-\infty}^{\infty} \phi_C(\Delta t) e^{-j2\pi\lambda\,\Delta t}\, d\Delta t \tag{14-1-18}$$

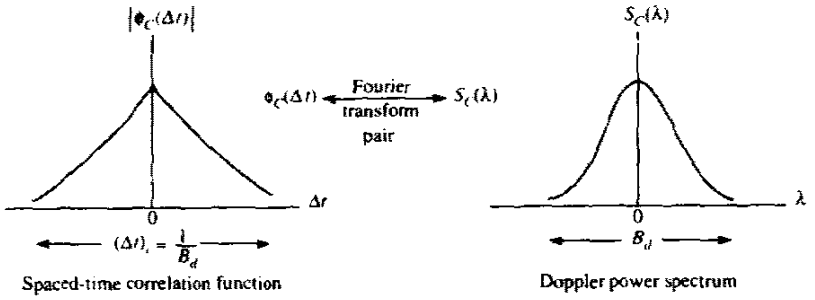

FIGURE 14-1-4 Relationship between $\phi_C(\Delta t)$ and $S_C(\lambda)$.

The function $S_C(\lambda)$ is a power spectrum that gives the signal intensity as a function of the Doppler frequency λ. Hence, we call $S_C(\lambda)$ the *Doppler power spectrum of the channel.*

From (14-1-18), we observe that if the channel is time-invariant, $\phi_C(\Delta t) = 1$ and $S_C(\lambda)$ becomes equal to the delta function $\delta(\lambda)$. Therefore, when there are no time variations in the channel, there is no spectral broadening observed in the transmission of a pure frequency tone.

The range of values of λ over which $S_C(\lambda)$ is essentially nonzero is called the *Doppler spread B_d of the channel.* Since $S_C(\lambda)$ is related to $\phi_C(\Delta t)$ by the Fourier transform, the reciprocal of B_d is a measure of the coherence time of the channel. That is,

$$(\Delta t)_c \approx \frac{1}{B_d} \tag{14-1-19}$$

where $(\Delta t)_c$ denotes the *coherence time.* Clearly, a slowly changing channel has a large coherence time or, equivalently, a small Doppler spread. Figure 14-1-4 illustrates the relationship between $\phi_C(\Delta t)$ and $S_C(\lambda)$.

We have now established a Fourier transform relationship between $\phi_C(\Delta f; \Delta t)$ and $\phi_c(\tau; \Delta t)$ involving the variables $(\tau, \Delta f)$, and a Fourier transform relationship between $\phi_C(\Delta f; \Delta t)$ and $S_C(\Delta f; \lambda)$ involving the variables $(\Delta t, \lambda)$. There are two additional Fourier transform relationships that we can define, which serve to relate $\phi_c(\tau; \Delta t)$ to $S_C(\Delta f; \lambda)$ and, thus, close the loop. The desired relationship is obtained by defining a new function, denoted by $S(\tau; \lambda)$, to be the Fourier transform of $\phi_c(\tau; \Delta t)$ in the Δt variable. That is,

$$S(\tau; \lambda) = \int_{-\infty}^{\infty} \phi_c(\tau; \Delta t) e^{-j2\pi\lambda\,\Delta t}\, d\Delta t \tag{14-1-20}$$

It follows that $S(\tau; \lambda)$ and $S_C(\Delta f; \lambda)$ are a Fourier transform pair. That is,

$$S(\tau; \lambda) = \int_{-\infty}^{\infty} S_C(\Delta f; \lambda) e^{j2\pi\tau\,\Delta f}\, d\Delta f \tag{14-1-21}$$

Furthermore, $S(\tau; \lambda)$ and $\phi_C(\Delta f; \Delta t)$ are related by the double Fourier transform

$$S(\tau; \lambda) = \int_{-\infty}^{\infty} \int_{-\infty}^{\infty} \phi_C(\Delta f; \Delta t) e^{-j2\pi\lambda\,\Delta t} e^{j2\pi\tau\,\Delta f}\, d\Delta t\, d\Delta f \qquad (14\text{-}1\text{-}22)$$

This new function $S(\tau; \lambda)$ is called the *scattering function of the channel.* It provides us with a measure of the average power output of the channel as a function of the time delay τ and the Doppler frequency λ.

The relationships among the four functions $\phi_C(\Delta f; \Delta t)$, $\phi_c(\tau; \Delta t)$, $\phi_C(\Delta f; \lambda)$, and $S(\tau; \lambda)$ are summarized in Fig. 14-1-5.

FIGURE 14-1-5 Relationships among the channel correlation functions and power spectra. [*From Green (1962), with permission.*]

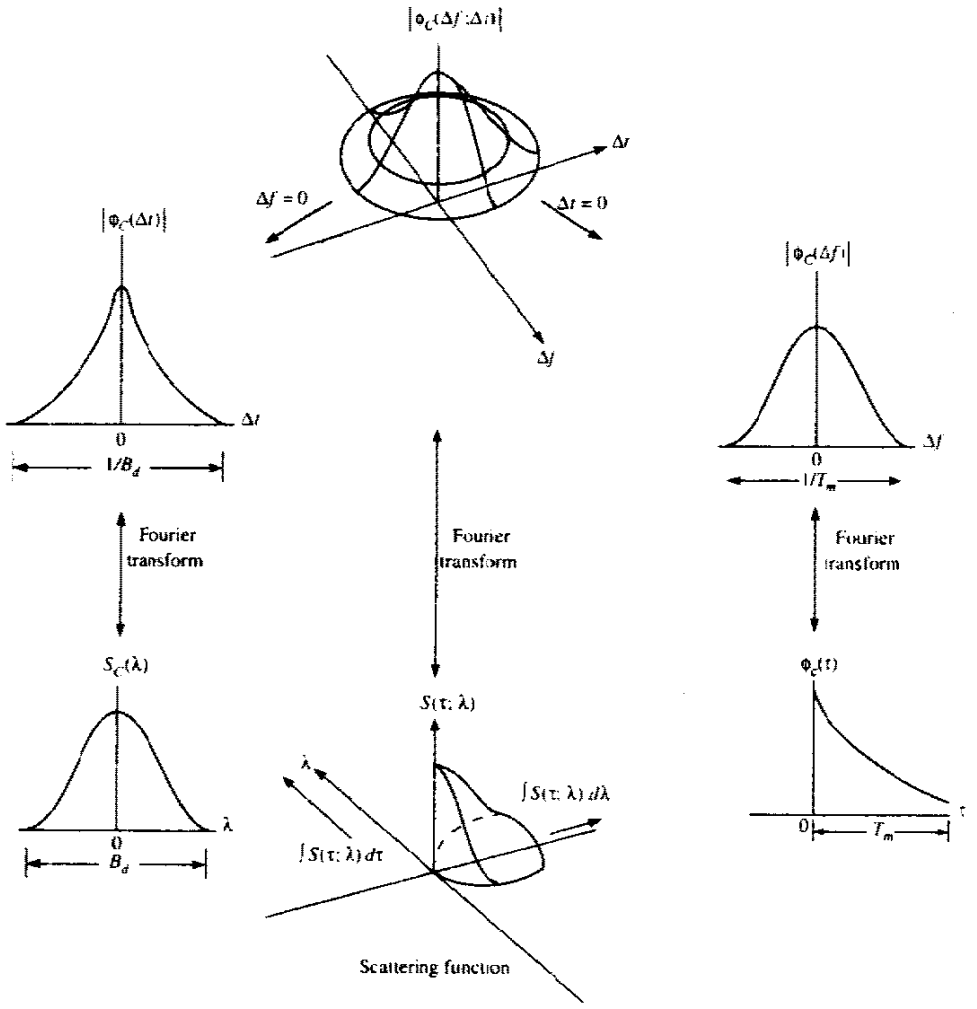

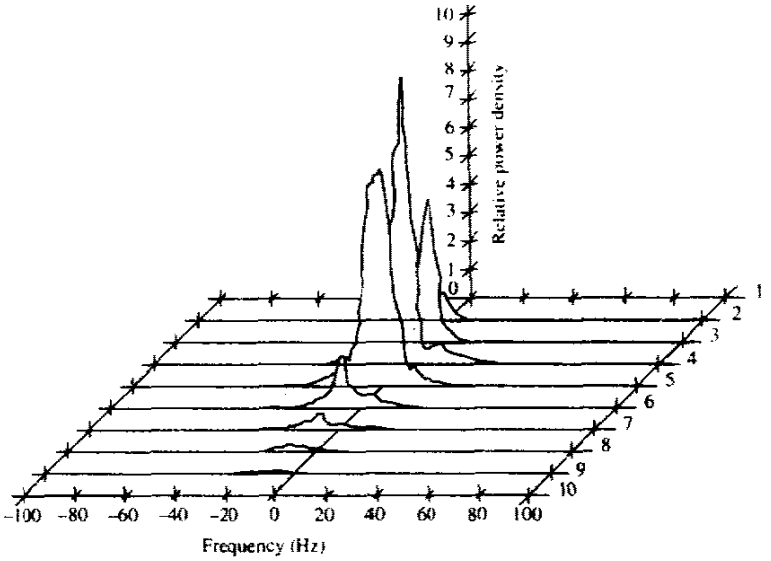

FIGURE 14-1-6 Scattering function of a medium-range tropospheric scatter channel. The taps delay increment is 0.1 μs.

The scattering function $S(\tau; \lambda)$ measured on a 150 mi tropospheric scatter link is shown in Fig. 14-1-6. The signal used to probe the channel had a time resolution of 0.1 μs. Hence, the time-delay axis is quantized in increments of 0.1 μs. From the graph, we observe that the multipath spread $T_m = 0.7$ μs. On the other hand, the Doppler spread, which may be defined as the 3 dB bandwidth of the power spectrum for each signal path, appears to vary with each signal path. For example, in one path it is less than 1 Hz, while in some other paths it is several hertz. For our purposes, we shall take the largest of these 3 dB bandwidths of the various paths and call that the *Doppler spread.*

14-1-2 Statistical Models for Fading Channels

There are several probability distributions that can be considered in attempting to model the statistical characteristics of the fading channel. When there are a large number of scatterers in the channel that contribute to the signal at the receiver, as is the case in ionospheric or tropospheric signal propagation, application of the central limit theorem leads to a gaussian process model for the channel impulse response. If the process is zero-mean, then the envelope of the channel response at any time instant has a Rayleigh probability distribution and the phase is uniformly distributed in the interval $(0, 2\pi)$. That is,

$$p_R(r) = \frac{2r}{\Omega} e^{-r^2/\Omega}, \quad r \geq 0 \tag{14-1-23}$$

where

$$\Omega = E(R^2) \tag{14-1-24}$$

We observe that the Rayleigh distribution is characterized by the single parameter $E(R^2)$.

An alternative statistical model for the envelope of the channel response is the Nakagami-m distribution given by the pdf in (2-1-147). In constrast to the Rayleigh distribution, which has a single parameter that can be used to match the fading channel statistics, the Nakagami-m is a two-parameter distribution, namely, involving the parameter m and the second moment $\Omega = E(R^2)$. As a consequence, this distribution provides more flexibility and accuracy in matching the observed signal statistics. The Nakagami-m distribution can be used to model fading channel conditions that are either more or less severe than the Rayleigh distribution, and it includes the Rayleigh distribution as a special case ($m = 1$). For example, Turin (1972) and Suzuki (1977) have shown that the Nakagami-m distribution is the best fit for data signals received in urban radio multipath channels.

The Rice distribution is also a two-parameter distribution. It may be expressed by the pdf given in (2-1-141), where the parameters are s and σ^2. Recall that s^2 is called the *noncentrality parameter* in the equivalent chi-square distribution. It represents the power in the nonfading signal components, sometimes called *specular components*, of the received signal.

There are many radio channels in which fading is encountered that are basically line-of-sight (LOS) communication links with multipath components arising from secondary reflections, or signal paths, from surrounding terrain. In such channels, the number of multipath components is small, and, hence, the channel may be modeled in a somewhat simpler form. We cite two channel models as examples.

As the first example, let us consider an airplane to ground communication link in which there is the direct path and a single multipath component at a delay t_0 relative to the direct path. The impulse response of such a channel may be modeled as

$$c(\tau; t) = \alpha\delta(\tau) + \beta(t)\delta(\tau - \tau_0(t)) \tag{14-1-25}$$

where α is the attenuation factor of the direct path and $\beta(t)$ represents the time-variant multipath signal component resulting from terrain reflections. Often, $\beta(t)$ can be characterized as a zero-mean gaussian random process. The transfer function for this channel model may be expressed as

$$C(f; t) = \alpha + \beta(t)e^{-j2\pi f\tau_0(t)} \tag{14-1-26}$$

This channel fits the Ricean fading model defined previously. The direct path with attenuation α represents the specular component and $\beta(t)$ represents the Rayleigh fading component.

A similar model has been found to hold for microwave LOS radio channels

used for long-distance voice and video transmission by telephone companies throughout the world. For such channels, Rummler (1979) has developed a three-path model based on channel measurements performed on typical LOS links in the 6 GHz frequency band. The differential delay on the two multipath components is relatively small, and, hence, the model developed by Rummler is one that has a channel transfer function

$$C(f) = \alpha[1 - \beta e^{-j2\pi(f-f_0)\tau_0}] \tag{14-1-27}$$

where α is the overall attenuation parameter, β is called a shape parameter which is due to the multipath components, f_0 is the frequency of the fade minimum, and τ_0 is the relative time delay between the direct and the multipath components. This simplified model was used to fit data derived from channel measurements.

Rummler found that the parameters α and β may be characterized as random variables that, for practical purposes, are nearly statistically independent. From the channel measurements, he found that the distribution of β has the form $(1-\beta)^{2.3}$. The distribution of α is well modeled by the lognormal distribution, i.e., $-\log \alpha$ is gaussian. For $\beta > 0.5$, the mean of $-20 \log \alpha$ was found to be 25 dB and the standard deviation was 5 dB. For smaller values of β, the mean decreases to 15 dB. The delay parameter determined from the measurements was $\tau_0 = 6.3$ ns. The magnitude-square response of $C(f)$ is

$$|C(f)|^2 = \alpha^2[1 + \beta^2 - 2\beta \cos 2\pi(f - f_0)\tau_0] \tag{14-1-28}$$

$|C(f)|$ is plotted in Fig. 14-1-7 as a function of the frequency $f - f_0$ for $\tau_0 = 6.3$ ns. Note that the effect of the multipath component is to create a deep attenuation at $f = f_0$ and at multiples of $1/\tau_0 \approx 159$ MHz. By comparison, the typical channel bandwidth is 30 MHz. This model was used by Lundgren and Rummler (1979) to determine the error rate performance of digital radio systems.

FIGURE 14-1-7 Magnitude frequency response of LOS channel model

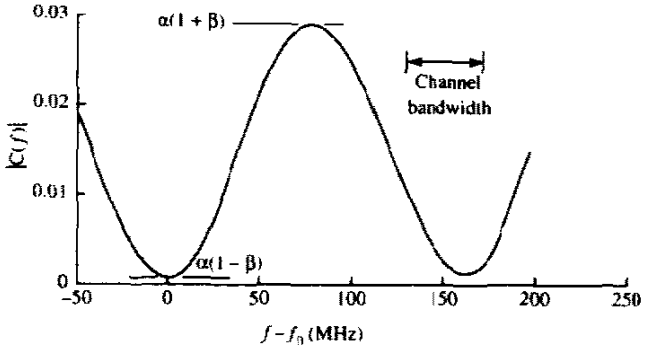

14-2 THE EFFECT OF SIGNAL CHARACTERISTICS ON THE CHOICE OF A CHANNEL MODEL

Having discussed the statistical characterization of time-variant multipath channels generally in terms of the correlation functions described in Section 14-1, we now consider the effect of signal characteristics on the selection of a channel model that is appropriate for the specified signal. Thus, let $s_l(t)$ be the equivalent lowpass signal transmitted over the channel and let $S_l(f)$ denote its frequency content. Then the equivalent lowpass received signal, exclusive of additive noise, may be expressed either in terms of the time domain variables $c(\tau; t)$ and $s_l(t)$ as

$$r_l(t) = \int_{-\infty}^{\infty} c(\tau; t) s_l(t - \tau)\, d\tau \tag{14-2-1}$$

or in terms of the frequency functions $C(f; t)$ and $S_l(f)$ as

$$r_l(t) = \int_{-\infty}^{\infty} C(f; t) S_l(f) e^{j2\pi ft}\, df \tag{14-2-2}$$

Suppose we are transmitting digital information over the channel by modulating (either in amplitude, or in phase, or both) the basic pulse $s_l(t)$ at a rate $1/T$, where T is the signaling interval. It is apparent from (14-2-2) that the time-variant channel characterized by the transfer function $C(f; t)$ distorts the signal $S_l(f)$. If $S_l(f)$ has a bandwidth W greater than the coherence bandwidth $(\Delta f)_c$ of the channel, $S_l(f)$ is subjected to different gains and phase shifts across the band. In such a case, the channel is said to be *frequency-selective*. Additional distortion is caused by the time variations in $C(f; t)$. This type of distortion is evidenced as a variation in the received signal strength, and has been termed *fading*. It should be emphasized that the frequency selectivity and fading are viewed as two different types of distortion. The former depends on the multipath spread or, equivalently, on the coherence bandwidth of the channel relative to the transmitted signal bandwidth W. The latter depends on the time variations of the channel, which are grossly characterized by the coherence time $(\Delta t)_c$ or, equivalently, by the Doppler spread B_d.

The effect of the channel on the transmitted signal $s_l(t)$ is a function of our choice of signal bandwidth and signal duration. For example, if we select the signaling interval T to satisfy the condition $T \gg T_m$, the channel introduces a negligible amount of intersymbol interference. If the bandwidth of the signal pulse $s_l(t)$ is $W \approx 1/T$, the condition $T \gg T_m$ implies that

$$W \ll \frac{1}{T_m} \approx (\Delta f)_c \tag{14-2-3}$$

That is, the signal bandwidth W is much smaller than the coherence bandwidth of the channel. Hence, the channel is frequency-nonselective. In other words,

all of the frequency components in $S_l(f)$ undergo the same attenuation and phase shift in transmission through the channel. But this implies that, within the bandwidth occupied by $S_l(f)$, the time-variant transfer function $C(f;t)$ of the channel is a complex-valued constant in the frequency variable. Since $S_l(f)$ has its frequency content concentrated in the vicinity of $f = 0$, $C(f;t) = C(0;t)$. Consequently, (14-2-2) reduces to

$$r_l(t) = C(0;t)\int_{-\infty}^{\infty} S_l(f)e^{j2\pi ft}\,df$$

$$= C(0;t)s_l(t) \tag{14-2-4}$$

Thus, when the signal bandwidth W is much smaller than the coherence bandwidth $(\Delta f)_c$ of the channel, the received signal is simply the transmitted signal multiplied by a complex-valued random process $C(0;t)$, which represents the time-variant characteristics of the channel. In this case, we say that the multipath components in the received are not resolvable because $W \ll (\Delta f)_c$.

The transfer function $C(0;t)$ for a frequency-nonselective channel may be expressed in the form

$$C(0;t) = \alpha(t)e^{-j\phi(t)} \tag{14-2-5}$$

where $\alpha(t)$ represents the envelope and $\phi(t)$ represents the phase of the equivalent lowpass channel. When $C(0;t)$ is modeled as a zero-mean complex-valued gaussian random process, the envelope $\alpha(t)$ is Rayleigh-distributed for any fixed value of t and $\phi(t)$ is uniformly distributed over the interval $(-\pi, \pi)$. The rapidity of the fading on the frequency-nonselective channel is determined either from the correlation function $\phi_C(\Delta t)$ or from the Doppler power spectrum $S_C(\lambda)$. Alternatively, either of the channel parameters $(\Delta t)_c$ or B_d can be used to characterize the rapidity of the fading.

For example, suppose it is possible to select the signal bandwidth W to satisfy the condition $W \ll (\Delta f)_c$ and the signaling interval T to satisfy the condition $T \ll (\Delta t)_c$. Since T is smaller than the coherence time of the channel, the channel attenuation and phase shift are essentially fixed for the duration of at least one signaling interval. When this condition holds, we call the channel a *slowly fading channel.* Furthermore, when $W \approx 1/T$, the conditions that the channel be frequency-nonselective and slowly fading imply that the product of T_m and B_d must satisfy the condition $T_m B_d < 1$.

The product $T_m B_d$ is called the *spread factor* of the channel. If $T_m B_d < 1$, the channel is said to be *underspread*; otherwise, it is *overspread.* The multipath spread, the Doppler spread, and the spread factor are listed in Table 14-2-1 for several channels. We observe from this table that several radio channels, including the moon when used as a passive reflector, are underspread. Consequently, it is possible to select the signal $s_l(t)$ such that these channels are frequency-nonselective and slowly fading. The slow-fading condition

TABLE 14-2-1 MULTIPATH SPREAD, DOPPLER SPREAD, AND SPREAD FACTOR FOR SEVERAL TIME-VARIANT MULTIPATH CHANNELS

Type of channel	Multipath duration	Doppler spread	Spread factor
Shortwave ionospheric propagation (HF)	10^{-3}–10^{-2}	10^{-1}–1	10^{-4}–10^{-2}
Ionospheric propagation under disturbed auroral conditions (HF)	10^{-3}–10^{-2}	10–100	10^{-2}–1
Ionospheric forward scatter (VHF)	10^{-4}	10	10^{-3}
Tropospheric scatter (SHF)	10^{-6}	10	10^{-5}
Orbital scatter (X band)	10^{-4}	10^{3}	10^{-1}
Moon at max. libration ($f_0 = 0.4$ kmc)	10^{-2}	10	10^{-1}

implies that the channel characteristics vary sufficiently slowly that they can be measured.

In Section 14-3, we shall determine the error rate performance for binary signaling over a frequency-nonselective slowly fading channel. This channel model is, by far, the simplest to analyze. More importantly, it yields insight into the performance characteristics for digital signaling on a fading channel and serves to suggest the type of signal waveforms that are effective in overcoming the fading caused by the channel.

Since the multipath components in the received signal are not resolvable when the signal bandwidth W is less than the coherence bandwidth $(\Delta f)_c$ of the channel, the received signal appears to arrive at the receiver via a single fading path. On the other hand, we may choose $W \gg (\Delta f)_c$, so that the channel becomes frequency-selective. We shall show later that, under this condition, the multipath components in the received signal are resolvable with a resolution in time delay of $1/W$. Thus, we shall illustrate that the frequency-selective channel can be modeled as a tapped delay line (transversal) filter with time-variant tap coefficients. We shall then derive the performance of binary signaling over such a frequency-selective channel model.

14-3 FREQUENCY-NONSELECTIVE, SLOWLY FADING CHANNEL

In this section, we derive the error rate performance of binary PSK and binary FSK when these signals are transmitted over a frequency-nonselective, slowly fading channel. As described in Section 14-2, the frequency-nonselective channel results in multiplicative distortion of the transmitted signal $s_l(t)$. Furthermore, the condition that the channel fades slowly implies that the multiplicative process may be regarded as a constant during at least one

signaling interval. Consequently, if the transmitted signal is $s_i(t)$, the received equivalent lowpass signal in one signaling interval is

$$r_l(t) = \alpha e^{-j\phi} s_l(t) + z(t), \quad 0 \leq t \leq T \tag{14-3-1}$$

where $z(t)$ represents the complex-valued white gaussian noise process corrupting the signal.

Let us assume that the channel fading is sufficiently slow that the phase shift ϕ can be estimated from the received signal without error. In that case, we can achieve ideal coherent detection of the received signal. Thus, the received signal can be processed by passing it through a matched filter in the case of binary PSK or through a pair of matched filters in the case of binary FSK. One method that we can use to determine the performance of the binary communications systems is to evaluate the decision variables and from these determine the probability of error. However, we have already done this for a fixed (time-invariant) channel. That is, for a fixed attenuation α, we have previously derived the probability of error for binary PSK and binary FSK. From (5-2-5), the expression for the error rate of binary PSK as a function of the received SNR γ_b is

$$P_2(\gamma_b) = Q(\sqrt{2\gamma_b}) \tag{14-3-2}$$

where $\gamma_b = \alpha^2 \mathscr{E}_b / N_0$. The expression for the error rate of binary FSK, detected coherently, is given by (5-2-10) as

$$P_2(\gamma_b) = Q(\sqrt{\gamma_b}) \tag{14-3-3}$$

We view (14-3-2) and (14-3-3) as conditional error probabilities, where the condition is that α is fixed. To obtain the error probabilities when α is random, we must average $P_2(\gamma_b)$, given in (14-3-2) and (14-3-3), over the probability density function of γ_b. That is, we must evaluate the integral

$$P_2 = \int_0^\infty P_2(\gamma_b) p(\gamma_b)\, d\gamma_b \tag{14-3-4}$$

where $p(\gamma_b)$ is the probability density function of γ_b when α is random.

Rayleigh Fading Since α is Rayleigh-distributed, α^2 has a chi-square probability distribution with two degrees of freedom. Consequently, γ_b also is chi-square-distributed. It is easily shown that

$$p(\gamma_b) = \frac{1}{\bar{\gamma}_b} e^{-\gamma_b/\bar{\gamma}_b}, \quad \gamma_b \geq 0 \tag{14-3-5}$$

where $\bar{\gamma}_b$ is the average signal-to-noise ratio, defined as

$$\bar{\gamma}_b = \frac{\mathscr{E}_b}{N_0} E(\alpha^2) \tag{14-3-6}$$

The term $E(\alpha^2)$ is simply the average value of α^2.

Now we can substitute (14-3-5) into (14-3-4) and carry out the integration for $P_2(\gamma_b)$ as given by (14-3-2) and (14-3-3). The result of this integration for binary PSK is

$$P_2 = \frac{1}{2}\left(1 - \sqrt{\frac{\bar{\gamma}_b}{1 + \bar{\gamma}_b}}\right) \tag{14-3-7}$$

If we repeat the integration with $P_2(\gamma_b)$ given by (14-3-3), we obtain the probability of error for binary FSK, detected coherently, in the form

$$P_2 = \frac{1}{2}\left(1 - \sqrt{\frac{\bar{\gamma}_b}{2 + \bar{\gamma}_b}}\right) \tag{14-3-8}$$

In arriving at the error rate results in (14-3-7) and (14-3-8), we have assumed that the estimate of the channel phase shift, obtained in the presence of slow fading, is noiseless. Such an ideal condition may not hold in practice. In such a case, the expressions in (14-3-7) and (14-3-8) should be viewed as representing the best achievable performance in the presence of Rayleigh fading. In Appendix C we consider the problem of estimating the phase in the presence of noise and we evaluate the error rate performance of binary and multiphase PSK.

On channels for which the fading is sufficiently rapid to preclude the estimation of a stable phase reference by averaging the received signal phase over many signaling intervals, DPSK, is an alternative signaling method. Since DPSK requires phase stability over only two consecutive signaling intervals, this modulation technique is quite robust in the presence of signal fading. In deriving the performance of binary DPSK for a fading channel, we begin again with the error probability for a nonfading channel, which is

$$P_2(\gamma_b) = \tfrac{1}{2}e^{-\gamma_b} \tag{14-3-9}$$

This expression is substituted into the integral in (14-3-4) along with $p(\gamma_b)$ obtained from (14-3-5). Evaluation of the resulting integral yields the probability of error for binary DPSK, in the form

$$P_2 = \frac{1}{2(1 + \bar{\gamma}_b)} \tag{14-3-10}$$

If we choose not to estimate the channel phase shift at all, but instead employ a noncoherent (envelope or square-law) detector with binary, orthogonal FSK signals, the error probability for a nonfading channel is

$$P_2(\gamma_b) = \tfrac{1}{2}e^{-\gamma_b/2} \tag{14-3-11}$$

When we average $P_2(\gamma_b)$ over the Rayleigh fading channel attenuation, the resulting error probability is

$$P_2 = \frac{1}{2 + \bar{\gamma}_b} \tag{14-3-12}$$

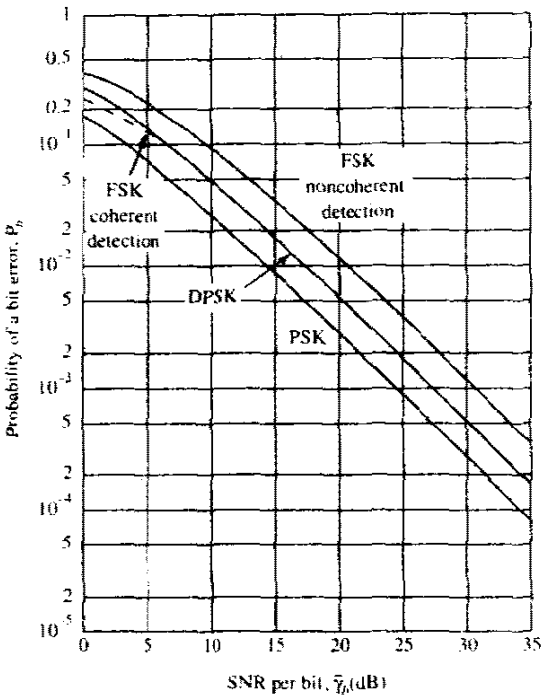

FIGURE 14-3-1 Performance of binary signaling on a Rayleigh fading channel.

The error probabilities in (14-3-7), (14-3-8), (14-3-10), and (14-3-12) are illustrated in Fig. 14-3-1. In comparing the performance of the four binary signaling systems, we focus our attention on the probabilities of error for large SNR, i.e., $\bar{\gamma}_b \gg 1$. Under this condition, the error rates in (14-3-7), (14-3-8), (14-3-10), and (14-3-12) simplify to

$$P_2 \approx \begin{cases} 1/4\bar{\gamma}_b & \text{for coherent PSK} \\ 1/2\bar{\gamma}_b & \text{for coherent, orthogonal FSK} \\ 1/2\bar{\gamma}_b & \text{for DPSK} \\ 1/\bar{\gamma}_b & \text{for noncoherent, orthogonal FSK} \end{cases} \tag{14-3-13}$$

From (14-3-13), we observe that coherent PSK is 3 dB better than DPSK and 6 dB better than noncoherent FSK. More striking, however, is the observation that the error rates decrease only inversely with SNR. In contrast, the decrease in error rate on a nonfading channel is exponential with SNR. This means that, on a fading channel, the transmitter must transmit a large amount of power in order to obtain a low probability of error. In many cases, a large amount of power is not possible, technically and/or economically. An alternative solution to the problem of obtaining acceptable performance on a fading channel is the use of redundancy, which can be obtained by means of diversity techniques, as discussed in Section 14-4.

Nakagami Fading If α is characterized statistically by the Nakagami-m distribution, the random variable $\gamma = \alpha^2 \mathcal{E}_b / N_0$ has the pdf (see Problem 14-15)

$$p(\gamma) = \frac{m^m}{\Gamma(m)\bar{\gamma}^m} \gamma^{m-1} e^{-m\gamma/\bar{\gamma}} \tag{14-3-14}$$

where $\bar{\gamma} = E(\alpha^2)\mathcal{E}/N_0$.

The average probability of error for any of the modulation methods is simply obtained by averaging the appropriate error probability for a nonfading channel over the fading signal statistics.

As an example of the performance obtained with Nakagami-m fading statistics, Fig. 14-3-2 illustrates the probability of error of binary PSK with m as a parameter. We recall that $m = 1$ corresponds to Rayleigh fading. We observe that the performance improves as m is increased above $m = 1$, which is indicative of the fact that the fading is less severe. On the other hand, when $m < 1$, the performance is worse than Rayleigh fading.

Other Fading Signal Statistics Following the procedure described above, one can determine the performance of the various modulation methods for other types of fading signal statistics, such as the Rice distribution.

Error probability results for Rice-distributed fading statistics can be found in the paper by Lindsey (1964), while for Nakagami-m fading statistics, the

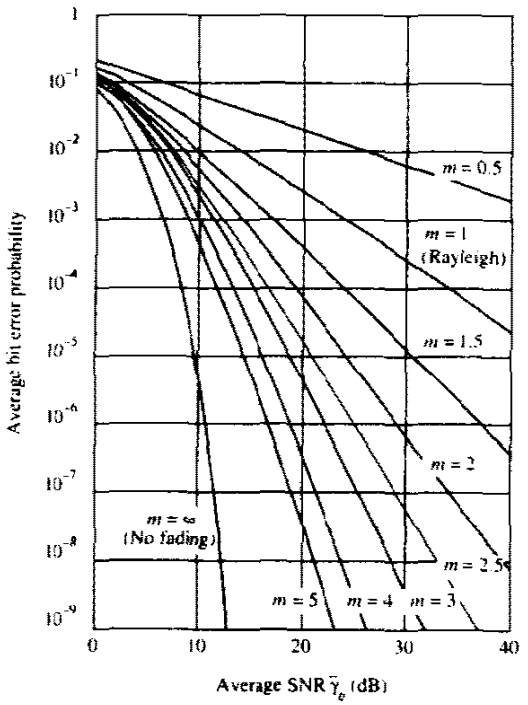

FIGURE 14-3-2 Average error probability for two-phase PSK symbol in nondiversity reception.

reader may refer to the papers by Esposito (1967), Miyagaki *et al.* (1978), Charash (1979), Al-Hussaini *et al.* (1985), and Beaulieu *et al.* (1991).

14-4 DIVERSITY TECHNIQUES FOR FADING MULTIPATH CHANNELS

Diversity techniques are based on the notion that errors occur in reception when the channel attenuation is large, i.e., when the channel is in a deep fade. If we can supply to the receiver several replicas of the same information signal transmitted over independently fading channels, the probability that all the signal components will fade simultaneously is reduced considerably. That is, if p is the probability that any one signal will fade below some critical value then p^L is the probability that all L independently fading replicas of the same signal will fade below the critical value. There are several ways in which we can provide the receiver with L independently fading replicas of the same information-bearing signal.

One method is to employ *frequency diversity*. That is, the same information-bearing signal is transmitted on L carriers, where the separation between successive carriers equals or exceeds the coherence bandwidth $(\Delta f)_c$ of the channel.

A second method for achieving L independently fading versions of the same information-bearing signal is to transmit the signal in L different time slots, where the separation between successive time slots equals or exceeds the coherence time $(\Delta t)_c$ of the channel. This method is called *time diversity*.

Note that the fading channel fits the model of a bursty error channel. Furthermore, we may view the transmission of the same information either at different frequencies or in difference time slots (or both) as a simple form of repetition coding. The separation of the diversity transmissions in time by $(\Delta t)_c$ or in frequency by $(\Delta f)_c$ is basically a form of block-interleaving the bits in the repetition code in an attempt to break up the error bursts and, thus, to obtain independent errors. Later in the chapter, we shall demonstrate that, in general, repetition coding is wasteful of bandwidth when compared with nontrivial coding.

Another commonly used method for achieving diversity employs multiple antennas. For example, we may employ a single transmitting antenna and multiple receiving antennas. The latter must be spaced sufficiently far apart that the multipath components in the signal have significantly different propagation delays at the antennas. Usually a separation of at least 10 wavelengths is required between two antennas in order to obtain signals that fade independently.

A more sophisticated method for obtaining diversity is based on the use of a signal having a bandwidth much greater than the coherence bandwidth $(\Delta f)_c$ of the channel. Such a signal with bandwidth W will resolve the multipath components and, thus, provide the receiver with several independently fading signal paths. The time resolution is $1/W$. Consequently, with a multipath

spread of T_m s, there are $T_m W$ resolvable signal components. Since $T_m \approx 1/(\Delta f)_c$, the number of resolvable signal components may also be expressed as $W/(\Delta f)_c$. Thus, the use of a wideband signal may be viewed as just another method for obtaining frequency diversity of order $L \approx W/(\Delta f)_c$. The optimum receiver for processing the wideband signal will be derived in Section 14-5. It is called a *RAKE correlator* or a *RAKE matched filter* and was invented by Price and Green (1958).

There are other diversity techniques that have received some consideration in practice, such as angle-of-arrival diversity and polarization diversity. However, these have not been as widely used as those described above.

14-4-1 Binary Signals

We shall now determine the error rate performance for a binary digital communications system with diversity. We begin by describing the mathematical model for the communications system with diversity. First of all, we assume that there are L diversity channels, carrying the same information-bearing signal. Each channel is assumed to be frequency-nonselective and slowly fading with Rayleigh-distributed envelope statistics. The fading processes among the L diversity channels are assumed to be mutually statistically independent. The signal in each channel is corrupted by an additive zero-mean white gaussian noise process. The noise processes in the L channels are assumed to be mutually statistically independent, with identical autocorrelation functions. Thus, the equivalent low-pass received signals for the L channels can be expressed in the form

$$r_{lk}(t) = \alpha_k e^{-j\phi_k} s_{km}(t) + z_k(t), \quad k = 1, 2, \ldots, L, \quad m = 1, 2 \qquad (14\text{-}4\text{-}1)$$

where $\{\alpha_k e^{-j\phi_k}\}$ represent the attenuation factors and phase shifts for the L channels, $s_{km}(t)$ denotes the mth signal transmitted on the kth channel, and $z_k(t)$ denotes the additive white gaussian noise on the kth channel. All signals in the set $\{s_{km}(t)\}$ have the same energy.

The optimum demodulator for the signal received from the kth channel consists of two matched filters, one having the impulse response

$$b_{k1}(t) = s_{k1}^*(T - t) \qquad (14\text{-}4\text{-}2)$$

and the other having the impulse response

$$b_{k2}(t) = s_{k2}^*(T - t) \qquad (14\text{-}4\text{-}3)$$

Of course, if binary PSK is the modulation method used to transmit the information, then $s_{k1}(t) = -s_{k2}(t)$. Consequently, only a single matched filter is required for binary PSK. Following the matched filters is a combiner that forms the two decision variables. The combiner that achieves the best performance is one in which each matched filter output is multiplied by the corresponding complex-valued (conjugate) channel gain $\alpha_k e^{j\phi_k}$. The effect of this multiplication is to compensate for the phase shift in the channel and to

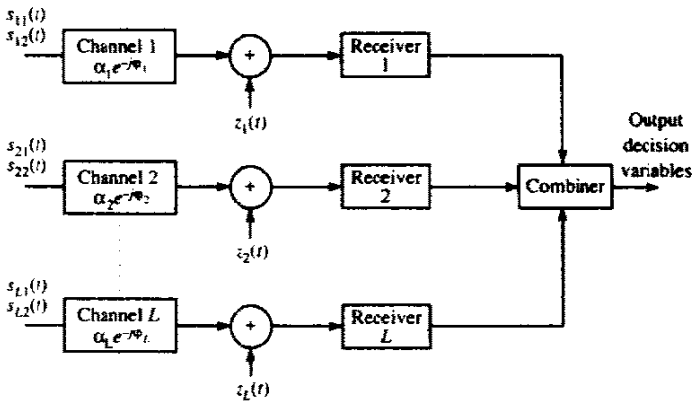

FIGURE 14-4-1 Model of binary digital communications system with diversity.

weight the signal by a factor that is proportional to the signal strength. Thus, a strong signal carries a larger weight than a weak signal. After the complex-valued weighting operation is performed, two sums are formed. One consists of the real parts of the weighted outputs from the matched filters corresponding to a transmitted 0. The second consists of the real part of the outputs from the matched filters corresponding to a transmitted 1. This optimum combiner is called a *maximal ratio combiner* by Brennan (1959). Of course, the realization of this optimum combiner is based on the assumption that the channel attenuations $\{\alpha_k\}$ and the phase shifts $\{\phi_k\}$ are known perfectly. That is, the estimates of the parameters $\{\alpha_k\}$ and $\{\phi_k\}$ contain no noise. (The effect of noisy estimates on the error rate performance of multiphase PSK is considered in Appendix C.

A block diagram illustrating the model for the binary digital communications system described above is shown in Fig. 14-4-1.

Let us first consider the performance of binary PSK with Lth-order diversity. The output of the maximal ratio combiner can be expressed as a single decision variable in the form

$$U = \mathrm{Re}\left(2\mathscr{E}\sum_{k=1}^{L}\alpha_k^2 + \sum_{k=1}^{L}\alpha_k N_k\right)$$
$$= 2\mathscr{E}\sum_{k=1}^{L}\alpha_k^2 + \sum_{k=1}^{L}\alpha_k N_{kr} \tag{14-4-4}$$

where N_{kr} denotes the real part of the complex-valued gaussian noise variable

$$N_k = e^{j\phi_k}\int_0^T z_k(t)s_k^*(t)\,dt \tag{14-4-5}$$

We follow the approach used in Section 14-3 in deriving the probability of error. That is, the probability of error conditioned on a fixed set of attenuation

factors $\{\alpha_k\}$ is obtained first. Then the conditional probability of error is averaged over the probability density function of the $\{\alpha_k\}$.

Rayleigh Fading For a fixed set of $\{\alpha_k\}$ the decision variable U is gaussian with mean

$$E(U) = 2\mathscr{E}\sum_{k=1}^{L}\alpha_k^2 \tag{14-4-6}$$

and variance

$$\sigma_U^2 = 2\mathscr{E}N_0\sum_{k=1}^{L}\alpha_k^2 \tag{14-4-7}$$

For these values of the mean and variance, the probability that U is less than zero is simply

$$P_2(\gamma_b) = Q(\sqrt{2\gamma_b}) \tag{14-4-8}$$

where the SNR per bit, γ_b, is given as

$$\begin{aligned}\gamma_b &= \frac{\mathscr{E}}{N_0}\sum_{k=1}^{L}\alpha_k^2 \\ &= \sum_{k=1}^{L}\gamma_k\end{aligned} \tag{14-4-9}$$

where $\gamma_k = \mathscr{E}\alpha_k^2/N_0$ is the instantaneous SNR on the kth channel. Now we must determine the probability density function $p(\gamma_b)$. This function is most easily determined via the characteristic function of γ_b. First of all, we note that for $L = 1$, $\gamma_b \equiv \gamma_1$ has a chi-square probability density function given in (14-3-5). The characteristic function of γ_1 is easily shown to be

$$\begin{aligned}\psi_{\gamma_1}(jv) &= E(e^{jv\gamma_1}) \\ &= \frac{1}{1 - jv\bar{\gamma}_c}\end{aligned} \tag{14-4-10}$$

where $\bar{\gamma}_c$ is the average SNR per channel, which is assumed to be identical for all channels. That is,

$$\bar{\gamma}_c = \frac{\mathscr{E}}{N_0}E(\alpha_k^2) \tag{14-4-11}$$

independent of k. This assumption applies for the results throughout this section. Since the fading on the L channels is mutually statistically independent, the $\{\gamma_k\}$ are statistically independent, and, hence, the characteristic function for the sum γ_b is simply the result in (14-4-10) raised to the Lth power, i.e.,

$$\psi_{\gamma_b}(jv) = \frac{1}{(1 - jv\bar{\gamma}_c)^L} \tag{14-4-12}$$

But this is the characteristic function of a chi-square-distributed random variable with $2L$ degrees of freedom. It follows from (2-1-107) that the probability density function $p(\gamma_b)$ is

$$p(\gamma_b) = \frac{1}{(L-1)!\bar{\gamma}_c^L}\gamma_b^{L-1}e^{-\gamma_b/\bar{\gamma}_c} \tag{14-4-13}$$

The final step in this derivation is to average the conditional error probability given in (14-4-8) over the fading channel statistics. Thus, we evaluate the integral

$$P_2 = \int_0^\infty P_2(\gamma_b)p(\gamma_b)\,d\gamma_b \tag{14-4-14}$$

There is a closed-form solution for (14-4-14), which can be expressed as

$$P_2 = [\tfrac{1}{2}(1-\mu)]^L \sum_{k=0}^{L-1}\binom{L-1+k}{k}[\tfrac{1}{2}(1+\mu)]^k \tag{14-4-15}$$

where, by definition,

$$\mu = \sqrt{\frac{\bar{\gamma}_c}{1+\bar{\gamma}_c}} \tag{14-4-16}$$

When the average SNR per channel, $\bar{\gamma}_c$, satisfies the condition $\bar{\gamma}_c \gg 1$, the term $\frac{1}{2}(1+\mu) \approx 1$ and the term $\frac{1}{2}(1-\mu) \approx 1/4\bar{\gamma}_c$. Furthermore,

$$\sum_{k=0}^{L-1}\binom{L-1+k}{k} = \binom{2L-1}{L} \tag{14-4-17}$$

Therefore, when $\bar{\gamma}_c$ is sufficiently large (greater than 10 dB), the probability of error in (14-4-15) can be approximated as

$$P_2 \approx \left(\frac{1}{4\bar{\gamma}_c}\right)^L\binom{2L-1}{L} \tag{14-4-18}$$

We observe from (14-4-18) that the probability of error varies as $1/\bar{\gamma}_c$ raised to the Lth power. Thus, with diversity, the error rate decreases inversely with the Lth power of the SNR.

Having obtained the performance of binary PSK with diversity, we now turn our attention to binary, orthogonal FSK that is detected coherently. In this case, the two decision variables at the output of the maximal ratio combiner may be expressed as

$$\begin{aligned} U_1 &= \mathrm{Re}\left(2\mathscr{E}\sum_{k=1}^{L}\alpha_k^2 + \sum_{k=1}^{L}\alpha_k N_{k1}\right) \\ U_2 &= \mathrm{Re}\left(\sum_{k=1}^{L}\alpha_k N_{k2}\right) \end{aligned} \tag{14-4-19}$$

where we have assumed that signal $s_{k1}(t)$ was transmitted and where $\{N_{k1}\}$ and $\{N_{k2}\}$ are the two sets of noise component at the output of the matched filters.

The probability of error is simply the probability that $U_2 > U_1$. This computation is similar to the one performed for PSK, except that we now have twice the noise power. Consequently, when the $\{\alpha_k\}$ are fixed, the conditional probability of error is

$$P_2(\gamma_b) = Q(\sqrt{\gamma_b}) \tag{14-4-20}$$

We use (14-4-13) to average $P_2(\gamma_b)$ over the fading. It is not surprising to find that the result given in (14-4-15) still applies, with $\bar{\gamma}_c$ replaced by $\frac{1}{2}\bar{\gamma}_c$. That is, (14-4-15) is the probability of error for binary, orthogonal FSK with coherent detection, where the parameter μ is defined as

$$\mu = \sqrt{\frac{\bar{\gamma}_c}{2 + \bar{\gamma}_c}} \tag{14-4-21}$$

Furthermore, for large values of $\bar{\gamma}_c$, the performance P_2 can be approximated as

$$P_2 \approx \left(\frac{1}{2\bar{\gamma}_c}\right)^L \binom{2L-1}{L} \tag{14-4-22}$$

In comparing (14-4-22) with (14-4-18), we observe that the 3 dB difference in performance between PSK and orthogonal FSK with coherent detection, which exists in a nonfading, nondispersive channel, is the same also in a fading channel.

In the above discussion of binary PSK and FSK, detected coherently, we assumed that noiseless estimates of the complex-valued channel parameters $\{\alpha_k e^{-j\phi_k}\}$ were used at the receiver. Since the channel is time-variant, the parameters $\{\alpha_k e^{-j\phi_k}\}$ cannot be estimated perfectly. In fact, on some channels, the time variations may be sufficiently fast to preclude the implementation of coherent detection. In such a case, we should consider using either DPSK or FSK with noncoherent detection.

Let us consider DPSK first. In order for DPSK to be a viable digital signaling method, the channel variations must be sufficiently slow so that the channel phase shifts $\{\phi_k\}$ do not change appreciably over two consecutive signaling intervals. In our analysis, we assume that the channel parameters $\{\alpha_k e^{-j\phi_k}\}$ remain constant over two successive signaling intervals. Thus the combiner for binary DPSK will yield as an output the decision variable

$$U = \mathrm{Re}\left[\sum_{k=1}^{L} (2\mathscr{E}\alpha_k e^{-j\phi_k} + N_{k2})(2\mathscr{E}\alpha_k e^{j\phi_k} + N_{k1}^*)\right] \tag{14-4-23}$$

where $\{N_{k1}\}$ and $\{N_{k2}\}$ denote the received noise components at the output of the matched filters in the two consecutive signaling intervals. The probability of error is simply the probability that $U < 0$. Since U is a special case of the general quadratic form in complex-valued gaussian random variables treated in Appendix B, the probability of error can be obtained directly from the results given in that appendix. Alternatively, we may use the error probability given in (12-1-3), which applies to binary DPSK transmitted over L time-invariant

channels, and average it over the Rayleigh fading channel statistics. Thus, we have the conditional error probability

$$P_2(\gamma_b) = (\tfrac{1}{2})^{2L-1} e^{-\gamma_b} \sum_{k=0}^{L-1} b_k \gamma_b^2 \tag{14-4-24}$$

where γ_b is given by (14-4-9) and

$$b_k = \frac{1}{k!} \sum_{n=0}^{L-1-k} \binom{2L-1}{n} \tag{14-4-25}$$

The average of $P_2(\gamma_b)$ over the fading channel statistics given by $p(\gamma_b)$ in (14-4-13) is easily shown to be

$$P_2 = \frac{1}{2^{2L-1}(L-1)!(1+\bar{\gamma}_c)^L} \sum_{k=0}^{L-1} b_k (L-1+k)! \left(\frac{\bar{\gamma}_c}{1+\bar{\gamma}_c}\right)^k \tag{14-4-26}$$

We indicate that the result in (14-4-26) can be manipulated into the form given in (14-4-15), which applies also to coherent PSK and FSK. For binary DPSK, the parameter μ in (14-4-15) is defined as (see Appendix C)

$$\mu = \frac{\bar{\gamma}_c}{1+\bar{\gamma}_c} \tag{14-4-27}$$

For $\bar{\gamma}_c \gg 1$, the error probability in (14-4-26) can be approximated by the expression

$$P_2 \approx \left(\frac{1}{2\bar{\gamma}_c}\right)^L \binom{2L-1}{L} \tag{14-4-28}$$

Orthogonal FSK with noncoherent detection is the final signaling technique that we consider in this section. It is appropriate for both slow and fast fading. However, the analysis of the performance presented below is based on the assumption that the fading is sufficiently slow so that the channel parameters $\{\alpha_k e^{-j\phi_k}\}$ remain constant for the duration of the signaling interval. The combiner for the multichannel signals is a square-law combiner. Its output consists of the two decision variables

$$\begin{aligned} U_1 &= \sum_{k=1}^{L} |2\mathscr{E}\alpha_k e^{-j\phi_k} + N_{k1}|^2 \\ U_2 &= \sum_{k=1}^{L} |N_{k2}|^2 \end{aligned} \tag{14-4-29}$$

where U_1 is assumed to contain the signal. Consequently the probability of error is the probability that $U_2 > U_1$.

As in DPSK, we have a choice of two approaches in deriving the performance of FSK with square-law combining. In Section 12-1, we indicated that the expression for the error probability for square-law combined FSK is the same as that for DPSK with γ_b replaced by $\frac{1}{2}\gamma_b$. That is, the FSK system requires 3 dB of additional SNR to achieve the same performance on a time-invariant channel. Consequently, the conditional error probability for DPSK given in (14-4-24) applies to square-law-combined FSK when γ_b is replaced by $\frac{1}{2}\gamma_b$. Furthermore, the result obtained by averaging (14-4-24) over the fading, which is given by (14-4-26), must also apply to FSK with $\bar{\gamma}_c$ replaced by $\frac{1}{2}\bar{\gamma}_c$. But we also stated previously that (14-4-26) and (14-4-15) are equivalent. Therefore, the error probability given in (14-4-15) also applies to square-law-combined FSK with the parameter μ defined as

$$\mu = \frac{\bar{\gamma}_c}{2 + \bar{\gamma}_c} \tag{14-4-30}$$

An alternative derivation used by Pierce (1958) to obtain the probability that the decision variable $U_2 > U_1$ is just as easy as the method described above. It begins with the probability density functions $p(U_1)$ and $p(U_2)$. Since the complex-valued random variables $\{\alpha_k e^{-j\phi_k}\}$, $\{N_{k1}\}$, and $\{N_{k2}\}$ are zero-mean gaussian-distributed, the decision variables U_1 and U_2 are distributed according to a chi-square probability distribution with $2L$ degrees of freedom. That is,

$$p(U_1) = \frac{1}{(2\sigma_1^2)^L (L-1)!} U_1^{L-1} \exp\left(-\frac{U_1}{2\sigma_1^2}\right) \tag{14-4-31}$$

where

$$\begin{aligned}\sigma_1^2 &= \tfrac{1}{2}E(|2\mathscr{E}\alpha_k e^{-j\phi_k} + N_{k1}|^2) \\ &= 2\mathscr{E}N_0(1 + \bar{\gamma}_c)\end{aligned}$$

Similarly,

$$p(U_2) = \frac{2}{(2\sigma_2^2)^L (L-1)!} U_2^{L-1} \exp\left(-\frac{U_2}{2\sigma_2^2}\right) \tag{14-4-32}$$

where

$$\sigma_2^2 = 2\mathscr{E}N_0$$

The probability of error is just the probability that $U_2 > U_1$. It is left as an exercise for the reader to show that this probability is given by (14-4-15), where μ is defined by (14-4-30).

When $\bar{\gamma}_c \gg 1$, the performance of square-law-detected FSK can be simplified as we have done for the other binary multichannel systems. In this case, the error rate is well approximated by the expression

$$P_2 \approx \left(\frac{1}{\bar{\gamma}_c}\right)^L \binom{2L-1}{L} \tag{14-4-33}$$

The error rate performance of PSK, DPSK, and square-law-detected

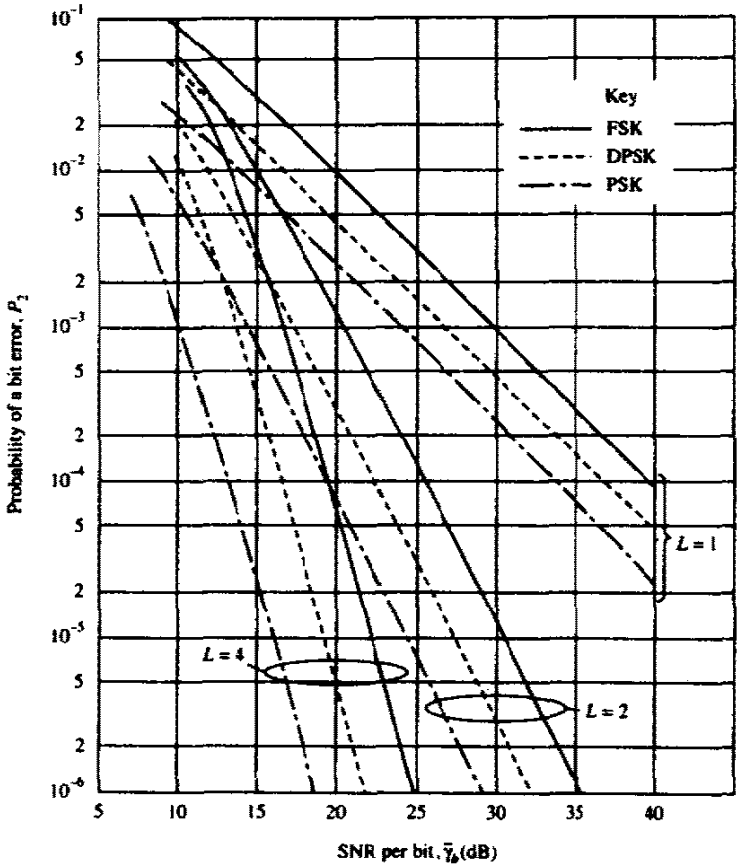

FIGURE 14-4-2 Performance of binary signals with diversity.

orthogonal FSK is illustrated in Fig. 14-4-2 for $L = 1$, 2, and 4. The performance is plotted as a function of the average SNR per bit, $\bar{\gamma}_b$, which is related to the average SNR per channel, $\bar{\gamma}_c$, by the formula

$$\bar{\gamma}_b = L\bar{\gamma}_c \tag{14-4-34}$$

The results in Fig. 14-4-2 clearly illustrate the advantage of diversity as a means for overcoming the severe penalty in SNR caused by fading.

14-4-2 Multiphase Signals

Multiphase signaling over a Rayleigh fading channel is the topic presented in some detail in Appendix C. Our main purpose in this section is to cite the general result for the probability of a symbol error in M-ary PSK and DPSK systems and the probability of a bit error in four-phase PSK and DPSK.

The general result for the probability of a symbol error in M-ary PSK and DPSK is

$$P_M = \frac{(-1)^{L-1}(1-\mu^2)^L}{\pi(L-1)!}\left(\frac{\partial^{L-1}}{\partial b^{L-1}}\left\{\frac{1}{b-\mu^2}\left[\frac{\pi}{M}(M-1)\right.\right.\right.$$
$$\left.\left.\left. - \frac{\mu \sin(\pi/M)}{\sqrt{b-\mu^2\cos^2(\pi/M)}}\cot^{-1}\frac{-\mu\cos(\pi/M)}{\sqrt{b-\mu^2\cos^2(\pi/M)}}\right]\right\}\right)_{b=1} \quad (14\text{-}4\text{-}35)$$

where

$$\mu = \sqrt{\frac{\bar{\gamma}_c}{1+\bar{\gamma}_c}} \quad (14\text{-}4\text{-}36)$$

for coherent PSK and

$$\mu = \frac{\bar{\gamma}_c}{1+\bar{\gamma}_c} \quad (14\text{-}4\text{-}37)$$

for DPSK. Again, $\bar{\gamma}_c$ is the average received SNR per channel. The SNR per bit is $\bar{\gamma}_b = L\bar{\gamma}_c/k$, where $k = \log_2 M$.

The bit error rate for four-phase PSK and DPSK is derived on the basis that the pair of information bits is mapped into the four phases according to a Gray code. The expression for the bit error rate derived in Appendix C is

$$P_b = \frac{1}{2}\left[1 - \frac{\mu}{\sqrt{2-\mu^2}}\sum_{k=0}^{L-1}\binom{2k}{k}\left(\frac{1-\mu^2}{4-2\mu^2}\right)^k\right] \quad (14\text{-}4\text{-}38)$$

where μ is again given by (14-4-36) and (14-4-37) for PSK and DPSK, respectively.

Figure 14-4-3 illustrates the probability of a symbol error of DPSK and coherent PSK for $M = 2$, 4, and 8 with $L = 1$. Note that the difference in performance between DPSK and coherent PSK is approximately 3 dB for all three values of M. In fact, when $\bar{\gamma}_b \gg 1$ and $L = 1$, (14-4-35) is well approximated as

$$P_M \approx \frac{M-1}{(M\log_2 M)[\sin^2(\pi/M)]\bar{\gamma}_b} \quad (14\text{-}4\text{-}39)$$

for DPSK and as

$$P_M \approx \frac{M-1}{(M\log_2 M)[\sin^2(\pi/M)]2\bar{\gamma}_b} \quad (14\text{-}4\text{-}40)$$

for PSK. Hence, at high SNR, coherent PSK is 3 dB better than DPSK on a Rayleigh fading channel. This difference also holds as L is increased.

Bit error probabilities are depicted in Fig. 14-4-4 for two-phase, four-phase, and eight-phase DPSK signaling with $L = 1$, 2, and 4. The expression for the bit error probability of eight-phase DPSK with Gray encoding is not given here, but it is available in the paper by Proakis (1968). In this case, we observe

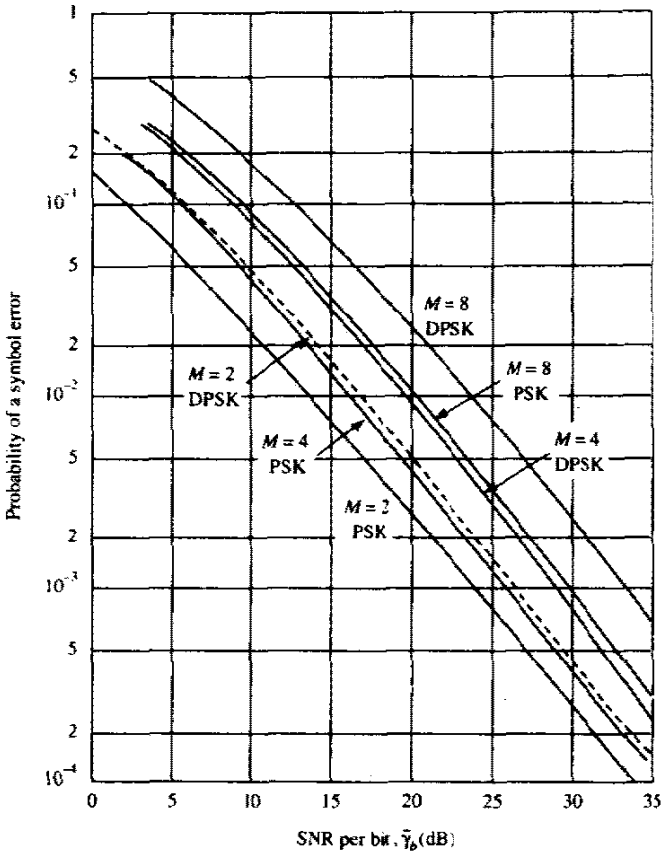

FIGURE 14-4-3 Probability of symbol error for PSK and DPSK for Rayleigh fading.

that the performances for two- and four-phase DPSK are (approximately) the same, while that for eight-phase DPSK is about 3 dB poorer. Although we have not shown the bit error probability for coherent PSK, it can be demonstrated that two- and four-phase coherent PSK also yield approximately the same performance.

14-4-3 *M*-ary Orthogonal Signals

In this sub-section, we determine the performance of M-ary orthogonal signals transmitted over a Rayleigh fading channel and we assess the advantages of higher-order signal alphabets relative to a binary alphabet. The orthogonal signals may be viewed as M-ary FSK with a minimum frequency separation of an integer multiple of $1/T$, where T is the signaling interval. The same information-bearing signal is transmitted on L diversity channels. Each diversity channel is assumed to be frequency-nonselective and slowly fading, and the fading processes on the L channels are assumed to be mutually

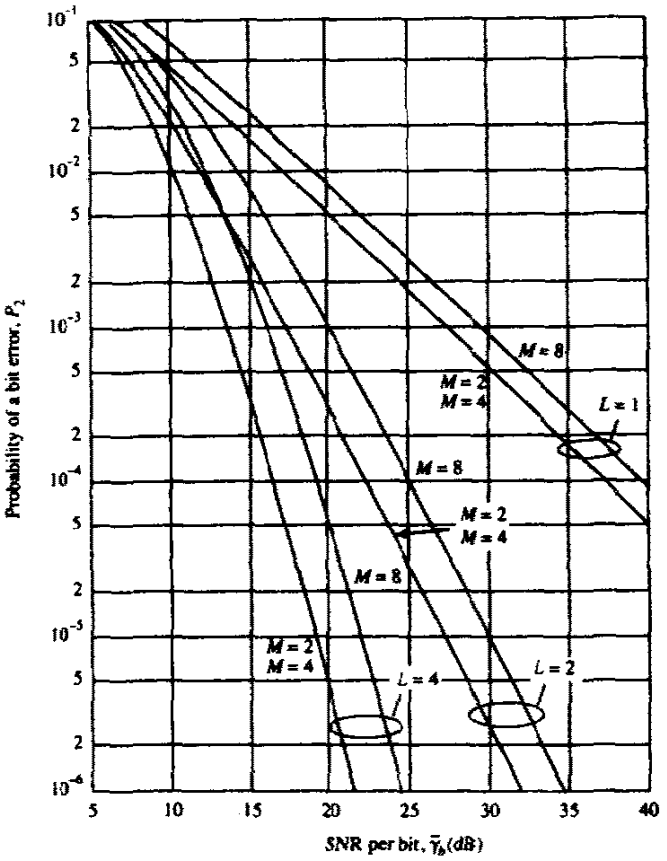

FIGURE 14-4-4 Probability of a bit error for DPSK with diversity for Rayleigh fading.

statistically independent. An additive white gaussian noise process corrupts the signal on each diversity channel. We assume that the additive noise processes are mutually statistically independent.

Although it is relatively easy to formulate the structure and analyze the performance of a maximal ratio combiner for the diversity channels in the M-ary communication system, it is more likely that a practical system would employ noncoherent detection. Consequently, we confine our attention to square-law combining of the diversity signals. The output of the combiner containing the signal is

$$U_1 = \sum_{k=1}^{L} |2\mathcal{E}\alpha_k e^{-j\phi_k} + N_{k1}|^2 \tag{14-4-41}$$

while the outputs of the remaining $M-1$ combiners are

$$U_m = \sum_{k=1}^{L} |N_{km}|^2, \quad m = 2, 3, 4, \ldots, M \tag{14-4-42}$$

The probability of error is simply 1 minus the probability that $U_1 > U_m$ for $m = 2, 3, \ldots, M$. Since the signals are orthogonal and the additive noise processes are mutually statistically independent, the random variables $U_1, U_2, \ldots, U_M$ are also mutually statistically independent. The probability density function of U_1 was given in (14-4-31). On the other hand, $U_2, \ldots, U_M$ are identically distributed and described by the marginal probability density function in (14-4-32). With U_1 fixed, the joint probability $P(U_2 < U_1, U_3 < U_1, \ldots, U_m < U_1)$ is equal to $P(U_2 < U_1)$ raised to the $M-1$ power. Now,

$$P(U_2 < U_1) = \int_0^{U_1} p(U_2)\, dU_2$$
$$= 1 - \exp\left(-\frac{U_1}{2\sigma_2^2}\right) \sum_{k=0}^{L-1} \frac{1}{k!} \left(\frac{U_1}{2\sigma_2^2}\right)^k \tag{14-4-43}$$

where $\sigma_2^2 = 2\mathcal{E}N_0$. The $M-1$ power of this probability is then averaged over the probability density function of U_1 to yield the probability of a correct decision. If we subtract this result from unity, we obtain the probability of error in the form given by Hahn (1962)

$$P_M = 1 - \int_0^\infty \frac{1}{(2\sigma_1^2)^L (L-1)!} U_1^{L-1} \exp\left(-\frac{U_1}{2\sigma_2^2}\right)$$
$$\times \left[1 - \exp\left(-\frac{U_1}{2\sigma_2^2}\right) \sum_{k=0}^{L-1} \frac{1}{k!} \left(\frac{U_1}{2\sigma_2^2}\right)^k\right]^{M-1} dU_1$$
$$= 1 - \int_0^\infty \frac{1}{(1+\bar{\gamma}_c)^L (L-1)!} U_1^{L-1} \exp\left(-\frac{U_1}{1+\bar{\gamma}_c}\right)$$
$$\times \left(1 - e^{-U_1} \sum_{k=0}^{L-1} \frac{U_1^k}{k!}\right)^{M-1} dU_1 \tag{14-4-44}$$

where $\bar{\gamma}_c$ is the average SNR per diversity channel. The average SNR per bit is $\bar{\gamma}_b = L\bar{\gamma}_c / \log_2 M = L\bar{\gamma}_c / k$.

The integral in (14-4-44) can be expressed in closed form as a double summation. This can be seen if we write

$$\left(\sum_{k=0}^{L-1} \frac{U_1^k}{k!}\right)^m = \sum_{k=0}^{m(L-1)} \beta_{km} U_1^k \tag{14-4-45}$$

where β_{km} is the set of coefficients in the above expansion. Then it follows that (14-4-44) reduces to

$$P_M = \frac{1}{(L-1)!} \sum_{m=1}^{M-1} \frac{(-1)^{m+1} \binom{M-1}{m}}{(1+m+m\bar{\gamma}_c)^L}$$
$$\times \sum_{k=0}^{m(L-1)} \beta_{km} (L-1+k)! \left(\frac{1+\bar{\gamma}_c}{1+m+m\bar{\gamma}_c}\right)^k \tag{14-4-46}$$

When there is no diversity ($L = 1$), the error probability in (14-4-46) reduces to the simple form

$$P_M = \sum_{m=1}^{M-1} \frac{(-1)^{m+1}\binom{M-1}{m}}{1+m+m\bar{\gamma}_c} \tag{14-4-47}$$

The symbol error rate P_M may be converted to an equivalent bit error rate by multiplying P_M with $2^{k-1}/(2^k-1)$.

Although the expression for P_M given in (14-4-46) is in closed form, it is computationally cumbersome to evaluate for large values of M and L. An alternative is to evaluate P_M by numerical integration using the expression in (14-4-44). The results illustrated in the following graphs were generated from (14-4-44).

First of all, let us observe the error rate performance of M-ary orthogonal signaling with square-law combining as a function of the order of diversity. Figures 14-4-5 and 14-4-6 illustrate the characteristics of P_M for $M = 2$ and 4 as

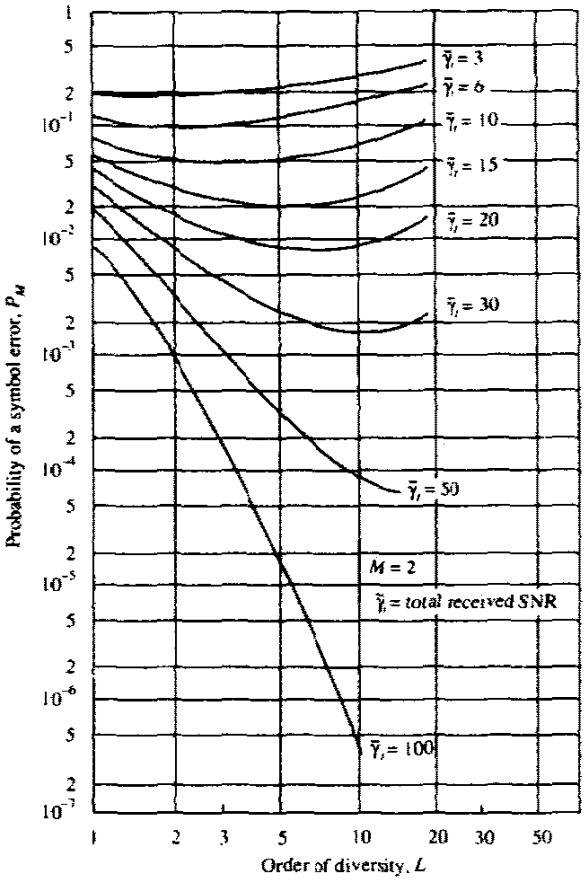

FIGURE 14-4-5 Performance of square-law-detected binary orthogonal signals as a function of diversity.

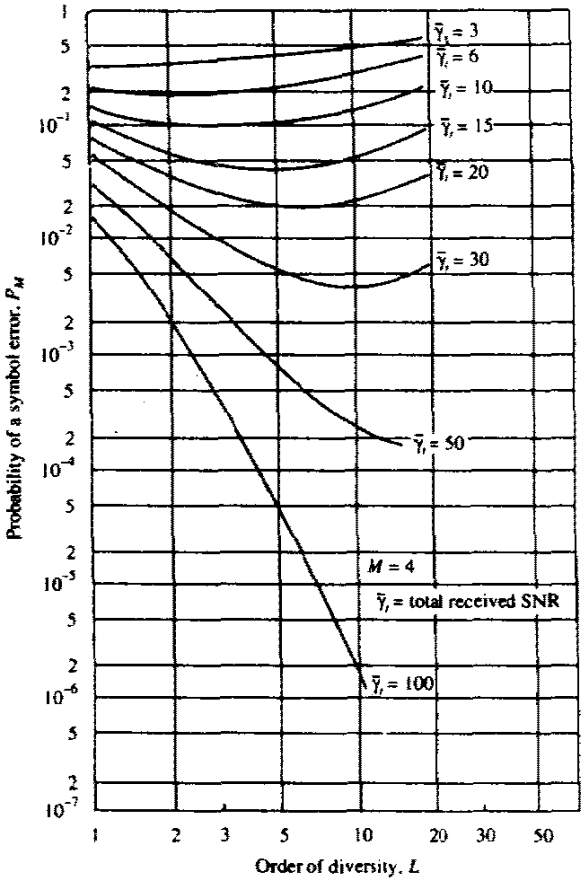

FIGURE 14-4-6 Performance of square-law-detected $M = 4$ orthogonal signals as a function of diversity.

a function of L when the total SNR, defined as $\bar{\gamma}_t = L\bar{\gamma}_c$, remains fixed. These results indicate that there is an optimum order of diversity for each $\bar{\gamma}_t$. That is, for any $\bar{\gamma}_t$, there is a value of L for which P_M is a minimum. A careful observation of these graphs reveals that the minimum in P_M is obtained when $\bar{\gamma}_c = \bar{\gamma}_t/L \approx 3$. This result appears to be independent of the alphabet size M.

Second, let us observe the error rate P_M as a function of the average SNR per bit, defined as $\bar{\gamma}_b = L\bar{\gamma}_c/k$. (If we interpret M-ary orthogonal FSK as a form of coding† and the order of diversity as the number of times a symbol is repeated in a repetition code then $\bar{\gamma}_b = \bar{\gamma}_c/R_c$, where $R_c = k/L$ is the code rate.) The graphs of P_M versus $\bar{\gamma}_b$ for $M = 2, 4, 8, 16, 32$ and $L = 1, 2, 4$ are shown in Fig. 14-4-7. These results illustrate the gain in performance as M increases and L increases. First, we note that a significant gain in performance is obtained by increasing L. Second, we note that the gain in performance obtained with an increase in M is relatively small when L is small. However,

† In Section 14-6, we show that M-ary orthogonal FSK with diversity may be viewed as a block orthogonal code.

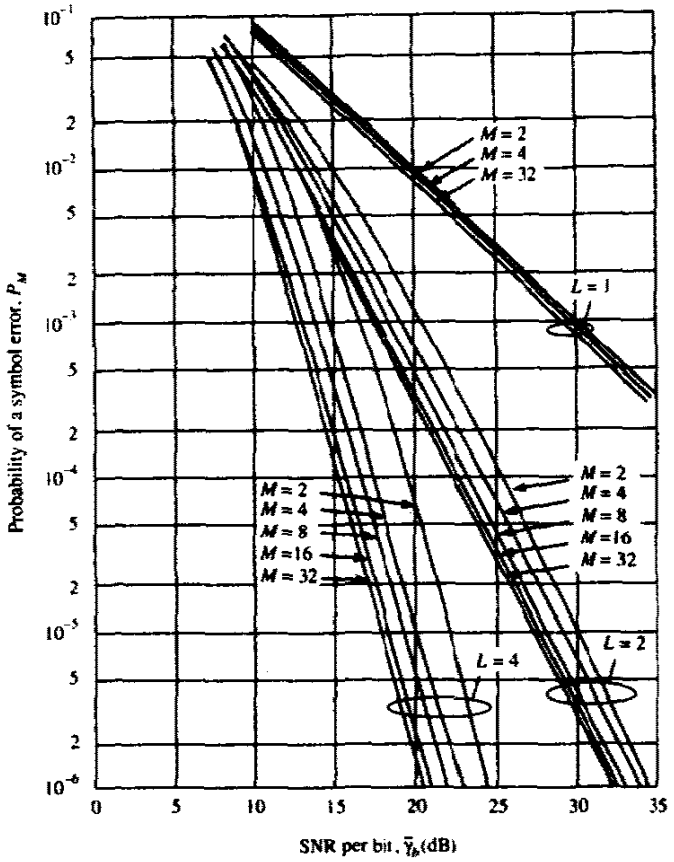

FIGURE 14-4-7 Performance of orthogonal signaling with M and L as parameters.

as L increases, the gain achieved by increasing M also increases. Since an increase in either parameter results in an expansion of bandwidth, i.e.,

$$B_e = \frac{LM}{\log_2 M}$$

the results illustrated in Fig. 14-4-7 indicate that an increase in L is more efficient than a corresponding increase in M. As we shall see in Section 14-6, coding is a bandwidth-effective means for obtaining diversity in the signal transmitted over the fading channel.

Chernoff Bound Before concluding this section, we develop a Chernoff upper bound on the error probability of binary orthogonal signaling with Lth-order diversity, which will be useful in our discussion of coding for fading channels, the topic of Section 14-6. Our starting point is the expression for the two decision variables U_1 and U_2 given by (14-4-29), where U_1 consists of the

square-law-combined signal-plus-noise terms and U_2 consists of square-law-combined noise terms. The binary probability of error, denoted here by $P_2(L)$, as

$$\begin{aligned} P_2(L) &= P(U_2 - U_1 > 0) \\ &= P(X > 0) = \int_0^\infty p(x)\,dx \end{aligned} \tag{14-4-48}$$

where the random variable X is defined as

$$X = U_2 - U_1 = \sum_{k=1}^{L} (|N_{k2}|^2 - |2\mathcal{E}\alpha_k + N_{k1}|^2) \tag{14-4-49}$$

The phase terms $\{\phi_k\}$ in U_1 have been dropped since they do not affect the performance of the square-law detector.

Let $S(X)$ denote the unit step function. Then the error probability in (14-4-48) can be expressed in the form

$$P_2(L) = E[S(X)] \tag{14-4-50}$$

Following the development in Section 2-1-5, the Chernoff bound is obtained by overbounding the unit step function by an exponential function. That is,

$$S(X) \leq e^{\zeta X}, \quad \zeta \geq 0 \tag{14-4-51}$$

where the parameter ζ is optimized to yield a tight bound. Thus, we have

$$P_2(L) = E[S(X)] \leq E(e^{\zeta X}) \tag{14-4-52}$$

Upon substituting for the random variable X from (14-4-49) and noting that the random variables in the summation are mutually statistically independent, we obtain the result

$$P_2(L) \leq \prod_{k=1}^{L} E(e^{\zeta|N_{k2}|^2}) E(e^{-\zeta|2\mathcal{E}\alpha_k + N_{k1}|^2}) \tag{14-4-53}$$

But

$$E(e^{\zeta|N_{k2}|^2}) = \frac{1}{1 - 2\zeta\sigma_2^2}, \quad \zeta < \frac{1}{2\sigma_2^2} \tag{14-4-54}$$

and

$$E(e^{-\zeta|2\mathcal{E}\alpha_k + N_{k1}|^2}) = \frac{1}{1 + 2\zeta\sigma_1^2}, \quad \zeta > \frac{-1}{2\sigma_1^2} \tag{14-4-55}$$

where $\sigma_2^2 = 2\mathcal{E}N_0$, $\sigma_1^2 = 2\mathcal{E}N_0(1 + \bar{\gamma}_c)$, and $\bar{\gamma}_c$ is the average SNR per diversity channel. Note that σ_1^2 and σ_2^2 are independent of k, i.e., the additive noise terms on the L diversity channels as well as the fading statistics are identically distributed. Consequently, (14-4-53) reduces to

$$P_2(L) \leq \left[\frac{1}{(1 - 2\zeta\sigma_2^2)(1 + 2\zeta\sigma_1^2)}\right]^L, \quad 0 \leq \zeta \leq \frac{1}{2\sigma_2^2} \tag{14-4-56}$$

By differentiating the right-hand side of (14-4-56) with respect to ζ, we find that the upper bound is minimized when

$$\zeta = \frac{\sigma_1^2 - \sigma_2^2}{4\sigma_1^2\sigma_2^2} \tag{14-4-57}$$

Substitution of (14-4-57) for ζ into (14-4-56) yields the Chernoff upper bound in the form

$$P_2(L) \leq \left[\frac{4(1+\bar{\gamma}_c)}{(2+\bar{\gamma}_c)^2}\right]^L \tag{14-4-58}$$

It is interesting to note that (14-4-58) may also be expressed as

$$P_2(L) \leq [4p(1-p)]^L \tag{14-4-59}$$

where $p = 1/(2+\bar{\gamma}_c)$ is the probability of error for binary orthogonal signaling on a fading channel without diversity.

A comparison of the Chernoff bound in (14-4-58) with the exact error probability for binary orthogonal signaling and square-law combining of the L diversity signals, which is given by the expression

$$\begin{aligned} P_2(L) &= \left(\frac{1}{1+\bar{\gamma}_c}\right)^L \sum_{k=0}^{L-1} \binom{L-1+k}{k} \left(\frac{1+\bar{\gamma}_c}{2+\bar{\gamma}_c}\right)^k \\ &= p^L \sum_{k=0}^{L-1} \binom{L-1+k}{k} (1-p)^k \end{aligned} \tag{14-4-60}$$

reveals the tightness of the bound. Figure (14-4-8) illustrates this comparison.

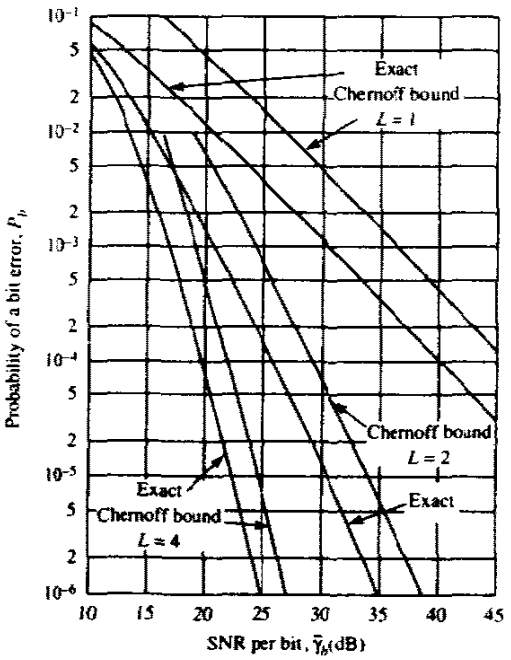

FIGURE 14-4-8 *Comparison of Chernoff bound with exact error probability.*

We observe that the Chernoff upper bound is approximately 6 dB from the exact error probability for $L = 1$, but, as L increases, it becomes tighter. For example, the difference between the bound and the exact error probability is about 2.5 dB when $L = 4$.

Finally we mention that the error probability for M-ary orthogonal signaling with diversity can be upper-bounded by means of the union bound

$$P_M \leq (M-1)P_2(L) \tag{14-4-61}$$

where we may use either the exact expression given in (14-4-60) or the Chernoff bound in (14-4-58) for $P_2(L)$.

14-5 DIGITAL SIGNALING OVER A FREQUENCY-SELECTIVE, SLOWLY FADING CHANNEL

When the spread factor of the channel satisfies the condition $T_m B_d \ll 1$, it is possible to select signals having a bandwidth $W \ll (\Delta f)_c$ and a signal duration $T \ll (\Delta t)_c$. Thus, the channel is frequency-nonselective and slowly fading. In such a channel, diversity techniques can be employed to overcome the severe consequences of fading.

When a bandwidth $W \gg (\Delta f)_c$ is available to the user, the channel can be subdivided into a number of frequency-division multiplexed (FDM) subchannels having a mutual separation in center frequencies of at least $(\Delta f)_c$. Then the same signal can be transmitted on the FDM subchannels, and, thus, frequency diversity is obtained. In this section, we describe an alternative method.

14-5-1 A Tapped-Delay-Line Channel Model

As we shall now demonstrate, a more direct method for achieving basically the same result is to employ a wideband signal covering the bandwidth W. The channel is still assumed to be slowly fading by virtue of the assumption that $T \ll (\Delta t)_c$. Now suppose that W is the bandwidth occupied by the real bandpass signal. Then the band occupancy of the equivalent lowpass signal $s_l(t)$ is $|f| \leq \frac{1}{2}W$. Since $s_l(t)$ is band-limited to $|f| \leq \frac{1}{2}W$, application of the sampling theorem results in the signal representation

$$s_l(t) = \sum_{n=-\infty}^{\infty} s_l\left(\frac{n}{W}\right) \frac{\sin[\pi W(t - n/W)]}{\pi W(t - n/W)} \tag{14-5-1}$$

The Fourier transform of $s_l(t)$ is

$$S_l(f) = \begin{cases} \dfrac{1}{W} \displaystyle\sum_{n=-\infty}^{\infty} s_l(n/W) e^{-j2\pi fn/W} & (|f| \leq \frac{1}{2}W) \\ 0 & (|f| > \frac{1}{2}W) \end{cases} \tag{14-5-2}$$

The noiseless received signal from a frequency-selective channel was previously expressed in the form

$$r_l(t) = \int_{-\infty}^{\infty} C(f;t)S_l(f)e^{j2\pi ft}\,df \tag{14-5-3}$$

where $C(f;t)$ is the time-variant transfer function. Substitution for $S_l(f)$ from (14-5-2) into (14-5-3) yields

$$\begin{aligned} r_l(t) &= \frac{1}{W}\sum_{n=-\infty}^{\infty} s_l(n/W)\int_{-\infty}^{\infty} C(f;t)e^{j2\pi f(t-n/W)}\,df \\ &= \frac{1}{W}\sum_{n=-\infty}^{\infty} s_l(n/W)c(t-n/W;t) \end{aligned} \tag{14-5-4}$$

where $c(\tau;t)$ is the time-variant impulse response. We observe that (14-5-4) has the form of a convolution sum. Hence, it can also be expressed in the alternative form

$$r(t) = \frac{1}{W}\sum_{n=-\infty}^{\infty} s_l(t-n/W)c(n/W;t) \tag{14-5-5}$$

It is convenient to define a set of time-variable channel coefficients as

$$c_n(t) = \frac{1}{W}c\left(\frac{n}{W};t\right) \tag{14-5-6}$$

Then (14-5-5) expressed in terms of these channel coefficients becomes

$$r(t) = \sum_{n=-\infty}^{\infty} c_n(t)s_l(t-n/W) \tag{14-5-7}$$

The form for the received signal in (14-5-7) implies that the time-variant frequency-selective channel can be modeled or represented as a tapped delay line with tap spacing $1/W$ and tap weight coefficients $\{c_n(t)\}$. In fact, we deduce from (14-5-7) that the lowpass impulse response for the channel is

$$c(\tau;t) = \sum_{n=-\infty}^{\infty} c_n(t)\delta(\tau-n/W) \tag{14-5-8}$$

and the corresponding time-variant transfer function is

$$C(f;t) = \sum_{n=-\infty}^{\infty} c_n(t)e^{-j2\pi fn/W} \tag{14-5-9}$$

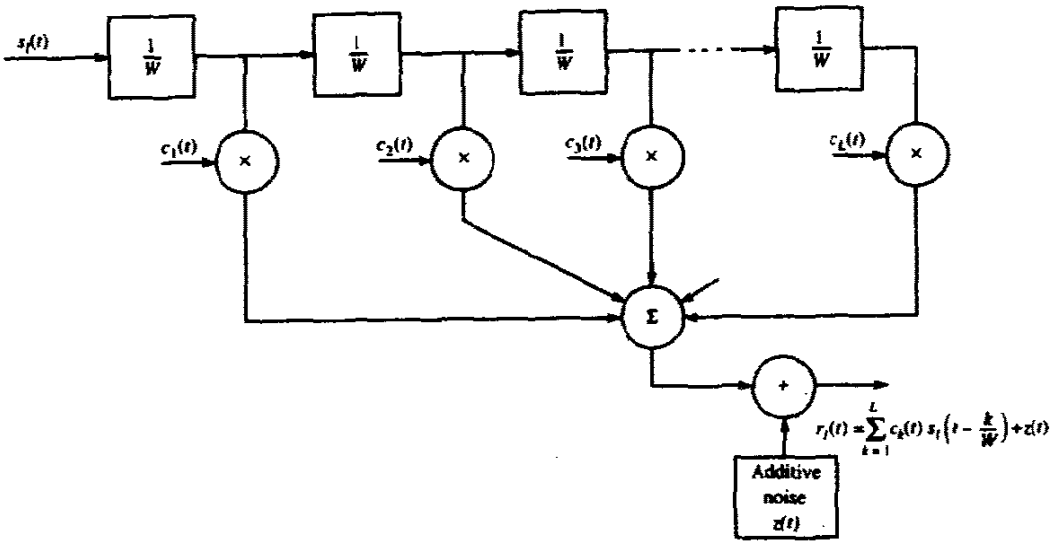

FIGURE 14-5-1 Trapped delay line model of frequency-selective channel.

Thus, with an equivalent lowpass signal having a bandwidth $\frac{1}{2}W$, where $W \gg (\Delta f)_c$, we achieve a resolution of $1/W$ in the multipath delay profile. Since the total multipath spread is T_m, for all practical purposes the tapped delay line model for the channel can be truncated at $L = [T_m W] + 1$ taps. Then the noiseless received signal can be expressed in the form

$$r_l(t) = \sum_{n=1}^{L} c_n(t) s_l\left(t - \frac{n}{W}\right) \tag{14-5-10}$$

The truncated tapped delay line model is shown in Fig. 14-5-1. In accordance with the statistical characterization of the channel presented in Section 14-1, the time-variant tap weights $\{c_n(t)\}$ are complex-valued stationary random processes. In the special case of Rayleigh fading, the magnitudes $|c_n(t)| = \alpha_n(t)$ are Rayleigh-distributed and the phases $\phi_n(t)$ are uniformly distributed. Since the $\{c_n(t)\}$ represent the tap weights corresponding to the L different delays $\tau = n/W$, $n = 1, 2, \ldots, L$, the uncorrelated scattering assumption made in Section 7-1 implies that the $\{c_n(t)\}$ are mutually uncorrelated. When the $\{c_n(t)\}$ are gaussian random processes, they are statistically independent.

14-5-2 The RAKE Demodulator

We now consider the problem of digital signaling over a frequency-selective channel that is modeled by a tapped delay line with statistically independent time-variant tap weights $\{c_n(t)\}$. It is apparent at the outset, however, that the tapped delay line model with statistically independent tap weights provides us

with L replicas of the same transmitted signal at the receiver. Hence, a receiver that processes the received signal in an optimum manner will achieve the performance of an equivalent Lth-order diversity communications system.

Let us consider binary signaling over the channel. We have two equal-energy signals $s_{i1}(t)$ and $s_{i2}(t)$, which are either antipodal or orthogonal. Their time duration T is selected to satisfy the condition $T \gg T_m$. Thus, we may neglect any intersymbol interference due to multipath. Since the bandwidth of the signal exceeds the coherent bandwidth of the channel, the received signal is expressed as

$$\begin{aligned} r_i(t) &= \sum_{k=1}^{L} c_k(t) s_{ii}(t - k/W) + z(t) \\ &= v_i(t) + z(t), \quad 0 \leq t \leq T, \quad i = 1, 2 \end{aligned} \tag{14-5-11}$$

where $z(t)$ is a complex-valued zero-mean white gaussian noise process. Assume for the moment that the channel tap weights are known. Then the optimum receiver consists of two filters matched to $v_1(t)$ and $v_2(t)$, followed by samplers and a decision circuit that selects the signal corresponding to the largest output. An equivalent optimum receiver employs cross correlation instead of matched filtering. In either case, the decision variables for coherent detection of the binary signals can be expressed as

$$\begin{aligned} U_m &= \text{Re}\left[\int_0^T r_l(t) v_m^*(t)\, dt\right] \\ &= \text{Re}\left[\sum_{k=1}^{L} \int_0^T r_l(t) c_k^*(t) s_{lm}^*(t - k/W)\, dt\right], \quad m = 1, 2 \end{aligned} \tag{14-5-12}$$

Figure 14-5-2 illustrates the operations involved in the computation of the decision variables. In this realization of the optimum receiver, the two reference signals are delayed and correlated with the received signal $r_l(t)$.

An alternative realization of the optimum receiver employs a single delay line through which is passed the received signal $r_l(t)$. The signal at each tap is correlated with $c_k(t)s_{lm}^*(t)$, where $k = 1, 2, \ldots, L$ and $m = 1, 2$. This receiver structure is shown in Fig. 14-5-3. In effect, the tapped delay line receiver attempts to collect the signal energy from all the received signal paths that fall within the span of the delay line and carry the same information. Its action is somewhat analogous to an ordinary garden rake and, consequently, the name "RAKE receiver" has been coined for this receiver structure by Price and Green (1958).

14-5-3 Performance of RAKE Receiver

We shall now evaluate the performance of the RAKE receiver under the condition that the fading is sufficiently slow to allow us to estimate $c_k(t)$ perfectly (without noise). Furthermore, within any one signaling interval, $c_k(t)$

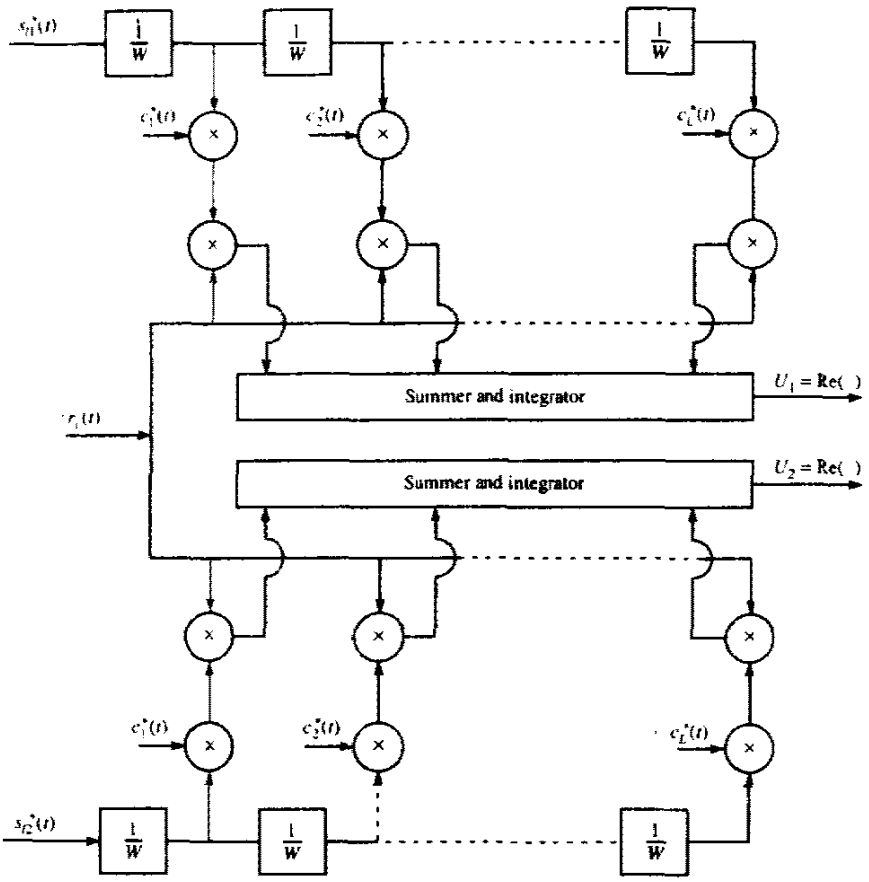

FIGURE 14-5-2 Optimum demodulator for wideband binary signals (delayed reference configuration).

is treated as a constant and denoted as c_k. Thus the decision variables in (14-5-12) may be expressed in the form

$$U_m = \text{Re}\left[\sum_{k=1}^{L} c_k^* \int_0^T r(t) s_{lm}^*(t - k/W)\, dt\right], \quad m = 1, 2 \tag{14-5-13}$$

Suppose the transmitted signal is $s_{l1}(t)$; then the received signal is

$$r_l(t) = \sum_{n=1}^{L} c_n s_{l1}(t - n/W) + z(t), \quad 0 \leq t \leq T \tag{14-5-14}$$

Substitution of (14-5-14) into (14-5-13) yields

$$U_m = \text{Re}\left[\sum_{k=1}^{L} c_k^* \sum_{n=1}^{L} c_n \int_0^T s_{l1}(t - n/W) s_{lm}^*(t - k/W)\, dt\right] + \text{Re}\left[\sum_{k=1}^{L} c_k^* \int_0^T z(t) s_{lm}^*(t - k/W)\, dt\right], \quad m = 1, 2 \tag{14-5-15}$$

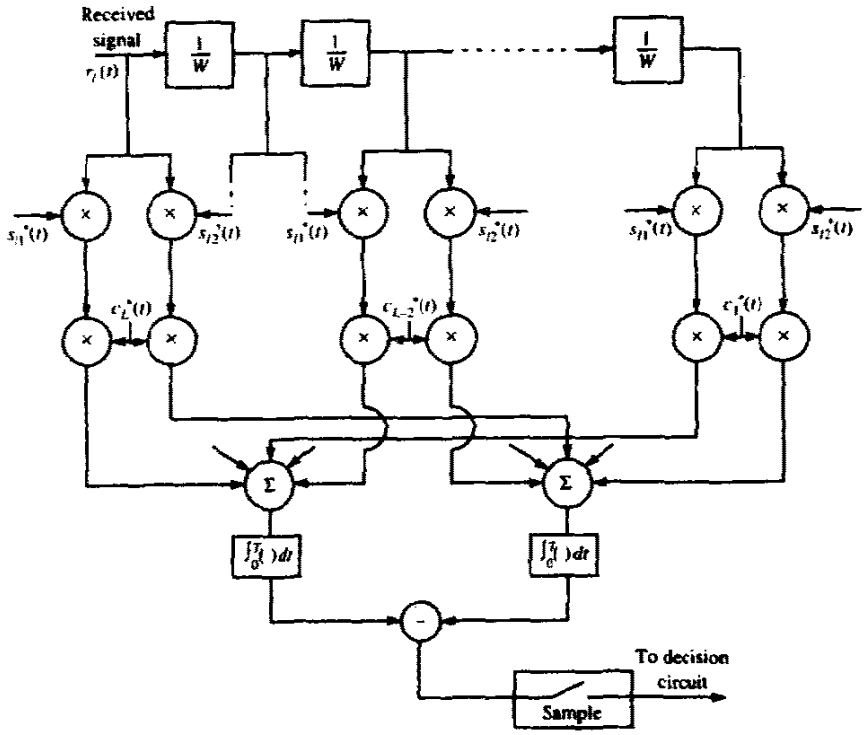

FIGURE 14-5-3 Optimum demodulator for wideband binary signals (delayed received signal configuration).

Usually the wideband signals $s_{l1}(t)$ and $s_{l2}(t)$ are generated from pseudo-random sequences, which result in signals that have the property

$$\int_0^T s_{li}(t - n/W)s_{li}^*(t - k/W)\,dt \approx 0, \quad k \neq n, \quad i = 1, 2 \qquad (14\text{-}5\text{-}16)$$

If we assume that our binary signals are designed to satisfy this property then (14-5-15) simplifies to†

$$U_m = \text{Re}\left[\sum_{k=1}^{L} |c_k|^2 \int_0^T s_{l1}(t - k/W)s_{lm}^*(t - k/W)\,dt\right] + \text{Re}\left[\sum_{k=1}^{L} c_k^* \int_0^T z(t)s_{lm}^*(t - k/W)\,dt\right], \quad m = 1, 2 \qquad (14\text{-}5\text{-}17)$$

† Although the orthogonality property specified by (14-5-16) can be satisfied by proper selection of the pseudo-random sequences, the cross-correlation of $s_{l1}(t - n/W)$ with $s_{lk}^*(t - k/W)$ gives rise to a signal-dependent self-noise, which ultimately limits the performance. For simplicity, we do not consider the self-noise term in the following calculations. Consequently, the performance results presented below should be considered as lower bounds (ideal RAKE). An approximation to the performance of the RAKE can be obtained by treating the self-noise as an additional gaussian noise component with noise power equal to its variance.

When the binary signals are antipodal, a single decision variable suffices. In this case, (14-5-17) reduces to

$$U_1 = \text{Re}\left(2\mathscr{E}\sum_{k=1}^{L}\alpha_k^2 + \sum_{k=1}^{L}\alpha_k N_k\right) \tag{14-5-18}$$

where $\alpha_k = |c_k|$ and

$$N_k = e^{j\phi_k}\int_0^T z(t)s_1^*(t - k/W)\,dt \tag{14-5-19}$$

But (14-5-18) is identical to the decision variable given in (14-4-4), which corresponds to the output of a maximal ratio combiner in a system with Lth-order diversity. Consequently, the RAKE receiver with perfect (noiseless) estimates of the channel tap weights is equivalent to a maximal ratio combiner in a system with Lth-order diversity. Thus, when all the tap weights have the same mean-square value, i.e., $E(\alpha_k^2)$ is the same for all k, the error rate performance of the RAKE receiver is given by (14-4-15) and (14-4-16). On the other hand, when the mean square values $E(\alpha_k^2)$ are not identical for all k, the derivation of the error rate performance must be repeated since (14-4-15) no longer applies.

We shall derive the probability of error for binary antipodal and orthogonal signals under the condition that the mean-square values of $\{\alpha_k\}$ are distinct. We begin with the conditional error probability

$$P_2(\gamma_b) = Q(\sqrt{\gamma_b(1-\rho_r)}) \tag{14-5-20}$$

where $\rho_r = -1$ for antipodal signals, $\rho_r = 0$ for orthogonal signals, and

$$\begin{aligned}\gamma_b &= \frac{\mathscr{E}}{N_0}\sum_{k=1}^{L}\alpha_k^2 \\ &= \sum_{k=1}^{L}\gamma_k\end{aligned} \tag{14-5-21}$$

Each of the $\{\gamma_k\}$ is distributed according to a chi-squared distribution with two degrees of freedom. That is,

$$p(\gamma_k) = \frac{1}{\bar{\gamma}_k}e^{-\gamma_k/\bar{\gamma}_k} \tag{14-5-22}$$

where $\bar{\gamma}_k$ is the average SNR for the kth path, defined as

$$\bar{\gamma}_k = \frac{\mathscr{E}}{N_0}E(\alpha_k^2) \tag{14-5-23}$$

Furthermore, from (14-4-10) we know that the characteristic function of γ_k is

$$\psi_{\gamma_k}(jv) = \frac{1}{1 - jv\bar{\gamma}_k} \tag{14-5-24}$$

Since γ_b is the sum of L statistically independent components $\{\gamma_k\}$, the characteristic function of γ_b is

$$\psi_{\gamma_b}(jv) = \prod_{k=1}^{L} \frac{1}{1 - jv\bar{\gamma}_k} \tag{14-5-25}$$

The inverse Fourier transform of the characteristic function in (14-5-25) yields the probability density function of γ_b in the form

$$p(\gamma_b) = \sum_{k=1}^{L} \frac{\pi_k}{\bar{\gamma}_k} e^{-\gamma_b/\bar{\gamma}_k}, \qquad \gamma_b \geq 0 \tag{14-5-26}$$

where π_k is defined as

$$\pi_k = \prod_{\substack{i=1 \\ i \neq k}}^{L} \frac{\bar{\gamma}_k}{\bar{\gamma}_k - \bar{\gamma}_i} \tag{14-5-27}$$

When the conditional error probability in (14-5-20) is averaged over the probability density function given in (14-5-26), the result is

$$P_2 = \tfrac{1}{2} \sum_{k=1}^{L} \pi_k \left[1 - \sqrt{\frac{\bar{\gamma}_k(1 - \rho_r)}{2 + \bar{\gamma}_k(1 - \rho_r)}} \right] \tag{14-5-28}$$

This error probability can be approximated as ($\bar{\gamma}_k \gg 1$)

$$P_2 \approx \binom{2L-1}{L} \prod_{k=1}^{L} \frac{1}{2\bar{\gamma}_k(1 - \rho_r)} \tag{14-5-29}$$

By comparing (14-5-29) for $\rho_r = -1$ with (14-4-18), we observe that the same type of asymptotic behavior is obtained for the case of unequal SNR per path and the case of equal SNR per path.

In the derivation of the error rate performance of the RAKE receiver, we assumed that the estimates of the channel tap weights are perfect. In practice, relatively good estimates can be obtained if the channel fading is sufficiently slow, e.g., $(\Delta t)_c/T \geq 100$, where T is the signaling interval. Figure 14-5-4 illustrates a method for estimating the tap weights when the binary signaling waveforms are orthogonal. The estimate is the output of the lowpass filter at each tap. At any one instant in time, the incoming signal is either $s_{l1}(t)$ or $s_{l2}(t)$. Hence, the input to the lowpass filter used to estimate $c_k(t)$ contains signal plus noise from one of the correlators and noise only from the other correlator. This method for channel estimation is not appropriate for antipodal signals, because the addition of the two correlator outputs results in signal cancellation. Instead, a single correlator can be employed for antipodal signals. Its output is fed to the input of the lowpass filter after the information-bearing signal is removed. To accomplish this, we must introduce a delay of one signaling interval into the channel estimation procedure, as illustrated in Fig. 14-5-5.

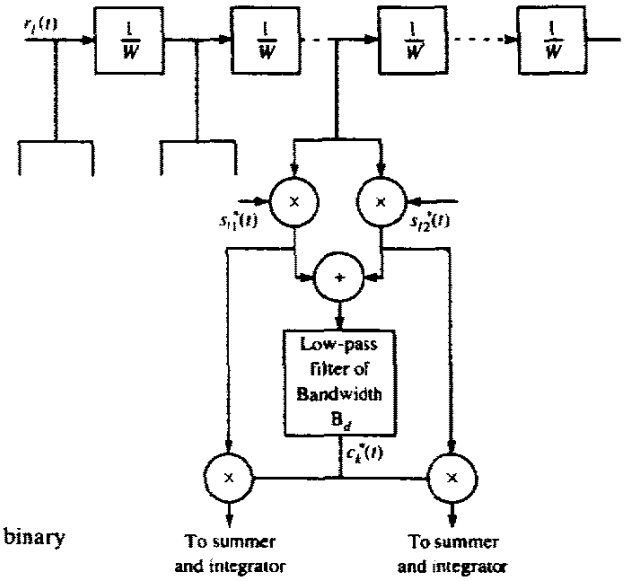

FIGURE 14-5-4 Channel tap weight estimation with binary orthogonal signals.

FIGURE 14-5-5 Channel tap weight estimation with binary antipodal signals.

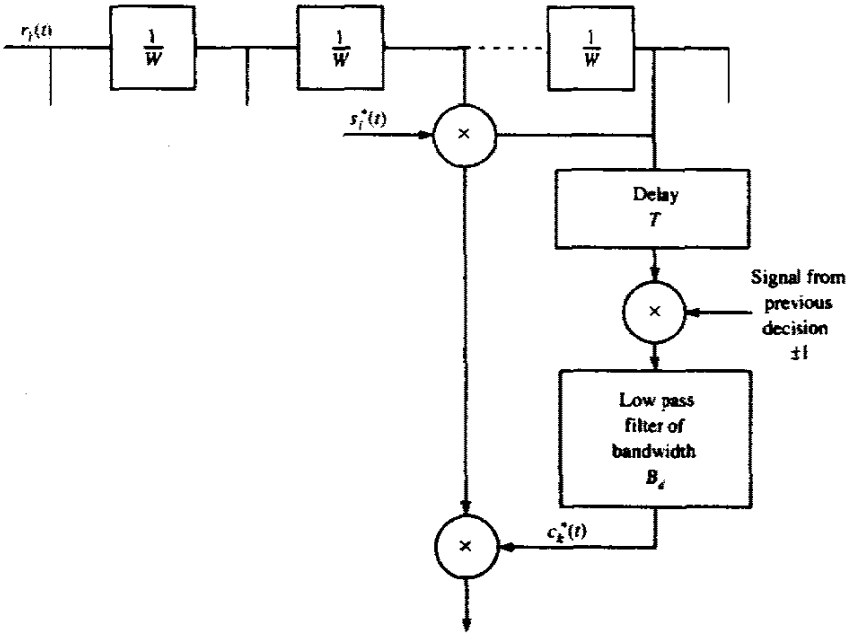

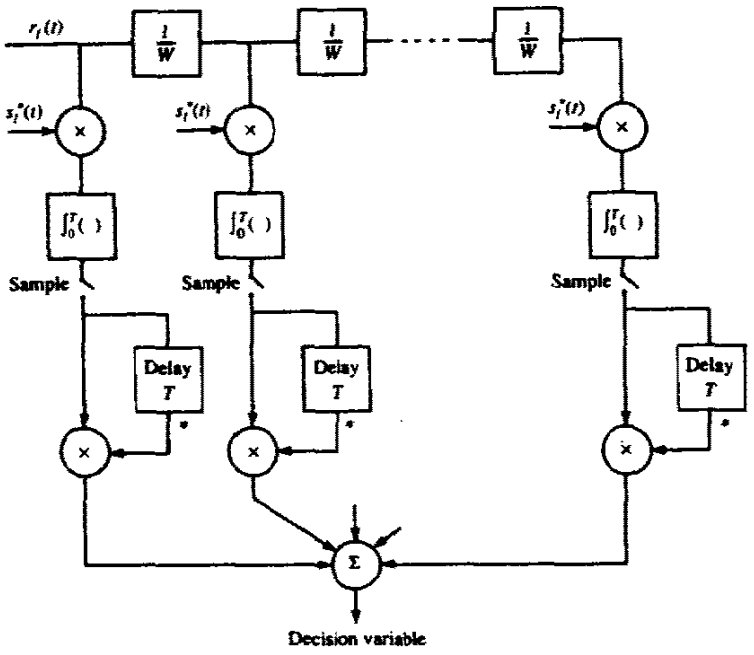

FIGURE 14-5-6 RAKE demodulator for DPSK signals.

That is, first the receiver must decide whether the information in the received signal is $+1$ or -1 and, then, it uses the decision to remove the information from the correlator output prior to feeding it to the lowpass fiter.

If we choose not to estimate the tap weights of the frequency-selective channel, we may use either DPSK signaling or noncoherently detected orthogonal signaling. The RAKE receiver structure for DPSK is illustrated in Fig 14-5-6. It is apparent that when the transmitted signal waveform $s_l(t)$ satisfies the orthogonality property given in (14-5-16), the decision variable is identical that given in (14-4-23) for an Lth-order diversity system. Consequently, the error rate performance of the RAKE receiver for a binary DPSK is identical to that given in (14-4-15) with $\mu = \bar{\gamma}_c/(1 + \bar{\gamma}_c)$, when all the signal paths have the same SNR $\bar{\gamma}_c$. On the other hand, when the SNRs $\{\bar{\gamma}_k\}$ are distinct, the error probability can be obtained by averaging (14-4-24), which is the probability of error conditioned on a time-invariant channel, over the probability density function of γ_b given by (14-5-26). The result of this integration is

$$P_2 = \left(\tfrac{1}{2}\right)^{2L-1} \sum_{m=0}^{L-1} m! b_m \sum_{k=1}^{L} \frac{\pi_k}{\bar{\gamma}_k} \left(\frac{\bar{\gamma}_k}{1 + \bar{\gamma}_k}\right)^{m+1} \tag{14-5-30}$$

where π_k is defined in (14-5-27) and b_m in (14-4-25).

Finally, we consider binary orthogonal signaling over the frequency-selective channel with square-law detection at the receiver. This type of signal

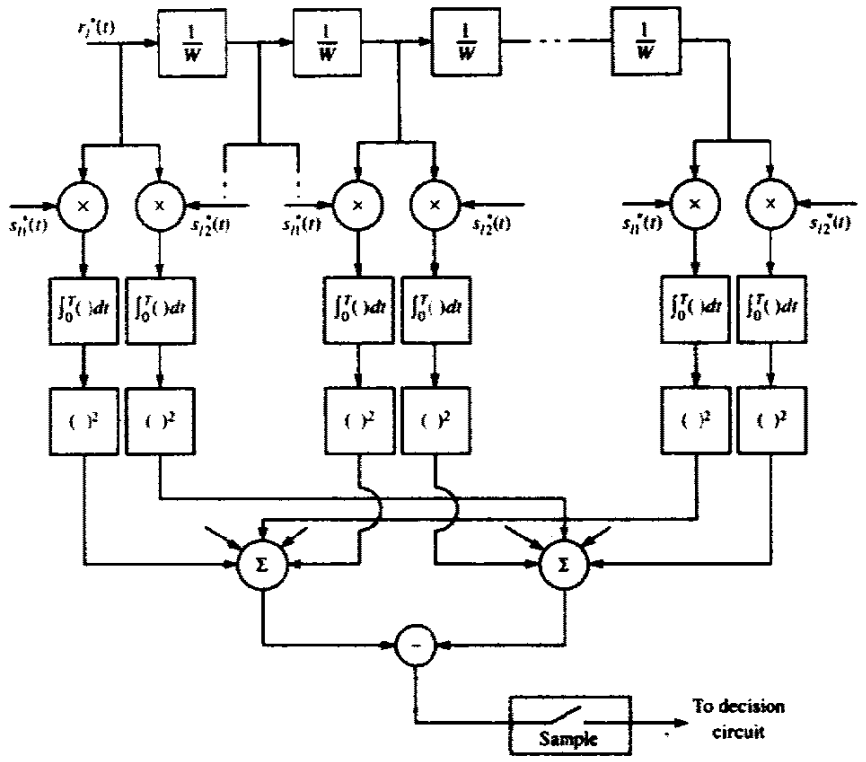

FIGURE 14-5-7 RAKE demodulator for square-law combination of orthogonal signals.

is appropriate when either the fading is rapid enough to preclude a good estimate of the channel tap weights or the cost of implementing the channel estimators is high. The RAKE receiver with square-law combining of the signal from each tap is illustrated in Fig. 14-5-7. In computing its performance, we again assume that the orthogonality property given in (14-5-16) holds. Then the decision variables at the output of the RAKE are

$$U_1 = \sum_{k=1}^{L} |2\mathscr{E}c_k + N_{k1}|^2$$
$$U_2 = \sum_{k=1}^{L} |N_{k2}|^2 \tag{14-5-31}$$

where we have assumed that $s_{j1}(t)$ was the transmitted signal. Again we observe that the decision variables are identical to the ones given in (14-4-29), which apply to orthogonal signals with Lth-order diversity. Therefore, the performance of the RAKE receiver for square-law-detected orthogonal signals is given by (14-4-15) with $\mu = \bar{\gamma}_c/(2 + \bar{\gamma}_c)$ when all the signal paths have the same SNR. If the SNRs are distinct, we can average the conditional error probability given by (14-4-24), with γ_b replaced by $\frac{1}{2}\gamma_b$, over the probability

density function $p(\gamma_k)$ given in (14-5-26). The result of this averaging is given by (14-5-30), with $\bar{\gamma}_k$ replaced by $\frac{1}{2}\bar{\gamma}_k$.

In the above analysis, the RAKE demodulator shown in Fig. 14-5-7 for square-law combination of orthogonal signals is assumed to contain a signal component at each delay. If that is not the case, its performance will be degraded, since some of the tap correlators will contribute only noise. Under such conditions, the low-level, noise-only contributions from the tap correlators should be excluded from the combiner, as shown by Chyi *et al.* (1988).

This concludes our discussion of signaling over a frequency-selective channel. The configurations of the RAKE receiver presented in this section can be easily generalized to multilevel signaling. In fact, if M-ary PSK or DPSK is chosen, the RAKE structures presented in this section remain unchanged. Only the PSK and DPSK detectors that follow the RAKE correlator are different.

14-6 CODED WAVEFORMS FOR FADING CHANNELS

Up to this point, we have demonstrated that diversity techniques are very effective in overcoming the detrimental effects of fading caused by the time-variant dispersive characteristics of the channel. Time- and/or frequency-diversity techniques may be viewed as a form of repetition (block) coding of the information sequence. From this point of view, the combining techniques described previously represent soft-decision decoding of the repetition code. Since a repetition code is a trivial form of coding, we shall now consider the additional benefits derived from more efficient types of codes. In particular, we demonstrate that coding provides an efficient means for obtaining diversity on a fading channel. The amount of diversity provided by a code is directly related to its minimum distance.

As explained in Section 14-4, time diversity is obtained by transmitting the signal components carrying the same information in multiple time intervals mutually separated by an amount equal to or exceeding the coherence time $(\Delta t)_c$ of the channel. Similarly, frequency diversity is obtained by transmitting the signal components carrying the same information in multiple frequency slots mutually separated by an amount of at least equal to the coherence bandwidth $(\Delta f)_c$ of the channel. Thus, the signal components carrying the same information undergo statistically independent fading.

To extend these notions to a coded information sequence, we simply require that the signal waveform corresponding to a particular code or code symbol fade independently of the signal waveform corresponding to any other code bit or code symbol. This requirement may result in inefficient utilization of the available time-frequency space, with the existence of large unused portions in this two-dimensional signaling space. To reduce the inefficiency, a number of code words may be interleaved in time or in frequency or both, in such a manner that the waveform corresponding to the bits or symbols of a given code word fade independently. Thus, we assume that the time-frequency signaling

space is partitioned into nonoverlapping time-frequency cells. A signal waveform corresponding to a code bit or code symbol is transmitted within such a cell.

In addition to the assumption of statistically independent fading of the signal components of a given code word, we also assume that the additive noise components corrupting the received signals are white gaussian processes that are statistically independent and identically distributed among the cells in the time-frequency space. Also, we assume that there is sufficient separation between adjacent cells so that intercell interference is negligible.

An important issue is the modulation technique that is used to transmit the coded information sequence. If the channel fades slowly enough to allow the establishment of a phase reference then PSK or DPSK may be employed. If this is not possible then FSK modulation with noncoherent detection at the receiver is appropriate. In our treatment, we assume that it is not possible to establish a phase reference or phase references for the signals in the different cells occupied by the transmitted signal. Consequently, we choose FSK modulation with noncoherent detection.

A model of the digital communications system for which the error rate performance will be evaluated is shown in Fig. 14-6-1. The encoder may be binary, nonbinary, or a concatenation of a nonbinary encoder with a binary encoder. Furthermore, the code generated by the encoder may be a block code, a convolutional code, or, in the case of concatenation, a mixture of a block code and a convolutional code.

In order to explain the modulation, demodulation, and decoding for FSK-type (orthogonal) signals, consider a linear binary block code in which k information bits are encoded into a block of n bits. For simplicity and without loss of generality, let us assume that all n bits of a code word are transmitted simultaneously over the channel on multiple frequency cells. A code word $\mathbf{C}_i$ having bits $\{c_{ij}\}$ is mapped into FSK signal waveforms in the following way. If $c_{ij} = 0$, the tone f_{0j} is transmitted, and if $c_{ij} = 1$, the tone f_{1j} is transmitted. This means that $2n$ tones or cells are available to transmit the n bits of the code word, but only n tones are transmitted in any signaling interval. Since each code word conveys k bits of information, the bandwidth expansion factor for FSK is $B_e = 2n/k$.

The demodulator for the received signal separates the signal into $2n$

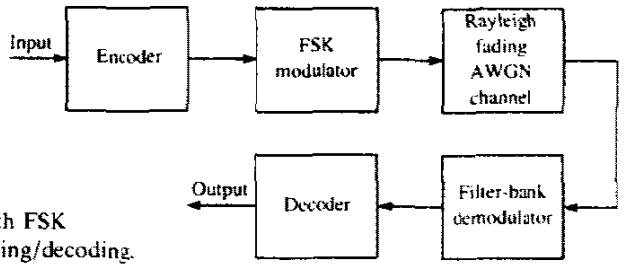

FIGURE 14-6-1 Model of communications system with FSK modulation/demodulation and encoding/decoding.

spectral components corresponding to the available tone frequencies at the transmitter. Thus, the demodulator can be realized as a bank of $2n$ filters, where each filter is matched to one of the possible transmitted tones. The outputs of the $2n$ filters are detected noncoherently. Since the Rayleigh fading and the additive white gaussian noises in the $2n$ frequency cells are mutually statistically independent and identically distributed random processes, the optimum maximum-likelihood soft-decision decoding criterion requires that these filter responses be square-law-detected and appropriately combined for each code word to form the $M = 2^k$ decision variables. The code word corresponding to the maximum of the decision variables is selected. If hard-decision decoding is employed, the optimum maximum-likelihood decoder selects the code word having the smallest Hamming distance relative to the received code word.

Although the discussion above assumed the use of a block code, a convolutional encoder can be easily accommodated in the block diagram shown in Fig. 14-6-1. For example, if a binary convolutional code is employed, each bit in the output sequence may be transmitted by binary FSK. The maximum-likelihood soft-decision decoding criterion for the convolutional code can be efficiently implemented by means of the Viterbi algorithm, in which the metrics for the surviving sequences at any point in the trellis consist of the square-law-combined outputs for the corresponding paths through the trellis. On the other hand, if hard-decision decoding is employed, the Viterbi algorithm is implemented with Hamming distance as the metric.

14-6-1 Probability of Error for Soft-Decision Decoding of Linear Binary Block Codes

Consider the decoding of a linear binary (n, k) code transmitted over a Rayleigh fading channel, as described above. The optimum soft-decision decoder, based on the maximum-likelihood criterion, forms the $M = 2^k$ decision variables

$$U_i = \sum_{j=1}^{n} [(1 - c_{ij})\,|y_{0j}|^2 + c_{ij}\,|y_{1j}|^2]$$

$$= \sum_{j=1}^{n} [|y_{0j}|^2 + c_{ij}(|y_{1j}|^2 - |y_{0j}|^2)], \qquad i = 1, 2, \ldots, 2^k \tag{14-6-1}$$

where $|y_{rj}|^2$, $j = 1, 2, \ldots, n$, and $r = 0, 1$ represent the squared envelopes at the outputs of the $2n$ filters that are tuned to the $2n$ possible transmitted tones. A decision is made in favor of the code word corresponding to the largest decision variable of the set $\{U_i\}$.

Our objective in this section is the determination of the error rate performance of the soft-decision decoder. Toward this end, let us assume that the all-zero code word $\mathbf{C}_1$ is transmitted. The average received signal-to-noise

ratio per tone (cell) is denoted by $\bar{\gamma}_c$. The total received SNR for the n tones in $n\bar{\gamma}_c$ and, hence, the average SNR per bit is

$$\begin{aligned}\bar{\gamma}_b &= \frac{n}{k}\bar{\gamma}_c \\ &= \frac{\bar{\gamma}_c}{R_c}\end{aligned} \tag{14-6-2}$$

where R_c is the code rate.

The decision variable U_1 corresponding to the code word $\mathbf{C}_1$ is given by (14-6-1) with $c_{ij} = 0$ for all j. The probability that a decision is made in favor of the mth code word is just

$$\begin{aligned}P_2(m) &= P(U_m > U_1) = P(U_1 - U_m < 0) \\ &= P\left[\sum_{j=1}^{n}(c_{1j} - c_{mj})(|y_{1j}|^2 - |y_{0j}|^2) < 0\right] \\ &= P\left[\sum_{j=1}^{w_m}(|y_{0j}|^2 - |y_{1j}|^2) < 0\right]\end{aligned} \tag{14-6-3}$$

where w_m is the weight of the mth code word. But the probability in (14-6-3) is just the probability of error for square-law combining of binary orthogonal FSK with w_mth-order diversity. That is,

$$P_2(m) = p^{w_m}\sum_{k=0}^{w_m-1}\binom{w_m - 1 + k}{k}(1-p)^k \tag{14-6-4}$$

$$\leq p^{w_m}\sum_{k=0}^{w_m-1}\binom{w_m - 1 + k}{k} = \binom{2w_m - 1}{w_m}p^{w_m} \tag{14-6-5}$$

where

$$p = \frac{1}{2 + \bar{\gamma}_c} = \frac{1}{2 + R_c\bar{\gamma}_b} \tag{14-6-6}$$

As an alternative, we may use the Chernoff upper bound derived in Section 14-4, which in the present notation is

$$P_2(m) \leq [4p(1-p)]^{w_m} \tag{14-6-7}$$

The sum of the binary error events over the $M - 1$ nonzero-weight code words gives an upper bound on the probability of error. Thus,

$$P_M \leq \sum_{m=2}^{M} P_2(m) \tag{14-6-8}$$

Since the minimum distance of the linear code is equal to the minimum weight, it follows that

$$(1 + R_c\bar{\gamma}_b)^{-w_m} \leq (2 + R_c\bar{\gamma}_b)^{-d_{\min}}$$

The use of this relation in conjunction with (14-6-5) and (14-6-8) yields a simple, albeit looser, upper bound that may be expressed in the form

$$P_M < \frac{\sum_{m=2}^{M} \binom{2w_m - 1}{w_m}}{(2 + R_c \bar{\gamma}_b)^{d_{\min}}} \tag{14-6-9}$$

This simple bound indicates that the code provides an effective order of diversity equal to $d_{\min}$. An even simpler bound is the union bound

$$P_M < (M - 1)[4p(1 - p)]^{d_{\min}} \tag{14-6-10}$$

which is obtained from the Chernoff bound given in (14-6-7).

As an example serving to illustrate the benefits of coding for a Rayleigh fading channel, we have plotted in Fig. 14-6-2 the performance obtained with the extended Golay (24, 12) code and the performance of binary FSK and quarternay FSK each with dual diversity. Since the extended Golay code requires a total of 48 cells and $k = 12$, the bandwidth expansion factor $B_e = 4$. This is also the bandwidth expansion factor for binary and quaternary FSK with $L = 2$. Thus, the three types of waveforms are compared on the basis of the same bandwidth expansion factor. Note that at $P_b = 10^{-4}$, the Golay code outperforms quaternary FSK by more than 6 dB, and at $P_b = 10^{-5}$, the difference is approximately 10 dB.

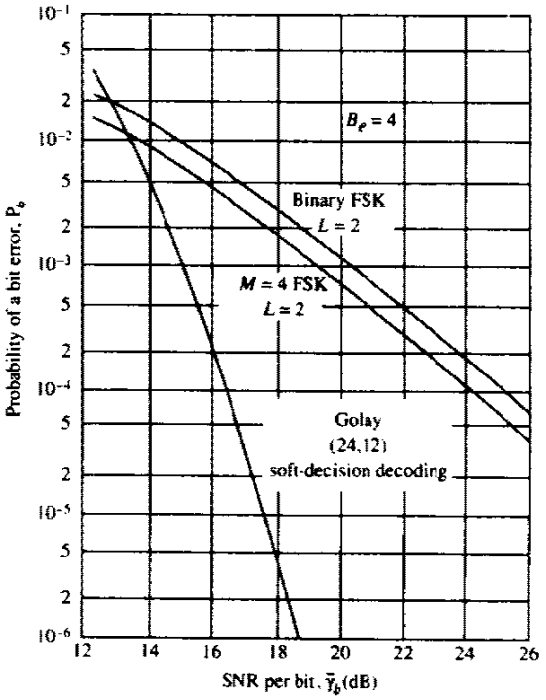

FIGURE 14-6-2 Example of performance obtained with conventional diversity versus coding for $B_e = 4$.

The reason for the superior performance of the Golay code is its large minimum distance ($d_{\min} = 8$), which translates into an equivalent eighth-order ($L = 8$) diversity. In contrast, the binary and quaternary FSK signals have only second-order diversity. Hence, the code makes more efficient use of the available channel bandwidth. The price that we must pay for the superior performance of the code is the increase in decoding complexity.

14-6-2 Probability of Error for Hard-Decision Decoding of Linear Binary Block Codes

Bounds on the performance obtained with hard-decision decoding of a linear binary (n, k) code have already been given in Section 8-1-5. These bounds are applicable to a general binary-input binary-output memoryless (binary symmetric) channel and, hence, they apply without modification to a Rayleigh fading AWGN channel with statistically independent fading of the symbols in the code word. The probability of a bit error needed to evaluate these bounds when binary FSK with noncoherent detection is used as the modulation and demodulation technique is given by (14-6-6).

A particularly interesting result is obtained when we use the Chernoff upper bound on the error probability for hard-decision decoding given by (8-1-89). That is,

$$P_2(m) \leq [4p(1-p)]^{m/2} \tag{14-6-11}$$

and P_M is upper-bounded by (14-6-8). In comparison, the Chernoff upper bound for $P_2(m)$ when soft-decision decoding is employed is given by (14-6-7). We observe that the effect of hard-decision decoding is a reduction in the distance between any two code words by a factor of 2. When the minimum distance of a code is relatively small, the reduction of the distances by a factor of 2 is much more noticeable in a fading channel than in a nonfading channel.

For illustrative pruposes we have plotted in Fig. 14-6-3 the performance of the Golay (23, 12) code when hard-decision and soft-decision decoding are used. The difference in performance at $P_b = 10^{-5}$ is approximately 6 dB. This is a significant difference in performance compared with the 2 dB difference between soft- and hard-decision decoding in a nonfading AWGN channel. We also note that the difference in performance increases as P_b decreases. In short, these results indicate the benefits of a soft-decision decoding over hard-decision decoding on a Rayleigh fading channel.

14-6-3 Upper Bounds on the Performance of Convolutional Codes for a Rayleigh Fading Channel

In this subsection, we derive the performance of binary convolutional codes when used on a Rayleigh fading AWGN channel. The encoder accepts k binary digits at a time and puts out n binary digits at a time. Thus, the code rate is $R_c = k/n$. The binary digits at the output of the encoder are transmitted

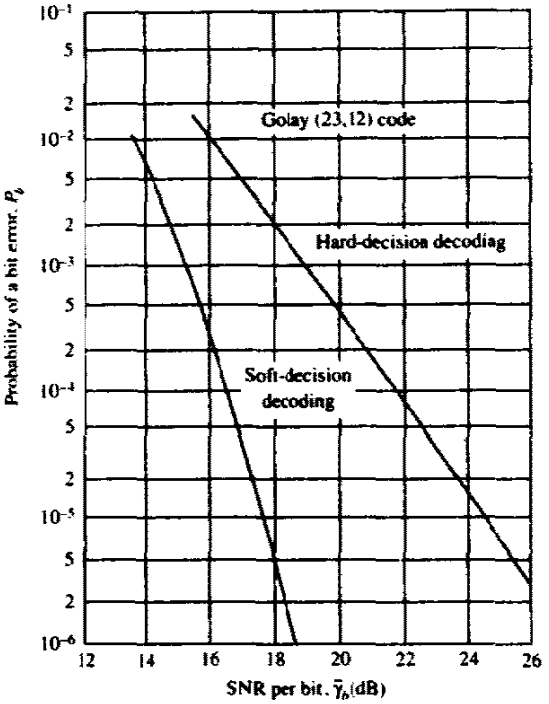

FIGURE 14-6-3 Comparison of performance between hard- and soft-decision decoding.

over the Rayleigh fading channel by means of binary FSK, which is square-law-detected at the receiver. The decoder for either soft- or hard-decision decoding performs maximum-likelihood sequence estimation, which is efficiently implemented by means of the Viterbi algorithm.

First, we consider soft-decision decoding. In this case, the metrics computed in the Viterbi algorithm are simply sums of square-law-detected outputs from the demodulator. Suppose the all-zero sequence is transmitted. Following the procedure outlined in Section 8-2-3, it is easily shown that the probability of error in a pairwise comparison of the metric corresponding to the all-zero sequence with the metric corresponding to another sequence that merges for the first time at the all-zero state is

$$P_2(d) = p^d \sum_{k=0}^{d-1} \binom{d-1+k}{k} (1-p)^k \tag{14-6-12}$$

where d is the number of bit positions in which the two sequences differ and p is given by (14-6-6). That is, $P_2(d)$ is just the probability of error for binary FSK with square-law detection and dth-order diversity. Alternatively, we may use the Chernoff bound in (14-6-7) for $P_2(d)$. In any case, the bit error probability is upperbounded, as shown in Section 8-2-3 by the expression

$$P_b < \frac{1}{k} \sum_{d=d_{\text{free}}}^{\infty} \beta_d P_2(d) \tag{14-6-13}$$

where the weighting coefficients $\{\beta_d\}$ in the summation are obtained from the expansion of the first derivative of the transfer function $T(D, N)$, given by (8-2-25).

When hard-decision decoding is performed at the receiver, the bounds on the error rate performance for binary convolutional codes derived in Section 8-2-4 apply. That is, P_b is again upper-bounded by the expression in (14-6-13), where $P_2(d)$ is defined by (8-2-28) for odd d and by (8-2-29) for even d, or upper-bounded (Chernoff bound) by (8-2-31), and p is defined by (14-6-6).

As in the case of block coding, when the respective Chernoff bounds are used for $P_2(d)$ with hard-decision and soft-decision decoding, it is interesting to note that the effect of hard-decision decoding is to reduce the distances (diversity) by a factor of 2 relative to soft-decision decoding.

The following numerical results illustrate the error rate performance of binary, rate $1/n$, maximal free distance convolutional codes for $n = 2$, 3, and 4 with soft-decision Viterbi decoding. First of all, Fig. 14-6-4 shows the performance of the rate 1/2 convolutional codes for constraint lengths 3, 4, and 5. The bandwidth expansion factor for binary FSK modulation is $B_e = 2n$. Since an increase in the constraint length results in an increase in the complexity of the decoder to go along with the corresponding increase in the minimum free distance, the system designer can weigh these two factors in the selection of the code.

Another way to increase the distance without increasing the constraint

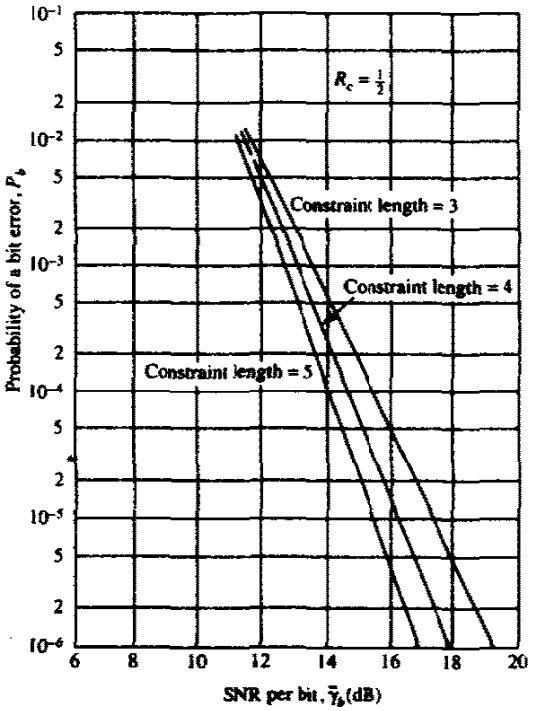

FIGURE 14-6-4 Performance of rate 1/2 binary convolutional codes with soft decision decoding.

length of the code is to repeat each output bit m times. This is equivalent to reducing the code rate by a factor of m or expanding the bandwidth by the same factor. The result is a convolutional code that has a minimum free distance of md_{free}, where d_{free} is the minimum free distance of the original code without repetitions. Such a code is almost as good, from the viewpoint of minimum distance, as a maximum free distance, rate $1/mn$ code. The error rate performance with repetitions is upper-bounded by

$$P_b < \frac{1}{k} \sum_{d_{free}}^{\infty} \beta_d P_2(md) \tag{14-6-14}$$

where $P_2(md)$ is given by (14-6-12). Figure (14-6-5) illustrates the performance of the rate 1/2 codes with repetitions ($m = 1, 2, 3, 4$) for constraint length 5.

14-6-4 Use of Constant-Weight Codes and Concatenated Codes for a Fading Channel

Our treatment of coding for a Rayleigh fading channel to this point was based on the use of binary FSK as the modulation technique for transmitting each of the binary digits in a code word. For this modulation technique, all the 2^k code

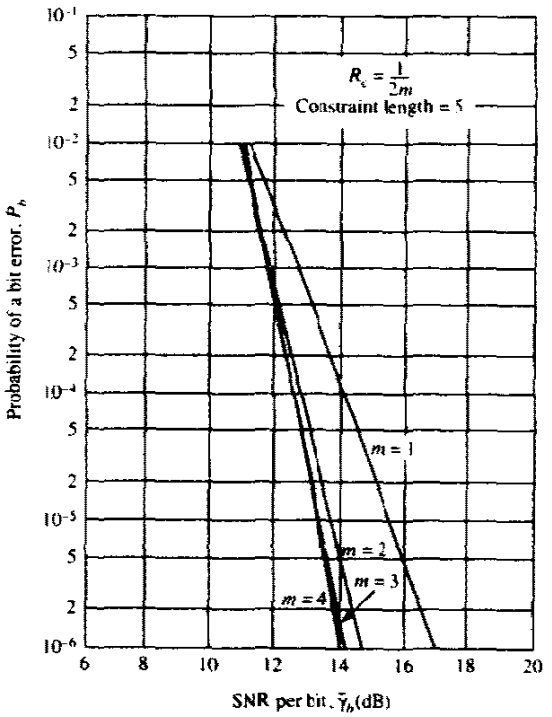

FIGURE 14-6-5 Performance of rate $1/2m$, constraint length 5, binary convolutional codes with soft-decision decoding.

words in the (n, k) code have identical transmitted energy. Furthermore, under the condition that the fading on the n transmitted tones is mutually statistically independent and identically distributed, the average received signal energy for the $M = 2^k$ possible code words is also identical. Consequently, in a soft-decision decoder, the decision is made in favor of the code word having the largest decision variable.

The condition that the received code words have identical average SNR has an important ramification in the implementation of the receiver. If the received code words do not have identical average SNR, the receiver must provide bias compensation for each received code word so as to render it equal energy. In general, the determination of the appropriate bias terms is difficult to implement because it requires the estimation of the average received signal power; hence, the equal-energy condition on the received code words considerably simplifies the receiver processing.

There is an alternative modulation method for generating equal-energy waveforms from code words when the code is constant-weight, i.e., when every code word has the same number of 1s. Note that such a code is nonlinear. Nevertheless, suppose we assign a single tone or cell to each bit position of the 2^k code words. Thus, an (n, k) binary block code has n tones assigned. Waveforms are constructed by transmitting the tone corresponding to a particular bit in a code word if that bit is a 1; otherwise, that tone is not transmitted for the duration of the interval. This modulation technique for transmitting the coded bits is called *on–off keying* (OOK). Since the code is constant-weight, say w, every coded waveform consists of w transmitted tones that depend on the positions of the 1s in each of the code words.

As in FSK, all tones in the OOK signal that are transmitted over the channel are assumed to fade independently across the frequency band and in time from one code word to another. The received signal envelope for each tone is described statistically by the Rayleigh distribution. Statistically independent additive white gaussian noise is assumed to be present in each frequency cell.

The receiver employs maximum-likelihood (soft-decision) decoding to map the received waveform into one of the M possible transmitted code words. For this purpose, n matched filters are employed, each matched to one of the n frequency tones. For the assumed statistical independence of the signal fading for the n frequency cells and additive white gaussian noise, the envelopes of the matched filter outputs are squared and combined to form the M decision variables

$$U_i = \sum_{j=1}^{n} c_{ij} |y_j|^2, \quad i = 1, 2, \ldots, 2^k \tag{14-6-15}$$

where $|y_j|^2$ corresponds to the squared envelope of the filter corresponding to the jth frequency, where $j = 1, 2, \ldots, n$.

It may appear that the constant-weight condition severely restricts our choice of codes. This is not the case, however. To illustrate this point, we

briefly describe some methods for constructing constant-weight codes. This discussion is by no means exhaustive.

Method 1: Nonlinear Transformation of a Linear Code In general, if in each word of an arbitrary binary code we substitute one binary sequence for every occurrence of a 0 and another sequence for each 1, a constant-weight binary block code will be obtained if the two substitution sequences are of equal weights and lengths. If the length of the sequence is v and the original code is an (n, k) code then the resulting constant-weight code will be an (vn, k) code. The weight will be n times the weight of the substitution sequence, and the minimum distance will be the minimum distances of the original code times the distances between the two substitution sequences. Thus, the use of complementary sequences when v is even results in a code with minimum distance $vd_{\min}$ and weight $\frac{1}{2}vn$.

The simplest form of this method is the case $v = 2$, in which every 0 is replaced by the pair 01 and every 1 is replaced by the complementary sequence 10 (or vice versa). As an example, we take as the initial code the (24, 12) extended Golay code. The parameters of the original and the resultant constant-weight code are given in Table 14-6-1.

Note that this substitution process can be viewed as a separate encoding. This secondary encoding clearly does not alter the information content of a code word—it merely changes the form in which it is transmitted. Since the new code word is composed of pairs of bits—one "on" and one "off"—the use of OOK transmission of this code word produces a waveform that is identical to that obtained by binary FSK modulation for the underlying linear code.

Method 2: Expurgation In this method, we start with an arbitrary binary block code and select from it a subset consisting of all words of a certain weight. Several different constant-weight codes can be obtained from one initial code by varying the choice of the weight w. Since the code words of the resulting expurgated code can be viewed as a subset of all possible permutations of any one code word in the set, the term *binary expurgated permutation modulation* (BEXPERM) has been used by Gaarder (1971) to describe such a code. In fact, the constant-weight binary block codes constructed by the other

TABLE 14-6-1 EXAMPLE OF CONSTANT-WEIGHT CODE FORMED BY METHOD 1

Code parameters	Original Golay	Constant-weight
n	24	48
k	12	12
M	4096	4096
$d_{\min}$	8	16
w	variable	24

TABLE 14-6-2 EXAMPLES OF CONSTANT-WEIGHT CODES FORMED BY EXPURGATION

Parameters	Original	Constant weight No. 1	Constant weight No. 2
n	24	24	24
k	12	9	11
M	4096	759	2576
$d_{\min}$	8	≥ 8	≥ 8
w	variable	8	12

methods may also be viewed as BEXPERM codes. This method of generating constant-weight codes is in a sense opposite to the first method in that the word length n is held constant and the code size M is changed. The minimum distance for the constant-weight subset will clearly be no less than that of the original code. As an example, we consider the Golay (24, 12) code and form the two different constant-weight codes shown in Table 14-6-2.

Method 3: Hadamard Matrices This method might appear to form a constant-weight binary block code directly, but it actually is a special case of the method of expurgation. In this method, a Hadamard matrix is formed as described in Section 8-1-2, and a constant-weight code is created by selection of rows (code words) from this matrix. Recall that a Hadamard matrix is an $n \times n$ matrix (*n* even integer) of 1s and 0s with the property that any row differs from any other row in exactly $\frac{1}{2}n$ positions. One row of the matrix is normally chosen as being all 0s.

In each of the other rows, half of the elements are 0s and the other half 1s. A Hadamard code of size $2(n-1)$ code words is obtained by selecting these $n-1$ rows and their complements. By selecting $M = 2^k \leq 2(n-1)$ of these code words, we obtain a Hadamard code, which we denote by $H(n, k)$, where each code word conveys k information bits. The resulting code has constant weight $\frac{1}{2}n$ and minimum distance $d_{\min} = \frac{1}{2}n$.

Since n frequency cells are used to transmit k information bits, the bandwidth expansion factor for the Hadamard $H(n, k)$ code is defined as

$$B_e = \frac{n}{k} \text{ cells per information bit}$$

which is simply the reciprocal of the code rate. Also, the average signal-to-noise ratio (SNR) per bit, denoted by $\bar{\gamma}_b$, is related to the average SNR per cell, $\bar{\gamma}_c$, by the expression

$$\begin{aligned} \bar{\gamma}_c &= \frac{k}{\frac{1}{2}n}\bar{\gamma}_b \\ &= 2\frac{k}{n}\bar{\gamma}_b = 2R_c\bar{\gamma}_b = \frac{2\bar{\gamma}_b}{B_e} \end{aligned} \tag{14-6-16}$$

Let us compare the performance of the constant-weight Hadamard codes under a fixed bandwidth constraint with a conventional M-ary orthogonal set of waveforms where each waveform has diversity L. The M orthogonal waveforms with diversity are equivalent to a block orthogonal code having a block length $n = LM$ and $k = \log_2 M$. For example, if $M = 4$ and $L = 2$, the code words of the block orthogonal code are

$$\mathbf{C}_1 = [1 \quad 1 \quad 0 \quad 0 \quad 0 \quad 0 \quad 0 \quad 0]$$

$$\mathbf{C}_2 = [0 \quad 0 \quad 1 \quad 1 \quad 0 \quad 0 \quad 0 \quad 0]$$

$$\mathbf{C}_3 = [0 \quad 0 \quad 0 \quad 0 \quad 1 \quad 1 \quad 0 \quad 0]$$

$$\mathbf{C}_4 = [0 \quad 0 \quad 0 \quad 0 \quad 0 \quad 0 \quad 1 \quad 1]$$

To transmit these code words using OOK modulation requires $n = 8$ cells, and since each code word conveys $k = 2$ bits of information, the bandwidth expansion factor $B_e = 4$. In general, we denote the block orthogonal code as $O(n, k)$. The bandwidth expansion factor is

$$B_e = \frac{n}{k} = \frac{LM}{k} \tag{14-6-17}$$

Also, the SNR per bit is related to the SNR per cell by the expression

$$\begin{aligned} \bar{\gamma}_c &= \frac{k}{L}\bar{\gamma}_b \\ &= M\left(\frac{k}{n}\right)\bar{\gamma}_b = M\frac{\bar{\gamma}_b}{B_e} \end{aligned} \tag{14-6-18}$$

Now we turn our attention to the performance characteristics of these codes. First, the exact probability of a code word (symbol) error for M-ary orthogonal signaling over a Rayleigh fading channel with diversity was given in closed form in Section 14-4. As previously indicated, this expression is rather cumbersome to evaluate, especially if either L or M or both are large. Instead, we shall use a union bound that is very convenient. That is, for a set of M orthogonal waveforms, the probability of a symbol error can be upper-bounded as

$$\begin{aligned} P_M &\leq (M-1)P_2(L) \\ &= (2^k - 1)P_2(L) < 2^k P_2(L) \end{aligned} \tag{14-6-19}$$

where $P_2(L)$, the probability of error for two orthogonal waveforms, each with diversity L, is given by (14-6-12) with $p = 1/(2 + \bar{\gamma}_c)$. The probability of bit error is obtained by multiplying P_M by $2^{k-1}/(2^k - 1)$, as explained previously.

A simple upper (union) bound on the probability of a code word error for the Hadamard $H(n, k)$ code is obtained by noting the probability of error in deciding between the transmitted code word and any other code word is bounded from above by $P_2(\frac{1}{2}d_{\min})$, where $d_{\min}$ is the minimum distance of the code. Therefore, an upper bound on P_M is

$$P_M \leq (M-1)P_2(\tfrac{1}{2}d_{\min}) < 2^k P_2(\tfrac{1}{2}d_{\min}) \qquad (14\text{-}6\text{-}20)$$

Thus the "effective order of diversity" of the code for OOK modulation is $\frac{1}{2}d_{\min}$. The bit error probability may be approximated as $\frac{1}{2}P_M$, or slightly overbounded by multiplying P_M by the factor $2^{k-1}/(2^k-1)$, which is the factor used above for orthogonal codes. The latter was selected for the error probability computations given below.

Figures 14-6-6 and 14-6-7 illustrate the error rate performance of a selected number of Hadamard codes and block orthogonal codes, respectively, for several bandwidth expansion factors. The advantage resulting from an increase in the size M of the alphabet (or k, since $k = \log_2 M$) and an increase in the bandwidth expansion factor is apparent from observation of these curves. Note, for example, that the $H(20, 5)$ code when repeated twice results in a code that is denoted by ${}_2H(20, 5)$ and has a bandwidth expansion factor $B_e = 8$. Figure 14-6-8 shows the performance of the two types of codes compared on the basis of equal bandwidth expansion factors. It is observed that the error rate curves for the Hadamard codes are steeper than the corresponding curves

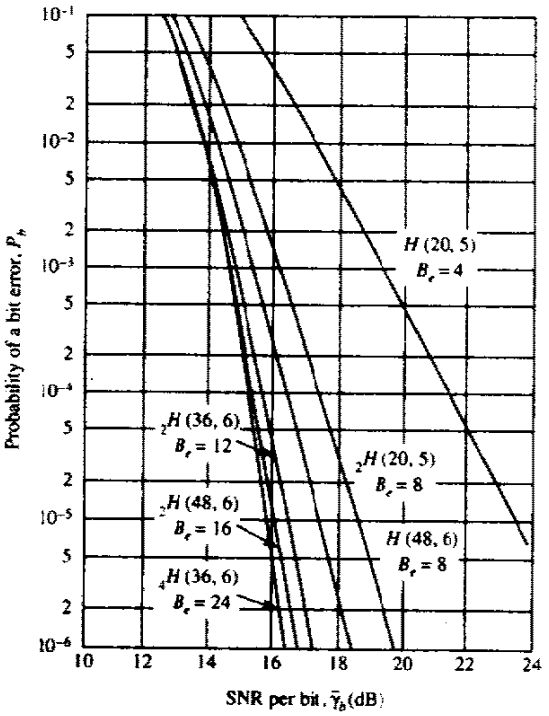

FIGURE 14-6-6 Performance of Hadamard codes.

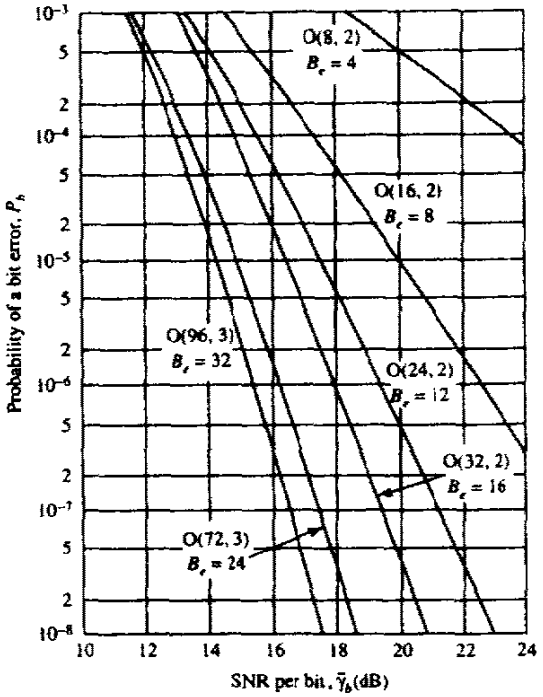

FIGURE 14-6-7 Performance of block orthogonal codes.

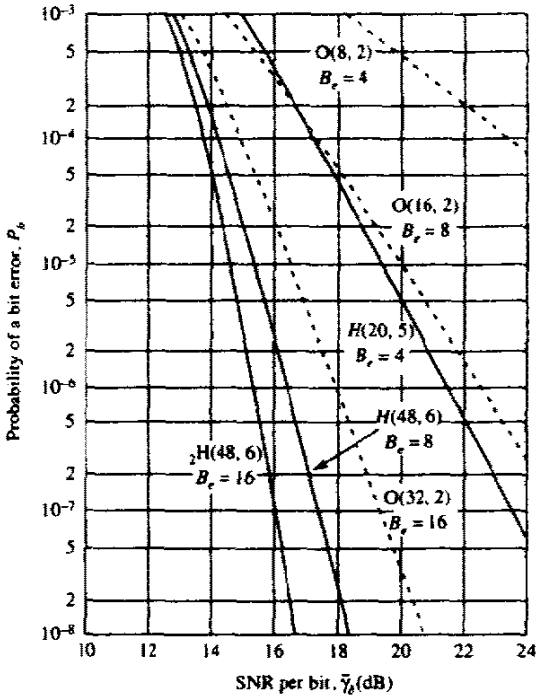

FIGURE 14-6-8 Comparison of performance between Hadamard codes and block orthogonal codes.

for the block orthogonal codes. This characteristic behavior is due simply to the fact that, for the same bandwidth expansion factor, the Hadamard codes provide more diversity than block orthogonal codes. Alternatively, one may say that Hadamard codes provide better bandwidth efficiency than block orthogonal codes. It should be mentioned, however, that at low SNR, a lower-diversity code outperforms a higher-diversity code as a consequence of the fact that, on a Rayleigh fading channel, there is an optimum distribution of the total received SNR among the diversity signals. Therefore, the curves for the block orthogonal codes will cross over the curves for the Hadamard codes at the low-SNR (high-error-rate) region.

Method 4: Concatenation In this method, we begin with two codes: one binary and the other nonbinary. The binary code is the inner code and is an (n, k) constant-weight (nonlinear) block code. The nonbinary code, which may be linear, is the outer code. To distinguish it from the inner code, we use uppercase letters, e.g., an (N, K) code, where N and K are measured in terms of symbols from a q-ary alphabet. The size q of the alphabet over which the outer code is defined cannot be greater than the number of words in the inner code. The outer code, when defined in terms of the binary inner code words rather than q-ary symbols, is the new code.

An important special case is obtained when $q = 2^k$ and the inner code size is chosen to be 2^k. Then the number of words is $M = 2^{kK}$ and the concatenated structure is an (nN, kK) code. The bandwidth expansion factor of this concatenated code is the product of the bandwidth expansions for the inner and outer codes.

Now we shall demonstrate the performance advantages obtained on a Rayleigh fading channel by means of code concatenation. Specifically, we construct a concatenated code in which the outer code is a dual-k (nonbinary) convolutional code and the inner code is either a Hadamard code or a block orthogonal code. That is, we view the dual-k code with M-ary ($M = 2^k$) orthogonal signals for modulation as a concatenated code. In all cases to be considered, soft-decision demodulation and Viterbi decoding are assumed.

The error rate performance of the dual-k convolutional codes is obtained from the derivation of the transfer function given by (8-2-39). For a rate-1/2, dual-k code with no repetitions, the bit error probability, appropriate for the case in which each k-bit output symbol from the dual-k encoder is mapped into one of $M = 2^k$ orthogonal code words, is upper-bounded as

$$P_b < \frac{2^{k-1}}{2^k - 1} \sum_{m=4}^{\infty} \beta_m P_2(m) \tag{14-6-21}$$

where $P_2(m)$ is given by (14-6-12).

For example, a rate-1/2, dual-2 code may employ a 4-ary orthogonal code O(4, 2) as the inner code. The bandwidth expansion factor of the resulting concatenated code is, of course, the product of the bandwidth expansion

factors of the inner and outer codes. Thus, in this example, the rate of the outer code is 1/2 and the inner code is 1/2. Hence, $B_c = (4/2)(2) = 4$.

Note that if every symbol of the dual-k is repeated r times, this is equivalent to using an orthogonal code with diversity $L = r$. If we select $r = 2$ in the example given above, the resulting orthogonal code is denoted as O(8, 2) and the bandwidth expansion factor for the rate-1/2, dual-2 code becomes $B_c = 8$. Consequently, the term $P_2(m)$ in (14-6-21) must be replaced by $P_2(mL)$ when the orthogonal code has diversity L. Since a Hadamard code has an "effective diversity" $\frac{1}{2}d_{\min}$, it follows that when a Hadamard code is used as the inner code with a dual-k outer code, the upper bound on the bit error probability of the resulting concatenated code given by (14-6-21) still applies if $P_2(m)$ is replaced by $P_2(\frac{1}{2}md_{\min})$. With these modifications, the upper bound on the bit error probability given by (14-6-21) has been evaluated for rate-1/2, dual-k convolutional codes with either Hadamard codes or block orthogonal codes as inner codes. Thus the resulting concatenated code has a bandwidth expansion factor equal to twice the bandwidth expansion factor of the inner code.

First, we consider the performance gains due to code concatenation. Figure 14-6-9 illustrates the performance of dual-k codes with block orthogonal inner codes compared with the performance of block orthogonal codes for bandwidth expansion factors $B_c = 4$, 8, 16, and 32. The performance gains due to concatenation are very impressive. For example, at an error rate of 10^{-6} and $B_c = 8$, the dual-k code outperforms the orthogonal block code by 7.5 dB. In

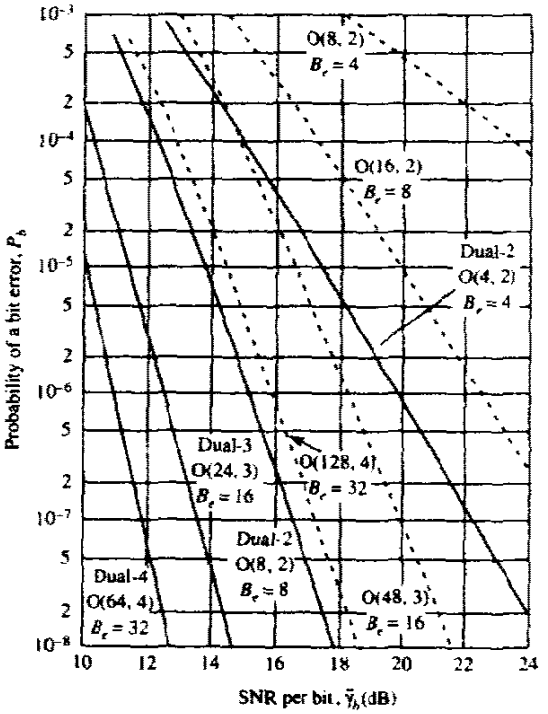

FIGURE 14-6-9 Comparison of performance between block orthogonal codes and dual-k with block orthogonal inner codes.

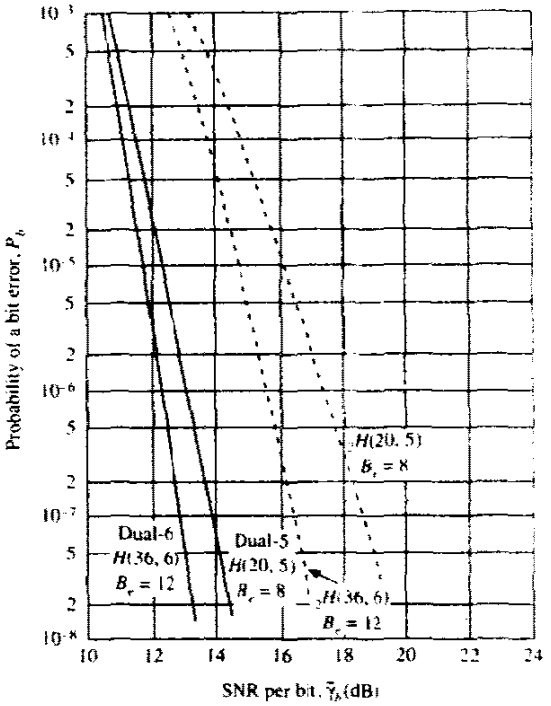

FIGURE 14-6-10 Comparison of performance between Hadamard codes and dual-k codes with Hadamard inner codes.

short, this gain may be attributed to the increased diversity (increase in minimum distance) obtained via code concatenation. Similarly, Fig. 14-6-10 illustrates the performance of two dual-k codes with Hadamard inner codes compared with the performance of the Hadamard codes alone for $B_e = 8$ and 12. It is observed that the performance gains due to code concatenation are still significant, but certainly not as impressive as those illustrated in Fig. 14-6-9. The reason is that the Hadamard codes alone yield a large diversity, so that the increased diversity arising from concatenation does not result in as large a gain in performance for the range of error rates covered in Fig. 14-6-10.

Next, we compare the performance for the two types of inner codes used with dual-k outer codes. Figure 14-6-11 shows the comparison for $B_e = 8$. Note that the $_2H(4, 2)$ inner code has $d_{\min} = 4$, and, hence, it has an effective order of diversity equal to 2. But this dual diversity is achieved by transmitting four frequencies per code word. On the other hand, the orthogonal code $O(8, 2)$ also gives dual diversity, but this is achieved by transmitting only two frequencies per code word. Consequently, the $O(8, 2)$ code is 3 dB better than the $_2H(4, 2)$. This difference in performance is maintained when the two codes are used as inner codes in conjunction with dual-2 code. On the other hand, for $B_e = 8$, one can use the $H(20, 5)$ as the inner code of a dual-5 code, and its performance is significantly better than that of the dual-2 code at low error rates. This improvement in performance is achieved at the expense of an increase in decoding complexity. Similarly, in Fig. 14-6-12, we compare the

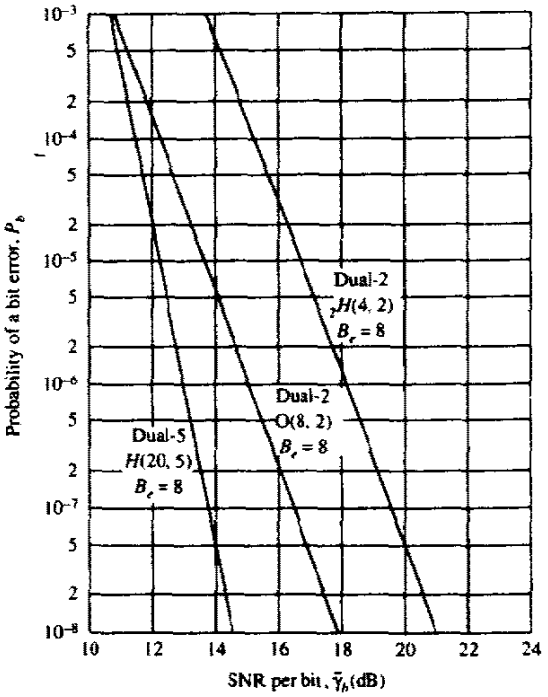

FIGURE 14-6-11 Performance of dual-k codes with either Hadamard or block orthogonal inner code for $B_c = 8$.

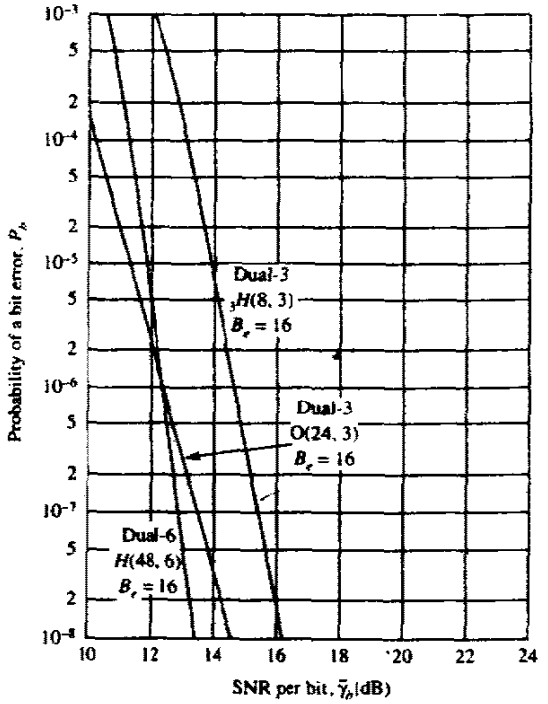

FIGURE 14-6-12 Performance of dual-k codes with either Hadamard or block orthogonal inner code for $B_c = 16$.

performance of the dual-k codes with two types of inner codes for $B_c = 16$. Note that the ${}_3H(8, 3)$ inner code has $d_{\min} = 12$, and, hence, it yields an effective diversity of 6. This diversity is achieved by transmitting 12 frequencies per code word. The orthogonal inner code O(24, 3) gives only third-order diversity, which is achieved by transmitting three frequencies per code word. Consequently the O(24, 3) inner code is more efficient at low SNR, that is, for the range of error rates covered in Fig. 14-6-12. At large SNR, the dual-3 code with the Hadamard ${}_3H(8, 3)$ inner code outperforms its counterpart with the O(24, 3) inner code due to the large diversity provided by the Hadamard code. For the same bandwidth expansion factor $B_c = 16$, one may use a dual-6 code with a $H(48, 6)$ code to achieve an improvement over the dual-3 code with the ${}_3H(8, 3)$ inner code. Again, this improvement in performance (which in this case is not as impressive as that shown in Fig. 14-6-11), must be weighed against the increased decoding complexity inherent in the dual-6 code.

The numerical results given above illustrate the performance advantages in using codes with good distance properties and soft-decision decoding on a Rayleigh fading channel as an alternative to conventional M-ary orthogonal signaling with diversity. In addition, the results illustrate the benefits of code concatenation on such a channel, using a dual-k convolutional code as the outer code and either a Hadamard code or a block orthogonal code as the inner code. Although dual-k codes were used for the outer code, similar results are obtained when a Reed–Solomon code is used for the outer code. There is an even greater choice in the selection of the inner code.

The important parameter in the selection of both the outer and the inner codes is the minimum distance of the resultant concatenated code required to achieve a specified level of performance. Since many codes will meet the performance requirements, the ultimate choice is made on the basis of decoding complexity and bandwidth requirements.

14-6-5 System Design Based on the Cutoff Rate

In the above treatment of coded waveforms, we have demonstrated the effectiveness of various codes for fading channels. In particular, we have observed the benefits of soft-decision decoding and code concatenation as a means for increasing the minimum distance and, hence, the amount of diversity in the coded waveforms. In this subsection, we consider randomly selected code words and derive an upper (union) bound on the error probability that depends on the cutoff rate parameter for the Rayleigh fading channel.

Let us consider the model for the communication system illustrated in Fig. 14-6-1. The modulator has a q-ary orthogonal FSK alphabet. Code words of block length n are mapped into waveforms by selecting n tones from the alphabet of q tones. The demodulation is performed by passing the signal through a bank of q matched filters followed by square-law detectors. The decoding is assumed to be soft-decision. Thus, the square-law detected outputs

from the demodulator are appropriately combined (added) with equal weighting to form M decision variables corresponding to the M possible transmitted code words.

To evaluate the union bound on the probability of error in a Rayleigh fading channel with AWGN, we first evaluate the binary error probability involving the decision variable U_1, which corresponds to the transmitted code word, and any of the other $M-1$ decision variables corresponding to the other code words. Let U_2 be the other decision variable and suppose that U_1 and U_2 have l tones in common. Hence, the contributions to U_1 and U_2 from these l tones are identical and, therefore, cancel out when we form the difference $U_1 - U_2$. Since the two decision variables differ in $n-l$ tones, the probability of error is simply that for a binary orthogonal FSK system with $n-l$ order diversity. The exact form for this probability of error is given by (14-6-4), where $p = 1/(2+\bar{\gamma}_c)$, and $\bar{\gamma}_c$ is the average SNR per tone. For simplicity, we choose to use the Chernoff bound for this binary event error probability, given by (14-6-7), i.e.,

$$P_2(U_1, U_2 \mid l) \leq [4p(1-p)]^{n-l} \tag{14-6-22}$$

Now, let us average over the ensemble of binary communication systems. There are q^n possible code words, from which we randomly select two code words. Thus, each code word is selected with equal probability. Then, the probability that two randomly selected code words have l tones in common is

$$P(l) = \binom{n}{l}\left(\frac{1}{q}\right)^l\left(1-\frac{1}{q}\right)^{n-l} \tag{14-6-23}$$

When we average (14-6-22) over the probability distribution of l given by (14-6-23), we obtain

$$\begin{aligned}\overline{P_2(U_1, U_2)} &= \sum_{l=0}^{n} P_2(U_1, U_2 \mid l)P(l) \\ &\leq \left\{\sum_{l=0}^{n}\binom{n}{l}\left(\frac{1}{q}\right)^l\left[4\left(1-\frac{1}{q}\right)p(1-p)\right]^{n-l}\right. \\ &\leq \left\{\frac{1}{q}[1+4(q-1)p(1-p)]\right\}^n\end{aligned} \tag{14-6-24}$$

Finally, the union bound for communication systems that use $M = 2^k$ randomly selected code words is simply

$$\bar{P}_M \leq (M-1)\overline{P_2(U_1, U_2)} < M\overline{P_2(U_1, U_2)} \tag{14-6-25}$$

By combining (14-6-24) with (14-6-25), we obtain the upper bound on the symbol error probability as

$$\bar{P}_M < 2^{-n(R_0 - R_c)} \tag{14-6-26}$$

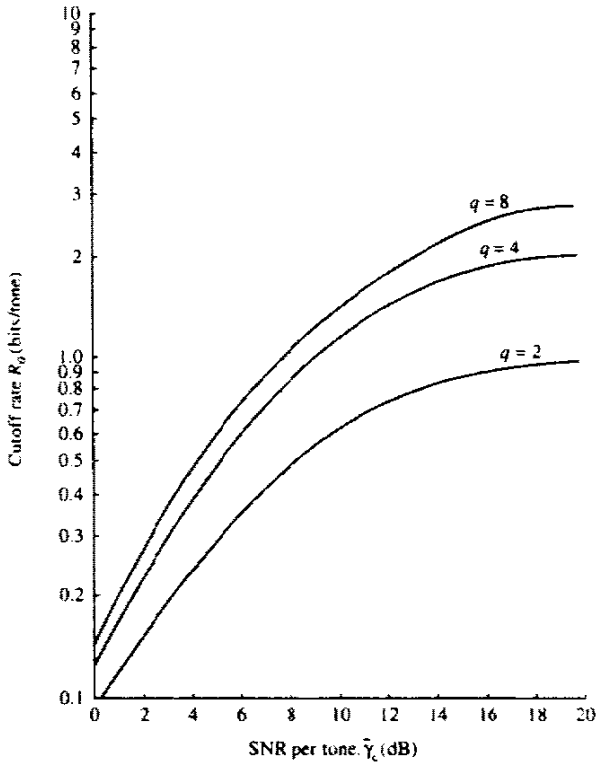

URE 14-6-13 Cutoff rate as a function of $\bar{\gamma}_c$ for Rayleigh fading channel.

where $R_c = k/n$ is the code rate and R_0 is the cutoff rate defined as

$$R_0 = \log_2 \frac{q}{1 + 4(q-1)p(1-p)} \tag{14-6-27}$$

with

$$p = \frac{1}{2 + \bar{\gamma}_c} \tag{14-6-28}$$

Graphs of R_0 as a function of $\bar{\gamma}_c$ are shown in Fig. 14-6-13 for $q = 2$, 4, and 8.

A more interesting form of (14-6-26) is obtained if we express $\bar{P}_M$ in terms of the SNR per bit. In particular, (14-6-26) may be expressed as

$$\bar{P}_M < 2^{-k[\bar{\gamma}_b R(q,\bar{\gamma}_c)-1]} \tag{14-6-29}$$

where, by definition,

$$\begin{aligned} g(q, \bar{\gamma}_c) &= \frac{R_0}{\bar{\gamma}_c} \\ &= \frac{1}{\bar{\gamma}_c} \log_2 \left[\frac{q}{1 + 4(q-1)p(1-p)} \right] \end{aligned} \tag{14-6-30}$$

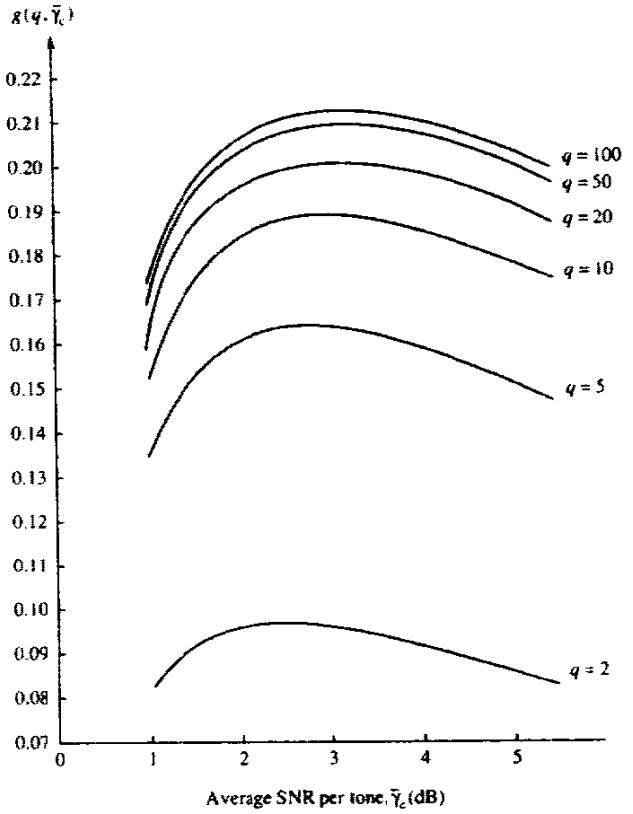

FIGURE 14-6-14 Graph of function $g(q, \bar{\gamma}_c)$.

Graphs of $g(q, \bar{\gamma}_c)$ as a function of $\bar{\gamma}_c$ are plotted in Fig. 14-6-14, with q as a parameter. First, we note thate is an optimum $\bar{\gamma}_c$ for each value of q that minimizes the probability of error. For large q, this value is approximately $\bar{\gamma}_c = 3$ (5 dB), which is consistent with our previous observation for ordinary square-law diversity combining. Furthermore, as $q \to \infty$, the function $g(q, \bar{\gamma}_c)$ approaches a limit, which is

$$\lim_{q \to \infty} g(q, \bar{\gamma}_c) = g_\infty(\bar{\gamma}_c) = \frac{1}{\bar{\gamma}_c} \log_2 \left[\frac{(2 + \bar{\gamma}_c)^2}{4(1 + \bar{\gamma}_c)} \right] \tag{14-6-31}$$

The value of $g_\infty(\bar{\gamma}_c)$ evaluated at $\bar{\gamma}_c = 3$ is

$$\begin{aligned} g_\infty(3) &= \max_{\bar{\gamma}_c} g_\infty(\bar{\gamma}_c) \\ &= 0.215 \end{aligned} \tag{14-6-32}$$

Therefore, the error probability in (14-6-29) for this optimum division of total SNR is

$$\bar{P}_M < 2^{-0.215k(\bar{\gamma}_b - 4.65)} \tag{14-6-33}$$

This result indicates that the probability of error can be made arbitrarily small with optimum SNR per code chip, if the average SNR per bit $\bar{\gamma}_b > 4.65$ (6.7 dB). Even a relatively modest value of $q = 20$ comes close to this minimum value. As seen from Fig. 14-6-14, $g(20, 3) = 0.2$, so that $P_M \to 0$, provided $\bar{\gamma}_b > 5$ (7 dB). On the other hand, if $q = 2$, the maximum value of $g(2, \bar{\gamma}_c) \approx 0.096$ and the corresponding minimum SNR per bit is 10.2 dB.

In the case of binary FSK waveforms ($q = 2$), we may easily compare the cutoff rate for the unquantized (soft-decision) demodulator output with the cutoff rate for binary quantization, for which

$$R_Q = 1 - \log[1 + \sqrt{4p(1-p)}], \qquad Q = 2$$

as was given in (8-1-104). Figure 14-6-15 illustrates the graphs for R_0 and R_Q. Note that the difference between R_0 and R_Q is approximately 3 dB for rates below 0.3 and the difference increases rapidly at high rates. This loss may be reduced significantly by increasing the number of quantization levels to $Q = 8$ (three bits).

Similar comparisons in the relative performance between unquantized soft-decision decoding and quantized decision decoding can also be made for $q > 2$.

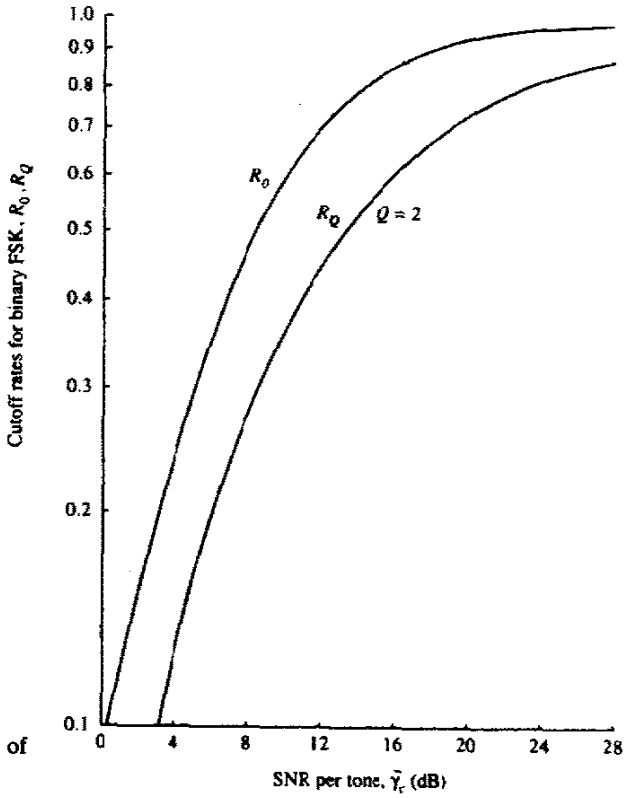

FIGURE 14-6-15 Cutoff rate for (unquantized) soft-decision and hard-decision decoding of coded binary FSK.

14-6-6 Trellis-Coded Modulation

Trellis-coded modulation was described in Section 8-3 as a means for achieving a coding gain on bandwidth-constrained channels, where we wish to transmit at a bit-rate-to-bandwidth ratio $R/W > 1$. For such channels, the digital communication system is designed to use bandwidth-efficient multilevel or multiphase modulation (PAM, PSK, DPSK, or QAM), which allows us to achieve an $R/W > 1$. When coding is applied in signal design for a bandwidth constrained channel, a coding gain is desired without expanding the signal bandwidth. This goal can be achieved, as described in Section 8-3, by increasing the number of signal points in the constellation over the corresponding uncoded system to compensate for the redundancy introduced by the code, and designing the trellis code so that the euclidean distance in a sequence of transmitted symbols corresponding to paths that merge at any node in the trellis is larger than the euclidean distance per symbol in an uncoded system.

In contrast, the coding schemes that we have described above in conjunction with FSK modulation expand the bandwidth of the modulated signal for the purpose of achieving signal diversity. Coupled with FSK modulation, which is not bandwidth-efficient, the coding schemes we have described are inappropriate for use on bandwidth-constrained channels.

In designing trellis-coded signal waveforms for fading channels, we may use the same basic principles that we have learned and applied in the design of conventional coding schemes. In particular, the most important objective in any coded signal design for fading channels is to achieve as large a signal diversity as possible. This implies that successive output symbols from the encoder must be interleaved or sufficiently separated in transmission, either in time or in frequency, so as to achieve independent fading in a sequence of symbols that equals or exceeds the minimum free distance of the trellis code. Therefore, we may represent such a trellis-coded modulation system by the block diagram in Fig. 14-6-16, where the interleaver is viewed broadly as a device that separates the successive coded symbols so as to provide independent fading on each symbol (through frequency or time separation of symbols) in the sequence. The receiver consists of a signal demodulator whose output is deinterleaved and fed to the trellis decoder.

FIGURE 14-6-16 Block diagram of trellis-coded modulation systems.

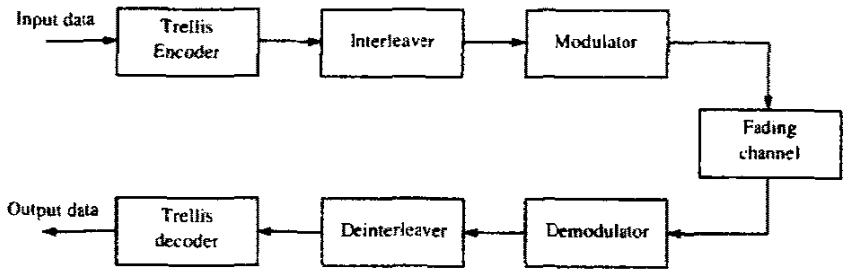

As indicated above, the candidate modulation methods that achieve high bandwidth efficiency are M-ary PSK, DPSK, QAM and PAM. The choice depends to a large extent on the channel characteristics. If there are rapid amplitude variations in the received signal, QAM and PAM may be particularly vulnerable, because a wideband automatic gain control (AGC) must be used to compensate for the channel variations. In such a case, PSK or DPSK are more suitable, since the information is conveyed by the signal phase and not by the signal amplitude. DPSK provides the additional benefit that carrier phase coherence is required only over two successive symbols. However, there is an SNR degradation in DPSK relative to PSK.

In the design of the trellis code, our objective is to achieve as large a free distance as possible, since this parameter is equivalent to the amount of diversity in the received signal. In conventional Ungerboeck trellis coding, each branch in the trellis corresponds to a single M-ary (PSK, DPSK, QAM) output channel symbol. Let us define the *shortest error event path* as the error event path with the smallest number of nonzero distances between itself and the correct path, and let L be its length. In other words, L is the Hamming distance between the M-ary symbols on the shortest error event path and those in the correct path. Hence, if we assume that the transmitted sequence corresponds to the all-zero path in the trellis, L is the number of branches in the shortest-length path with a nonzero M-ary symbol. In a trellis diagram with parallel paths, the paths are constrained to have a shortest error event length of one branch, so that $L = 1$. This means that such a trellis code provides no diversity in a fading channel and, hence, the probability of error is inversely proportional to the SNR per symbol. Therefore, in conventional trellis coding for a fading channel, it is undesirable to design a code that has parallel paths in its trellis, because such a code yields no diversity. This is the case in a conventional rate-$m/(m + 1)$ trellis code, where we are forced to have parallel paths when the number of states is less than 2^m.

One possible way to increase the minimum free distance and, thus, the order of diversity in the code, is to introduce asymmetry in the signal point constellation. This approach appears to be somewhat effective, and has been investigated by Simon and Divsalar (1985), Divsalar and Yuen (1984), and Divsalar *et al.* (1987).

A more effective way to increase the distance L and, thus, the order of diversity is to employ multiple trellis-coded modulation (MTCM). In MTCM, illustrated in Fig. 14-6-17, b input bits to the encoder are coded into c output bits, which are then subdivided into k groups, each of m bits, such that $c = km$. Each m-bit group is mapped into an M-ary symbol. Thus, we obtain the M-ary output symbols. The special case $k = 1$ corresponds to the conventional Ungerboeck codes. With k M-ary output symbols, it is possible to design trellis codes with parallel paths having a distance $L = k$. Thus, we can achieve an error probability that decays inversely as $(\mathscr{E}/N_0)^k$.

An important consideration in the design of the decoder for the trellis code is the use of any side information regarding the channel attenuation for each

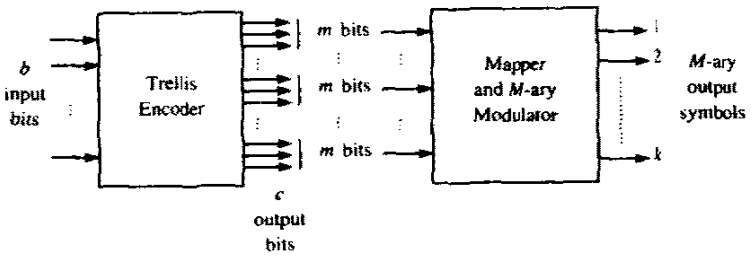

FIGURE 14-6-17 Block diagram of MTCM transmitter.

symbol. In the case of FSK modulation with square-law combination at the decoder to form the decision metrics, it is not necessary to know the channel attenuation for demodulated symbols. However, with coherent detection, the optimum euclidean distance metric for each demodulated symbol is of the form $|r_n - \alpha_n s_n|^2$, where α_n is the channel attenuation for the transmitted symbol s_n and r_n is the demodulation output. Hence, the sum of branch metrics for any given path through the trellis is of the form

$$D(\mathbf{r}, \mathbf{s}^{(i)}) = \sum_n |r_n - \alpha_n s_n^{(i)}|^2$$

where the superscript (i) indicates the ith path through the trellis. Therefore, the estimation of the channel attenuation must be performed in order to realize the optimum trellis decoder. The estimation of the channel attenuation and phase shift, is considered in Appendix C for the case of PSK modulation and demodulation. The effect of the quality of the attenuation and phase estimates on the performance of PSK (uncoded) modulation is also assessed in Appendix C.

14-7 BIBLIOGRAPHICAL NOTES AND REFERENCES

In this chapter, we have considered a number of topics concerned with digital communications over a fading multipath channel. We began with a statistical characterization of the channel and then described the ramifications of the channel characteristics on the design of digital signals and on their performance. We observed that the reliability of the communication system is enhanced by the use of diversity transmission and reception. Finally we demonstrated that channel encoding and soft-decision decoding provide a bandwidth-efficient means for obtaining diversity over such channels.

The pioneering work on the characterization of fading multipath channels and on signal and receiver design for reliable digital communications over such channels was done by Price (1954, 1956). This work was followed by additional significant contributions from Price and Green (1958, 1960), Kailath (1960, 1961), and Green (1962). Diversity transmission and diversity combining techniques under a variety of channel conditions have been considered in the papers by Pierce (1958), Brennan (1959), Turin (1961, 1962), Pierce and Stein

(1960), Barrow (1963), Bello and Nelin (1962a, b, 1963), Price (1962a, b), and Lindsey (1964).

Our treatment of coding for fading channels has relied on contributions from a number of researchers. In particular, the use of dual-k codes with M-ary orthogonal FSK was proposed in publications by Viterbi and Jacobs (1975) and Odenwalder (1976). The importance of coding for digital communications over a fading channel was also emphasized in a paper by Chase (1976). The benefits derived from concatenated coding with soft-decision decoding for a fading channel were demonstrated by Pieper *et al.* (1978). There, a Reed–Solomon code was used for the outer code and a Hadamard code was selected as the inner code. The performance of dual-k codes with either block orthogonal codes or Hadamard codes as inner code were investigated by Proakis and Rahman (1979). The error rate performance of maximal free distance binary convolutional codes was evaluated by Rahman (1981). Finally, the derivation of the cutoff rate for Rayleigh fading channels is due to Wozencraft and Jacobs (1965).

Trellis-coded modulation for fading channels has been investigated by many researchers, whose work was motivated to a large extent by applications to mobile and cellular communications. The book by Biglieri *et al.* (1991) gives a tutorial treatment of this topic and contains a large number of references to the technical literature.

Our treatment of digital communications over fading channels focused primarily on the Rayleigh fading channel model. For the most part, this is due to the wide acceptance of this model for describing the fading effects on many radio channels and to its mathematical tractability. Although other statistical models, such as a Ricean fading model or the Nakagami fading model may be more appropriate for characterizing fading on some real channels, the general approach in the design of reliable communications presented in this chapter carries over.

PROBLEMS

14-1 The scattering function $S(\tau; \lambda)$ for a fading multipath channel is nonzero for the range of values $0 \leq \tau \leq 1$ ms and -0.1 Hz $\leq \lambda \leq 0.1$ Hz. Assume that the scattering function is approximately uniform in the two variables.

a Give numerical values for the following parameters:

(i) the multipath spread of the channel;
(ii) the Doppler spread of the channel;
(iii) the coherence time of the channel;
(iv) the coherence bandwidth of the channel;
(v) the spread factor of the channel.

b Explain the meaning of the following, taking into consideration the answers given in (a):

(i) the channel is frequency-nonselective;
(ii) the channel is slowly fading;
(iii) the channel is frequency-selective.

c Suppose that we have a frequency allocation (bandwidth) of 10 kHz and we wish to transmit at a rate of 100 bits/s over this channel. Design a binary communications system with frequency diversity. In particular, specify (i) the type of modulation, (ii) the number of subchannels, (iii) the frequency separation between adjacent carriers, and (iv) the signaling interval used in your design. Justify your choice of parameters.

14-2 Consider a binary communications system for transmitting a binary sequence over a fading channel. The modulation is orthogonal FSK with third-order frequency diversity ($L = 3$). The demodulator consists of matched filters followed by square-law detectors. Assume that the FSK carriers fade independently and identically according to a Rayleigh envelope distribution. The additive noises on the diversity signals are zero-mean gaussian with autocorrelation functions $\frac{1}{2}E[z_k^*(t)z_k(t+\tau)] = N_0\delta(\tau)$. The noise processes are mutually statistically independent.

a The transmitted signal may be viewed as binary FSK with square-law detection, generated by a repetition code of the form

$$1 \rightarrow \mathbf{C}_1 = [1 \quad 1 \quad 1], \qquad 0 \rightarrow \mathbf{C}_0 = [0 \quad 0 \quad 0]$$

Determine the error rate performance P_{2h} for a hard-decision decoder following the square-law-detected signals.

b Evaluate P_{2h} for $\bar{\gamma}_c = 100$ and 1000.

c Evaluate the error rate P_{2s} for $\bar{\gamma}_c = 100$ and 1000 if the decoder employs soft-decision decoding.

d Consider the generalization of the result in (a). If a repetition code of block length L (L odd) is used, determine the error probability P_{2h} of the hard-decision decoder and compare that with P_{2s}, the error rate of the soft-decision decoder. Assume $\bar{\gamma} \gg 1$.

14-3 Suppose that the binary signal $s_i(t)$ is transmitted over a fading channel and the received signal is

$$r_i(t) = \pm a s_i(t) + z(t), \qquad 0 \leq t \leq T$$

where $z(t)$ is zero-mean white gaussian noise with autocorrelation function

$$\phi_{zz}(\tau) = N_0\delta(\tau)$$

The energy in the transmitted signal is $\mathscr{E} = \frac{1}{2}\int_0^T |s_i(t)|^2\,dt$. The channel gain a is specified by the probability density function

$$p(a) = 0.1\delta(a) + 0.9\delta(a-2)$$

a Determine the average probability of error P_2 for the demodulator that employs a filter matched to $s_i(t)$.

b What value does P_2 approach as $\mathscr{E}/N_0$ approaches infinity.

c Suppose that the same signal is transmitted on two statistically *independently fading* channels with gains a_1 and a_2, where

$$p(a_k) = 0.1\delta(a_k) + 0.9\delta(a_k - 2), \qquad k = 1, 2$$

The noises on the two channels are statistically independent and identically distributed. The demodulator employs a matched filter for each channel and

simply adds the two filter outputs to form the decision variable. Determine the average P_2.

d For the case in (c) what value does P_2 approach as $\mathscr{E}/N_0$ approaches infinity.

14-4 A multipath fading channel has a multipath spread of $T_m = 1$ s and a Doppler spread $B_d = 0.01$ Hz. The total channel bandwidth at bandpass available for signal transmission is $W = 5$ Hz. To reduce the effects of intersymbol interference, the signal designer selects a pulse duration $T = 10$ s.

a Determine the coherence bandwidth and the coherence time.

b Is the channel frequency selective? Explain.

c Is the channel fading slowly or rapidly? Explain.

d Suppose that the channel is used to transmit binary data via (antipodal) coherently detected PSK in a frequency diversity mode. Explain how you would use the available channel bandwidth to obtain frequency diversity and determine how much diversity is available.

e For the case in (d), what is the *approximate* SNR required per diversity to achieve an error probability of 10^{-6}?

f Suppose that a wideband signal is used for transmission and a RAKE-type receiver is used for demodulation. How many taps would you use in the RAKE receiver?

g Explain whether or not the RAKE receiver can be implemented as a coherent receiver with maximal ratio combining.

h If binary orthogonal signals are used for the wideband signal with square-law postdetection combining in the RAKE receiver, what is the *approximate* SNR required to achieve an error probability of 10^{-6}? (assume that all taps have the same SNR.)

14-5 In the binary communications system shown in Fig. P14-5, $z_1(t)$ and $z_2(t)$ are statistically independent white gaussian noise processes with zero mean and identical autocorrelation functions $\phi_{zz}(\tau) = N_0\delta(\tau)$. The sampled values U_1 and U_2 represent the *real parts* of the matched filter outputs. For example, if $s_1(t)$ is transmitted, then we have

$$U_1 = 2\mathscr{E} + N_1$$
$$U_2 = N_1 + N_2$$

where $\mathscr{E}$ is the transmitted signal energy and

$$N_k = \text{Re}\left[\int_0^T s_i^*(t) z_k(t)\, dt\right], \quad k = 1, 2$$

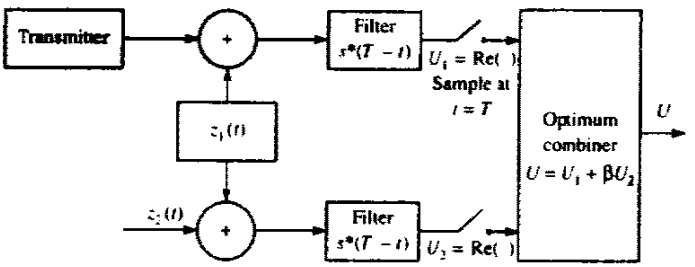

FIGURE P14-5

It is apparent that U_1 and U_2 are correlated gaussian variables while N_1 and N_2 are independent gaussian variables. Thus,

$$p(n_1) = \frac{1}{\sqrt{2\pi}\sigma} \exp\left(-\frac{n_1^2}{2\sigma^2}\right)$$

$$p(n_2) = \frac{1}{\sqrt{2\pi}\sigma} \exp\left(-\frac{n_2^2}{2\sigma^2}\right)$$

where the variance of N_k is $\sigma^2 = 2\mathscr{E}N_0$.

a Show that the joint probability density function for U_1 and U_2 is

$$p(U_1, U_2) = \frac{1}{2\pi\sigma^2} \exp\left\{-\frac{1}{2\sigma^2}[(U_1 - 2\mathscr{E})^2 - U_2(U_1 - 2\mathscr{E}) + \tfrac{1}{2}U_2^2]\right\}$$

if $s(t)$ is transmitted and

$$p(U_1, U_2) = \frac{1}{2\pi\sigma^2} \exp\left\{-\frac{1}{2\sigma^2}[(U_1 + 2\mathscr{E})^2 - U_2(U_1 + 2\mathscr{E}) + \tfrac{1}{2}U_2^2]\right\}$$

if $-s(t)$ is transmitted.

b Based on the likelihood ratio, show that the optimum combination of U_1 and U_2 results in the decision variable

$$U = U_1 + \beta U_2$$

where β is a constant. What is the optimum value of β?

c Suppose that $s(t)$ is transmitted. What is the probability density function of U?

d What is the probability of error assuming that $s(t)$ was transmitted? Express your answer as a function for the SNR $\mathscr{E}/N_0$.

e What is the loss in performance if only $U = U_1$ is the decision variable?

14-6 Consider the model for a binary communications system with diversity as shown in Fig. P14-6. The channels have fixed attenuations and phase shifts. The $\{z_k(t)\}$ are

FIGURE P14-6

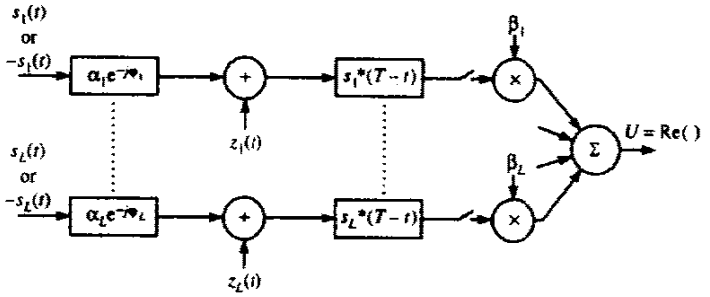

complex-valued white gaussian noise processes with zero mean and autocorrelation functions

$$\phi_{z_k}(t) = \tfrac{1}{2}E[z_k^*(t)z_k(t+\tau)] = N_{0k}\delta(\tau)$$

(Note that the spectral densities $\{N_{0k}\}$ are all different.) Also, the noise processes $\{z_k(t)\}$ are mutually statistically independent. The $\{\beta_k\}$ are complex-valued weighting factors to be determined. The decision variable from the combiner is

$$U = \text{Re}\left(\sum_{k=1}^{L} \beta_k U_k\right) \gtrless_{-1}^{1} 0$$

a Determine the pdf $p(U)$ when $+1$ is transmitted.
b Determine the probability of error P_2 as a function of the weights $\{\beta_k\}$.
c Determine the values of $\{\beta_k\}$ that minimize P_2.

14-7 Determine the probability of error for binary orthogonal signaling with Lth-order diversity over a Rayleigh fading channel. The pdfs of the two decision variables are given by (14-4-31) and (14-4-32).

14-8 The rate-1/3, $L = 3$, binary convolutional code with transfer function given by (8-2-5) is used for transmitting data over a Rayleigh fading channel via binary PSK.
a Determine and plot the probability of error for hard-decision decoding. Assume that the transmitted waveforms corresponding to the coded bits fade independently.
b Determine and plot the probability of error for soft-decision decoding. Assume that the waveforms corresponding to the coded bits fade independently.

14-9 A binary sequence is transmitted via binary antipodal signaling over a Rayleigh fading channel with Lth-order diversity. When $s_i(t)$ is transmitted, the received equivalent lowpass signals are

$$r_k(t) = \alpha_k e^{-j\phi_k} s_i(t) + z_k(t), \quad k = 1, 2, \ldots, L$$

The fading among the L subchannels is statistically independent. The additive noise terms $\{z_k(t)\}$ are zero-mean, statistically independent and identically distributed white gaussian noise processes with autocorrelation function $\phi_{z_k}(\tau) = N_0\delta(\tau)$. Each of the L signals is passed through a filter matched to $s_i(t)$ and the output is phase-corrected to yield

$$U_k = \text{Re}\left[e^{j\phi_k}\int_0^T r_k(t)s_i^*(t)\,dt\right], \quad k = 1, 2, \ldots, L$$

The $\{U_k\}$ are combined by a linear combiner to form the decision variable

$$U = \sum_{k=1}^{L} U_k$$

a Determine the pdf of U conditional on fixed values for the $\{a_k\}$.
b Determine the expression for the probability of error when the $\{\alpha_k\}$ are statistically independent and identically distributed Rayleigh random variables.

14-10 The Chernoff bound for the probability of error for binary FSK with diversity L in Rayleigh fading was shown to be

$$P_2(L) < [4p(1-p)]^L = \left[4\frac{1+\bar{\gamma}_c}{(2+\bar{\gamma}_c)^2}\right]^L$$
$$< 2^{-\bar{\gamma}_b g(\bar{\gamma}_c)}$$

where

$$g(\bar{\gamma}_c) = \frac{1}{\bar{\gamma}_c}\log_2\left[\frac{(2+\bar{\gamma}_c)^2}{4(1+\bar{\gamma}_c)}\right]$$

a Plot $g(\bar{\gamma}_c)$ and determine its approximate maximum value and the value of $\bar{\gamma}_c$ where the maximum occurs.

b For a given $\bar{\gamma}_b$, determine the optimal order of diversity.

c Compare $P_2(L)$, under the condition that $g(\bar{\gamma}_c)$ is maximized (optimal diversity), with the error probability for binary FSK in AWGN with no fading, which is

$$P_2 = \tfrac{1}{2}e^{-\gamma_b/2}$$

and determine the penalty in SNR due to fading and noncoherent (square-law) combining.

14-11 A DS spread-spectrum system is used to resolve the multipath signal components in a two-path radio signal propagation scenario. If the path length of the secondary path is 300 m longer than that of the direct path, determine the minimum chip rate necessary to resolve the multipath components.

14-12 A baseband digital communication system employs the signals shown in Fig. P14-12(*a*) for the transmission of two equiprobable messages. It is assumed that the communication problem studied here is a "one-shot" communication problem; that is, the above messages are transmitted just once and no transmission takes place afterward. The channel has no attenuation ($\alpha = 1$), and the noise is AWG with power spectral density $\frac{1}{2}N_0$.

a Find an appropriate orthonormal basis for the representation of the signals.

b In a block diagram, give the precise specifications of the optimum receiver using matched filters. Label the diagram carefully.

c Find the error probability of the optimum receiver.

d Show that the optimum receiver can be implemented by using just *one* filter

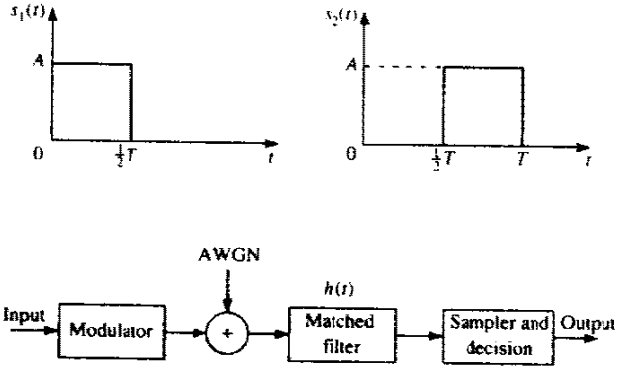

FIGURE P14-12

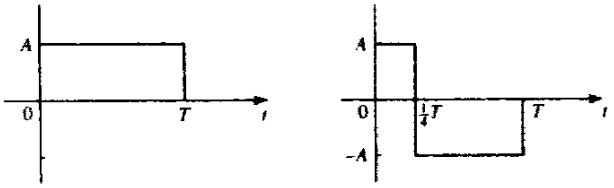

FIGURE P14-14

(see the block diagram in Fig. P14-12(*b*). What are the characteristics of the matched filter and the sampler and decision device?

e Now assume that the channel is not ideal but has an impulse response of $c(t) = \delta(t) + \frac{1}{2}\delta(t - \frac{1}{2}T)$. Using the same matched filter as (d), design an optimum reciever.

f Assuming that the channel impulse response is $c(t) = \delta(t) + a\delta(t - \frac{1}{2}T)$, where a is a random variable uniformly distributed on [0, 1], and using the same matched filter as in (d), design the optimum receiver.

14-13 A communication system employs dual antenna diversity and binary orthogonal FSK modulation. The received signals at the two antennas are

$$r(t) = \alpha_1 s(t) + n_1(t)$$
$$r_2(t) = \alpha_2 s(t) + n_2(t)$$

where α_1 and α_2 are statistically iid Rayleigh random variables, and $n_1(t)$ and $n_2(t)$ are statistically independent, zero-mean white gaussian random processes with power-spectral density $\frac{1}{2}N_0$. The two signals are demodulated, squared and then combined (summed) prior to detection.

a Sketch the functional block diagram of the entire receiver, including the demodulator, the combiner and the detector.

b Plot the probability of error for the detector and compare the result with the case of no diversity.

14-14 The two equivalent lowpass signals shown in Fig. P14-14 are used to transmit a binary sequence. The equivalent lowpass impulse response of the channel is $h(t) = 4\delta(t) - 2\delta(t - T)$. To avoid pulse overlap between successive transmissions, the transmission rate in bits/s is selected to be $R = 1/2T$. The transmitted signals are equally probable and are corrupted by additive zero-mean white gaussian noise having an equivalent lowpass representation $z(t)$ with an autocorrelation function

$$\phi_{zz}(\tau) = \tfrac{1}{2}E[z^*(t)z(t + \tau)] = N_0\delta(\tau)$$

a Sketch the two possible equivalent lowpass noise-free *received* waveforms.

b Specify the optimum receiver and sketch the equivalent lowpass impulse responses of all filters used in the optimum receiver. Assume *coherent detection* of the signals.

14-15 Verify the relation in (14-3-14) by making the change of variable $\gamma = \alpha^2\mathcal{E}_b/N_0$ in the Nakagami-m distribution.

15

MULTIUSER COMMUNICATIONS

Our treatment of communication systems up to this point has been focused on a single communication link involving a transmitter and a receiver. In this chapter, the focus shifts to multiple users and multiple communication links. We explore the various ways in which the multiple users access a common channel to transmit information. The multiple access methods that are described in this chapter form the basis for current and future wireline and wireless communication networks, such as satellite networks, cellular and mobile communication networks, and underwater acoustic networks.

15-1 INTRODUCTION TO MULTIPLE ACCESS TECHNIQUES

It is instructive to distinguish among several types of multiuser communication systems. One type is a multiple access system in which a large number of users share a common communication channel to transmit information to a receiver. Such a system is depicted in Fig. 15-1-1. The common channel may be the up-link in a satellite communication system, or a cable to which are connected a set of terminals that access a central computer, or some frequency band in the radio spectrum that is used by multiple users to communicate with a radio receiver. For example, in a mobile cellular communication system, the users are the mobile transmitters in any particular cell of the system and the receiver resides in the base station of the particular cell.

A second type of multiuser communication system is a broadcast network in which a single transmitter sends information to multiple receivers as depicted

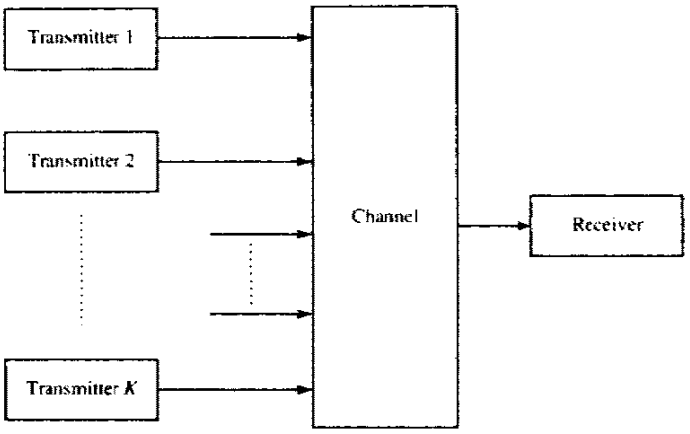

FIGURE 15-1-1 A multiple access system.

in Fig. 15-1-2. Examples of broadcast systems include the common radio and TV broadcast systems, as well as the down-links in a satellite system.

The multiple access and broadcast networks are probably the most common multiuser communication systems. A third type of multiuser system is a store-and-forward network, as depicted in Fig. 15-1-3. Yet a fourth type is the two-way communication system shown in Fig. 15-1-4.

In this chapter, we focus on multiple access methods for multiuser communications. In general, there are several different ways in which multiple users can send information through the communication channel to the receiver. One simple method is to subdivide the available channel bandwidth into a number, say N, of frequency nonoverlapping subchannels, as shown in Fig. 15-1-5, and to assign a subchannel to each user upon request by the users. This

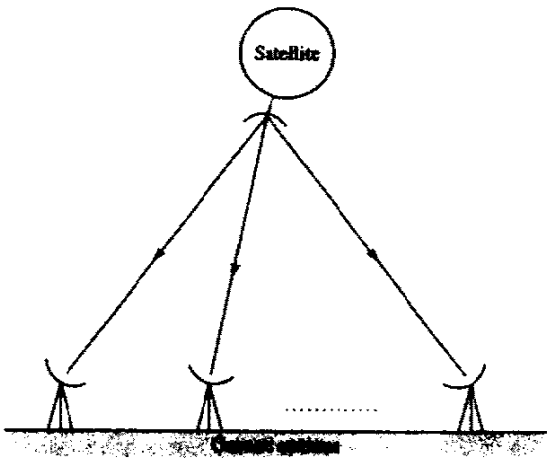

FIGURE 15-1-2 A broadcast network.

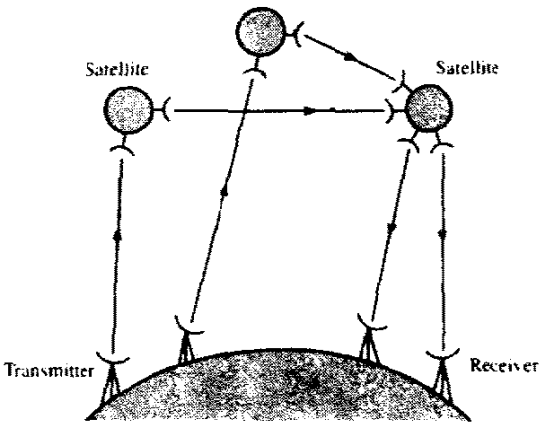

FIGURE 15-1-3 A store-and-forward communication network with satellite relays.

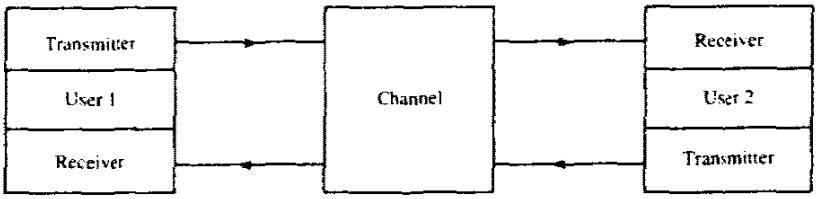

FIGURE 15-1-4 A two-way communication channel.

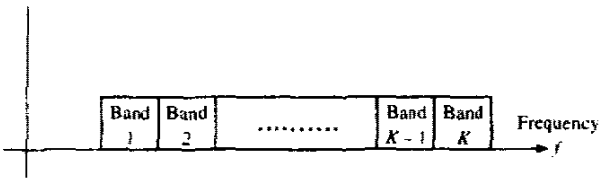

FIGURE 15-1-5 Subdivisions of the channel into nonoverlapping frequency bands.

method is generally called *frequency-division multiple access* (FDMA), and is commonly used in wireline channels to accommodate multiple users for voice and data transmission.

Another method for creating multiple subchannels for multiple access is to subdivide the duration T_f, called the *frame duration*, into, say, N nonoverlapping subintervals, each of duration T_f/N. Then each user who wishes to transmit information is assigned to a particular time slot within each frame. This multiple access method is called *time-division multiple access* (TDMA) and it is frequently used in data and digital voice transmission.

We observe that in FDMA and TDMA, the channel is basically partitioned into independent single-user subchannels. In this sense, the communication

system design methods that we have described for single-user communication are directly applicable and no new problems are encountered in a multiple access environment, except for the additional task of assigning users to available channels.

The interesting problems arise when the data from the users accessing the network is bursty in nature. In other words, the information transmissions from a single user are separated by periods of no transmission, where these periods of silence may be greater than the periods of transmission. Such is the case generally with users at various terminals in a computer communications network that contains a central computer. To some extent, this is also the case in mobile cellular communication systems carrying digitized voice, since speech signals typically contain long pauses.

In such an environment where the transmission from the various users is bursty and low-duty-cycle, FDMA and TDMA tend to be inefficient because a certain percentage of the available frequency slots or time slots assigned to users do not carry information. Ultimately, an inefficiently designed multiple access system limits the number of simultaneous users of the channel.

An alternative to FDMA and TDMA is to allow more than one user to share a channel or subchannel by use of direct-sequence spread spectrum signals. In this method, each user is assigned a unique code sequence or *signature sequence* that allows the user to spread the information signal across the assigned frequency band. Thus signals from the various users are separated at the receiver by cross-correlation of the received signal with each of the possible user signature sequences. By designing these code sequences to have relatively small cross-correlations, the crosstalk inherent in the demodulation of the signals received from multiple transmitters is minimized. This multiple access method is called *code-division multiple access* (CDMA).

In CDMA, the users access the channel in a random manner. Hence, the signal transmissions among the multiple users completely overlap both in time and in frequency. The demodulation and separation of these signals at the receiver is facilitated by the fact that each signal is spread in frequency by the pseudo-random code sequence. CDMA is sometimes called *spread-spectrum multiple access* (SSMA).

An alternative to CDMA is nonspread random access. In such a case, when two users attempt to use the common channel simultaneously, their transmissions collide and interfere with each other. When that happens, the information is lost and must be retransmitted. To handle collisions, one must establish protocols for retransmission of messages that have collided. Protocols for scheduling the retransmission of collided messages are described below.

15-2 CAPACITY OF MULTIPLE ACCESS METHODS

It is interesting to compare FDMA, TDMA, and CDMA in terms of the information rate that each multiple access method achieves in an ideal AWGN channel of bandwidth W. Let us compare the capacity of K users, where each

user has average power $P_i = P$, for all $1 \leq i \leq K$. Recall that in an ideal band-limited AWGN channel of bandwidth W, the capacity of a single user is

$$C = W \log_2\left(1 + \frac{P}{WN_0}\right) \tag{15-2-1}$$

where $\frac{1}{2}N_0$ is the power spectral density of the additive noise.

In FDMA, each user is allocated a bandwidth W/K. Hence, the capacity of each user is

$$C_K = \frac{W}{K}\log_2\left[1 + \frac{P}{(W/K)N_0}\right] \tag{15-2-2}$$

and the total capacity for the K users is

$$KC_K = W \log_2\left(1 + \frac{KP}{WN_0}\right) \tag{15-2-3}$$

Therefore, the total capacity is equivalent to that of a single user with average power $P_{av} = KP$.

It is interesting to note that for a fixed bandwidth W, the total capacity goes to infinity as the number of users increases linearly with K. On the other hand, as K increases, each user is allocated a smaller bandwidth (W/K) and, consequently, the capacity per user decreases. Figure 15-2-1 illustrates the capacity C_K per user normalized by the channel bandwidth W, as a function of $\mathscr{E}_b/N_0$, with K as a parameter. This expression is given as

$$\frac{C_K}{W} = \frac{1}{K}\log_2\left[1 + K\frac{C_K}{W}\left(\frac{\mathscr{E}_b}{N_0}\right)\right] \tag{15-2-4}$$

A more compact form of (15-2-4) is obtained by defining the normalized

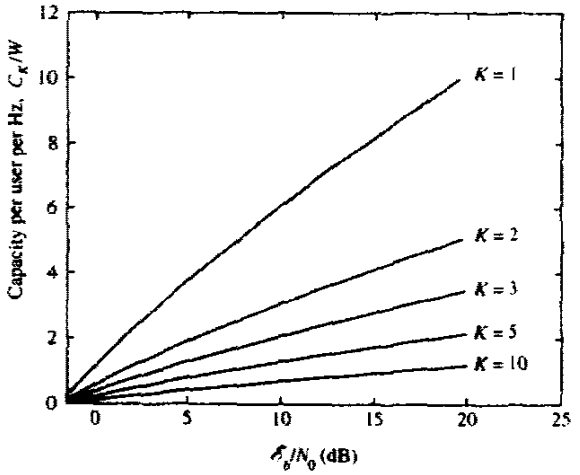

FIGURE 15-2-1 Normalized capacity as a function of $\mathscr{E}_b/N_0$ for FDMA.

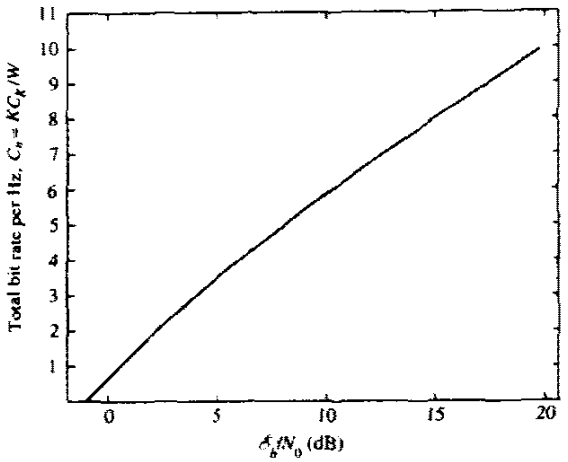

FIGURE 15-2-2 Total capacity per hertz as a function of $\mathscr{E}_b/N_0$ for FDMA.

total capacity $C_n = KC_K/W$, which is the total bit rate for all K users per unit of bandwidth. Thus, (15-2-4) may be expressed as

$$C_n = \log_2\left(1 + C_n\frac{\mathscr{E}_b}{N_0}\right) \tag{15-2-5}$$

or, equivalently,

$$\frac{\mathscr{E}_b}{N_0} = \frac{2^{C_n} - 1}{C_n} \tag{15-2-6}$$

The graph of C_n versus $\mathscr{E}_b/N_0$ is shown in Fig. 15-2-2. We observe that C_n increases as $\mathscr{E}_b/N_0$ increases above the minimum value of ln 2.

In a TDMA system, each user transmits for $1/K$ of the time through the channel of bandwidth W, with average power KP. Therefore, the capacity per user is

$$C_K = \left(\frac{1}{K}\right)W\log_2\left(1 + \frac{KP}{WN_0}\right) \tag{15-2-7}$$

which is identical to the capacity of an FDMA system. However, from a practical standpoint, we should emphasize that, in TDMA, it may not be possible for the transmitters to sustain a transmitter power of KP when K is very large. Hence, there is a practical limit beyond which the transmitter power cannot be increased as K is increased.

In a CDMA system, each user transmits a pseudo-random signal of a bandwidth W and average power P. The capacity of the system depends on the level of cooperation among the K users. At one extreme is noncooperative CDMA, in which the receiver for each user signal does not know the spreading waveforms of the other users, or chooses to ignore them in the demodulation process. Hence, the other users signals appear as interference at the receiver of each user. In this case, the multiuser receiver consists of a bank of K

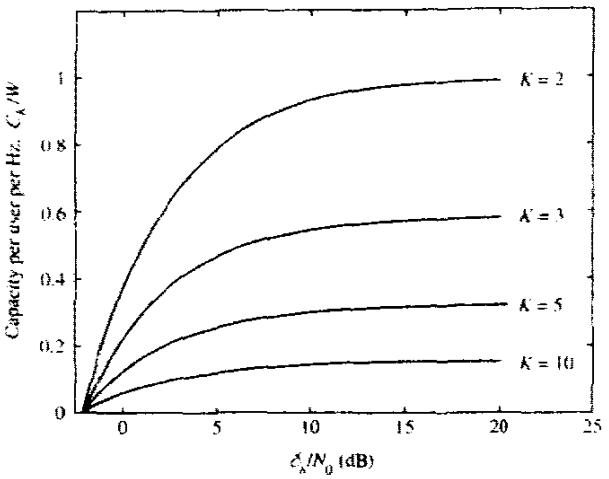

FIGURE 15-2-3 Normalized capacity as a function of $\mathscr{E}_b/N_0$ for noncooperative CDMA.

single-user receivers. If we assume that each user's pseudorandom signal waveform is gaussian then each user signal is corrupted by gaussian interference of power $(K-1)P$ and additive gaussian noise of power WN_0. Therefore, the capacity per user is

$$C_K = W \log_2 \left[1 + \frac{P}{WN_0 + (K-1)P} \right] \tag{15-2-8}$$

or, equivalently,

$$\frac{C_K}{W} = \log_2 \left[1 + \frac{C_K}{W} \frac{\mathscr{E}_b/N_0}{1 + (K-1)(C_K/W)\mathscr{E}_b/N_0} \right] \tag{15-2-9}$$

Figure 15-2-3 illustrates the graph of C_K/W versus $\mathscr{E}_b/N_0$, with K as a parameter.

For a large number of users, we may use the approximation $\ln(1+x) \leq x$. Hence,

$$\frac{C_K}{W} \leq \frac{C_K}{W} \frac{\mathscr{E}_b/N_0}{1 + K(C_K/W)(\mathscr{E}_b/N_0)} \log_2 e \tag{15-2-10}$$

or, equivalently,

$$\begin{aligned} C_n &\leq \log_2 e - \frac{1}{\mathscr{E}_b/N_0} \\ &\leq \frac{1}{\ln 2} - \frac{1}{\mathscr{E}_b/N_0} < \frac{1}{\ln 2} \end{aligned} \tag{15-2-11}$$

In this case, we observe that the total capacity does not increase with K as in TDMA and FDMA.

On the other hand, suppose that the K users cooperate by transmitting synchronously in time, and the multiuser receiver knows the spreading

waveforms of all users and jointly demodulates and detects all the users' signals. Thus, each user is assigned a rate R_i, $1 \leq i \leq K$, and a codebook containing a set of 2^{nR_i} codewords of power P. In each signal interval, each user selects an arbitrary codeword, say $\mathbf{X}_i$, from its own codebook and all users transmit their codewords simultaneously. Thus, the decoder at the receiver observes

$$\mathbf{Y} = \sum_{i=1}^{K} \mathbf{X}_i + \mathbf{Z} \tag{15-2-12}$$

where $\mathbf{Z}$ is an additive noise vector. The optimum decoder looks for the K codewords, one from each codebook, that have a vector sum closest to the received vector $\mathbf{Y}$ in euclidean distance.

The achievable K-dimensional rate region for the K users in an AWGN channel, assuming equal power for each user, is given by the following equations:

$$R_i < W \log_2 \left(1 + \frac{P}{WN_0}\right), \quad 1 \leq i \leq K \tag{15-2-13}$$

$$R_i + R_j < W \log_2 \left(1 + \frac{2P}{WN_0}\right), \quad 1 \leq i, j \leq K \tag{15-2-14}$$

$$\vdots$$

$$\sum_{i=1}^{K} R_i < W \log_2 \left(1 + \frac{KP}{WN_0}\right) \tag{15-2-15}$$

In the special case when all the rates are identical, the inequality (15-2-15) is dominant over the other $K - 1$ inequalities. It follows that if the rates $\{R_i, 1 \leq i \leq K\}$ for the K cooperative synchronous users are selected to fall in the capacity region specified by the inequalities given above then the probabilities of error for the K users tend to zero as the code block length n tends to infinity.

From the above discussion, we conclude that the sum of the rates of the K users goes to infinity with K. Therefore, with cooperative synchronous users, the capacity of CDMA has a form similar to that of FDMA and TDMA. Note that if all the rates in the CDMA system are selected to be identical to R then (15-2-15) reduces to

$$R < \frac{W}{K} \log_2 \left(1 + \frac{KP}{WN_0}\right) \tag{15-2-16}$$

which is identical to the rate constraint in FDMA and TDMA. In this case, CDMA does not yield a higher rate than TDMA and FDMA. However, if the rates of the K users are selected to be unequal such that the inequalities (15-2-13)–(15-2-15) are satisfied then it is possible to find the points in the achievable rate region such that the sum of the rates for the K users in CDMA exceeds the capacity of FDMA and TDMA.

Example 15-2-1

Consider the case of two users in a CDMA system that employs coded signals as described above. The rates of the two users must satisfy the inequalities

$$R_1 < W \log_2\left(1 + \frac{P}{WN_0}\right)$$

$$R_2 < W \log_2\left(1 + \frac{P}{WN_0}\right)$$

$$R_1 + R_2 < W \log_2\left(1 + \frac{2P}{WN_0}\right)$$

where P is the average transmitted power of each user and W is the signal bandwidth. Let us determine the capacity region for the two-user CDMA system.

The capacity region for the two-user CDMA system with coded signal waveforms has the form illustrated in Fig. 15-2-4, where

$$C_i = W \log_2\left(1 + \frac{P_i}{WN_0}\right), \quad i = 1, 2$$

are the capacities corresponding to the two users with $P_1 = P_2 = P$. We note that if user 1 is transmitting at capacity C_1, user 2 can transmit up to a maximum rate

$$R_{2m} = W \log_2\left(1 + \frac{2P}{WN_0}\right) - C_1$$

$$= W \log_2\left(1 + \frac{P}{P + WN_0}\right) \tag{15-2-17}$$

which is illustrated in Fig. 15-2-4 as point A. This result has an interesting

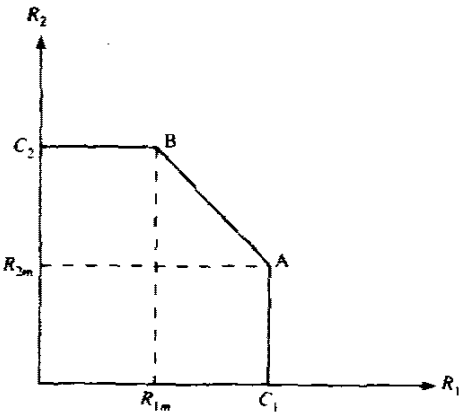

FIGURE 15-2-4 Capacity region of two-user CDMA multiple access gaussian channel.

interpretation. We note that rate R_{2m} corresponds to the case in which the signal from user 1 is considered as an equivalent additive noise in the detection of the signal of user 2. On the other hand, user 1 can transmit at capacity C_1, since the receiver knows the transmitted signal from user 2 and, hence, it can eliminate its effect in detecting the signal of user 1.

Due to symmetry, a similar situation exists if user 2 is transmitting at capacity C_2. Then, user 1 can transmit up to a maximum rate $R_{1m} = R_{2m}$, which is illustrated in Fig. 15.2.4 as point B. In this case, we have a similar interpretation as above, with an interchange in the roles of user 1 and user 2.

The points A and B are connected by a straight line. It is easily seen that this straight line is the boundary of the achievable rate region, since any point on the line corresponds to the maximum rate $W \log_2 (1 + 2P/WN_0)$, which can be obtained by simply time-sharing the channel between the two users.

In the next section, we consider the problem of signal detection for a multiuser CDMA system and assess the performance and the computational complexity of several receiver structures.

15-3 CODE-DIVISION MULTIPLE ACCESS

As we have observed, TDMA and FDMA are multiple access methods in which the channel is partitioned into independent, single-user subchannels, i.e., nonoverlapping time slots or frequency bands, respectively. In CDMA, each user is assigned a distinct signature sequence (or waveform), which the user employs to modulate and spread the information-bearing signal. The signature sequences also allow the receiver to demodulate the message transmitted by multiple users of the channel, who transmit simultaneously and, generally, asynchronously.

In this section, we treat the demodulation and detection of multiuser CDMA signals. We shall see that the optimum maximum-likelihood detector has a computational complexity that grows exponentially with the number of users. Such a high complexity serves as a motivation to devise suboptimum detectors having lower computational complexities. Finally, we consider the performance characteristics of the various detectors.

15-3-1 CDMA Signal and Channel Models

Let us consider a CDMA channel that is shared by K simultaneous users. Each user is assigned a signature waveform $g_k(t)$ of duration T, where T is the symbol interval. A signature waveform may be expressed as

$$g_k(t) = \sum_{n=0}^{L-1} a_k(n) p(t - nT_c), \qquad 0 \leq t \leq T \tag{15-3-1}$$

where $\{a_k(n), 0 \leq n \leq L-1\}$ is a pseudo-noise (PN) code sequence consisting of L chips that take values $\{\pm 1\}$, $p(t)$ is a pulse of duration T_c, and T_c is the chip interval. Thus, we have L chips per symbol and $T = LT_c$. Without loss of generality, we assume that all K signature waveforms have unit energy, i.e.,

$$\int_0^T g_k^2(t)\,dt = 1 \tag{15-3-2}$$

The cross-correlations between pairs of signature waveforms play an important role in the metrics for the signal detector and on its performance. We define the following cross-correlations:

$$\rho_{ij}(\tau) = \int_0^T g_i(t)g_j(t-\tau)\,dt, \qquad i \leq j \tag{15-3-3}$$

$$\rho_{ji}(\tau) = \int_0^T g_i(t)g_j(t+T-\tau)\,dt, \qquad i \leq j \tag{15-3-4}$$

For simplicity, we assume that binary antipodal signals are used to transmit the information from each user. Hence, let the information sequence of the kth user be denoted by $\{b_k(m)\}$, where the value of each information bit may be ± 1. It is convenient to consider the transmission of a block of bits of some arbitrary length, say N. Then, the data block from the kth user is

$$\mathbf{b}_k = [b_k(1) \quad \ldots \quad b_k(N)]' \tag{15-3-5}$$

and the corresponding equivalent lowpass, transmitted waveform may be expressed as

$$s_k(t) = \sqrt{\mathscr{E}_k} \sum_{i=1}^{N} b_k(i)g_k(t-iT) \tag{15-3-6}$$

where $\mathscr{E}_k$ is the signal energy per bit. The composite transmitted signal for the K users may be expressed as

$$\begin{aligned} s(t) &= \sum_{k=1}^{K} s_k(t-\tau_k) \\ &= \sum_{k=1}^{K} \sqrt{\mathscr{E}_k} \sum_{i=1}^{N} b_k(i)g_k(t-iT-\tau_k) \end{aligned} \tag{15-3-7}$$

where $\{\tau_k\}$ are the transmission delays, which satisfy the condition $0 \leq \tau_k < T$ for $1 \leq k \leq K$. Without loss of generality, we assume that $0 \leq \tau_1 \leq \tau_2 \leq \ldots \leq \tau_k < T$. This is the model for the multiuser transmitted signal in an asynchronous mode. In the special case of synchronous transmission, $\tau_k = 0$ for $1 \leq k \leq K$. The values of τ of interest in the cross-correlations given by (15-3-3) and (15-3-4) may also be restricted to $0 \leq \tau < T$, without loss of generality.

The transmitted signal is assumed to be corrupted by AWGN. Hence, the received signal may be expressed as

$$r(t) = s(t) + n(t) \tag{15-3-8}$$

where $s(t)$ is given by (15-3-7) and $n(t)$ is the noise, with power spectral density $\frac{1}{2}N_0$.

15-3-2 The Optimum Receiver

The optimum receiver is defined as the receiver that selects the most probable sequence of bits $\{b_k(n), 1 \leq n \leq N, 1 \leq k \leq K\}$ given the received signal $r(t)$ observed over the time interval $0 \leq t \leq NT + 2T$. First, let us consider the case of synchronous transmission; later, we shall consider asynchronous transmission.

Synchronous Transmission In synchronous transmission, each (user) interferer produces exactly one symbol which interferes with the desired symbol. In additive white gaussian noise, it is sufficient to consider the signal received in one signal interval, say $0 \leq t \leq T$, and determine the optimum receiver. Hence, $r(t)$ may be expressed as

$$r(t) = \sum_{k=1}^{K} \sqrt{\mathscr{E}_k} b_k(1) g_k(t) + n(t), \quad 0 \leq t \leq T \tag{15-3-9}$$

The optimum maximum-likelihood receiver computes the log-likelihood function

$$\Lambda(\mathbf{b}) = \int_0^T \left[r(t) - \sum_{k=1}^{K} \sqrt{\mathscr{E}_k} b_k(1) g_k(t) \right]^2 dt \tag{15-3-10}$$

and selects the information sequence $\{b_k(1), 1 \leq k \leq K\}$ that minimizes $\Lambda(\mathbf{b})$. If we expand the integral in (15-3-10), we obtain

$$\Lambda(\mathbf{b}) = \int_0^T r^2(t)\, dt - 2 \sum_{k=1}^{K} \sqrt{\mathscr{E}_k} b_k(1) \int_0^T r(t) g_k(t)\, dt + \sum_{j=1}^{K} \sum_{k=1}^{K} \sqrt{\mathscr{E}_j \mathscr{E}_k} b_k(1) b_j(1) \int_0^T g_k(t) g_j(t)\, dt \tag{15-3-11}$$

We observe that the integral involving $r^2(t)$ is common to all possible sequences $\{b_k(1)\}$ and is of no relevance in determining which sequence was transmitted. Hence, it may be neglected. The term

$$r_k = \int_0^T r(t) g_k(t)\, dt, \quad 1 \leq k \leq K \tag{15-3-12}$$

represents the cross-correlation of the received signal with each of the K signature sequences. Instead of cross-correlators, we may employ matched filters. Finally, the integral involving $g_k(t)$ and $g_j(t)$ is simply

$$\rho_{jk}(0) = \int_0^T g_j(t) g_k(t)\, dt \tag{15-3-13}$$

Therefore, (15-3-11) may be expressed in the form of correlation metrics

$$C(\mathbf{r}_K, \mathbf{b}_K) = 2 \sum_{k=1}^{K} \sqrt{\mathscr{E}_k} b_k(1) r_k - \sum_{j=1}^{K} \sum_{k=1}^{K} \sqrt{\mathscr{E}_j \mathscr{E}_k} b_k(1) b_j(1) \rho_{jk}(0) \tag{15-3-14}$$

These correlation metrics may also be expressed in vector inner product form as

$$C(\mathbf{r}_K, \mathbf{b}_K) = 2\mathbf{b}_K'\mathbf{r}_K - \mathbf{b}_K'\mathbf{R}_s\mathbf{b}_K \tag{15-3-15}$$

where

$$\mathbf{r}_K = [r_1 \quad r_2 \quad \cdots \quad r_K]', \qquad \mathbf{b}_K = [\sqrt{\mathscr{E}_1}b_1(1) \quad \cdots \quad \sqrt{\mathscr{E}_K}b_K(1)]$$

and $\mathbf{R}_s$ is the correlation matrix, with elements $\rho_{jk}(0)$. It is observed that the optimum detector must have knowledge of the received signal energies in order to compute the correlation metrics.

There are 2^K possible choices of the bits in the information sequence of the K users. The optimum detector computes the correlation metrics for each sequence and selects the sequence that yields the largest correlation metric. We observe that the optimum detector has a complexity that grows exponentially with the number of users, K.

In summary, the optimum receiver for symbol-synchronous transmission consists of a bank of K correlators or matched filters followed by a detector that computes the 2^K correlation metrics given by (15-3-15) corresponding to the 2^K possible transmitted information sequences. Then, the detector selects the sequence corresponding to the largest correlation metric.

Asynchronous Transmission In this case, there are exactly two consecutive symbols from each interferer that overlap a desired symbol. We assume that the receiver knows the received signal energies $\{\mathscr{E}_k\}$ for the K users and the transmission delays $\{\tau_k\}$. Clearly, these parameters must be measured at the receiver or provided to the receiver as side information by the users via some control channel.

The optimum maximum-likelihood receiver computes the log-likelihood function

$$\begin{aligned}\Lambda(\mathbf{b}) &= \int_0^{NT+2T}\left[r(t) - \sum_{k=1}^{K}\sqrt{\mathscr{E}_k}\sum_{i=1}^{N}b_k(i)g_k(t-iT-\tau_k)\right]^2 dt \\ &= \int_0^{NT+2T} r^2(t)\,dt - 2\sum_{k=1}^{K}\sqrt{\mathscr{E}_k}\sum_{i=1}^{N}b_k(i)\int_0^{NT+2T} r(t)g_k(t-iT-\tau_k)\,dt \\ &\quad + \sum_{k=1}^{K}\sum_{l=1}^{K}\sqrt{\mathscr{E}_k\mathscr{E}_l}\sum_{i=1}^{N}\sum_{j=1}^{N}b_k(i)b_l(j)\int_0^{NT+2T} g_k(t-iT-\tau_k)g_l(t-jT-\tau_l)\,dt\end{aligned} \tag{15-3-16}$$

where $\mathbf{b}$ represents the data sequences from the K users. The integral involving $r^2(t)$ may be ignored, since it is common to all possible information sequences. The integral

$$r_k(i) \equiv \int_{iT+\tau_k}^{(i+1)T+\tau_k} r(t)g_k(t-iT-\tau_k)\,dt, \qquad 1 \le i \le N \tag{15-3-17}$$

represents the outputs of the correlator or matched filter for the kth user in each of the signal intervals. Finally, the integral

$$\int_0^{NT+2T} g_k(t - iT - \tau_k)g_l(t - jT - \tau_l)\,dt = \int_{-iT-\tau_k}^{NT+2T-iT-\tau_k} g_k(t)g_l(t + iT - jT + \tau_k - \tau_l)\,dt \quad (15\text{-}3\text{-}18)$$

may be easily decomposed into terms involving the cross-correlation $\rho_{kl}(\tau) = \rho_{kl}(\tau_k - \tau_l)$ for $k \leq l$ and $\rho_{lk}(\tau)$ for $k > l$. Therefore, we observe that the log-likelihood function may be expressed in terms of a correlation metric that involves the outputs $\{r_k(i), 1 \leq k \leq K, 1 \leq i \leq N\}$ of K correlators or matched filters—one for each of the K signature sequences. Using vector notation, it can be shown that the NK correlator or matched filter outputs $\{r_k(i)\}$ can be expressed in the form

$$\mathbf{r} = \mathbf{R}_N\mathbf{b} + \mathbf{n} \quad (15\text{-}3\text{-}19)$$

where, by definition

$$\mathbf{r} = [\mathbf{r}'(1) \quad \mathbf{r}'(2) \quad \dots \quad \mathbf{r}'(N)]' \qquad \mathbf{r}(i) = [r_1(i) \quad r_2(i) \quad \dots \quad r_K(i)]' \quad (15\text{-}3\text{-}20)$$

$$\mathbf{b} = [\mathbf{b}'(1) \quad \mathbf{b}'(2) \quad \dots \quad \mathbf{b}'(N)]' \qquad \mathbf{b}(i) = [\sqrt{\mathscr{E}_1}b_1(i) \quad \sqrt{\mathscr{E}_2}b_2(i) \quad \dots \quad \sqrt{\mathscr{E}_K}b_K(i)]' \quad (15\text{-}3\text{-}21)$$

$$\mathbf{n} = [\mathbf{n}'(1) \quad \mathbf{n}'(2) \quad \dots \quad \mathbf{n}'(N)]' \qquad \mathbf{n}(i) = [n_1(i) \quad n_2(i) \quad \dots \quad n_K(i)]' \quad (15\text{-}3\text{-}22)$$

$$\mathbf{R}_N = \begin{bmatrix} \mathbf{R}_a(0) & \mathbf{R}_a'(1) & \mathbf{0} & \dots & \dots & \mathbf{0} \\ \mathbf{R}_a(1) & \mathbf{R}_a(0) & \mathbf{R}_a'(1) & \mathbf{0} & \dots & \mathbf{0} \\ \vdots & \vdots & \vdots & \vdots & \vdots & \vdots \\ \mathbf{0} & \mathbf{0} & \mathbf{0} & \mathbf{R}_a(1) & \mathbf{R}_a(0) & \mathbf{R}_a'(1) \\ \mathbf{0} & \mathbf{0} & \mathbf{0} & \mathbf{0} & \mathbf{R}_a(1) & \mathbf{R}_a(0) \end{bmatrix} \quad (15\text{-}3\text{-}23)$$

and $\mathbf{R}_a(m)$ is a $K \times K$ matrix with elements

$$R_{kl}(m) = \int_{-\infty}^{\infty} g_k(t - \tau_k)g_l(t + mT - \tau_l)\,dt \quad (15\text{-}3\text{-}24)$$

The gaussian noise vectors $\mathbf{n}(i)$ have zero mean and autocorrelation matrix

$$E[\mathbf{n}(k)\mathbf{n}'(j)] = \tfrac{1}{2}N_0\mathbf{R}_a(k - j) \quad (15\text{-}3\text{-}25)$$

Note that the vector $\mathbf{r}$ given by (15-3-19) constitutes a set of sufficient statistics for estimating the transmitted bits $b_k(i)$.

If we adopt a block processing approach, the optimum ML detector must compute 2^{NK} correlation metrics and select the K sequences of length N that correspond to the largest correlation metric. Clearly, such an approach is much too complex computationally to be implemented in practice, especially

when K and N are large. An alternative approach is ML sequence estimation employing the Viterbi algorithm. In order to construct a sequential-type detector, we make use of the fact that each transmitted symbol overlaps at most with $2K-2$ symbols. Thus, a significant reduction in computational complexity is obtained with respect to the block size parameter N, but the exponential dependence on K cannot be reduced.

It is apparent that the optimum ML receiver employing the Viterbi algorithm involves such a high computational complexity that its use in practice is limited to communication systems where the number of users is extremely small, e.g., $K < 10$. For larger values of K, one should consider a sequential-type detector that is akin to either the sequential decoding or the stack algorithms described in Chapter 8. Below, we consider a number of suboptimums detectors whose complexity grows linearly with K.

15-3-3 Suboptimum Detectors

In the above discussion, we observed that the optimum detector for the K CDMA users has a computational complexity, measured in the number of arithmetic operations (additions and multiplications/divisions) per modulated symbol, that grows exponentially with K. In this subsection we describe suboptimum detectors with computational complexities that grow linearly with the number of users, K. We begin with the simplest suboptimum detector, which we call the conventional (single-user) detector.

Conventional Single-User Detector In conventional single-user detection, the receiver for each user consists of a demodulator that correlates (or match-filters) the received signal with the signature sequence of the user and passes the correlator output to the detector, which makes a decision based on the single correlator output. Thus, the conventional detector neglects the presence of the other users of the channel or, equivalently, assumes that the aggregate noise plus interference is white and gaussian.

Let us consider synchronous transmission. Then, the output of the correlator for the kth user for the signal in the interval $0 \leq t \leq T$ is

$$r_k = \int_0^T r(t) g_k(t)\, dt \tag{15-3-26}$$

$$= \sqrt{\mathscr{E}_k} b_k(1) + \sum_{\substack{j=1 \\ j \neq k}}^{K} \sqrt{\mathscr{E}_j} b_j(1) \rho_{jk}(0) + n_k(1) \tag{15-3-27}$$

where the noise component $n_k(1)$ is given as

$$n_k(1) = \int_0^T n(t) g_k(t)\, dt \tag{15-3-28}$$

Since $n(t)$ is white gaussian noise with power spectral density $\frac{1}{2}N_0$, the variance of $n_k(1)$ is

$$E[n_k^2(1)] = \tfrac{1}{2}N_0 \int_0^T g_k^2(t)\, dt = \tfrac{1}{2}N_0 \tag{15-3-29}$$

Clearly, if the signature sequences are orthogonal, the interference from the other users given by the middle term in (15-3-27) vanishes and the conventional single-user detector is optimum. On the other hand, if one or more of the other signature sequences are not orthogonal to the user signature sequence, the interference from the other users can become excessive if the power levels of the signals (or the received signal energies) of one or more of the other users is sufficiently larger than the power level of the kth user. This situation is generally called the *near–far problem* in multiuser communications, and necessitates some type of power control for conventional detection.

· In asynchronous transmission, the conventional detector is more vulnerable to interference from other users. This is because it is not possible to design signature sequences for any pair of users that are orthogonal for all time offsets. Consequently, interference from other users is unavoidable in asynchronous transmission with the conventional single-user detection. In such a case, the near–far problem resulting from unequal power in the signals transmitted by the various users is particularly serious. The practical solution generally requires a power adjustment method that is controlled by the receiver via a separate communication channel that all users are continuously monitoring. Another option is to employ one of the multiuser detectors described below.

Decorrelating Detector We observe that the conventional detector has a complexity that grows linearly with the number of users, but its vulnerability to the near–far problem requires some type of power control. We shall now devise another type of detector that also has a linear computational complexity but does not exhibit the vulnerability to other-user interference.

Let us first consider the case of symbol-synchronous transmission. In this case, the received signal vector $\mathbf{r}_K$ that represents the output of the K matched filters is

$$\mathbf{r}_K = \mathbf{R}_s\mathbf{b}_K + \mathbf{n}_K \tag{15-3-30}$$

where $\mathbf{b}_K = [\sqrt{\mathscr{E}_1}b_1(1)\ \sqrt{\mathscr{E}_2}b_2(1)\ \ldots\ \sqrt{\mathscr{E}_K}b_K(1)]^t$ and the noise vector with elements $\mathbf{n}_K = [n_1(1)\ n_2(1)\ \ldots\ n_K(1)]^t$ has a covariance

$$E(\mathbf{n}_K\mathbf{n}_K^t) = \mathbf{R}_s \tag{15-3-31}$$

Since the noise is gaussian, $\mathbf{r}_K$ is described by a K-dimensional gaussian pdf with mean $\mathbf{R}_s\mathbf{b}_K$ and covariance $\mathbf{R}_s$. That is,

$$p(\mathbf{r}_K \mid \mathbf{b}_K) = \frac{1}{\sqrt{(2\pi)^K \det \mathbf{R}_s}} \exp\left[-\tfrac{1}{2}(\mathbf{r}_K - \mathbf{R}_s\mathbf{b}_K)^t\mathbf{R}_s^{-1}(\mathbf{r}_K - \mathbf{R}_s\mathbf{b}_K)\right] \tag{15-3-32}$$

The best linear estimate of $\mathbf{b}_K$ is the value of $\mathbf{b}_K$ that minimizes the likelihood function

$$\Lambda(\mathbf{b}_K) = (\mathbf{r}_K - \mathbf{R}_s\mathbf{b}_K)^t\mathbf{R}_s^{-1}(\mathbf{r}_K - \mathbf{R}_s\mathbf{b}_K) \tag{15-3-33}$$

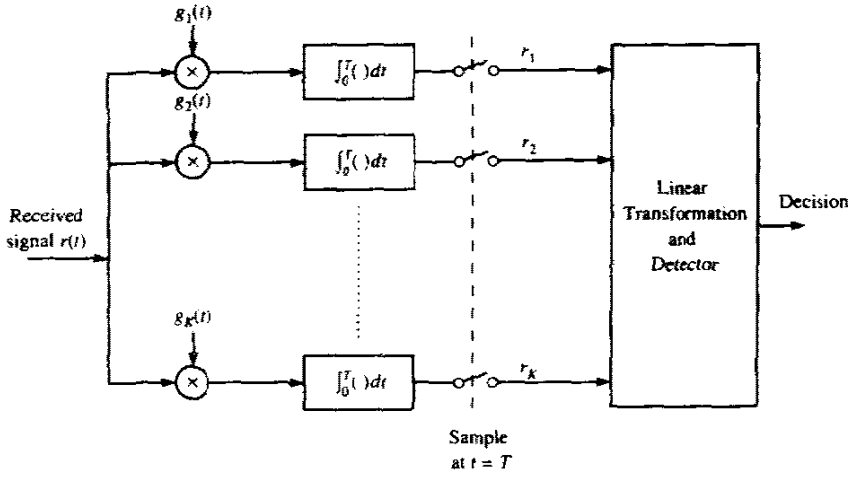

FIGURE 15-3-1 Receiver structure for decorrelation receiver.

The result of this minimization yields

$$\mathbf{b}_K^0 = \mathbf{R}_s^{-1}\mathbf{r}_K \tag{15-3-34}$$

Then, the detected symbols are obtained by taking the sign of each element of $\mathbf{b}_K^0$, i.e.

$$\hat{\mathbf{b}}_K = \text{sgn}\,(\mathbf{b}_K^0) \tag{15-3-35}$$

Figure 15-3-1 illustrates the receiver structure. Note from (15-3-34) and (15-3-35) that the decorrelator requires knowledge of the relative delays, in general, to form $\mathbf{R}_s$; no knowledge of the signal amplitudes is required.

Since the estimate $\mathbf{b}_K^0$ is obtained by performing a linear transformation on the vector of correlator outputs, the computational complexity is linear in K.

The reader should observe that the best (maximum-likelihood) linear estimate of $\mathbf{b}_K$ given by (15-3-34) is different from the optimum nonlinear ML sequence detector that finds the best discrete-valued $\{\pm 1\}$ sequence that maximizes the likelihood function. It is also interesting to note that the estimate $\mathbf{b}_K^0$ is the best linear estimate that maximizes the correlation metric given by (15-3-15).

An interesting interpretation of the detector that computes $\mathbf{b}_K^0$ as in (15-3-34) and makes decisions according to (15-3-35) is obtained by considering the case of $K = 2$ users. In this case,

$$\mathbf{R}_s = \begin{bmatrix} 1 & \rho \\ \rho & 1 \end{bmatrix} \tag{15-3-36}$$

$$\mathbf{R}_s^{-1} = \frac{1}{1-\rho^2}\begin{bmatrix} 1 & -\rho \\ -\rho & 1 \end{bmatrix} \tag{15-3-37}$$

where

$$\rho = \int_0^T g_1(t)g_2(t)\,dt \tag{15-3-38}$$

Then, if we correlate the received signal

$$r(t) = \sqrt{\mathscr{E}_1}b_1g_1(t) + \sqrt{\mathscr{E}_2}b_2g_2(t) + n(t) \tag{15-3-39}$$

with $g_1(t)$ and $g_2(t)$, we obtain

$$\mathbf{r}_2 = \begin{bmatrix} \sqrt{\mathscr{E}_1}b_1 + \rho\sqrt{\mathscr{E}_2}b_2 + n_1 \\ \rho\sqrt{\mathscr{E}_1}b_1 + \sqrt{\mathscr{E}_2}b_2 + n_2 \end{bmatrix} \tag{15-3-40}$$

where n_1 and n_2 are the noise components at the output of the correlators. Therefore,

$$\begin{aligned} \mathbf{b}_2^0 &= \mathbf{R}_s^{-1}\mathbf{r}_2 \\ &= \begin{bmatrix} \sqrt{\mathscr{E}_1}b_1 + (n_1 - \rho n_2)/(1-\rho^2) \\ \sqrt{\mathscr{E}_2}b_2 + (n_2 - \rho n_1)/(1-\rho^2) \end{bmatrix} \end{aligned} \tag{15-3-41}$$

This is a very interesting result, because the transformation $\mathbf{R}_s^{-1}$ has eliminated the interference components between the two users. Consequently, the near–far problem is eliminated and there is no need for power control.

It is interesting to note that a result similar to (15-3-41) is obtained if we correlate $r(t)$ given by (15-3-39) with the two modified signature waveforms

$$g_1'(t) = g_1(t) - \rho g_2(t) \tag{15-3-42}$$

$$g_2'(t) = g_2(t) - \rho g_1(t) \tag{15-3-43}$$

This means that, by correlating the received signal with the modified signature waveforms,[1] we have tuned out or *decorrelated* the multiuser interference. Hence, the detector based on (15-3-34) is called a *decorrelating detector.*

In asynchronous transmission, the received signal at the output of the correlators is given by (15-3-19). Hence, the log-likelihood function is given as

$$\Lambda(\mathbf{b}) = (\mathbf{r} - \mathbf{R}_N\mathbf{b})'\mathbf{R}_N^{-1}(\mathbf{r} - \mathbf{R}_N\mathbf{b}) \tag{15-3-44}$$

where $\mathbf{R}_N$ is defined by (15-3-23) and $\mathbf{b}$ is given by (15-3-21). It is relatively easy to show that the vector $\mathbf{b}$ that minimizes $\Lambda(\mathbf{b})$ is

$$\mathbf{b}^0 = \mathbf{R}_N^{-1}\mathbf{r} \tag{15-3-45}$$

This is the ML estimate of $\mathbf{b}$ and it is again obtained by performing a linear transformation of the outputs from the bank of correlators of matched filters.

Since $\mathbf{r} = \mathbf{R}_N\mathbf{b} + \mathbf{n}$, it follows from (15-3-45) that

$$\mathbf{b}^0 = \mathbf{b} + \mathbf{R}_N^{-1}\mathbf{n} \tag{15-3-46}$$

Therefore, $\mathbf{b}^0$ is an unbiased estimate of $\mathbf{b}$. This means that the multiuser

interference has been eliminated, as in the case of symbol-synchronous transmission. Hence, this detector for asynchronous transmission is also called a *decorrelating detector.*

A computationally efficient method for obtaining the solution given by (15-3-45) is the square-root factorization method described in Appendix D. Of course, there are many other methods that may be used to invert the matrix $\mathbf{R}_N$. Iterative methods to decorrelate the signals have also been explored.

Minimum Mean-Square-Error Detector In the above discussion, we showed that the linear ML estimate of $\mathbf{b}$ is obtained by minimizing the quadratic log-likelihood function in (15-3-44). Thus, we obtained the result given by (15-3-45), which is an estimate derived by performing a linear transformation on the outputs of the bank of correlators or matched filters.

Another, somewhat different, solution is obtained if we seek the linear transformation $\mathbf{b}^0 = \mathbf{A}\mathbf{r}$, where the matrix $\mathbf{A}$ is to be determined so as to minimize the mean square error (MSE)

$$\begin{aligned} J(\mathbf{b}) &= E[(\mathbf{b} - \mathbf{b}^0)'(\mathbf{b} - \mathbf{b}^0)] \\ &= E[(\mathbf{b} - \mathbf{A}\mathbf{r})'(\mathbf{b} - \mathbf{A}\mathbf{r})] \end{aligned} \tag{15-3-47}$$

It is easily shown that the optimum choice of $\mathbf{A}$ that minimizes $J(\mathbf{b})$ is

$$\mathbf{A}^0 = (\mathbf{R}_N + \tfrac{1}{2}N_0\mathbf{I})^{-1} \tag{15-3-48}$$

and, hence,

$$\mathbf{b}^0 = (\mathbf{R}_N + \tfrac{1}{2}N_0\mathbf{I})^{-1}\mathbf{r} \tag{15-3-49}$$

The output of the detector is then $\hat{\mathbf{b}} = \text{sgn}(\mathbf{b}^0)$.

The estimate given by (15-3-49) is called the *minimum MSE* (MMSE) estimate of $\mathbf{b}$. Note that when $\frac{1}{2}N_0$ is small compared with the diagonal elements of $\mathbf{R}_N$, the MMSE solution approaches the ML solution given by (15-3-45). On the other hand, when the noise level is large compared with the signal level in the diagonal elements of $\mathbf{R}_N$, $\mathbf{A}^0$ approaches the identity matrix (scaled by $\frac{1}{2}N_0$). In this low-SNR case, the detector basically ignores the interference from other users, because the additive noise is the dominant term. It should also be noted that the MMSE criterion produces a biased estimate of $\mathbf{b}$. Hence, there is some residual multiuser interference.

To perform the computations that lead to the values of $\mathbf{b}$, we solve the set of linear equations

$$(\mathbf{R}_N + \tfrac{1}{2}N_0\mathbf{I})\mathbf{b} = \mathbf{r} \tag{15-3-50}$$

This solution may be computed efficiently using a square-root factorization of the matrix $\mathbf{R}_N + \frac{1}{2}N_0\mathbf{I}$ as indicated above. Thus, to detect NK bits requires $3NK^2$ multiplications. Therefore, the computational complexity is $3K$ multiplications per bit, which is independent of the block length N and is linear in K.

Other Types of Detectors The decorrelating detector and the MMSE detector described above involve performing linear transformations on a block of data from a bank of K correlators or matched filters. The MMSE detector is akin to the linear MSE equalizer described in Chapter 10. Consequently, MMSE multiuser detection can be implemented by employing a tapped-delay-line filter with adjustable coefficients for each user and selecting the filter coefficients to minimize the MSE for each user signal. Thus, the received information bits are estimated sequentially with finite delay, instead of as a block.

The estimate $\mathbf{b}^{(1)}$ given by (15-3-46), which is obtained by processing a block of N bits by a decorrelating detector, can also be computed sequentially. Xie *et al.* (1990) have demonstrated that the transmitted bits may be recovered sequentially from the received signal, by employing a form of a decision-feedback equalizer with finite delay. Thus, there is a similarity between the detection of signals corrupted by ISI in a single-user communication system and the detection of signals in a multiuser system with asynchronous transmission.

15-3-4 Performance Characteristics of Detectors

The bit error probability is generally the desirable performance measure in multiuser communications. In evaluating the effect of multiuser interference on the performance of the detector for a single user, we may use as a benchmark the probability of a bit error for a single-user receiver in the absence of other users of the channel, which is

$$P_k(\gamma_k) = Q(\sqrt{2\gamma_k}) \tag{15-3-51}$$

where $\gamma_k = \mathscr{E}_k/N_0$, $\mathscr{E}_k$ is the signal energy per bit and $\frac{1}{2}N_0$ is the power spectral density of the AWGN.

In the case of the optimum detector for either synchronous or asynchronous transmission, the probability of error is extremely difficult and tedious to evaluate. In this case, we may use (15-3-51) as a lower bound and the performance of a suboptimum detector as an upper bound.

Let us consider, first, the suboptimum, conventional single-user detector. For synchronous transmission, the output of the correlator for the kth user is given by (15-3-27). Therefore, the probability of error for the kth user, conditional on a sequence $\mathbf{b}_i$ of bits from other users, is

$$P_k(\mathbf{b}_i) = Q\left(\sqrt{2\left[\sqrt{\mathscr{E}_k} + \sum_{\substack{j=1 \\ j\neq k}}^{K} \sqrt{\mathscr{E}_j} b_j(1)\rho_{jk}(0)\right]^2 \Big/ N_0}\right) \tag{15-3-52}$$

Then, the average probability of error is simply

$$P_k = (\tfrac{1}{2})^{K-1} \sum_{\substack{i=1 \\ i\neq k}}^{K} P_k(\mathbf{b}_i) \tag{15-3-53}$$

The probability in (15-3-53) will be dominated by the term that has the smallest argument in the Q function. The smallest argument will result in an SNR of

$$(SNR)_{\min} = \frac{1}{N_0}\left[\sqrt{\mathscr{E}_k} - \sum_{\substack{j=1 \\ j\neq k}}^{K} \sqrt{\mathscr{E}_j}\,|\rho_{jk}(0)|\right]^2 \tag{15-3-54}$$

Therefore,

$$(\tfrac{1}{2})^{K-1}Q(\sqrt{2(SNR)_{\min}}) < P_k < (\tfrac{1}{2})^{K-1}(K-1)Q(\sqrt{2(SNR)_{\min}}) \tag{15-3-55}$$

A similar development can be used to obtain bounds on the performance for asynchronous transmission.

In the case of a decorrelating detector, the other-user interference is completely eliminated. Hence, the probability of error may be expressed as

$$P_k = Q(\mathscr{E}_k/\sigma_k^2) \tag{15-3-56}$$

where σ_k^2 is the variance of the noise in the kth element of the estimate $\mathbf{b}^0$.

Example 15-3-1

Consider the case of synchronous, two-user transmission, where $\mathbf{b}_2^0$ is given by (15-3-41). Let us determine the probability of error.

The signal component for the first term in (15-3-41) is $\sqrt{\mathscr{E}_1}$. The noise component is

$$n = \frac{n_1 - \rho n_2}{1-\rho^2}$$

where ρ is the correlation between the two signature signals. The variance of this noise is

$$\sigma_1^2 = \frac{E[(n_1 - \rho n_2)]^2}{(1-\rho^2)^2} = \frac{1}{1-\rho^2}\frac{N_0}{2} \tag{15-3-57}$$

and

$$P_1 = Q\left(\sqrt{\frac{2\mathscr{E}_1}{N_0}(1-\rho^2)}\right) \tag{15-3-58}$$

A similar result is obtained for the performance of the second user. Therefore, the noise variance has increased by the factor $(1-\rho^2)^{-1}$. This noise enhancement is the price paid for the elimination of the multiuser interference by the decorrelation detector.

The error rate performance of the MMSE detector is similar to that for the decorrelation detector when the noise level is low. For example, from

(15-3-49), we observe that when N_0 is small relative to the diagonal elements of the signal correlation matrix $\mathbf{R}_N$,

$$\mathbf{b}^{(0)} \approx \mathbf{R}_N^{-1}\mathbf{r} \tag{15-3-59}$$

which is the solution for the decorrelation detector. For low multiuser interference, the MMSE detector results in a smaller noise enhancement compared with the decorrelation detector, but has some residual bias resulting from the other users. Thus, the MMSE detector attempts to strike a balance between the residual interference and the noise enhancement.

An alternative to the error probability as a figure of merit that has been used to characterize the performance of a multiuser communication system is the ratio of SNRs with and without the presence of interference. In particular, (15-3-51) gives the error probability of the kth user in the absence of other-user interference. In this case, the SNR is $\gamma_k = \mathscr{E}_k/N_0$. In the presence of multiuser interference, the user that transmits a signal with energy $\mathscr{E}_k$ will have an error probability P_k that exceeds $P_k(\gamma_k)$. The *effective SNR* γ_{ke} is defined as the SNR required to achieve the error probability

$$P_k = P_k(\gamma_{ke}) = Q(\sqrt{2\gamma_{ke}}) \tag{15-3-60}$$

The *efficiency* is defined as the ratio γ_{ke}/γ_k and represents the performance loss due to the multiuser interference. The desirable figure of merit is the *asymptotic efficiency*, defined as

$$\eta_k = \lim_{N_0 \to 0} \frac{\gamma_{ke}}{\gamma_k} \tag{15-3-61}$$

This figure of merit is often simpler to compute than the probability of error.

Example 15-3-2

Consider the case of two symbol-synchronous users with signal energies $\mathscr{E}_1$ and $\mathscr{E}_2$. Let us determine the asymptotic efficiency of the conventional detector.

In this case, the probability of error is easily obtained from (15-3-52) and (15-3-53) as

$$P_1 = \tfrac{1}{2}Q\left(\sqrt{2(\sqrt{\mathscr{E}_1} + \rho\sqrt{\mathscr{E}_2})^2/N_0}\right) + \tfrac{1}{2}Q\left(\sqrt{2(\sqrt{\mathscr{E}_1} - \rho\sqrt{\mathscr{E}_2})^2/N_0}\right)$$

However, the asymptotic efficiency is much easier to compute. It follows from the definition (15-3-61) and from (15-3-52) that

$$\eta_1 = \left[\max\left(0, 1 - \sqrt{\frac{\mathscr{E}_2}{\mathscr{E}_1}}|\rho|\right)\right]^2$$

A similar expression is obtained for η_2.

The asymptotic efficiency of the optimum and suboptimum detectors that we have described has been evaluated by Verdu (1986), Lupas and Verdu

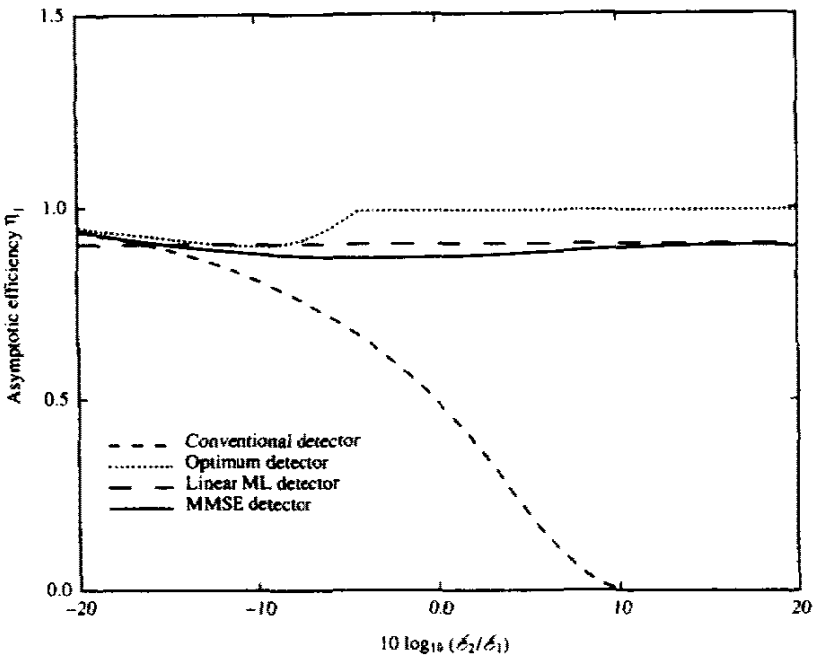

FIGURE 15-3-2 Asymptotic efficiencies of optimum (Viterbi) detector, conventional detector, MMSE detector, and linear ML detector in a two-user synchronous DS/SSMA system. [*From Xie* et al. *(1990),* ©*IEEE.*]

(1989), and Xie *et al.* (1990). Figure 15-3-2 illustrates the asymptotic efficiencies of these detectors when $K = 2$ users are transmitting synchronously. These graphs show that when the interference is small ($\mathscr{E}_2 \rightarrow 0$), the asymptotic efficiencies of these detectors are relatively large (near unity) and comparable. As $\mathscr{E}_2$ increases, the asymptotic efficiency of the conventional detector deteriorates rapidly. However, the other linear detectors perform relatively well compared with the optimum detector. Similar conclusions are reached by computing the error probabilities, but these computations are often more tedious.

15-4 RANDOM ACCESS METHODS

In this section, we consider a multiuser communication system in which users transmit information in packets over a common channel. In contrast to the CDMA method described in Section 15-3, the information signals of the users are not spread in frequency. As a consequence, simultaneous transmission of signals from multiple users cannot be separated at the receiver. The access methods described below are basically random, because packets are generated according to some statistical model. Users access the channel when they have one or more packets to transmit. When more than one user attempts to transmit packets simultaneously, the packets overlap in time, i.e., they collide,

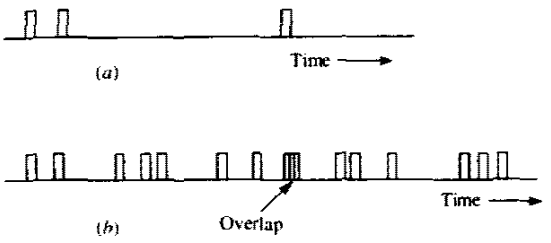

FIGURE 15-4-1 Random access packet transmission: (*a*) packets from a typical user; (*b*) packets from several users.

and, hence, a conflict results, which must be resolved by devising some channel protocol for retransmission of the packets. Below, we describe several random access channel protocols that resolve conflicts in packet transmission.

15-4-1 ALOHA Systems and Protocols

Suppose that a random access scheme is employed where each user transmits a packet as soon as it is generated. When a packet is transmitted by a user and no other user transmits a packet for the duration of the time interval then the packet is considered successfully transmitted. However, if one or more of the other users transmits a packet that overlaps in time with the packet from the first user, a collision occurs and the transmission is unsuccessful. Figure 15-4-1 illustrates this scenario. If the users know when their packets are transmitted successfully and when they have collided with other packets, it is possible to devise a scheme, which we may call a *channel access protocol*, for retransmission of collided packets.

Feedback to the users regarding the successful or unsuccessful transmission of packets is necessary and can be provided in a number of ways. In a radio broadcast system, such as one that employs a satellite relay as depicted in Fig. 15-4-2, the packets are broadcast to all the users on the down-link. Hence, all

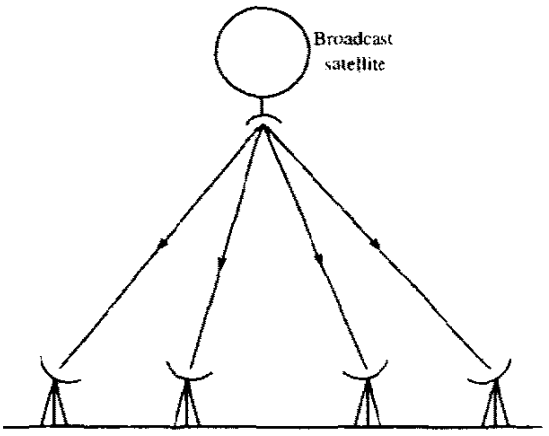

FIGURE 15-4-2 Broadcast system.

the transmitters can monitor their transmissions and, thus, obtain the following ternary information: no packet was transmitted, or a packet was transmitted successfully, or a collision occurred. This type of feedback to the transmitters is generally denoted as $(0, 1, c)$ feedback. In systems that employ wireline or filter-optic channels, the receiver may transmit the feedback signal on a separate channel.

The ALOHA system devised by Abramson (1973, 1977) and others at the University of Hawaii employs a satellite repeater that broadcasts the packets received from the various users who access the satellite. In this case, all the users can monitor the satellite transmissions and, thus, establish whether or not their packets have been transmitted successfully.

There are basically two types of ALOHA systems: *synchronized or slotted* and *unsynchronized or unslotted.* In an unslotted ALOHA system, a user may begin transmitting a packet at any arbitrary time. In a slotted ALOHA, the packets are transmitted in time slots that have specified beginning and ending times.

We assume that the start time of packets that are transmitted is a Poisson point process having an average rate of λ packets/s. Let T_p denote the time duration of a packet. Then, the normalized channel traffic G, also called the *offered channel traffic*, is defined as

$$G = \lambda T_p \tag{15-4-1}$$

There are many channel access protocols that can be used to handle collisions. Let us consider the one due to Abramson (1973). In Abramson's protocol, packets that have collided are retransmitted with some delay τ, where τ is randomly selected according to the pdf

$$p(\tau) = \alpha e^{-\alpha\tau} \tag{15-4-2}$$

where α is a design parameter. The random delay τ is added to the time of the initial transmission and the packet is retransmitted at the new time. If a collision occurs again, a new value of τ is randomly selected and the packet is retransmitted with a new delay from the time of the second transmission. This process is continued until the packet is transmitted successfully. The design parameter α determines the average delay between retransmissions. The smaller the value of α, the longer the delay between retransmissions.

Now, let λ', where $\lambda' < \lambda$, be the rate at which packets are transmitted successfully. Then, the normalized channel throughput is

$$S = \lambda' T_p \tag{15-4-3}$$

We can relate the channel throughput S to the offered channel traffic G by making use of the assumed start time distribution. The probability that a packet will not overlap a given packet is simply the probability that no packet

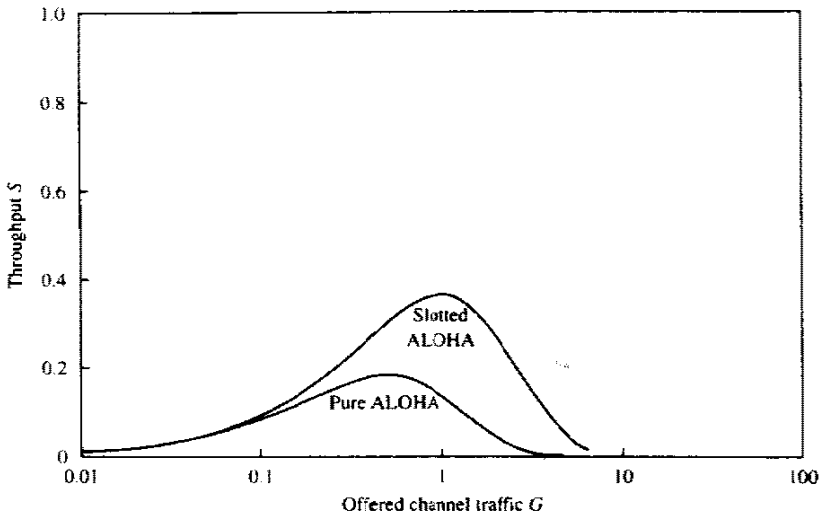

FIGURE 15-4-3 Throughput in ALOHA systems.

begins T_p s before or T_p s after the start time of the transmitted packet. Since the start time of all packets is Poisson-distributed, the probability that a packet will not overlap is $\exp(-2\lambda T_p) = \exp(-2G)$. Therefore,

$$S = Ge^{-2G} \tag{15-4-4}$$

This relationship is plotted in Fig. 15-4-3. We observe that the maximum throughput is $S_{\max} = 1/2e = 0.184$ packets per slot, which occurs at $G = \frac{1}{2}$. When $G > \frac{1}{2}$, the throughput S decreases. The above development illustrates that an unsynchronized or unslotted random access method has a relatively small throughput and is inefficient.

Throughput for slotted ALOHA To determine the throughput in a slotted ALOHA system, let G_i be the probability that the ith user will transmit a packet in some slot. If all the K users operate independently and there is no statistical dependence between the transmission of the user's packet in the current slot and the transmission of the user's packet in previous time slots, the total (normalized) offered channel traffic is

$$G = \sum_{i=1}^{K} G_i \tag{15-4-5}$$

Note that, in this case, G may be greater than unity.

Now, let $S_i \leq G_i$ be the probability that a packet transmitted in a time slot is received without a collision. Then, the normalized channel throughput is

$$S = \sum_{i=1}^{K} S_i \tag{15-4-6}$$

The probability that a packet from the ith user will not have a collision with another packet is

$$Q_i = \prod_{\substack{j=1 \\ j \neq i}}^{K} (1 - G_j) \tag{15-4-7}$$

Therefore,

$$S_i = G_i Q_i \tag{15-4-8}$$

A simple expression for the channel throughput is obtained by considering K identical users. Then,

$$S_i = \frac{S}{K}, \qquad G_i = \frac{G}{K}$$

and

$$S = G\left(1 - \frac{G}{K}\right)^{K-1} \tag{15-4-9}$$

Then, if we let $K \to \infty$, we obtain the throughput

$$S = Ge^{-G} \tag{15-4-10}$$

This result is also plotted in Fig. 15-4-3. We observe that S reaches a maximum throughput of $S_{max} = 1/e = 0.368$ packets per slot at $G = 1$, which is twice the throughput of the unslotted ALOHA system.

The performance of the slotted ALOHA system given above is based on Abramson's protocol for handling collisions. A higher throughput is possible by devising a better protocol.

A basic weakness in Abramson's protocol is that it does not take into account the information on the amount of traffic on the channel that is available from observation of the collisions that occur. An improvement in throughput of the slotted ALOHA system can be obtained by using a tree-type protocol devised by Capetanakis (1979). In this algorithm, users are not allowed to transmit new packets that are generated until all earlier collisions are resolved. A user can transmit a new packet in a time slot immediately following its generation, provided that all previous packets that have collided have been transmitted successfully. If a new packet is generated while the channel is clearing the previous collisions, the packet is stored in a buffer. When a new packet collides with another, each user assigns its respective packet to one of two sets, say A or B, with equal probability (by flipping a coin). Then, if a packet is put in set A, the user transmits it in the next time slot. If it collides again, the user will again randomly assign the packet to one of two sets and the process of transmission is repeated. This process continues until all packets contained in set A are transmitted successfully. Then, all packets in set B are transmitted following the same procedure. All the users

monitor the state of the channel, and, hence, they know when all the collisions have been serviced.

When the channel becomes available for transmission of new packets, the earliest generated packets are transmitted first. To establish a queue, the time scale is subdivided into subintervals of sufficiently short duration such that, on average, approximately one packet is generated by a user in a subinterval. Thus, each packet has a "time tag" that is associated with the subinterval in which it was generated. Then, a new packet belonging to the first subinterval is transmitted in the first available time slot. If there is no collision then a packet from the second subinterval is transmitted, and so on. This procedure continues as new packets are generated and as long as any backlog of packets for transmission exists. Capetanakis has demonstrated that this channel access protocol achieves a maximum throughput of 0.43 packets per slot.

In addition to throughput, another important performance measure in a random access system is the average transmission delay in transmitting a packet. In an ALOHA system, the average number of transmissions per packet is G/S. To this number we may add the average waiting time between transmissions and, thus, obtain an average delay for a successful transmission. We recall from the above discussion that in the Abramson protocol, the parameter α determines the average delay between retransmissions. If we select α small, we obtain the desirable effect of smoothing out the channel load at times of peak loading, but the result is a long retransmission delay. This is the trade-off in the selection of α in (15-4-2). On the other hand, the Capetanakis protocol has been shown to have a smaller average delay in the transmission of packets. Hence, it outperforms Abramson's protocol in both average delay and throughput.

Another important issue in the design of random access protocols is the stability of the protocol. In our treatment of ALOHA-type channel access protocols, we implicitly assumed that for a given offered load, an equilibrium point is reached where the average number of packets entering the channel is equal to the average number of packets transmitted successfully. In fact, it can be demonstrated that any channel access protocol, such as the Abramson protocol, that does not take into account the number of previous unsuccessful transmissions in establishing a retransmission policy is inherently unstable. On the other hand, the Capetanakis algorithm differs from the Abramson protocol in this respect and has been proved to be stable. A thorough discussion of the stability issues of random access protocols is found in the paper by Massey (1988).

15-4-2 Carrier Sense Systems and Protocols

As we have observed, ALOHA-type (slotted and unslotted) random-access protocols yield relatively low throughput. Furthermore, a slotted ALOHA system requires that users transmit at synchronized time slots. In channels where transmission delays are relatively small, it is possible to design random

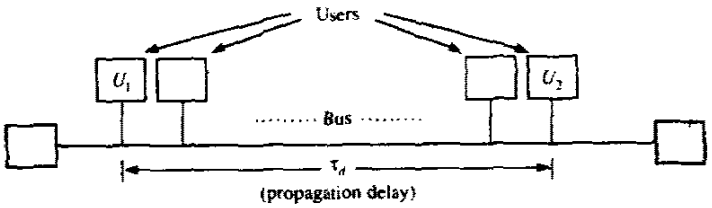

FIGURE 15-4-4 Local area network with bus architecture.

access protocols that yield higher throughput. An example of such a protocol is *carrier sensing* with collision detection, which is used as a standard Ethernet protocol in local area networks. This protocol is generally known as *carrier sense multiple access with collision detection* (CSMA/CD).

The CSMA/CD protocol is simple. All users listen for transmissions on the channel. A user who wishes to transmit a packet seizes the channel when it senses that the channel is idle. Collisions may occur when two or more users sense an idle channel and begin transmission. When the users that are transmitting simultaneously sense a collision, they transmit a special signal, called a *jam signal*, that serves to notify all users of the collision and abort their transmissions. Both the carrier sensing feature and the abortion of transmission when a collision occurs result in minimizing the channel down-time and, hence, yield a higher throughput.

To elaborate on the efficiency of CSMA/CD, let us consider a local area network having a bus architecture, as shown in Fig. 15-4-4. Consider two users U_1 and U_2 at the maximum separation, i.e., at the two ends of the bus, and let τ_d be the propagation delay for a signal to travel the length of the bus. Then, the (maximum) time required to sense an idle channel is τ_d. Suppose that U_1 transmits a packet of duration T_p. User U_2 may seize the channel τ_d s later by using carrier sensing, and begins to transmit. However, user U_1 would not know of this transmission until τ_d s after U_2 begins transmission. Hence, we may define the time interval $2\tau_d$ as the (maximum) time interval to detect a collision. If we assume that the time required to transmit the jam signal is negligible, the CSMA/CD protocol yields a high throughput when $2\tau_d \ll T_p$.

There are several possible protocols that may be used to reschedule transmissions when a collision occurs. One protocol is called *nonpersistent CSMA*, a second is called *1-persistent CSMA*, and a generalization of the latter is called p-persistant CSMA.

Nonpersistent CSMA In this protocol, a user that has a packet to transmit senses the channel and operates according to the following rule.

(a) If the channel is idle, the user transmits a packet.
(b) If the channel is sensed busy, the user schedules the packet

transmission at a later time according to some delay distribution. At the end of the delay interval, the user again senses the channel and repeats steps (a) and (b).

1-Persistent CSMA This protocol is designed to achieve high throughput by not allowing the channel to go idle if some user has a packet to transmit. Hence, the user senses the channel and operates according to the following rule.

(a) If the channel is sensed idle, the user transmits the packet with probability 1.

(b) If the channel is sensed busy, the user waits until the channel becomes idle and transmits a packet with probability one. Note that in this protocol, a collision will always occur when more than one user has a packet to transmit.

***p*-Persistent CSMA** To reduce the rate of collisions in 1-persistent CSMA and increase the throughput, we should randomize the starting time for transmission of packets. In particular, upon sensing that the channel is idle, a user with a packet to transmit sends it with probability p and delays it by τ with probability $1-p$. The probability p is chosen in a way that reduces the probability of collisions while the idle periods between consecutive (nonoverlapping) transmissions is kept small. This is accomplished by subdividing the time axis into minislots of duration τ and selecting the packet transmission at the beginning of a minislot. In summary, in the p-persistent protocol, a user with a packet to transmit proceeds as follows.

(a) If the channel is sensed idle, the packet is transmitted with probability p, and with probability $1-p$ the transmission is delayed by τ s.

(b) If at $t=\tau$, the channel is still sensed to be idle, step (a) is repeated. If a collision occurs, the users schedule retransmission of the packets according to some preselected transmission delay distribution.

(c) If at $t=\tau$, the channel is sensed busy, the user waits until it becomes idle, and then operates as in (a) and (b) above.

Slotted versions of the above protocol can also be constructed.

The throughput analysis for the nonpersistent and the p-persistent CSMA/CD protocols has been performed by Kleinrock and Tobagi (1975), based on the following assumptions:

1 the average retransmission delay is large compared with the packet duration T_p;

2 the interarrival times of the point process defined by the start times of all the packets plus retransmissions are independent and exponentially distributed.

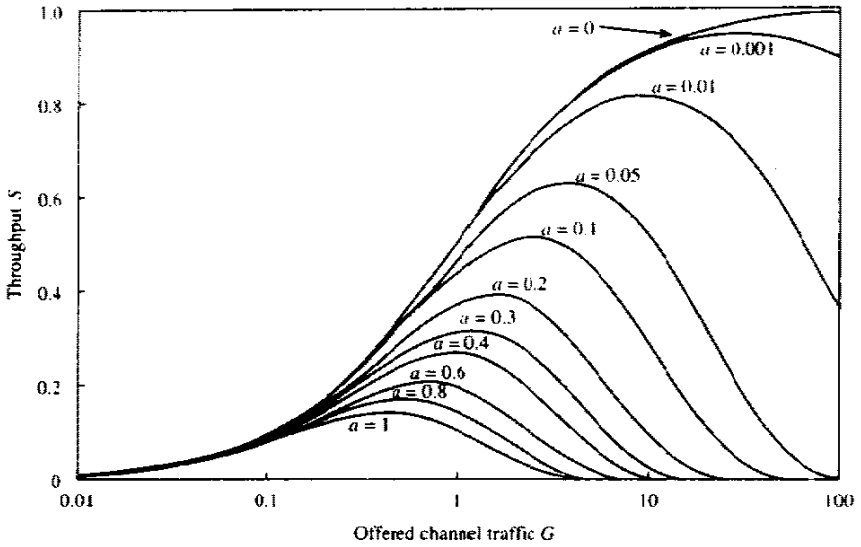

FIGURE 15-4-5 Throughput in nonpersistent CSMA. [*From Kleinrock and Tobagi (1975), © IEEE.*]

For the nonpersistent CSMA, the throughput is

$$S = \frac{Ge^{-aG}}{G(1+2a) + e^{-aG}} \tag{15-4-11}$$

where the parameter $a = \tau_d/T_p$. Note that as $a \to 0$, $S \to G/(1+G)$. Figure 15-4-5 illustrates the throughput versus the offered traffic G, with a as a parameter. We observe that $S \to 1$ as $G \to \infty$ for $a = 0$. For $a > 0$, the value of $S_{\max}$ decreases.

For the 1-persistent protocol, the throughput obtained by Kleinrock and Tobagi (1975) is

$$S = \frac{G[1+G+aG(1+G+\frac{1}{2}aG)]e^{-G(1+2a)}}{G(1+2a) - (1-e^{-aG}) + (1+aG)e^{-G(1+a)}} \tag{15-4-12}$$

In this case,

$$\lim_{a \to 0} S = \frac{G(1+G)e^{-G}}{G+e^{-G}} \tag{15-4-13}$$

which has a smaller peak value than the nonpersistent protocol.

By adopting the p-persistent protocol, it is possible to increase the throughput relative to the 1-persistent scheme. For example, Fig. 15-4-6 illustrates the throughput versus the offered traffic with $a = \tau_d/T_p$ fixed and with p as a parameter. We observe that as p increases toward unity, the maximum throughput decreases.

The transmission delay was also evaluated by Kleinrock and Tobagi (1975). Figure 15-4-7 illustrates the graphs of the delay (normalized by T_p) versus the

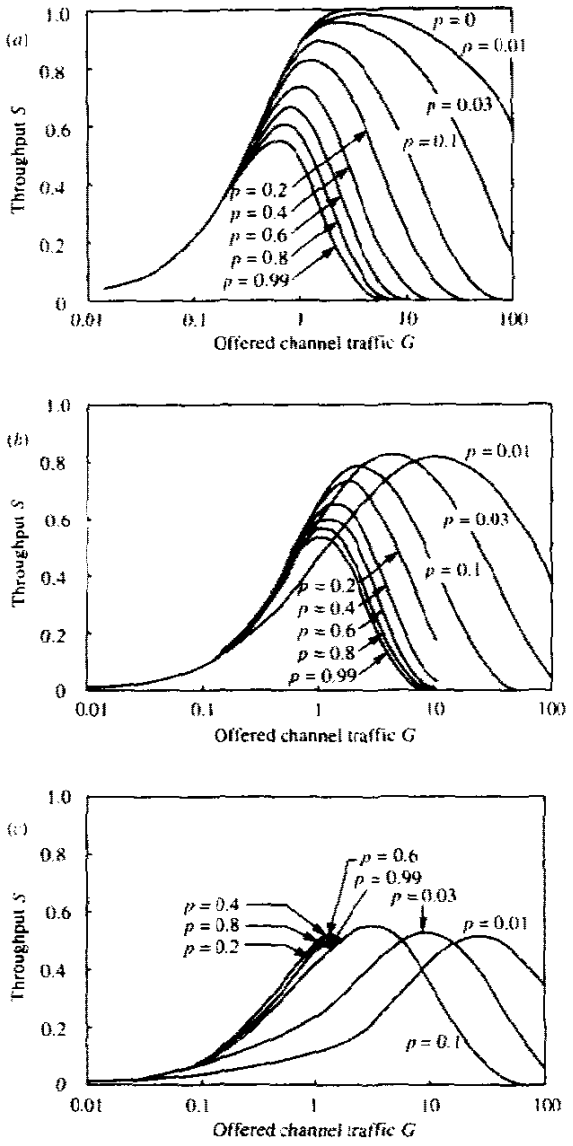

FIGURE 15-4-6 Channel throughput in p-persistent CSMA: (*a*) $a = 0$; (*b*) $a = 0.01$; (*c*) $a = 0.1$ [*From Kleinrock and Tobagi (1975). © IEEE.*]

throughput S for the slotted nonpersistent and p-persistent CSMA protocols. Also shown for comparison is the delay versus throughput characteristic of the ALOHA slotted and unslotted protocols. In this simulation, only the newly generated packets are derived independently from a Poisson distribution. Collisions and uniformly distributed random retransmissions are handled without further assumptions. These simulation results illustrate the superior performance of the p-persistent and the nonpersistent protocols relative to the ALOHA protocols. Note that the graph labeled "optimum p-persistent" is

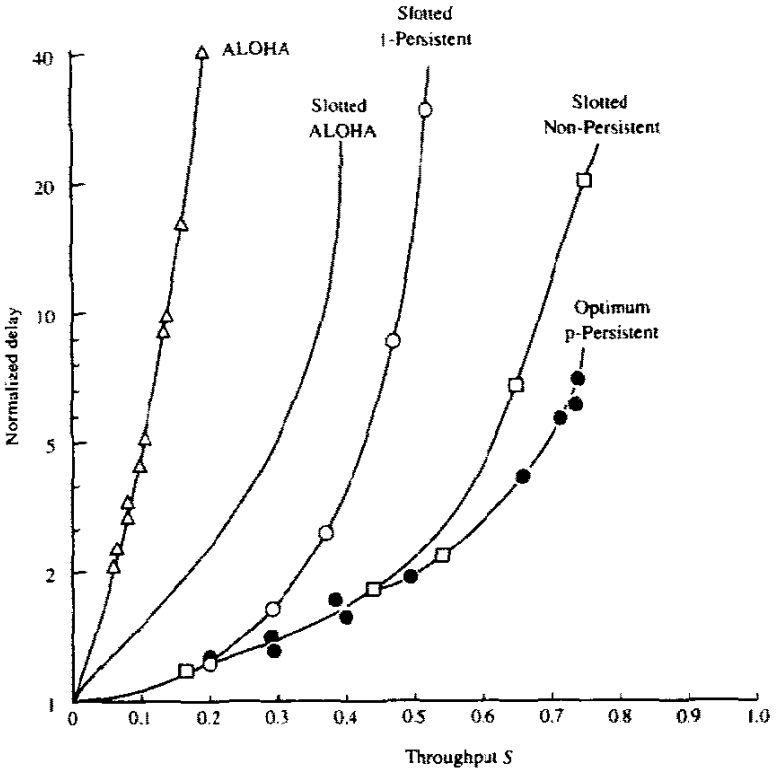

FIGURE 15-4-7 Throughput versus delay from simulation ($a = 0.01$). [*From Kleinrock and Tobagi (1975), © IEEE.*]

obtained by finding the optimum value of p for each value of the throughput. We observe that for small values of the throughput, the 1-persistent ($p = 1$) protocol is optimal.

15-5 BIBLIOGRAPHICAL NOTES AND REFERENCES

FDMA was the dominant multiple access scheme that has been used for decades in telephone communication systems for analog voice transmission. With the advent of digital speech transmission using PCM, DPCM, and other speech coding methods, TDMA has replaced FDMA as the dominant multiple access scheme in telecommunications. CDMA and random access methods, in general, have been developed over the past three decades, primarily for use in wireless signal transmission and in local area wireline networks.

Multiuser information theory deals with basic information-theoretic limits in source coding for multiple sources, and channel coding and modulation for multiple access channels. A large amount of literature exists on these topics. In the context of our treatment of multiple access methods, the reader will find

the papers by Cover (1972), El Gamal and Cover (1980) Bergmans and Cover (1974), and Hui (1984) particularly relevant. The capacity of a cellular CDMA system has been considered in the paper by Gilhousen *et al.* (1991).

Signal demodulation and detection for multiuser communications has received considerable attention in recent years. The reader is referred to the papers by Verdu (1986a–c, 1989), Lupas and Verdu (1990), Xie *et al.* (1990a, b), Poor and Verdu (1988), Zhang and Brady (1993), and Zvonar and Brady (1995). Earlier work on signal design and demodulation for multiuser communications is found in the papers by Van Etten (1975, 1976), Horwood and Gagliardi (1975), and Kaye and George (1970).

The ALOHA system, which was one of the earliest random access systems, is treated in the papers by Abramson (1970, 1977) and Roberts (1975). These papers contain the throughput analysis for unslotted and slotted systems. Stability issues regarding the ALOHA protocols may be found in the papers by Carleial and Hellman (1975), Ghez *et al.* (1988), and Massey (1988). Stable protocols based on tree algorithms for random access channels were first given by Capetanakis (1977). The carrier sense multiple access protocols that we described are due to Kleinrock and Tobagi (1975). Finally, we mention the IEEE Press book edited by Abramson (1993), which contains a collection of papers dealing with multiple access communications.

PROBLEMS

15-1 In the formulation of the CDMA signal and channel models described in Section 15-3-1, we assumed that the received signals are real. For $K > 1$, this assumption implies phase synchronism at all transmitters, which is not very realistic in a practical system. To accommodate the case where the carrier phases are not synchronous, we may simply alter the signature waveforms for the K users, given by (15-3-1), to be complex-valued, of the form

$$g_k(t) = e^{j\theta_k} \sum_{n=0}^{L-1} a_k(n) p(t - nT_c), \quad 1 \leq k \leq K$$

where θ_k represents the constant phase offset of the kth transmitter as seen by the common receiver.

a Given this complex-valued form for the signature waveforms, determine the form of the optimum ML receiver that computes the correlation metrics analogous to (15-3-15).

b Repeat the derivation for the optimum ML detector for asynchronous transmission that is analogous to (15-3-19).

15-2 Consider a TDMA system where each user is limited to a transmitted power P, independent of the number of users. Determine the capacity per user, C_K, and the total capacity KC_K. Plot C_K and KC_K as functions of $\mathcal{E}_b/N_0$ and comment on the results as $K \to \infty$.

15-3 Consider an FDMA system with $K = 2$ users, in an AWGN channel, where user 1 is assigned a bandwidth $W_1 = \alpha W$ and user 2 is assigned a bandwidth $W_2 = (1 - \alpha)W$, where $0 \leq \alpha \leq 1$. Let P_1 and P_2 be the average powers of the two users.

a Determine the capacities C_1 and C_2 of the two users and their sum $C = C_1 + C_2$ as a function of α. On a two-dimensional graph of the rates R_2 versus R_1, plot the graph of the points (C_2, C_1) as α varies in the range $0 \leq \alpha \leq 1$.

b Recall that the rates of the two users must satisfy the conditions

$$R_1 < W_1 \log_2\left(1 + \frac{P_1}{W_1 N_0}\right)$$

$$R_2 < W_2 \log_2\left(1 + \frac{P_2}{W_2 N_0}\right)$$

$$R_1 + R_2 < W \log_2\left(1 + \frac{P_1 + P_2}{W N_0}\right)$$

Determine the total capacity C when $P_1/\alpha = P_2/(1-\alpha) = P_1 + P_2$, and, thus, show that the maximum rate is achieved when $\alpha/(1-\alpha) = P_1/P_2 = W_1/W_2$.

15-4 Consider a TDMA system with $K = 2$ users in an AWGN channel. Suppose that the two transmitters are peak-power-limited to P_1 and P_2, and let user 1 transmit for $100\alpha\%$ of the available time and user 2 transmit $100(1-\alpha)\%$ of the time. The available bandwidth is W.

a Determine the capacities C_1, C_2, and $C = C_1 + C_2$ as functions of α.

b Plot the graph of the points (C_2, C_1) as α varies in the range $0 \leq \alpha \leq 1$.

15-5 Consider a TDMA system with $K = 2$ users in an AWGN channel. Suppose that the two transmitters are average-power-limited, with powers P_1 and P_2. User 1 transmits $100\alpha\%$ of the time and user 2 transmits $100(1-\alpha)\%$ of the time. The channel bandwidth is W.

a Determine the capacities C_1, C_2, and $C = C_1 + C_2$ as functions of α.

b Plot the graph of the points (C_2, C_1) as α varies in the range $0 \leq \alpha \leq 1$.

c What is the similarity between this solution and the FDMA system in Problem 15-3.

15-6 Consider the two-user, *synchronous*, multiple-access channel and the signature sequences shown in Fig. P15-6. The parameter $A \geq 0$ describes the relative strength between the two users, and $0 \leq B \leq 1$ describes the degree of correlation between the waveforms. Let

$$r(t) = \sum_{k=1}^{2} \sum_{i=-\infty}^{\infty} b_k(i) s_k(t-i) + n(t)$$

FIGURE P15-6

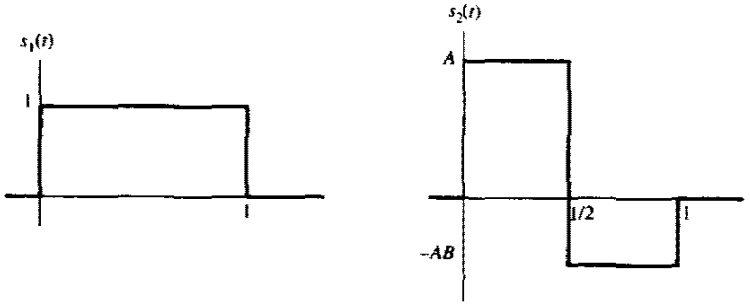

denote the received waveform at time t, where $n(t)$ is white gaussian noise with power spectral density σ^2, and $b_k(i) \in \{-1, +1\}$. In the following problems, you will compare the structure of the conventional multiuser detector to optimimum receiver structures for various values of A, $0 \leq B \leq 1$, and σ^2.

a Show that, given the observation $\{r(t), -\infty < t \leq 1\}$, a sufficient statistic for the data $b_1(0)$ and $b_2(0)$ is the observation during $t \in [0, 1]$.

b Conventional (suboptimum) multiuser detection chooses the data $b_k(0)$ according to the following rule:

$$b_k(0) = \operatorname{sgn}(y_k)$$

where

$$y_k = \int_0^1 r(t)s_k(t)\,dt$$

Determine an expression for the probability of bit error for user 1, using the notation

$$w_k = \int_0^1 s_k^2(t)\,dt$$

$$\rho_{12} = \int_0^1 s_1(t)s_2(t)\,dt.$$

c What is the form of this expression for $A \to 0$, $B < 1$, and arbitrary σ^2?

d What is the form of this expression for arbitrarily large A, $B < 1$, and arbitrary σ^2? What does this say about conventional detection?

e What is the form of this expression for $B = 1$, and arbitrary σ^2 and A? Why does this differ from the result in (d)?

f Determine the form of this expression for arbitrarily large σ^2, arbitrary A, and $B < 1$.

g Determine the form of this expression for $\sigma^2 \to 0$, arbitrary A, and $B < 1$.

15-7 Refer to Problem 15-6. The maximum-likelihood sequence receiver for this channel selects the data $b_1(0)$ and $b_2(0)$ transmitted during the interval $[0, 1]$ according to the rule

$$(\widehat{b_1(0)}, \widehat{b_2(0)}) = \underset{b_1, b_2}{\operatorname{argmax}} \Lambda[\{r(t), 0 < t < 1\} \mid b_1, b_2]$$

where $\Lambda[\{r(t), 0 < t < 1\} \mid b_1, b_2]$ is the likelihood function of b_1 and b_2 given an observation of $\{r(t), 0 < t < 1\}$. It will be helpful to write this maximization as

$$(\widehat{b_1(0)}, \widehat{b_2(0)}) = \underset{b_1}{\operatorname{argmax}} \underset{b_2}{\operatorname{argmax}} \Lambda[\{r(t), 0 < t < 1\} \mid b_1, b_2]$$

where the value b_2^* that satisfies the inner maximization may depend on b_1. Note that the need for "sequence detection" is obviated.

a Express this maximization in the *simplest* possible terms, using the same notation as in Problem 15-6(b). Reduce this maximization to simplest form, using facts like

$$\underset{x}{\operatorname{argmax}}\, Ke^{f_1(x)} = \underset{x}{\operatorname{argmax}}\, f_1(x)$$

if, say, K is independent of x.

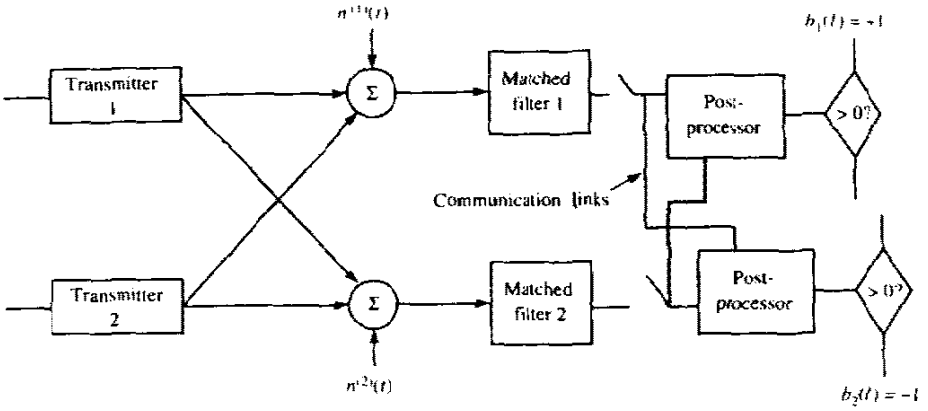

FIGURE P15-8

b What is the simplest structure of the MLS receiver as the relative strength of the interferer vanishes, $A \to 0$? How does it compare with conventional detection?

c What is the simplest structure of the MLS receiver for $B = 1$ and arbitrary A and σ^2? How does it compare with conventional detection? Why?

d What is the simplest structure of the MLS receiver for arbitrarily large σ^2 and arbitrary A and B? How does it compare with conventional detection? Determine the error rate for user 1 in this case. [*Hint:* Use the fact that $\text{sgn}(y_2) = \text{sgn}(y_2 \pm \rho_{12})$ with high probability in this case.]

e Determine the error probability of user 1 of the MLS receiver for $\sigma^2 \to 0$, and arbitrarily large A and $B < 1$? How does it compare with conventional detection?

f What is the structure of the MLS receiver for arbitrarily large A, and $B < 1$, and arbitrary σ_2? How does it compare with conventional detection? What does this say about conventional detection in this case? [*Hint:* Use the fact that $E|y_2|$ is roughly A times greater than $E|y_1|$.]

15-8 Consider the asynchronous communication system shown in Fig. P15-8. The two receivers are not colocated, and the white noise processes $n^{(1)}(t)$ and $n^{(2)}(t)$ may be considered to be independent. The noise processes are identically distributed, with power spectral density σ^2 and zero mean. Since the receivers are not colocated, the relative delays between the users are not the same—denote the relative delay of user k at receiver i by $\tau_k^{(i)}$. All other signal parameters coincide for the receivers, and the received signal at receiver i is

$$r^{(i)}(t) = \sum_{k=1}^{2} \sum_{l=-\infty}^{\infty} b_k(l) s_k(t - lT - \tau_k^{(i)}) + n^{(i)}(t)$$

where s_k has support on $[0, T]$. You may assume that the receiver i has full knowledge of the waveforms, energies, and relative delays $\tau_1^{(i)}$ and $\tau_2^{(i)}$. Although receiver i is eventually interested only in the data from transmitter i, note that there is a free communication link between the sampler of one receiver, and the postprocessing circuitry of the other. Following each postprocessor, the decision is attained by threshold detection. In this problem, you will consider options for postprocessing and for the communication link in order to improve performance.

a What is the bit error probability for users 1 and 2 of a receiver pair that does not utilize the communication link, and does not perform postprocessing. Use the following notation:

$$y_k(l) = \int s_k(t - lT - \tau_k^{(k)}) r^{(k)}(t)\, dt$$

$$\rho_{12}^{(l)} = \int s_1(t - \tau_1^{(l)}) s_2(t - \tau_2^{(l)})\, dt$$

$$\rho_{21}^{(l)} = \int s_1(t - \tau_1^{(l)}) s_2(t + T - \tau_2^{(l)})\, dt$$

$$w_k = \int s_k^2(t - \tau_k^{(1)})\, dt = \int s_k^2(t - \tau_k^{(2)})\, dt$$

b Consider a postprocessor for receiver 1 that accepts $y_2(l-1)$ and $y_2(l)$ from the communication link, and implements the following postprocessing on $y_1(l)$

$$z_1(l) = y_1(l) - \rho_{21}^{(l)} \operatorname{sgn}[y_2(l-1)] - \rho_{12}^{(l)} \operatorname{sgn}[y_2(l)].$$

Determine an exact expression for the bit error rate for user 1.

c Determine the asymptotic multiuser efficiency of the receiver proposed in (b), and compare with that in (a). Does this receiver always perform better than that proposed in (a)?

15-9 The baseband waveforms shown in Fig. P15-6 are assigned to two users who share the same *asynchronous*, narrowband channel. Assume that $B = 1$ and $A = 4$. We should like to compare the performance of several receivers, with a criterion of $\mathcal{P}_1(0)$. Since this expression is too complicated in some cases, we shall also be interested in comparing the asymptotic multiuser efficiency η_1 of each receiver. Assume that $\tau_1 = 0$ but that $0 < \tau_2 < T$ is fixed and known at the receiver, and assume that we have *infinite horizon transmission*, $2M + 1 \to \infty$.

a For the conventional, multiuser detector:

(i) Find the exact bit probability of error for user 1. Express this result in terms of w_1, ρ_{12}, ρ_{21}, and σ^2. [*Hint:* Conditioning on $b_2(-1)$ and $b_2(0)$ will help.]

(ii) Plot the asymptotic multiuser efficiency η_1 as a function of τ_2. Indicate and explain the maximum and minimum values of η_1 in this plot.

b For the MLS receiver:

(i) Plot η_1 as a function of τ_2. Explain maximum and minimum values, and compare with (a)(ii).

(ii) Which error sequences are most likely for each value of τ_2?

c For the limiting decorrelating detector:

(i) Find an exact expression for the probability of error for user 1, with similar parameters as in (a)(i) [*Hint:* Don't forget to normalize ρ_{12} and ρ_{21}.]

(ii) Plot η_1 as a function of τ_2. Explain the minimum value of η_1 in this case, and compare with (a)(ii).

15-10 The symbol-by-symbol detector that minimizes the probability of a symbol error differs from the maximum-likelihood sequence detector. The former is more completely described as the detector that selects each $b_k(0)$ according to the rule

$$\widehat{b_k(0)} = \underset{b_k(0)}{\operatorname{argmax}} \Lambda[\{r(t), 0 < t < 1\} \mid b_k(0)]$$

a Show that this decision rule minimizes $\Lambda[b_k(0) \neq \widehat{b_k(0)}]$ among all decision rules with observation $\{r(t), 0 < t < 1\}$. Subject to this criteria, it is superior to the MLS receiver.

b Show that the simplest structure of the minimum-probability-of-error receiver for user 1 is given by

$$\widehat{b_1(0)} = \underset{b_1}{\operatorname{argmax}} \left[\exp\left(\frac{b_1 y_1}{\sigma^2}\right) \cosh\left(\frac{y_2 - b_1 \rho_{12}}{\sigma^2}\right) \right] .$$

c Find the simplest form of the minimum-probability-of-error receiver for $B = 1$ and arbitrary A and σ^2. How does this compare with the above receivers?

d Find the limiting form of the minimum-probability-of-error receiver for arbitrarily large σ^2 and arbitrary A and B. Compare with the above receivers.

e Find the limiting form of the minimum-probability-of-error receiver for $A \gg 1$ and arbitrary σ^2 and B. Compare with the above receivers.

f Find the limiting form of the minimum-probability-of-error receiver for $A \gg 1$ $\sigma^2 \to 0$ and arbitrary B. Compare with the above receivers.

15-11 In a pure ALOHA system, the channel bit rate is 2400 bits/s. Suppose that each terminal transmits a 100 bit message every minute on the average.

a Determine the maximum number of terminals that can use the channel.

b Repeat (a) if slotted ALOHA is used.

15-12 Determine the maximum input traffic for the pure ALOHA and slotted ALOHA protocols.

15-13 For a Poisson process, the probability of k arrivals in a time interval T is

$$P(k) = \frac{e^{-\lambda T}(\lambda T)^k}{k!}, \quad k = 0, 1, 2, \ldots$$

a Determine the average number or arrivals in the interval T.

b Determine the variance σ^2 in the number of arrivals in the interval T.

c What is the probability of at least one arrival in the interval T?

d What is the probability of exactly one arrival in the interval T?

15-14 Refer to Problem 15-13. The average arrival rate is $\lambda = 10$ packets/s. Determine

a the average time between arrivals;

b the probability that another packet will arrive within 1 s; within 100 ms.

15-15 Consider a pure ALOHA system that is operating with a throughput $G = 0.1$ and packets are generated with a Poisson arrival rate λ. Determine

a the value of λ;

b the average number of attempted transmissions to send a packet.

15-16 Consider a CSMA/CD system in which the transmission rate on the bus is 10 Mbits/s. The bus is 2 km and the propagation delay is 5 μs/km. Packets are 1000 bits long. Determine

a the end-to-end delay τ_d;

b the packet duration T_p;

c the ratio τ_d / T_p;

d the maximum utilization of the bus and the maximum bit rate.

APPENDIX A

THE LEVINSON–DURBIN ALGORITHM

The Levinson–Durbin algorithm is an order-recursive method for determining the solution to the set of linear equations

$$\mathbf{\Phi}_p \mathbf{a}_p = \boldsymbol{\phi}_p \tag{A-1}$$

where $\mathbf{\Phi}_p$ is a $p \times p$ Toeplitz matrix, $\mathbf{a}_p$ is the vector of predictor coefficients expressed as

$$\mathbf{a}_p' = [a_{p1} \quad a_{p2} \quad \cdots \quad a_{pp}]$$

and $\boldsymbol{\phi}_p$ is a p-dimensional vector with elements

$$\boldsymbol{\phi}_p' = [\phi(1) \quad \phi(2) \quad \cdots \quad \phi(p)]$$

For a first-order ($p = 1$) predictor, we have the solution

$$\phi(0)a_{11} = \phi(1)$$

$$a_{11} = \phi(1)/\phi(0) \tag{A-2}$$

The residual mean square error (MSE) for the first-order predictor is

$$\begin{aligned} \mathscr{E}_1 &= \phi(0) - a_{11}\phi(1) \\ &= \phi(0) - a_{11}^2\phi(0) \\ &= \phi(0)(1 - a_{11}^2) \end{aligned} \tag{A-3}$$

In general, we may express the solution for the coefficients of an mth-order

predictor in terms of the coefficients of the $(m-1)$th-order predictor. Thus, we express $\mathbf{a}_m$ as the sum of two vectors, namely,

$$\mathbf{a}_m = \begin{bmatrix} a_{m1} \\ a_{m2} \\ \vdots \\ a_{mm} \end{bmatrix} = \begin{bmatrix} \mathbf{a}_{m-1} \\ \hline 0 \end{bmatrix} + \begin{bmatrix} \mathbf{d}_{m-1} \\ \hline k_m \end{bmatrix} \tag{A-4}$$

where the vector $\mathbf{d}_{m-1}$ and the scalar k_m are to be determined. Also, $\mathbf{\Phi}_m$ may be expressed as

$$\mathbf{\Phi}_m = \begin{bmatrix} \mathbf{\Phi}_{m-1} & \vdots & \boldsymbol{\phi}'_{m-1} \\ \hline \boldsymbol{\phi}'_{m-1} & \vdots & \phi(0) \end{bmatrix} \tag{A-5}$$

where $\boldsymbol{\phi}'_{m-1}$ is just the vector $\boldsymbol{\phi}_{m-1}$ in reverse order.

Now

$$\begin{bmatrix} \mathbf{\Phi}_{m-1} & \vdots & \boldsymbol{\phi}'_{m-1} \\ \hline \boldsymbol{\phi}'_{m-1} & \vdots & \phi(0) \end{bmatrix} \left(\begin{bmatrix} \mathbf{a}_{m-1} \\ \hline 0 \end{bmatrix} + \begin{bmatrix} \mathbf{d}_{m-1} \\ \hline k_m \end{bmatrix} \right) = \begin{bmatrix} \boldsymbol{\phi}_{m-1} \\ \hline \phi(m) \end{bmatrix} \tag{A-6}$$

From (A-6), we obtain two equations. The first is the matrix equation

$$\mathbf{\Phi}_{m-1}\mathbf{a}_{m-1} + \mathbf{\Phi}_{m-1}\mathbf{d}_{m-1} + k_m\boldsymbol{\phi}'_{m-1} = \boldsymbol{\phi}_{m-1} \tag{A-7}$$

But $\mathbf{\Phi}_{m-1}\mathbf{a}_{m-1} = \boldsymbol{\phi}_{m-1}$. Hence, (A-7) simplifies to

$$\mathbf{\Phi}_{m-1}\mathbf{d}_{m-1} + k_m\boldsymbol{\phi}'_{m-1} = \mathbf{0} \tag{A-8}$$

This equation has the solution

$$\mathbf{d}_{m-1} = -k_m\mathbf{\Phi}_{m-1}^{-1}\boldsymbol{\phi}'_{m-1} \tag{A-9}$$

But $\boldsymbol{\phi}'_{m-1}$ is just $\boldsymbol{\phi}_{m-1}$ in reverse order. Hence, the solution in (A-9) is simply $\mathbf{a}_{m-1}$ in reverse order multiplied by $-k_m$. That is,

$$\mathbf{d}_{m-1} = -k_m \begin{bmatrix} a_{m-1,m-1} \\ a_{m-1,m-2} \\ \vdots \\ a_{m-1,1} \end{bmatrix} \tag{A-10}$$

The second equation obtained from (A-6) is the scalar equation

$$\boldsymbol{\phi}'_{m-1}\mathbf{a}_{m-1} + \boldsymbol{\phi}'_{m-1}\mathbf{d}_{m-1} + \phi(0)k_m = \phi(m) \tag{A-11}$$

We eliminate $\mathbf{d}_{m-1}$ from (A-11) by use of (A-10). The resulting equation gives us k_m. That is,

$$\begin{aligned} k_m &= \frac{\phi(m) - \boldsymbol{\phi}'_{m-1}\mathbf{a}_{m-1}}{\phi(0) - \boldsymbol{\phi}'_{m-1}\mathbf{\Phi}_{m-1}^{-1}\boldsymbol{\phi}'_{m-1}} \\ &= \frac{\phi(m) - \boldsymbol{\phi}'_{m-1}\mathbf{a}_{m-1}}{\phi(0) - \mathbf{a}'_{m-1}\boldsymbol{\phi}_{m-1}} \\ &= \frac{\phi(m) - \boldsymbol{\phi}'_{m-1}\mathbf{a}_{m-1}}{\mathscr{E}_{m-1}} \end{aligned} \tag{A-12}$$

where $\mathscr{E}_{m-1}$ is the residual MSE given as

$$\mathscr{E}_{m-1} = \phi(0) - \mathbf{a}'_{m-1}\boldsymbol{\phi}_{m-1} \tag{A-13}$$

By substituting (A-10) for $\mathbf{d}_{m-1}$ in (A-4), we obtain the order-recursive relation

$$a_{mk} = a_{m-1,k} - k_m a_{m-1,m-k}, \quad k = 1, 2, \ldots, m-1, \quad m = 1, 2, \ldots, p \tag{A-14}$$

and

$$a_{mm} = k_m$$

The minimum MSE may also be computed recursively. We have

$$\mathscr{E}_m = \phi(0) - \sum_{k=1}^{m} a_{mk}\phi(k) \tag{A-15}$$

Using (A-14) in (A-15), we obtain

$$\mathscr{E}_m = \phi(0) - \sum_{k=1}^{m-1} a_{m-1,k}\phi(k) - a_{mm}\left[\phi(m) - \sum_{k=1}^{m-1} a_{m-1,m-k}\phi(k)\right] \tag{A-16}$$

But the term in square brackets in (A-16) is just the numerator of k_m in (A-12). Hence,

$$\begin{aligned}\mathscr{E}_m &= \mathscr{E}_{m-1} - a_{mm}^2\mathscr{E}_{m-1} \\ &= \mathscr{E}_{m-1}(1 - a_{mm}^2)\end{aligned} \tag{A-17}$$

APPENDIX **B**

ERROR PROBABILITY FOR MULTICHANNEL BINARY SIGNALS

In multichannel communication systems that employ binary signaling for transmitting information over the AWGN channel, the decision variable at the detector can be expressed as a special case of the general quadratic form

$$D = \sum_{k=1}^{L} (A|X_k|^2 + B|Y_k|^2 + CX_kY_k^* + C^*X_k^*Y_k) \tag{B-1}$$

in complex-valued gaussian random variables. A, B, and C are constants; X_k and Y_k are a pair of correlated complex-valued gaussian random variables. For the channels considered, the L pairs $\{X_k, Y_k\}$ are mutually statistically independent and identically distributed.

The probability of error is the probability that $D < 0$. This probability is evaluated below.

The computation begins with the characteristic function, denoted by $\psi_D(jv)$, of the general quadratic form. The probability that $D < 0$, denoted here as the probability of error P_b, is

$$P_b = P(D < 0) = \int_{-\infty}^{0} p(D)\,dD \tag{B-2}$$

where $p(D)$, the probability density function of D, is related to $\psi_D(jv)$ by the Fourier transform, i.e.,

$$p(D) = \frac{1}{2\pi}\int_{-\infty}^{\infty} \psi_D(jv)e^{-jvD}\,dv$$

Hence,

$$P_b = \int_{-\infty}^{0} dD \frac{1}{2\pi} \int_{-\infty}^{\infty} \psi_D(jv) e^{-jvD} dv \tag{B-3}$$

Let us interchange the order of integration and carry out first the integration with respect to D. The result is

$$P_b = -\frac{1}{2\pi j} \int_{-\infty+j\varepsilon}^{\infty+j\varepsilon} \frac{\psi_D(jv)}{v} dv \tag{B-4}$$

where a small positive number ε has been inserted in order to move the path of integration away from the singularity at $v = 0$ and which must be positive in order to allow for the interchange in the order of integration.

Since D is the sum of statistically independent random variables, the characteristic function of D factors into a product of L characteristic functions, with each function corresponding to the individual random variables d_k, where

$$d_k = A|X_k|^2 + B|Y_k|^2 + CX_kY_k^* + C^*X_k^*Y_k$$

The characteristic function of d_k is

$$\phi_{d_k}(jv) = \frac{v_1 v_2}{(v + jv_1)(v - jv_2)} \exp\left[\frac{v_1 v_2(-v^2\alpha_{1k} + jv\alpha_{2k})}{(v + jv_1)(v - jv_2)}\right] \tag{B-5}$$

where the parameters v_1, v_2, α_{1k}, and α_{2k} depend on the means $\bar{X}_k$ and $\bar{Y}_k$ and the second (central) moments μ_{xx}, μ_{yy}, and μ_{xy} of the complex-vlaued gaussian variables X_k and Y_k through the following definitions ($|C|^2 - AB > 0$):

$$\begin{aligned}
v_1 &= \sqrt{w^2 + \frac{1}{4(\mu_{xx}\mu_{yy} - |\mu_{xy}|^2)(|C|^2 - AB)}} - w \\
v_2 &= \sqrt{w^2 + \frac{1}{4(\mu_{xx}\mu_{yy} - |\mu_{xy}|^2)(|C|^2 - AB)}} + w \\
w &= \frac{A\mu_{xx} + B\mu_{yy} + C\mu_{xy}^* + C^*\mu_{xy}}{4(\mu_{xx}\mu_{yy} - |\mu_{xy}|^2)(|C|^2 - AB)} \\
\alpha_{1k} &= 2(|C|^2 - AB)(|\bar{X}_k|^2\mu_{yy} + |\bar{Y}_k|^2\mu_{xx} - \bar{X}_k^*\bar{Y}_k\mu_{xy} - \bar{X}_k\bar{Y}_k^*\mu_{xy}^*) \\
\alpha_{2k} &= A|\bar{X}_k|^2 + B|\bar{Y}_k|^2 + C\bar{X}_k^*\bar{Y}_k + C^*\bar{X}_k\bar{Y}_k^* \\
\mu_{xv} &= \tfrac{1}{2}E[(X_k - \bar{X}_k)(Y_k - \bar{Y}_k)^*]
\end{aligned} \tag{B-6}$$

Now, as a result of the independence of the random variables d_k, the characteristic function of D is

$$\begin{aligned}
\psi_D(jv) &= \prod_{k=1}^{L} \psi_{d_k}(jv) \\
\psi_D(jv) &= \frac{(v_1 v_2)^L}{(v + jv_1)^L(v - jv_2)^L} \exp\left[\frac{v_1 v_2(jv\alpha_2 - v^2\alpha_1)}{(v + jv_1)(v - jv_2)}\right]
\end{aligned} \tag{B-7}$$

where

$$\alpha_1 = \sum_{k=1}^{L} \alpha_{1k}, \qquad \alpha_2 = \sum_{k=1}^{L} \alpha_{2k} \tag{B-8}$$

The result (B-7) is substituted for $\psi_D(jv)$ in (B-4), and we obtain

$$P_b = -\frac{(v_1 v_2)^L}{2\pi j} \int_{-\infty+jr}^{\infty+jr} \frac{dv}{v(v+jv_1)^L (v-jv_2)^L} \exp\left[\frac{v_1 v_2 (jv\alpha_2 - v^2\alpha_1)}{(v+jv_1)(v-jv_2)}\right] \tag{B-9}$$

This integral is evaluated as follows.

The first step is to express the exponential function in the form

$$\exp\left(-A_1 + \frac{jA_2}{v+jv_1} - \frac{jA_3}{v-jv_2}\right)$$

where one can easily verify that the constants A_1, A_2, and A_3 are given as

$$\begin{aligned} A_1 &= \alpha_1 v_1 v_2 \\ A_2 &= \frac{v_1^2 v_2}{v_1+v_2}(\alpha_1 v_1 + \alpha_2) \\ A_3 &= \frac{v_1 v_2^2}{v_1+v_2}(\alpha_1 v_2 - \alpha_2) \end{aligned} \tag{B-10}$$

Second, a conformal transformation is made from the v plane onto the p plane via the change in variable

$$p = -\frac{v_1}{v_2}\frac{v-jv_2}{v+jv_1} \tag{B-11}$$

In the p plane, the integral given by (B-9) becomes

$$P_b = \frac{\exp\left[v_1 v_2(-2\alpha v_1 v_2 + \alpha_2 v_1 - \alpha_2 v_2)/(v_1+v_2)^2\right]}{(1+v_2/v_1)^{2L-1}} \frac{1}{2\pi j}\int_\Gamma f(p)\,dp \tag{B-12}$$

where

$$f(p) = \frac{[1+(v_2/v_1)p]^{2L-1}}{p^L(1-p)} \exp\left[\frac{A_2(v_2/v_1)}{v_1+v_2}p + \frac{A_3(v_1/v_2)}{v_1+v_2}\frac{1}{p}\right] \tag{B-13}$$

and Γ is a circular contour of radius less than unity that encloses the origin.

The third step is to evaluate the integral

$$\begin{aligned} \frac{1}{2\pi j}\int_\Gamma f(p)\,dp = \frac{1}{2\pi j}\int_\Gamma &\frac{(1+(v_2/v_1)p)^{2L-1}}{p^L(1-p)} \\ &\times \exp\left[\frac{A_2(v_2/v_1)}{v_1+v_2}p + \frac{A_3(v_1/v_2)}{v_1+v_2}\frac{1}{p}\right]dp \end{aligned} \tag{B-14}$$

In order to facilitate subsequent manipulations, the constants $a \geq 0$ and $b \geq 0$ are introduced and defined as follows:

$$\tfrac{1}{2}a^2 = \frac{A_3(v_1/v_2)}{v_1+v_2}, \qquad \tfrac{1}{2}b^2 = \frac{A_2(v_2/v_1)}{v_1+v_2} \tag{B-15}$$

Let us also expand the function $[1 + (v_2/v_1)p]^{2L-1}$ as a binomial series. As a result, we obtain

$$\frac{1}{2\pi j}\int_\Gamma f(p)\,dp = \sum_{k=0}^{2L-1}\binom{2L-1}{k}\left(\frac{v_2}{v_1}\right)^k \times \frac{1}{2\pi j}\int_\Gamma \frac{p^k}{p^L(1-p)}\exp\left(\tfrac{1}{2}a^2\frac{1}{p} + \tfrac{1}{2}b^2 p\right)dp \qquad \text{(B-16)}$$

The contour integral given in (B-16) is one representation of the Bessel function. It can be solved by making use of the relations

$$I_n(ab) = \begin{cases} \dfrac{1}{2\pi j}\left(\dfrac{a}{b}\right)^n \displaystyle\int_\Gamma \frac{1}{p^{n+1}}\exp\left(\tfrac{1}{2}a^2\frac{1}{p} + \tfrac{1}{2}b^2 p\right)dp \\ \dfrac{1}{2\pi j}\left(\dfrac{b}{a}\right)^n \displaystyle\int_\Gamma p^{n-1}\exp\left(\tfrac{1}{2}a^2\frac{1}{p} + \tfrac{1}{2}b^2 p\right)dp \end{cases}$$

where $I_n(x)$ is the nth order modified Bessel function of the first kind and the series representation of Marcum's Q function in terms of Bessel functions, i.e.,

$$Q_1(a, b) = \exp\left[-\tfrac{1}{2}(a^2 + b^2)\right] + \sum_{n=0}^{\infty}\left(\frac{a}{b}\right)^n I_n(ab)$$

First, consider the case $0 \le k \le L-2$ in (B-16). In this case, the resulting contour integral can be written in the form†

$$\frac{1}{2\pi j}\int_\Gamma \frac{1}{p^{L-k}(1-p)}\exp\left(\tfrac{1}{2}a^2\frac{1}{p} + \tfrac{1}{2}b^2 p\right)dp = Q_1(a, b)\exp\left[\tfrac{1}{2}(a^2 + b^2)\right] + \sum_{n=1}^{L-k-1}\left(\frac{b}{a}\right)^n I_n(ab) \qquad \text{(B-17)}$$

Next, consider the term $k = L-1$. The resulting contour integral can be expressed in terms of the Q function as follows:

$$\frac{1}{2\pi j}\int_\Gamma \frac{1}{p(1-p)}\exp\left(\tfrac{1}{2}a^2\frac{1}{p} + \tfrac{1}{2}b^2 p\right)dp = Q_1(a, b)\exp\left[\tfrac{1}{2}(a^2 + b^2)\right] \qquad \text{(B-18)}$$

Finally, consider the case $L \le k \le 2L-1$. We have

$$\begin{aligned}\frac{1}{2\pi j}\int_\Gamma \frac{p^{k-L}}{1-p}\exp\left(\tfrac{1}{2}a^2\frac{1}{p} + \tfrac{1}{2}b^2 p\right)dp &= \sum_{n=0}^{\infty}\frac{1}{2\pi j}\int_\Gamma p^{k-L+n}\exp\left(\tfrac{1}{2}a^2\frac{1}{p} + \tfrac{1}{2}b^2 p\right)dp \\ &= \sum_{n=k+1-L}^{\infty}\left(\frac{a}{b}\right)^n I_n(ab) = Q_1(a, b)\exp\left[\tfrac{1}{2}(a^2 + b^2)\right] - \sum_{n=0}^{k-L}\left(\frac{a}{b}\right)^n I_n(ab) \qquad \text{(B-19)}\end{aligned}$$

Collecting the terms that are indicated on the right-hand side of (B-16) and using

† This contour integral is related to the generalized Marcum Q function, defined as

$$Q_m(a, b) = \int_b^{\infty} x(x/a)^{m-1}\exp\left[-\tfrac{1}{2}(x^2 + a^2)\right]I_{m-1}(ax)\,dx, \qquad m \ge 1$$

in the following manner:

$$Q_m(a, b)\exp\left[\tfrac{1}{2}(a^2 + b^2)\right] = \frac{1}{2\pi j}\int_\Gamma \frac{1}{p^m(1-p)}\exp\left(\tfrac{1}{2}a^2\frac{1}{p} + \tfrac{1}{2}b^2 p\right)dp$$

the results given in (B-17)–(B-19), the following expression for the contour integral is obtained after some algebra:

$$\frac{1}{2\pi j}\int_{\Gamma} f(p)\,dp = \left(1+\frac{v_2}{v_1}\right)^{2L-1}\left[\exp\left[\tfrac{1}{2}(a^2+b^2)\right]Q_1(a,b) - I_0(ab)\right] + I_0(ab)\sum_{k=0}^{L-1}\binom{2L-1}{k}\left(\frac{v_2}{v_1}\right)^k + \sum_{n=1}^{L-1} I_n(ab)\sum_{k=0}^{L-1-n}\binom{2L-1}{k}\left[\left(\frac{b}{a}\right)^n\left(\frac{v_2}{v_1}\right)^k - \left(\frac{a}{b}\right)^n\left(\frac{v_2}{v_1}\right)^{2L-1-k}\right] \tag{B-20}$$

Equation (B-20) in conjunction with (B-12) gives the result for the probability of error. A further simplification results when one uses the following identity, which can easily be proved:

$$\exp\left[\frac{v_1 v_2}{(v_1+v_2)^2}(-2\alpha_1 v_1 v_2 + \alpha_2 v_1 - \alpha_2 v_2)\right] = \exp\left[-\tfrac{1}{2}(a^2+b^2)\right]$$

Therefore, it follows that

$$\begin{aligned} P_b &= Q_1(a,b) - I_0(ab)\exp\left[-\tfrac{1}{2}(a^2+b^2)\right] \\ &\quad + \frac{I_0(ab)\exp\left[-\frac{1}{2}(a^2+b^2)\right]}{(1+v_2/v_1)^{2L-1}}\sum_{k=0}^{L-1}\binom{2L-1}{k}\left(\frac{v_2}{v_1}\right)^k + \frac{\exp\left[-\frac{1}{2}(a^2+b^2)\right]}{(1+v_2/v_1)^{2L-1}} \\ &\quad \times \sum_{n=1}^{L-1} I_n(ab)\sum_{k=0}^{L-1-n}\binom{2L-1}{k} \\ &\quad \times \left[\left(\frac{b}{a}\right)^n\left(\frac{v_2}{v_1}\right)^k - \left(\frac{a}{b}\right)^n\left(\frac{v_2}{v_1}\right)^{2L-1-k}\right] \quad (L>1) \end{aligned} \tag{B-21}$$

$$P_b = Q_1(a,b) - \frac{v_2/v_1}{1+v_2/v_1} I_0(ab)\exp\left[-\tfrac{1}{2}(a^2+b^2)\right] \quad (L=1)$$

This is the desired expression for the probability of error. It is now a simple matter to relate the parameters a and b to the moments of the pairs $\{X_k, Y_k\}$. Substituting for A_2 and A_3 from (B-10) into (B-15), we obtain

$$\begin{aligned} a &= \left[\frac{2v_1^2 v_2(\alpha_1 v_2 - \alpha_2)}{(v_1+v_2)^2}\right]^{1/2} \\ b &= \left[\frac{2v_1 v_2^2(\alpha_1 v_1 + \alpha_2)}{(v_1+v_2)^2}\right]^{1/2} \end{aligned} \tag{B-22}$$

Since v_1, v_2, α_1, and α_2 have been given in (B-6) and (B-8) directly in terms of the moments of the pairs X_k and Y_k, our task is completed.

APPENDIX C

ERROR PROBABILITIES FOR ADAPTIVE RECEPTION OF M-PHASE SIGNALS

In this appendix, we derive probabilities of error for two- and four-phase signaling over an L-diversity-branch time-invariant additive guassian noise channel and for M-phase signaling over an L-diversity-branch Rayleigh fading additive gaussian noise channel. Both channels corrupt the signaling waveforms transmitted through them by introducing additive white gaussian noise and an unknown or random multiplicative gain and phase shift in the transmitted signal. The receiver processing consists of cross-correlating the signal plus noise received over each diversity branch by a noisy reference signal, which is derived either from the previously received information-bearing signals or from the transmission and reception of a pilot signal, and adding the outputs from all L-diversity branches to form the decision variable.

C-1 MATHEMATICAL MODEL FOR AN M-PHASE SIGNALING COMMUNICATIONS SYSTEM

In the general case of M-phase signaling, the signaling waveforms at the transmitter are†

$$s_i(t) = \mathrm{Re}\left[s_{li}(t)e^{j2\pi f_c t}\right]$$

† The complex representation of real signals is used throughout. Complex conjugation is denoted by an asterisk.

where

$$s_{in}(t) = g(t) \exp\left[j\frac{2\pi}{M}(n-1)\right], \quad n = 1, 2, \ldots, M, \quad 0 \leq t \leq T \tag{C-1}$$

and T is the time duration of the signaling interval.

Consider the case in which one of these M waveforms is transmitted, for the duration of the signaling interval, over L channels. Assume that each of the channels corrupts the signaling waveform transmitted through it by introducing a multiplicative gain and phase shift, represented by the complex-valued number g_k, and an additive noise $z_k(t)$. Thus, when the transmitted waveform is $s_{in}(t)$, the waveform received over the kth channel is

$$r_{ik}(t) = g_k s_{in}(t) + z_k(t), \quad 0 \leq t \leq T, \quad k = 1, 2, \ldots, L \tag{C-2}$$

The noises $\{z_k(t)\}$ are assumed to be sample functions of a stationary white gaussian random process with zero mean and autocorrleation function $\phi_z(\tau) = N_0\delta(\tau)$, where N_0 is the value of the spectral density. These sample functions are assumed to be mutually statistically independent.

At the demodulator, $r_{ik}(t)$ is passed through a filter whose impulse response is matched to the waveform $g(t)$. The output of this filter, sampled at time $t = T$, is denoted as

$$X_k = 2\mathscr{E}g_k \exp\left[j\frac{2\pi}{M}(n-1)\right] + N_k \tag{C-3}$$

where $\mathscr{E}$ is the transmitted signal energy per channel and N_k is the noise sample from the kth filter. In order for the demodulator to decide which of the M phases was transmitted in the signaling interval $0 \leq t \leq T$, it attempts to undo the phase shift introduced by each channel. In practice, this is accomplished by multiplying the matched filter output X_k by the complex conjugate of an estimate $\hat{g}_k$ of the channel gain and phase shift. The result is a weighted and phase-shifted sampled output from the kth-channel filter, which is then added to the weighted and phase-shifted sampled outputs from the other $L - 1$ channel filters.

The estimate $\hat{g}_k$ of the gain and phase shift of the kth channel is assumed to be derived either from the transmission of a pilot signal or by undoing the modulation on the information-bearing signals received in previous signaling intervals. As an example of the former, suppose that a pilot signal, denoted by $s_{pk}(t)$, $0 \leq t \leq T$, is transmitted over the kth channel for the purpose of measuring the channel gain and phase shift. The received waveform is

$$g_k s_{pk}(t) + z_{pk}(t), \quad 0 \leq t \leq T$$

where $z_{pk}(t)$ is a sample function of a stationary white gaussian random process with zero mean and autocorrelation function $\phi_p(\tau) = N_0\delta(\tau)$. This signal plus noise is passed through a filter matched to $s_{pk}(t)$. The filter output is sampled at time $t = T$ to yield the random variable $X_{pk} = 2\mathscr{E}_p g_k + N_{pk}$, where $\mathscr{E}_p$ is the energy in the pilot signal, which is assumed to be identical for all channels, and N_{pk} is the additive noise sample. An estimate of g_k is obtained by properly normalizing X_{pk}, i.e., $\hat{g}_k = g_k + N_{pk}/2\mathscr{E}_p$.

On the other hand, an estimate of g_k can be obtained from the information-bearing signal as follows. If one knew the information component contained in the matched filter output then an estimate of g_k could be obtained by properly normalizing this

output. For example, the information component in the filter output given by (C-3) is $2\mathscr{E}g_k \exp[j(2\pi/M)(n-1)]$, and hence, the estimate is

$$\hat{g}_k = \frac{X_k}{2\mathscr{E}} \exp\left[-j\frac{2\pi}{M}(n-1)\right] = g_k + \frac{N_k'}{2\mathscr{E}}$$

where $N_k' = N_k \exp[-j(2\pi/M)(n-1)]$ and the pdf of N_k' is identical to the pdf of N_k. An estimate that is obtained from the information-bearing signal in this manner is called a *clairvoyant estimate*. Although a physically realizable receiver does not possess such clairvoyance, it can approximate this estimate by employing a time delay of one signaling interval and by feeding back the estimate of the transmitted phase in the previous signaling interval.

Whether the estimate of g_k is obtained from a pilot signal or from the information-bearing signal, the estimate can be improved by extending the time interval over which it is formed to include several prior signaling intervals in a way that has been described by Price (1962a, b). As a result of extending the measurement interval, the signal-to-noise ratio in the estimate of g_k is increased. In the general case where the estimation interval is the infinite past, the normalized *pilot signal estimate* is

$$\hat{g}_k = g_k + \sum_{i=1}^{\infty} c_i N_{pki} \Big/ 2\mathscr{E}_p \sum_{i=1}^{\infty} c_i \tag{C-4}$$

where c_i is the weighting coefficient on the subestimate of g_k derived from the ith prior signal interval and N_{pki} is the sample of additive gaussian noise at the output of the filter matched to $s_{pk}(t)$ in the ith prior signaling interval. Similarly, the clairvoyant estimate that is obtained from the information-bearing signal by undoing the modulation over the infinite past is

$$\hat{g}_k = g_k + \sum_{i=1}^{\infty} c_i N_{ki} \Big/ 2\mathscr{E} \sum_{i=1}^{\infty} c_i \tag{C-5}$$

As indicated, the demodulator forms the product between $\hat{g}_k^*$ and X_k and adds this to the products of the other $L-1$ channels. The random variable that results is

$$\begin{aligned} z &= \sum_{k=1}^{L} X_k \hat{g}_k^* = \sum_{k=1}^{L} X_k Y_k^* \\ &= z_r + jz_i \end{aligned} \tag{C-6}$$

where, by definition, $Y_k = \hat{g}_k$, $z_r = \mathrm{Re}(z)$, and $z_i = \mathrm{Im}(z)$. The phase of z is the decision variable. This is simply

$$\theta = \tan^{-1}\left(\frac{z_i}{z_r}\right) = \tan^{-1}\left[\mathrm{Im}\left(\sum_{k=1}^{L} X_k Y_k^*\right) \Big/ \mathrm{Re}\left(\sum_{k=1}^{L} X_k Y_k^*\right)\right] \tag{C-7}$$

C-2 CHARACTERISTIC FUNCTION AND PROBABILITY DENSITY FUNCTION OF THE PHASE θ

The following derivation is based on the assumption that the transmitted signal phase is zero, i.e., $n = 1$. If desired, the pdf of θ conditional on any other transmitted signal phase can be obtained by translating $p(\theta)$ by the angle $2\pi(n-1)/M$. We also assume

that the complex-valued numbers $\{g_k\}$, which characterize the L channels, are mutually statistically independent and identically distributed zero-mean gaussian random variables. This characterization is appropriate for slowly Rayleigh fading channels. As a consequence, the rrandom variables (X_k, Y_k) are correlated, complex-valued, zero-mean, gaussian, and statistically independent, but identically distributed with any other pair (X_i, Y_i).

The method that has been used in evaluating the probability density $p(\theta)$ in the general case of diversity reception is as follows. First, the characteristic function of the joint probability distribution function of z_r and z_i, where z_r and z_i are two components that make up the decision variable θ, is obtained. Second, the double Fourier transform of the characteristic function is performed and yields the density $p(z_r, z_i)$. Then the *transformation*

$$r = \sqrt{z_r^2 + z_i^2}, \qquad \theta = \tan^{-1}\left(\frac{z_i}{z_r}\right) \tag{C-8}$$

yields the joint pdf of the envelope r and the phase θ. Finally, integration of this joint pdf over the random variable r yields the pdf of θ.

The joint characteristic function of the random variables z_r and z_i can be expressed in the form

$$\psi(jv_1, jv_2) = \left[\frac{\dfrac{4}{m_{xx}m_{yy}(1-|\mu|^2)}}{\left(v_1 - j\dfrac{2|\mu|\cos\varepsilon}{\sqrt{m_{xx}m_{yy}}(1-|\mu|^2)}\right)^2 + \left(v_2 - j\dfrac{2|\mu|\sin\varepsilon}{\sqrt{m_{xx}m_{yy}}(1-|\mu|^2)}\right)^2 + \dfrac{4}{m_{xx}m_{yy}(1-|\mu|^2)^2}}\right]^L \tag{C-9}$$

where, by definition,

$$\begin{aligned} m_{xx} &= E(|X_k|^2) \qquad \text{identical for all } k \\ m_{yy} &= E(|Y_k|^2) \qquad \text{identical for all } k \\ m_{xy} &= E(X_k Y_k^*) \qquad \text{identical for all } k \\ \mu &= \frac{m_{xy}}{\sqrt{m_{xx}m_{yy}}} = |\mu| e^{j\varepsilon} \end{aligned} \tag{C-10}$$

The result of Fourier-transforming the function $\psi(jv_1, jv_2)$ with respect to the variables v_1 and v_2 is

$$\begin{aligned} p(z_r, z_i) = \frac{(1-|\mu|^2)^L}{(L-1)!\pi 2^L}&(\sqrt{z_r^2 + z_i^2})^{L-1} \\ &\times \exp[|\mu|(z_r\cos\varepsilon + z_i\sin\varepsilon)]K_{L-1}(\sqrt{z_r^2 + z_i^2}) \end{aligned} \tag{C-11}$$

where $K_n(x)$ is the modified Hankel function of order n. Then the transformation of random variables, as indicated in (C-8) yields the joint pdf of the envelope r and the phase θ in the form

$$p(r, \theta) = \frac{(1-|\mu|^2)^L}{(L-1)!\pi 2^L} r^L \exp[|\mu| r\cos(\theta - \varepsilon)]K_{L-1}(r) \tag{C-12}$$

Now, integration over the variable r yields the marginal pdf of the phase θ. We have evaluated the integral to obtain $p(\theta)$ in the form

$$p(\theta) = \frac{(-1)^{L-1}(1-|\mu|^2)^L}{2\pi(L-1)!}\left\{\frac{\partial^{L-1}}{\partial b^{L-1}}\left[\frac{1}{b-|\mu|^2\cos^2(\theta-\varepsilon)}\right.\right.$$
$$\left.\left.+\frac{|\mu|\cos(\theta-\varepsilon)}{[b-|\mu|^2\cos^2(\theta-\varepsilon)]^{3/2}}\cos^{-1}\left(-\frac{|\mu|\cos(\theta-\varepsilon)}{b^{1/2}}\right)\right]\right\}\Bigg|_{b=1} \tag{C-13}$$

In this equation, the notation

$$\frac{\partial^L}{\partial b^L} f(b,\mu)\Big|_{b=1}$$

denotes the Lth partial derivative of the function $f(b,\mu)$ evaluated at $b=1$.

C-3 ERROR PROBABILITIES FOR SLOWLY RAYLEIGH FADING CHANNELS

In this section, the probability of a character error and the probability of a binary digit error are derived for M-phase signaling. The probabilities are evaluated via the probability density function and the probability distribution function of θ.

The Probability Distribution Function of the Phase In order to evaluate the probability of error, we need to evaluate the definite integral

$$P(\theta_1 \le \theta \le \theta_2) = \int_{\theta_1}^{\theta_2} p(\theta)\,d\theta$$

where θ_1 and θ_2 are limits of integration and $p(\theta)$ is given by (C-13). All subsequent calculations are made for a real cross-correlation coefficient μ. A real-valued μ implies that the signals have symmetric spectra. This is the usual situation encountered. Since a complex-valued μ causes a shift of ε in the pdf of θ, i.e., ε is simply a bias term, the results that are given for real μ can be altered in a trivial way to cover the more general case of complex-valued μ.

In the integration of $p(\theta)$, only the range $0 \le \theta \le \pi$ is considered, because $p(\theta)$ is an even function. Furthermore, the continuity of the integrand and its derivatives and the fact that the limits θ_1 and θ_2 are independent of b allow for the interchange of integration and differentiation. When this is done, the resulting integral can be evaluated quite readily and can be expressed as follows:

$$\int_{\theta_1}^{\theta_2} p(\theta)\,d\theta = \frac{(-1)^{L-1}(1-\mu^2)^L}{2\pi(L-1)!}$$
$$\times\frac{\partial^{L-1}}{\partial b^{L-1}}\left\{\frac{1}{b-\mu^2}\left[\frac{\mu\sqrt{1-(b/\mu^2-1)x^2}}{b^{1/2}}\cot^{-1}x\right.\right.$$
$$\left.\left.-\cot^{-1}\left(\frac{xb^{1/2}\mu}{\sqrt{1-(b/\mu^2-1)x^2}}\right)\right]\right\}\Bigg|_{x_1}^{x_2}\Bigg|_{b=1} \tag{C-14}$$

where, by definition,

$$x_i = \frac{-\mu\cos\theta_i}{\sqrt{b-\mu^2\cos\theta_i}}, \quad i=1,2 \tag{C-15}$$

Probability of a Symbol Error The probability of a symbol error for any M-phase signaling system is

$$P_M = 2\int_{\pi/M}^{\pi} p(\theta)\, d\theta$$

When (C-14) is evaluated at these two limits, the result is

$$P_M = \frac{(-1)^{L-1}(1-\mu^2)^L}{\pi(L-1)!}\frac{\partial^{L-1}}{\partial b^{L-1}}\left\{\frac{1}{b-\mu^2}\left[\frac{\pi}{M}(M-1) - \frac{\mu \sin(\pi/M)}{\sqrt{b-\mu^2\cos^2(\pi/M)}}\cot^{-1}\left(\frac{-\mu\cos(\pi/M)}{\sqrt{b-\mu^2\cos^2(\pi/M)}}\right)\right]\right\}\Bigg|_{b=1} \tag{C-16}$$

Probability of a Binary Digit Error First, let us consider two-phase signaling. In this case, the probability of a binary digit error is obtained by integrating the pdf $p(\theta)$ over the range $\frac{1}{2}\pi < \theta < 3\pi$. Since $p(\theta)$ is an even function and the signals are a priori equally likely, this probability can be written as

$$P_2 = 2\int_{\pi/2}^{\pi} p(\theta)\, d\theta$$

It is easily verified that $\theta_1 = \frac{1}{2}\pi$ implies $x_1 = 0$ and $\theta_2 = \pi$ implies $x_2 = \mu/\sqrt{b-\mu^2}$. Thus,

$$P_2 = \frac{(-1)^{L-1}(1-\mu^2)^L}{2(L-1)!}\frac{\partial^{L-1}}{\partial b^{L-1}}\left[\frac{1}{b-\mu^2} - \frac{\mu}{b^{1/2}(b-\mu^2)}\right]\Bigg|_{b=1} \tag{C-17}$$

After performing the differentiation indicated in (C-17) and evaluating the resulting function at $b = 1$, the probability of a binary digit error is obtained in the form

$$P_2 = \frac{1}{2}\left[1 - \mu\sum_{k=0}^{L-1}\binom{2k}{k}\left(\frac{1-\mu^2}{4}\right)^k\right] \tag{C-18}$$

Next, we consider the case of four-phase signaling in which a Gray code is used to map pairs of bits into phases. Assuming again that the transmitted signal is $s_{i1}(t)$, it is clear that a single error is committed when the received phase is $\frac{1}{4}\pi < \theta < \frac{3}{4}\pi$, and a double error is committed when the received phase is $\frac{3}{4}\pi < \theta < \pi$. That is, the probability of a binary digit error is

$$P_{4b} = \int_{\pi/4}^{3\pi/4} p(\theta)\, d\theta + 2\int_{3\pi/4}^{\pi} p(\theta)\, d\theta \tag{C-19}$$

It is easily established from (C-14) and (C-19) that

$$P_{4b} = \frac{(-1)^{L-1}(1-\mu^2)^L}{2(L-1)!}\frac{\partial^{L-1}}{\partial b^{L-1}}\left[\frac{1}{b-\mu^2} - \frac{\mu}{(b-\mu^2)(2b-\mu^2)^{1/2}}\right]\Bigg|_{b=1}$$

Hence, the probability of a binary digit error for four-phase signaling is

$$P_{4b} = \frac{1}{2}\left[1 - \frac{\mu}{\sqrt{2-\mu^2}}\sum_{k=0}^{L-1}\binom{2k}{k}\left(\frac{1+\mu^2}{4-2\mu^2}\right)^k\right] \tag{C-20}$$

Note that if one defines the quantity $\rho = \mu/\sqrt{2-\mu^2}$, the expression for P_{4b} in terms of ρ is

$$P_{4b} = \frac{1}{2}\left[1 - \rho\sum_{k=0}^{L-1}\binom{2k}{k}\left(\frac{1-\rho^2}{4}\right)^k\right] \tag{C-21}$$

In other words, P_{4b} has the same form as P_2 given in (C-18). Furthermore, note that ρ, just like μ, can be interpreted as a cross-correlation coefficient, since the range of ρ is $0 \leq \rho \leq 1$ for $0 \leq \mu \leq 1$. This simple fact will be used in Section C-4.

The above procedure for obtaining the bit error probability for an M-phase signal with a Gray code can be used to generate results for $M = 8$, 16, etc., as shown by Proakis (1968).

Evaluation of the Cross-Correlation Coefficient The expressions for the probabilities of error given above depend on a single parameter, namely, the cross-correlation coefficient μ. The clairvoyant estimate is given by (C-5), and the matched filter output, when signal waveform $s_{i1}(t)$ is transmitted, is $X_k = 2\mathscr{E}g_k + N_k$. Hence, the cross-correlation coefficient is

$$\mu = \frac{\sqrt{\nu}}{\sqrt{(\bar{\gamma}_c^{-1} + 1)(\bar{\gamma}_c^{-1} + \nu)}} \tag{C-22}$$

where, by definition,

$$\begin{aligned} \nu &= \left|\sum_{i=1}^{\infty} c_i\right|^2 \Big/ \sum_{i=1}^{\infty} |c_i|^2 \\ \bar{\gamma}_c &= \frac{\mathscr{E}}{N_0} E(|g_k|^2), \quad k = 1, 2, \ldots, L \end{aligned} \tag{C-23}$$

The parameter ν represents the effective number of signaling intervals over which the estimate is formed, and $\bar{\gamma}_c$ is the average SNR per channel.

In the case of differential phase signaling, the weighting coefficients are $c_1 = 1$, $c_i = 0$ for $i \neq 1$. Hence, $\nu = 1$ and $\mu = \bar{\gamma}_c/(1 + \bar{\gamma}_c)$.

When $\nu = \infty$, the estimate is perfect and

$$\lim_{\nu \to \infty} \mu = \sqrt{\frac{\bar{\gamma}_c}{\bar{\gamma}_c + 1}}$$

Finally, in the case of a pilot signal estimate, given by (C-4) the cross-correlation coefficient is

$$\mu = \left[\left(1 + \frac{r+1}{r\bar{\gamma}_t}\right)\left(1 + \frac{r+1}{\nu\bar{\gamma}_t}\right)\right]^{-1/2} \tag{C-24}$$

where, by definition,

$$\begin{aligned} \bar{\gamma}_t &= \frac{\mathscr{E}_t}{N_0} E(|g_k|^2) \\ \mathscr{E}_t &= \mathscr{E} + \mathscr{E}_p \\ r &= \mathscr{E}/\mathscr{E}_p \end{aligned}$$

The values of μ given above are summarized in Table C-1.

C-4 ERROR PROBABILITIES FOR TIME-INVARIANT AND RICEAN FADING CHANNELS

In Section C-2, the complex-valued channel gains $\{g_k\}$ were characterized as zero-mean gaussian random variables, which is appropriate for Rayleigh fading channels. In this section, the channel gains $\{g_k\}$ are assumed to be nonzero-mean gaussian random variables. Estimates of the channel gains are formed by the demodulator and are used

TABLE C-1 RAYLEIGH FADING CHANNEL

Type of estimate	Cross-correlation coefficient μ
Clairvoyant estimate	$\dfrac{\sqrt{\nu}}{\sqrt{(\bar{\gamma}_c^{-1}+1)(\bar{\gamma}_c^{-1}+\nu)}}$
Pilot signal estimate	$\dfrac{\sqrt{r\nu}}{(r+1)\sqrt{\left(\dfrac{1}{\bar{\gamma}_t}+\dfrac{r}{r+1}\right)\left(\dfrac{1}{\bar{\gamma}_t}+\dfrac{\nu}{r+1}\right)}}$
Differential phase signaling	$\dfrac{\bar{\gamma}_c}{\bar{\gamma}_c+1}$
Perfect estimate	$\sqrt{\dfrac{\bar{\gamma}_c}{\bar{\gamma}_c+1}}$

as described in Section C-1. Moreover, the decision variable θ is defined again by (C-7). However, in this case, the gaussian random variables X_k and Y_k, which denote the matched filter output and the estimate, respectively, for the kth channel, have nonzero means, which are denoted by $\bar{X}_k$ and $\bar{Y}_k$. Furthermore, the second moments are

$$m_{xx} = E(|X_k - \bar{X}_k|^2) \qquad \text{identical for all channels}$$
$$m_{yy} = E(|Y_k - \bar{Y}_k|^2) \qquad \text{identical for all channels}$$
$$m_{xy} = E[(X_k - \bar{X}_k)(Y_k^* - \bar{Y}_k^*)] \qquad \text{identical for all channels}$$

and the normalized covariance is defined as

$$\mu = \frac{m_{xy}}{\sqrt{m_{xx}m_{yy}}}$$

Error probabilities are given below only for two- and four-phase signaling with this channel model. We are interested in the special case in which the fluctuating component of each of the channel gains $\{g_k\}$ is zero, so that the channels are time-invariant. If, in addition to this time invariance, the noises between the estimate and the matched filter output are uncorrelated then $\mu = 0$.

In the general case, the probability of error for two-phase signaling over L statistically independent channels characterized in the manner described above can be obtained from the results in Appendix B. In its most general form, the expresssion for the binary error rate is

$$\begin{aligned} P_2 &= Q_1(a,b) - I_0(a)\exp\left[-\tfrac{1}{2}(a^2+b^2)\right] \\ &\quad + \frac{I_0(ab)\exp\left[-\frac{1}{2}(a^2+b^2)\right]}{[2/(1-\mu)]^{2L-1}}\sum_{k=0}^{L-1}\binom{2L-1}{k}\left(\frac{1+\mu}{1-\mu}\right)^k \\ &\quad + \frac{\exp\left[-\frac{1}{2}(a^2+b^2)\right]}{[2/(1-\mu)]^{2L-1}} \\ &\quad \times \sum_{k=1}^{L-1} I_n(ab)\sum_{k=0}^{L-1-n}\binom{2L-1}{k}\left[\left(\frac{b}{a}\right)^n\left(\frac{1+\mu}{1-\mu}\right)^k - \left(\frac{a}{b}\right)^n\left(\frac{1+\mu}{1-\mu}\right)^{2L-1-k}\right] \quad (L \geq 2) \\ P_2 &= Q_1(a,b) - \tfrac{1}{2}(1+\mu)I_0(ab)\exp\left[-\tfrac{1}{2}(a^2+b^2)\right] \quad (L=1) \end{aligned} \tag{C-25}$$

where, by definition,

$$a = \left(\tfrac{1}{2}\sum_{k=1}^{L}\left|\frac{\bar{X}_k}{\sqrt{m_{xx}}} - \frac{\bar{Y}_k}{\sqrt{m_{yy}}}\right|^2\right)^{1/2}$$
$$b = \left(\tfrac{1}{2}\sum_{k=1}^{L}\left|\frac{\bar{X}_k}{\sqrt{m_{xx}}} + \frac{\bar{Y}_k}{\sqrt{m_{yy}}}\right|^2\right)^{1/2} \tag{C-26}$$
$$Q_1(a, b) = \int_b^\infty x \exp\left[-\tfrac{1}{2}(a^2 + x^2)\right] I_0(ax)\, dx$$

$I_n(x)$ is the modified Bessel function of the first kind and of order n.

Let us evaluate the constants a and b when the channel is time-invariant, $\mu = 0$, and the channel gain and phase estimates are those given in Section C-1. Recall that when signal $s_1(t)$ is transmitted, the matched filter output is $X_k = 2\mathscr{E}g_k + N_k$. The clairvoyant estimate is given by (C-5). Hence, for this estimate, the moments are $\bar{X}_k = 2\mathscr{E}g_k$, $\bar{Y}_k = g_k$, $m_{xx} = 4\mathscr{E}N_0$, and $m_{yy} = N_0/\mathscr{E}v$, where $\mathscr{E}$ is the signal energy, N_0 is the value of the noise spectral density, and v is defined in (C-23). Substitution of these moments into (C-26) results in the following expressions for a and b:

$$a = \sqrt{\tfrac{1}{2}\gamma_b}\,|\sqrt{v} - 1|$$
$$b = \sqrt{\tfrac{1}{2}\gamma_b}\,|\sqrt{v} + 1| \tag{C-27}$$
$$\gamma_b = \frac{\mathscr{E}}{N_0}\sum_{k=1}^{L}|g_k|^2$$

This is a result originally derived by Price (1962).

The probability of error for differential phase signaling can be obtained by setting $v = 1$ in (C-27).

Next, consider a pilot signal estimate. In this case, the estimate is given by (C-4) and the matched filter output is again $X_k = 2\mathscr{E}g_k + N_k$. When the moments are calculated and these are substituted into (C-26), the following expressions for a and b are obtained:

$$a = \sqrt{\frac{\gamma_t}{2}}\left|\sqrt{\frac{v}{r+1}} - \sqrt{\frac{r}{r+1}}\right|$$
$$b = \sqrt{\frac{\gamma_t}{2}}\left(\sqrt{\frac{v}{r+1}} + \sqrt{\frac{r}{r+1}}\right) \tag{C-28}$$

where

$$\gamma_t = \frac{\mathscr{E}_t}{N_0}\sum_{k=1}^{L}|g_k|^2$$
$$\mathscr{E}_t = \mathscr{E} + \mathscr{E}_p$$
$$r = \mathscr{E}/\mathscr{E}_p$$

Finally, we consider the probability of a binary digit error for four-phase signaling over a time-invariant channel for which the condition $\mu = 0$ obtains. One approach that can be used to derive this error probability is to determine the pdf of θ and then to integrate this over the appropriate range of values of θ. Unfortunately, this approach proves to be intractable mathematically. Instead, a simpler, albeit roundabout, method may be used that involves the Laplace transform. In short, the integral in (14-4-14) of the text that relates the error probability $P_2(\gamma_b)$ in an AWGN channel to the error

TABLE C-2 TIME-INVARIANT CHANNEL

Type of estimate	a	b
	Two-phase signaling	
Clairvoyant estimate	$\sqrt{\frac{1}{2}\gamma_b}\lvert\sqrt{\nu}-1\rvert$	$\sqrt{\frac{1}{2}\gamma_b}(\sqrt{\nu}+1)$
Differential phase signaling	0	$\sqrt{2\gamma_b}$
Pilot signal estimate	$\sqrt{\frac{\gamma_t}{2}}\left\lvert\sqrt{\frac{\nu}{r+1}}-\sqrt{\frac{r}{r+1}}\right\rvert$	$\sqrt{\frac{\gamma_t}{2}}\left(\sqrt{\frac{\nu}{r+1}}+\sqrt{\frac{r}{r+1}}\right)$
	Four-phase signaling	
Clairvoyant estimate	$\sqrt{\frac{1}{2}\gamma_b}\lvert\sqrt{\nu+1+\sqrt{\nu^2+1}}$ $-\sqrt{\nu+1-\sqrt{\nu^2+1}}\rvert$	$\sqrt{\frac{1}{2}\gamma_b}(\sqrt{\nu+1-\sqrt{\nu^2+1}}$ $+\sqrt{\nu+1-\sqrt{\nu^2+1}})$
Differential phase signaling	$\sqrt{\frac{1}{2}\gamma_b}(\sqrt{2+\sqrt{2}}-\sqrt{2-\sqrt{2}})$	$\sqrt{\frac{1}{2}\gamma_b}(\sqrt{2+\sqrt{2}}+\sqrt{2-\sqrt{2}})$
Pilot signal estimate	$\sqrt{\frac{\gamma_t}{4(r+1)}}\lvert\sqrt{\nu+r+\sqrt{\nu^2+r^2}}$ $-\sqrt{\nu+r-\sqrt{\nu^2+r^2}}\rvert$	$\sqrt{\frac{\gamma_t}{4(r+1)}}(\sqrt{\nu+r+\sqrt{\nu^2+r^2}}$ $+\sqrt{\nu+r-\sqrt{\nu^2+r^2}})$

probability P_2 in a Rayleigh fading channel is a Laplace transform. Since the bit error probabilities P_2 and P_{4h} for a Rayleigh fading channel, given by (C-18) and (C-21), respectively, have the same form but differ only in the correlation coefficient, it follows that the bit error probabilities for the time-invariant channel also have the same form. That is, (C-25) with $\mu = 0$ is also the expression for the bit error probability of a four-phase signaling system with the parameters a and b modified to reflect the difference in the correlation coefficient. The detailed derivation may be found in the paper by Proakis (1968). The expressions for a and b are given in Table C-2.

APPENDIX **D**

SQUARE-ROOT FACTORIZATION

Consider the solution of the set of linear equations

$$\mathbf{R}_N\mathbf{C}_N = \mathbf{U}_N \tag{D-1}$$

where $\mathbf{R}_N$ is an $N \times N$ positive-definite symmetric matrix, $\mathbf{C}_N$ is an N-dimensional vector of coefficients to be determined, and $\mathbf{U}_N$ is an arbitrary N-dimensional vector. The equations in (D-1) can be solved efficiently by expressing $\mathbf{R}_N$ in the factored form

$$\mathbf{R}_N = \mathbf{S}_N\mathbf{D}_N\mathbf{S}_N' \tag{D-2}$$

where $\mathbf{S}_N$ is a lower triangular matrix with elements $\{s_{ik}\}$ and $\mathbf{D}_N$ is a diagonal matrix with diagonal elements $\{d_k\}$. The diagonal elements of $\mathbf{S}_N$ are set to unity, i.e., $s_{ii} = 1$. Then we have

$$\begin{aligned} r_{ij} &= \sum_{k=1}^{j} s_{ik}d_k s_{jk}, \quad 1 \leq j \leq i-1, \quad i \geq 2 \\ r_{11} &= d_1 \end{aligned} \tag{D-3}$$

where $\{r_{ij}\}$ arte the elements of $\mathbf{R}_N$. Consequently, the elements $\{s_{ik}\}$ and $\{d_k\}$ are determined from (D-3) according to the equations

$$\begin{aligned} d_1 &= r_{11} \\ s_{ij}d_j &= r_{ij} - \sum_{k=1}^{j-1} s_{ik}d_k s_{jk}, \quad 1 \leq j \leq i-1, \quad 2 \leq i \leq N \\ d_i &= r_{ii} - \sum_{k=1}^{i-1} s_{ik}^2 d_k, \quad 2 \leq i \leq N \end{aligned} \tag{D-4}$$

Thus, (D-4) define $\mathbf{S}_N$ and $\mathbf{D}_N$ in terms of the elements of $\mathbf{R}_N$.

The solution to (D-1) is performed in two steps. With (D-2) substituted into (D-1) we have

$$\mathbf{S}_N\mathbf{D}_N\mathbf{S}_N'\mathbf{C}_N = \mathbf{U}_N$$

Let

$$\mathbf{Y}_N = \mathbf{D}_N\mathbf{S}_N'\mathbf{C}_N \tag{D-5}$$

Then

$$\mathbf{S}_N\mathbf{Y}_N = \mathbf{U}_N \tag{D-6}$$

First we solve (D-6) for $\mathbf{Y}_N$. Because of the triangular form of $\mathbf{S}_N$, we have

$$\begin{aligned} y_1 &= u_1 \\ y_i &= u_i - \sum_{j=1}^{i-1} s_{ij} y_j, \qquad 2 \le i \le N \end{aligned} \tag{D-7}$$

Having obtained $\mathbf{Y}_N$, the second step is to compute $\mathbf{C}_N$. That is,

$$\mathbf{D}_N\mathbf{S}_N'\mathbf{C}_N = \mathbf{Y}_N$$
$$\mathbf{S}_N'\mathbf{C}_N = \mathbf{D}_N^{-1}\mathbf{Y}_N$$

Beginning with

$$c_N = y_N/d_N \tag{D-8}$$

the remaining coefficients of $\mathbf{C}_N$ are obtained recursively as follows:

$$c_i = \frac{y_i}{d_i} - \sum_{j=i+1}^{N} s_{ij} c_j, \qquad 1 \le i \le N-1 \tag{D-9}$$

The number of multiplications and divisions required to perform the factorization of $\mathbf{R}_N$ is proportional to N^3. The number of multiplications and divisions required to compute $\mathbf{C}_N$, once $\mathbf{S}_N$ is determined, is proportional to N^2. In contrast, when $\mathbf{R}_N$ is Toeplitz the Levinson–Durbin algorithm should be used to determine the solution of (D-1), since the number of multiplications and divisions is proportional to N^2. On the other hand, in a recursive least-squares formulation, $\mathbf{S}_N$ and $\mathbf{D}_N$ are not computed as in (D-3), but they are updated recursively. The update is accomplished with N^2 operations (multiplications and divisions). Then the solution for the vector $\mathbf{C}_N$ follows the steps (D-5)–(D-9). Consequently, the computational burden of the recursive least-squares formulation is proportional to N^2.

REFERENCES AND BIBLIOGRAPHY

Abend, K. and Fritchman, B. D. (1970). "Statistical Detection for Communication Channels with Intersymbol Interference," *Proc. IEEE*, pp. 779–785, May.

Abramson, N. (1963). *Information Theory and Coding*, McGraw-Hill, New York.

Abramson, N. (1970). "The ALOHA System—Another Alternative for Computer Communications," *1970 Fall Joint Comput. Conf., AFIDS Conf. Proc.*, vol. 37, pp. 281–285, AFIPS Press, Montvale, N.J.

Abramson, N. (1977). "The Throughput of Packet Broadcasting Channels," *IEEE Trans. Commun.*, vol. COM-25, pp. 117–128, January.

Abramson, N. (1993). *Multiple Access Communications*, IEEE Press, New York.

Adler, R. L., Coppersmith, D., and Hassner, M. (1983). "Algorithms for Sliding Block Codes," *IEEE Trans. Inform. Theory*, vol. IT-29, pp. 5–22, January.

Al-Hussaini, E. and Al-Bassiouni (1985). "Performance of MRC Diversity Systems for the Detection of Signals with Nakagami Fading," *IEEE Trans. Commun.*, vol. COM-33, pp. 1315–1319, December.

Altekar, S. A. and Beaulieu, N. C. (1993). "Upper Bounds on the Error Probability of Decision Feedback Equalization," *IEEE Trans. Inform. Theory*, vol. IT-39, pp. 145–156, January.

Anderberg, M. R. (1973). *Cluster Analysis for Applications*, Academic, New York.

Anderson, J. B., Aulin, T., and Sundberg, C. W. (1986). *Digital Phase Modulation*, Plenum, New York.

Anderson, R. R. and Salz, J. (1965). "Spectra of Digital FM," *Bell Syst. Tech. J.*, vol. 44 pp. 1165–1189, July–August.

Ash, R. B. (1965). *Information Theory*, Interscience, New York.

Aulin, T. (1980). "Viterbi Detection of Continuous Phase Modulated Signals," *Nat. Telecommun. Conf. Record*, pp. 14.2.1–14.2.7, Houston, Texas, November.

Aulin, T., Rydbeck, N., and Sundberg, C. W. (1981). "Continuous Phase Modulation—Part II: Partial Response Signaling," *IEEE Trans. Commun.*, vol. COM-29, pp. 210–225, March.

Aulin, T. and Sundberg, C. W. (1981). "Continuous Phase Modulation—Part I: Full Response Signaling," *IEEE Trans. Commun.*, vol. COM-29, pp. 196–209, March.

Aulin, T. and Sundberg, C. W. (1982a). "On the Minimum Euclidean Distance for a Class of Signal Space Codes," *IEEE Trans. Inform. Theory*, vol. IT-28, pp. 43–55, January.

Aulin, T. and Sundberg, C. W. (1982b). "Minimum Euclidean Distance and Power Spectrum for a Class of Smoothed Phase Modulation Codes with Constant Envelope," *IEEE Trans. Commun.*, vol. COM-30, pp. 1721–1729, July.

Aulin, T. and Sundberg, C. W. (1984). "CPM—An Efficient Constant Amplitude Modulation Scheme," *Int. J. Satellite Commun.*, vol. 2, pp. 161–186.

Austin, M. E. (1967). "Decision-Feedback Equalization for Digital Communication Over Dispersive Channels," MIT Lincoln Laboratory, Lexington, Mass., Tech. Report No. 437, August

Barrow, B. (1963). "Diversity Combining of Fading Signals with Unequal Mean Strengths," *IEEE Trans. Commun., Syst.*, vol. CS-11, pp. 73–78, March.

Beaulieu, N. C. (1990). "An Infinite Series for the Computation of the Complementary Probability Distribution Function of a Sum of Independent Random Variables and Its Application to the Sum of Rayleigh Random Variables," *IEEE Trans. Commun.*, vol. COM-38, pp. 1463–1474, September.

Beaulieu, N. C. and Abu-Dayya, A. A. (1991). "Analysis of Equal Gain Diversity on Nakagami Fading Channels," *IEEE Trans. Commun.*, vol. COM-39, pp. 225–234, February.

Bekir, N. E., Scholtz, R. A., and Welch, L. R. (1978). "Partial-Period Correlation Properties of PN Sequences," *1978 Nat. Telecommun. Conf. Record*, pp. 35.1.1–25.1.4, Birmingham, Alabama, November.

Belfiore, C. A. and Park, J. H., Jr. (1979). "Decision-Feedback Equalization," *Proc. IEEE*, vol. 67, pp. 1143–1156, August.

Bellini, J. (1986). "Bussgang Techniques for Blind Equalization," *Proc. GLOBECOM'86*, pp. 46.1.1–46.1.7, Houston, Texas, December.

Bello, P. A. and Nelin, B. D. (1962a). "Predetection Diversity Combining with Selectivity Fading Channels," *IRE Trans. Commun. Syst.*, vol. CS-10, pp. 32–42, March.

Bello, P. A. and Nelin, B. D. (1962b). "The Influence of Fading Spectrum on the Binary Error Probabilities of Incoherent and Differentially Coherent Matched Filter Receivers," *IRE Trans. Commun. Syst.*, vol. CS-10, pp. 160–168, June.

Bello, P. A. and Nelin, B. D. (1963). "The Effect of Frequency Selective Fading on the Binary Error Probabilities of Incoherent and Differentially Coherent Matched Filter Receivers," *IEEE Trans. Commun. Syst.*, vol. CS-11, pp. 170–186, June.

Bennett, W. R. and Davey, J. R. (1965). *Data Transmission*, McGraw-Hill, New York.

Bennett, W. R. and Rice, S. O. (1963). "Spectral Density and Autocorrelation Functions Associated with Binary Frequency-Shift Keying," *Bell Syst. Tech. J.*, vol. 42, pp. 2355–2385, September.

Benveniste, A. and Goursat, M. (1984). "Blind Equalizers," *IEEE Trans. Commun.*, vol. COM-32, pp. 871–883, August.

Berger, T. (1971). *Rate Distortion Theory*, Prentice-Hall, Englewood Cliffs, N.J.

Berger, T. and Tufts, D. W. (1967). "Optimum Pulse Amplitude Modulation, Part I: Transmitter-Receiver Design and Bounds from Information Theory," *IEEE Trans. Inform. Theory*, vol. IT-13, pp. 196–208.

Bergmans, P. P. and Cover, T. M. (1974). "Cooperative Broadcasting," *IEEE Trans. Inform. Theory*, vol. IT-20, pp. 317–324, May.

Berlekamp, E. R. (1968). *Algebraic Coding Theory*, McGraw-Hill, New York.

Berlekamp, E. R. (1973). "Goppa Codes," *IEEE Trans. Inform. Theory*, vol. IT-19, pp. 590–592.

Berlekamp, E. R. (1974). *Key Papers in the Development of Coding Theory*, IEEE Press, New York.

Bierman, G. J. (1977). *Factorization Methods for Discrete Sequential Estimation*, Academic, New York.

Biglieri, E., Divsalar, D., McLane, P. J., and Simon, M. K. (1991). *Introduction to Trellis-Coded Modulation with Applications*, Macmillan, New York.

Bingham, J. A. C. (1990). "Multicarrier Modulation for Data Transmission: An Idea Whose Time Has Come," *IEEE Commun. Mag.*, vol. 28, pp. 5–14, May.

Blahut, R. E. (1983). *Theory and Practice of Error Control Codes*, Addison-Wesley, Reading, Mass.

Blahut, R. E. (1987). *Principles and Practice of Information Theory*, Addison-Wesley, Reading, Mass.

Bose, R. C. and Ray-Chaudhuri, D. K. (1960a). "On a Class of Error Correcting Binary Group Codes," *Inform. Control*, vol. 3, pp. 68–79, March.

Bose, R. C. and Ray-Chaudhuri, D. K. (1960b). "Further Results in Error Correcting Binary Group Codes," *Inform. Control*, vol. 3, pp. 279–290, September.

Brennan, D. G. (1959). "Linear Diversity Combining Techniques," *Proc. IRE.*, vol. 47, pp. 1075–1102.

Busgang, J. J. (1952). "Crosscorrelation Functions of Amplitude-Distored Gaussian Signals," MIT RLE Tech. Report 216.

Bucher, E. A. (1980). "Coding Options for Efficient Communications on Non-Stationary Channels," *Rec. IEEE Int. Conf. Commun.*, pp. 4.1.1–4.1.7.

Burton, H. O. (1969). "A Class of Asymptotically Optimal Burst Correcting Block Codes," *Proc. ICCC*, Boulder, Col., June.

Buzo, A., Gray, A. H., Jr., Gray, R. M., and Markel, J. D. (1980). "Speech Coding Based Upon Vector Quantization," *IEEE Trans. Acoust., Speech, Signal Processing*, Vol. ASSP-28 pp. 562–574, October.

Cahn, C. R. (1960). "Combined Digital Phase and Amplitude Modulation Communication Systems," *IRE Trans. Commun. Syst.*, vol. CS-8, pp. 150–155, September.

Calderbank, A. R. and Sloane, N. J. A. (1987). "New Trellis Codes Based on Lattices and Cosets," *IEEE Trans. Inform. Theory*, vol. IT-33, pp. 177–195, March.

Campanella, S. J. and Robinson, G. S. (1971). "A Comparison of Orthogonal Transformations for Digital Speech Processing," *IEEE Trans. Commun.*, vol. COM-19, pp. 1045–1049, December.

Campopiano, C. N. and Glazer, B. G. (1962). "A Coherent Digital Amplitude and Phase Modulation Scheme," *IRE Trans. Commun. Syst.*, vol. CS-10, pp. 90–95, June.

Capetanakis, J. I. (1979). "Tree Algorithms for Packet Broadcast Channels," *IEEE Trans. Inform. Theory*, vol. IT-25, pp. 505–515, September.

Caraiscos, C. and Liu, B. (1984). "A Roundoff Error Analysis of the LMS Adaptive Algorithm," *IEEE Trans. Acoust., Speech, Signal Processing*, Vol. ASSP-32, pp. 34–41, January.

Carayannis, G., Manolakis, D. G., and Kalouptsidis, N. (1983). "A Fast Sequential Algorithm for Least-Squares Filtering and Prediction," *IEEE Trans. Acoust., Speech, Signal Processing*, Vol. ASSP-31, pp. 1394–1402, December.

Carayannis, G. Manolakis, D. G., and Kalouptsidis, N. (1986). "A Unified View of Parametric Processing Algorithms for Prewindowed Signals," *Signal Processing*, vol. 10, pp. 335–368, June.

Carleial, A. B. and Hellman, M. E. (1975). "Bistable Behavior of ALOHA-Type Systems," *IEEE Trans. Commun.*, vol. COM-23, pp. 401–410, April 1975.

Carlson, A. B. (1975). *Communication Systems*, McGraw-Hill, New York.

Chang, D. Y., Gersho, A., Ramamurthi, B., and Shohan, Y. (1984). "Fast Search Algorithms for Vector Quantization and Pattern Matching," *Proc. IEEE Int. Conf. Acoust., Speech, Signal Processing*, paper 9.11, San Diego, Calif., March.

Chang, R. W. (1966). "Synthesis of Band-Limited Orthogonal Signals for Multichannel Data Transmission," *Bell Syst. Tech. J.*, vol. 45, pp. 1775–1796, December.

Charash, U. (1979). "Reception Through Nakagami Fading Multipath Channels with Random Delays," *IEEE Trans. Commun.*, vol. COM-27, pp. 657–670, April.

Chase, D. (1972). "A Class of Algorithms for Decoding Block Codes With Channel Measurement Information," *IEEE Trans. Inform. Theory*, vol. IT-18, pp. 170–182, January.

Chase, D. (1976). "Digital Signal Design Concepts for a Time-Varying Ricean Channel," *IEEE Trans. Commun.*, vol. COM-24, pp. 164–172, February.

Chien, R. T. (1964). "Cyclic Decoding Procedures for BCH Codes," *IEEE Trans. Inform. Theory*, vol. IT-10, pp. 357–363, October.

Chow, J. S., Tu, J. C., and Cioffi, J. M. (1991). "A Discrete Multitone Transceiver System for HDSL Applications," *IEEE J. Selected Areas Commun.*, vol. SAC-9, pp. 895–908, August.

Chyi, G. T., Proakis, J. G., and Keller, C. M. (1988). "Diversity Selection/Combining Schemes with Excess Noise-Only Diversity Receptions Over a Rayleigh-Fading Multipath Channel." *Proc. Conf. Inform. Sci. Syst.*, Princeton University, Princeton, N.J. March.

Cioffi, J. M. and Kailath, T. (1984). "Fast Recursive-Least Squares Transversal Filters for Adaptive Filtering," *IEEE Trans. Acoust., Speech, Signal Processing*, vol. ASSP-32, pp. 304–337, April.

Cook, C. E., Ellersick, F. W., Milstein, L. B., and Schilling, D. L. (1983). *Spread Spectrum Communcations*, IEEE Press, New York.

Costas, J. P. (1956). "Synchronous Communications," *Proc. IRE*, vol. 44, pp. 1713–1718, December.

Cover, T. M. (1972). "Broadcast Channels," *IEEE Trans. Inform. Theory*, vol. IT-18, pp. 2–14, January.

Cramér, H. (1946). *Mathematical Methods of Statistics*, Princeton University Press, Princeton, N.J.

Daut, D. G., Modestino, J. W., and Wismer, L. D. (1982). "New Short Constraint Length Convolutional Code Construction for Selected Rational Rates," *IEEE Trans. Inform. Theory*, vol. IT-28, pp. 793–799, September.

Davenport, W. B., Jr. (1970). *Probability and Random Processes*, McGraw-Hill, New York.

Davenport, W. B. Jr. and Root, W. L. (1958). *Random Signals and Noise*, McGraw-Hill, New York.

Davisson, L. D. (1973). "Universal Noiseless Coding," *IEEE Trans. Inform. Theory*, vol. IT-19, pp. 783–795.

Davisson, L. D., McEliece, R. J., Pursley, M. B., and Wallace, M. S. (1981). "Efficient Universal Noiselss Source Codes," *IEEE Trans. Inform. Theory*, vol. IT-27, pp. 269–279.

deBuda, R. (1972). "Coherent Demodulation of Frequency Shift Keying with Low Deviation Ratio," *IEEE Trans. Commun.*, vol. COM-20, pp. 429–435, June.

Deller, J. P., Proakis, J. G., and Hansen, H. L. (1993). *Discrete-Time Processing of Speech Signals*, MacMillan, New York.

Ding, Z. (1990). *Application Aspects of Blind Adaptive Equalizers in QAM Data Communications*, Ph.D. Thesis, Department of Electrical Engineering, Cornell University.

Ding, Z., Kennedy, R. A., Anderson, B. D. O., and Johnson, C. R. (1989). "Existence and Avoidance of Ill-Convergence of Godard Blind Equalizers in Data Communication Systems," *Proc. 23rd Conf. on Inform. Sci. Systems*, Baltimore, Md.

Divsalar, D., Simon, M. K., and Yuen, J. H. (1987). "Trellis Coding with Asymmetric Modulation," *IEEE Trans. Commun.*, vol. COM-35, pp. 130–141, February.

Divsalar, D. and Yuen, J. H. (1984). "Asymmetric MPSK for Trellis Codes," *Proc. GLOBECOM'84*, pp. 20.6.1–20.6.8, Atlanta, Georgia, November.

Dixon, R. C. (1976). *Spread Spectrum Techniques*, IEEE Press, New York.

Doelz, M. L., Heald, E. T., and Martin, D. L. (1957). "Binary Data Transmission Techniques for Linear Systems," *Proc. IRE*, vol. 45, pp. 656–661, May.

Drouilhet, P. R., Jr. and Bernstein, S. L. (1969). "TATS—A Bandspread Modulation-Demodulation System for Multiple Access Tactical Satellite Communication," *1969 IEEE Electronics and Aersopace Systems (EASCON) Conv. Record*, Washington, D.C., pp. 126–132, October 27–29.

Duffy, F. P. and Tratcher, T. W. (1971). "Analog Transmission Performance on the Switched Telecommunications Network," *Bell Syst. Tech. J.*, vol. 50, pp. 1311–1347, April.

Durbin, J. (1959). "Efficient Estimation of Parameters in Moving-Average Models," *Biometrika*, vol. 46, parts 1 and 2, pp. 306–316.

Duttweiler, D. L., Mazo, J. E., and Messerschmitt, D. G. (1974). "Error Propagation in Decision-Feedback Equalizers," *IEEE Trans. Inform. Theory*, vol. IT-20, pp. 490–497, July.

Eleftheriou, E. and Falconer, D. D. (1987). "Adaptive Equalization Techniques for HF Channels," *IEEE J. Selected Areas Commun.*, vol. SAC-5 pp. 238–247, February.

El Gamal, A. and Cover, T. M. (1980). "Multiple User Information Theory," *Proc. IEEE*, vol. 68, pp. 1466–1483, December.

Elias, P. (1954). "Error-Free Coding," *IRE Trans. Inform. Theory*, vol. IT-4, pp. 29–37, September.

Elias, P. (1955). "Coding for Noisy Channels," *IRE Convention Record*, vol. 3, part 4, 37–46.

Esposito, R. (1967). "Error Probabilities for the Nakagami Channel," *IEEE Trans. Inform. Theory*, vol. IT-13, pp. 145–148, January.

Eyuboglu, V. M. (1988). "Detection of Coded Modulation Signals on Linear, Severely Distorted Channels Using Decision-Feedback Noise Prediction with Interleaving," *IEEE Trans. Commun.*, vol. COM-36, pp. 401–409, April.

Falconer, D. D. (1976). "Jointly Adaptive Equalization and Carrier Recovery in Two-Dimensional Digital Communication Systems," *Bell Syst. Tech. J.*, vol. 55, pp. 317–334, March.

Falconer, D. D. and Ljung, L. (1978). "Application of Fast Kalman Estimation to Adaptive Equalization," *IEEE Trans. Commun.*, vol. COM-26, pp. 1439–1446, October.

Falconer, D. D. and Salz, J. (1977). "Optimal Reception of Digital Data Over the Gaussian Channel with Unknown Delay and Phase Jitter," *IEEE Trans. Inform. Theory*, vol. IT-23, pp. 117–126, January.

Fano, R. M. (1961). *Transmission of Information*, MIT Press, Cambridge, Mass.

Fano, R. M. (1963). "A Heuristic Discussion of Probabilistic Coding," *IEEE Trans. Inform. Theory*, vol. IT-9, pp. 64–74, April.

Feinstein, A. (1958). *Foundations of Information Theory*, McGraw-Hill, New York.

Fire, P. (1959). "A Class of Multiple-Error-Correcting Binary Codes for Non-Independent Errors," Sylvania Report No. RSL-E-32, Sylvania Electronic Defense Laboratory, Mountain View, Calif., March.

Flanagan, J. L., et al. (1979). "Speech Coding," *IEEE Trans. Commun.*, vol. COM-27, pp. 710–736, April.

Forney, G. D., Jr. (1965). "One Decoding BCH Codes," *IEEE Trans. Inform. Theory*, vol. IT-11, pp. 549–557, October.

Forney, G. D., Jr. (1966a). *Concatenated Codes*, MIT Press, Cambridge, Mass.

Forney, G. D., Jr. (1966b). "Generalized Minimum Distance Decoding," *IEEE Trans. Inform. Theory*, vol. IT-12, pp. 125–131, April.

Forney, G. D., Jr. (1968). "Exponential Error Bounds for Erasure, List, and Decision-Feedback Schemes," *IEEE Trans. Inform. Theory*, vol. IT-14, pp. 206–220, March.

Forney, G. D., Jr. (1970a). "Coding and Its Application in Space Communications," *IEEE Spectrum*, vol. 7, pp. 47–58, June.

Forney, G. D., Jr. (1970b). "Convolutional Codes I: Algebraic Structure," *IEEE Trans. Inform. Theory*, vol. IT-16, pp. 720–738, November.

Forney, G. D., Jr. (1971). "Burst Correcting Codes for the Classic Bursty Channel," *IEEE Trans. Commun. Tech.*, vol. COM-19, pp. 772–781, October.

Forney, G. D., Jr. (1972). "Maximum-Likelihood Sequence Estimation of Digital Sequences in the Presence of Intersymbol Interference," *IEEE Trans. Inform. Theory*, vol. IT-18, pp. 363–378, May.

Forney, G. D., Jr. (1974). "Convolutional Codes III: Sequential Decoding," *Inform. Control*, vol. 25, pp. 267–297, July.

Forney, G. D., Jr. (1988). "Coset Codes I: Introduction and Geometrical Classification," *IEEE Trans. Inform. Theory*, vol. IT-34, pp. 671–680, September.

Forney, G. D., Jr., Gallager, R. G., Lang, G. R., Longstaff, F. M., and Qureshi, S. U. (1984). "Efficient Modulation for Band-Limited Channels," *IEEE J. Selected Areas Commun.*, vol. SAC-2, pp. 632–647, September.

Foschini, G. J. (1984). "Contrasting Performance of Faster-Binary Signaling with QAM," *Bell Syst. Tech. J.*, vol. 63, pp. 1419–1445, October.

Foschini, G. J. (1985). "Equalizing Without Altering or Detecting Data, *Bell Syst. Tech. J.*, vol. 64, pp. 1885–1911, October.

Foschini, G. J., Gitlin, R. D., and Weinstein, S. B. (1974). "Optimization of Two-Dimensional Signal Constellations in the Presence of Gaussian Noise," *IEEE Trans. Commun.*, vol. COM-22, pp. 28–38, January.

Franaszek, P. A. (1968). "Sequence-State Coding for Digital Transmission," *Bell Syst. Tech. J.*, vol. 27, p. 143.

Franaszek, P. A. (1969). "On Synchronous Variable Length Coding for Discrete Noiseless Channels," *Inform. Control*, vol. 15, pp. 155–164.

Franaszek, P. A. (1970). "Sequence-State Methods for Run-Length-Limited Coding," *IBM J. Res. Dev.*, pp. 376–383, July.

Franks, L. E. (1969). *Signal Theory*, Prentice-Hall, Englewood Cliff, N.J.

Franks, L. E. (1983). "Carrier and Bit Synchronization in Data Communication—A Tutorial Review," *IEEE Trans. Commun.*, vol. COM-28, pp. 1107–1121, August.

Franks, L. E. (1981). "Synchronization Subsystems: Analysis and Design," *in Digital Communications, Satellite/Earth Station Engineering*, K. Feher (ed.), Prentice-Hall, Englewood Cliffs, N.J.

Fredricsson, S. (1975). "Pseudo-Randomness Properties of Binary Shift Register Sequences," *IEEE Trans. Inform. Theory*, vol. IT-21, pp. 115–120, January.

Freiman, C. E. and Wyner, A. D. (1964). "Optimum Block Codes for Noiseless Input Restricted Channels," *Inform. Control*, vol. 7, pp. 398–415.

Gaarder, N. T. (1971). "Signal Design for Fast-Fading Gaussian Channels," *IEEE Trans. Inform. Theory*, vol. IT-17, pp. 247–256, May.

Gabor, A. (1967). "Adaptive Coding for Self Clocking Recording," *IEEE Trans. Electronic Comp.* vol. EC-16, p. 866.

Gallager, R. G. (1965). "Simple Derivation of the Coding Theorem and Some Applications," *IEEE Trans. Inform. Theory*, vol. IT-11, pp. 3–18, January.

Gallager, R. G. (1968). *Information Theory and Reliable Communication*, Wiley, New York.

Gardner, F. M. (1979). *Phaselock Techniques*, Wiley, New York.

Gardner, W. A. (1984). "Learning Characteristics of Stochastic-Gradient Descent Algorithms: A General Study, Analysis, and Critique," *Signal Processing*, vol. 6, pp. 113–133, April.

George, D. A., Bowen, R. R., and Storey, J. R. (1971). "An Adaptive Decision-Feedback Equalizer," *IEEE Trans. Commun. Tech.*, vol. COM-19, pp. 281–293, June.

Gersho, A. (1982). "On the Structure of Vector Quantizers," *IEEE Trans. Inform. Theory*, vol. IT-28, pp. 157–166, March.

Gersho, A. and Gray, R. M. (1992). *Vector Quantization and Signal Compression*, Kluwer Academic Publishers, Boston.

Gersho, A. and Lawerence, V. B. (1984). "Multidimensional Signal Constellations for Voiceband Data Transmission," *IEEE J. Selected Areas Commun.*, vol. SAC-2, pp. 687–702, September.

Gerst, I. and Diamond, J. (1961). "The Elimination of Intersymbol Interference by Input Pulse Shaping," *Proc. IRE*, vol. 53, July.

Ghez, S., Verdu, S., and Schwartz, S. C. (1988). "Stability Properties of Slotted Aloha with Multipacket Reception Capability," *IEEE Trans. Autom. Control*, vol. 33, pp. 640–649, July.

Ghosh, M. and Weber, C. L. (1991). "Maximum likelihood Blind Equalization," *Proc. 1991 SPIE Conf.*, San Diego, Calif. July.

Gilbert, E. N. (1952). "A Comparison of Signaling Alphabets," *Bell Syst. Tech. J.*, vol. 31, pp. 504–522, May.

Gilhousen, K. S., Jacobs, I. M., Podovani, R., Viterbi, A. J., Weaver, L. A., and Wheatley, G. E. III (1991). "On the Capacity of a Cellular CDMA System," *IEEE Trans. Vehicular Tech.*, vol. 40, pp. 303–312, May.

Gitlin, R. D. Meadors, H. C., and Weinstein, S. B. (1982). "The Tap Leakage Algorithm: An Algorithm for the Stable Operation of a Digitally Implemented Fractionally Spaced, Adaptive Equalizer," *Bell Syst. Tech. J.*, vol. 61, pp. 1817–1839, October.

Gitlin, R. D. and Weinstein, S. B. (1979). "On the Required Tap-Weight Precision for Digitally Implemented Mean-Squared Equalizers," *Bell Syst. Tech. J.*, vol. 58, pp. 301–321, February.

Gitlin, R. D. and Weinstein, S. B. (1981). "Fractionally-Spaced Equalization: An Improved Digital Transversal Equalizer," *Bell Syst. Tech. J.*, vol. 60, pp. 275–296, February.

Glave, F. E. (1972). "An Upper Bound on the Probability of Error due to Intersymbol Interference for Correlated Digital Signals," *IEEE Trans. Inform. Theory*, vol. IT-18, pp. 356–362, May.

Goblick, T. J., Jr. and Holsinger, J. L. (1967). "Analog Source Digitization: A Comparison of Theory and Practice," *IEEE Trans. Inform. Theory*, vol. IT-13, pp. 323–326, April.

Godard, D. N. (1974). "Channel Equalization Using a Kalman Filter for Fast Data Transmission," *IBM J. Res. Dev.*, vol. 18, pp. 267–273, May.

Godard, D. N. (1980). "Self-Recovering Equalization and Carrier Tracking in Two-Dimensional Data Communications Systems," *IEEE Trans. Commun.*, vol. COM-28, pp. 1867–1875, November.

Golay, M. J. E. (1949). "Note on Digital Coding," *Proc. IRE*, vol. 37, p. 657, June.

Gold, R. (1967). "Optimal Binary Sequences for Spread Spectrum Multiplexing," *IEEE Trans. Inform. Theory*, vol. IT-13, pp. 619–621, October.

Gold, R. (1968). "Maximal Recursive Sequences with 3-Valued Recursive Cross Correlation Functions," *IEEE Trans. Inform. Theory*, vol. IT-14, pp. 154–156, January.

Golomb, S. W. (1967). *Shift Register Sequences*, Holden-Day, San Francisco, Calif.

Goppa, V. D. (1970). "New Class of Linear Correcting Codes," *Probl. Peredach. Inform.*, vol. 6, pp. 24–30.

Goppa, V. D. (1971). "Rational Presentation of Codes and (L, g)-Codes," *Probl. Peredach. Inform.*, vol 7, pp. 41–49.

Gray, R. M. (1975). "Sliding Block Source Coding," *IEEE Trans. Inform. Theory*, vol. IT 21, pp. 357–368, July.

Gray, R. M. (1990). *Source Coding Theory*, Kluwer Academic Publishers, Boston.

Greefkes, J. A. (1970). "A Digitally Companded Delta Modulation Modem for Speech Transmission," *Proc. IEEE Int. Conf. on Commun.* pp. 7.33–7.48, June.

Green, P. E., Jr. (1962). "Radar Astronomy Measurement Techniques," MIT Lincoln Laboratory, Lexington, Mass., Tech. Report No. 282, December.

Gronemeyer, S. A. and McBride, A. L. (1976). "MSK and Offset QPSK Modulation," *IEEE Trans. Commun.*, vol. COM-24, pp. 809–820, August.

Gupta, S. C. (1975). "Phase-Locked Loops," *Proc. IEEE*, vol. 63, pp. 291–306, February.

Hahn, P. M. (1962). "Theoretical Diversity Improvement in Multiple Frequency Shift Keying," *IRE Trans. Commun. Syst.*, vol. CS-10, pp. 177–184, June.

Hamming, R. W. (1950). "Error Detecting and Error Correcting Codes," *Bell Syst. Tech. J.*, vol. 29, pp. 147–160, April.

Hamming, R. W. (1986). *Coding and Information Theory*, Prentice-Hall, Englewood Cliffs, N.J.

Hancock, J. C. and Lucky, R. W. (1960). "Performance of Combined Amplitude and Phase-Modulated Communication Systems," *IRE Trans. Commun. Syst.*, vol. CS-8, pp. 232–237, December.

Hartley, R. V. (1928). "Transmission of Information," *Bell Syst. Tech. J.*, vol. 7, p. 535.

Hatzinakos, D. and Nikias, C. L. (1991). "Blind Equalization Using a Tricepstrum-Based Algorithm," *IEEE Trans. Commun.*, vol. COM-39, pp. 669–682, May.

Hecht, M. and Guida, A. (1969). "Delay Modulation," *Proc. IEEE*, vol. 57, pp. 1314–1316, July.

Heller, J. A. (1968). "Short Constraint Length Convolutional Codes," Jet Propulsion Laboratory, California Institue of Technology, Pasadena, Calif., *Space Program Summary* 37–54, vol. 3, pp. 171–174, December.

Heller, J. A. (1975). "Feedback Decoding of Convolutional Codes," in *Advances in Communication Systems*, vol. 4, A. J. Viterbi (ed.), Academic, New York.

Heller, J. A. and Jacobs, I. M. (1971). "Viterbi Decoding for Satellite and Space Commmunication," *IEEE Trans. Commun. Tech.*, vol. COM-19, pp. 835–848, October.

Helstrom, C. W. (1955). "The Resolution of Signals in White Gaussian Noise," *Proc. IRE*, vol. 43, pp. 1111–1118, September.

Helstrom, C. W. (1968). *Statistical Theory of Signal Detection*, Pergamon, London.
Helstrom, C. W. (1991). *Probability and Stochastic Processes for Engineers*, Macmillan, New York.
Hildebrand, F. B. (1960). *Methods of Applied Mathematics*, Prentice-Hall, Englewood Cliffs, N.J.
Hirosaki, B. (1981). "An Orthogonality Multiplexed QAM System Using the Discrete Fourier Transform," *IEEE Trans. Commun.*, vol. COM-29, pp. 982–989, July.
Hirosaki, B., Hasegawa, S., and Sabato, A. (1986). "Advanced Group-Band Modem Using Orthogonally Multiplexed QAM Techniques," *IEEE Trans. Commun.*, vol. COM-34, pp. 587–592, June.
Ho, E. Y. and Yeh, Y. S. (1970). "A New Approach for Evaluating the Error Probability in the Presence of Intersymbol Interference and Additive Gaussian Noise," *Bell Syst. Tech. J.*, vol. 49, pp. 2249–2265, November.
Hocquenghem, A. (1959). "Codes Correcteurs d'Erreurs," *Chiffres*, vol. 2, pp. 147–156.
Holmes, J. K. (1982). *Coherent Spread Spectrum Systems*, Wiley-Interscience, New York.
Horwood, D. and Gagliardi, R. (1975). "Signal Design for Digital Multiple Access Communications," *IEEE Trans. Commun.*, vol. COM-23, pp. 378–383, March.
Hsu, F. M. (1982). "Square-Root Kalman Filtering for High-Speed Data Received over Fading Dispersive HF Channels," *IEEE Trans. Inform. Theory*, vol. IT-28, pp. 753–763, September.
Huffman, D. A. (1952). "A Method for the Construction of Minimum Redundancy Codes," *Proc. IRE*, vol. 40, pp. 1098–1101, September.
Hui, J. Y. N. (1984). "Throughput Analysis for Code Division Multiple Accessing of the Spread Spectrum Channel," *IEEE J. Selected Areas Commun.*, vol. SAC-2, pp. 482–486, July.
Immink, K. A. S. (1990). "Runlength-Limited Sequences," *Proc. IEEE*, vol. 78, pp. 1745–1759, November.
Itakura, F. (1975). "Minimum Prediction Residual Principle Applied to Speech Recognition," *IEEE Trans. Acoust., Speech, Signal Processing*, vol. ASSP-23, pp. 67–72, February.
Itakura, F. and Saito, S. (1968). "Analysis Synthesis Telephony Based on the Maximum-Likelihood Methods," *Proc. 6th Int. Congr. Acoust.*, Tokyo, Japan, pp. C17–C20.
Jacobs, I. M. (1974). "Practial Applications of Coding," *IEEE Trans. Inform. Theory*, vol. IT-20, pp. 305–310, May.
Jacoby, G. V. (1977). "A New Look-Ahead Code for Increased Data Density," *IEEE Trans. Magnetics*, vol. MAG-13, 1202–1204.
Jayant, N. S. (1970). "Adaptive Delta Modulation with a One-Bit Memory," *Bell Syst. Tech. J.*, pp. 321–342, March.
Jayant, N. S. (1974). "Digital Coding of Speech Waveforms: PCM, DPCM, and DM Quantizers," *Proc. IEEE*, vol. 62, pp. 611–632, May.
Jayant, N. S. (1976). *Waveform Quantization and Coding*, IEEE Press, New York.
Jayant, N. S. and Noll, P. (1984). *Digital Coding of Waveforms*, Prentice-Hall, Englewood Cliffs, N.J.
Jelinek, F. (1968). *Probabilistic Information Theory*, McGraw-Hill, New York.
Jelinek, F. (1969). "Fast Sequential Decoding Algorithm Using a Stack," *IBM J. Res. Dev.*, vol. 13, pp. 675–685, November.
Johnson, C. R. (1991). "Admissibility in Blind Adaptive Channel Equalization," *IEEE Control Syst. Mag.*, pp. 3–15, January.
Jones, S. K., Cavin, R. K. and Reed, W. M. (1982). "Analysis of Error-Gradient Adaptive Linear Equalizers for a Class of Stationary-Dependent Processes," *IEEE Trans. Inform. Theory*, vol. IT-28, pp. 318–329, March.
Jordan, K. L., Jr. (1966). "The Performance of Sequential Decoding in Conjunction with Efficient Modulation," *IEEE Trans. Commun. Syst.*, vol. CS-14, pp. 283–287, June.
Justesen, J. (1972). "A Class of Constructive Asymptotically Good Algebraic Codes," *IEEE Trans. Inform. Theory*, vol. IT-18, pp. 652–656, September.
Kailath, T. (1960). "Correlation Detection of Signals Perturbed by a Random Channel," *IRE Trans. Inform. Theory*, vol. IT-6, pp. 361–366, June.

Kailath, T. (1961). "Channel Characterization: Time-Variant Dispersive Channels, In *Lectures on Communication System Theory*, Chap. 6. E. Baghdady (ed.), McGraw-Hill, New York.

Kalet, I. (1989). "The Multitone Channel," *IEEE Trans. Commun.*, vol. COM-37, pp. 119–124, February.

Karabed, R. and Siegel, P. H. (1991). "Matched-Spectral Null Codes for Partial-Response Channels," *IEEE Trans. Inform. Theory*, vol. IT-37, pp. 818–855, May.

Kasami, T. (1966). "Weight Distribution Formula for Some Class of Cyclic Codes," Coordinated Science Laboratory, University of Illinois, Urbana, Ill., Tech. Report No. R-285, April.

Kaye, A. R. and George, D. A. (1970). "Transmission of Multiplexed PAM Signals over Multiple Channel and Diversity Systems," *IEEE Trans. Commun.*, vol. COM-18, pp. 520–525, October.

Kelly, E. J., Reed, I. S., and Root, W. L. (1960). "The Detection of Radar Echoes in Noise, Pt. I." *J. SIAM*, vol. 8, pp. 309–341, September.

Kleinrock, L. and Tobagi, F. A. (1975). "Packet Switching in Radio Channels: Part I—Carrier Sense Multiple-Access Modes and Their Throughput-Delay Characteristics," *IEEE Trans. Commun.*, vol. COM-23, pp. 1400–1416, December.

Kobayashi, H. (1971). "Simultaneous Adaptive Estimation and Decision Algorithm for Carrier Modulated Data Transmission Systems," *IEEE Trans. Commun. Tech.*, vol. COM-19, pp. 268–280, June.

Kotelnikov, V. A. (1947). "The Theory of Optimum Noise Immunity," Ph.D. Dissertation, Molotov Energy Institute, Moscow. [Translated by R. A. Silverman, McGraw-Hill, New York.]

Kretzmer, E. R. (1966). "Generalization of a Technique for Binary Data Communication," *IEEE Trans. Commun. Tech.*, vol. COM-14, pp. 67–68, February.

Larsen, K. J. (1973). "Short Convolutional Codes with Maximal Free Distance for Rates 1/2, 1/3, and 1/4," *IEEE Trans. Inform. Theory*, vol. IT-19, pp. 371–372, May.

Lender, A. (1963). "The Duobinary Technique for High Speed Data Transmission," *AIEE Trans. Commun. Electronics*, vol. 82, pp. 214–218.

Leon-Garcia, A. (1994). *Probability and Random Processes for Electrical Engineering*, Addison-Wesley, Reading, Mass.

Levinson, N. (1947). "The Wiener RMS (Root Mean Square) Error Criterion in Filter Design and Prediction," *J. Math. and Phys.*, vol. 25, pp. 261–278.

Lin, S. and Costello, D. J., Jr. (1983). *Error Control Coding: Fundamentals and Applications*, Prentice-Hall, Englewood Cliffs, N.J.

Linde, Y., Buzo, A., and Gray, R. M. (1980). "An Algorithm for Vector Quantizer Design." *IEEE Trans. Commun. vol. COM-28*, pp. 84–95, January.

Lindell, G. (1985). "On Coded Continuous Phase Modulation," Ph.D. Dissertation, Telecommunication Theory, University of Lund, Lund, Sweden, May.

Lindholm, J. H. (1968). "An Analysis of the Pseudo-Randomness Properties of Subsequences of Long m-Sequences," *IEEE Trans. Inform. Theory*, vol. IT-14, pp. 569–576, July.

Lindsey, W. C. (1964). "Error Probabilities for Ricean Fading Multichannel Reception of Binary and N-Ary Signals," *IEEE Trans. Inform. Theory*, vol. IT-10, pp. 339–350, October.

Lindsey, W. C. (1972). *Synchronization Systems in Communications*, Prentice-Hall, Englewood Cliffs, N.J.

Lindsey, W. C. and Chie, C. M. (1981). "A Survey of Digital Phase-Locked Loops," *Proc. IEEE*, vol. 69, pp. 410–432.

Lindsey, W. C. and Simon, M. K. (1973). *Telecommunication Systems Engineering*, Prentice-Hall, Englewood Cliffs, N.J.

Ling, F. (1988). "Convergence Characteristics of LMS and LS Adaptive Algorithms for Signals with Rank-Deficient Correlation Matrices," *Proc. Int. Conf. Acoust., Speech, Signal Processing*, New York, 25.D.4.7, April.

Ling, F., Manolakis, D. G., and Proakis, J. G. (1986a). "Finite Word-Length Effects in Recursive Least Squares Algorithms with Application to Adaptive Equalization," *Annales des Telecommunications*, vol. 41, pp. 1–9, May–June.

Ling, F., Manolakis, D. G., and Proakis, J. G. (1986b). "Numerically Robust Least-Squares Lattice-Ladder Alghorithms with Direct Updating of the Reflection Coefficients," *IEEE Trans. Acoust., Speech, Signal Processing*, vol. ASSP-34, pp. 837–845, August.

Ling, F. and Proakis, J. G. (1982). "Generalized Least Squares Lattice and Its Applications to DFE," *Proc. 1982, IEEE Int. Conf. on Acoustics, Speech, Signal Processing*, Paris, France, May.

Ling, F. and Proakis, J. G. (1984a), "Numerical Accuracy and Stability: Two Problems of Adaptive Estimation Algorithms Caused by Round-Off Error," *Proc. Int. Conf. Acoust., Speech, Signal Processing*, pp. 30.3.1–30.3.4, San Diego, Calif., March.

Ling, F. and Proakis, J. G. (1984b). "Nonstationary Learning Characteristics of Least Squares Adaptive Estimation Algorithms," *Proc. Int. Conf. Acoust., Speech, Signal Processing*, pp. 3.7.1–3.7.4, San Diego, Calif., March.

Ling, F. and Proakis, J. G. (1984c). "A Generalized Multichannel Least-Squares Lattice Algorithm with Sequential Processing Stages," *IEEE Trans. Acoust., Speech, Signal Processing*, vol. ASSP-32, pp. 381–389, April.

Ling, F. and Proakis, J. G. (1985). "Adaptive Lattice Decision-Feedback Equalizers—Their Performance and Application to Time-Variant Multipath Channels," *IEEE Trans. Commun.*, vol. COM-33, pp. 348–356, April.

Ling, F. and Proakis, J. G. (1986). "A Recursive Modified Gram–Schmidt Algorithm," *IEEE Trans. Acoust., Speech, Signal Processing*, vol. ASSP-34, pp. 829–836, August.

Ling, F. and Quershi, S. U. H. (1986). "Lattice Predictive Decision-Feedback Equalizer for Digital Communication Over Fading Multipath Channels," *Proc. GLOBECOM '86*, Houston, Texas, December.

Ljung, S. and Ljung, L. (1985). "Error Propagation Properties of Recursive Least-Squares Adaptation Algorithms," *Automatica*, vol. 21, pp. 159–167.

Lloyd, S. P. (1982). "Least Squares Quantization in PCM," *IEEE Trans. Inform. Theory*, vol. IT-28, pp. 129–137, March.

Loeve, M. (1955). *Probability Theory*, Van Nostrand, Princeton, N.J.

Long, G., Ling, F., and Proakis, J. G. (1987). "Adaptive Transversal Filters with Delayed Coefficient Adaptation," *Proc. Int. Conf. Acoust., Speech, Signal Processing*, Dallas, Texas, March.

Long, G., Ling, F., and Proakis, J. G. (1988a). "Fractionally-Spaced Equalizers Based on Singular-Value Decomposition," *Proc. Int. Conf. Acoust., Speech, Signal Processing*, New York, 25.D.4.10, April.

Long, G., Ling, F., and Proakis, J. G. (1988b). "Applications of Fractionally-Spaced Decision-Feedback Equalizers to HF Fading Channels," *Proc. MILCOM*, San Diego, Calif., October.

Long, G., Ling, F., and Proakis, J. G. (1989). "The LMS Algorithm with Delayed Coefficient Adaptation, "*IEEE Trans. Acoust., Speech, Signal Processing*, vol. ASSP-37, October.

Lucky, R. W. (1965). "Automatic Equalization for Digital Communications, *Bell Syst. Tech. J.*, vol. 44, pp. 547–588, April.

Lucky, R. W. (1966). "Techniques for Adaptive Equalization of Digital Communication," *Bell Syst. Tech. J.*, vol. 45, pp. 255–286.

Lucky, R. W. and Hancock, J. C. (1962). "On the Optimum Performance of N-ary Systems Having Two Degrees of Freedom," *IRE Trans. Commun. Syst.*, vol. CS-10, pp. 185–192, June.

Lucky, R. W., Salz, J., and Weldon, E. J., Jr. (1968). *Principles of Data Communication*, McGraw-Hill, New York.

Lugannani, R. (1969). "Intersymbol Interference and Probability of Error in Digital Systems," *IEEE Trans. Inform. Theory*, vol. IT-15, pp. 682–688, November.

Lundgren, C. W. and Rummler, W. D. (1979). "Digital Radio Outage Due to Selective Fading—Observation vs. Prediction from Laboratory Simulation," *Bell Syst. Tech. J.*, vol. 58, pp. 1074–1100, May–June.

Lupas, R. and Verdu, S. (1989). "Linear Multiuser Detectors for Synchronous Code-Division Multiple-Access Channels," *IEEE Trans. Inform. Theory*, vol. IT-35, pp. 123–136, January.

Lupas, R. and Verdu, S. (1990). "Near–Far Resistance of Multiuser Detectors in Asynchronous Channels," *IEEE Trans. Commun.*, vol. COM-38, pp. 496–508, April.

MacKenchnie, L. R. (1973). "Maximum Likelihood Receivers for Channels Having Memory," Ph.D. Dissertation, Department of Electrical Engineering, University of Notre Dame, Notre Dame, Ind., January.

MacWilliams, F. J. and Sloane, J. J. (1977). *The Theory of Error Correcting Codes*, North Holland, New York.

Magee, F. R. and Proakis, J. G. (1973). "Adaptive Maximum-Likelihood Sequence Estimation for Digital Signaling in the Presence of Intersymbol Interference," *IEEE Trans. Inform. Theory*, vol. IT-19, pp. 120–124, January.

Makhoul, J. (1978). "A Class of All-Zero Lattice Digital Filters: Properties and Applications," *IEEE Trans. Acoust., Speech, Signal Processing*, vol. ASSP-26, pp. 304–314, August.

Makhoul, J., Roucos, S., and Gish, H. (1985). "Vector Quantization in Speech Coding," *Proc. IEEE*, vol. 73, pp. 1551–1587, November.

Martin, D. R. and McAdam, P. L. (1980). "Convolutional Code Performance with Optimal Jamming," *Conf. Rec. Int. Conf. Commun.*, pp. 4.3.1–4.3.7, May.

Massey, J. L. (1963). *Threshold Decoding*, MIT Press, Cambridge, Mass.

Massey, J. L. (1965). "Step-by-Step Decoding of the BCH Codes," *IEEE Trans. Inform. Theory*, vol. IT-11, pp. 580–585, October.

Massey, J. L. (1988). "Some New Approaches to Random Access Communications," *Performance '87*, pp. 551–569. [Reprinted 1993 in *Multiple Access Communications*, N. Abramson (ed.), IEEE Press, New York.]

Massey, J. L. and Sain, M. (1968). "Inverses of Linear Sequential Circuits," *IEEE Trans. Comput.*, vol. C-17, pp. 330–337, April.

Matis, K. R. and Modestino, J. W. (1982). "Reduced-State Soft-Decision Trellis Decoding of Linear Block Codes," *IEEE Trans. Inform. Theory*, vol. IT-28, pp. 61–68, January.

Max, J. (1960). "Quantizing for Minimum Distortion," *IRE Trans. Inform. Theory*, vol. IT-6, pp. 7–12, March.

Mazo, J. E. (1975). "Faster-Than-Nyquist Signaling," *Bell Syst. Tech. J.*, vol. 54, pp. 1451–1462, October.

Mazo, J. E. (1979). "On the Independence Theory of Equalizer Convergence," *Bell Syst. Tech. J.*, vol. 58, pp. 963–993, May.

McMahon, M. A. (1984). *The Making of a Profession—A Century of Electrical Engineering in America*, IEEE Press, New York.

Mengali, U. (1977). "Joint Phase and Timing Acquisition in Data Transmission," *IEEE Trans. Commun.*, vol. COM-25, pp. 1174–1185, October.

Meyers, M. H. and Franks, L. E. (1980). "Joint Carrier Phase and Symbol Timing for PAM Systems," *IEEE Trans. Commun.*, vol. COM-28, pp. 1121–1129, August.

Meyr, H. and Ascheid, G. (1990). *Synchronization in Digital Communications*, Wiley Interscience, New York.

Miller, K. S. (1964). *Multidimensional Gaussian Distributions*, Wiley, New York.

Millman, S. (ed.) (1984). *A History of Engineering and Science in the Bell System—Communication Sciences (1925–1980)*, AT&T Bell Laboratoreis.

Miyagaki, Y., Morinaga, N., and Namekawa, T. (1978). "Error Probability Characteristics for CPSK Signal Through m-Distributed Fading Channel," *IEEE Trans. Commun.*, vol. COM-26, pp. 88–100, January.

Monsen, P. (1971). "Feedback Equalization for Fading Dispersive Channels," *IEEE Trans. Inform. Theory*, vol. IT-17, pp. 56–64, January.

Morf, M. (1977). "Ladder Forms in Estimation and System Identification," *Proc. 11th Annual Asilomar Conf. on Circuits, Systems and Computers*, Monterey, Calif., Nov. 7–9.

Morf, M., Dickinson, B., Kailath, T., and Vieira, A. (1977). "Efficient Solution of Covariance Equations for Linear Prediction," *IEEE Trans. Acoust., Speech, Signal Processing*, vol. ASSP-25, pp. 429–433, October.

Morf, M. and Lee, D. (1979). "Recursive Lest Squares Ladder Forms for Fast Parameter

Tracking," *Proc. 1978 IEEE Conf. on Decision and Control*, San Diego, Calif., pp. 1362–1367, January 12.

Morf, M., Lee, D., Nickolls, J. and Vieira, A. (1977). "A Classification of Algorithms for ARMA Models and Ladder Realizations," *Proc. 1977 IEEE Int. Conf on Acousuics, Speech, Signal Processing*, Hartford, Conn., pp. 13–19, May.

Morf, M., Vieira, A., and Lee, D. (1977). "Ladder Forms for Identification and Speech Processing," *Proc. 1977 IEEE Conf. on Decision and Control*, New Orleans, La, pp. 1074–1078, December.

Mueller, K. H. and Muller, M. S. (1976). "Timing Recovery in Digital Synchronous Data Receivers," *IEEE Trans. Commun.*, vol. COM-24, pp. 516–531, May.

Muller, D. E. (1954). "Application of Boolean Algebra to Switching Circuit Design and to Error Detection," *IRE Trans. Electronic Comput.*, vol. EC-3, pp. 6–12, September.

Mulligan, M. G. (1988). "Multi-Amplitude Continuous Phase Modulation with Convolutional Coding," Ph.D. Dissertation, Department of Electrical and Computer Engineering, Northeastern University, June.

Nakagami, M. (1960). "The m-Distribution—A General Formula of Intensity Distribution of Rapid Fading," in *Statistical Methods of Radio Wave Propagation*, W. C. Hoffman (ed.), pp. 3–36, Pergamon Press, New York.

Natali, F. D. and Walbesser, W. J. (1969). "Phase-Locked Loop Detection of Binary PSK Signals Utilizing Decision Feedback," *IEEE Trans. Aerospace Electronic Syst.*, vol. AES-5, pp. 83–90, January.

Neyman, J. and Pearson, E. S. (1933). "On the Problem of the Most Efficient Tests of Statistical Hypotheses," *Phil. Trans. Roy. Soc. London, Series A*, vol. 231, 289–337.

North, D. O. (1943). "An Analysis of the Factors Which Determine Signal/Noise Discrimination in Pulse-Carrier Systems," RCA Tech. Report No. 6 PTR-6C.

Nyquist, H. (1924). "Certain Factors Affecting Telegraph Speed," *Bell Syst. Tech. J.*, vol. 3, pp. 324.

Nyquist, H. (1928). "Certain Topics in Telegraph Transmission Theory," *AIEE Trans.*, vol. 47, pp. 617–644.

Odenwalder, J. P. (1970). "Optimal Decoding of Convolutional Codes," Ph.D. Dissertation, Department of Systems Sciences, School of Engineering and Applied Sciences, University of California, Los Angeles.

Odenwalder, J. P. (1976). "Dual-k Convolutional Codes for Noncoherently Demodulated Channels," *Proc. Int. Telemetering Conf.* vol. 12, pp. 165–174, September.

Olsen, J. D. (1977). "Nonlinear Binary Sequences with Asymptotically Optimum Periodic Cross Correlation," Ph.D. Dissertation, University of Southern California, December.

Omura, J. (1971). "Optimal Receiver Design for Convolutional Codes and Channels with Memory Via Control Theoretical Concepts," *Inform. Sci.*, vol. 3, pp. 243–266.

Omura, J. K. and Levitt, B. K. (1982). "Code Error Probability Evaluation for Antijam Communication Systems," *IEEE Trans. Commun.*, vol. COM-30, pp. 896–903, May.

Osborne, W. P. and Luntz, M. B. (1974). "Coherent and Noncoherent Detection of CPFSK," *IEEE Trans. Commun.*, vol. COM-22, pp. 1023–1036, August.

Paaske, E. (1974). "Short Binary Convolutional Codes with Maximal Free Distance for Rates 2/3 and 3/4," *IEEE Trans. Inform. Theory*, vol. IT-20, pp. 683–689, September.

Paez, M. D. and Glisson, T. H. (1972). "Minimum Mean Squared Error Quantization in Speech PCM and DPCM Systems," *IEEE Trans. Commun.*, vol. COM-20, pp. 225–230, April.

Pahlavan, K. (1985). "Wireless Communications for Office Information Networks," *IEEE Commun. Mag.*, vol. 23, pp. 18–27, June.

Papoulis, A. (1984). *Probability, Random Variables, and Stochastic Processes*, McGraw-Hill, New York.

Paul, D. B. (1983). "An 800 bps Adaptive Vector Quantization Vocoder Using a Preceptual Distance Measure," *Proc. IEEE Int. Conf. Acoust., Speech, Signal Processing*, Boston, Mass, pp. 73–76, April.

Pearson, K., (1965). *Tables of the Incomplete Γ-Function*, Cambridge University Press, London.

Peebles, P. Z. (1987). *Probability, Random Variables, and Random Signal Principles*, McGraw-Hill, New York.

Peterson, W. W. (1960). "Encoding and Error-Correction Procedures for Bose-Chaudhuri Codes," *IRE Trans. Inform. Theory*, vol. IT-6, pp. 459–470, September.

Peterson, W. W. and Weldon, E. J., Jr. (1972). *Error-Correcting Codes*, 2d ed., MIT Press, Cambrdige, Mass.

Picci, G. and Prati, G. (1987). "Blind Equalization and Carrier Recovery Using a Stop-and-Go Decision Directed Algorithm," *IEEE Trans. Commun.*, vol. COM-35, pp. 877–887, September.

Picinbono, B. (1978). "Adaptive Signal Processing for Detection and Communication," in *Communication Systems and Random Process Theory*, J. K. Skwirzynski (ed.), Sijthoff & Nordhoff, Alphen aan den Rijn, The Netherlands.

Pickholtz, R. L., Schilling, D. L., and Milstein, L. B. (1982). "Theory of Spread Spectrum Communications—A Tutorial," *IEEE Trans. Commun.*, vol. COM-30, pp. 855–884, May.

Pieper, J. F., Proakis, J. G., Reed, R. R., and Wolf, J. K. (1978). "Design of Efficient Coding and Modulation for a Rayleigh Fading Channel," *IEEE Trans. Inform. Theory*, vol. IT-24, pp. 457–468, July.

Pierce, J. N. (1958). "Theoretical Diversity Improvement in Frequency-Shift Keying," *Proc. IRE*, vol. 46, pp. 903–910, May.

Pierce, J. N. and Stein, S. (1960). "Multiple Diversity with Non-Independent Fading," *Proc. IRE*, vol. 48, pp. 89–104, January.

Plotkin, M. (1960). "Binary Codes with Specified Minimum Distance," *IRE Trans. Inform. Theory*, vol. IT-6, pp. 445–450, September.

Poor, H. V. and Verdu, S. (1988). "Single-User Detectors for Multiuser Channels," *IEEE Trans. Commun.*, vol. 36, pp. 50–60, January.

Price, R. (1954). "The Detection of Signals Perturbed by Scatter and Noise," *IRE Trans. Inform. Theory*, vol. PGIT-4, pp. 163–170, September.

Price, R. (1956). "Optimum Detection of Random Signals in Noise, with Application to Scatter-Multipath Communicaton," *IRE Trans. Inform. Theory*, vol. IT-2, pp. 125–135, December.

Price, R. (1962a). "Error Probabalities for Adaptive Multichannel Reception of Binary Signals," MIT Lincoln Laboratory, Lexington, Mass., Tech. Report No. 258, July.

Price, R. (1962b). "Error Probabilities for Adaptive Multichannel Reception of Binary Signals," *IRE Trans. Inform. Theory*, vol. IT-8, pp. 305–316, September.

Price, R. (1972). "Nonlinearly Feedback-Equalized PAM vs. Capacity," *Proc. 1972 IEEE Int Conf. on Commun.* Philadelphia, Penn., pp. 22.12–22.17, June.

Price, R. and Green, P. E., Jr. (1958). "A Communication Technique for Multipath Channels," *Proc. IRE*, vol. 46, pp. 555–570, March.

Price, R. and Green, P. E., Jr. (1960). "Signal Processing in Radar Astronomy—Communication via Fluctuating Multipath Media," MIT Lincoln Laboratory, Lexington, Mass., Tech. Report No. 234, October.

Proakis, J. G. (1968). "Probabilities of Error for Adaptive Reception of M-Phase Signals," *IEEE Trans. Commun. Tech.*, vol. COM-16, pp. 71–81, February.

Proakis, J. G. (1975). "Advances in Equalization for Intersymbol Interference," in *Advances in Communication Systems*, vol. 4, A. J. Viterbi (ed.), Academic, New York.

Proakis, J. G., Drouilhet, P. R., Jr., and Price, R. (1964). "Performance of Coherent Detection Systems Using Decision-Directed Channel Measurement," *IEEE Trans. Commun. Syst.*, vol. CS-12, pp. 54–63, March.

Proakis, J. G. and Ling, F. (1984). "Recursive Least Squares Algorithms for Adaptive Equalization of Time-Variant Multipath Channels," *Proc. Int. Conf. Commun.* Amsterdam, The Netherlands, May.

Proakis, J. G. and Manolakis, D. G. (1988). *Introduction to Digital Processing*, Macmillan, New York.

Proakis, J. G. and Miller, J. H. (1969). "Adaptive Receiver for Digital Signaling through

Channels with Intersymbol Interference," *IEEE Trans. Inform. Theory*, vol. IT-15, pp. 484–497, July.

Proakis, J. G. and Rahman, I. (1979). "Performance of Concatenated Dual-*k* Codes on a Rayleigh Fading Channel with a Bandwidth Constraint," *IEEE Trans. Commun.*, vol. COM-27, pp. 801–806, May.

Pursley, M. B. (1979). "On the Mean-Square Partial Correlation of Periodic Sequences," *Proc. 1979 Conf. Inform. Science and Systems*, Johns Hopkins University, Baltimore, Md., pp. 377–379, March.

Qureshi, S. U. H. (1976). "Timing Recovery for Equalized Partial Response Systems," *IEEE Trans. Commun.*, vol. COM-24, pp. 1326–1331, December.

Qureshi, S. U. H. (1985). "Adaptive Equalization," *Proc. IEEE*, vol. 53, pp. 1349–1387, September.

Qureshi, S. U. H. and Forney, G. D., Jr. (1977). "Performance and Properties of a *T*/2 Equalizer," *Natl. Telecom. Conf. Record*, pp. 11.1.1–11.1.14, Los Angeles, Calif., December.

Rabiner, L. R. and Schafer, R. W. (1978). *Digital Processing of Speech Signals*, Prentice-Hall, Englewood Cliffs, N.J.

Raheli, R., Polydoros, A., and Tzou, C.-K. (1995). "The Principle of Per-Survivor Processing: A General Approach to Approximate and Adaptive MLSE," *IEEE Trans. Commun.*, vol. COM-43 (to appear).

Rahman, I. (1981). "Bandwidth Constrained Signal Design for Digital Communication over Rayleigh Fading Channels and Partial Band Interference Channels," Ph.D. Dissertation, Department of Electrical Engineering, Northeastern University, Boston, Mass.

Ramsey, J. L. (1970). "Realization of Optimum Interleavers," *IEEE Trans. Inform. Theory*, vol. IT-16, pp. 338–345.

Reed, I. S. (1954). "A Class of Multiple-Error Correcting Codes and the Decoding Scheme," *IRE Trans. Inform.*, vol. IT-4, pp. 38–49, September.

Reed, I. S. and Solomon, G. (1960). "Polynomial Codes Over Certain Finite Fields," *SIAM J.*, vol. 8, pp. 300–304, June.

Rizos, A. D., Proakis, J. G., and Nguyen, T. Q. (1994). "Comparison of DFT and Cosine Modulated Filter Banks in Multicarrier Modulation," *Proc. Globecom '94*, pp. 687–691, San Francisco. Calif., November.

Roberts, L. G. (1975). "Aloha Packet System with and without Slots and Capture," *Comp. Commun. Rev.*, vol. 5, pp. 28–42, April.

Roucos, S., Schwartz, R., and Makhoul, J. (1982). "Segment Quantization for Very-Low-Rate Speech Coding," *Proc. Int. Conf. Acoust., Speech, Signal Processing*, Paris, France, pp. 1565–569, May.

Rowe, H. E. and Prabhu, V. K. (1975). "Power Spectrum of a Digital Frequency Modulation Signal," *Bell Syst. Tech. J.*, vol. 54, pp. 1095–1125, July–August.

Rummler, W. D. (1979). "A New Selective Fading Model: Application to Propagation Data," *Bell Syst. Tech. J.*, vol. 58, pp. 1037–1071, May–June.

Ryder, J. D. and Fink, D. G. (1984). *Engineers and Electronics*, IEEE Press, New York.

Saltzberg, B. R. (1967). "Performance of an Efficient Parallel Data Transmission System," *IEEE Trans. Commun.*, vol. COM-15, pp. 805–811, December.

Saltzberg, B. R. (1968). "Intersymbol Interference Error Bounds with Application to Ideal Bandlimited Signaling," *IEEE Trans. Inform. Theory*, vol. IT-14, pp. 563–568, July.

Salz, J. (1973). "Optimum Mean-Square Decision Feedback Equalization," *Bell Syst. Tech. J.*, vol. 52, pp. 1341–1373, October.

Salz, J., Sheehan, J. R., and Paris, D. J. (1971). "Data Transmission by Cominbed AM and PM," *Bell Syst. Tech. J.*, vol. 50, pp. 2399–2419, September.

Sarwate, D. V. and Pursley, M. B. (1980). "Crosscorrelation Properties of Pseudorandom and Related Sequences," *Proc. IEEE*, vol. 68, pp. 593–619, May.

Sato, Y. (1975). "A Method of Self-Recovering Equalization for Multilevel Amplitude-Modulation Systems," *IEEE Trans. Commun.*, vol. COM-23, pp. 679–682, June.

Sato, Y. *et al.* (1986). "Blind Suppression of Time Dependency and its Extension to Multi-Dimensional Equalization," *Proc. ICC'86*, pp. 46.4.1–46.4.5.

Satorius, E. H. and Alexander, S. T. (1979). "Channel Equalization Using Adaptive Lattice Algorithms," *IEEE Trans. Commun.*, vol. COM-27, pp. 899–905, June.

Satorius, E. H. and Pack, J. D. (1981). "Application of Least Squares Lattice Algorithms to Adaptive Equalization," *IEEE Trans. Commun.*, vol. COM-29, pp. 136–142, February.

Savage, J. E. (1966). "Sequential Decoding—The Computation Problem," *Bell Syst. Tech. J.*, vol. 45, pp. 149–176, January.

Scholtz, R. A. (1977). "The Spread Spectrum Concept," *IEEE Trans. Commun.*, vol. COM-25, pp. 748–755, August.

Scholtz, R. A. (1979). "Optimal CDMA Codes," *1979 Nat. Telecommun. Conf. Rec.*, Washington, D.C., pp. 54.2.1–54.2.4, November.

Scholtz, R. A. (1982). "The Origins of Spread Spectrum," *IEEE Trans. Commun.*, vol. COM-30, pp. 822–854, May.

Schonhoff, T. A. (1976). "Symbol Error Probabilities for M-ary CPFSK: Coherent and Noncoherent Detection," *IEEE Trans. Commun.*, vol. COM-24, pp. 644–652, June.

Seshadri, N. (1994). "Joint Data and Channel Estimation Using Fast Blind Trellis Search Techniques," *IEEE Trans. Commun.*, vol. COM-42, pp. 1000–1011, March.

Shalvi, O. and Weinstein, E. (1990). "New Criteria for Blind Equalization of Nonminimum Phase Systems Channels," *IEEE Trans. Inform. Theory*, vol. IT-36, pp. 312–321, March.

Shannon, C. E. (1948a). "A Mathematical Theory of Communication," *Bell Syst. Tech. J.*, vol. 27, pp. 379–423, July.

Shannon, C. E. (1948b). "A Mathematical Theory of Communication," *Bell Syst. Tech. J.*, vol. 27, pp. 623–656, October.

Shannon, C. E. (1949). "Communication in the Presence of Noise," *Proc. IRE*, vol. 37, pp. 10–21, January.

Shannon, C. E. (1959a). "Coding Theorems for a Discrete Source with a Fidelity Criterion," *IRE Nat. Conv. Rec.*, pt. 4, pp. 142–163, March.

Shannon, C. E. (1959b). "Probability of Error for Optimal Codes in a Gaussian Channel," *Bell Syst. Tech. J.*, vol. 38, pp. 611–656, May.

Shannon, C. E., Gallager, R. G., and Berlekamp, E. R. (1967). "Lower Bounds to Error Probability for Coding on Discrete Memoryless Channels, I and II," *Inform. Control.*, vol. 10, pp. 65–103, January; pp. 527–552, May.

Shimbo, O. and Celebiler, M. (1971). "The Probability of Error due to Intersymbol Interference and Gaussian Noise in Digital Communication Systems," *IEEE Trans. Commun. Tech.*, vol. COM-19, pp. 113–119, April.

Simon, M. K. and Divsalar, D. (1985). "Combined Trellis Coding with Asymmetric MPSK Modulation," *JPL Publ. 85-24*, Pasadena, Calif, May.

Simon, M. K., Omura, J. K., Scholtz, R. A., and Levitt, B. K. (1985). *Spread Spectrum Communications Vol. I, II, III*, Computer Science Press, Rockville, Md.

Simon, M. K. and Smith, J. G. (1973). "Hexagonal Multiple Phase-and-Amplitude-Shift Keyed Signal Sets," *IEEE Trans. Commun.*, vol. COM-21, pp. 1108–1115, October.

Slepian, D. (1956). "A Class of Binary Signaling Alphabets," *Bell Syst. Tech. J.*, vol. 35, pp. 203–234, January.

Slepian, D. (1974). *Key Papers in the Development of Information Theory*, IEEE Press, New York.

Slepian, D. and Wolf, J. K. (1973). "A Coding Theorem for Multiple Access Channels with Correlated Sources," *Bell Syst. Tech. J.*, vol. 52, pp. 1037–1076.

Sloane, N. J. A. and Wyner, A. D. (1993). *The Collected Papers of Shannon*, IEEE Press, New York.

Slock, D. T. M. and Kailath, T. (1988). "Numerically Stable Fast Recursive Least-Squares Transversal Filters," *Proc. Int. Conf. Acoust., Speech, Signal Processing*, pp. 1365–1368, New York, April.

Smith, J. W. (1965). "The Joint Optimization of Transmitted Signal and Receiving Filter for Data Transmission Systems," *Bell Syst. Tech. J.*, vol. 44, pp. 1921–1942, December.

Stenbit, J. P. (1964). "Table of Generators for BCH Codes," *IEEE Trans. Inform. Theory*, vol. IT-10, pp. 390–391, October.

Stiffler, J. J. (1971). *Theory of Synchronous Communications*, Prentice-Hall, Englewood Cliffs, N.J.

Sundberg, C. E. (1986). "Continuous Phase Modulation," *IEEE Commun. Mag.*, vol. 24, pp. 25–38, April.

Suzuki, H. (1977). "A Statistical Model for Urban Multipath Channels with Random Delay," *IEEE Trans. Commun.*, vol. COM-25, pp. 673–680, July.

Tang, D. L. and Bahl, L. R. (1970). "Block Codes for a Class of Constrained Noiseless Channels," *Inform. Control*, vol. 17, pp. 436–461.

Titsworth, R. C. and Welch, L. R. (1961). "Power Spectra of Signals Modulated by Random and Pseudorandom Sequences," *JPL Tech. Rep. 32-140*, October 10.

Thomas, C. M., Weidner, M. Y., and Durrani, S. H. (1974). "Digital Amplitude-Phase-Keying with *M*-ary Alphabets," *IEEE Trans. Commun.*, vol. COM-22, pp. 168–180, February.

Tong, L. Xu, G., and Kailath, T. (1994). "Blind Identification and Equalization Based on Second-Order Statistics," *IEEE Trans. Inform. Theory*, vol. IT-40, pp. 340–349, March.

Tufts, D. W. (1965). "Nyquist's Problem—The Joint Optimization of Transmitter and Receiver in Pulse Amplitude Modulation," *Proc. IEEE*, vol. 53, pp. 248–259, March.

Turin, G. L. (1961). "On Optimal Diversity Reception," *IRE Trans. Inform. Theory*, vol. IT-7, pp. 154–166, July.

Turin, G. L. (1962). "On Optimal Diversity Reception II," *IRE Trans. Commun. Syst.*, vol. CS-12, pp. 22–31, March.

Turin, G. L. *et al.* (1972). "Simulation of Urban Vehicle Monitoring Systems," *IEEE Trans. Vehicular Tech.*, pp. 9–16, February.

Tzannes, M. A., Tzannes, M. C., Proakis, J. G., and Heller, P. N. (1994). "DMT Systems, DWMT Systems and Digital Filter Banks," *Proc. Int. Conf. Commun.*, pp. 311–315, New Orleans, Louisiana, May 1–5.

Ungerboeck, G. (1972). "Theory on the Speed of Convergence in Adaptive Equalizers for Digital Communication," *IBM J. Res. Dev.*, vol. 16, pp. 546–555, November.

Ungerboeck, G. (1974). "Adaptive Maximum-Likelihood Receiver for Carrier-Modulated Data-Transmission Systems," *IEEE Trans. Commun.*, vol. COM-22, pp. 624–636, May.

Ungerboeck, G. (1976). "Fractional Tap-Spacing Equalizer and Consequences for Clock Recovery in Data Modems," *IEEE Trans. Commun.*, vol. COM-24, pp. 856–864, August.

Ungerboeck, G. (1982). "Channel Coding with Multilevel/Phase Signals," *IEEE Trans. Inform. Theory*, vol. IT-28, pp. 55–67, January.

Ungerboeck, G. (1987). "Trellis-Coded Modulation with Redundant Signal Sets, Parts I and II," *IEEE Commun. Mag.*, vol. 25, pp. 5–21, February.

Ungerboeck, G. and Csajka, I. (1976). "On Improving Data-Link Performance by Increasing the Channel Alphabet and Introducing Sequence Coding, *1976 Int. Conf. Inform. Theory, Ronneby, Sweden*, June.

Vaidyanathan, P. P. (1993). *Multirate Systems and Filter Banks*, Prentice-Hall, Englewood Cliffs, N.J.

Van Etten, W. (1975). "An Optimum Linear Receiver for Multiple Channel Digital Transmission Systems," *IEEE Trans. Commun.*, vol. COM-23, pp. 828–834, August.

Van Etten, W. (1976). "Maximum Likelihood Receiver for Multiple Channel Transmission Systems," *IEEE Trans. Commun.*, vol. COM-24, pp. 276–283, February.

Van Trees, H. L. (1968). *Detection, Estimation, and Modulation Theory, Part I*, Wiley, New York.

Varsharmov, R. R. (1957). "Estimate of the Number of Signals in Error Correcting Codes," *Doklady Akad. Nauk, S.S.S.R.*, vol. 117, pp. 739–741.

Verdu, S. (1986a). "Minimum Probability of Error for Asynchronous Gaussian Multiple-Access Channels," *IEEE Trans. Inform. Theory*, vol. IT-32, pp. 85–96, January.

Verdu, S. (1986b). "Multiple-Access Channels with Point-Process Observation: Optimum Demodulation," *IEEE Trans. Inform. Theory*, vol. IT-32, pp. 642–651, September.

Verdu, S. (1986c). "Optimum Multiuser Asymptotic Efficiency," *IEEE Trans. Commun.*, vol. COM-34, pp. 890–897, September.

Verdu, S. (1989). "Recent Progress in Multiuser Detection," *Advances in Communications and Signal Processing*, Springer-Verlag, Berlin. [Reprinted in *Multiple Access Communications*, N. Abramson (ed.), IEEE Press, New York.]

Viterbi, A. J. (1966). *Principles of Coherent Communication*, McGraw-Hill, New York.

Viterbi, A. J. (1967). "Error Bounds for Convolutional Codes and an Asymptotically Optimum Decoding Algorithm," *IEEE Trans. Inform. Theory*, vol. IT-13, pp. 260–269, April.

Viterbi, A. J. (1969). "Error Bounds for White Gaussian and Other Very Noisy Memoryless Channels with Generalized Decision Regions," *IEEE Trans. Inform. Theory*, vol. IT-15, pp. 279–287, March.

Viterbi, A. J. (1971). "Convolutional Codes and Their Performance in Communication Systems," *IEEE Trans. Commun. Tech.*, vol. COM-19, pp. 751–772, October.

Viterbi, A. J. (1978). "A Processing Satellite Transponder for Multiple Access by Low-Rate Mobile Users," *Proc. Fourth Int. Conf. on Digital Satellite Communications*, Montreal, Canada, pp. 166–174, October.

Viterbi, A. J. (1979). "Spread Spectrum Communication—Myths and Realities," *IEEE Commun. Mag.*, vol. 17, pp. 11–18, May.

Viterbi, A. J. (1985). "When Not to Spread Spectrum—A Sequel," *IEEE Commun. Mag.*, vol. 23, pp. 12–17, April.

Viterbi, A. J. and Jacobs, I. M. (1975). "Advances in Coding and Modulation for Noncoherent Channels Affected by Fading, Partial Band, and Multiple-Access Interference," in *Advances in Communication Systems*, vol. 4, A. J. Viterbi (ed.), Academic, New York.

Viterbi, A. J. and Omura, J. K. (1979). *Principles of Digital Communication and Coding*, McGraw-Hill, New York.

Wainberg, S. and Wolf, J. K. (1970). "Subsequences of Pseudo-Random Sequences," *IEEE Trans. Commun. Tech.*, vol. COM-18, pp. 606–612, October.

Wainberg, S. and Wolf, J. K. (1973). "Algebraic Decoding of Block Codes Over a q-ary Input, Q-ary Output Channel, $Q > q$," *Inform. Control*, vol. 22, pp. 232–247, April.

Wald, A. (1947). *Sequential Analysis*, Wiley, New York.

Ward, R. B. (1965). "Acquisition of Pseudonoise Signals by Sequential Estimation," *IEEE Trans. Commun. Tech.*, vol. COM-13, pp. 474–483, December.

Ward, R. B. and Yiu, K. P. (1977). "Acquisition of Pseudonoise Signals by Recursion-Aided Sequential Estimation," *IEEE Trans. Commun.*, vol. COM-25, pp. 784–794, August.

Weber, W. J., III, Stanton, P. H., and Sumida, J. T. (1978). "A Bandwidth Compressive Modulation System Using Multi-Amplitude Minimum-Shift Keying (MAMSK)," *IEEE Trans. Commun.*, vol. COM-26, pp. 543–551, May.

Wei, L. F. (1984a). "Rotationally Invariant Convolutional Channel Coding with Expanded Signal Space, Part I: 180°," *IEEE J. Selected Areas Commun.*, vol. SAC-2, pp. 659–671, September.

Wei, L. F. (1984b). "Rotationally Invariant Convolutional Channel Coding with Expanded Signal Space, Part II: Nonlinear Codes," *IEEE J. Selected Areas Commun.*, vol. SAC-2, pp. 672–686, September.

Wei, L. F. (1987). "Trellis-Coded Modulation with Multi-Dimensional Constellations," *IEEE Trans. Inform. Theory*, vol. IT-33, pp. 483–501, July.

Weinstein, S. B. and Ebert, P. M. (1971). "Data Transmission by Frequency-Division Multiplexing Using the Discrete Fourier Transform," *IEEE Trans. Commun.*, vol. COM-19, pp. 628–634, October.

Welch, L. R. (1974). "Lower Bounds on the Maximum Cross Correlation of Signals," *IEEE Trans. Inform. Theory*, vol. IT-20, pp. 397–399, May.

Weldon, E. J., Jr. (1971). "Decoding Binary Block Codes on Q-ary Output Channels," *IEEE Trans. Inform. Theory*, vol. IT-17, pp. 713–718, November.

Widrow, B. (1966). "Adaptive Filters, I: Fundamentals," Stanford Electronics Laboratory, Stanford University, Stanford, Calif., Tech Report No. 6764-6, December.

Widrow, B. (1970). "Adaptive Filters," *Aspects of Network and System Theory*, R. E. Kalman and N. DeClaris (eds.), Holt, Rinehart and Winston, New York.

Widrow, B. and Hoff, M. E., Jr. (1960). "Adaptive Switching Circuits," *IRE WESCON Conv. Rec.*, pt. 4, pp. 96–104.

Widrow, B. *et al.* (1975). "Adaptive Noise Cancelling: Principles and Applications," *Proc. IEEE*, vol. 63, pp. 1692–1716, December.

Wiener, N. (1949). *The Extrapolation, Interpolation, and Smoothing of Stationary Time Series with Engineering Applications*, Wiley, New York (reprint of original work published as an MIT Radiation Laboratory Report in 1942).

Wintz, P. A. (1972). "Transform Picture Coding," *Proc. IEEE*, vol. 60, pp. 880–920, July.

Wolf, J. K. (1978). "Efficient Maximum Likelihood Decoding of Linear Block Codes Using a Trellis," *IEEE Trans. Inform. Theory*, vol. IT-24, pp. 76–81, January.

Wozencraft, J. M. (1957). "Sequential Decoding for Reliable Communication," *IRE Nat. Conv. Rec.*, vol. 5, pt. 2, pp. 11–25.

Wozencraft, J. M. and Jacobs, I. M. (1965). *Principles of Communication Engineering*, Wiley, New York.

Wozencraft, J. M. and Kennedy, R. S. (1966). "Modulation and Demodulation for Probabilistic Decoding," *IEEE Trans. Inform. Theory*, vol. IT-12, pp. 291–297, July.

Wozencraft, J. M. and Rieffen, B. (1961). *Sequential Decoding*, MIT Press, Cambridge, Mass.

Wyner, A. D. (1965). "Capacity of the Band-Limited Gaussian Channel," *Bull. Syst. Tech. J.*, vol. 45, pp. 359–371, March.

Xie, Z., Rushforth, C. K., and Short, R. T. (1990a). "Multiuser Signal Detection Using Sequential Decoding," *IEEE Trans. Commun.*, vol. COM-38, pp. 578–583, May.

Xie, Z., Short, R. T., and Rushforth, C. K. (1990b). "A Family of Suboptimum Detectors for Coherent Multiuser Communications," *IEEE J. Selected Areas Commun.*, vol. SAC-8, pp. 683–690, May.

Yao, K. (1972). "On Minimum Average Probability of Error Expression for Binary Pulse-Communication System with Intersymbol Interference," *IEEE Trans. Inform. Theory*, vol. IT-18, pp. 528–531, July.

Yao, K. and Tobin, R. M. (1976). "Moment Space Upper and Lower Error Bounds for Digital Systems with Intersymbol Interference," *IEEE Trans. Inform. Theory*, vol. IT-22, pp. 65–74, January.

Yue, O. (1983). "Spread Spectrum Mobile Radio 1977–1982," *IEEE Trans. Vehicular Tech.*, vol. VT-32, pp. 98–105, February.

Zelinski, P. and Noll, P. (1977). "Adaptive Transform Coding of Speech Signals," *IEEE Trans. Acoustics, Speech, Signal Processing*, vol. ASSP-25, pp. 299–309, August.

Zervas, E., Proakis, J. G., and Eyuboglu, V. (1991). "A Quantized Channel Approach to Blind Equalization," *Proc. ICC'91*, Chicago, Il, June.

Zhang, X. and Brady, D. (1993). "Soft-Decision Multistage Detection of Asynchronous AWGN Channels," *Proc. 31st Allerton Conf. on Commun., Contr., Comp.* Allerton, Il., October.

Zhou, K. and Proakis, J. G. (1988). "Coded Reduced-Bandwidth QAM with Decision-Feedback Equalization," *Conf. Rec. IEEE Int. Conf. Commun.*, Philadelphia, Penn., pp. 12.6.1–12.6.5, June.

Zhou, K., Proakis, J. G., and Ling, F. (1987). "Decision-Feedback Equalization of Fading Dispersive Channels with Trellis-Coded Modulation," *Int. Conf. Commun. Tech.*, Nanjing, China, November.

Zhou, K., Proakis, J. G., and Ling, F. (1990). "Decision-Feedback Equalization of Time-Dispersive Channels with Coded Modulation," *IEEE Trans. Commun.*, vol. COM-38, pp. 18–24, January.

Ziemer, R. E. and Peterson, R. L. (1985). *Digital Communications and Spread Spectrum Systems*, Macmillan, New York.

Zigangirov, K. S. (1966). "Some Sequential Decoding Procedures," *Probl. Peredach. Inform.*, vol. 2, pp. 13–25.

Ziv, J. (1985). "Universal Quantization," *IEEE Trans. Inform. Theory*, vol. 31, pp. 344–347.

Ziv, J. and Lempel, A. (1977). "A Universal Algorithm for Sequential Data Compression," *IEEE Trans. Inform. Theory*, vol. IT-23, pp. 337–343.

Ziv, J. and Lempel, A. (1978). "Compression of Individual Sequences via Variable-Rate Coding," *IEEE Trans. Inform. Theory*, vol. IT-24, pp. 530–536.

Zvonar, Z. and Brady, D. (1995). "Differentially Coherent Multiuser Detection in Asynchronous CDMA Flat Rayleigh Fading Channels," *IEEE Trans. Commun.*, vol. COM-43, to appear.

INDEX

Adaptive equalization, 636–676
Adaptive equalizers, 636–676 (*See also* Equalizers)
  blind, 664–675
  decision-feedback, 621–625, 649–650
  linear, 584–601, 648–649
    baseband, 648
    passband, 648–649
  maximum likelihood sequence estimator, 607–616, 652–654
Adaptive transform coding, 137
Algorithm:
  Constant-modulus, 670
  Godard, 670–673
  Huffman, 99–103
  K means, 122
  Lempel-Ziv, 106–108
  Levinson-Durbin, 128, 139, 879–881
  LMS (MSE), 639–642
  recursive least-squares (RLS), 654–664
  RLS (fast), 660
  RLS (Kalman), 656–658
  RLS lattice, 660–664
  RLS square-root, 660
  stochastic gradient, 668
  zero-forcing, 637–638
Amplitude distortion, 535
Analog sources, 82
  quantization of, 108–125
    optimum, 113
    scalar, 113–118
    vector, 118
  sampling of, 72–73
Antenna:
  beamwidth, 317
  effective area, 316
  effective radiated power, 316
  illumination efficiency factor, 317
A posteriori probability, 21
A priori probability, 21
Autocorrelation function, 64
  at output of linear system, 68–70
  of cyclostationary process, 75–76
Autocovariance function, 64
Automotic gain control (AGC), 336
Average power density spectrum, 77
Averages, 33–37
  central moments, 33
  characteristic function, 35–37
    for sum of statistically independent random variables, 36
  correlation, 34
  covariance, 34
  covariance matrix, 34
  expected value (mean), 33
  joint moments, 34
    of stochastic processes, 64–67
  variance, 33
  AWGN (additive white Gaussian noise) channel, 233–234

Band-limited channels, 534–540 (*See also* Channels)
Bandpass signals, 152–157
  complex envelope of, 159
  envelope of, 155

Bandpass signals (*Cont.*):
phase of, 155
quadrature components, 155
Bandpass system, 157–159
response of, 157–159
Bandwidth efficiency, 283–284
Bandwidth expansion factor, 444, 807
Baseband signals, 176
delay modulation, 188
Miller, 188
NRZ, 187
NRZI, 187
power spectra of, 220–223
Baudot code, 13
Bayes' theorem, 21
BCH (Bose-Chaudhuri–Hocquenghem) codes, 435–436
Bibliography, 899–916
Binary symmetric channel (BSC), 381
capacity of, 381
transition probability, 376–377
Binomial distribution, 37–38
Biorthogonal signals, 183
Bit interval, 174
Blind equalization, 664–675
constant modulus algorithm, 670
Godard algorithm, 670–673
joint data and channel estimation, 667–668
maximum-likelihood algorithms, 664–667
stochastic gradient algorithms, 668–669
with second-order moments, 673–675
Block codes, 413–468
binary, 4
concatenated, 467–468
cyclic, 423–436
Bose–Chaudhuri–Hocquenghem (BCH), 435–436
encoders for, 430–435
generator polynomial for, 437–438
Golay, 433
Hamming, 433
maximum-length shift-register (MLSR), 433–435
table of MLSR connections, 435
dual code, 426
equivalent, 418
error correction capability, 451–452
error detection capability, 451–452
extended, 420
fixed-weight, 414
generator matrix, 417
generator polynomial, 424
Golay, 423, 433
extended, 423
generator polynomial of, 433
performance on AWGN channel, 454–455
weight distribution, 423
Block codes (*Cont.*):
Hadamard, 422–423
Hamming, 421–422
hard-decision decoding, 445–456
linear, 413–468
maximum-distance-separable, 461
message polynomial, 424
minimum distance bounds, 461–464
Elias, 463
Gilbert–Varsharmov, 463
Hamming, 462
Plotkin, 462
nonbinary, 464–468
nonsystematic, 418
null space, 416
parity-check matrix, 419
parity polynomial, 426
perfect, 453
quasi-perfect, 454
rate, 2, 414
reciprocal polynomial, 426
Reed-Solomon, 464–466
shortened, 421
soft-decision decoding, 436–445
standard array, 447
syndrome, 449–451
systematic, 418
Block length, 414
Burst errors, 469
Burst error correction capability, 469

Capacity (*see* Channel capacity)
Carrier, 159
Carrier phase estimation
Costas loop, 355–356
decision-directed, 347–350
ML methods, 339–341
nondecision directed, 350–358
phase-locked loop, 341–346
squaring loop, 353–355
Carrier recovery, 336–358
Canchy-Schwartz inequality, 165
Central limit theorem, 61–62
Central moments, 33
Channel:
additive white gaussian noise (AWGN), 233–234
band-limited, 534–540
binary symmetric, 375–376
capacity, 380–386
AWGN, 381–386
band limited AWGN, 383–386
DMC, 376–377
infinite bandwidth AWGN, 385
coherence bandwidth, 764

Channel (*Cont.*):
coherence time, 765
cutoff rate, 394
for system design, 400–406
discrete memoryless (*DMC*), 376–377
discrete-time model, 586–588
distortion, 534–540
amplitude, 535
envelope delay, 535
frequency offset, 538
impulse noise, 538
nonlinear, 537
phase jitter, 535
squared-error, 108
thermal noise, 538
Distortion-rate function, 110
Doppler power spectrum, 765
Doppler spread, 765
encoder, 1–2
code rate, 2, 414
code word, 2
fading multipath: characterization of, 759–769
correlation functions for, 763–767
impulse response, 760–761
models for, 767–769
transfer function, 763
fiber optic, 5
frequency nonselective, 764, 772–795
digital signaling over, 772–795
frequency selective, 764, 798–806
digital signaling over, 795–806
error rate for, 798–806
RAKE demodulator for, 797–806
tap weight estimation of, 801–803
tapped delay line model of, 795–797
microwave LOS, 767–769
models for, 11–13, 375–380
additive noise, 11
binary symmetric, 375–376
discrete memoryless, 376–377
discrete-time, 586–588
linear filter, 11
linear, time-variant filter, 12
waveform, 378–380
multipath spread, 763
Nakagami fading, 762
overspread, 771
Rayleigh fading, 761
binary signaling over, 772–776
coded waveforms for, 806–832
cutoff rate for, 825–832
frequency nonselective, 764
M-ary orthogonal signaling over, 787–792
multiphase signaling over, 785–787
Channel (*Cont.*):
Ricean fading, 761
scattering function, 766
spread factor, 771
table, 772
storage, 10
underspread, 771
underwater acoustic, 9
wireless, 5
wireline, 4
Channel encoder, 2
Channel reliability function, 389
Characteristic function, 35–37
of binomial, 38
of chi-square, 42–44
of gaussian, 41
of multivariate gaussian, 49–52
of uniform, 39
Chebyshev inequality, 52–54
Chernoff bound, 53–57
for BSC, 455
for Rayleigh fading channel, 792–794
Chi-square distribution, 41–45
central, 42–43
noncentral, 42–44
Code division multiple access (CDMA)
asynchronous, 852–854
effective SNR, 861
efficiency of, 861
optimum receiver for, 851–854
suboptimum detectors for, 854–861
decorrelating, 855–857
MMSE, 858–859
performance, 859
single user, 854
synchronous, 851–852
Code rate, 2
Code word, 2
fixed length, 94
variable length (Huffman), 96–103
Coded modulation, 511–526
Codes:
source:
instantaneously decodable, 96
uniquely decodable, 96
(*See also* Block codes; Convolutional codes)
Coding:
entropy, 97, 117
for AWGN channel: block codes, 413–468
convolutional codes, 470–511
for BSC (*see* Block codes; Convolutional codes)
for Rayleigh fading channel, 806–832
concatenated, 814–825
constant-weight codes, 814–825

Coding (*Cont.*):
for Rayleigh fading channel (*Cont.*):
convolutional codes, 811–814
cutoff rate, 825–829
linear block codes, 808–814
trellis codes, 830–832
Huffman (entropy), 96–103
noiseless, 93–108
speech, 143–144
Coding gain, 441, 507, 733
Compandor, 127
Comparison of digital modulation, 282–284
Complementary error function, 40
Complete orthonormal functions, 165–168
Complex envelope, 155
of narrowband process, 155
Computational cutoff rate, 503
(*See also* cutoff rate)
Concatenated block codes, 467–468
Concatenated convolutional codes, 449–500
Conditional cdf (cumulative distribution function), 26–28
Conditional pdf (probability density function), 25
Conditional probability, 20
Consistent estimate (*see* Estimate)
Constraint length, 470
Continuous-phase frequency-shift keying (CPFSK), 190–191
performance of, 284–301
power density spectrum of, 209–219
representation of, 284–285
Continuous-phase modulation (CPM), 191–203
demodulation:
maximum-likelihood sequence estimation, 284–289
multiamplitude, 200–203
multi-h, 295
performance of, 290–296
symbol-by-symbol, 296–300
full response, 192
minimum-shift keying (MSK), 196–199
modulation index, 191
multiamplitude, 200–203
multi-h, 295
partial response, 192
phase cylinder, 195
phase trees of, 192
power spectrum of, 209–219
representation of, 190–196
signal space diagram for, 199–200
state trellis, 196
trellis of, 195
Continuously variable slope delta modulation (CVSD), 135
Convolutional codes, 470–511
applications of, 506–511
binary, 470–476
Convolutional codes (*Cont.*):
catastrophic error propagation, 482
concatenated, 492, 499–500
constraint length, 470
decoding, 483–486
Fano algorithm, 500–503
feedback, 505–506
sequential, 500–502
stack algorithm, 503–504
Viterbi, 483–486
distance properties of, 492–496
dual-k, 492–499
encoder, 470–478
generators, 471–472
hard-decision decoding, 489–492
minimum free distance, 479
nonbinary, 492–499
optimum decoding of, 483–485
performance on AGWN channel, 486–492
performance on BSC, 489–491
performance on Rayleigh fading channel, 811–814
quantized metrics, 508–510
soft-decision decoding, 486–489
state diagram, 474–477
table of generators for maximum free distance, 493–497
transfer function, 477–480
tree diagram, 472
trellis diagram, 473
Correlation demodulator, 234–238
metrics for, 246
Correlative state vector, 286
Coset, 447
Coset leader, 447
Covariance, 34
Covariance function, 65
Cross-correlation function, 65
Cross-power density spectrum, 68
Cumulative distribution function (cdf), 23
Cutoff rate, 394
comparison with channel capacity, 399–400
for binary coded signals, 396
for M-ary input, M-ary output vector channel, 403
for multiamplitude signals, 397–399
for noncoherent channel, 405–406
for q-ary input Q-ary output channel, 400–401
system design with, 400–406
CW jamming, 706
Cyclic codes (*see* Block codes, cyclic)
Cyclostationary process, 75–76, 205

Data compression, 1
Data translation codes, 566
Decision-feedback equalizer (*see* Equalizers, decision-feedback)

Decoding of block codes:
for fading channels: hard-decision, 811
soft-decision, 808–811
hard-decision, 445–456
bounds on performance for BSC, 452–455
Chernoff bound, 455
syndrome, 449–451
table lookup method, 447–448
soft-decision, 436–445
bounds on performance for AWGN, 440–443
comparison with hard-decision decoding, 456–461
Decoding of convolutional codes:
for fading channel, performance, 811–814
feedback, 505–506
hard-decision, 489–492
performance on AWGN channel, 486–492
performance on BSC, 489–491
sequential, 500–502
soft decision, 486–489
stack algorithm, 503–504
Viterbi algorithm, 483–486
Delay distortion, 535
Delay power spectrum, 762
Delta modulation (*see* Source, encoding)
Demodulation/Detection
carrier recovery for, 337–358
Costas loop, 355–356
decision-directed, 347–350
ML methods, 339–341
non-decision-directed, 350–358
squaring PLL, 353–355
coherent:
of binary signals, 257–260
of biorthogonal signals, 264–266
comparison of, 282–284
of DPSK signals, 274–278
of equicorrelated signals, 266
of M-ary binary coded signals, 266–267
optimum, 244–257
of orthogonal signals, 260–264
of PAM signals, 267–269
of PSK signals, 269–274
of QAM signals, 278–282
correlation-type, 234–238
of CPFSK, 284–289
performance, 289–301
for intersymbol interference, 584–627
matched filter-type, 238–244
maximum-likelihood, 244–254
maximum likelihood sequence, 249–254
noncoherent, 302–313
of binary signals, 302–308
of M-ary orthogonal signals, 308–312
multichannel, 680–686
Demodulation/Detection (*Cont.*):
noncoherent (*Cont.*):
optimum, 302–312
symbol-by-symbol, 254–256
Differential encoding, 187
Differential entropy, 92
Differential phase-shift keying (DPSK), 274–278
Digital communication system model, 1–3
Digital modulator, 2
Direct sequence (*see* Spread spectrum signals)
Discrete memoryless channel (DMC), 376–377
Discrete random variable, 23
Distance (*see* Block codes; Convolutional codes, minimum free distance)
Distortion (*See also* Channel distortion):
from quantization, 113–125
granular noise, 134
slope overload, 134
Distortion rate function, 110
Distributions (*see* Probability distributions)
Diversity:
antenna, 777
frequency, 777
performance of, 777–795
polarization, 778
RAKE, 778
time, 777
Double-sideband modulation, 176
DPCM (Differential pulse code modulation) (*see* Source, encoding)
DPSK (differential phase-shift keying), 274–278
Dual code, 426
Dual-k codes, 492–499
Duobinary signal, 548–549

Early-late gate synchronizer, 362–365
Effective antenna area, 316
Effective radiated power, 316
Eigenvalue, 164
Eigenvector, 164
Elias bound, 461–463
Encoding (*see* Block codes; Conventional codes)
Energy, 156
Ensemble averages, 64–65
Entropy, 88
conditional, 88
differential, 92
discrete memoryless sources, 94–103
discrete stationary sources, 103–106
Entropy coding, 96, 117
Envelope, 155
Envelope detection, 306
Equalizers (*See also* Adaptive equalizers)
decision-feedback, 621–627, 649–650

Equalizers (*Cont.*):
decision-feedback (*Cont.*):
adaptive, 649–652
examples of performance, 622–623
of trellis-coded signals, 650–652
minimum MSE, 622
predictive form, 626–627
linear, 601–620, 648–649
adaptive, 636–644
convergence of MSE algorithm, 642–644
error probability, 613–617
examples of performance, 613–617
excess MSE, 644–648
fractionally spaced, 617–620
LMS (MSE) algorithm, 639–642
limit on step size, 645–646
mean-square error (MSE) criterion, 607–620
minimum MSE, 610–611
output SNR for, 605, 610
peak distortion, 602
peak distortion criterion, 602–607
zero-forcing, 603–604, 637–638
maximum-likelihood sequence estimation, 584–586, 589–593, 607–616
self-recovering (blind), 644–675
with trellis-coded modulation, 650–652
using the Viterbi algorithm, 589–593
channel estimator for, 652–654
performance of, 593–601
Equivalent codes, 418
Equivalent lowpass impulse response, 157–158
Equivalent lowpass signal, 155
Equivocation, 90
Error function, 40
Error probability:
coherent demodulation:
binary coded, 266–267
for binary signals, 257–260
for DPSK, 274–278
for M-ary biorthogonal, 264–265
for M-ary equicorrelated, 266
for M-ary orthogonal, 260–263
for M-ary PAM, 267–269
for PSK, 269–274
for QAM, 278–282
union bound for, 263–264
multichannel, 680–686
noncoherent demodulation, 301–313
for binary signals, 301–308
for M-ary orthogonal, 308–312
Estimate:
biased, 367
consistent, 59, 368
efficient, 368
Estimate (*Cont.*):
unbiased, 367
Estimate of phase (*See also* Carrier phase estimation)
clairvoyant, 889
pilot signal, 889
Estimation, maximum-likelihood sequence (MLSE), 249–254
Estimation:
maximum likelihood, 334–335
of carrier phase, 337–358
of signal parameters, 333–335
of symbol timing, 358–365
of symbol timing and carrier phase, 365–371
performance of, 367–370
Euclidean:
distance, 251
weight, 595
Events, 18
intersection of, 19
joint, 19
mutually exclusive, 19
null, 19
probability of, 19
union of, 19
Excess bandwidth, 546
Excess MSE, 644–648
Expected value, 33
Expurgated codes, 816–817
Extended code, 420
Extension field, 415
Eye pattern, 541

Fading channels, 8, 758–839 (*See also* Channels)
Feedback decoding, 505–506
FH spread spectrum signals (*see* Spread spectrum signals)
Filter:
integrator, 238
matched, 239
Folded spectrum, 606
Follower jammer, 731
Fourier transform, 35
Free euclidian distance, 517
Free-space path loss, 317
Frequency diversity, 777
Frequency division multiple access (FDMA), 842–844
Frequency-hopped (FH) spread spectrum (*see* Spread spectrum signals)
Frequency-shift keying (FSK), 181–183, 190–191
continuous-phase (CPFSK): performance of, 284–301
power density spectrum of, 213–217
representation of, 190–191
Functions of random variables, 28–32

Galois field, 415
Gamma function, 42
Gaussian distribution, 39–41
  multivariate, 49–52
Gaussian noise, 11
Gaussian random process, 65
Gaussian random variables, linear transformation of, 50–52
Generator matrix, 417
Generator polynomial, 424
Gilbert–Varsharmov bound, 463
Golay codes, 423, 433
  extended, 423
  generator polynomial of, 433
  performance on AWGN channel, 454–455
Gold sequences, 727
Gram–Schmidt procedure, 167–173
Granular noise, 134
Gray encoding, 175

Hadamard codes, 422–423, 817–821
Hamming bound on minimum distance, 462
Hamming codes, 421–422, 433
Hamming distance, 415
Hard-decision decoding:
  block codes, 445–456
  convolutional codes, 489–492
Hilbert transform, 154
Huffman coding, 96–103

Illumination efficiency factor, 317
Impulse noise, 538
Impulse response, 68
Independent events, 21
Independent random variables, 28
Inforamtion, 84–85
  equivocation, 90
  measure of, 84–91
  mutual, 84
    average, 87
  self-, 85
    average (entropy), 88
  sequence, 3, 83
Interleaving, 468–470
  block, 469
  convolutional, 470
Intersymbol interference, 536–537
  controlled (*see* Partial response signals)
  discrete-time model for, 586–589
  equivalent white noise filter model, 588
  optimum demodulator for, 584–593
Inverse filter, 603

Jacobian, 32
Jamming margin, 707
Joint cdf (cumulative distribution function), 25
Joint pdf (probabiltiy density function), 25
Joint processes, 65

Kalman (RLS) algorithm, 656–658
  fast, 660
Kasami sequences, 729
Kraft inequality, 97–98

Laplace probability density function, 56
Lattice:
  filter, 660–664
  recursive least-squares, 664
Law of large numbers (weak), 59
Least favorable pdf, 305
Least-squares algorithms, 654–664
Lempel-Ziv algorithm, 106–108
Levinson-Durbin algorithm, 128, 139, 879–881
Likelihood ratio, 304
Line codes, 566
Linear codes (*see* Block codes, linear; Convolutional codes)
Linear equalization (*see* Equalizers, linear)
Linear-feedback shift-register, maximal length, 433–435, 724–727
Linear prediction, 128–130, 138–144, 660–664
  backward, 661–662
  forward, 661–662
  residuals, 663
Linear predictive coding (LPC):
  speech, 138–144
Linear time-invariant system, 68–69
  response to stochastic input, 68–72
Linear transformation of random variables, 28–29, 50–52
Link budget analysis, 316–319
Link margin, 319
Lloyd–Max quantizer, 113
Lowpass signal, 155
Lowpass system, 157
Low probability of intercept, 696, 715–716

Magnetic recording, 567–568
  normalized density, 567
Majority logic decoder, 506
Mapping by set partitioning, 512
Marginal probability density, 26
Marcum's Q-function, 44
Markov chain, 189
  transition probability matrix of, 189
Matched filter, 238–244
Maximal ratio combining, 779
  performance of, 780–782

Maximum a posteriori probability (MAP)
criterion, 245, 254–257
Maximum free distance codes, tables of, 492–496
Maximum length shift-register codes, 433–435, 724–727
Maximum likelihood:
parameter estimation, 333–335, 339–341
for carrier phase, 339–341
for joint carrier and symbol, 365–367
for symbol timing, 358–364
performance of, 367–370
Maximum-likelihood criterion, 245–246
Maximum-likelihood receiver, 233–257
Maximum-likelihood sequence estimation (MLSE), 249–254
Mean-square error (MSE) criterion, 607–617
Mean value, 33
Microwave LOS channel, 768–769
Miller code, 188, 575
Minimum distance:
bounds on, 461–464
definition, 416
Euclidean, 173
Hamming, 416
Minimum-shift keying (MSK), 196–199
power spectrum of, 213–219
Models:
channel, 375–386
source, 82–84, 93–95
Modified duobinary signal, 549–550
Modulation:
binary, 257–260
biorthogonal, 264–266
comparison of, 282–284
continuous-phase FSK (CPFSK), 190–191
power spectrum, 213–219
DPSK, 274–278
equicorrelated (simplex), 266
index, 191
linear, 174–186
power spectrum of, 204–209
M-ary orthogonal, 260–264
multichannel, 680–686
nonlinear, 190–203
offset QPSK, 198
PAM (ASK), 267–269
PSK, 269–274
QAM, 278–282
Modulation codes, 566–576 (*See also* Partial response signals)
capacity of, 569
Miller code, 573
NRZ, 574
NRZI, 566, 568, 574–575
run-length limited, 568–576
Modulation codes (*Cont.*):
run-length limited (*Cont.*):
fixed rate, 572
state dependent, 571
state independent, 571
Modulator:
binary, 2
digital, 2
M-ary, 2
Moments, 33
Morse Code, 13
Multicarrier communications
capacity of, 687–689
FFT-based system, 689–692
Multichannel communications, 680–686
with binary signals, 682–684
with M-ary orthogonal signals, 684–686
Multipath channels, 8, 758–839
Multipath intensity profile, 762
Multipath spread, 763
Multiple access methods, 840–849
capacity of, 843–849
CDMA, 843, 849–862
FDMA, 842
random access, 962–872
TDMA, 842
Multiuser communications, 840–872
Multivariate gaussian distribution, 49–52
Mutual information, 84
average, 87–88
Mutually exclusive events, 18

Narrowband interference, 704–706
Narrowband process, 152
carrier frequency of, 153
Narrowband signal, 152
Noise:
gaussian, 162
white, 162–163
Noisy channel coding theorem, 386–387
Noncoherent combining loss 683–684
Nonlinear distortion, 537
Nonlinear modulation, 190
Nonstationary stochastic process, 63
Norm, 165
Normal equations, 128
Normal random variables (*see* Gaussian distribution)
Null event, 18
Null space, 416
Nyquist criterion, 542–547
Nyquist rate, 14, 72

Offset quadrature PSK (OQPSK), 198
On-off signalling (OOK), 321

Optimum demodulation: (*see* Demodulation/Detection)
Orthogonal signals, 165–166
Orthogonality principle, mean-square estimation, 608
Orthonormal:
  expansion, 165–173
  functions, 165–166

Parity check, 417
  matrix, 419
Parity polynomial, 426
Partial-band interference, 734–741
Partial response signals, 548–560
  duobinary, 548–549
  error probability of, 562–565
  modified duobinary, 549
  precoding for, 551–555
Partial-time (pulsed) jamming, 717–724
Peak distortion criterion, 602–607
Peak frequency deviation, 190
Perfect codes, 453–454
Periodically stationary, wide sense, 75–76, 205
Phase jitter, 538
Phase-locked loop (PLL), 341–346
  Costas, 355–356
  decision-directed, 347–350
  M-law type, 356–358
  non-decision-directed, 350–351
  square-law type, 353–355
Phase-shift keying (PSK), 177–178, 269–274
  adaptive reception of, 887–896
  pdf of phase, 270–271
  performance for AWGN channel, 271–274
  performance for Rayleigh fading channel, 780–787, 887–894
Plotkin bound on minimum distance, 462
Power density spectrum, 67–68, 204–223
  at output of linear system, 69
  of digitally modulated signals, 204–223
Prediction (*see* Linear prediction)
Preferred sequences, 727
Prefix condition, 96
Probability:
  a priori, 21
  a posteriori, 21
  conditional, 20, 26–28
  of events, 18
  joint, 19, 25–26
Probability density function (pdf), 24
Probability distribution function, 23
Probability distributions, 37–52
  binomial, 37–38
  chi-square, 41–45
    central, 42–43
    noncentral, 42–44

Probability distributions (*Cont.*):
  gamma, 43
  gaussian, 39–41
  multivariate gaussian, 49–52
  Nakagami, 48–49
  Rayleigh, 45–46
  Rice, 47–48
  uniform, 39
Probability transition matrix, 377
Processing gain, 707
Pseudo-noise (PN) sequences:
  autocorrelation function, 725–726
  generation via shift register, 724–729
  Gold, 727
  Kasami, 729
  maximal-length, 725–726
  peak cross-correlation, 726–727
  preferred, 727
  (*See also* Spread spectrum signals)
Pulse amplitude modulation (PAM), 174–176, 267–269
Pulse code modulation (PCM), 125–133
  adaptive (ADPCM), 131–133
  differential (DPCM), 127–129
Pulsed interference, 717
  effect on error rate performance, 717–724

Quadrature amplitude modulation (QAM), 178–180, 278–282
Quadrature components, 155
  of narrowband process, 155–156
  properties of, 161–162
Quantization, 108–125
  block, 118–125
  optimization (Lloyd-Max), 113–118
  scalar, 113–118
  vector, 118–125
Quantization error, 125–133
Quasiperfect codes, 454

Raised cosine spectrum, 546
  excess bandwidth, 546
  rolloff parameter, 546
RAKE correlator, 797–798
RAKE receiver:
  for binary antipodal signals, 798–803
  for binary orthogonal signals, 801–802
  for DPSK signals, 804
  for noncoherent detection of orthogonal signals, 805
RAKE matched filter, 799–800
Random access, 862–872
  ALOHA, 863–867
  carrier sense, 867–872
    with collision detection, 868
    non persistent, 868

Random access (*Cont.*):
carrier sense (*Cont.*):
1-persistent, 869
p-persistent, 869
offered channel traffic, 864
slotted ALOHA, 864
throughput, 865–867
unslotted, 864
Random coding, 390–400
binary coded signals, 390–397
multiamplitude signals, 397–399
Random Processes (*see* Stochastic processes)
Random variables, 22–28
function of, 28–32
multiple, 25
orthogonal, 35
single, 22–24
statistically independent, 28
sums of, 58–63
central limit theorem, 61–62
transformation of, 28–32
Jacobian of, 32
linear, 28, 32, 49–52
uncorrelated, 34
Rate:
code, 2, 414
of encoded information (*see* Source encoding)
Rate distortion function, 108–113
of bandlimited gaussian source, 112
of memoryless gaussian source, 109–110
table of, 112
Rayleigh distribution, 45–46
Rayleigh fading (*see* Channel, fading multipath; Channel, Rayleigh fading)
Reciprocal polynomial, 426
Recursive least squares (RLS) algorithms, 654–664
fast RLS, 660
RLS Kalman, 656–660
RLS lattice, 660–664
Reed-Solomon codes, 464–466
References, 899–916
Reflection coefficients, 140
Regenerative repeaters, 314–316
Residuals, 663
Rice distribution, 47–48
Ricean fading channel, 761
Run-length limited codes, 568–576
fixed rate, 572
state dependent, 571
state independent, 571

Sample function, 63
Sample mean, 58
Sample space, 17–18
Sampling theorem, 72–73
Scattering function, 766
Self-information, 85
average (entropy), 88
Sequential decoding, 501–503
Set partitioning, 512
Shannon limit, 264
Shortened code, 421
Signal constellations:
PAM, 174–176
PSK, 177–178
QAM, 178–180
Signal design, 540–576
for band-limited channel, 540–551
for channels with distortion, 557–560
for no intersymbol interference, 540–547
with partial response pulses, 548–551
with raised cosine spectral pulse, 546–547
Signal-to-noise ratio (SNR), 258
Signals:
bandpass, 152–157
baseband, 176, 186–189
binary antipodal, 257
binary coded, 266–267
binary orthogonal, 258
biorthogonal, 183–184, 264–266
carrier of, 159
characterization of, 152–163
complex envelope of, 155
digitally modulated, 173–209
cyclostationary, 204–206
representation of, 173–202
spectral characteristics of, 202–223
discrete-time, 74–76
energy of, 156
envelope of, 155
equivalent lowpass, 155
lowpass, 155
M-ary orthogonal, 181–183
multiamplitude, 174–176
multidimensional, 180–181
multiphase, 177–178
narrowband, 152
optimum demodulation of, 233–257
quadrature amplitude modulated (QAM), 178–180
quadrature components of, 155–156
properties of, 161–162
simplex, 184, 266
speech, 143–144
stochastic, 62–77, 159–163
autocorrelation of, 64, 68–70, 75–76
autocovariance, 64
bandpass stationary, 159–163
cross correlation of, 65

Signals (*Cont.*):
stochastic (*Cont.*):
ensemble averages of, 64–65
power density spectrum, 67–68, 204–223
properties of quadrature components, 161–162
white noise, 162–163
Signature sequence, 843
Simplex signals, 266
Single-sideband modulation, 176
Skin depth, 9
Slope overload distortion, 134
Slope overload distortion, 134
Soft decision decoding:
block codes, 436–445
convolutional codes, 486–489
Source:
analog, 82–83
binary, 83
discrete memoryless (DMS), 82–83
discrete stationary, 103–106
endoding, 93–144
adaptive DM, 135–136
adaptive DPCM, 131–133
adaptive PCM, 131–133
delta modulation (DM), 133–136
differential pulse code modulation (DPCM), 127–129
discrete memoryless, 94–103
Huffman, 99–103
Lempel–Ziv, 106–108
linear predictive coding (LPC), 138–142
pulse code modulation (PCM), 125–127
models, 82–84
speech, 143–144
spectral, 136–138
waveform, 125–144
Source coding, 82–144
Spaced-frequency, spaced-time correlation function, 763
Spectrum:
of CPFSK and CPM, 209–219
of digital signals, 203–223
of linear modulation, 204–209
of signals with memory, 220–223
Spread factor, 771
table of, 771
Spread spectrum multiple access (SSMA), 716
Spread spectrum signals:
acquisition of, 774–748
for antijamming, 712–715
for code division multiple access (CDMA), 696, 716–717, 741–743
concatenated codes for, 711–712, 740–741
direct sequence, 697–700
applications of, 712–717
coding for, 710–712
Spread spectrum signals (*Cont.*):
direct sequence (*Cont.*):
demodulation of, 701–702
performance of, 702–712
with pulse interference, 717–724
examples of DS, 712–717
frequency-hopped (FH), 729–743
block hopping, 731
follower jammer for, 731
performance of, 732–734
with partial-band interference, 734, 741
hybrid combinations, 743–744
for low-probability of intercept (LPI), 696, 715–716
for multipath channels, 795–806
synchronization of, 744–752
time-hopped (TH), 743
tracking of, 748
uncoded PN, 708
Spread spectrum system model, 697–698
Square-law detection, 306
Square-root factorization, 660, 897–898
Staggered quadrature PSK (SQPSK), 198
State diagram, 196, 474–477
Stationary stochastic processes, 63–64
strict-sense, 63–64
wide-sense, 64
Statistical averages, 64–67
Steepest-descent (gradient) algorithm, 639–642
Stochastic process, 62–72, 159–163
cyclostationary, 75–76
discrete-time, 74–76
narrowband, 159
nonstationary, 63
strict-sense stationary, 63–64
wide-sense stationary, 64
Storage channel, 10
Strict-sense stationary, 63–64
Subband coding, 137
Symbol interval, 174
Synchronization:
carrier, 337–358
effect of noise, 343–346
for multiphase signals, 356–358
with Costas loop, 355–356
with decision-feedback loop, 347–350
with phase-locked loop (PLL), 341–346
with squaring loop, 353–355
of spread spectrum signals, 744–752
sliding correlator, 747
symbol, 336–337
Syndrome, 446
Syndrome decoding, 446–451
System, linear, 68–72
autocorrelation function at output, 69

System, linear (*Cont.*):
bandpass, response of, 157–159
power density spectrum at output, 69–70
Systematic code, 418

Tail probability bounds, 53–57
Chebyshev inequality, 53–54
Chernoff bound, 54–57
TATS (tactical transmission system), 741–743
Telegraphy, 13
Telephone channels, 4, 563–538
Thermal noise, 3, 11
Threshold decoder, 506
Time diversity, 777
Time division multiple access (TDMA), 842–844
Toeplitz matrix, 879
Transfer function:
of convolutional code, 477–483
of linear system, 68–72
Transformation of random variables, 29–32, 49–52
Transition probabilities, 189
Transition probability matrix, 189
for channel, 375–378
for delay modulation, 189–190
Tree diagram, 192–195, 471–472
Trellis-coded modulation, 511–526
free Euclidean distance, 517
subset decoding, 519
tables of coding gains for, 522–523
Trellis diagram, 473

Uncorrelated random variables, 34
Uniform distribution, 39
Union bound, 263–264, 387–389
Union of events, 18
Uniquely decodable, 96
Universal source coding, 106

Variable-length encoding, 95–103
Variance, 33
Vector space, 163–165
Vector quantization, 118–125
Viterbi algorithm, 251, 287–289, 483–486
Vocal tract, 141–143
Voltage-controlled oscillator (VCO), 341–343

Weak law of large numbers, 59
Weight:
of code word, 414
distribution, 414
for Golay, 423
Welch bound, 728
White noise, 162–163
Whitening filter, 587–588
Wide-sense stationary, 64
Wiener filter, 14

Yule–Walker equations, 128

Z transform, 587
Zero-forcing equalizer, 602–605
Zero-forcing filter, 603–604